Late Quaternary vegetation and climate history reconstructed from palynology of marine cores off southwestern New Zealand

A thesis submitted in fulfilment of the requirements for the
degree of Doctor of Philosophy in Earth Sciences
at
Victoria University of Wellington

By
Matthew Thomas Ryan

School of Geography, Environment and Earth Sciences
Victoria University of Wellington
2017

Supervised by:
Prof. Rewi Newnham
Dr. Gavin Dunbar
Dr. Marcus Vandergoes

Frontispiece: The marine-terrestrial interface at Jackson Bay south Westland.

Abstract

Little is known about how mid-latitude Southern Hemisphere terrestrial vegetation responded during glacial terminations and the warmer phases of the Late Quaternary, especially beyond the last glacial cycle where records are commonly fragmentary and poorly-dated. The timing, magnitude and sequence of environmental changes are investigated here for terminations (T) I, II and V and their subsequent warm interglacials of MIS 1, 5e and 11 by direct correlation of terrestrial palynomorphs (pollen and spores) and marine climate indicators in marine piston cores MD06-2990/2991 recovered from the East Tasman Sea, west of South Island, New Zealand. The climate there is strongly influenced by the prevailing mid-latitude westerly wind belt that generates significant amounts of orographic rainfall and the proximity of the ocean which moderates temperature variability. Chronological constraint for the cores is provided by $\delta^{18}O$ stratigraphy, radiocarbon chronology and the identification of two widespread silicic tephra horizons (25.6 ka Kawakawa/Oruanui Tephra (KOT); ~345 ka Rangitawa Tephra (RtT)) sourced from the central North Island.

Similar vegetation changes over the last two glacial cycles at MD06-2991 and in the adjacent nearby on land record of vegetation-climate change from Okarito Bog permit transfer of the well resolved Marine Isotope Stage (MIS) chronology to Okarito for the pre radiocarbon dated interval (~139-28 ka). Placing both sequences on a common age scale nonetheless assumes there is minimal lag between pollen production and final deposition on the seafloor. However, the timing of Late Pleistocene palynomorph events and KOT between independently dated marine and terrestrial sedimentary sequences are found in this study to be indistinguishable, which supports the direct transfer of terrestrially derived ages to the marine realm and vice versa.

Vegetation change in southwestern New Zealand is of similar structure during T-I and T-II, despite different amplitudes of forcing (i.e., insolation rise, CO_2 concentrations). In a climate amelioration scenario, shrubland-grassland gave rise to dominantly podocarp-broadleaf forest taxa, with accompanying rises in mean annual air temperature (MAAT) estimated from Okarito pollen typically synchronous with nearby ocean temperatures. The T-II amelioration commenced after ~139 ka in response to increasing boreal summer insolation intensity, with prominent ocean-atmosphere warming over the period from ~133-130 ka. In contrast, northern mid-high latitude paleoclimate records display cooling over Heinrich Stadial 11

(~135-130 ka), and are prominently warm from ~130-128 ka, while southwestern New Zealand and the adjacent ocean displays cooling. Such millennial-scale climate asynchrony between the hemispheres is most likely a result of a systematic, but non-linear re-organisation of the ocean-atmosphere circulation system in response to orbital forcing. The subsequent MIS 5e climatic optimum in Westland was between ~128-123 ka, with maximum temperatures reconstructed in the ocean and atmosphere of 2.5°C and 1.5°C higher than present.

Similarities revealed between land and sea pollen records in southwestern New Zealand over the last ~160 ka offer confidence for assessing vegetation and climate for older intervals, including T-V/MIS 11, for which no adjacent terrestrial equivalents currently exist. Vegetation change over T-V is similar to T-II and T-I, with southern warming antiphased with northern mid-high latitude cooling. Tall trees and the thermophilous shrub *Ascarina lucida* define interglacial conditions in the study region between ~428-396 ka. East Tasman Sea surface temperatures rose in two phases; 435-426 ka (MIS 12a-MIS 11e) and 417-407 ka (MIS 11c climatic optimum), reaching at least ~1.5-2°C warmer than present over the latter. Similarly, *Ascarina lucida* dominance over MIS 11c is akin to that displayed during the early Holocene climatic optimum (11.5-9 ka) in west-central North Island, where MAAT average ~3°C higher today. This contrasts markedly with the dominance of the tall tree conifer *Dacrydium cupressinum* for the Holocene (MIS 1) and last interglacial (MIS 5e) in southwestern New Zealand. Biogeographic barriers are proposed to have inhibited the migration of species from more northerly latitudes better adapted to warmer climatic conditions over MIS 5e and MIS 11.

Acknowledgements

No academic thesis is possible without good supervision. First and foremost, I express my deepest gratitude to my supervisors Prof. Rewi Newnham, Dr. Gavin Dunbar and Dr. Marcus Vandergoes for their patience, guidance, and recommendations through this thesis. Thank you for providing me with such a great project and for attempting to keep me on a leash and focused, I know how much of a Jack Russell I am. Rewi, thanks for persisting with me, you are truly world class and I have learnt an incredible amount under your leadership. Gavin, thanks for being a right hand man and stepping in, you're a vibrant researcher and you always challenge me. Marcus, thanks for your valuable input and direction as an extra set of eyes when it was needed and access to published and unpublished (Okarito Bog) data used in the study.

Thanks to the officers and crew from the MATACORE *R.V Marion Dufresne* cruise MD-152 for the collection of the cores and on-board data used in this study. I am grateful to NIWA, in particular to Helen Neil and Helen Bostock for allowing access to the cores, and data used in the study, and for helpful advice. Big Bad Brent "Victor" Alloway, you are an amazing guy and I'm honoured to call you a really good mate. Cheers BVA, I'll try keep being the mini tomb raider. Many thanks to Andrew Rees, for help with OxCal and for helping provide guidance. Thanks to Lou for positivity and Manks Tarn discussions. Thanks to Brian Anderson for tying himself to the Totara River bridge while it was in flood. Thanks to Marcus Vandergoes and Janet Wilmshurst for the pollen-climate reconstructions and Marcus Vandergoes and Xun Li for additional pollen analysis from Okarito Bog. Thanks go to George Scott, Bruce Hayward and Ashwaq Sabaa for discussions on ocean temperature reconstructions. Many appreciations to Euan Smith for help with age model uncertainties. Credits go to Ralph Tiedemann and Silke Steph for acquisition of MD06-2990 data. Thanks to Shaun Eaves for calculation of ^{10}Be reanalysis.

Thanks to Bill McLea and Dallas Mildenhall for discussions on New Zealand palynology and flora. Thanks to Linda Heusser and Joe Prebble for providing me with the DSDP Site 594 data used in this study. I am appreciative of Christopher Bronk Ramsey for his advice on OxCal v4.2.4. Chapter 3 benefited from constructive comments by Katie Collins and Christine Prior. Thanks to Lionel Carter for being you, your enthusiasm is simply infectious and you always make me laugh. You are my idol. To Mike "Dog", for making sure I'm alive, and that I eventually finished. To the Antarctic Research Centre (ARC) staff, Peter, A-Mac,

Fester, Nick, Cliff, Big T, and Mantis for helpful suggestions over the years and for including me in your activities. Thanks to technical staff Jane, Deno, A-Rae.

Thanks to all of the other past and present postgraduate students and staff at Victoria for providing me with lots of laughs and memories, there are too many to thank. If you're reading this then you are special to me. Katie, thanks for being such a great office mate in the "Danger Zone", you helped me so much matey! Condor, my fellow dactyl, you rock. Dez, lad, my man. Nachito, been a pleasure to go on this journey with you lad. Hammer, Bella, Rich, Juliet, Jenny, Shaun, Viking, Cam, Kraus, Creech, Sam, Barks, Elliot, Shano, Heidi, Coop, Georgia, Val, Dom, Kayt, Aidan, Zrb. Thanks to Fi for your motivational words of wisdom. To K.B, you're a fun and caring girl, love the adventures with you. Thanks to VUWFC for taking my mind away from study, and for all the good times (Rowe, Willy, Inky, CC, Errrobbo, Si, Mitch), and to the old Geol crew (Kim, Bass, Molnar, Rach, Boot, James, Dog, Moon, Bod, Bull, Rood). Shot to the Dev and Moala. Thanks to N. Lakes peeps, Pistol, Blick, Amanda, Kirsty, Latu, Koz, Tamlyn. Thanks to Griggs, Tom, O.B peeps Loli and Nic, and sauna crew. To Ash, thanks for being amazing during all the late nights writing. Thanks for making sure I took breaks, and for sharing amazing holidays together. Even though we have parted our ways, I'll never forget. Thank you to Ron and Karen for their help during this time as well.

Finally, most importantly, thanks to my family and extended family for which I owe everything for, and love lots. Nana and Poppa for making me laugh on weekends at afternoon tea; it really took the stress off. Taking you out over the last few years have been amazing. Thank you for always being there for me. To my sisters Nicole and Julia, and brother-in-law Adrian, thanks for always caring, understanding and helping me when I most needed it. I couldn't have done this without you. To my lovely nieces, Michaela, Ava and Pippa, thanks for making me smile, you all mean the world to me, and I'll always be there for you. Mum, for supporting me and loving me. Thanks for always checking up on me, making sure I'm alright, and seeing how things are going, love you lots. Extended thanks go to Kevin's family, although not for the "are you finished yet"?

Most definitely the hardest part to write, and to those I couldn't tell in person, to my step-dad Kevin, and to my dad. Thank you for everything you helped me achieve in life, I strive to be the pillars that you both were for me one day, I love you and miss you lots.

M.T. Ryan.

This thesis is dedicated to my family

In particular to Nana and Poppa, thank you for your constant support.
You are truly inspirational. I'm glad I got to show you this both before Poppa passed away.

Love you so much.

Table of Contents

Abstract v

Acknowledgements vii

Table of Contents xi

List of Figures xv

List of Tables xvii

List of Appendices xviii

List of Abbreviations xxii

1. Introduction and Rationale 1

1.1 Overview 1

1.2 Previous research and research aims of this thesis 8

1. *Poor age control of terrestrial paleoenvironmental records beyond radiocarbon timescales* 8

2. *Assumption of negligible timing for pollen transfer to the ocean* 8

3. *Assessment of leads and lags in the climate system from discrete sequences* 9

4. *The scarcity of quantifiable estimates of air temperature for the last interglacial (LIG)* 9

5. *Length of terrestrial paleoclimate record* 9

1.3 Key themes of this thesis 11

1.4 Rationale for the site location, and review of aims and key themes 11

1.5 Structure of the thesis 15

1.6 Statement on the contributions made to this thesis by the author, supervisors and collaborators 16

1.7 Conference presentations resulting from this thesis 18

1.8 Awards resulting from this thesis 19

1.9 Scholarships and funding contributing to this thesis 19

2. Background 20

2.1 Present-day vegetation/pollen relationships for paleoecology 20

2.1.1 Representivity of terrestrial palynomorphs 21

2.1.2 Pollen taphonomy and residence pathways of terrestrial pollen reaching the marine realm 23

2.1.3 Marine-terrestrial core comparison in southwestern New Zealand 25

2.2 Key taxa used in climate reconstructions 29

2.3 Climate event stratigraphy for southwestern New Zealand and the adjacent ocean over the last 450 ka 31

2.3.1 Chronological constraint 31

2.3.2 Glacial climate 35

2.3.3 Climate amelioration over T-I and T-II and hemispheric asynchronies 38

2.3.4 Interglacial climate 40

2.4 Climate variables and vegetation 41

2.5 Modern vegetation of Westland 45
2.6 Summary 46
3. Exploring the source-to-sink residence time of terrestrial pollen deposited offshore Westland, New Zealand 48
3.1 Introduction 48
3.2 Study region 50
3.2.1 Terrestrial environment 50
3.2.2 Marine environment 52
3.2.3 Westland's late Pleistocene palynomorph sequence 53
3.3 Methods 53
3.3.1 Radiocarbon dating of fluvially-transported material 53
3.3.2 Radiocarbon dating and numerical methods 55
3.3.3 Comparing the timing of key events in marine and terrestrial records 56
3.3.4 MD06-2991 palynology 59
3.3.5 Kawakawa/Oruanui Tephra (KOT) at MD06-2991 and onshore correlatives 60
3.4 Results 62
3.4.1 Radiocarbon dating of fluvially-transported material 62
3.4.2 Comparing the timing of key events in marine and terrestrial records 62
3.5 Discussion 65
3.5.1 Radiocarbon dating of fluvially-transported component 65
3.5.2 Comparing the timing of key events in marine and terrestrial records 66
3.5.3 The Kawakawa/Oruanui Tephra 68
3.6 Conclusions 68
3.7 Contributions 69
4. Ocean and atmospheric interactions from south-west New Zealand over the last two terminations and interglacials 70
4.1 Introduction 71
4.2 Materials and methods 77
4.2.1 Sample selection and processing for MD06-2991 77
4.2.2 MD06-2991 chronology 78
4.2.3 MD06-2991 sea surface temperature (SST) estimates 82
4.2.4 MD06-2991 $CaCO_3$ and siliciclastic sediment content 82
4.2.5 Okarito bog chronology and palynology (153-9.5 kyr) 83
4.2.6 CONISS and Regional Pollen Assemblage Zones (RPAZ) 87
4.2.7 Okarito mean annual air temperature reconstruction (MAAT) 87
4.3 Results 89
4.3.1 MD06-2991 (Sedimentation, $CaCO_3$, $\delta^{18}O$, SST, pollen) 89
4.3.2 Pollen and SST change from southwestern New Zealand 89
4.4 Discussion 101
4.4.1 Palynomorph taphonomy, representivity, and paleovegetation reconstruction 102
4.4.2 The onset of Okarito Bog sedimentation 104

4.4.3 Climate event stratigraphy and chronological uncertainty for MIS 6-5 from southwestern New Zealand 105
4.4.4 Radiocarbon chronology of Termination I in southwest New Zealand 109
4.4.5 The 'local' Penultimate Glacial maxima 118
4.4.6 The penultimate glacial-interglacial transition (PGIT) 121
4.4.7 The timing and duration of the last interglacial (LIG) in southwestern New Zealand (~128-116 ka) 127
4.4.8 The amplitude of LIG temperature change and seasonality 129
4.5 Conclusion 137
4.6 Contributions 140
5. Ocean-atmosphere reconstructions over MIS 11 from southwestern New Zealand 141
5.1 Introduction 143
5.2 Environmental framework: 146
5.2.1 Umutekai Bog (early Holocene analogue) 147
5.2.2 Rangitawa Tephra (RtT) 147
5.3 Materials and methods 149
5.3.1 Core information and sampling and chronology 149
5.3.2 Chronological uncertainty 150
5.3.3 Rangitawa Tephra (RtT) 154
5.3.4 MD06-2990 sea surface temperature (SST) estimates 154
5.4 Results 156
5.4.1 Southwestern New Zealand profiles (palynology and SST) 156
5.4.2 Rangitawa Tephra 161
5.5 Discussion 163
5.5.1 The MIS 12 glacial 163
5.5.2 Climate amelioration over Termination V in southwestern New Zealand 164
5.5.3 South Island vegetation change during early MIS 11(e-d) 171
5.5.4 The timing and amplitude of the MIS 11c climatic optimum (417-407 ka) 173
5.5.5 Progressive cooling and sub-orbital climate variability from MIS 11b-10a 178
5.5.6 The deposition of Rangitawa Tephra (RtT) and its significance for T-IV 179
5.6 Contributions 184
6. Synthesis 185
6.1 What is the source-to-sink residence time (RT) of terrestrial pollen deposited offshore Westland, New Zealand? 185
6.2 What is the sequence of environmental changes for terminations I, II and V and their subsequent warm interglacials (MIS 1, 5e, 11) from southwestern New Zealand? How do their timing and magnitude relate to climate forcing, paradigms of terminations, and existing climate observations? 187
6.2.1 The termination of glacial conditions during MIS 12, 6 and 2 in southwestern New Zealand and the ETS 187

6.2.2 Climate amelioration over land and ocean in southwestern New Zealand and the East Tasman Sea during terminations 192
6.2.3 Does each termination register the appearance of millennial scale climate reversals as noted globally for T-I? 193
6.2.4 Is the pattern of climate amelioration between land and sea synchronous for all three interglacials or is there evidence for lags in the climate system? 194
6.2.5 Are vegetation changes in the southwestern New Zealand during interglacials of similar character and magnitude? 194
6.2.6 Were past interglacials (MIS 1, 5e and 11) in southwestern New Zealand warmer than present, and what do they tell us about future climate in a warming world? 195
6.3 Summary 197
References 198
Appendix One Supplementary Figures 229
Appendix Two Supplementary Tables 285
Appendix Three Exploring the source-to-sink residence time of terrestrial pollen deposited offshore Westland, New Zealand 293

List of Figures

Chapter 1

Fig. 1.1 Paleoclimate records and orbital parameters over the last 450 ka 2

Fig. 1.2 Essential elements of a termination following Denton et al. (2010) 5

Fig. 1.3 Peak global mean temperature, atmospheric CO_2, maximum global mean sea level (GMSL), and source(s) of meltwater 6

Fig. 1.4 Regional setting of the study area 13

Fig. 1.5 Regional distribution of modern annual sea surface temperature (SST) and water masses 14

Chapter 2

Fig. 2.1 Relationship between the size of the terrestrial sites in Westland 23

Fig. 2.2 Source-to-sink transport pathways and the residence time of fluvially transported palynomorphs (RT) from Westland to the East Tasman Sea 27

Fig. 2.3 Key palynomorph taxa from TAN0513-14 and Okarito Bog (last two glacial cycles) 28

Fig. 2.4 Selected pollen and spore types and their correlation with mean annual air temperature 31

Fig. 2.5 Studies of terrestrial palynology from south to north Westland, South Island, NZ 34

Fig. 2.6 NZ INTIMATE Climate Event Stratigraphy (30-0 ka) 35

Fig. 2.7 Distribution of the Kawakawa/Oruanui Tephra (KOT) in the New Zealand region 36

Fig. 2.8 Vegetation cover of New Zealand at 21 ka 38

Fig. 2.9 Modern climate variables (A-E) influencing Westland vegetation 45

Fig. 2.10 Flooding and bank erosion vs. low flow and no erosion, Westland 45

Chapter 3

Fig. 3.1 Regional setting showing sampling sites and locations 52

Fig. 3.2 Age-depth model and stratigraphy for MD06-2991 59

Fig. 3.3 Glass shard major element bivariate plots of Kawakawa/Oruanui Tephra (KOT) 62

Fig. 3.4 Principal components analysis of fluvially-transported radiocarbon data set 64

Fig. 3.5 Summary pollen percentage diagram for MD06-2991 and location of key palynomorph events since 30 cal kyr BP 65

Fig. 3.6 Calibrated calendar year ages and error range of the KOT and four palynomorph events at MD06-2991 and their correlatives in Westland terrestrial records 68

Chapter 4

Fig. 4.1 Location of key sites around the globe referred to in text 75

Fig. 4.2 Regional setting of the study area 77

Fig. 4.3 MD06-2991 age model and SST reconstruction 82

Fig. 4.4 Chronostratigraphic correlation of event based palynomorph calibration points (PCPs) between MD06-2991 and Okarito Bog over the interval 160-95 ka (MIS 6c to 5c) 86

Fig. 4.5 Partial percentage pollen diagram showing the prominent dryland pollen taxa for MD06-2991 over 27-9 cal ka BP 94

Fig. 4.6 Partial percentage pollen diagram showing the prominent dryland pollen taxa for Okarito Bog over 27-9.5 cal ka BP 95

Fig. 4.7 Partial percentage pollen diagram showing the prominent dryland pollen taxa for T-II to MIS 5c at MD06-2991 100

Fig. 4.8 Partial percentage pollen diagram showing the prominent dryland pollen taxa for T-II to MIS 5c at Okarito Bog (aligned to the MD06-2991 chronology) 101

Fig. 4.9 Southwestern New Zealand climate event stratigraphy (160-98 ka) 109

Fig. 4.10 Integration of Ice, Marine and Terrestrial (INTIMATE) records from 18-9.5 cal ka BP..... 111

Fig. 4.11 Three reconstructions of the Southern Subtropical Front–S-STF (yellow line) and Dynamical Subtropical Front–DSTF for the southwest Pacific Ocean 113

Fig. 4.12 Integration of key Ice, Marine and Terrestrial (INTIMATE) records from 160-98 ka 121

Fig. 4.13 Comparison between TI and T-II 125

Fig. 4.14 Map of MIS 5e SST anomalies 135

Chapter 5

Fig. 5.1 Location of all land and sea records which encompass the MIS 11 interglacial. 148

Fig. 5.2 MD06-2991 age model and SST reconstruction 154

Fig. 5.3 MD06-2990 age model and SST reconstruction 155

Fig. 5.4 Core stratigraphy, age model and partial percentage dryland pollen diagram from T-V to T-IV for MD06-2990 161

Fig. 5.5 Core stratigraphy, age model and partial percentage dryland pollen diagram from T-V to T-IV for MD06-2991 162

Fig. 5.6 Glass shard major element bivariate plots of Rangitawa Tephra (RtT) 164

Fig. 5.7 Integration of key Ice, Marine and Terrestrial records from 460-335 ka 170

Fig. 5.8 Comparison between T-I and T-V 172

Chapter 6

Fig. 6.1 Comparison between T-I, T-II and T-V 191

Fig. 6.2 Paleoceanographic reconstructions around New Zealand during: (a) modern, (b) interglacials MIS 11 and 5e, (c) MIS 2 193

List of Tables

Chapter 1

Table 1.1 Timing and duration of key climate events included in this thesis 3

Table 1.2 Datasets discussed in this thesis (published and unpublished), their source, and the contribution or revision of that data by M.T. Ryan 17

Chapter 2

Table 2.1 Palynological indicators of vegetation and climatic change in southwestern New Zealand 32

Chapter 3

Table 3.1 Organic material samples collected from Westland rivers submitted for ^{14}C dating 56

Table 3.2 Details of radiocarbon age measurements from MD06-291 58

Chapter 4

Table 4.1 Radiometric Datum List for speleothem vs. LR04 stack correlation after Caballero-Gill et al. (2012a). 80

Table 4.2 MD06-2991 palynostratigraphic calibration points (PCPs) to Okarito Bog 87

Table 4.3 Key palynomorph changes at MD06-2991 and Okarito Bog, and the respective estimates of sea surface temperature (SST) and mean annual air temperature (MAAT) across Termination I (T-I) 93

Table 4.4 Comparison between vegetation changes recorded at MD06-2991 and Okarito Bog, and their respective estimates of SST and MAAT 99

Chapter 5

Table 5.1 Key palynomorph changes and their vegetation inferences drawn for southwestern New Zealand from MD06-2990/MD06-2991, in relation to marine isotope stages (MIS) determined from the $\delta^{18}O$ for this core and SST estimates 160

Table 5.2 Comparison of SST reconstructions adjacent to South Island New Zealand for the warm interglacial periods 177

List of Appendices

Appendix 1 (Supplementary Figures)

Supplementary Figures for Chapter 2

Suppl. Fig. 2.1 Median annual total rainfall for West Coast, South Island, New Zealand 230

Suppl. Fig. 2.2 Median annual temperature (°C) for West Coast, South Island, New Zealand 231

Supplementary Figures for Chapter 3

Suppl. Fig. 3.1 Age-depth model and stratigraphy for the Okarito Bog record 232

Suppl. Fig. 3.2 Age-depth model and core stratigraphy for the Galway Tarn 233

Suppl. Fig. 3.3 Age-model and core stratigraphy for the Gillespies Beach Rd (GBR) record 234

Suppl. Fig. 3.4 Age-depth model for the Manks Tarn record 235

Suppl. Fig. 3.5 Summary pollen diagram for Okarito Bog 236

Suppl. Fig. 3.6 Summary pollen diagram for Galway tarn 237

Suppl. Fig. 3.6 Summary pollen diagram for Gillespies Beach Rd 238

Suppl. Fig. 3.7 Summary pollen diagram for Manks Tarn 239

Suppl. Fig. 3.8 Field emission scanning electron microprobe image of an organic particle from MD06-2991 240

Supplementary Figures for Chapter 4

Suppl. Fig. 4.1 $\delta^{18}O$ record from ODP 1146 (light blue) tuned to LR04 benthic $\delta^{18}O$ chronology (Lisiecki and Raymo, 2005) and $\delta^{18}O$ radiometric U/Th chronology composite record from Sanbao and Hulu Caves 241

Suppl. Fig. 4.2 LR04 benthic $\delta^{18}O$ record vs. SPECMAP $\delta^{18}O$ record 242

Suppl. Fig. 4.3 Original and resampled ^{18}O curves for LR04 and MD2991 (158-28 ka) 244

Suppl. Fig. 4.4 MD06-2991 (158-28 ka) best fit 245

Suppl. Fig. 4.5 Original and resampled ^{18}O curves for LR04 and MD2991) (158-98 ka) 246

Suppl. Fig. 4.6 MD06-2991 (158-98 ka) best fit 247

Suppl. Fig. 4.7 Distribution of faunal foraminiferal-based core top samples from the Pacific region, contributing to 1223 samples applied in the SH0911 database 248

Suppl. Fig. 4.8 Comparison of MD06-2991 and MD06-2986 age model and SST estimates 249

Suppl. Fig. 4.9 The 95% confidence interval for the mean C2RF500 estimates 250

Suppl. Fig. 4.10 Palynostratigraphic calibration points from MD06-2991 to Okarito Bog 251

Suppl. Fig. 4.11 Inverse sedimentation rate for Okarito Bog 252

Suppl. Fig. 4.12 Age-depth model and associated age uncertainty for pollen sample depths from the Okarito Bog pollen profile 253

Suppl. Fig. 4.13 Depth error bar model and comparison of palynomorph taxa between Okarito Bog and MD06-2991 254

Suppl. Fig. 4.14 Schematic displaying the transfer of PCPs from MD06-2991 (MD) to generate the chronology and uncertainty for Okarito Bog (OB) over ~T-II 255

Suppl. Fig. 4.15 MD06-2991 chronology, SST estimates and palynology 256-258

Suppl. Fig. 4.16 Variability in the dominant species in the biogeographic groups of foraminifera across MIS 6-1 259

Suppl. Fig. 4.17 Comparison of Okarito Bog (OB) age models derived by palynostratigraphic approaches from the $\delta^{18}O$ dated MD06-2991 record and that from TAN0513-14 260

Suppl. Fig. 4.18 Revised Okarito Bog pollen percentage diagram 261-263

Suppl. Fig. 4.19 Recalibrated radiocarbon (^{14}C) ages of wood from glacial sediments preserved in Canavans Knob 264

Suppl. Fig. 4.20 Revised age model for DSDP-594 and additional proxies 265

Suppl. Fig. 4.21 Prominent dryland pollen taxa for Greens Beach 266

Suppl. Fig. 4.22 Prominent dryland pollen taxa for Chesterfield 267

Suppl. Fig. 4.23 Prominent dryland pollen taxa for Candle Light 267

Supplementary Figures for Chapter 5

Suppl. Fig. 5.1 Original and resampled ^{18}O curves for LR04 and MD2990 (~500-0 ka) 268

Suppl. Fig. 5.2 MD06-2990 (~500-0 ka) best fit 269

Suppl. Fig. 5.3 Colourless and vesicular cuspate Rangitawa Tephra (RtT) glass shards in palynological slides (<2.0 g cm^3) from MD06-2991 270

Suppl. Fig. 5.4 Glass shards containing mineral inclusions assigned to Rangitawa Tephra (RtT) in palynological slides (<2.0 g cm^3) from MD06-2990 271

Suppl. Fig. 5.5 Uncertainty calculated for SST estimates for MD06-2990 272

Suppl. Fig. 5.6 MD06-2990 chronology, SST estimates and palynology 273-276

Suppl. Fig. 5.7 MD06-2991 chronology, SST estimates and palynology 277-279

Suppl. Fig. 5.8 DSDP-594 age model (MIS 12-10) and additional core properties 280-281

Suppl. Fig. 5.9 Age-model and core stratigraphy for the Umutekai Bog record 282-283

Suppl. Fig. 5.10 Summary pollen diagram for selected taxa from Umutekai Bog for the late glacial to early Holocene 284

Appendix 2 (Supplementary Tables)

Supplementary Tables Figures for Chapter 3

Suppl. Table 3.1. Mean major element composition of glass shards from East Tasman Sea marine cores compared with South Island & offshore Kawakawa/Oruanui Tephra (KOT) correlatives 286

Supplementary Tables Figures for Chapter 4

Suppl. Table 4.1. Mean Age-depth model and sampling resolution ($\delta^{18}O$ measurements, SST estimates and palynology) undertaken on MD06-2991 287

Suppl. Table 4.2. Okarito bog $\delta^{18}O$ chronology 288

Supplementary Tables Figures for Chapter 5

Suppl. Table 5.1. Site location and analysis 289

Suppl. Table 5.2. Sedimentation rate and sample resolution for marine cores 290

Suppl. Table 5.3. Mean major element composition of glass shards from MD06-2991 and DSDP-594, compared with selected offshore and onshore Rangitawa Tephra correlatives 291

Suppl. Table 5.4. DSDP Site 594 revised isotope stratigraphy 292

Appendix 3 (PDF in back pocket)

Matthew T. Ryan, Rewi M. Newnham (corresponding author), Gavin B. Dunbar, Marcus J. Vandergoes, Andrew B.H. Rees, Helen L. Neil, S. Louise Callard, Brent V. Alloway, Helen Bostock, Quan Hua, Brian M. Anderson (2016). Exploring the source-to-sink residence time of terrestrial pollen deposited offshore Westland, New Zealand. *Review of Paleobotany and Palynology*, 230, pp. 37-46.

Digital Appendix

OxCal Scripts (MD06-2991/Galway Tarn/Okarito Bog/Galway Tarn/Gillespies Beach Rd/Umutekai Bog)

Random Forest uncertainty MD06-2990/1

Faunal based SST counts MD06-2990/2991

Pollen counts from MD06-2990 and 2991

Oxygen isotope data/MD06-2991 age depth model

Oxygen isotope data/MD06-2990 age depth model

Okarito Bog MAAT data (22-6 ka and 153-98 ka), and MD06-2991 age model aligned to Okarito Bog depths

PDF of Ryan et al. (2016)

List of Abbreviations

AASW	Antarctic Surface Water
ACC	Antarctic Circumpolar Current
ACR	Antarctic Cold Reversal
AIM	Antarctic Isotope Maxima
AMOC	Atlantic Meridional Overturning Circulation
AMS	Accelerated Mass Spectrometry
ANN	Artificial Neural Network
ANSTO	Australian Nuclear Science and Technology Organisation
APIS	Antarctic Peninsula Ice Sheet
BST	Boundary Stream Tarn
CA	Cascade Plateau moraines
$CaCO_3$	Calcium carbonate
CK	Canavans Knob
CONISS	Constrained cluster analysis
CT	Cropp Till
DCA	Detrended Correspondence Analysis
DF	Degrees of Freedom
DPS	Dryland pollen sum
DRE	Dense Rock Equivalent
DSDP	Deep Sea Drilling Project
EAC	East Australian Current
EACe	East Australian Current extension
EAIS	East Antarctic Ice Sheet
EDC	EPICA Dome C (ice core)
EDML	EPICA Dronning-Maudland (ice core)
EPICA	European Project for Ice Coring in Antarctica
ESI	East South Island
ES	Estuarine Storage
ESI	East South Island
ETS	Eastern Tasman Sea
FD	Final Deposition
GBR	Gillespies Beach Road
GHG	Greenhouse Gases
G-IG	Glacial-Interglacial
GIS	Greenland Ice Sheet
GMSL	Global Mean Sea Level
GT	Galway Tarn
HS	Heinrich Stadial
Ht	Heinrich "type"
INTIMATE	Integration of Ice Marine and Terrestrial archives
IPD	Initial Pollen Deposition
IRD	Ice Rafted Debris
IRSL	Infrared stimulated Luminescence
ITCZ	Inter-Tropical Convergence Zone
KOT	Kawakawa/Oruanui Tephra
LC	Leewin Current
LGCP	Last Glacial Cold Period
LGI	Last Glacial Inception
LGIT	Last Glacial-Interglacial Transition

LGM	Last Glacial Maximum
LIG	Last Interglacial
LINZ	Land Information New Zealand
LR04	Lisiecki and Raymo $\delta^{18}O$-age reference curve
MASL	Metres above sea level
MAAT	Mean Annual Air Temperature
MAT	Modern Analogue Technique
MBE	Mid-Brunhes Event
MBSF	Metres below sea floor
MD	*Marion Dufresne*
MIS	Marine Isotope Stage
MISE	Mean Integrated Square Error
MLSH	Mid-latitude Southern Hemisphere
MOR	Macro Organic Residue
MPT	Mid-Pleistocene Climate Transition
MT	Manks Tarn
MWP	Melt Water Pulse
NCEP	National Centres for Environmental Prediction
NEEM	North Greenland Eemian Ice Drilling
NGRIP	North Greenland Ice core Project
NH	Northern Hemisphere
NIWA	National Institute of Water and Atmosphere
NZ	New Zealand
NZCES	New Zealand INTIMATE Climate Event Stratigraphy
OB	Okarito Bog
ODP	Ocean Drilling Program
OR	Organic Residue
PC1/2	Principal Component Axes
PC	Pollen Concentrate
PCA	Principle Component Analysis
PCP	Palynostratigraphic Calibration Point
PF	Polar Front
PGCP	Penultimate Glacial Cold Period
PGIT	Penultimate Glacial-Interglacial Transition
PLS	Partial Least Squares Regression
P/P	*Podocarpus/Prumnopitys*
PPMV	Parts per Million (volume)
RF	Random Forest
RMSEP	Root Mean Square of Predictions Error
RPAZ	Regional Pollen Assemblage Zone
RT	Residence Time
RtT	Rangitawa Tephra
R/V	Research Vessel
SAF	Subantarctic Front
SAW	Sub-Antarctic Surface Waters
SC	Southland Current
SH	Southern Hemisphere
SHWW	Southern Hemisphere Westerly Winds
SM	Shallow marine
SPD	Secondary pollen deposition
Spp.	Species (genus level)
SPT	Sodium polytungstate

SST	Sea Surface Temperature
STF	Sub-Tropical Front
STW	Sub-Tropical Surface Waters
TDP	Total Dry Land Pollen
TF	Tasman Front
TVZ	Taupo Volcanic Zone
VPDB	Vienna Peede belemnite
VSMOW	Vienna Standard Mean Ocean Water
WAIS	West Antarctic Ice Sheet
WC	Westland Current
WMI	Weak Monsoon Interval
WSI	Western South Island
YD	Younger Dryas
^{14}C	Radiocarbon

Time units

a	annum
BP	Before Present
cal	calibrated
ka	kiloannum (one thousand years)
AD	Anno Domini
kyr	thousand years

Following Aubry et al. (2009), I use 'annus' ('a') to denote absolute time and 'year' ('yr') for durations.

Chapter One

1. Introduction and Rationale

1.1 Overview

Paleoclimate reconstructions of the Late Quaternary reveal oscillations between glacial and interglacial (G-I) conditions (Fig. 1.1; Imbrie et al., 1992; Imbrie et al., 1993; Berger and Jansen, 1994). Long periods of gradual cooling (~70-90 kyr) are characterised by the growth of large Northern Hemisphere (NH) ice sheets (Clark et al., 2009), a ca.120 m fall of global mean sea level (Rohling et al., 2014), and reduced greenhouse gases (GHG) with atmospheric CO_2 up to 100 ppmv lower (Monnin et al., 2001). These periods are followed by abrupt warming (~10 kyr) known as terminations (Broecker and Donk, 1970), with the development of interglacial climate (Denton et al., 2010), before the cycle is repeated.

Glacial-interglacial cycles are paced by changes in the geometry of Earth's orbit ("Milankovitch orbital frequencies") which induce changes in the seasonal distribution of insolation (Hays et al., 1976; Tziperman et al., 2006; Huybers, 2011). The mechanisms that link insolation to global climate particularly during terminations remain elusive (Raymo and Huybers, 2008). First, rising insolation alone is considered to be insufficient to explain terminations as they have occurred during times of both low and high amplitude NH summer insolation (Denton et al., 2010; Schaefer et al., 2015), with insolation antiphased between the hemispheres (Broecker and Denton, 1990; Berger, 1999; Denton et al., 1999; Broecker, 2000). Second, the contribution of eccentricity to insolation (which changes not just the distribution of insolation over the Earth's surface, but the total amount received) is too small to drive terminations directly (Imbrie et al., 1993; Paillard, 1998; Schulz and Zeebe, 2006; Cheng et al., 2009).

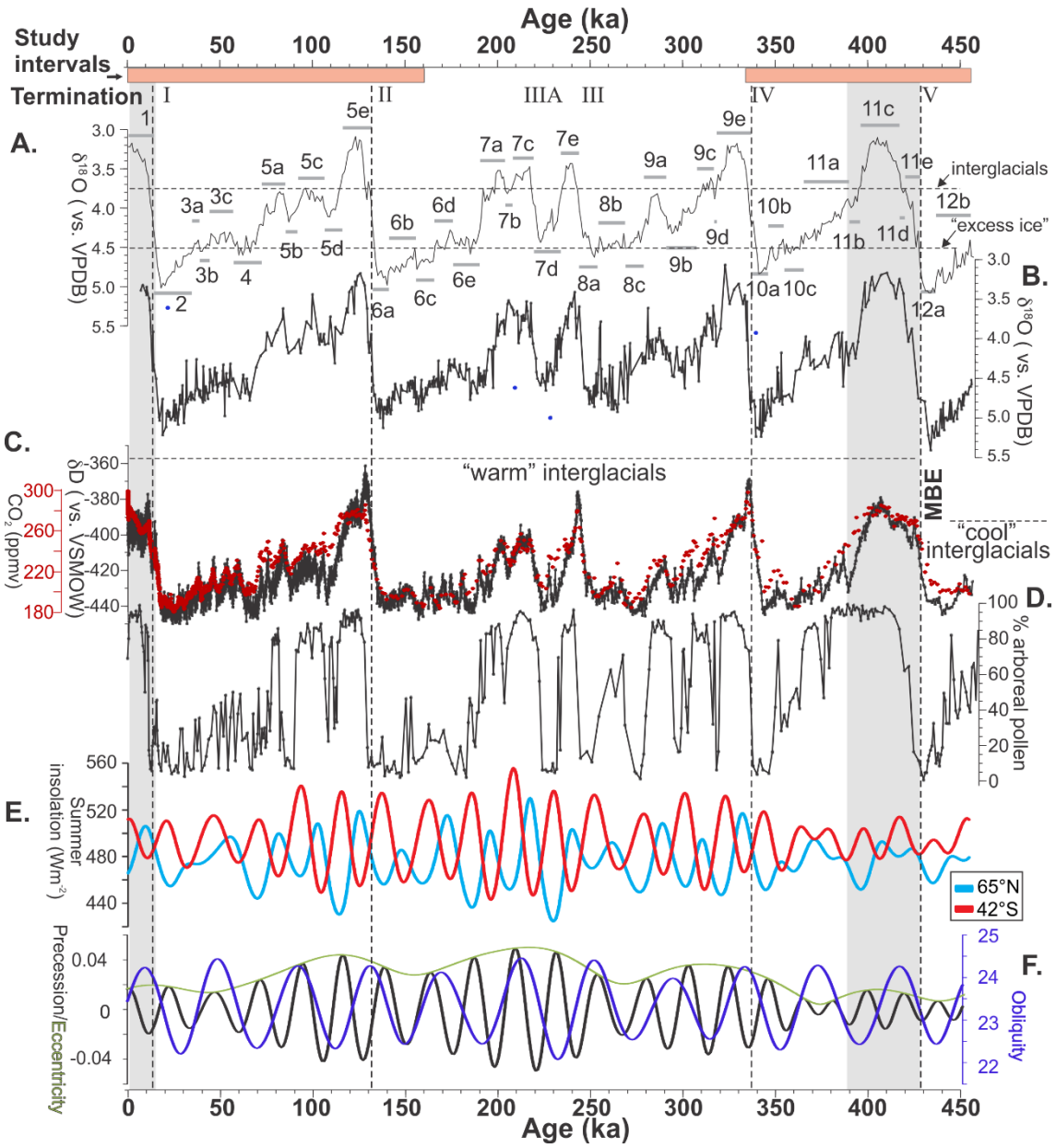

Fig. 1.1. A comparison of various paleoclimate records and orbital parameters over the last 450 ka of the Late Pleistocene. The study intervals for this thesis are indicated by pink horizontal boxes (top). This captures the terminations (roman numerals) I, II, V, and to a lesser extent IV which are illustrated by a vertical dashed line, and key interglacials 1, 5e and 11. **A.** Reference stacked marine benthic oxygen isotope record, LR04 (Lisiecki and Raymo, 2005), with key marine isotope substages (MIS) lettered and their length indicated by horizontal bars (Railsback et al., 2015). Interglacials as defined by past interglacials working group of PAGES (2016) are displayed above top dashed line (3.75‰). Glacial periods containing "excess ice" which are critical for a termination are bellow bottom dashed line (4.5‰) following Raymo (1997). **B.** Southwest Pacific marine oxygen isotope record of Elderfield et al. (2012) from ODP Site 1123, 1100 km offshore from eastern New Zealand aligned to LR04 (outliers in blue dots). **C.** EPICA Dome C (EDC) Antarctic ice core record (deuterium isotopes that act as a proxy for air temperature (EPICA, 2004; Jouzel et al., 2007)), and Antarctic CO_2 composite record (red circles; Luthi et al., 2008; Schneider et al., 2013), placed on the chronology of Veres et al. (2013) and Bazin et al. (2013). The shift from "cool" interglacials to "warm" interglacials which occurs from MIS 13 to MIS 11 is termed the mid-Brunhes Event (labelled MBE), and is indicated by a dashed horizontal line. **D.** Aboreal pollen percentage record from Tenaghi Phillipon, Greece (Tzedakis et al., 2006). **E.** Summer insolation for 42°S (21 Dec) and 65°N (21 June) and; **F.** Orbital components of eccentricity, obliquity and precession cycles derived from Laskar et al. (2004). The low "eccentricity" interglacials of MIS 1 and MIS 11 are highlighted by grey vertical bars, and are compared in this thesis.

.

Superimposed on these cycles are millennial frequency, high amplitude oscillations in climate considered to be produced by factors internal to the Earth's atmosphere and ocean system (Alley et al., 1999; Chiang et al., 2014; Landais et al., 2015), and are antiphased between the polar regions of each hemisphere (Bender et al., 1994; Broecker, 2000; WAIS Divide Project Members, 2013). Abrupt warming phases in Greenland ice core records are shown to lead Antarctic cooling by ~200 years, and climate oscillations in Antarctic records are more subdued (EPICA Community Members, 2004; North Greenland Ice Core Project members, 2004; WAIS Divide Project Members, 2015). Causes and mechanisms for these bipolar seesaws in temperature have been connected with the release of icebergs from glacial ice sheets, changes in sea ice extent, surface salinity and temperature, and reorganisations of the thermohaline circulation (Heinrich, 1988; Bond et al., 1992; Broecker et al., 1992; McManus et al., 1999). Six major influxes of ice-rafted debris (IRD) associated with iceberg discharges from NH ice sheets are documented for the last glacial cycle (Hemming, 2004), with each cold phase noted in Greenland associated with a respective IRD layer, termed a Heinrich stadial (HS) (Barker et al., 2009; Harrison and Sánchez Goñi, 2010). Major IRD layers which characterise the last five terminations are termed Heinrich stadials or Heinrich "type" events (Heinrich, 1988; Oppo et al., 1998; Oppo et al., 2006; Rodrigues et al., 2011; Barker et al., 2015). The timing and duration of key past climate events (e.g., Heinrich events) that are referred to in this thesis are outlined in Table 1.1.

Table 1.1: Timing and duration of key past climate events included in this thesis

Climate event	Acronym	Lower boundary (ka BP)	Upper boundary (ka BP)	Duration (ka)	Marine Isotope stage (MIS) correlatives	Reference
Younger Dryas	**YD**	12.9	11.7	1.2	1	Rasmussen et al. (2006)
Antarctic Cold Reversal	**ACR**	14.6	12.8	1.8	2/1	Lemieux-Dudson et al. (2010)
Heinrich Stadial 1	**HS-1**	17.8	14.7	3.1	2	Bard et al. (2000)
Last glacial-interglacial transition	**LGIT**	18 (T-I onset)	11.88	6.12	2	Barrell et al. (2013)
Last glacial-cold period	**LGCP**	30	18	12	2	Barrell et al. (2013)
Last glacial inception	**LGI**	~116	–	–	5e/5d boundary	Lisiecki and Raymo (2005); Bazin et al. (2013)
Last interglacial 'acme'	**LIG**	129.4	120.3	9.1	5e	Govin et al. (2015)
Last interglacial	**LIG**	130	116	14	5e	Lisiecki and Raymo (2005)
Heinrich Stadial 11	**HS-11**	135 ± 1 (2σ)	130 ± 2	5	6	Marino et al. (2015)
Penultimate glacial-interglacial transition	**PGIT**	139.3 (T-II onset)	130	9.3	6	*This study*
Penultimate glacial cold period	**PGCP**	undefined	139.3	–	6	*This study*
Heinrich type 4+5	**Ht-5/4**	~437	~428	9	12	Rodrigues et al. (2011); Barker et al. (2015)

One chain of events considered to result in an antiphased temperature signal between the hemispheres during terminations is outlined by Denton et al. (2010), and invokes the role of very large NH ice sheets with marine based components (Fig. 1.2). These ice sheets are considered to have been vulnerable to unstable collapse due to weak but increasing boreal summer isolation at the onset of each of the last five glacial terminations (Fig. 1.1; Denton and Hughes, 1983; Raymo, 1997; Cheng et al., 2009; Denton et al., 2010; Meckler et al., 2012; Abe-Ouchi et al., 2013). The increased flux of ice and massive inflows of meltwater to the ocean from such a collapse could have been significant enough to slow down the Atlantic meridional overturning current (AMOC), cooling the NH and conserving heat in the SH, i.e., the bipolar seesaw mechanism (Broecker et al., 1985; Crowley, 1992; Broecker, 1998; Stocker et al., 2000). A reduced AMOC and increased sea ice from longer winters caused NH cooling (Denton et al., 2005; Margari et al., 2014; Martrat et al., 2014), and thus facilitated a Heinrich event.

The effects of northern millennial-scale stadial/interstadial events may have also been rapidly transferred into the SH from a complimentary southward shift of the Intertropical Convergence Zone (ITCZ) resulting from an aforementioned decreased AMOC (Anderson et al., 2009; Toggweiler, 2009; Bostock et al., 2013). This facilitated a southward shift of the Southern Hemisphere westerly wind (SHWW) belt, resulting in increased upwelling of CO_2-rich water in the Southern Ocean (Ahn and Brook, 2008; Bostock et al., 2013; Parrenin et al., 2013). Antarctic ice core records suggest that Southern Ocean CO_2 outgassing lagged NH insolation by millennia during each of the last four terminations (Kawamura et al., 2007). Despite this lag, outgassing was of sufficient magnitude to synchronise the climate system of both hemispheres, and achieve interglacial conditions (Cheng et al., 2009). However, the paucity of well dated mid-latitude SH records beyond the last termination makes it difficult to assess the nature and extent of any asynchronous interhemispheric pattern. It is widely accepted that well-dated, continuous records of the timing and amplitude of SH climate change under a range of insolation, ice volume and CO_2 conditions can therefore contribute directly to our understanding of these processes.

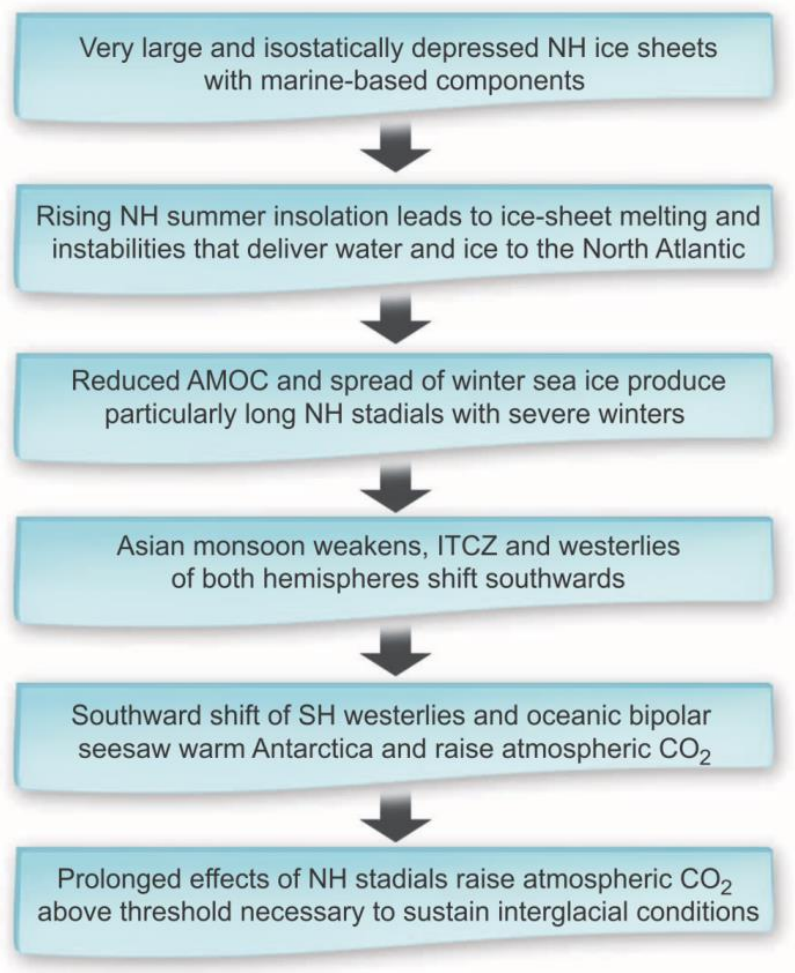

Fig.1.2: Essential elements of a termination following Denton et al. (2010). A summary of the conditions and processes described in the text that contribute to the termination of a Late Pleistocene ice age (e.g. T-I to T-V displayed in Fig. 1.1).

Past interglacials with climates warmer than the present are regularly studied to better understand the impact of anticipated human-induced warm climate on ecological and geomorphic systems of the current Holocene interglacial (Tzedakis et al., 2009a; Masson-Delmotte et al., 2013; Past Interglacials Working Group of PAGES, 2016). The climate optimums of the last interglacial (LIG), which is represented by Marine Isotope Stage (MIS) 5e (ca. 132-116 ka), and that of MIS 11c (~417-396 ka), are globally distinctive with evidence for warmer conditions than the present (Kukla, 2000; Lang and Wolff, 2011; Past Interglacials Working Group of PAGES, 2016). Sea levels were 6-9 m higher during the LIG and 6-13 m higher during MIS 11 (Fig. 1.3; Masson-Delmotte et al., 2013; repeated by Dutton et al., 2015a), with higher average atmospheric CO_2 concentrations (~20 ppmv) than the pre-industrial period (Lüthi et al., 2008; Schneider et al., 2013). Both intervals provide analogues to future warm climate (Imbrie and Imbrie, 1980; Loutre and Berger, 2000; EPICA Community Members, 2004; Yin and Berger, 2012), with MIS 11 characterised by similar orbital configuration to the present day (Fig. 1.1). The interplay of insolation cycles with

internal climate system feedbacks which can be either rapid (i.e., sea ice, CO_2 feedbacks, atmospheric water vapour, vegetation cover, ocean surface temperatures, ocean circulation) or sluggish (i.e., ice sheet extent and thickness, sea level), have profoundly influenced the climate system in both hemispheres (Clark et al., 1999; Broecker, 2000). Resolving the drivers and mechanisms of these changes during terminations and their subsequent interglacials remains an outstanding goal of paleoclimate science.

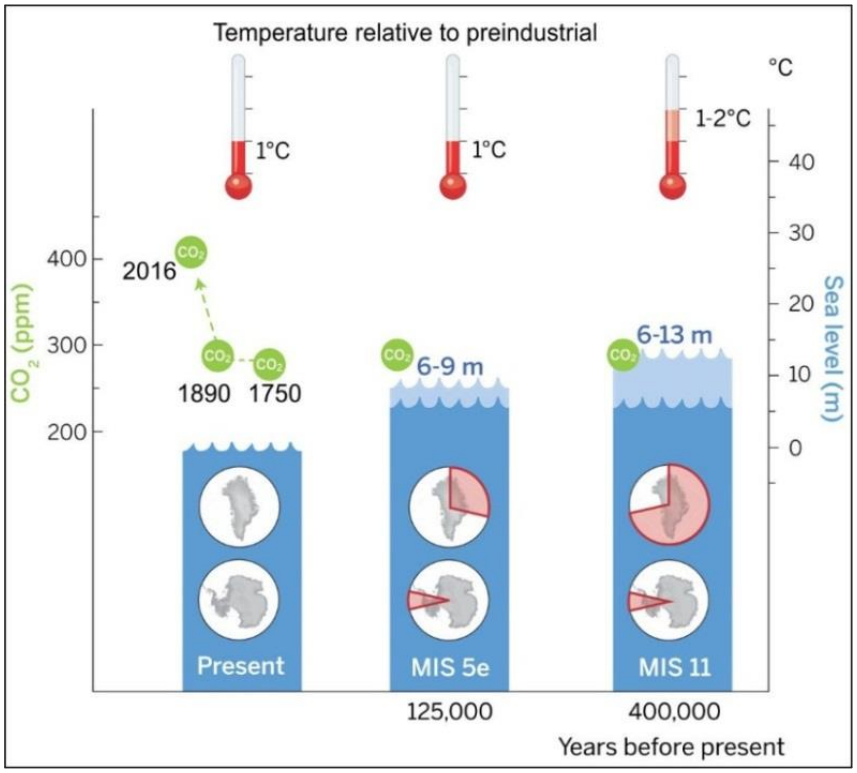

Fig. 1.3. Peak global mean temperature, atmospheric CO_2, maximum global mean sea level (GMSL), and source(s) of meltwater. Light blue shading indicates uncertainty of GMSL maximum. Red pie charts over Greenland and Antarctica denote fraction (not location) of ice retreat. Modified after Dutton et al. (2015a), with present anthropogenically enhanced CO_2 levels of ~409 ppmv from April 2016 (Keeling et al., 2016).

Records of past ocean and atmospheric change can offer valuable insights into the environmental effects of predicted future warming. Last year the planet achieved its record warmth for the second consecutive year, where temperatures exceeded the average values for the mid to late 19th century by more than 1°C for the first time (Blunden and Arndt, 2016). By the end of this century global mean surface temperatures may be as high as 4.8°C above pre-industrial values (Meinshausen et al., 2011; Stocker et al., 2013). Estimates of future warming couched in terms of global mean values are useful for identifying the environmental problems Earth will soon face but do not acknowledge the possibility of marked regional differences in timing and magnitude of climate change. Whilst observations of recent regional warming and models of future regional warming are providing a predictions relevant to policymakers (IPCC, 2014), paleoclimate archives and models

provide deeper insights to how regional climate changed during past periods of global warmth, and allow models used for projections to be tested (Masson-Delmotte et al., 2013). Therefore, paleoclimate studies such as this thesis provide important insights into the pattern of regional climate change and processes that are involved.

This thesis utilises pollen and spores from terrestrial plants to reconstruct changes in vegetation, and thus climate, over the past 450 ka from marine cores from the East Tasman Sea. Particular emphasis is placed on vegetation changes during glacial-interglacial terminations and 'super-warm' interglacial periods. Glacial terminations represent periods of rapid global warming, yet with sufficiently refined age models it is possible to explore inter hemispheric relationships in the response of the climate system. Terrestrial records from the SH (including New Zealand) display warming during the post-Termination-I amelioration (~18-15.6 ka, Barrell et al., 2013), while equivalent NH records display cooling (Denton et al., 2010). It remains uncertain if this pattern recurs during every termination, as well dated long terrestrial records from the Southern Hemisphere mid-latitudes are few.

This thesis also examines the response of forest elements from the southwestern New Zealand during MIS 5e (125 ka) and MIS 11 (~410 ka). Data from the Northern Hemisphere and Antarctica both suggest these were periods when global temperatures were significantly warmer than present (Past Interglacials Working Group of PAGES, 2016), although terrestrial paleo-environmental data for these periods from New Zealand are equivocal or are absent (e.g. Vandergoes et al., 2005). Whilst there are numerous pollen records illustrating step-changes in New Zealand vegetation due to warming since the Last Glacial Maximum (Termination I), there are far fewer that capture the vegetation response to significantly warmer-than-present conditions. Reconstruction of multi-proxy paleo environmental records for these periods help to provide a better understanding of southwest Pacific and New Zealand regional climate change, but perhaps just as importantly allow the ecological response of significant vegetation community of the west coast of the South Island to warmer-than-present conditions to be evaluated. While progressive warming may not lead to progressive changes in vegetation, there appear to be critical thresholds that exist within the existing West Coast Rimu-dominated forest that leave it vulnerable to warming >~3ºC.

1.2 Previous research and research aims of this thesis

During 2006, the R/V *Marion Dufresne* (MD) collected giant piston cores for the MATACORE transit voyage (MD152) in order to assess "the tectonic and climate controls on sediment budget" for New Zealand (NZ). The paleoclimate component of this research focused on identifying the New Zealand response to past rapid climate changes from records with high temporal resolution, and provide an understanding of future instability of the ocean and atmosphere system (Proust et al., 2006; Proust et al., 2008). This PhD research primarily focuses on two terrestrially influenced marine cores (MD06-2990 and 2991) collected from the Challenger Plateau (Fig. 1.3), in the East Tasman Sea (ETS). The goal is to form an understanding of how terrestrial pollen, and by inference vegetation, in southwestern New Zealand responded to orbital and millennial scale climatic change over terminations (T) I, II, V and their subsequent warm interglacials of MIS 1, 5e and 11 (Fig. 1.1). This research is motivated by the scarcity of continuous, well dated and quantifiable reconstructions of past environmental change over the past 450 ka in the mid-high Southern Hemiphere latitudes. Limitations of previous work, with a particular focus on southwestern New Zealand, are outlined as follows:

1. *Poor age control of terrestrial paleoenvironmental records beyond radiocarbon timescales*

The timing and duration of paleoenvironmental changes identified in continuous terrestrial sequences from New Zealand extending beyond radiocarbon timescales remain poorly constrained, i.e., 30 ka uncertainty at the onset of the last interglacial (LIG) at Okarito Bog, southwestern New Zealand (Fig.1.4; Vandergoes et al., 2005). This uncertainty was partly circumvented via the generation of the adjacent ~210 ka pollen profile at ~2kyr sampling resolution from a 3.27 m long piston core (TAN0513-14; 42°18'S, 169°53'E; 950 m water depth; Fig. 1.4) situated on the continental slope to the west of New Zealand's South Island, and~110 km NNW of Okarito bog. The TAN0513-14 record developed from Ryan et al. (2012) displays remarkable similarity to variations in the pollen content at Okarito, but with greater chronological precision achieved beyond radiocarbon dating timescale (up to 4 kyr (1σ) over the last 1 Ma via the LR04 δ^{18}O-age reference curve (Lisiecki and Raymo, 2005).

2. *Assumption of negligible timing for pollen transfer to the ocean*

Previous investigation of past vegetation changes reconstructed from TAN0513-14 assumed negligible residence times to the ocean (Ryan et al., 2012). This assumption was critical for transferring the marine chronology of TAN0513-14 to the adjacent pre ^{14}C dated Okarito Bog sequence, but was not rigorously tested. Surface sampling between land and ocean in

that study indicated terrestrial pollen and spores (collectively termed "terrestrial palynomorphs" in this thesis) were primarily transported to the coast via fluvial processes.

3. *Assessment of leads and lags in the climate system from discrete sequences*

Phase relationships between pollen and $\delta^{18}O$ have previously highlighted major environmental changes over the past 210 ka from TAN0513-14 (Fig.1.4). However, reconstructed changes in vegetation were compared to regional estimates of sea surface temperature (SST) change undertaken on nearby core SO136-GC3 (Fig. 1.4; Pelejero et al., 2003; Pelejero et al., 2006; Barrows et al., 2007a), and introduce possible offsets in their association due to age model differences.

4. *The scarcity of quantifiable estimates of air temperature for the last interglacial (LIG)*

Low resolution reconstructions of vegetation change from pollen assemblages of land and sea sequences for southwestern New Zealand have failed to reconcile whether there is evidence for a short period of greatly enhanced warmth for early MIS 5e. Pollen assemblages imply regional land surface temperatures were similar to modern or perhaps slightly cooler (Vandergoes et al., 2005). Quantified estimates of regional land surface temperatures for MIS 5e from terrestrial sequences from New Zealand are scarce, with the sole South Island record recently undertaken at Okarito Bog (unpublished) and constrained to the TAN0513-14 age model of Ryan et al. (2012). Equivalent quantitative reconstructions of terrestrial climate change have yet to be undertaken on marine sequences in this region due to taphonomic issues and are outlined in Chapter 2.

5. *Length of terrestrial paleoclimate record*

At present there are no terrestrial sequences containing T-V and the climatic optimum of MIS 11 reported from New Zealand. In contrast, existing reconstructions of marine sea surface changes from the East Tasman Sea extend to 1 Ma (Hayward et al., 2012).

The net result of these limitations led to the development of these three key aims for this thesis.

Aim one: Evaluate the time taken between the production and eventual seafloor deposition of terrestrial palynomorphs for southwestern New Zealand; here referred to as source-to-sink residence time.

- This approach serves two purposes. First, it tests the assumption that marine and terrestrial indicators of climate change derived from the same marine sequence can be directly compared in time with confidence. This circumvents potential

chronological uncertainties which may arise when comparing indicators from separate marine and terrestrial records. Second, it provides a means for transferring MIS chronologies (MD06-2991) to long terrestrial records (e.g., Okarito Bog) that extend beyond the range of radiocarbon dating using equivalent palynomorph events.

Aim two: To determine the sequence of climate events associated with T-I, T-II and T-V and their subsequent interglacials from southwestern New Zealand.

- The sequence of climate events, including their timing and magnitude, is well constrained for T-I and the Holocene interglacial from discrete marine-terrestrial sequences from this region. However, little is known about the timing and magnitude of these changes during previous terminations and their following interglacials. Long, well dated, high sedimentation marine sequences from the East Tasman Sea capture all of these intervals (T-I, T-II, T-V) and enable their similarities and differences to be explored. Key questions involve; What is the representivity of terrestrial palynomorphs between adjacent land and sea profiles? Is the pattern of climate amelioration between land and sea synchronous or is there evidence for lags in the climate system? Does each termination register the appearance of millennial scale climate reversals as noted globally for T-I? Are vegetation changes of similar character and magnitude during each termination and following interglacial?

Aim three: How do the timing, magnitude and sequence of climate events over T-I, T-II and T-V and their post-termination interglacials in southwestern New Zealand relate to climate forcing, and how do they compare with paradigms of terminations and existing observations?

- Does the sequence of climate events revealed for terminations from southwestern New Zealand and the adjacent East Tasman Sea follow previous paradigms outlined such as that of Denton et al. (2010) for T-I? Is the magnitude of temperature change similar between adjacent land and sea records? Is there evidence for regional differences in the climate amelioration of terrestrial New Zealand during terminations? How does the timing and magnitude of major environmental change in New Zealand compare to that revealed to records developed from the NH? Were

past interglacials in southwestern New Zealand warmer than present, and what is New Zealand's potential future climate in a warming world?

1.3 Key themes of this thesis

Key themes elaborated throughout this thesis comprise;

- **A.** The representativeness of pollen in adjacent land-sea pollen records
- **B.** The source-to-sink transport time of palynomorphs and tephra from land to sea (residence time)
- **C.** Regionally dispersed palynomorphs/tephra as chronostratigraphic tools for correlation between land and sea records
- **D.** Comparison of land and sea temperature estimates
- **E.** Inter-hemispheric phasing of climate events
- **F.** Past warmth during interglacials MIS 1, 5e and 11, and New Zealand's potential future climate in a warming world

1.4 Rationale for the site location, and review of aims and key themes

New Zealand is one of only two Southern Hemisphere mid-latitude landmasses and is therefore ideally located to contribute to understanding climate processes on glacial-interglacial timescales (McGlone et al., 1993; Alloway et al., 2007a). The climate of New Zealand is influenced by northern tropical and southern subpolar ocean currents (Fig. 1.5), and is thus ideally positioned to examine antiphased relationships in the ocean-atmosphere circulation system that exist between hemispheres (Pahnke et al., 2003; Carter et al., 2008). New Zealand's mountainous landscape intercepts the Southern Hemisphere westerly wind belt and result in high sediment erosion rates, which are considered to be rapidly deposited onto adjacent sedimentary basins through effective conduits (Proust et al., 2008). The South Island of New Zealand is a small landmass with high altitude (~3000 m) N-S trending mountains which support the largest and most climatically sensitive of New Zealand's glaciers, and a number of short, steep river catchments located along the western flank of the Southern Alps. These catchments in turn support a diverse range of vegetation, whose areal extent is strongly dependent on temperature and (on the eastern side of the island) rainfall (Wardle, 1979). This relationship between vegetation, temperature and precipitation has enabled the timing and magnitude of past regional and global environmental change to be investigated in this region using palynomorphs recovered from terrestrial (Moar and Suggate, 1996; Newnham et al., 2007a; Vandergoes et al., 2005) and marine (Ryan et al., 2012) sedimentary sequences over the last two glacial-interglacial cycles (**key theme A**).

The extensive history of glaciation in Westland (Suggate, 1990; Suggate and Almond, 2005; Barrell, 2011) has created a landscape in which paleovegetation records of more than 150 kyr in duration are often fragmentary in nature and poorly dated beyond the range of ^{14}C dating (≥40 ka). Therefore, non-conventional methods must be used to explore the paleoclimatic history of the region over longer timescales. Terrestrial palynomorphs extracted from continuous marine sedimentary sequences circumvent this problem, as they can be dated using oxygen isotope ($\delta^{18}O$) stratigraphy (Lisiecki and Raymo, 2005), and correlated to MIS. Independent evidence for oceanic (in particular, SST) and ice volume change through time can also be obtained from geochemical proxies from the same record (Barrows et al., 20007a).

Long continuous and well dated terrestrially influenced marine archives collected from the East Tasman Sea are examined in this thesis to help to resolve outstanding questions. The MD06-2990/1 core sites are situated seaward of the narrow continental shelf adjacent to Westland, thus limiting changes in the palynomorph source area (i.e., palynomorphs would be largely sourced from the Hokitika River catchment) as sea level rises and falls (Ryan et al., 2012). Large sediment-laden rivers that drain Westland supply abundant palynomorphs along a relatively short transport pathway and potentially limit the difference in time between palynomorph production and deposition at the core site (a hypothesis tested in aim one of this thesis and in **key theme B**). Minimal residence times allow direct comparison of the magnitude and timing of terrestrial and oceanic climate change from marine cores MD06-2990/1, thus avoiding comparison of paleoclimate records which may be far apart and have associated problems of age model differences.

The similarity between land-sea records permits the transfer of marine core chronologies to terrestrial sequences beyond the radiocarbon dated interval, such as that from Okarito Bog (Fig. 1.4), allowing the assessment of both records on a common time scale (aim two; **key theme C**). Comparison of reconstructions of vegetation change from land and sea profiles help determine the relative sensitivity of the offshore palynomorph record to climate change, which will in turn help constrain the interpretation of older sections preserved in the marine record such as the entire MIS 11c interglacial, for which there are no well-dated terrestrial equivalents. Further, direct comparisons from these adjacent environments are important as they allow the scale and timing of past climatic changes in each to be assessed (**aim two and three; key theme D**), and permit comparison to climate events farther afield (**key theme E**). This provides insight into the nature of changes in the ocean and atmosphere circulation

systems under higher temperatures, thus providing useful analogues to how these systems may perform under anticipated future climate warming (**key theme F**).

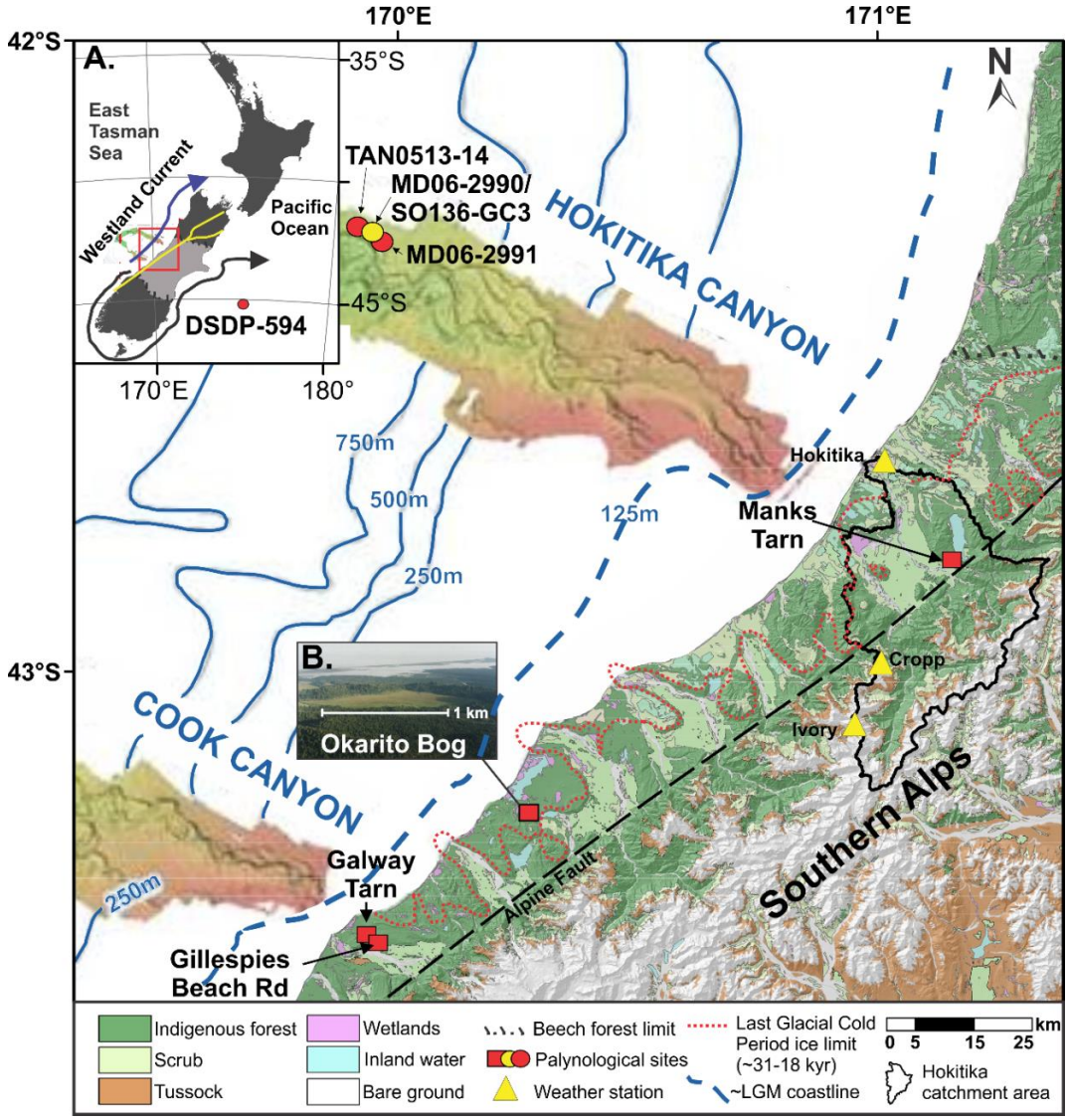

Fig. 1.4: Regional setting of the study area showing the locations of climate stations, and key marine and terrestrial core sites containing palynological reconstructions discussed. The distribution of vegetation in central-southern Westland is broadly approximated by altitudinal range on the map. The approximate northern limit of the central Westland southern beech gap is delineated (Wardle 1984), and is discussed in Chapter 2.5. **Inset A;** The extent of the Biotic Gap zone is highlighted in light grey, with the NE-SW trending yellow line representing the Alpine Fault along the Southern Alps (Hill et al., 2009). The Westland Current (blue) and the Southland Current (black) are illustrated (Carter, 1975; Heath, 1985). The digital elevation model shown is derived from Land Information New Zealand (LINZ) digital topographic contours and spot heights (Crown Copyright reserved), with bathymetric data supplied by National Institute of Water and Atmosphere (NIWA). Note the Okarito Bog site is illustrated outside of the Last Glacial Coldest Period (LGCP) ice limit defined by Barrell (2011) and Barrows et al. (2013) and is pictured (**Inset B**). The Last Glacial Maximum (LGM) coastline defined by the ~120 m bathymetric contour.

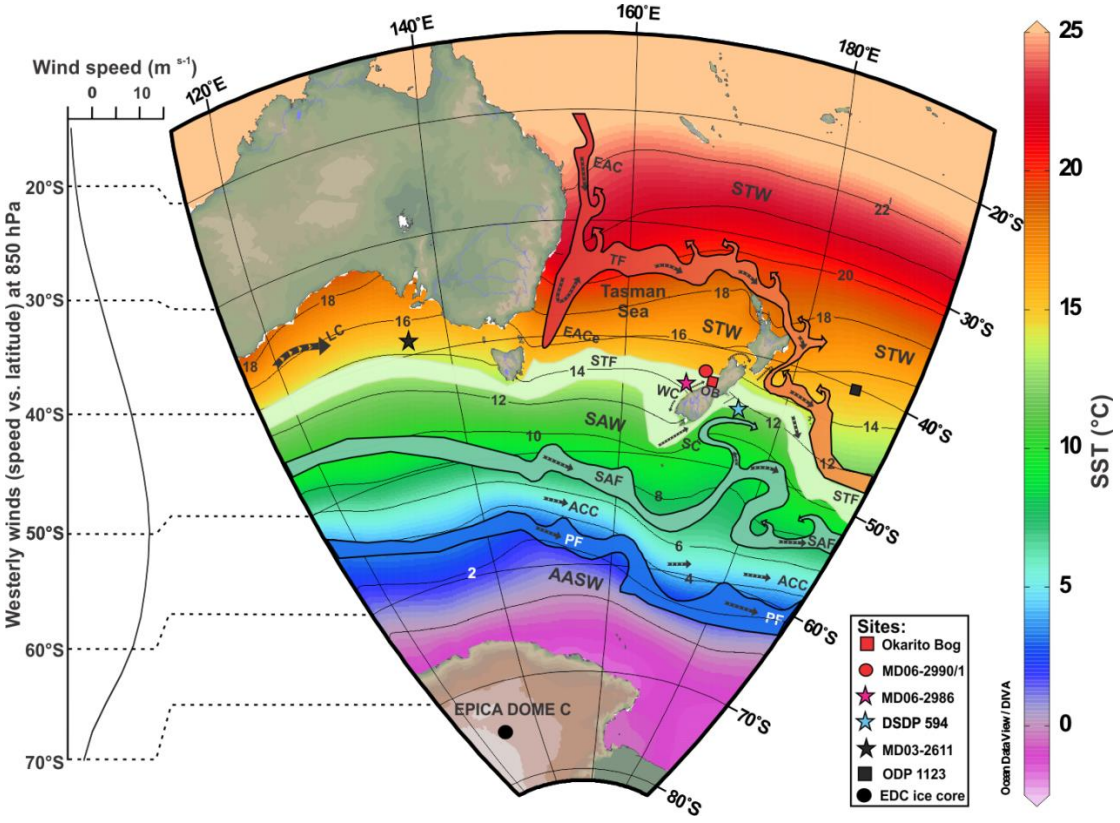

Fig. 1.5: Regional distribution of modern annual sea surface temperature (SST) and water masses (Subtropical Water – STW, Subantarctic Surface Water – SAW, Antarctic Circumpolar Current – ACC, Antarctic Surface Water– AASW), fronts (Tasman Front – TF, Subtropical Front – STF, Subantarctic Front – SAF, Polar Front – PF) and flow pathways (arrows) across the Southwest Pacific. The STF in the Tasman Sea is density compensated and has no flow associated with it, while east of New Zealand the STF boundary is dynamical with a strong flow (Chiswell et al., 2015). The positions of the Leewin Current (LC), East Australian Current (EAC), including its southernmost extension (EACe), the Westland Current (WC) and the Southland Current (SC) are labelled, along with the position of paleoclimate records referred to in text (Chapter 3-5). All modern watermass and currents illustrated follow Bostock et al. (2013; 2015); Smith et al. (2013); Chiswell et al. (2015). The modern SST is 15.5°C at the MD06-2991 core site and is determined by annual SST data (1955-2012) from World Ocean Atlas 13 (Locarnini et al., 2013) and plotted in Ocean Data View v.4.6.4 (Schlitzer, 2012). Westerly wind speed (m $^{s-1}$) vs. southerly latitude at 850 hPa is from a NCEP1 50 yr (1948-1999) reanalysis (Kistler et al., 2001).

1.5 Structure of the thesis

Chapter one (introduction and rationale) presents a brief overview of paleoclimate, previous research and limitations in the study region, the rationale and research questions, and statement of authorship. Chapter two (background) presents background material regarding the use of palynology in paleoenvironmental reconstructions over the Late Quaternary, and the modern-day vegetation and climate variables of Westland. Chapters 3, 4 and 5 are formatted as scientific journal articles, with individual abstract, introduction, methods, results and discussion sections, but their formats adhere to the overall thesis style. Background material such as the climate of southwestern New Zealand for Chapters 4 and 5 is contained in Chapters 2 and 3 to avoid repetition. Chapter three has been published in *Review of Paleobotany and Palynology* (with online version attached in Appendix 3). Chapter 6 (synthesis) integrates the datasets and key findings presented in the three previous chapters, where the key aims introduced in Chapter 1 are addressed and future research objectives are suggested.

The paragraphs below detail the aims and general method of each data chapter.

Chapter three:

Exploring the source-to-sink residence time of terrestrial pollen deposited offshore Westland, New Zealand

This chapter investigates the source to sink residence time of the transport and deposition of terrestrial palynomorphs using two approaches. The radiocarbon dating of terrestrial palynomorphs and organic residue transported or deposited in modern Westland river systems was undertaken in approach one. The second approach focuses on a paleo perspective, by comparing palynomorph events and tephra common to regional and independently constrained land-sea sequences from southwestern New Zealand and the ETS. Author list: Matthew T. Ryan, Rewi M. Newnham (corresponding author), Gavin B. Dunbar, Marcus J. Vandergoes, Andrew B.H. Rees, Helen Neil, S. Louise Callard, Brent V. Alloway, Helen Bostock, Quan Hua, Brian M. Anderson (PDF of manuscript in Appendix 3).

Chapter four:

Ocean and atmospheric interactions from southwestern New Zealand over the last two terminations and interglacials

This chapter investigates ocean-atmosphere change for southwestern New Zealand over the last two terminations and their following interglacials from marine core MD06-2991. This is matched to New Zealand's longest continuous terrestrial sequence of paleoenvironmental

change from Okarito Bog using palynostratigraphic correlation, and allows both adjacent land-sea records to be placed on a common timescale. Combined, these records provide insight into the nature, timing and magnitude of ocean-atmosphere change during T-I and T-II and the subsequent interglacials.

Chapter five:

MIS 11 ocean-atmosphere reconstructions from southwestern New Zealand

This chapter investigates ocean-atmosphere change over MIS 12-10 from southwestern New Zealand. It introduces core MD06-2990 retrieved from the same submarine canyon system as MD06-2991 which was introduced in paleoclimate reconstructions in Chapter 3 and 4. Previously published terrestrial sequences from western North Island spanning late MIS 11c-MIS 10 and the early Holocene climatic optimum provide the basis for comparison with data of MIS 12-10 age generated in this study.

1.6 Statement on the contributions made to this thesis by the author, supervisors and collaborators

I present original research designed and carried out by myself, and identify the extent of my contribution and that of supervisors and collaborators following each of Chapters 3-5. This project was supervised by Prof. Rewi Newnham (VUW), Dr Gavin Dunbar (VUW/ARC), and Dr Marcus Vandergoes (GNS Science) (RMN, GBD and MJV respectively). Supervisor contributions include: i) project guidance which involved the discussion and contribution of scientific ideas and concepts and the editorial advice on the write up of this thesis; ii) published and unpublished datasets; iii) part funding for SST determinations, funding of lab materials and dating associated with this thesis; and (iv) funding the PhD scholarship and fees of the candidate (3 years) through VUW and through the GNS Science Global Change Through Time Programme. Contributions were made from Dr H.L. Neil (HLN), Dr H. Bostock (HB), A. Prof B.V. Alloway (BVA), Dr A.B.H Rees (ABHR), Dr S.L Callard (SLC), Dr Q. Hua (QA), Dr B.M Anderson (BMA), Prof. E.G.C Smith (EGCS), Dr A.T Sabaa (ATS), Dr B. W Hayward (BWH), Dr G.H Scott (GHS), Dr J.M Wilmshurst (JMW), Dr X. Li (XL), Dr S. Steph (SS), Dr R. Tiedemann (RT), Dr J. Prebble (JP), D.J. Lowe (DJL). Published and unpublished data and their sources are outlined in Table 1.2.

Table. 1.2 Datasets discussed in this thesis (published and unpublished), their source, and the contribution or revision of that data by M.T.Ryan

External data sources contributing to this thesis	Source/Analysist	Reference	Revision or contribution from M.T Ryan
Chapter 3			
West Coast flood and suspended load samples and 14C ages*	GBD, BMA	Ryan et al. (2016)	Sample processing, Calibration of ^{14}C dates
MD06-2991 ^{14}C ages**	HLN	Helen Neil & Rewi Newnham, unpublished	Revised calibration of ^{14}C dates and depositional modelling under guidance of ABHR
Okarito Bog palynology and age model	MJV, RMN	Vandergoes et al. (2005); Newnham et al. (2007a)	Revised calibration of ^{14}C dates and depositional modelling under guidance of ABHR
Gillespies Beach Rd palynology and age model	MJV	Vandergoes and Fitzsimons, (2003); Turney et al (2006)	Revised calibration of ^{14}C dates and depositional modelling under guidance of ABHR
Galway Tarn palynology and age model	MJV	Vandergoes et al. (2013a; 2013b) and unpublished	Revised calibration of ^{14}C dates and depositional modelling under guidance of ABHR
Manks Tarn palynology and age model	SLC, MJV, RMN	Callard (2011)	Revised calibration of ^{14}C dates and depositional modelling under guidance of ABHR
Chapter 4			
δ^{18}O MD06-2991 ***	HLN	Williams et al. (2015); high resolution work: Helen Neil, unpublished	Sampling, foraminifera picked for high resolution δ^{18}O , contruction of age model
MD06-2991 $CaCO_3$ data ***	HLN, HB	Helen Neil & Helen Bostok, unpublished	Alignment to age model
MD06-2991 SST determinations	BWH, ATS	Rewi Newnham, Gavin Dunbar & Matt Ryan, unpublished	Sample selection, sediment processing, alignment to age model
Okarito Bog revised pollen counts	MJV, XL	Marcus Vandergoes, unpublished	Alignment to age model
Okarito Bog revised MAAT	MJV , JMW, RMN	Marcus Vandergoes, Rewi Newnham & Janet Wilmshurst	Alignment to age model
Tephra geochemistry (KOT)	BVA	Brent Alloway, unpublished	Identification, counting and extraction of all glass shards
Kaipo Bog age model and MAAT	RMN, JMW, DJL	Newnham et al. (2012); Lowe et al. (2013)	Revised age model to align MAAT
Cropp Till	–	Basher and McSaveney (1989)	Revised calibration of ^{14}C dates
Canavans Knob	–	Turney et al. (2007)	Revised calibration of ^{14}C dates
Chapter 5			
δ^{18}O MD06-2990	SS, RT	Ronge et al. (2015) & Ralf Tiedemann & Silke Steph, unpublished	Construction of age model
MD06-2990 SST determinations	BWH, ATS	Rewi Newnham, Gavin Dunbar & Matt Ryan, unpublished	Sample selection, sediment processing, alignment to age model
Tephra geochemistry (RtT)	BVA	Brent Alloway, unpublished	Identification, counting and extraction of all glass shards, age model
DSDP-Site 594 palynology (MIS 12-10)	JP	J. Prebble PhD thesis (2012)	Alignment to Prebble et al. (2016) age model
DSDP-Site 594 δ^{18}O ***	HLN	Prebble et al. (2016)	Sample processing
Umutekai palynology and ^{14}C data	RMN, BVA	Newnham (1990); Newnham and Alloway (2001)	Revised calibration of ^{14}C dates and depositional modelling under guidance of ABHR

Refer to previous section for list of authors.

* 14C age determinations funded under AINSE Research Award ALNGRA11168 to Gavin Dunbar.

** 14C age determinations funded under AINSE Research Award ALNGRA12130P to Rewi Newnham and NIWA Coasts and Oceans Marine Physical Resources Core Funding.

*** Funded under NIWA Coasts And Oceans Marine Physical Resources Core Funding.

1.7 Conference presentations resulting from this thesis

(Presenter underlined with author in bold).

Ryan, M.T., Newnham, R.M., Dunbar, G.B., Vandergoes, M.J., Alloway, B.V., Neil, H., Bostock, H., Sabaa, A., Hayward, B; Scott, G.H., Rees, A.B.H., Prebble, J.G., Tiedemann, R. 2015. A high-resolution Southern Hemispheric terrestrial vegetation and SST reconstruction of the "super-warm" Interglacial of MIS 11 retrieved from the eastern Tasman Sea. INQUA XIX Congress, Nagoya, Japan, 26 July-2nd August.

Ryan, M.T., Newnham, R.M., Vandergoes, M.J., Dunbar, G.B., Smith, E.G.C., Neil, H., Bostock, H., Alloway, B.V., Rees, A.B.H., Sabaa, A., Hayward, B., Scott, G.H., Wilmshurst, J.M., Li, X. 2015. Ocean-atmospheric interactions from south-west New Zealand, over the last two glacial-interglacial cycles. INQUA XIX Congress, Nagoya, Japan, 26 July-2nd August.

Newnham, R., **Ryan, M.,** Dunbar, G., Vandergoes, M., Neil, H., Alloway, B., Bostock, H., Hua, Q. 2014. Marine-terrestrial comparisons and ocean ventilation in the East Tasman Sea during the last glacial-interglacial cycle. Geoscience Society of New Zealand Conference, New Plymouth, New Zealand, 25-28 November.

Ryan, M.T; Newnham, R.M; Vandergoes, M.J; Dunbar, G.B; Neil, H., Bostock, H., Alloway, B.V. 2013. Transferring marine age models and their uncertainties to a long ~150 kyr terrestrial record using palynostratigraphy, southwestern, New Zealand. INQUA Early Career Researcher Meeting, University of Wollongong, 2-6th December.

Ryan, M., Newnham, R., Vandergoes, M., Dunbar, G., Neil, H., Bostock, H., Alloway, B. 2012. Terrestrial vegetation and climate reconstruction from warm to super-warm interglacial stages 1, 5e, and 11, from marine sediment cores, South Island, New Zealand. Geoscience Society of New Zealand Conference, Hamilton, New Zealand, 25-28 November.

Ryan, M., Newnham, R., Dunbar, G., Vandergoes, M., Neil, H., Bostock, H. 2012. High-resolution Southern Hemisphere palynological records from interglacial stages 5e and 11 from a marine sediment core adjacent to Westland, New Zealand. *Japanese Journal of Palynology* Volume 58 (Special Issue). Abstract issue for the Joint Meeting of 13th International Palynological Congress (IPC-XIII) and 9th International Organisation of Palaeobotany Conference (IOPC-IX), Tokyo, Japan, 23-30 August (pp. 198-199).

Vandergoes, M., Newnham, R., **Ryan, M.,** Dunbar, G., Wilmshurst, J., Li, X., Neil, H., Bostock, H., Alloway, B. 2012. Evidence of a warmer world MIS 5(e) from terrestrial archives in New Zealand. We don't know as much as we need to! 34th International Geological Congress, Brisbane, Australia, 5-10 August (Keynote).

Ryan, M., Newnham, R., Dunbar, G., Vandergoes, M. Neil, H., Bostock, H. 2011. Mid-Late Quaternary vegetation and climate change reconstructed from palynology of marine cores off southwestern New Zealand. *XVIII INQUA Congress Quaternary Sciences - The View from the Mountains*, Bern, Switzerland, 21-27 July. (Poster). Abstract published in *Quaternary International* 279-280: 419-420.

Ryan, M., Newnham, R., Dunbar, G.B., Vandergoes, M.J., Neil H.L, Bostock, H., Hannah, M., Alloway, B.V. 2011. Terrestrial vegetation and climate reconstruction during the MIS 12-11 transition recorded from 4 sediment cores, Hokitika canyon, New Zealand. In: N.J. Litchfield and K. Clark (Eds.), Abstract volume, Geosciences Conference, Nelson, 27 November-1 December. *Geoscience Society of New Zealand Miscellaneous Publication 130A*: p. 97.

1.8 Awards resulting from this thesis

- INQUA XIX Congress, 2015, Nagoya, Japan, 26th–July-2nd August best student poster award.
- Hornibrook award stratigraphic correlation in the south-west Pacific, New Zealand Geosciences Conference, 2013.

1.9 Scholarships and funding contributing to this thesis

- Wellington Botanical Society Student Grant 2015
- Victoria University of Wellington
- Antarctic Research Centre Endowed Development Fund
- GNS Global Change Through Time programme (540GCT41)
- Australian Institute of Nuclear Science and Engineering (AINSE) award numbers (ALNGRA1116 and 10524)
- NIWA under the Marine Physical Resources and Processes Programme
- New Zealand Geosciences travel fund
- INQUA Travel Grant
- SGEES Faculty Research Grant for SST determinations

Chapter Two

2. Background

To achieve the aims and objectives set out in Chapter 1, I first discuss key components for the use of terrestrial palynomorphs as a paleoclimate proxy, and review palynological data from marine and terrestrial sequences over the Late Quaternary from southwestern New Zealand. The ecological affinities of key taxa used in climate reconstructions for this region are introduced, as is the environmental and paleo-environmental context of this region and the adjacent East Tasman Sea.

2.1 Present-day vegetation/pollen relationships for paleoecology

Pollen and spores (terrestrial palynomorphs) are small cellular bodies mostly 10-100 μm in size, produced as part of the reproductive cycle of plants (Traverse, 2007). Terrestrial palynomorphs provide useful data for interpreting past vegetation and by inference climatic change (Macphail and McQueen, 1983; Birks and Birks, 2006), as they are taxonomically distinctive and they can be widely dispersed (Moar et al., 2011). Most terrestrial palynomorph grains have a tough outer wall (exine) made of sporopollenin which is resistant to degradation, and thus enables them to be preserved in a range of terrestrial (e.g. lakes, bogs, rivers, soils) and marine environments (Brasier, 1980). Paleovegetation reconstructions using fossil palynomorphs requires knowledge of how numbers of these grains in modern or fossil material relate to the plant that produced them (i.e., their "representivity"), and how the distribution of vegetation relates to aspects of climate ("ecological affinity"). Factors influencing the representivity of palynomorphs include their occurrence, preservation, pollination mode, and production and dispersal mechanisms (Macphail and McQueen, 1983; Moar et al., 2011). Terrestrial palynomorphs extracted from marine sediments are also influenced by additional transport and deposition processes which are not experienced on land (McGlone, 2001), and these additional processes are addressed below (section 2.1.1-2.1.2).

2.1.1 Representivity of terrestrial palynomorphs

Production and dispersal

The number of terrestrial palynomorphs produced by any given plant species is largely dependent on dispersal strategy, with pollination occurring via wind, insects or animals (Batten, 1996). Typically, plants that are wind pollinated produce greater amounts of palynomorphs because of their "shotgun" reproductive strategy, resulting in large numbers of grains which are dispersed over a broad area in order to maximise the chance of finding a suitable receptor (Faegri and Iversen, 1989). In the New Zealand context, pollen produced by native conifers (i.e., *Dacrydium cupressinum, Podocarpus, Prumnopitys*) have large air-filled "wings" (sacci) connected to the body (corpus) of the grain, making them effective for wind pollination (Macphail and McQueen, 1983; Jarzen and Nichols, 1996; Moar et al., 2011).

In addition, the morphology of these grains increases their hydrodynamic performance, enabling them to float for long distances as suspended sediment and therefore avoid mechanical abrasion (Chaloner and Muir, 1968; Mudie, 1982; Smirnov et al., 1996; Traverse, 2007; Luo et al., 2014). This is considered to make these taxa over-represented in marine sediments compared to their terrestrial counterparts of the same age (Mildenhall and Orpin, 2010). By contrast pollination from insects or animals produces fewer pollen grains due to the direct transport from the source to the receptor, with smaller numbers typically found in palynological records (Moar, 1970; Macphail and McQueen, 1983; Moar et al., 2011). Investigating Westland's past vegetation from pollen profiles generated from lake sediments requires an appreciation of the region's productive and dispersal strategies. Jacobson and Bradshaw (1981) illustrate a generalised relationship between basin size with no inflowing stream and the relative contribution of pollen orginating from vegetation sources in and around that basin (Fig. 2.1). The diameter of four well dated palynological sequences which capture the Last Glacial–Interglacial Transition (LGIT) from Westland are depicted on Fig. 2.1, with each sites potential pollen contributions outlined. The smaller sites of Galway Tarn (Vandergoes et al., 2013a; 2013b), Manks Tarn (Callard, 2011), and Gillespies Beach Road (Vandergoes and Fitzsimons, 2003; Turney et al., 2006) - are considered to record a larger local signal of pollen rain which comes from plants from within 20 m of the site, while extra-local pollen is produced from plants up to ~20-300 m from the basin. The primary recorder of the regional pollen rain (pollen transported more than ~300 m from the basin of deposition) in this model is from Okarito Bog (Vandergoes et al., 2005; Newnham et al., 2007a), a ~1 km^2 moraine impounded basin at Okarito in South Westland (70 masl (metres above sea level)). The site is situated outside of the Last Glacial Coldest Period (LGCP; ~30-

18 kyr) ice limit (Fig. 1.4; Barrell, 2011), and is one of only two terrestrial records in the Southern Hemisphere mid-latitudes to capture past vegetation and past climate change over the full penultimate glacial-interglacial transition (PGIT). The comparison of the palynological changes reflected in these Westland sites and from sediment cores collected in the adjacent East Tasman Sea (ETS) over the LGIT help to; a) provide insight into palynomorph representivity in both realms for a period of major environmental change (**key theme A**); and b) explore the time taken for palynomorphs to transit from land to the deep sea (**key theme B**; residence time). These key themes are addressed in Chapter 3 (**aim 1**).

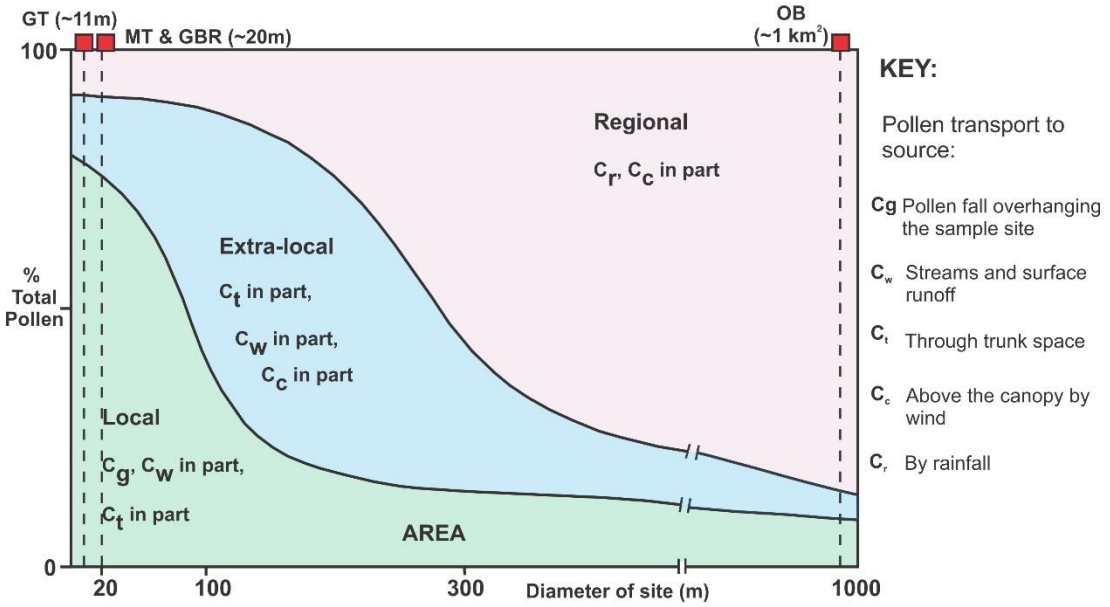

Fig. 2.1: Relationship between the size of the terrestrial sites in Westland with no inflowing streams and the relative proportion of pollen originating from different areas around the site. The sites are Galway Tarn (GT), Manks Tarn (MT), Gillespies Beach Rd (GBR), and Okarito Bog (OB). Figure modified from Macphail and McQueen (1983), based on the original figure in Jacobson and Bradshaw (1981).

High and frequent rainfall on the South Island's West Coast (>12,000 mm/yr) results from the predominantly warm westerly airflow which gathers moisture across the Tasman Sea and is forced orographically over the Southern Alps (Sturman and Tapper, 2006). This is considered to promote the rapid scavenging of lofted atmospheric particulates including pollen (Ryan et al., 2012). Terrestrial palynomorphs which fall onto the ground in this way are typically in good physical condition as they quickly become waterlogged, promoting sinking in both air and water (McDonald, 1962). On land, these grains can become transported in small streams and surface runoff (soil erosion), which can contribute to significant (85-90%) amounts of pollen to terrestrial lakes/swamps (Peck, 1973; Jacobson and Bradshaw, 1981) although this stream-borne contribution can be <50% where forests

deposit palynomorphs directly into the lake. Fluvial transport routes are considered the primary mechanism of palynomorph delivery onto the continental shelf west of New Zealand's South Island by the fact that prevailing winds are onshore, and by the greatly enhanced proportion of fern spores at the core site relative to terrestrial sites without inflowing streams (Ryan et al., 2012). Pollen that arrives in Westland and the ETS is also sourced from long distance transport (<1%) from Australia (Moar, 1969, 1970; Ryan, 2010).

2.1.2 Pollen taphonomy and residence pathways of terrestrial pollen reaching the marine realm

Reconstructions of vegetation change from marine sedimentary sequences are influenced sorting of grains by size and physical abrasion). The preservation of terrestrial palynomorphs in marine sediments can be variable depending on the original preservation state of the grains, the source, distance and travel mechanisms, and mechanical and chemical attack (Holmes, 1994; Mildenhall, 2003; Cundill et al., 2006). This may distort the "environmental signal" from marine cores compared to traditional terrestrial representivity studies (e.g. Moss et al., 2005; Wilmshurst and McGlone, 2005), reducing the confidence with which paleoclimate reconstructions can be made (Moss and Kershaw, 2000; Hope et al., 2004).

Land sea records can be further biased based on how long palynomorphs reside in soils, estuaries and coastal shelf sediments (McGlone, 2001; Moss et al., 2005). These times can change by up to an order of magnitude over G-I cycles due to erosion and sediment storage (Dosseto et al., 2010), or changes in coastal configuration (Dunbar et al., 2000; Carter et al., 2002; Carter and Manighetti, 2006). Large changes to the pollen source area over G-I cycles can distort the vegetation-climate signal (Hope et al., 2004), as large pollen catchment areas often comprise a much greater range of climatic conditions than those associated with coeval records from nearby terrestrial sites (McGlone, 2001; Mildenhall, 2003). However, such sorting of palynomorphs is not an inevitable consequence of fluvial and marine transport. Where river length is short or where rivers rapidly deposit their sedimentary loads, including any trapped palynomorphs, an unsorted palynomorph assemblage may result which faithfully reflects nearby plant communities (Smirnov et al., 1996; Wilmshurst et al., 1999; van der Kaars, 2001; Traverse, 2007). Once in the ocean, the particle can then become transported from coastal currents and surface waters as they settle through the water column (Heusser, 1990).

The assumed range of transport pathway of palynomorphs from Westland to the East Tasman Sea is illustrated in Fig. 2.2. The region is characterised by high catchment erosion rates (32,000 t/km^2/yr) and runoff, which is a consequence of high rainfall and steep gradients, with little interception in the small estuaries present (Hicks et al., 2011). This is hypothesised to result in negligible residence times to the East Tasman Sea, however this feature was not quantified (Ryan et al., 2012). The relatively narrow (~15 km) continental shelf seaward of Westland prevents large changes in the pollen source area over G-I cycles. By contrast, on the east coast of the South Island, the LGM shoreline was located up to 85 km east of the present shoreline, exerting a stronger influence on the pollen transport pathway of marine sediments in that region (i.e., DSDP Site 594; Fig. 1.4). Palynomorphs delivered to the Hokitika Canyon, a prominent highly sinuous submarine canyon system of the East Tasman Sea, are considered to have largely been sourced from the Hokitika River catchment over time (Ryan et al., 2012). This is one of the four largest suspended sediment producing rivers in Westland, and the second largest of the South Island, contributing 6.2 Mt.y^{-1} of the total 62 Mt.y^{-1} of sediment and organic matter delivered onto the continental margin of the East Tasman Sea (Hicks et al., 2011). The Hokitika canyon acts as an efficient conduit for this material eroded off the Southern Alps during all phases of sea level change (Neil, 2008; Hicks et al., 2011; Ryan et al., 2012; Larsen et al., 2014). The canyon has actively incised the continental shelf following post glacial sea level rise (Norris, 1978), with the canyon head ~8 km seaward of the modern shoreline and ~12 km from the modern Hokitika River mouth.

The primary delivery of sediment (and palynomorphs) to the levee banks along the submarine channel, and thus to marine core sites outlined in Fig. 1.4, occurs via dense hyperpycnal underflows and rapid submarine gravity flows (Bradford-Grieve et al., 2006; Radford, 2012), with a portion of the resulting fine material accumulating on levee banks (Peakall et al., 2000; Proust et al., 2006; Proust et al., 2008). Sediment can also be delivered by low-density hypopycnal overflows (Fig. 2.2), identifiable up to 75 km offshore (Moore and Murdoch, 1993). Fine sediment accumulating in the Hokitika Canyon levee may also be transported from distal locations by the wind driven, predominantly NE flowing, coast parallel Westland Current (Fig. 1.4; Carter, 1975; Carter and Heath, 1975; Stanton, 1976; Heath, 1985; Radford, 2012). Littoral sediment was likely diverted into the Hokitika canyon at the large promontory south of the canyon head, referred to as the 'seaward bulge', during sea-level low stands (Norris, 1978).

The length of time it takes between the release of palynomorphs until their deposition on the seafloor at the final site of interest is termed residence time. This is explored for the Last Glacial Coldest Period and the last termination amelioration (**aim 1; Chapter 3**). Negligible residence times over this period of major environmental change would help to justify the direct comparison of the magnitude and timing of terrestrial and oceanic climate change from marine cores, and the transfer of marine core chronologies to long terrestrial sequences in this region beyond radiocarbon timescales.

2.1.3 Marine-terrestrial core comparison in southwestern New Zealand

A comparison of some key taxa between the benchmark long terrestrial palynomorph record from Okarito Bog and the adjacent ~210 ka profile developed from marine core TAN0513-14 (Fig. 1.4), provides insight into palynomorph taphonomy during the source-to-sink transport from Westland to the East Tasman Sea over the last two glacial-interglacial cycles (Fig. 2.3). This comparison illustrates the usefulness of the marine record for reconstructing the dominant vegetation communities over longer time periods but also serves to highlight certain differences in pollen representivity. Marine records from the East Tasman Sea have higher numbers of more robust and non-anemophilous (i.e., not wind-pollinated) palynomorphs, such as Asteraceae and *Cyathea* spp. (tree fern spores), than terrestrial records (Ryan et al., 2012). These grains are not aerially transported far from source (Macphail and McQueen, 1983; Moar et al., 2011; van der Kaars, 2001), and so their vastly over-represented amounts at TAN0513-14 reflect a potentially long and arduous fluvial transport history from a relatively large altitudinal range. Their potential preservation is evidently aided by their robustness. Both records oscillate similarly over time, with more dominant tree ferns spores during interglacial periods and more dominant Asteraceae during glacial periods. Similar trends are recorded in land-ocean comparisons of modern and last glacial age from the New Zealand region (Dunbar et al., 1997; Wilmshurst et al., 1999; Mildenhall, 2003; Wilmshurst and McGlone, 2005; Crouch et al., 2010; Mildenhall and Orpin, 2010).

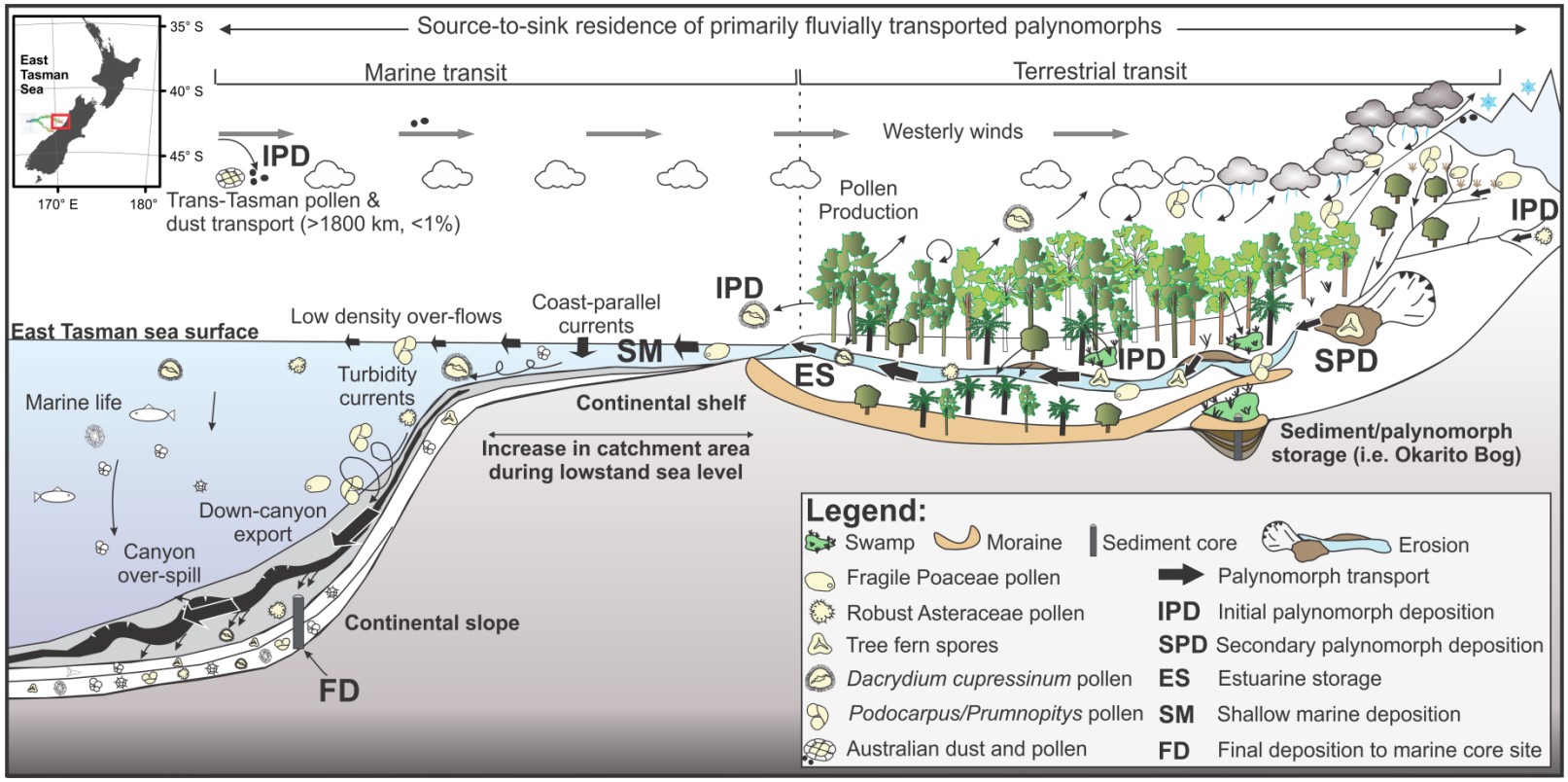

Fig. 2.2: Cartoon illustrating potential source-to-sink transport pathways prior to human influence and the residence of fluvially transported palynomorphs from Westland to its final destination in the East Tasman Sea. The initial transport and deposition of palynomorphs (IDP) to the ocean via fluvial processes is considered to occur relatively quickly with little storage in estuarine environments (ES). This process occurs against the prevailing westerly wind direction, also responsible for transporting low proportions of exotic taxa from Australia (Ryan, 2010). The exhumation of soil material from stream bank erosion and instabilities within the landscape (SPD) also likely contribute to palynomorphs deposited into the East Tasman Sea (Ryan et al., 2012). Widespread anthropogenic lowland forest disturbance of Westland catchments has altered this natural source-to-sink process. Once in the marine realm palynomorphs may reside in shallow marine settings (SM) prior to being exported down the Hokitika submarine canyon system until their final deposition (FD) via overbank spill (Ryan et al., 2012). Illustration idea adapted from one presented by Mudie and McCarty (2006).

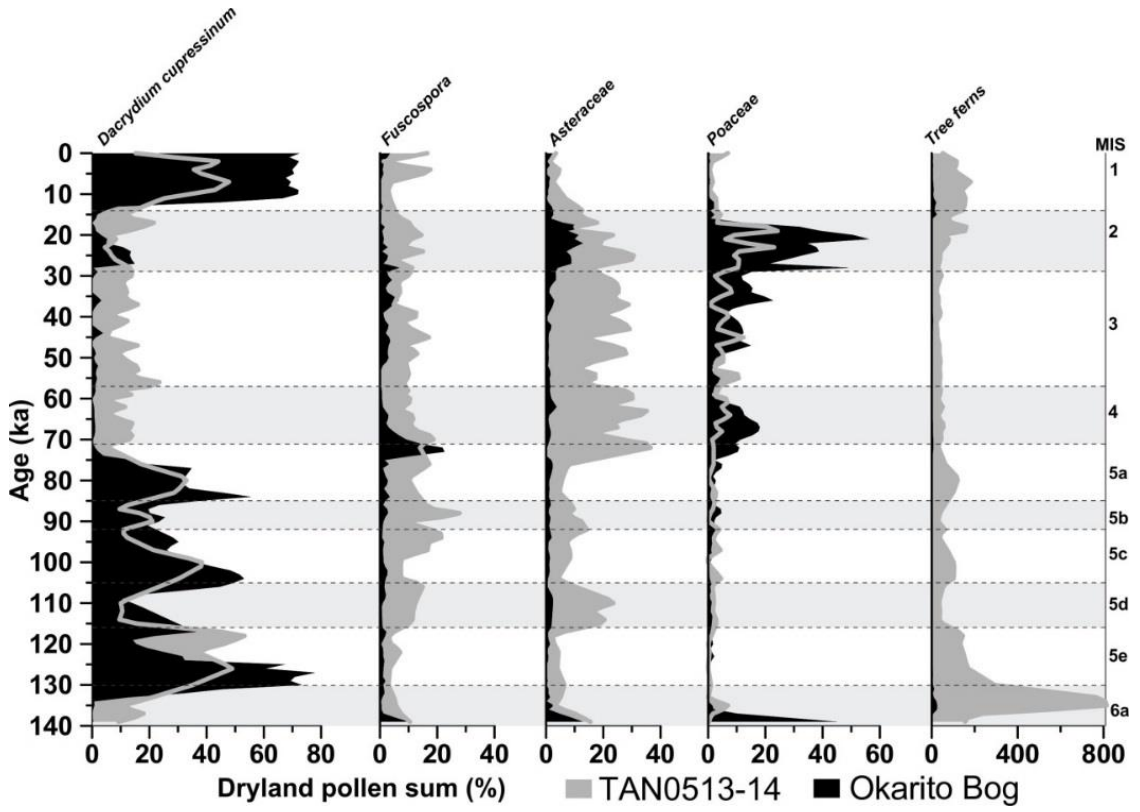

Fig. 2.3: Comparison between key palynomorph taxa from TAN0513-14 (grey) and Okarito Bog (black) of Ryan et al. (2012) over the last two glacial cycles. Palynomorph taxa are rescaled to common ages between both and are plotted on the TAN0513-14 age model. All taxa are proportions of the dryland pollen sum.

Central-south Westland terrestrial records (e.g. Galway Tarn and Okarito Bog; Newnham et al., 2013; Vandergoes et al., 2013a) contain a significantly greater proportion of typically over-represented, anemophilous (wind pollinated), and more delicate grass (Poaceae) pollen than is recorded in marine sediments. Importantly, similar variations in Poaceae reflected in three Westland terrestrial sequences of differing chronological constraint facilitated in the establishment of a regional vegetation-climate signal developed for the Last Glacial Coldest Period for Westland (Vandergoes et al., 2013a). Fewer numbers of Poaceae pollen are found offshore and likely result from their degradation during transit from source-to-sink (Ryan et al., 2012), with these grains preferentially degraded in soils exposed to oxidising conditions(Cushing, 1967; West, 1971; Jacobson and Bradshaw, 1981; Delusina, 2007; Traverse, 2007; Howarth et al., 2013). While preserved in lower abundances than on land, the similar patterns of occurrence evident in the marine records is useful for correlation between land and sea records more generally (Fig. 2.3).

Proportions of the tall tree conifer *Dacrydium cupressinum* show similar high relative abundances during interglacials at Okarito and TAN0513-14, although generally proportions are lower in the marine record. Conversely, greater proportions of *Dacrydium cupressinum* are

reflected at TAN0513-14 during glacial/stadial periods than Okarito (Fig. 2.3). This over-representation of podocarp grains is similarly reflected in sea-floor sediments around New Zealand of last glacial age, with the grains' superior hydrodynamic performance being lengthened along fluvial and oceanographic transport routes (McGlone, 2001; Mildenhall et al., 2004; Crouch et al., 2010; Williams et al., 2015). Palynomorphs transported to the ocean during glacial periods (sea level lowstand) are sourced from a larger pollen collection area than during interglacials. Pollen produced from comparatively small numbers of these trees, which likely persisted along the now submerged coastal fringe of Westland (Marske et al., 2009; Ryan et al., 2012), may be over-represented in the marine realm due to their capacity for wide-dispersal (Mudie, 1982; Crouch et al., 2010; Moar et al., 2011; Luo et al., 2014).

A final notable difference between both profiles is the greater over-representation of *Fuscospora* in modern and fossil marine sediments adjacent to Westland, despite the catchments of rivers that drain central Westland being currently devoid of Nothofagaceae (southern beech) forest. The so-called "central Westland biotic gap" (Wardle, 1984; Wardle, 1988) occurs between the Taramakau and Paringa rivers (Fig. 1.4, inset A). To the north and south of this gap, the prominent beech species are *Lophozonia* (formerly *Nothofagus*) *menziesii, Fuscospora fusca*, and at higher altitudes, *Fuscospora cliffortioides* (Wardle, 1988; Heenan and Smissen, 2013). Higher abundances of southern beech at TAN0513-14 over the last two glacial cycles occur during glacial/stadial intervals than interglacial/interstadial periods (Ryan et al., 2012). This dissimilarity has been attributed to the redistribution of these grains from north or south of the core site in the form of coast-parallel currents and wind (e.g., Cahill et al., 1991; Moore and Murdoch, 1993). These currents are poorly defined in this region and may flow in either direction in response to the prevailing winds, although the relatively greater wave energy from southerly swells would tend to favour southwest to northeast sediment transport (Carter and Heath, 1975). Pollen and DNA analysis have indicated that southern beech forest may have occupied this gap during the MIS 7 interglacial (Leschen et al., 2008; Ryan et al., 2012), and its pronounced geographic restriction occurred following the transition into T-II, where the slow spread of taxa to upland areas was outcompeted by the superior seed dispersal capabilities of podocarp-hardwood taxa during a period of warming climate and rapidly rising sea level (Hall and McGlone, 2006; Newnham et al., 2007a). Nevertheless, increasing levels of southern beech in terrestrial sequences attributed to the MIS 5b stadial in the Hokitika region suggests southern beech may have advanced south of its current northern limit under favourable climate conditions (Moar and Suggate 1996; Moar et al., 2008).

Despite the differences outlined between regional central-south Westland terrestrial records and adjacent reconstructions from marine sequences, coeval changes in the relative proportions of these taxa in response to climate change can be identified in both environments. The similarity between variations in regionally dispersed taxa (as opposed to the relative abundance of each taxon) presents the opportunity to transfer marine core chronologies to pre radiocarbon dated terrestrial sequences in this region (**key theme C**). However, this technique is only valid if it can be shown that the residence time of palynomorphs is negligible (undertaken in Chapter 3). The transfer of the aforementioned marine chronologies to long terrestrial counterparts which contain quantitative reconstructions of climate help overcome the biases faced in each of these environments, i.e., poor age control in terrestrial sequences and representivity issues in the marine realm (Chapter 4; **key theme D**).

2.2 Key taxa used in climate reconstructions

This section summarises key palynological indicators that are used to reconstruct changing vegetation and infer climate in southwestern New Zealand. A detailed description of the vegetation of Westland is described in section 2.5. Several key taxa with known ecological ranges that are used to reconstruct past climate are outlined (Table 2.1), with these key palynological indicators varying both over time and in geographical range. Quantitaive paleoclimate reconstructions using pollen-rain from pre-deforested sites has enabled the climate-vegetation relationships to be investigated from locations around New Zealand and the nearby Subantarctic Islands primarily over the LGIT and early Holocene (Wilmshurst et al., 2007; McGlone et al., 2010a; 2010b; Newnham et al., 2012; Sikes et al., 2013). Mean annual air temperature (MAAT), followed by mean annual precipitation, has the strongest influence on New Zealand vegetation than other climate variables in the pollen-climate calibration model (Wilmshurst et al., 2007). Prominent Westland taxa that are significantly correlated with high or low mean annual land surface temperatures are listed in Fig. 2.4 and Table 2.1.

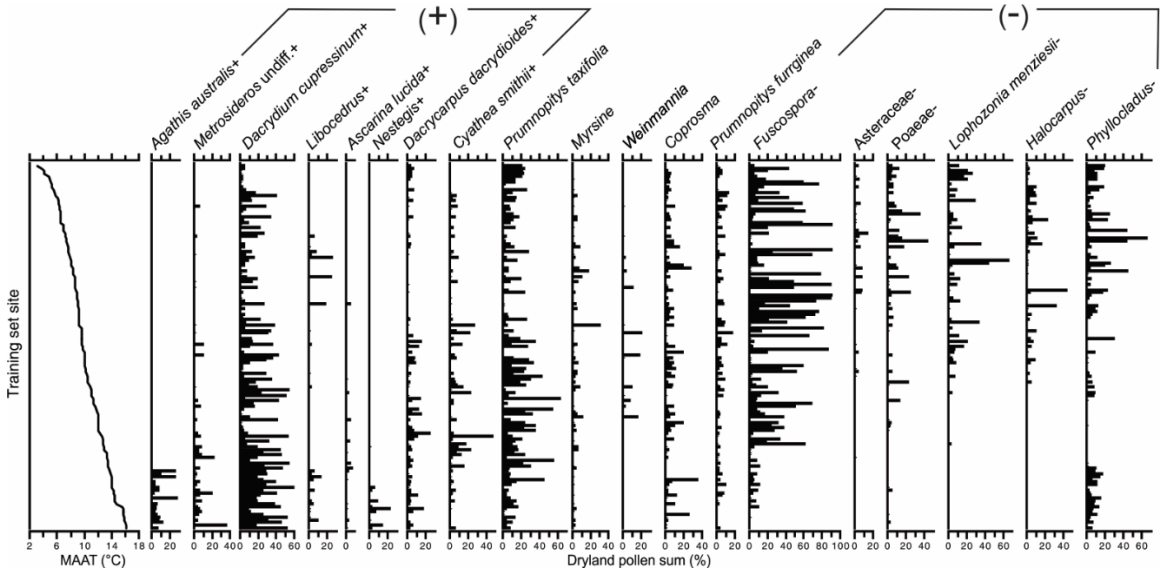

Fig. 2.4: Pollen diagram showing the relative abundance of selected pollen and spore types with samples (histogram bars) arranged from the coolest mean annual air temperatures (MAAT) (top) to the warmest (base) modified from Wilmshurst et al. (2007). Taxa are arranged from left to right according to the strength of their correlations with MAAT; taxa with significant correlations are followed by – or +.

Equivalent quantitative reconstructions of terrestrial climate change have yet to be undertaken on marine sequences from New Zealand due to taphonomic issues, and thus remain qualitative in nature (for example "wetter and cooler", "warmer and drier", etc). However, the technique of transfering marine age models to terrestrial sequences previously undertaken in this region offers potential for quantitaive paleoclimate reconstructions from terrestrial sites to be compared to those from adjacent marine cores beyond the Last Glacial-Interglacial Transition. Where these practices are not available, i.e., in the absence of terrestrial analogues, semi-quantitative paleoclimate information can be obtained from the presence of key "indicator" species whose climatic limits are well known. For example the presence in marine cores of the frost-and drought-intolerant *Ascarina lucida* and the frost-intolerant *Dodonaea viscosa* (Ryan et al., 2012) places useful constraints on temperature minima (McGlone and Topping, 1973; McGlone and Moar, 1977; Macphail and McQueen, 1983; Martin and Ogden, 2005).

Total dryland pollen assembledges from terrestrial profiles in southwestern New Zealand have been grouped by Vandergoes et al. (2005), and from Ryan et al. (2012) in marine sediment core TAN0513-14, according to four categories: podocarp-hardwoods (predominantly *Dacrydium cupressinum*, *Prumnopitys ferruginea*, *Prumnopitys taxifolia*, *Metrosideros*, *Weinmannia*, *Nestegis, Dacrycarpus dacrydiodies)*, beech (*Fuscospora*, *Lophozonia menziesii*), montane-subalpine trees (Asteraceae, *Coprosma*, *Halocarpus*, *Myrsine*, *Phyllocladus*) and shrubs, and herbs (Poaceae). These groups closely correspond to the altitudinal (≈temperature) zonation

described in section 2.5, with individual taxa and their correlation with MAAT displayed in Fig. 2.4. Several taxa nontheless extend wide altitudinal ranges (Table. 2.1), i.e., Poaceae is widely distrubuted and while it is dominant in the low-alpine zone (1200-1400 masl), it may be locally extensive on lowland river flats, slips and sand landforms (<400 masl). Reference to the relative abundance of terrestrial palynomorph taxa for terrestrial and marine sites in this thesis follow; rare typically <1%, common ~10-20%, abundant >20%.

Table 2.1 – Palynological indicators of vegetation and climatic change in southwestern New Zealand

Climate conditions	Vegetation indicator	Key palynological indicator and distribution
Extreme cold (glacial)	Grassland/herbfield and alpine shrubs	Poaceae^{L-A} (-0.49) and Asteraceae^{L-A} (-0.39).
Warming but cool	Cool climate small tree shrubs	*Coprosma* $^{L-A}$, *Myrsine* $^{M-S}$, possibly *Halocarpus* $^{M-S}$ (-0.59) and *Phyllocladus* $^{M-S}$ (-0.65).
Marked warming	Development of tall podocarp or podocarp-beech forest	*Metrosideros* $^{L-M}$, *Weinmannia* $^{L-M}$, *Dacrycarpus dacrydiodies* ^{L} (0.31), *Prumnopitys ferruginea* ^{L}, *Dacrydium cupressinum* ^{L} (0.51).
Warm (interglacial)	Tall podocarp-hardwood forest with frost and drought intolerant species	*Prumnopitys ferruginea, Dacrydium cupressinum, Nestegis* ^{L} (0.46), *Ascarina lucida* $^{L-M}$ (0.43), *Dodonaea viscosa* $^{L-M}$ (0.28).
Climate cooling	Decline in warmer climate flora, increase and spread of cool climate tolerate grassland-herbfield and small tree shrub species	Increasing Poaceae and Asteraceae, possibly *Halocarpus, Phyllocladus* , *Fuscospora* $^{M-S}$ (-0.38), and *Lophozonia menziesii* $^{M-S}$ (-0.51). Decreasing *Metrosideros, Weinmannia, Prumnopitys ferruginea, Dacrydium cupressinum.*

Significant spearman rank correlation r values for selected pollen types in the New Zealand pollen database (Wilmshurst et al., 2007) versus mean annual temperature (MAAT) are displayed in brackets. The strength of the correlation with MAAT is displayed, with positive associations to warmer temperatures and negative to colder. The altitudinal range of each taxa is indicated by a subscript; Lowland (L); Montane (M); Subalpine (S); low-alpine (A) after Macphail and McQueen (1983). Table modified after Vandergoes (2000) and Ryan (2010).

2.3 Climate event stratigraphy for southwestern New Zealand and the adjacent ocean over the last 450 ka

2.3.1 Chronological constraint

The western flank of New Zealand's South Island contains a recognised history of past ice sheet activity spanning multiple glacial-interglacial cycles over the late Pleistocene (Suggate et al., 1996; Suggate and Almond; 2005: Barrell, 2011; Barrell et al., 2011). These ice advances expanded from their valleys to form large piedmonts that extended ~700 km along the

Southern Alps (Suggate, 1990). The complex intercalation and fortuitous preservation of these glacial remnants, fragmentary infilled sedimentary depressions, and coastal shorelines arise from persistent uplift and movement along the Alpine Fault (Fig. 1.4). These deposits provide valuable climatostratigraphic information about past glacial and interglacial periods, often in the absence of precise chronological control. In particular, palynology of biogenic deposits represent snapshot and continuous records of past climate change, with recognisable differences in glacial and interglacial flora (Fig. 2.5; Moar and Suggate, 1996; Moar and McKellar, 2001; Moar et al., 2008; Newnham et al., 2007a). Prior to recent advancements in exposure age dating techniques, direct chronological control for the remnants of ice advances descending from the Southern Alps ice cap over the last two glacial cycles only existed at a few locations (Suggate and Almond; 2005). As a consequence, radiocarbon or luminescence ages primarily undertaken largely on fragmentary peat deposits amidst till and outwash largely underpinned the stratigraphy of the region (Fig. 2.5).

Fluctuations in the relative abundance of regionally dispersed grass pollen recorded from lacustrine sediments at Galway Tarn (Fig. 1.4), south Westland, provide key climatostratigraphic information for the period from ca. 30-18 cal ka BP (Barrell et al., 2013). This sequence was selected as the type record for the Last Glacial Coldest Period (LGCP) in the pollen based New Zealand-INTIMATE (Integration of Ice Marine and Terrestrial archives) Climate Event Stratigraphy (NZces) (Fig. 2.6). Chronological constraint for the sequence was provided from radiocarbon dating and from the occurrence of the widespread 25.4 cal ka BP Kawakawa/Oruanui Tephra (KOT) (Vandergoes et al., 2013a; 2013b), and is also identified in the nearby long pollen record at Okarito Bog (Fig. 2.5; 2.7). This tephra originates from the Taupo volcanic caldera in the central North Island of New Zealand, 630 km to the northeast (Wilson, 2001; Lowe et al., 2008; Wilson et al., 2009; Van Eaton et al., 2013), and is one of the most widespread Late Quaternary tephra in the New Zealand region (Fig. 2.7). KOT is the only Quaternary macroscopic tephra so far identified in terrestrial Westland cover-bed sequences (Mew et al., 1986; Almond, 1996; Almond et al., 2001; Suggate and Almond, 2005; Barrows et al., 2013). Cores collected from levee bank deposits in the East Tasman Sea contain KOT albeit cryptically (Ryan et al., 2012), as well as other tephra layers deposited over the last 1 Ma (Hayward et al., 2012), with all providing potentially valuable stratigraphic and chronological markers that support land-sea correlations.

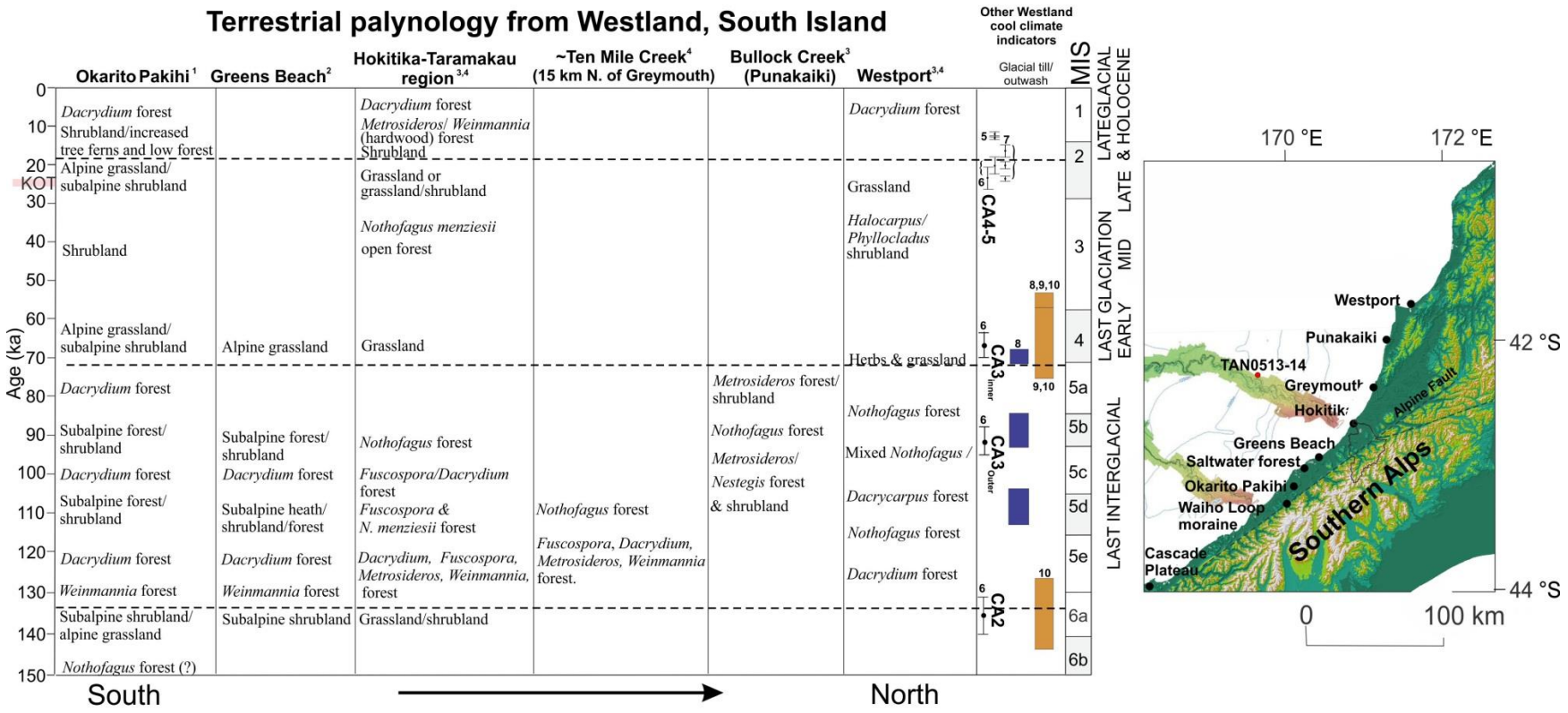

Fig. 2.5: Studies of terrestrial palynology from south to north Westland, South Island, modified from Moar and Suggate (1996). Studies included are Vandergoes et al. (2005)[1], Moar and McKellar (2001)[2], Moar and Suggate (1996)[3], Moar et al. (2008)[4]. The location of the 25.4 cal ka BP Kawakawa/Oruanui Tephra (KOT) is displayed (Vandergoes et al., 2013b). *Dacrydium cupressinum* has been abbreviated in this figure to *Dacrydium*. Additional cool-climate indicators for Westland are displayed (right) from; Waiho Loop moraine and Canavans Knob associated with re-advance of the Franz Josef Glacier (Denton and Hendy, 1994; Barrows et al., 2007b; Turney et al., 2007; Applegate et al., 2008)[5], Cascade Plateau (CA) moraines (Sutherland et al., 2007)[6], north Westland moraines (Barrows et al., 2013)[7], and various Westland outwash and till sequences Preusser et al. (2005)[8], Berger et al. (2001)[9], Almond et al. (2001)[10]. All ^{10}Be ages[5,6,7] are rescaled using the local production rate of Putnam et al. (2010a). Key vegetation transitions based on lowland forest expansions are displayed by dashed horizontal lines.

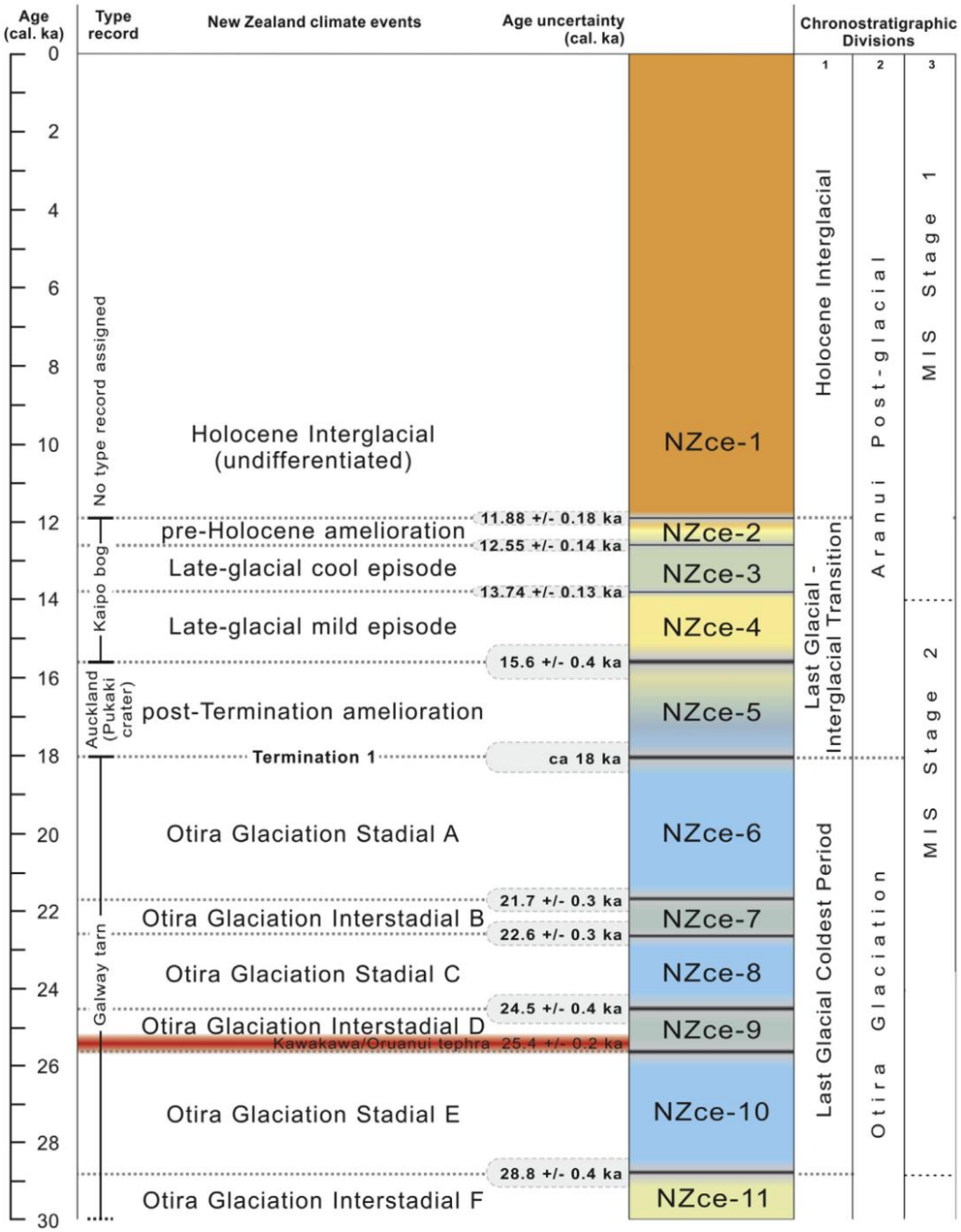

Fig. 2.6: The New Zealand-INTIMATE climate event stratigraphy based on boundaries derived from the composite stratotype (modified by Barrell et al., 2013). The colour scheme schematically illustrates characteristic atmospheric temperatures (orange = warmest, blue = coldest). Chronostratigraphic schemes are (1) major climate phases in New Zealand (Alloway et al., 2007a; Barrell et al., 2013); (2) New Zealand climate-based time-stratigraphic stages from Gage and Suggate (1958) and Suggate (1961); and (3) global marine-oxygen isotope scale (MIS) stages (Lisiecki and Raymo, 2005).

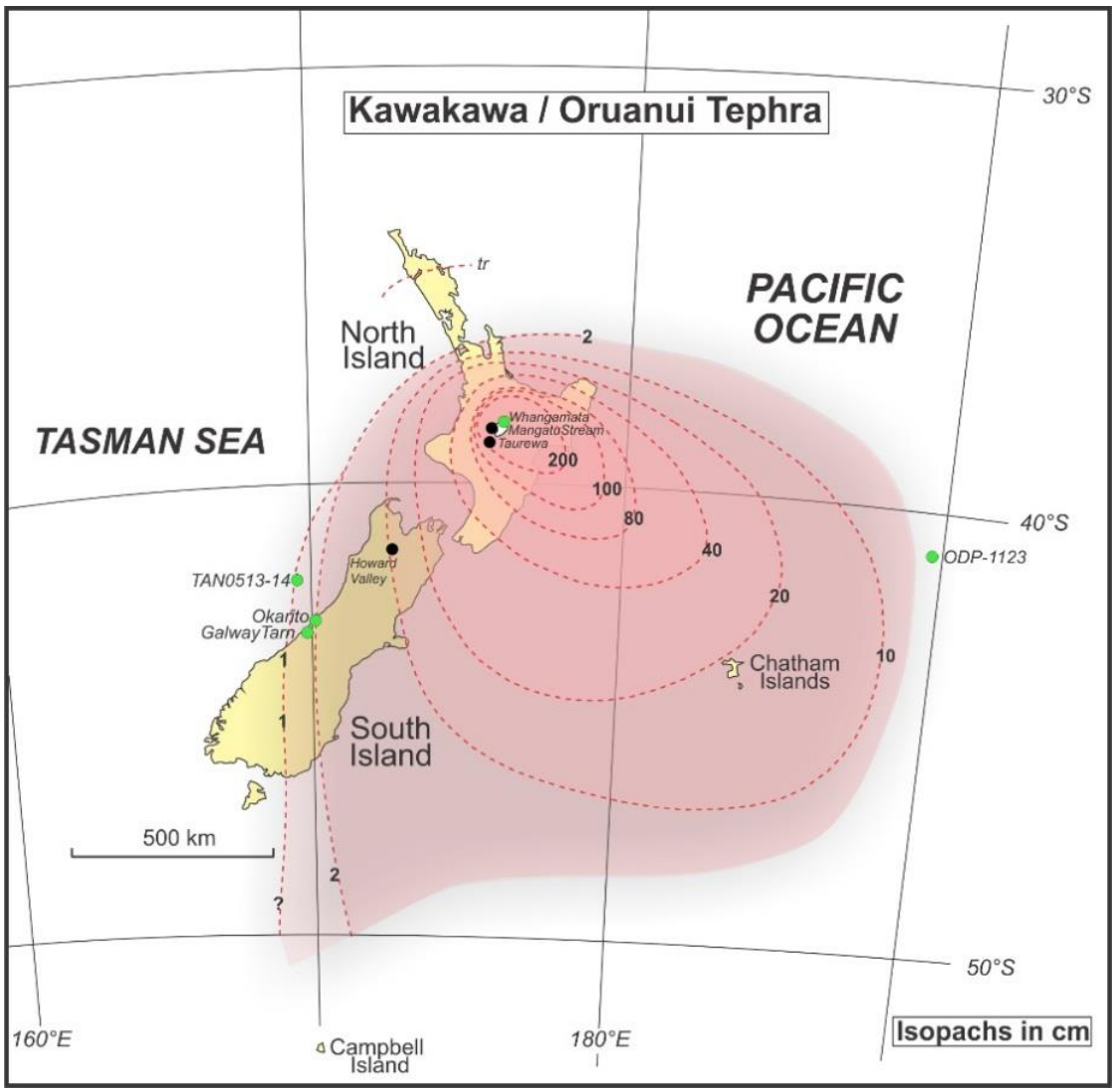

Fig. 2.7: Distribution of Kawakawa/Oruanui Tephra (KOT) in the New Zealand region. Sites with major element compositions displayed in Ryan et al. (2012) are shown in green circles. Sites used for determining the age of KOT by Vandergoes et al. (2013b) are shown in black circles. Map modified from Alloway et al. (2007b) and further revisions (Lowe et al., 2008; Vandergoes et al., 2013b).

2.3.2 Glacial climate

At present there are no published records of glacial-interglacial vegetation change from Westland which are recognised to have been deposited prior to the penultimate glacial (MIS 6). As such terrestrial palynomorphs extracted from marine sedimentary sequences offer potential for investigating climate and vegetation history of the region, in combination with ocean surface conditions prior to that period. The regional vegetation cover for the penultimate glacial from Westland is characterised by grassland-shrubland communities containing Poaceae, Asteraceae, *Coprosma* (Fig. 2.4; Moar and Suggate, 1996; Moar and McKellar, 2001; Vandergoes et al., 2005). High numbers (>50%) of non-arboreal pollen taxa associated with extreme cold conditions for MIS 6 are represented at Okarito (Vandergoes

et al., 2005), western Taranaki (Bussell, 1990), ~500 km to the north, and from the ~350 kyr record of eastern South Island terrestrial vegetation change from DSDP Site 594, situated ~300 km east (Fig. 1.4; Heusser and van de Geer, 1994). DSDP Site 594 is located within Subantarctic Waters (SAW), while sites in the East Tasman Sea sites lie in the vicinity of Subtropical Waters and the Subtropical Front (Fig. 1.5), with these waters influencing the variation in SST estimates (East Tasman Sea sites warmer), and the adjacent vegetation profiles. The pattern of vegetation change during the MIS 6 glacial resembles that reflected for the Last Glacial Coldest Period (Fig. 2.5 and 2.8), although insufficient chronological control prevents further examination of the timing of these changes (Newnham et al., 2007a).

Surface exposure age dating of glacial moraines have recently provided direct constraints on the timing of ice advances in this region since the penultimate glacial (Fig. 2.5; Sutherland et al., 2007; Barrows et al., 2007b; Barrows et al., 2013). Those representing past glacier positions in the Cascade Plateau (CA2-5; Fig. 2.5), south Westland (Sutherland et al., 2007), which have been revised to local production rates (Putnam et al., 2010a), show good correspondence with vegetation change and glacial outwash (Berger et al., 2001). Ocean surface temperatures were ~6-7°C colder in the East Tasman Sea than interglacials periods following the mid-Brunhes Event (Fig. 1.1, i.e. during MIS 12, 6, 2), and are associated with migrations of the Subtropical Front ~3-5° to the north from its current position (Fig. 1.5; Barrows et al., 2007a; Hayward et al., 2012; Bostock et al., 2013; 2015). In contrast, to the east of the South Island, ocean surface temperature reconstructions from DSDP site 594 were up to ~11-12°C colder during glacial periods than interglacial periods following the mid-Brunhes (Hayward et al., 2008).

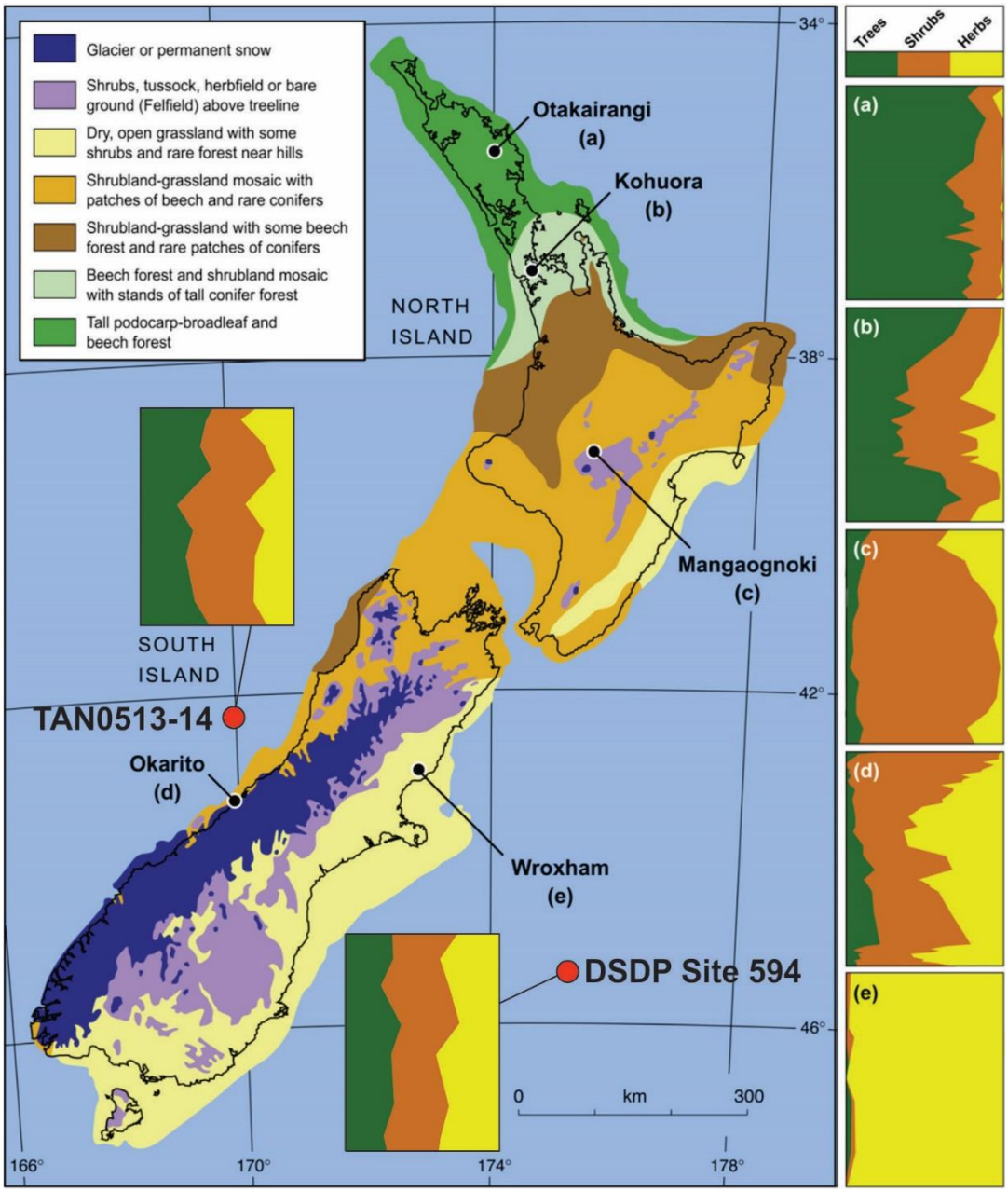

Fig. 2.8: Vegetation cover of New Zealand at 21 ka, as reconstructed from pollen, macrofossil, beetle and geomorphic evidence taken from Newnham et al. (2013). Panels to the right show time-stratigraphic sequences of the proportion of tree, shrub and herb pollen for the broader LGM interval (ca. 30-18 ka) for five distinctive regions. Note: trees (largely conifers) persisted at Okarito (site d) over this interval, although are less than northern counterparts. Marine core sites adjacent to the South Island are also displayed, with a greater representation of trees and concomitant reduced proportion of herb taxa reflected.

2.3.3 Climate amelioration over T-I and T-II and hemispheric asynchronies

Pollen profiles generated from Westland peat and lacustrine sediments depict a regional vegetation succession over the penultimate and last deglacial transitions, where a shrubland-grassland mosaic, including patches of southern beech and rare conifers, progressed into a mix of shrubs and conifers and then finally into a landscape dominated by tall conifer trees (Fig. 2.5; Moar and Suggate 1996; Newnham et al., 2007a; Newnham et al., 2012; Vandergoes et al., 2013a; Barrell et al., 2013). These vegetation changes are documented in both marine and terrestrial pollen records, and thus provide milestones to facilitate comparison between both environments (Ryan et al., 2012).

The onset of the termination one and the succeeding post termination amelioration (18-15.6 ka) reflected in pollen records is coeval with rapid glacier retreat each side of the Southern Alps (Putnam et al., 2013a; 2013b; Barrows et al., 2013; Vandergoes et al., 2013a). Glacial deposits indicative of past glacier position over the course of a deglacial termination from southwestern New Zealand are scarce, preventing the timing and magnitude of past environmental change from being assessed. Such absences are considered to result from topographic variability due to extremely high erosion rates and incision following ice retreat (Hicks et al., 2011; Larsen et al., 2014; Cogez et al., 2015), and variable regional climate controls on equilibrium lines (Barrows et al., 2013). Consequently, records east of the Southern Alps, which are similarly influenced by maritime climate changes (Doughty et al., 2015), complement records of past environmental change from southwestern New Zealand (e.g., Putnam et al., 2010b; 2013a; 2013b). Rapid warming over the post termination amelioration, reconstructed from the retreat of glaciers from eastern South Island, is connected with a concomitant rise in sea surface temperatures south of Australia from MD03-2611 (Fig. 1.5; De Deckker et al., 2012; Putnam et al., 2013a) and the East Tasman Sea (Barrows et al., 2013). However, the nature of this retreat has been questioned in the same region by Rother et al. (2014) who suggest it occurred gradually.

Warming of the Southern Hemisphere mid-latitudes over much of the Last Glacial Interglacial Transition has been linked to southwards migration of the ocean-atmosphere circulation system (Newnham et al., 2012; Putnam et al., 2013a). In contrast, coeval records across southern Europe display an advance in cool-climate vegetation and polar foraminifera over this time and are connected with a southwards migration of the ocean-atmosphere circulation system (Tzedakis et al., 2009a; 2009b). The succession of vegetation changes and rising sea surface temperatures over T-II (~139-130 ka) has been investigated from the nearby East Tasman Sea cores TAN0513-14 and SO136-GC3 (Fig. 1.4), with progressive

warming preceding the rapid warming of Northern Hemisphere ice sheets by up to ~4 kyr (Ryan et al., 2012). The low sedimentation rate of those two records (<3 cm.kyr^{-1}) and problems associated with core correlations precluded further assessment into higher order climate variability over millennia and comparisons between those sites and other far reaching records.

Newnham et al. (2007a) point out the similarity of a ~2 kyr millennial scale reversal in the progression of vegetation change at Okarito Bog, during both T-I as T-II, although the timing, magnitude and processes behind the T-II event remained unclear due to insufficient age control, with no strong evidence for cooling reflected in regional SSTs (Barrows et al., 2007a). The timing of the brief expansion of montane-subalpine shrub taxa during T-I, which reverses the progression of tall trees, is broadly consistent with evidence for cooling in the mid-high Southern Hemisphere latitudes. This is associated with a northwards propagation of the ocean-atmosphere system during the Antarctic Cold Reversal (ACR) between ~14.7-13 cal ka BP and within the Last Glacial-Interglacial Transition (Vandergoes and Fitzsimons, 2003; Vandergoes et al., 2005; Putnam et al., 2010b; De Deckker et al., 2012; Bostock et al., 2013; Pedro et al., 2015), and is asynchronous with the timing of warming displayed in Northern Hemisphere records (Bard et al., 2000; Barker et al., 2009; Cheng et al., 2009). Paleoclimate records (glacier, speleothem, vegetation) from the Southern Alps are increasingly being examined to better constrain the timing and magnitude of this event. The phasing of both T-I and T-II climate reversals are explored further in Chapter 4, in particular, how do these events compare with environmental changes reflected at Northern Hemisphere mid-latitude sites? (**key theme E**).

2.3.4 Interglacial climate

The climate optimums of the early Holocene (11.5-9 ka), MIS 5e (128-123 ka), and MIS 11c (417-407 ka) display evidence for global temperatures that are warmer than the present climate (Fig. 1.3). These intervals are regularly studied to better understand the impact of anticipated human-induced warm climate on ecological and geomorphic systems (Tzedakis et al., 2009a; Lang and Wolff, 2011; Past Interglacials Working Group of PAGES, 2016). Few well constrained quantitative estimates of ocean and atmosphere temperatures exist for the mid-high Southern Hemisphere latitudes for MIS 5e and MIS 11. Those of MIS 5e, being the most recent pre-Holocene analogue, display variability in time and the extent of warmth (Turney and Jones, 2010; Cortese et al., 2013; Capron et al., 2014; Govin et al., 2015). In the absence of continuous terrestrial sequences which covers all these interglacials, the only feasible method to assess the pattern of each interglacial is by extracting palynomorphs from marine cores adjacent to southwestern New Zealand, and thus is the prime motivation for the current study (**key theme F**).

Paleovegetation reconstructions from Westland and wider New Zealand constrain the timing of the Holocene amelioration by a rapid rise of podocarp-hardwood and frost intolerant pollen (Fig. 2.5; Moar and Suggate, 1996; Newnham et al., 2007a; Barrell et al., 2013). The timing of this event is similar to that of the global Pleistocene-Holocene parastratotype boundary at 11.88 ± 0.18 cal ka BP from Lake Maratoto in the Waikato lowlands (Walker et al., 2009), which could define the Holocene Interglacial on the New Zealand Climate Event Stratigraphy (NZces) 2-1 as proposed by Barrell et al. (2013) and is displayed in Fig. 2.6. Quantitative estimates for warming over New Zealand for the early Holocene (11-9 cal ka BP) suggest mean annual temperatures were ~1-1.5°C warmer than present (Wilmshurst et al., 2007; McGlone et al., 2010b), with lower regional treelines over the Southern Alps considered to reflect a reduced seasonality regime (i.e., cooler summers) (McGlone and Basher, 2012).

Surface ocean temperatures surrounding New Zealand during past interglacials appear to have been ~2-3°C warmer during MIS 5e and MIS 11c than the early Holocene (Hayward et al., 2012; Cortese et al., 2013; Prebble et al., 2016). While there is evidence for warm and moist conditions in reconstructions in vegetation change over MIS 5e from New Zealand (Bussell, 1990, 1992; Heusser and van de Geer, 1994; Mildenhall, 1995; Shulmeister et al., 1999; Carter and Lian, 2000; Carter, 2002; Marra, 2003; Newnham and Alloway, 2004; Ryan et al., 2012; Williams et al., 2015), reconstructions of temperature change have remained largely qualitative in nature. While not independently constrained, sites along Westland

previously correlated with the last interglacial (MIS 5e) on the basis that the palynomorph assemblage appear to be similar to that of the present interglacial palynomorph assemblage (Fig. 2.5). One notable difference is from the presence of pollen from the coastal hardwood tree *Nestegis* in sequences along Westland, where this species is otherwise not present. This suggest that either the distribution was much greater in the past and growing further south than its contemporary southern limit in the northern South Island (Moar, 1984; Moar and Suggate, 1996; Moar and McKellar, 2001; Newnham et al., 2007a), or alternatively that *Nestegis* pollen may have been transported from distant sources. A similar suggestion can be invoked for increased *Dodonaea viscosa* pollen in marine sediments associated with MIS 5e from TAN0513-14 (Ryan et al., 2012), as this species does not occur in contemporary forests south of Greymouth on the West Coast (Haase, 1990). While the comparison of land-sea pollen records and speleothem isotope profiles in this region have helped constrain the timing of MIS 5e in the terrestrial realm to ~128-117 ka (Ryan et al., 2012; Williams et al., 2015), the magnitude of atmospheric warming in terrestrial sites is poorly understood **(explored in aim 3, theme F)**. At present there are no terrestrial sequences containing T-V and the climatic optimum of MIS 11 reported from New Zealand **(theme F)**.

2.4 Climate variables and vegetation

The following section outlines the key climatic variables that influence the distribution of vegetation in Westland, i.e., air temperature, precipitation, sunshine hours and sea surface temperature in the study area. Non-climatic factors (e.g., soil type, geology, nutrients and drainage) may also be locally important on vegetation, but are considered secondary to temperature here (Wardle, 1991).

Rainfall

Rainfall is high in coastal regions (~2900 mm/yr^{-1}, Hokitika, NIWA 2014a; Fig. 1.4; Suppl. Fig. 2.1) and at altitude (11,200 mm/yr^{-1}, 902 masl, Hicks et al., 2011). The persistence of westerly airflow throughout the year (Renwick et al., 1998) means that there is little intra-annual variability in the distribution of rainfall with the wettest month (Dec.) averaging 275 mm at Hokitika, and the driest (Feb.) 189 mm (Fig. 2.9; Suppl. Fig. 2.2). Substantial rain falls in the upper Hokitika catchment all year round, with >25 mm on more than half of the days of the year (Griffiths and McSaveney, 1983a). The most extreme rainfall events in Westland have the ability to produce >350 mm of rainfall within 24 hours (Horrell et al., 2012). Flooding of the major Hokitika river (exceeding the 90th percentile of flow >160 m^3/s, NIWA, 2013) occurs regularly (~35 annual occurrences in 2013), and is characteristic of

many Westland catchments and can result in the erosion of stream bank material (Fig. 2.10). Consequently, periods of drought in Westland are rare, and relative humidity remains at 80-90% (Wardle, 1979). By contrast the orographic effect of the Southern Alps produces a rain shadow across the eastern South Island resulting in considerably less rainfall with an annual average of ~600-1500 mm occurring on the Canterbury plains at <500 masl (Griffiths and McSaveney, 1983b). Extensive snow and ice cover in winter in high altitude valleys along the Southern Alps can produce katabatic winds which sweep onto lowlands, creating extreme cold conditions and causing frosts in the winter in central Westland (Wardle, 1979). It is these moderately severe frosts rather than the hoar-frosts (i.e., those that form on cold clear nights) that damage plants on the Westland inland areas (Moar and Suggate, 1996).

Land surface temperatures

Climatically the study area is temperate, with a mean annual air temperature (MAAT) at the coastal town of Hokitika of 11.7°C (1981-2010; Fig. 2.9; Suppl. Fig. 2.2, a mean monthly maximum of ~15.7°C (~20°C in February the warmest month), and a monthly minimum of 7.7°C (~3°C July; the coolest month, NIWA, 2014a). Temperature decreases with altitude at a rate of ~5.6°C km^{-1} so that mean annual temperature is ~4°C at ~1400 masl (Stuart, 2009), with a maximum of 7.1°C (Feb.) and a minimum of 0°C (July, NIWA, 2014b). Mean MAATs at Okarito (~75 km south-west of Hokitika) are similar at 11.3°C (Whitehead et al., 2002). The distribution of native flora in the Westland region is strongly influenced by temperature and results in a marked altitudinal zonation (Wardle 1991).

Sunshine hours

The amount of sunshine hours per year is important for photosynthesis and is dependent on latitude, aspect, density of cloud cover and presence of overshadowing plants (Wardle, 1979). Annually, Hokitika receives 1893 hours of sunshine, which is close to the average of New Zealand's annual sunshine hours, despite the high degree of cloud cover and frequent rain (Garnier, 1958; Wardle, 1979). These combined effects of sunshine hours, cloud cover, precipitation and temperature produce a moist climate with mild winters and cool summers (Moar and McKellar, 2001).

Regional sea surface temperatures

Mean annual SSTs in the eastern Tasman Sea adjacent to Hokitika are 15.6°C (Fig. 2.9), with a mean monthly maximum of 18.8°C in January and minimum in late August to early September of 13.2-13.1°C (Locarnini et al., 2013). A lag of approximately 10 weeks occurs between the minimum monthly air temperature (June/July) and the minimum monthly SST (Aug/Sept) (Fig. 2.9) as a consequence of the influence of SST in moderating regional land surface temperatures. The SSTs are semi-parallel to the coast (Locarnini et al., 2013), where slightly lower temperatures occur inshore, with a maximum temperature ~130 km offshore of Westland (Bradford, 1983).

In maritime climates there is a strong relationship between SST and terrestrial air temperature. The higher specific heat, and heat capacity, of the ocean results in a reduction in the amplitude of the seasonal temperature cycle when compared to solid (land) surfaces which heat up and cool down much more quickly (Sutton and Roemmich, 2001). Therefore the annual temperature cycle of relatively small landmasses (e.g. New Zealand) surrounded by ocean are expected to be coupled to SST over time. This effect is reduced in the more continental regions of inland Otago and Canterbury (e.g. McGlone et al., 2003). This has important implications for paleo-vegetation studies because paleo-SSTs can be quantified with some confidence on glacial-interglacial timescales around the South Island of New Zealand (e.g. Pahnke et al., 2003; Pelejero et al., 2006; Barrows et al., 2007a; Hayward et al., 2008).

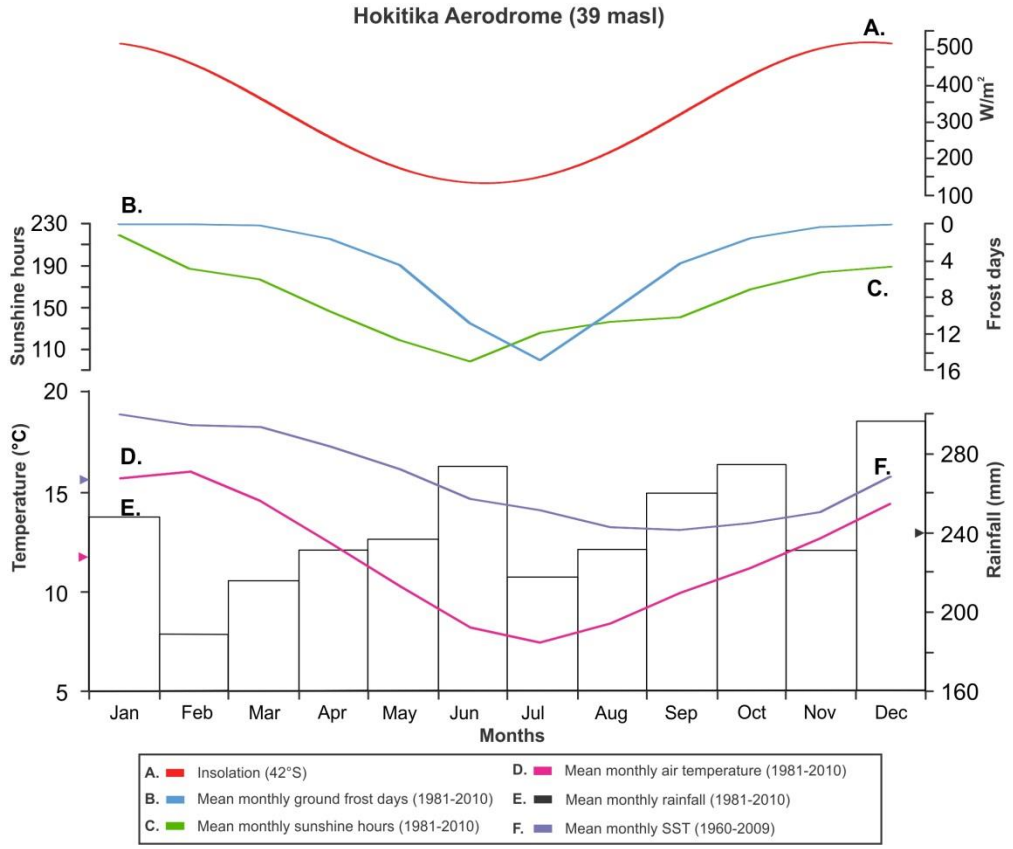

Fig. 2.9: Modern climate variables (A-E) influencing Westland vegetation measured from Hokitika Aerodrome climate station (39 masl) from 1981-2010 (NIWA, 2014a). **A.** Incoming solar radiation (W/m²) at the top of the atmosphere at 42°S calculated using the solution of Laskar et al. (2004); **B.** Mean monthly ground frost days; **C.** mean monthly sunshine hours; **D.** mean monthly air temperature and; **E.** mean monthly rainfall. Mean monthly SST's (1960-2006) from the position of the MD06-2991 core site at 169.5°E and 42.5°S (Locarnini et al., 2013) are shown in F.; Means for D-F are shown by coloured triangles adjacent to each plot.

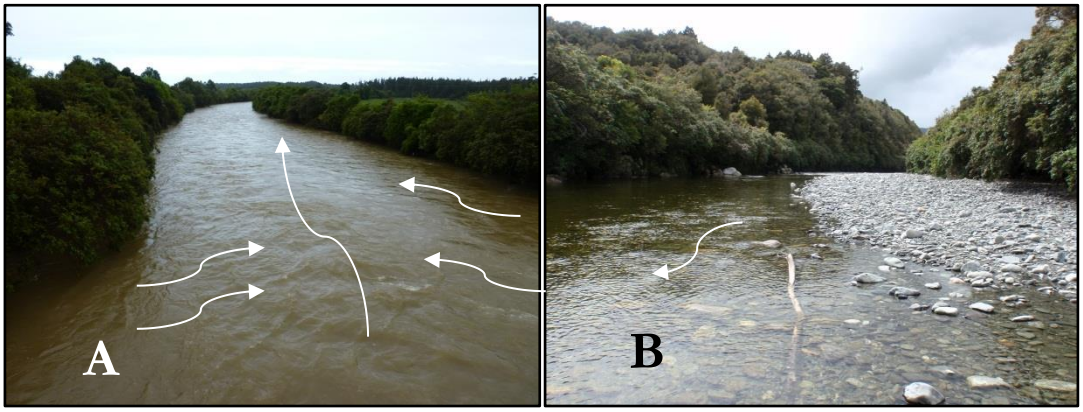

Fig. 2.10: Flooding and bank erosion vs. low flow and no erosion, Totara River, Westland, with direction of flow indicated from white arrows **A.** Photograph taken looking downstream (west) from the Totara River Bridge during a flood event (26/10/2011), with stream bank erosion contributing to the suspended sediment supply (Photo: Brian Anderson). **B.** Photograph taken looking upstream under the bridge of the Totara River during base-level conditions (18/11/12) (Photo: Gavin Dunbar).

2.5 Modern vegetation of Westland

In Westland there are a number of short, steep river catchments, which support a diverse range of vegetation, whose aerial extent is strongly dependent on primarily temperature and secondly rainfall (Wardle, 1979; 1991). Comprehensive studies of the vegetation of central Westland (Wardle, 1979; Reif and Allen, 1988) indicate that lowland podocarp forest is dominated by the thermophilous conifer *Dacrydium cupressinum* (Rimu), extending from sea level to ca. 400 masl, with *Prumnopitys ferruginea* (Miro), and *Dacrycarpus dacrydioides* (Kahikatea) as secondary emergent species. The lowland understorey is comprised largely of the drought and frost intolerant *Ascarina lucida* (Hutu; Sakai and Wardle, 1978; Martin and Ogden, 2005), *Pseudopanax* spp., *Coprosma* spp., *Myrsine* spp. and tree ferns (*Cyathea smithii*, *Cyathea colensoi*, *Dicksonia squarrosa*).

On the higher parts of the piedmont, and lower flanks of the range front (>400-800 masl), a montane podocarp-hardwood forest occurs and is characterised by *Metrosideros umbellata* (southern rātā), *Weinmannia racemosa* (Kāmahi), *Griselinia littoralis* and *Podocarpus hallii*. Sub-canopy trees include *Myrsine divaricata*, *Pseudopanax simplex*, *Pseudowintera colorata*, and *Coprosma foetidissima*. Many of these species remain common into the subalpine zone (>800-1200 masl) along with the small tree conifers *Phyllocladus alpinus* and *Libocedrus bidwillii*, collectively forming a dense shrubland up to the contemporary tree-line at ~1200 masl. Above the treeline, low-alpine open shrub grassland communities dominate, including shrubs of *Coprosma* spp., *Veronica (Pseudoveronica)* spp. ('hebes'), *Dracophyllum* spp., numerous species of Asteraceae, and tussock grasses of the genus *Chionochloa*. Tall grasses and low shrubs become sparse above 1400 masl and high alpine grassland communities consist of *Chionochloa* spp., *Poa colensoi*, *Aciphilla* spp., *Ranunculus lyalii* and *Celmisia* spp.

Alluvial valleys in central Westland have been extensively modified by the felling of native tall timber podocarp-hardwoods, gold mining practices (in the 1860s), and the planting of arable crops (such as exotic grasses). Exotic *Pinus* spp. were planted as a timber resource (1920s), while *Salix* spp. was planted along riverbanks for flood protection (Molloy, 1970). The presence of *Pinus* pollen in offshore surface sediment samples, located up to ~100 km offshore, provides evidence for the rapid delivery of terrigenous material to the marine realm (Ryan et al., 2012). Overall, past changes in the altitudinal extent of these vegetation zones in central Westland are reflected in the pollen spectra in terrestrial and marine vegetation profiles (Ryan et al., 2012; Vandergoes et al., 2013a), with fluvial drainage systems capable of

transporting palynomorphs from high and low elevations to the ocean via the highly effective conduit of the Hokitika submarine canyon.

2.6 Summary

This section has highlighted the use of terrestrial palynomorphs as a paleoclimate proxy and reviewed existing palynological data from marine and terrestrial sequences over the Late Quaternary from southwestern New Zealand in order to address the aims and key themes outlined in Chapter 1. The representivity of palynomorphs in adjacent land-sea sequences (**key theme A**), and the current understanding of the source-to-sink transport time of palynomorphs and tephra from land to sea (residence time; **key theme B**) was explored in this region (section 2.1.3). Chapter 3 explores the residence time between marine-terrestrial records in this region further, with palynomorphs and tephra used as chronostratigraphic tools between land and sea records in Chapter 4 (**key theme C**). Once aligned to a common age scale, land and sea temperature estimates can compared (**key theme D**), allowing the inter-hemispheric phasing of climate events (**key theme E**), and investigation of past warmth and potential future climate in a warming world to be explored (**key theme F**; section 2.3.4). Key themes **D-F** are investigated in detail in Chapters 4 and 5 for time intervals 18-9.5 ka (MIS 2-1), ~140-98 ka (MIS 6-5c) and MIS 12-10 (~456-338 ka).

Chapter Three

3. Exploring the source-to-sink residence time of terrestrial pollen deposited offshore Westland, New Zealand

This chapter has been published in *Review of Paleobotany and Palynology*.

Abstract:

The occurrence of terrestrial palynomorphs in Quaternary marine sedimentary sequences allows for direct land– sea correlations and provides a means for transferring Marine Isotope Stage chronologies to terrestrial records that extend beyond the range of radiocarbon dating. Both of these important applications require an implicit assumption that the lag between pollen release and final deposition on the seafloor – here referred to as source-to-sink residence time – is negligible in relation to the chronological resolution of the sedimentary sequence. Most studies implicitly assume zero lag, and where studies do take palynomorph residence time into account, its magnitude is rarely quantified. In Westland, New Zealand, fluvial transport is the main source of delivery of terrestrial pollen offshore to the adjacent East Tasman Sea. We radiocarbon-dated organic matter carried and deposited by contemporary Westland rivers that drain catchments with varying degrees of disturbance. The ages obtained ranged widely from essentially modern (i.e., −57 ± 22 cal yr BP) to 3583 ± 188 cal yr BP, suggesting that precisely constraining the residence time in this region is unlikely to be achieved. We also compared the timing of four palynomorph events characterising Westland's late Pleistocene, along with the well-dated Kawakawa/Oruanui Tephra (KOT), between marine core MD06-2991 and four terrestrial records from Westland. Critically, all palynomorph events and the KOT are chronologically indistinguishable with respect to the independently dated marine and terrestrial records, supporting the general principle of transferring the marine chronology onto the terrestrial records in this setting. In other regions, particularly those lacking the high soil production and erosion rates that characterise Westland, we suggest that similar tests of marine residence time should be conducted before assumptions of zero or negligible lag are invoked.

3.1 Introduction

Terrestrial pollen and spores (palynomorphs) preserved in marine sediments add two useful attributes to the Quaternary scientist's toolkit. First, marine palynomorph records generally

provide longer, more continuous archives of vegetation change than records recovered from terrestrial sites. Second, by identifying distinct palynomorph events common to both marine and terrestrial records, there is an opportunity to transfer the well-established Marine Isotope Stage chronology to sections of terrestrial records beyond the range of ^{14}C dating. By placing marine and terrestrial paleoclimate archives on a common timescale, long-term ocean and atmosphere interactions can be investigated, offering insights into both key feedbacks and leads and lags within the climate system (Tzedakis et al., 2004; Sánchez Goñi et al., 2013).

Although records of terrestrial palynomorphs from marine sequences possess clear advantages, the methodology is not without caveats. Palynomorphs deposited offshore have a complex transport history, via soil erosion, river entrainment and ocean currents, potentially resulting in a lengthy lag before final deposition on the ocean floor (Mudie and McCarthy, 1994; McGlone, 2001; Dupont and Wyputta, 2003; Van Der Kaars and De Deckker, 2003). Taphonomic processes, which are poorly understood compared to terrestrial realm counterparts, may alter how well the relative abundance of palynomorphs in marine records represent their parent plant communities, making these records difficult to interpret in terms of vegetation change (Wilmshurst et al., 1999; Wilmshurst and McGlone, 2005). Indeed, while this uncertainty is often mentioned in the literature, the time from initial palynomorph release to final deposition within a marine sequence is assumed to be negligible. However, the validity of this assumption is rarely tested (Heusser and van de Geer, 1994; Moss et al., 2005). Long residence times would significantly undermine the key objectives of marine–terrestrial comparisons.

In light of this, we investigate the residence time (RT) for palynomorphs terrestrially derived from Westland, New Zealand (Fig. 3.1), then delivered to the adjacent Tasman Sea. RT is defined as the total source-to-sink time for a terrestrial palynomorph to travel from its source plant to its final destination on the seafloor. We build on previous work in this region that shows most of the terrestrially derived palynomorphs recovered from marine sediment cores in the East Tasman Sea have been transported by rivers draining the adjacent Westland region (Ryan et al., 2012). In this study, we explore RT in Westland by two independent methods. First, we attempt to constrain the fluvially transported component of RT through direct ^{14}C age determinations of palynomorph concentrates and organic residues sampled from contemporary Westland rivers. Second, to assess overall source-to-sink residence time, we compare the relative timing of regionally discernible and independently dated palynomorph events, and of a widespread tephra marker common to both the marine and terrestrial records. Our ultimate goal is to assess the validity of comparing marine and

terrestrial palynomorph records in the time domain at a location where excellent, high resolution examples of both exist.

3.2 Study region

Investigating RT in this region requires an appreciation of the immense productive and erosive capacities of Westland's terrestrial environment as well as an understanding of the East Tasman Sea's submarine canyon system. It is also necessary to briefly summarise Westland's regional vegetation succession previously reported from Last Glacial–Interglacial Transition (LGIT) palynological records. These records provide the basis for evaluating the timing of equivalent events seen in the marine record.

3.2.1 Terrestrial environment

Westland catchments (Fig. 3.1) are humid, tectonically active and have high relief, encouraging extremely short palynomorph residence times. Climate is temperate, with mean annual, mean monthly maximum and mean monthly minimum land surface temperatures at the coastal town of Hokitika reaching 11.7, 15.7 and 7.7°C, respectively (NIWA, 2014b). Temperature decreases with altitude at a mean rate of ~5.6°C km^{-1}, so that mean annual temperature is 4.1°C at ~1400 masl, ranging from 7.1°C (Feb) to 0°C (Jul) (NIWA, 2014a). Rainfall is influenced by the adjacent East Tasman Sea and southern mid-latitude westerly winds. The predominantly warm westerly airflow gathers moisture across the Tasman Sea and is orographically forced over the Southern Alps, producing high rainfall in coastal regions (~2900 mm yr^{-1}, Hokitika, 39 masl) (NIWA, 2014b) and extreme rainfall at altitude (11,200 mm yr^{-1}, Cropp, 902 masl) (Hicks et al., 2011). This results in numerous perennial rivers (Fig. 3.1), high catchment erosion rates (32,000 t km^{-2} yr^{-1}) (Hicks et al., 2011) and soil production and weathering rates ranking among the fastest in the world (2.5 to 12 mm yr^{-1}) (Larsen et al., 2014). In south Westland, four rivers (Arawata, Hokitika, Haast and Whataroa) each deliver ~5–7 Mt yr^{-1} of sediment onto the continental margin of the East Tasman Sea (Hicks et al., 2011).

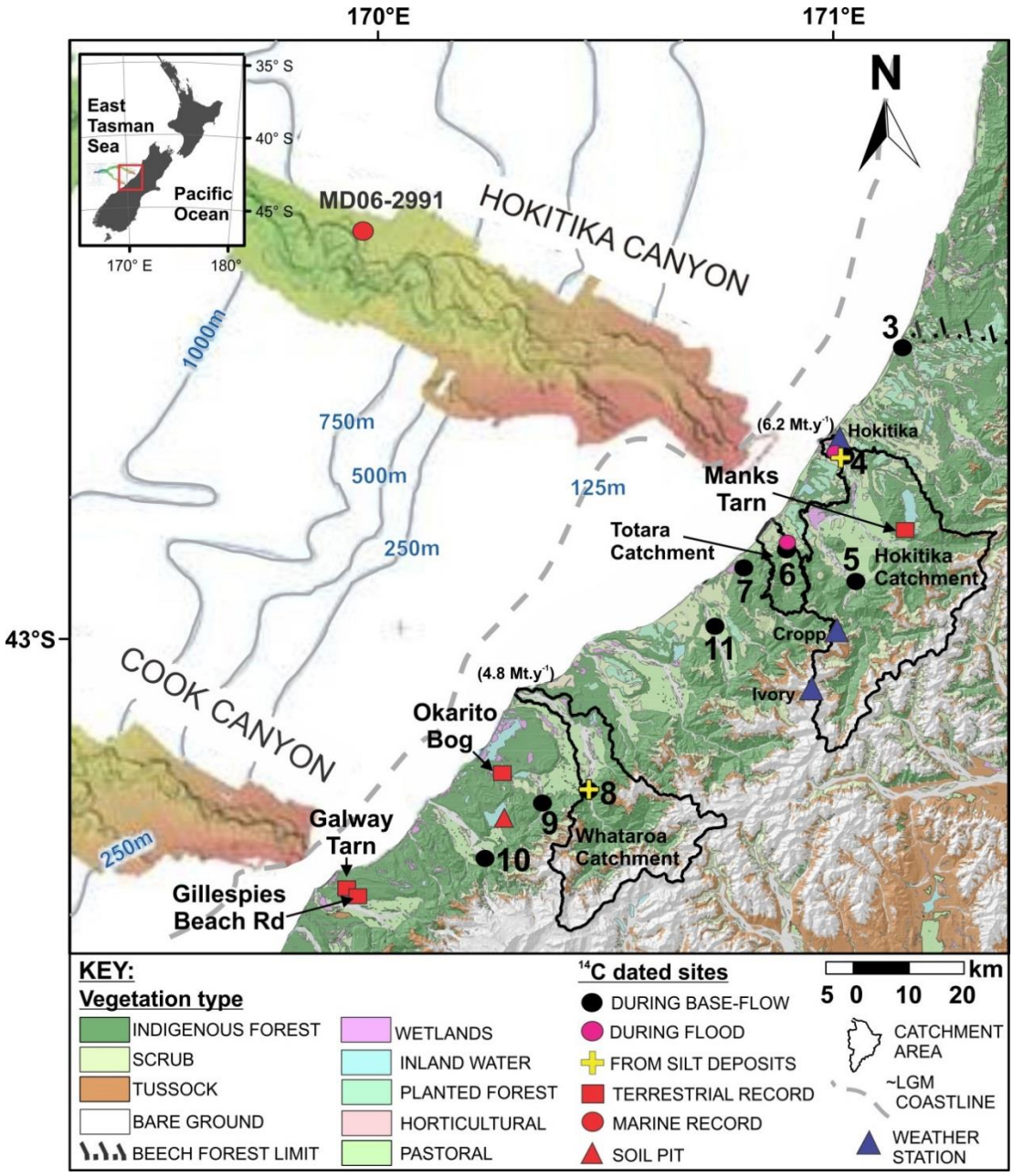

Fig. 3.1. Regional setting showing sampling sites and locations referred to in the text. Terrestrial sites include the following (from south to north): Gillespies Beach Road, Galway tarn, Okarito bog and Manks Tarn. Black circles 3 to 11 are sites sampled for ^{14}C material suspended in the river during base-flow conditions. Pink circles are locations sampled for ^{14}C material suspended during floods of the Totara and Hokitika Rivers. Yellow crosses are locations were riverbed silts were sampled for ^{14}C. Annual suspended sediment yields to the central south Westland coast are denoted at the mouths of the high sediment producing Hokitika and Whataroa Rivers (Hicks et al., 2011). The soil sample of Howarth et al. (2013), discussed in the text, is depicted as a red triangle. The digital elevation model is from Land Information New Zealand (LINZ) digital topographic contours and spot heights (Crown Copyright reserved), with bathymetric data supplied by NIWA.

3.2.2 Marine environment

The submarine canyon systems of the East Tasman Sea act as an efficient conduit for the large volumes of sediment and organic carbon that are eroded off the Southern Alps and deposited in the deep ocean (Neil, 2008; Hicks et al., 2011; Larsen et al., 2014). Prominent, highly sinuous submarine channel systems incise the relatively steep (0.3–0.5°), narrow (12–50 km) continental shelf and extend ~1600 km across the Challenger Plateau (Fig. 3.1). Down-canyon transport occurs via dense hyperpycnal underflows and rapid submarine gravity flows (Bradford-Grieve et al., 2006; Radford, 2012), with a portion of the resulting fine material accumulating on levee banks (Peakall et al., 2000; Proust et al., 2006). Sediment can also be delivered by low density hypopycnal overflows, identifiable up to 75 km offshore (Moore and Murdoch, 1993).

Terrigenous sediment is also carried northwards by longshore drift. These sediments can be diverted into the Hokitika and Cook submarine canyons at major promontories along the shoreline (Fig. 3.1) (Norris, 1978; Radford, 2012). The largest of these, a paleo-headland, referred to as the 'seaward bulge' by Norris, occurs directly south of the Hokitika submarine canyon head.

High rates of soil production and erosion, in conjunction with longshore drift and a predominantly westerly wind direction, result in palynomorphs that are deposited offshore primarily by fluvial routes (Ryan et al., 2012). However, taphonomic processes affect palynomorphs during fluvial and marine transport. In marine sediments, taxa with more robust, non-anemophilous (i.e., not wind-pollinated) palynomorphs, such as Asteraceae and *Cyathea* spp., often appear in greater relative abundance than in terrestrial depositional settings (Crouch et al., 2010; Mildenhall and Orpin, 2010; Ryan et al., 2012). Conversely, central-south Westland terrestrial records contain a wider array of palynomorphs, including some taxa that deteriorate beyond recognition during offshore transport (e.g., Newnham et al., 2013; Vandergoes et al., 2013a). These differences in pollen taphonomy between marine and terrestrial depositional settings can therefore result in selective biases that must be taken into account when direct comparisons are made between the two domains.

3.2.3 Westland's late Pleistocene palynomorph sequence

Pollen profiles generated from Westland lake sediments depict a regional vegetation succession over the LGIT. A shrubland–grassland mosaic, with patches of southern beech and rare conifers, progressed into a mix of shrubs and conifers and then finally into a landscape dominated by tall conifer trees (Moar and Suggate, 1996; Newnham et al., 2007a; Newnham et al., 2012; Vandergoes et al., 2013a). Palynologically, this sequence can be divided into four zones: (1) initially high proportions of Poaceae pollen (occasionally Asteraceae), followed by successively increasing proportions of *Coprosma* and *Myrsine* (occasionally *Halocarpus*); (2) then increasing tree ferns and the conifer species *Podocarpus/Prumnopitys*, maximum *Myrsine* and decreasing *Coprosma*, (3) followed by maximum *Podocarpus/Prumnopitys* and tree fern spores, culminating in (4) a high abundance of the tall conifer tree *Dacrydium cupressinum* and decreasing *Podocarpus/Prumnopitys*. The regional timing of these palynological zones provides the basis for marine and terrestrial comparisons.

3.3 Methods

3.3.1 Radiocarbon dating of fluvially-transported material

Organic fraction sizes

We collected a range of material for radiocarbon dating from eight Westland rivers to assess variability of the fluvially transported component (Fig. 3.1; Table 3.1). Material originated from catchments of differing size and degree of anthropogenic impact and comprised both suspended sediments from the water column and riverine silt deposits. Both sample classes were further sub-divided into three organic fraction sizes: macro-organic material (>90 μm), organic material (90 > to >45 μm) and palynomorph concentrate (45 > to >6 μm) (Table 1) following a variation on separation and concentration methodologies presented in Vandergoes and Prior (2003), Newnham et al. (2007b) and Howarth et al. (2013). This involved using HCl to remove $CaCO_3$ and KOH to remove humic acids, multiple sieving steps (90–6 μm) and organic matter concentration using pre-filtered at 1.2 μm sodium polytungstate (SPT) heavy liquid separation (2.0–1.1 s.g.). These methods were used to both isolate various fractions of organic material and exclude black carbonaceous particulate matter (potentially ^{14}C dead), which was observed in some samples. A subsample of each palynomorph and organic concentrate submitted for radiocarbon analysis was mounted on glass slides with glycerine jelly and inspected with a binocular microscope to determine contents.

Suspended sediment and silt deposit sampling

Suspended sediment samples were collected under baseline (57– 64 m^3s^{-1}) and flood (≥90th percentile of the 2003– 2013 flow regime) (NIWA, 2013) conditions between October and November, 2012. During baseline flow, a PVC pipe and socket (50 × 7 cm), fitted with a 15 μm nylon mesh, was pointed upstream to filter and collect material as water passed through. The pipe filled rapidly with water and was tilted upright to drain, then placed back in the river to refill; this process was repeated for 25 min, equivalent to filtering ~250 l of water. Some palynomorphs <15 μm were also retained on the 15 μm mesh due to clumping of the organic material. This component was added to the sample collected and subsequently filtered at 6 μm, thereby extending the lower limit of organic fractions sizes from 15 to 6 μm. Suspended sediments were also collected from the Hokitika and Totara Rivers during floods. These samples were used to evaluate whether or not organics eroded and entrained during a flood produced older ^{14}C ages than material transported during base flow. These rivers carry abundant sediment loads during floods, so organic material was able to be concentrated from just five litres of water from each river.

Riverine silt deposits were also collected from Hokitika and Whataroa Rivers, between January and February, 2008, due to concerns, subsequently confirmed, that the waterborne samples may not have sufficient material for ^{14}C dating. These deposits likely represent continuous deposition in the case of Hokitika River and a high discharge event in the case of Whataroa River. The Hokitika River silt deposit was collected between two boulders submerged during low flow, located ~1 km from the river's mouth (Fig. 3.1). These deposits have accumulated over an unknown time period. The exposed Whataroa riverbed silt situated adjacent to flowing water, was retrieved following a flood that occurred one day earlier. To limit the amount of aerially transported palynomorphs, the upper 2 cm of the Whataroa silt deposit was removed before sampling.

Table 3.1 Organic material samples collected from Westland rivers submitted for ^{14}C dating (n=14). Samples were submitted to the Rafter National Isotope Centre (GNS Science) and Australian Nuclear Science and Technology Organisation (ANSTO) for radiocarbon dating, and ^{14}C ages were calibrated with SHCal13 (Hogg et al., 2013) in OxCal v4.2.3. Organic residue represents macro-organic residue (MOR), micro-organic matter (OR) and pollen concentrate (PC), with the respective size faction and specific gravity of separation shown.

Sample	Organic residue	Fraction	Lab code	$\delta^{13}C$ (‰)	pMC ± 1σ	^{14}C age ± 1σ yr BP	Mean age ± 2σ cal. yr BP	Carbon mass (µg)
Suspended sed. base-flow	MOM	x>90 µm, x<2.0 s.g.	NZA55594	-40.3	-	1357 ± 46	1226 ± 102	100
Suspended sed. base-flow	OM/PC	90>x>6 µm, x<2.0 s.g.	NZA55590	-41.1	-	2543 ± 44	2581 ± 188	100
Whataroa silt 'flood' deposit	MOM	x>90 µm, x<1.6 s.g.	NZA55427	-27.1 ± 0.2	105.8 ± 0.24	Modern	-57 ± 22	1000
Whataroa silt 'flood' deposit	OM	90>x>45 µm, x<2.0 s.g.	NZA55592	-37.6	-	1707 ± 35	1577 ± 108	200
Whataroa silt 'flood' deposit	PC	45>x>6 µm, x<2.0 s.g.	NZA55591	-41.7	-	3384 ± 71	3583 ± 188	100
Hokitika silt deposit	MOM	x>90 µm, x<2.2 s.g.	NZA55423	-29.8 ± 0.2	105.8 ± 0.23	Modern	-57 ± 22	1000
Hokitika silt deposit	OM	90>x>45 µm, x<1.4 s.g.	NZA55424	-29.3 ± 0.2	-	658 ± 22	602 ± 54	1300
Hokitika silt deposit	PC	45>x>25 µm, 1.4>x>1.1 s.g.	NZA55425	-29.0 ± 0.2	-	822 ± 19	701 ± 32	1900
Hokitika silt deposit	PC	25>x>6 µm, 1.4>x>1.1s.g.	NZA55426	-29.9 ± 0.2	-	1091 ± 19	948 ± 34	1500
Totara River flood	MOM	x>90 µm, x<2.0 s.g.	NZA55428	-28.2 ± 0.2	104.8 ± 0.25	Modern	-33 ± 54	900
Totara River flood	OM	90>x>50 µm, x<2.2 s.g.	OZO850	-25.0*	-	540 ± 150	495 ± 270	72.9 ± 0.68
Totara River flood	PC/OM	50>x>10 µm, x<2.2 s.g.	OZO851	-28.3	-	645 ± 40	597 ± 66	47.38 ± 0.44
Hokitika River flood	MOM	x>50 µm, x< 2.0 s.g.	NZA55593	-44.5	-	933 ± 35	809 ± 66	200
Hokitika River flood	PC/OM	50>x>10 µm, x<2.2 s.g.	OZO849	-25.0*	-	3240 ± 150	3415 ± 306	150.33 ± 1.4

* An assumed $\delta^{13}C$ value due to limited sample material available for $\delta^{13}C$ determination.

3.3.2 Radiocarbon dating and numerical methods

All material for this study, including marine core MD06-2991 samples, was submitted to the Rafter National Isotope Centre (GNS Science) or Australian Nuclear Science and Technology Organisation (ANSTO) for AMS radiocarbon dating. Radiocarbon ages of terrestrial samples were calibrated in OxCal v4.2.4 (Bronk Ramsey, 2009b) using SHCal13 (Hogg et al., 2013) extended to AD 2012 by the SH Zone 1-2 data (Hua et al., 2013). A principal components analysis (PCA) of the fluvially-transported component was performed to summarise the complex relationships inherent to this data set. The PCA was run in R v3.1.2 (R-Core Team, 2014) with the FactoMineR library (Husson et al., 2013). Catchment disturbance and size, river length, carbon content, the abundance of fern spores in each sample, and sample age were all included in the ordination, scaled to unit variance. The categorical variables, namely sediment type (suspended sediment, riverine silt), flow (baseline, variable, flood), and organic fraction (palynomorph concentrate, organic material, macro-organic material) were included as supplementary variables. Note that this has been revised from that presented in Ryan et al. (2016) so that categorical variables were plotted in ordination space as supplementary data but did not affect sample score calculations.

3.3.3 Comparing the timing of key events in marine and terrestrial records

To investigate RT, we compared the timing of palynomorph events characteristic of Westland's late Pleistocene sequence, along with the deposition of the well-studied Kawakawa/Oruanui Tephra (KOT), between marine core MD06-2991 and four lake sediment records (Fig. 3.1). These lake sediment records are all proximal to the coast (1.6, 21.6 and 8.2 km = min, max and mean distance from the coast, respectively). Critically, if the timing of events overlaps in all records, within errors of the age-depth models, then RT is negligible, validating the assumption of near-contemporaneous deposition of palynomorphs at terrestrial and adjacent marine sites.

MD06-2991 radiocarbon chronology and recalibration of lake sediment records

Marine sediment core MD06-2991 was retrieved with a Calypso piston corer from the northern levee bank of the Hokitika submarine canyon system (42°21´06´´S, 169°59´59´´E, 886 mbsl) by the R.V *Marion Dufresne* (Proust et al., 2006). The late Pleistocene portion of the record encompassed the top 2.3 m of the 33 m core.

A chronology was developed from 15 AMS ^{14}C ages (Table 3.2; Fig. 3.2); dates were measured on whole mixed planktonic foraminifera tests (~10 mg of $CaCO_3$). The AMS radiocarbon ages were converted to calendar years using the Marine13 calibration curve (Reimer et al., 2013) and a regional reservoir correction (ΔR) of −24 yr (30 SD). The regional reservoir correction was estimated by averaging the ΔR of the ten closest locations to the core site from the marine reservoir correction database (http://intcal.qub.ac.uk/calib/), all of which are situated in a similar subtropical water mass. We have assumed that ΔR has remained constant over time. Although ΔR has been shown to vary over the time frame of this study in other situations (e.g., Sikes et al., 2000), we are unable to test this assumption rigorously from available data. However, we note that the age of KOT determined using our ΔR correction corresponds closely to the established age for the tephra (Fig. 3.2). Further, we point out that the relatively low temporal resolution of our records means that even potential variations in ΔR of several centuries will not impact our interpretation or conclusions. An age-depth model was generated with OxCal v4.2.4 (Bronk Ramsey, 2009a), using a P Sequence model (Bronk Ramsey, 2008) with a variable k parameter (Bronk Ramsey and Lee, 2013).

Chronologies for Okarito Bog (Vandergoes et al., 2005; Newnham et al., 2007a), Galway tarn (Vandergoes et al., 2013a, 2013b), Gillespie's Beach Rd. (Vandergoes and Fitzsimons, 2003; Turney et al., 2006) and Manks Tarn (Callard, 2011) were remodelled for this study (Suppl.

Figs. 3.1–3.4). Radiocarbon dates were recalibrated to SHCal13 (Hogg et al., 2013), and age-depth models were developed using a P_Sequence model (Bronk Ramsey, 2008) with a variable k parameter (Bronk Ramsey and Lee, 2013) in OxCal v4.2.4 (Bronk Ramsey, 2009a). The age of KOT was also remodelled using the chronological query code from Vandergoes et al. (2013b), modified to calibrate radiocarbon ages with SHCal13 (Hogg et al., 2013). The KOT was previously dated to 25,360 ± 162 cal yr BP (2σ) (Vandergoes et al., 2013b: Table S1), whereas the recalibrated age presented here is 25,590 ± 72 cal yr BP (2σ), producing a difference of 230 ± 178 cal yr BP (2σ). This recalculated KOT age was assigned to depth positions within sediment cores retrieved from Galway tarn and Okarito Bog where the KOT was present.

Table 3.2. Details of all radiocarbon age measurements from MD06-2991 presented in this study.

MD06-2991 depth (cmbsf)	Lab number	^{14}C age (yr BP)	± (1σ)	Unmodlled calibrated age (cal BP)	± (2σ)	Modelled calibrated calendar age range (cal BP)	± (2σ)
10 – 10.5	Wk-29317	1634	39	1,197	92	1,243	292
20 – 20.5	NZA-30916	3098	43	2,871	122	2,898	228
40 – 40.5	Wk-29318	4772	41	5,041	176	5,085	220
60 – 60.5	NZA-30917	7377	47	7,840	112	7,861	222
70 – 70.5	Wk-29319	8373	45	8,953	150	8,991	312
90 – 90.5	Wk-29320	10588	48	11,873	240	11,862	238
95 – 95.5	OZ-Q120	10700	47	12,106	244	12,168	384
105 – 105.5	OZ-Q122	10505	47	11,685	300	13,839	1444
110 – 110.5	WK-29321	13079	54	15,072	232	15,149	446
114 – 114.5	OZ-Q125	13880	52	16,219	200	16,272	446
120 – 120.5	OZ-Q127	15210	56	18,010	180	17,969	222
130 – 130.5	OZ-Q129	15510	65	18,356	208	18,443	382
160 – 160.5	NZA-32351	19270	103	22,730	278	22,641	578
190 – 190.5	Wk-29322	20672	69	24,337	230	24,375	298
230 – 230.5	Wk-29323	23416	101	27,337	220	27,352	228

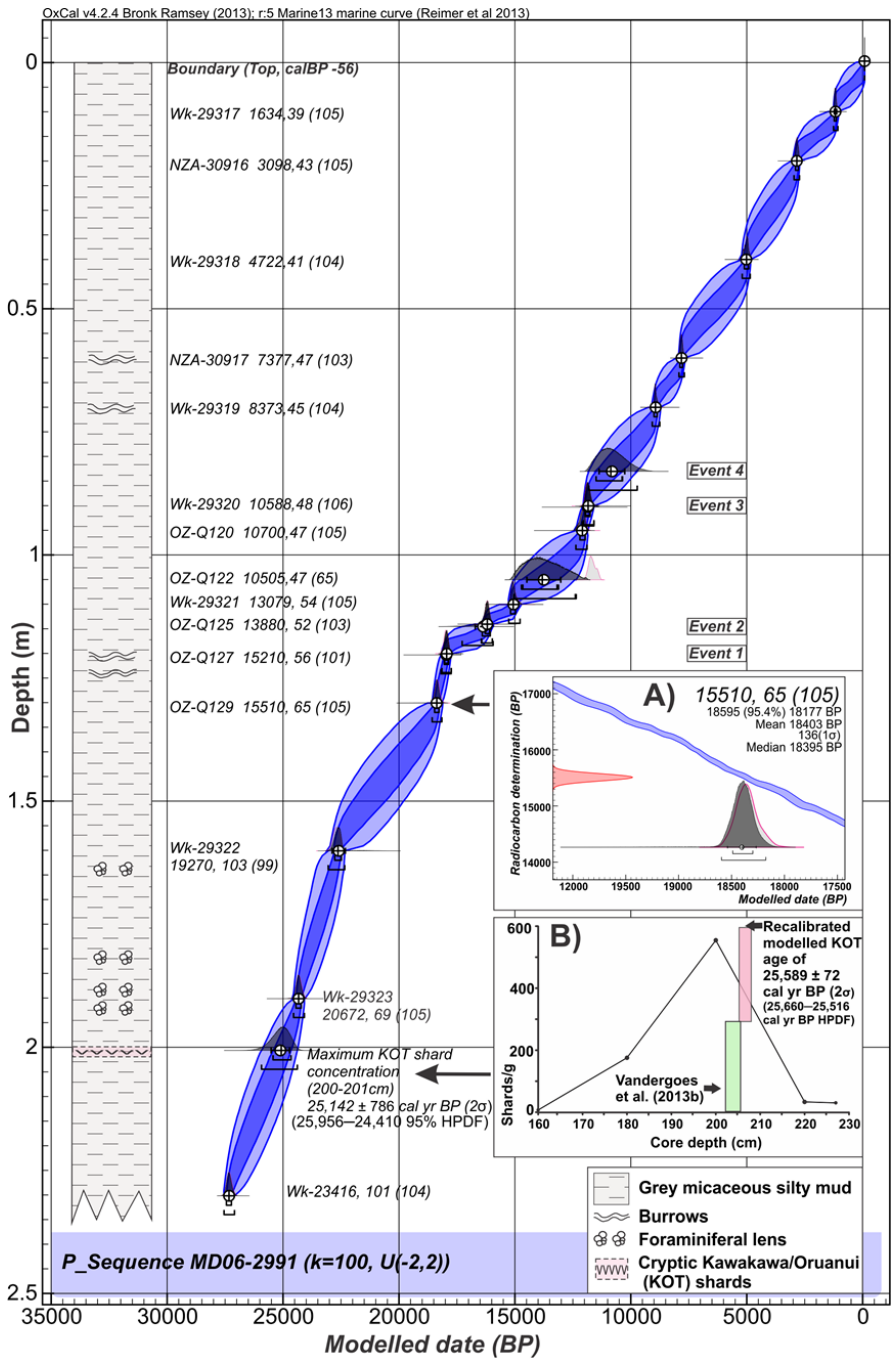

Fig. 3.2. Age-depth model and stratigraphy for MD06-2991 based on fifteen ^{14}C dates (Table 3.2). The model was produced in OxCal v4.2.4 using a P_Sequence (Bronk Ramsey, 2008), with a variable k (Bronk Ramsey and Lee, 2013); the Marine13 calibration curve (Reimer et al., 2013); and a regional reservoir correction (ΔR) of −24 yr (30 SD). The resulting model has an agreement (Amodel) of 102. The 68% (dark blue) and the 95% (light blue) confidence levels are shown. Sample agreement, in parentheses after the ^{14}C date with 1σ error; calendar age likelihoods, illustrated in dark pink (see Inset A for magnified example); and posterior probability density functions, in dark grey (see Inset A for magnified example), are shown. Inset A depicts a magnified profile, where the mean (white circle) and median (vertical line in circle) values are shown. Inset B shows the calculated maximum distribution of glass shards/g at MD06-2991 at 200.5–201 cm (25,142 ± 786 cal BP, 2σ), the recalibrated eruption age of the Kawakawa/Oruanui Ignimbrite (25,589 ± 72 cal BP, 2σ) presented here, and the original calibration (25,360 ± 160, 2σ cal BP) (Vandergoes et al., 2013b: Table S1). Regional palynomorph events 1-4 are shown

3.3.4 MD06-2991 palynology

We chose a palynomorph sampling strategy to evenly space samples in time. To accommodate sedimentation rates that varied from 6.7 cm kyr^{-1} to 11.8 cm kyr^{-1}, we collected 26 palynomorph samples at intervals ranging from 2 to 20 cm. This produced a resolution of 1.2 kyr per sample prior to 18 ka and 1.1 kyr thereafter. Palynomorphs were concentrated from 5 to 12 g of dry bulk sediment and mounted on slides following a method modified from Faegri and Iversen (1989). To determine absolute grain abundance, each sample was spiked with an exotic *Lycopodium* marker spore tablet (20,848 grains, SD 1546). Samples were digested in 10% HCl to remove CaCO3, disaggregated in hot sodium hexametaphosphate (0.5 g/L) for 30–45 min and treated with a hot 10% KOH bath (20 min) to remove humic acids. Acetolysis was undertaken (9:1 v/v solution of acetic acid and sulphuric acid) at 96°C for 5 min to remove cellulose. Organic and lithogenic materials were separated using a 2.0 specific gravity (s.g.) sodium–polytungstate heavy liquid. Floated material was washed through a 6 μm wet sieve, retaining the coarse fraction. The resulting residue was lightly stained with safranin to aid identification. Palynomorph identification was made using standard reference texts (Pocknall, 1981b, a; Large and Braggins, 1991; Moar, 1993) and the Victoria University of Wellington, New Zealand, pollen reference collection.

The relative abundance of each taxon was calculated using a total dryland pollen sum that ranged between 334 and 108 grains (mean=256). Dryland pollen were grouped according to the four categories of Vandergoes et al. (2005): podocarp-hardwoods, predominantly comprised of *Dacrydium cupressinum, Prumnopitys ferruginea, Prumnopitys taxifolia, Metrosideros* spp.; southern beech, with Nothofagaceae separated into *Fuscospora* and *Lophozonia* following Heenan and Smissen (2013); montane-subalpine trees and shrubs, including Asteraceae*, Coprosma* spp.*, Halocarpus* spp.*, Myrsine* spp.*, Phyllocladus* spp.; and herbs, primarily Poaceae. The proportions of non-dryland palynomorphs, including tree ferns (*Cyathea* spp.), ferns and fern allies, wetland and exotic pollen (*Casuarina* spp.), were calculated using the method defined by Faegri and Iversen (1989).

Four palynomorph 'events' from MD06-2991 were defined using prominent changes in the abundance, or first or last occurrence of key taxa identified in Westland's late Pleistocene terrestrial records (Suppl. Figs. 3.5–3.8). These pollen events are generally characteristic of Westland's palynostratigraphy and are documented widely in regional palynological and paleovegetation reconstructions (such as Moar, 1973, McGlone, 1995; Vandergoes and Fitzsimons, 2003; Vandergoes et al., 2013a, 2013b). To help visualise palynomorph trends, a detrended correspondence analysis (DCA), with rare taxa down weighted, was undertaken

using the vegan library (Oksanen et al., 2014) in R (R Core Team, 2014). Palynomorph profiles were also independently zoned with stratigraphically constrained cluster analysis (CONISS), using a square-root transformation performed for all dryland pollen taxa and the relative abundance of tree ferns, excluding values <2% (Grimm, 1987).

3.3.5 Kawakawa/Oruanui Tephra (KOT) at MD06-2991 and onshore correlatives

We compared the geochemical fingerprinting of cryptic volcanic glass in marine core MD06-2991 to terrestrial Westland records containing the KOT, including: Okarito Bog, Galway tarn, and other New Zealand sites (Fig. 3.3). This tephra layer provides an isochronous marker independent of the MD06-2991 radiocarbon chronology (Pillans et al., 1993; Lowe et al., 2008; Vandergoes et al., 2013b).

Glass shards from 180.5 to 181 cm below surface (cmbsf) were separated with 2.0 s.g. sodium–polytungstate. The separated fraction was wet sieved at 63 μm and glass shards in the >63 um fraction were analysed for major elements using a JEOL Superprobe (JXA-8230), housed at Victoria University of Wellington and corrected using the ZAF method. Analyses were performed using an accelerating voltage of 15 kV under a static electron beam operating at 8 nA. The electron beam was defocused to yield a spot size between 10 and 20 μm. The abundance of all elements was calculated on a water-free basis, with H_2O by difference from 100%. Total Fe was expressed as FeO_t, and all samples were normalised against glass standards ATHO-G (Jochum et al., 2000) and/or VG-568 (Jarosewich et al., 1980). The accuracy of maximum shard concentration was compared to our recalibrated terrestrial age of the KOT.

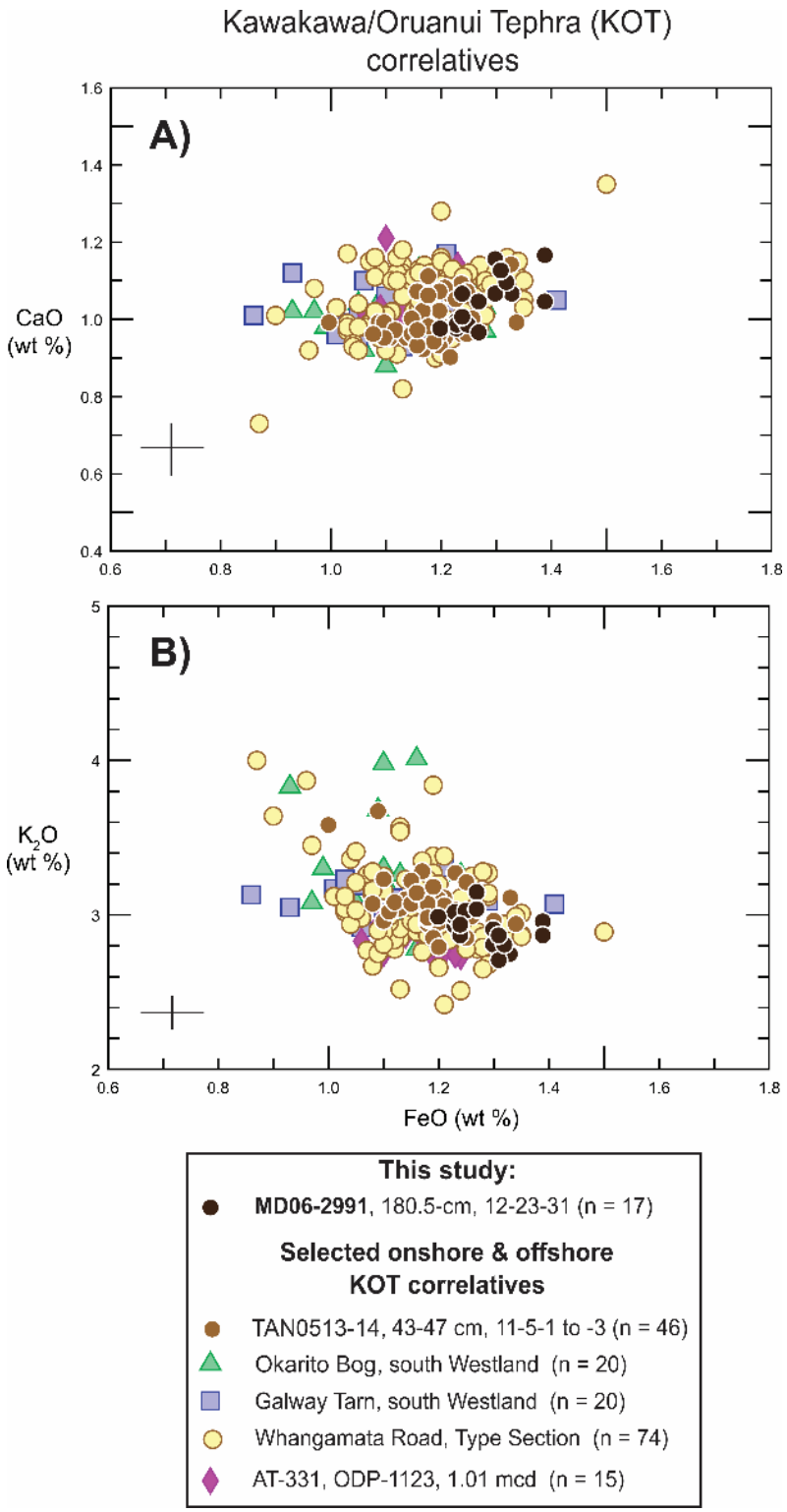

Fig. 3.3. Glass shard major element bivariate plots of a) CaO vs FeO (wt %) and b) K_2O vs FeO (wt %) from 180.5-181 cmbsf of MD06-2991 (n=17) compared to five previously published KOT analyses (using the same electron microprobe and under the same analytical conditions and standards). Crosses represent the 2σ error on individual analyses. The mean major element compositions, analyst and/or sources of analyses are given in Supplementary Table 3.1.

3.4 Results

3.4.1 Radiocarbon dating of fluvially-transported material

The ages of pollen samples collected from suspended and deposited sediment in modern rivers range from instantaneous (-57 ± 22 cal yr BP) to 3583 ± 188 cal yr BP (Table 3.1). Unfortunately, base flow suspended sediment sampling of individual rivers did not yield enough material to radiocarbon date, so the base flow samples from all rivers were amalgamated before submission. As these amalgamated samples were of mixed origins, they were excluded from the PCA. The first two axes of the PCA together explain 71% of the variance in the modern radiocarbon data set (Fig. 3.4). Principal component (PC) 1, explaining 46% of the variance, is positively associated with catchment size, river length and amount of carbon combusted. PC2, explaining 25% of the variance, is positively related to age of the sample and fern spore content. Smaller organic fractions (i.e., pollen concentrates) are associated with older ages.

3.4.2 Comparing the timing of key events in marine and terrestrial records

The upper 2.3 m of MD06-2991 consists of greenish-grey, foraminifera-rich muds, with iron staining in the uppermost 8 cm. One radiocarbon date, at 105-105.5 mbsf, is identified as an outlier (Table 3.2). However, weighting that date as an outlier produced an acceptable agreement of 65% and an overall agreement index for the model (A_{model}) of 102%. The resulting age-depth model possesses a fairly uniform sedimentation rate, despite a slowdown after roughly 18 cal kyr BP (Fig. 3.2).

MD06-2991 preserves a Westland palynomorph succession with salient features clearly recognisable from nearby terrestrial sites (Fig. 3.5). The Last Glacial Coldest Period (Newnham et al., 2007c) is characterised by the highest percentages of Poaceae and herbs for the entire record (>50%), and abundant *Coprosma* and Asteraceae. The base of the first palynomorph zone, characterised by maximum *Coprosma*, high abundances of Poaceae and herbs, and increasing *Myrsine*, occurs between 18.2 and 17.7 cal kyr BP. The base of the second zone, characterised by increasing podocarp-hardwoods, maximum *Myrsine* and decreasing *Coprosma*, occurs between 17.3 and 16 cal kyr BP. Maximum *Podocarpus/Prumnopitys* and tree fern spores appear around 12.1 to11.6 cal kyr BP, the third zone. Finally, the fourth zone, denoted by increasing *Dacrydium cupressinum* and decreasing *Podocarpus/Prumnopitys*, occurs between 11.9 and 9.8 cal kyr BP. Critically, the palynomorph events of MD06-2991 coincide with the 95% confidence limit of the same, independently dated events for the four lake sediment records (Fig. 3.6): Okarito Bog, Galway tarn,

Gillespie's Beach Rd and Manks Tarn (see Suppl. Fig. 3.5−3.8 for respective palynostratigraphies).

The maximum density of volcanic glass shards at MD06-2991 appears at 200.5-201 cm, corresponding to 25,140 ± 786 cal yr BP (2σ) based on the age-depth model (Fig. 3.2, Inset B). The recalibrated eruption age for the KOT is 25,589 ± 72 cal yr BP (2σ), which is statistically indistinguishable within error, from the independently calculated age for maximum KOT glass shard concentration at MD06-2991.

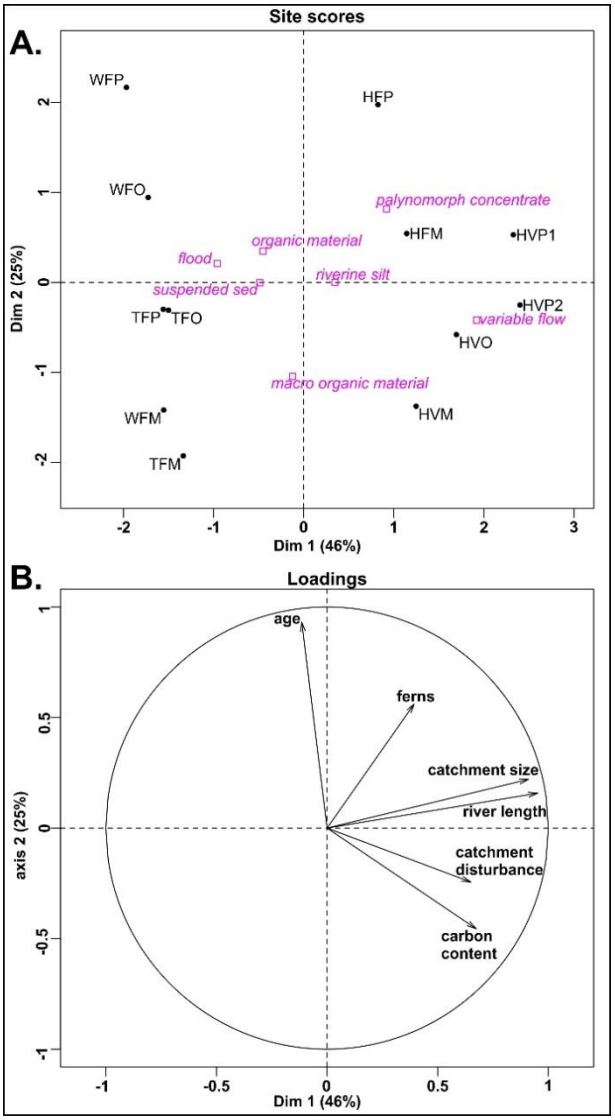

Fig. 3.4. Principal components analysis of fluvially-transported radiocarbon data set (Table 3.1) including plots of (a) site scores (black) with supplementary categorical data (pink) and (b) loadings. PC1 reflects the diversity of sampled material, while PC2 represents sample ages. Letters represent river (H=Hokitika, T=Totara, W=Whataroa), flow (V=varied, F=Flood), and organic fraction size (M=macro-organic material, O=organic material, P=pollen concentrate).

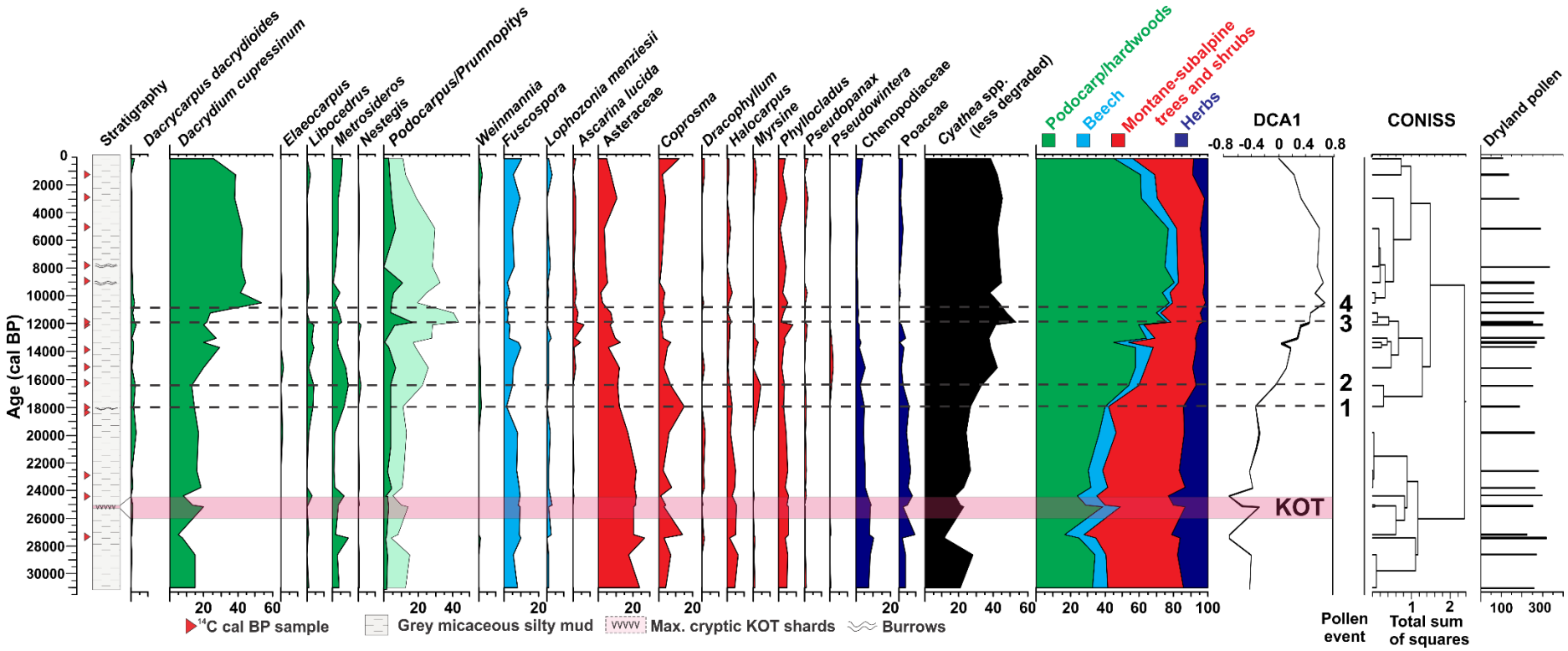

Fig. 3.5. Summary pollen percentage diagram for MD06-2991 and location of key palynomorph events since 30 cal kyr BP. The core stratigraphy and location of the calibrated AMS ^{14}C ages (red triangles) are shown on the left. The relative percentages of the main dryland pollen taxa are shown from left to right and are grouped into a cumulative dryland pollen diagram, which includes podocarp-hardwoods, beech, montane-subalpine trees and shrubs, and herbs. *Podocarpus* (green) and *Prumnopitys* (light green) are displayed grouped, although their respective relative percentages are differentiated by colour and a black line. The proportion of non-degraded *Cyathea* fern spores was calculated following Faegri and Iversen (1989), while the results of DCA axis 1 and the CONISS zonation are presented on the far right. The position of the Kawakawa/Oruanui Tephra (KOT) is shown.

3.5 Discussion

In this study, we set out to investigate RT, the time taken for a terrestrial palynomorph to be transported from its source plant to its final destination on the east Tasman seafloor. Evaluating this potential lag is crucial, where palynostratigraphies from marine archives are either compared to terrestrial counterparts or used to transfer marine chronologies to land-based proxies (e.g., Moss et al., 2007; Ryan et al., 2012). In the Westland region, the most important component of RT is likely to be fluvial transport to the marine environment. Traditional Quaternary techniques permit an approximation of this component, by radiocarbon dating material entrained by rivers, and of RT overall, by comparing the timing of stratigraphic events from lakes near the ocean to those same events archived in a marine core.

3.5.1 Radiocarbon dating of fluvially-transported component

In the PCA results (Fig. 3.4), PC1 reflects our diverse sampling regime – disturbed and undisturbed catchments, long and short river lengths, variable and high flow rates, and samples with differing amounts of carbon. However, PC2 provides insight with respect to varying residence time. Older samples (>0 on PC2) tend to consist of smaller size organic fractions (pollen concentrates and organic material), and samples with high fern spore abundance.

Previous studies highlight the comparatively high concentrations of robust tree fern spores, relative to dryland pollen taxa, in reworked sediments, for instance during glacial retreat (Newnham et al., 2007a) and by fluvial-driven erosion of catchment soils (Dunbar et al., 1997; Wilmshurst et al., 1999). Recent radiocarbon dating from soil profiles in Westland by Howarth et al. (2013) shows that fern spores are preferentially preserved relative to dryland pollen taxa and samples dominated by fern spores may produce ages significantly older than other material from the same horizon. Black carbonaceous particulate matter (potentially ^{14}C dead) found in some samples in the current study when inspected with the binocular microscope are another source of older carbon (Suppl. Fig. 3.9). The broad range of ages determined from the riverine samples are likely to reflect these sources of older carbon, reworked into the riverine sediments in the modern anthropogenically disturbed Westland environment and possibly accentuated by the small sample size (Table 3.1). The results of this part of the study therefore are inconclusive in terms of constraining the fluvial delivery

component of RT in Westland. Clearly some river-borne sediment is delivered to the coast in the modern setting with negligible lag, but not all.

3.5.2 Comparing the timing of key events in marine and terrestrial records

There is clear synchronicity between MD06-2991 and comparable terrestrial records, with respect to the four palynomorph events and KOT (Fig. 3.6). Considering three of the four terrestrial sites are small and lack significant tributaries, the spatially diverse, although temporally indistinguishable signals, are convincing evidence that the RT is negligible for Westland. This synchronicity persists throughout both the Last Glacial Coldest Period (Alloway et al., 2007a), when deposition rates of terrigenous material on the levees of the Hokitika and Haast canyons were almost double (Radford, 2012; Nelson et al., 2013) and the LGIT. During this latter period, global sea level rose from 120 to 95 m below present (Carter et al., 1986; Rohling et al., 2009), corresponding to a shoreline migration ~10 km landwards on gentler slopes (Radford, 2012). At the same time, regional climate also warmed substantially to interglacial values, causing glaciers to shrink and allowing vegetation to recolonise the region. Despite major environmental changes, RT remained negligible.

It is important to note that the palynomorph events used to compare marine and terrestrial records are based on trends rather than magnitude. While these marine and terrestrial records are similar, they also possess distinct differences related to taphonomic processes. For instance, terrestrial sites record higher relative abundances of anemophilous Poaceae pollen, which are less durable than other palynomorphs and degrade during fluvial and marine transport. Conversely, comparatively high abundances of entomophilous palynomorphs, like Asteraceae pollen, are recorded in marine sediments, which is attributed to the robustness of the pollen grain. Furthermore, Events 3 and 4 are reversed at Gillespie's Beach Rd. (Fig. 3.6, Supplementary Fig. 3.7). Gillespie's Beach Rd. possesses poor drainage conditions due to its location within sloping LGCP recessional moraines (Vandergoes and Fitzsimons, 2003; Turney et al., 2006). Consequently, the appearance of *D. cupressinum* before *Podocarpus/Prumnopitys* most likely reflects a local signal, as *D. cupressinum* can better tolerate boggy substrates (Norton et al., 1988).

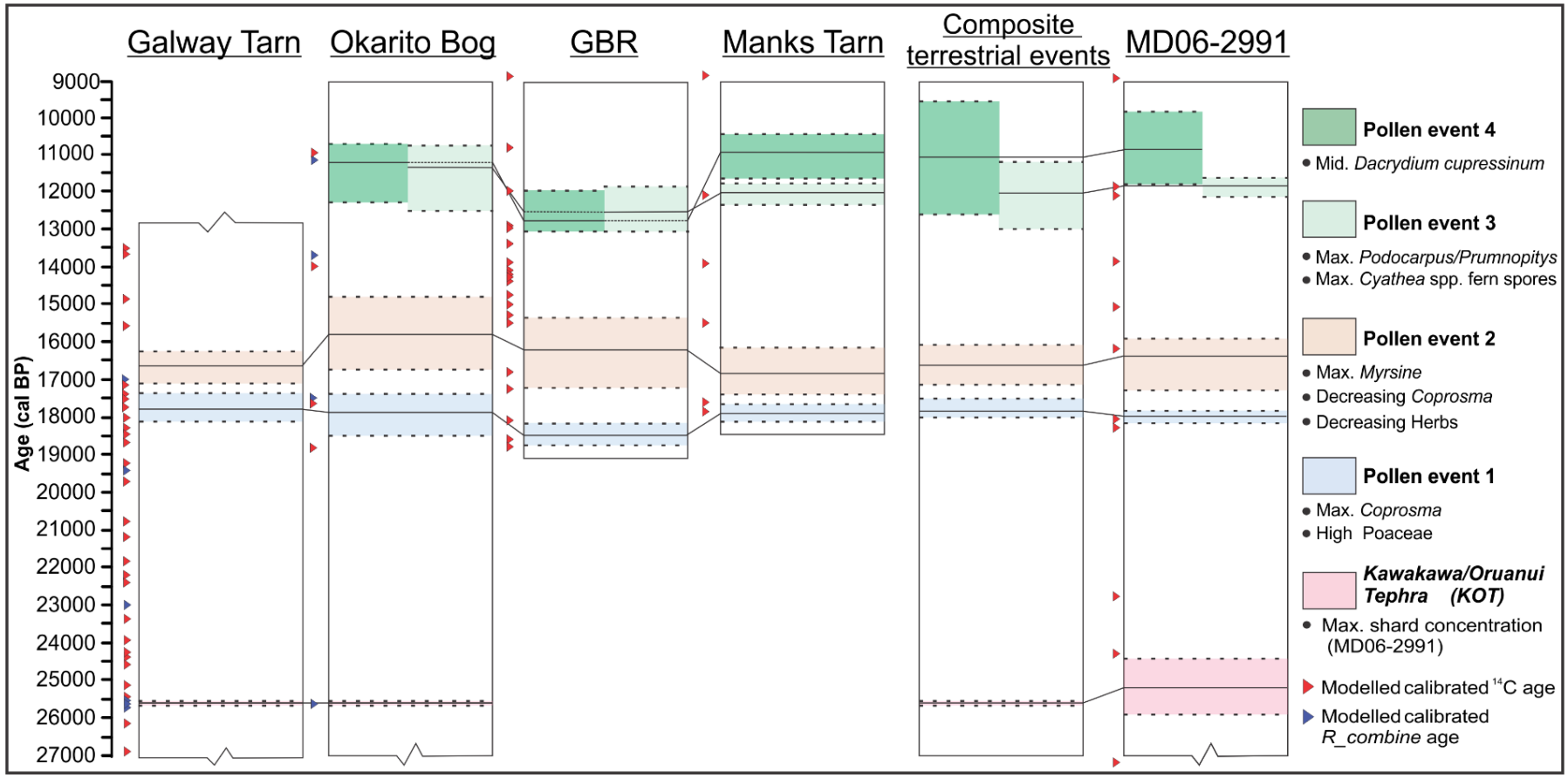

Fig. 3.6: Calibrated calendar year ages (black line) and error range (2σ, dashed line) of the KOT and four palynomorph events at MD06-2991 and their correlatives in Westland terrestrial records. Mean calibrated ^{14}C ages (red triangles) and *R_combine* ages (blue triangles) are shown next to each record. The weighted mean age and error of each palynomorph event in the terrestrial records are combined to produce a composite stratigraphy next to MD06-2991. Note, palynomorph event 4 for Gillespie's Beach Rd (GBR) was not included in the composite.

3.5.3 The Kawakawa/Oruanui Tephra

The KOT, which erupted from the central North Island of New Zealand over a short duration of weeks to months, provides an independent chronological link between marine and terrestrial sequences (Pillans et al., 1993; Carter et al., 1995; Wilson, 2001; Manville and Wilson, 2004; Vandergoes et al., 2013b). The delivery of the KOT to MD06-2991 likely followed similar pathways as terrestrial palynomorphs. After airborne deposition, the tephra would have been eroded off the adjacent landscape and delivered to the ocean via the paleo Hokitika, Totara and Waitaha Rivers (Norris, 1978). The age of deposition at Okarito Bog and Galway tarn, where it is clearly an airfall deposit is statistically indistinguishable from the independently dated horizon of highest shard concentration in MD06-2991. This provides further evidence that RT is less than the resolving power of our sedimentary records (i.e., a few hundred years), supporting both the comparison of marine and terrestrial palynomorph records and the transfer of marine chronologies to adjacent terrestrial settings.

3.6 Conclusions

We attempted to constrain RT, namely, the source-to-sink residence time for terrestrial palynomorphs to reach the ocean floor in Westland, New Zealand. By radiocarbon dating fluvially transported material, a critical component of RT, we determined that component ranged from being nearly instantaneous to lagging 3583 ± 188 cal yr BP in this anthropogenic setting, characterised by high rates of erosion. On the other hand, the synchronicity between MD06-2991 and four Westland archives, with respect to deposition of the KOT and regional palynomorph events, indicates that RT overall is negligible for Westland. We conclude that (1) terrestrial palynomorphs, deposited alongside marine proxies at MD06-2991, enable direct ocean-land comparisons to be confidently made, even over periods of major environmental change, and (2) the terrestrial palynomorph record of MD06-2991 can be used to transfer its independently derived $\delta^{18}O$ chronology to terrestrial sequences in Westland, beyond the period datable by radiocarbon, by alignment of palynomorph events common to both records. Nevertheless, radiocarbon ages of up to 3.5 ka for recent fluvially transported material in disturbed catchments provide a warning that RT in some settings has the potential to be much greater and we suggest that similar tests of terrestrial–marine RT should be conducted before assumptions of zero or negligible lag are invoked.

3.7 Contributions

MTR Writing and ideas of the early draft of this chapter. All figures and supplementary information. Collection of modern grab samples and processing of all ^{14}C samples of modern material. Identification and extraction of KOT glass shards at MD06-2991. Pollen processing and analysis for MD06-2991. CONISS analysis. Joint contribution of OxCal modelling of all sequences with A.B.R. Calibration of all ^{14}C dates.

All additional work provided by other parties for this chapter, with authors listed in order of appearance in *Reviews of Palaeobotany and Palynology* manuscript.

RMN Project guidance, intellectual input and written material to published manuscript.

GBD Project guidance, collection of spring samples from West Coast rivers, and intellectual input and written material to published manuscript.

MJV Project guidance, pollen analysis and ^{14}C sampling and dating for Gillespies Beach Rd, Galway Tarn and Okarito Bog.

ABHR Project guidance. Variance of ^{14}C ages for modern samples using the program R. Guidance and deposition modelling in OxCal for all sequences (50% contribution). Intellectual input and written material to published manuscript.

HLN Collection of foraminifera for ^{14}C chronology for MD06-2991. Sampling guidance.

LSC Pollen processing, pollen analysis and pollen concentrate ^{14}C dating for unpublished Manks Tarn record.

BVA Preparation and analysis of EMP mounts as well as acquisition and processing of major element compositional data of KOT glass shards from MD06-2991. Preparation of Fig. 3.3 and Supplementary Table 3.1.

HB Collection of foraminifera for ^{14}C chronology for MD06-2991. Sampling guidance.

QH Radiocarbon analysis of modern riverine samples (n=3) and MD06-2991 samples (n=5).

BA Collection of flood samples for modern ^{14}C samples.

Further contribution from:

EGCS Provided guidance and the equation in calculating the mean weighted age and uncertainty for the composite Westland terrestrial event stratigraphy.

GNS and **ANSTO staff** ^{14}C dating of target material.

Chapter Four

4. Ocean and atmospheric interactions from south-west New Zealand over the last two terminations and interglacials

Abstract:

The timing, magnitude and sequence of environmental changes associated with the last two terminations (T-I and T-II) in the Southern Hemisphere (SH) mid-latitudes are investigated here. Reconstructions of vegetation using terrestrial palynomorphs (pollen and spores), and sea-surface temperatures (SST) based on foraminifera, were undertaken on marine piston core MD06-2991 (42°21'06"S, 169°59'59"E), taken from west of New Zealand's South Island. Glacial to interglacial (G-I) changes in vegetation as reconstructed from terrestrial palynomorphs are marked by a change from dominantly shrubland-grassland to dominantly podocarp-broadleaf forest taxa. Vegetation changes are shown to be predominantly coupled with variations in SST, with the climate inferences developed from them displaying an asynchronous pattern to Northern Hemisphere (NH) counterparts. Similar variability is observed in regionally-dispersed palynomorphs in the nearby terrestrial Okarito Bog record. Mean annual air temperatures (MAATs) reconstructed from the Okarito pollen record are typically aligned with SST reconstructed at MD06-2991 over the last two G-I cycles. However, an apparent "decoupling" of land-sea temperatures occurs at the culmination of T-I and T-II, presumably resulting from regional climate factors such as seasonal variability, frost, and topographic factors such as ice cover. The two reconstructions of paleovegetation over T-I and T-II from western South Island (Westland), New Zealand display a similar structure despite different amplitudes of external forcing. The onset of the T-II climate amelioration occurs at ~139 ka, with cool but warming conditions as temperatures declined in the NH during Heinrich Stadial 11. Rapid warming prior to the culmination of T-II occurs between ~133-130 ka, and precedes NH counterparts by 2-3 ka. Land-sea temperatures decline in Westland from ~130-128 ka and are attributed to the northward migration of ocean-atmosphere heat transport at the onset of rapid NH warming. The MIS 5e climatic optimum in Westland was between ~127-123 ka, with maxima in reconstructed ocean-atmosphere temperatures of 2.5°C and 1.5°C higher than present.

4.1 Introduction

For the last half-million years, Earth's climate has oscillated between glacial and interglacial (G-I) conditions (Imbrie et al., 1992; 1993; Berger and Jansen, 1994). Long periods of gradual cooling (~70-90 kyr) are followed by abrupt warming (~10 kyr) known as terminations (Broecker and van Donk, 1970). These cycles are linked to Milankovitch orbital frequencies (Tziperman et al., 2006; Raymo and Huybers, 2008). The relationship between orbital forcing and terminations is poorly understood. The contribution of eccentricity to insolation is too small to drive terminations directly (Imbrie et al., 1993; Paillard, 1998; Schultz and Zeebe, 2006; Cheng et al 2009). Furthermore, rising insolation alone is considered to be insufficient to explain terminations as well as they have occurred during times of both low and high amplitude Northern Hemisphere (NH) summer insolation (Denton et al., 2010; Schaefer et al., 2015). What is observable is that late Pleistocene terminations coincide with the near-maxima of every second or third obliquity cycle (Huybers, 2004; Huybers and Wunsch, 2005; Huybers, 2007). These obliquity cycles, plus alignment of perihelion with precession (when the earth is closest to the sun), have been shown to force glacial cyclicity in the late Pleistocene (Raymo et al., 2006; Raymo and Huybers, 2008; Huybers, 2011).

A "fly in the ointment" of Milankovitch theory is that Southern Hemisphere (SH) paleoclimate records display a covariant warming and cooling pattern with NH summer insolation intensity over glacial-interglacial G-I cycles, despite antiphasing intensity of summer insolation between the hemispheres (Broecker and Denton, 1990; Denton et al., 1999; Berger, 1999; Broecker, 2000; Barrows et al., 2007a; Ryan et al., 2012; Doughty et al., 2015). The essential element of a glacial termination, according to Denton et al. (2010), is very large NH ice sheets with marine based components. These ice sheets containing "excess ice" would have been vulnerable to unstable collapse due to the weak but increasing boreal summer isolation at the onset of each of the last five glacial terminations (Raymo, 1997; Denton and Hughes, 1981; Cheng et al., 2009; Denton et al., 2010; Abe-Ouchi et al., 2013). The increased flux of ice and meltwater from such a collapse could have been significant enough to slow down the Atlantic meridional overturning current (AMOC), cooling the NH and conserving heat in the SH (Broecker et al., 1985; Crowley, 1992; Broecker, 1998; Stocker, 2000).

A reduced Atlantic meridional overturning current and increased sea ice from longer winters caused NH cooling (Margari et al., 2014; Martrat et al., 2014), termed Heinrich stadials (HS), and are characterised by influxes of ice-rafted debris (IRD) in the last five terminations

(McManus et al., 1999; Oppo et al., 1998; 2006; Barker et al., 2015). During terminations, there is an increased upwelling of CO_2-rich water in the Southern Ocean (Ahn and Brook, 2008; Parrenin et al., 2013; Bostock et al., 2013), which leads global ice volume by several millennia (Shackleton, 2000). While Antarctic ice cores suggest a small apparent lead of Antarctic temperature warming over increasing atmospheric CO_2 by 0-400 years between the LGM to Holocene (Pedro et al., 2012), the large increase in global average SSTs which lag CO_2 by up to 800 years suggests carbon cycle feedbacks are amplifiers in climatic change by facilitating global temperature rise (Shakun et al., 2012). Two mechanisms are proposed to explain this outgassing of CO_2. First, a southward shift of the Southern Hemisphere Westerly Winds (SHWW) caused by a southward shift of the Intertropical Convergence Zone (ITCZ; Fig. 4.1), in turn caused by the aforementioned decrease in the Atlantic meridional overturning current (Toggweiler, 2009; Anderson et al., 2009; Barker et al., 2009; Bostock et al., 2013). Second, an expanded Antarctic ice sheet could have stopped the formation of brine on the Antarctic margin, and thus the formation of sea ice, resulting in the initial CO_2 outgassing (Bouttes et al., 2010; He et al., 2013)

Antarctic ice core records suggest that SH CO_2 outgassing lagged NH insolation by millennia during each of the last four terminations (Kawamura et al., 2007). Despite this lag, the outgassing was apparently of sufficient magnitude to synchronise the climate system of both hemispheres, and achieve interglacial conditions (Cheng et al., 2009). Under this scenario, the regular reoccurrence of glacial terminations should be accompanied by similar spatiotemporal patterns of climate change. An alternate explanation of the CO_2 increase is that SH insolation triggered the initial rise, synchronising global climate over orbital timescales (Vandergoes et al., 2005; Huybers and Denton, 2008; Timmermann et al., 2009). If correct, this implies that SH summer insolation, which leads that of the NH, plays a direct role in initiation of glacial terminations (Schulz and Zeebe, 2006). While 'regional' southern drivers of climate over G-I cycles may occur (Wolff et al., 2006; Wolff et al., 2009; WAIS Divide Project Members, 2013; Fogwill et al., 2015), the precise mechanisms can be difficult to discriminate as they show similar patterns of change (Huybers, 2009). For example, the transmittance of heat from the north, following increasing NH summer intensity and long stadials, may be amplified in high southern latitudes which at the same time experience an orbitally induced lengthening of summers and shortening of winters (Huybers and Denton, 2008; Denton et al., 2010; Huybers, 2011).

Superimposed on these cycles at Milankovitch orbital frequencies are millennial frequency oscillations in climate considered to be produced by factors internal to the Earth's atmosphere and ocean system (Alley et al., 1999; Knutti et al., 2002; Chiang et al., 2014), and antiphased between hemispheres (Bender et al., 1994; Broecker, 2000; WAIS Divide Project Members, 2015), with the actual boundary of each hemispheres influence lying at about the latitude of New Zealand (Pahnke and Zahn, 2005; Carter et al., 2008). Abrupt warming's in Greenland are shown to lead Antarctic cooling by ~200 years, with oscillations in climate more subdued in southern records (EPICA Community Members, 2006; WAIS Divide Project Members, 2015). The interplay of insolation cycles with internal climate system feedbacks which can be rapid (i.e., sea ice, CO_2 feedbacks, atmospheric water vapour, vegetation cover, ocean surface temperatures, ocean circulation) and sluggish (i.e., ice sheet extent and thickness, sea level) have profoundly influenced the climate system in both hemispheres (Clark et al., 1999; Broecker, 2000).

The last interglacial (LIG; here defined between ~130-116 ka) has been shown to have atmospheric CO_2 levels similar to pre-industrial levels of the present interglacial (Luthi et al., 2008; Schneider et al., 2013), but within a different orbital configuration (Tzedakis et al., 2004; Yin and Berger, 2012). Temperatures were at least ~5°C above present at the poles (Jouzel et al., 2007; Sime et al., 2009; Rasmussen et al., 2013), and there is evidence for reduced ice in Greenland and Antarctica (Dutton and Lambeck, 2012; Rasmussen et al., 2013; Dutton et al., 2015a; Steig et al., 2015), with sea level on average 6-9 m higher (Masson-Delmotte et al., 2013; repeated by Dutton et al., 2015a). These deviations from the present interglacial suggest that interglacials can be highly variable in character with sub-millennial to millennial scale climate oscillations during warmer-than-present times (Müller et al., 2005; Masson-Delmotte et al., 2010; Koutsodendris et al., 2011; Pol et al., 2011; Wanner et al., 2011; Galaasen et al., 2014; Pol et al., 2014).

This chapter asks the following questions:

1- What is the sequence of vegetation changes and associated climate events during terminations T-I and T-II and subsequent interglacials from southwestern New Zealand?
2- How do the timing and magnitude of climate events in T-I and T-II relate to climate forcing, and how do they compare with existing observations and models of terminations?

3- What was the climate like in southwestern New Zealand during the LIG? How do the local paleoclimate data fit with global observations and paleoclimate simulations?

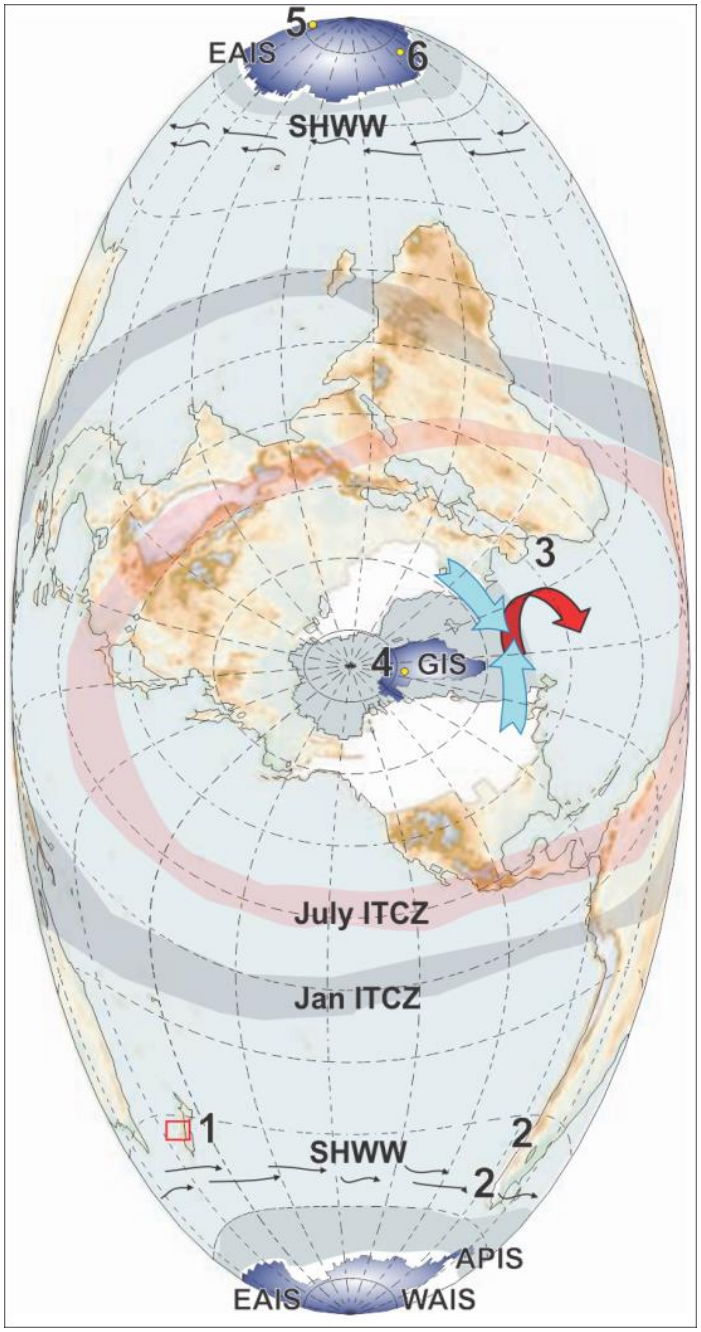

Fig. 4.1: Location of key sites referred to in text; the primary study region **1.** New Zealand (NZ) with study region highlighted by a red box, **2.** South America/Patagonia; **3.** Iberian Margin; Ice cores from **4.** North Greenland Eemian Ice Drilling (NEEM); **5.** EPICA (European Project for Ice Coring in Antarctica) Dome C (EDC); **6.** EPICA Dronning-Maudland (EDML). Map revised from Clark et al. (2009); with the general region of deepwater formation in the North Atlantic Ocean (red arrow), and the supply of freshwater and icebergs and IRD shown (blue arrows) from Denton et al. (2010). On the Southern Ocean, grey shading indicates maximum extent of winter sea ice. Two ice sheets (in blue) survived the last termination; one is in Greenland (GIS), the other in Antarctica which is divided into three components (EAIS, WAIS and APIS). These ice sheets are determined vulnerable to projected rising temperature and were reduced during the last interglacial (LIG; Dutton et al., 2015a). The location of the Intertropical Convergence Zone (ITCZ; Jan and July) and Southern Hemisphere westerly wind (SHWW) belt is displayed.

Investigating these questions involves utilising the strengths of both terrestrial and marine palynomorph records to overcome their respective shortcomings. Terrestrial records can faithfully capture the vegetation-climate signal although such records are often fragmentary in nature and poorly dated beyond the range of ^{14}C dating. Marine records can be well dated, and typically offer greater length and continuity than their terrestrial counterparts, although they are influenced by pollen taphonomy affecting quantitative climate reconstructions. Reconstructions of ocean-atmosphere from marine and terrestrial paleoclimate data from marine core MD06-2991 (42°21´06´´S, 169°59´59´´E, 886 mbsl, ~8.5 cm/kyr), retrieved west of the strongly maritime influenced South Island, New Zealand (Fig. 4.2) assess the termination paradigm of Denton et al. (2010) for the last two glacials.

Considerable effort has gone into producing the best constrained age model possible for MD06-2991 and the adjacent Okarito bog pollen record for the period preceding the ^{14}C-dated interval. The chronology is based on carefully quantifying the uncertainty associated with matching the $\delta^{18}O$ stratigraphy of MD06-2991 to the LR04 $\delta^{18}O$ reference stack (Lisiecki and Raymo, 2005), uncertainties in the reference stack itself (Caballero-Gill et al., 2012a), and in the correlation of palynomorph events between the MD06-2991 and Okarito records. This also builds on the observation that time lags between pollen production and delivery to the sea are negligible for the last deglaciation and the Holocene, and are less than is detectable given other age model uncertainties (Chapter 3). The resulting combined marine/terrestrial record for the last two G-I cycles for southwestern New Zealand permits a more detailed examination of the postulated mechanisms influencing the record than has been hitherto achieved (Vandergoes et al., 2005; Newnham et al., 2007a; Ryan et al., 2012). Specifically, this includes the penultimate deglaciation where a similar vegetation succession is shown to that which occurs over the LGIT (Newnham et al., 2007a), and the last interglacial, where a strong thermal maximum was not detected in the Okarito record at a low-resolution. The new data also provides an opportunity to examine in detail the phase relationship between changing local and global climate drivers and insight into their interaction (e.g., Allen et al., 1999; Tzedakis et al., 2004; Newnham et al., 2012; Sánchez Goñi et al., 2013; Govin et al., 2015).

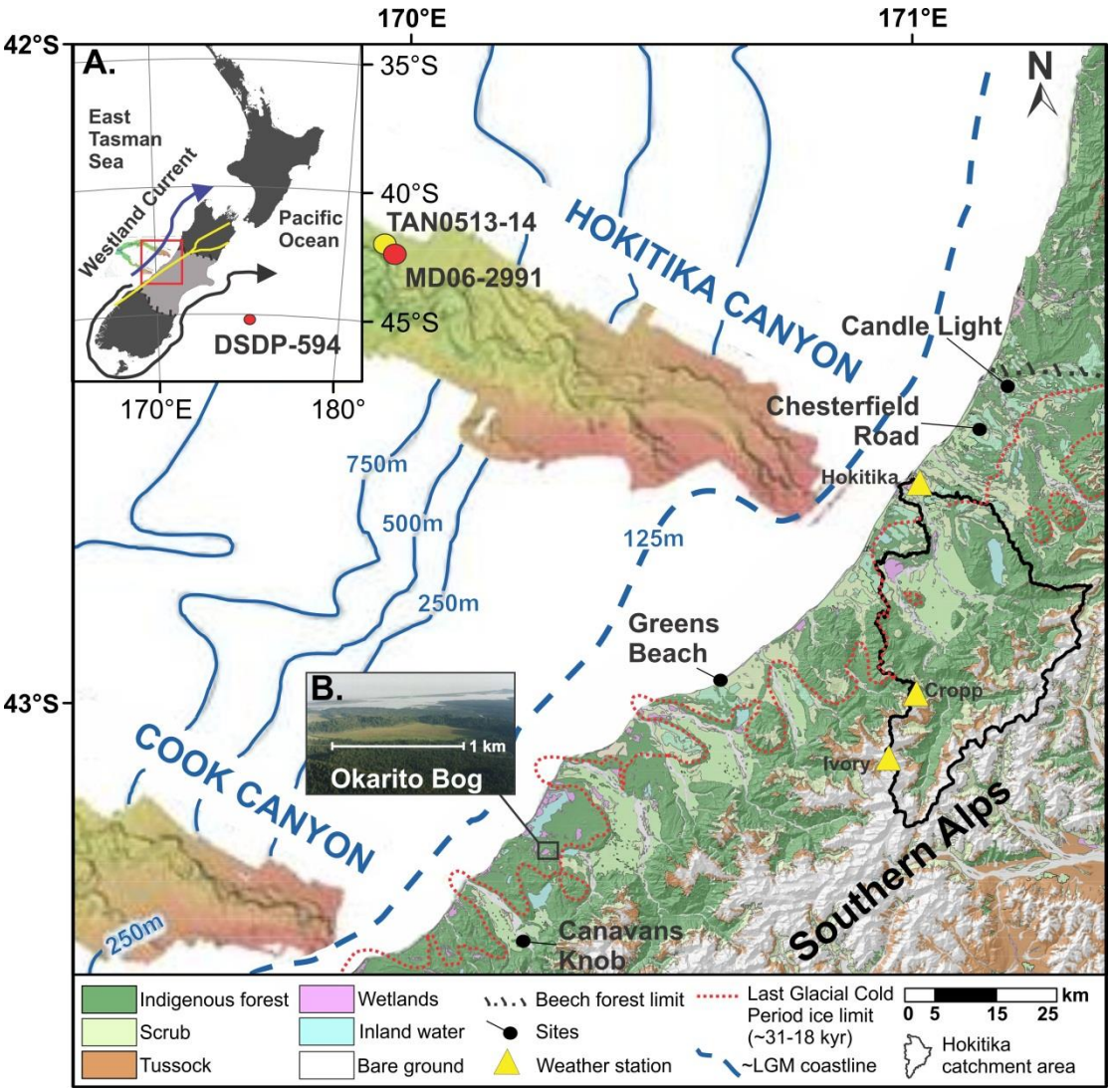

Fig. 4.2: Regional setting of the study area showing the locations of climate stations, marine and terrestrial core sites. The distribution of vegetation in central-southern Westland is broadly approximated by altitudinal range on the map as outlined in section 2.5. The approximate northern limit of the central Westland southern beech gap is delineated (Wardle 1984). **Inset A;** The extent of the Biotic Gap zone is highlighted in light grey (Section 2.1.3), with the NE-SW trending yellow line representing the Alpine Fault along the Southern Alps (Hill et al., 2009). The Westland Current (blue) and the Southland Current (black) are illustrated (Carter, 1975; Heath, 1985). The digital elevation model shown is derived from Land Information New Zealand (LINZ) digital topographic contours and spot heights (Crown Copyright reserved), with bathymetric data supplied by NIWA. Note the Okarito Bog site is illustrated outside of the LGCP ice limit defined by Barrell (2011) and Barrows et al. (2013) and is pictured (**Inset B**). Additional Termination II (T-II) profiles are discussed in text, with the LGM coastline defined by the ~120 m bathymetric contour.

4.2 Materials and methods

4.2.1 Sample selection and processing for MD06-2991

Piston core MD06-2991 was retrieved from the northern levee bank of the Hokitika submarine canyon system by the R.V *Marion Dufresne* with a Calypso piston corer (Proust et al., 2006; Fig. 4.2). This 33 m-long core consists of a greenish grey foraminifera-rich mud, with no turbidites observed. Samples of sediment (4-20 g dry weight) were taken from 0.5-1 cm thick slices at intervals between 0.5 and 20 cm, down to 11 m core depth. These samples were oven dried at 50°C, disaggregated in sodium hexametaphosphate (0.5 g/L), and wet sieved at 150 μm. The coarse fraction was retained for stable isotope analysis ($\delta^{18}O$ and $\delta^{13}C$) and planktonic foraminiferal assemblage counting. The fine fraction (<150 μm) of this sample, supplemented by an additional sample within 1 cm if sufficient material was not available, was processed for pollen analysis. This material was spiked with a *Lycopodium* tablet (20,848 grains, s.d. 1546) for determining absolute pollen abundance, dissolved in 10% HCl, and processed for palynology following the methods described in Chapter 3. The 11 m length of core examined contained an average of 250 (range 108-370 grains) dryland pollen grains from 113 palynological samples (86 additional from that presented in Chapter 3).

Stable oxygen and carbon isotope analyses were conducted on approximately three to four individual tests of the spinose planktonic foraminifer *Globigerina bulloides* (250-355 μm), identified using the taxonomy of Hemleben et al. (1989), and on the benthic foraminifera *Uvigerina peregrina*, using the taxonomy of Hayward et al. (2010). Oxygen isotopes ($\delta^{18}O$) were initially analysed every 20 cm down-core by NIWA from 0.5–530 cm (0–71.3 ka, MIS 5a), and between 1040-1110 cm (144.7–157.7 ka, MIS 6; Williams et al., 2015). To obtain a highly resolved record for the penultimate deglaciation, the sampling interval was reduced to 10 cm between 530–880 cm (71.3–114 ka, MIS 5d), and 5 cm between 880–1040 cm (114–144.7 ka, MIS 6; Suppl. Table 1), with foraminifera picked from those samples by Matt Ryan, Helen Neil and Helen Bostock.

All stable isotopes were analysed using the National Institute of Water and Atmospheric (NIWA) Research automated individual-carbonate reaction (Kiel) device coupled with a Finnigan MAT 252 mass spectrometer. The results are reported relative to the Vienna Peedee belemnite (vPDB) using the NBS-19 standard, where $\delta^{13}C$ has a value of +1.95‰ and $\delta^{18}O$ has a value of –2.20‰. Internal precision (within a run) of standard measurements was 0.02–

0.08‰ ($\delta^{18}O$), external precision was ±0.03 % relative to vPDB. Five splits of samples were analysed with internal variability of <0.3‰.

4.2.2 MD06-2991 chronology

Chronology for the upmost 230 cm of MD06-2991 was generated using 15 radiocarbon (^{14}C) dates on mixed planktonic foraminifera and is unchanged from that presented in Chapter 3. This provides an independent constraint for the position of the maximum concentration of KOT volcanic glass shards (200.5-201 cm) at 25.14 ± 0.8 cal kyr BP (2 σ), and is consistent with the associated onshore Oruanui eruption age of 25.59 ± 0.07 cal kyr BP (2 σ) revised from Vandergoes et al. (2013b). In addition, the occurrence of KOT provides support for the ^{14}C age model for the upper part of the core and the assumption of a constant reservoir for this period (~400 years). This is consistent with the findings of Sikes et al. (2016) who suggest an LGM age marine surface reservoir correction for the eastern New Zealand waters of ~700 years at the timing of KOT deposition.

Additional chronological constraint beyond the range of ^{14}C age control for the MD06-2991 sequence (~28 ka) is obtained by matching down-core $\delta^{18}O$ measurements on benthic foraminifera between 1110-231 cm core depth (158-28 ka) to the reference LR04 benthic $\delta^{18}O$ stack (Lisiecki and Raymo, 2005). The widely used LR04 benthic $\delta^{18}O$-age curve was selected as the target reference curve, as this facilitates comparison with a wide variety of global records. A notable inconsistency occurs between the radiocarbon and $\delta^{18}O$ chronologies between 100-80 cm core depths, where benthic $\delta^{18}O$ "wiggle-matching" suggests an age of 18-14 ka whereas the ^{14}C chronology is 13-10 ka for the same interval. This may reflect the relatively low resolution sampling of the $\delta^{18}O$ stratigraphy at MD06-2991 and therefore the ^{14}C chronology is used for this interval in the analysis and discussion that follows.

With all sources of errors incorporated, Lisiecki and Raymo (2005) suggest their widely used LR04 $\delta^{18}O$-age reference curve has an uncertainty of up to 4 kyr (1σ) at any point in time over the last million years, potentially compounded by regional differences in the timing of $\delta^{18}O$ change (Skinner and Shackleton, 2005). For example, Lisiecki and Raymo (2009) suggest that $\delta^{18}O$ changes in the Atlantic precede those in the Pacific by an average of 1.6 kyr for the last five terminations. To better constrain the timing and uncertainty of glacial terminations in the Pacific basin I have utilised the results of Caballero-Gill et al. (2012a),

who determine the average uncertainty in the LR04 stack to be 1.1 ± 0.7 kyr (1σ) over the last 240,000 years based on matching their benthic $\delta^{18}O$ record from ODP 1146 in the South China Sea to the nearby independently U/Th dated speleothems from Sanbao and Hulu Caves (last 160 ka displayed in Table 4.1; 2σ uncertainties plotted on LR04 stack on Fig. 4.3; Suppl. Fig. 4.1). Their results are broadly consistent with improved age uncertainties determined for the orbitally tuned SPECMAP chronology from radiometric dating of corals by Thompson and Goldstein (2006; Suppl. Fig. 4.2).

Table 4.1 Radiometric Datum List[a] for speleothem vs. LR04 stack.

Datum Number[b]	Depth (Rmcd09)	RC Age (ka)	Age Error (±kyr)	Speleothem	Minimum Age (kyr)	Minimum Speleothem Error (kyr)	Minimum Speleothem	Maximum Age (kyr)	Maximum Speleothem Error (kyr)	Maximum Speleothem	Comment	Reference[c]
1	14.34	60.02	0.43	MSL-125							tie point	
2	17.13	72.52	0.25	MSL-192							HC	1
3	18.09	77.00	0.70	SB22-237							HC	1
4	19.37	84.03			82.90	0.50	SB25-1-92	88.00	0.50	SB22-314	HC	1,2
5	19.96	86.90			82.90	0.50	SB25-1-92	88.00	0.50	SB22-314	HC	2
6	20.57	90.42			88.00	0.50	SB22-314	91.30	0.80	SB22-341	HC	2
7	21.98	99.36	1.30	SB23-88							HC	2
8	22.62	104.47			100.10	1.30	SB23-88	105.40	0.80	SB23-126	HC	2
9	23.38	109.69	1.10	SB23-156							tie point	2
10	24.57	121.73	1.00	SB23-261							HC	2
11	26.27	129.71	0.80	SB11-38							HC	2
12	27.05	134.19			131.10	1.60	SB11-63	136.40	0.90	SB11-87	HC	2
13	28.59	138.66	1.60	SB11-106							HC	2
14	34.06	160.70	1.30	SB11-245							HC	2

[a] High-confidence (HC) correlation points identified in ODP 1146 by Caballero-Gill et al. (2012a).
[b] Note age errors for HC do not include the ±0.09 kyr (2σ) uncertainty due to sample spacing in the ODP 1146 planktic record.
[c] References: 1, Wang et al. (2001); 2, Wang et al. (2008).
RC: Radiometric chronology with 2σ uncertainty.

Age uncertainties in the LR04 $\delta^{18}O$ reference curve are compounded by a degree of subjectivity in the fit (i.e., 'wiggle-match') between our down-core MD06-2991 $\delta^{18}O$ stratigraphy and the LR04 $\delta^{18}O$ stack. Therefore, in consultation with Prof. Euan Smith (VUW), an attempt was made to reduce the subjective aspects of wiggle-matching by minimising the mean integrated square error between the two age-models (detailed procedure outlined in supplementary material through Fig. 4.2-4.5). To do this, $\delta^{18}O$ data for MD06-2991 were resampled to a common time-base with 0.2 kyr spacing and a mean over the full time range. The optimum offset over the full time range of the samples (158-29 kyr) in the LR04 and MD06-2991 $\delta^{18}O$ curves was then estimated by minimising the mean integrated square error (MISE) between the two time models for a range of offsets equal to multiples of 0.2 kyr. A chi-squared random variable is the sum of "*n*" independent squared normal variables; where "*n*" is the degrees of freedom (*df*). Resampling the data increases the number of data points, but they are not independent. The number of independent points is the smaller of the number of samples in the two datasets being compared, which are LR04

and MD06-2991, with the former typically the smaller. The age uncertainty in the best fit between the age models is thus conservatively estimated using a chi-squared statistic with *df* equal to the size of the smaller sample.

The time offset which gives the best fit between the LR04 benthic $\delta^{18}O$ stack and the MD06-2991 $\delta^{18}O$ stratigraphy over the 158-28 ka time interval is 0.0 kyr (± 6 kyr, 95% level of confidence; Supplementary Fig. 4.3-4.5). For the high-resolution sampled interval between 158-98 kyr, the best fit time offset is 1.2 kyr (+ 7 kyr -5 kyr, 95% level of confidence; Supplementary Fig. 4.5-4.6). The uncertainties associated with this offset do not justify making a 1.2 kyr correction. Chapter 5 provides an example of where the level of fit is better resolved between the higher resolution $\delta^{18}O$ sampled MD06-2990 marine sediment core (situated ~1 km northwest of MD06-2991) and the LR04 stack. The uncertainty in the fit is reduced with improved sample resolution.

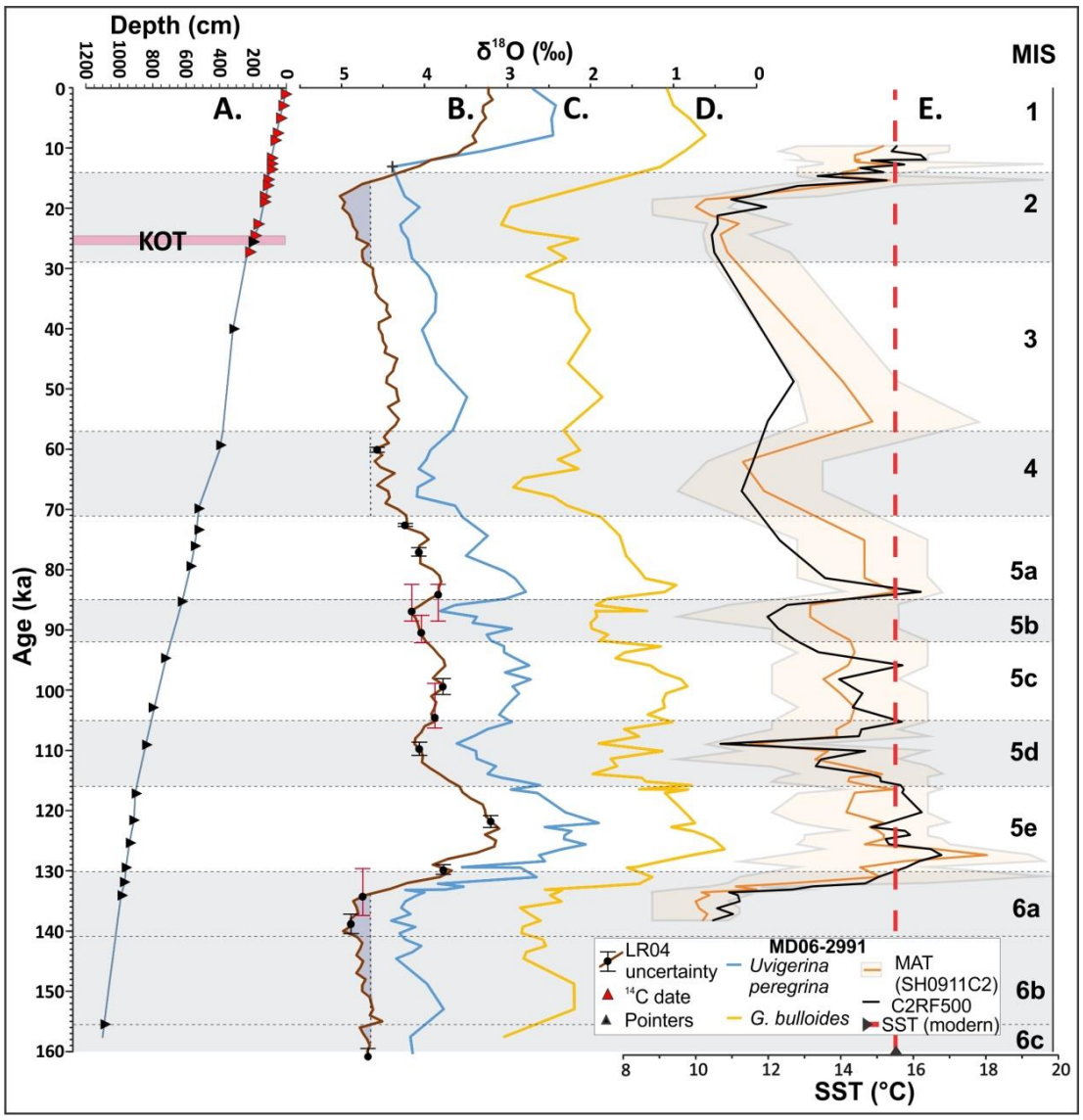

Fig. 4.3: MD06-2991 age model and SST reconstruction. **A.** Age-depth model with calibrated ^{14}C dates (red triangles, n=15) on planktonic foraminifera, the maximum concentration of KOT glass shards at MD06-299, and $\delta^{18}O$ tie-points (black triangles) which align down-core $\delta^{18}O$ measurements from MD06-2991 to **B.** the reference LR04 benthic $\delta^{18}O$ stack (Lisiecki and Raymo, 2005). Intervals of "excess ice" of Raymo (1997) considered necessary to achieve a termination are shown (purple shading, >4.5‰). Age uncertainties on the LR04 stack represent radiometrically dated speleothem samples tied to LR04 (black), while the red 2σ age uncertainties are for correlation points that lie between radiometrically dated samples (Caballero-Gill et al., 2012a). **C+D**; MD06-2991 oxygen isotope records for *Uvigerina peregrina* and *Globigerina bulloides*, with a black cross used to illustrate a potential outlier. **E.** SST estimates from planktic foraminifera based on the modern analogue technique (MAT) using the SH training set (SH0911C2) discussed in Cortese et al. (2013) with an associated uncertainty envelope. A random forest ensemble (C2RF500) based SST for the same foraminiferal counts are illustrated. The MIS boundaries of the LR04 stack are shown following the subdivision of Railsback et al. (2015), with the glacial stages and the stadial sub-stages represented in grey shading.

4.2.3 MD06-2991 sea surface temperature (SST) estimates

SST estimates since MIS 6 are based on planktic foraminiferal faunal assemblages undertaken by Ashwaq Sabaa and Bruce Hayward (Geomarine Research Ltd) and follow the methods of Hayward et al. (2012) and Cortese et al. (2013). The >150 μm size fraction from 72 samples was repeatedly split until approximately 300 (range 199-402) whole or nearly whole planktic foraminiferal tests remained, which were identified and counted. Twenty-three species of planktic foraminiferal taxa were discriminated, with most being used in the reconstruction of mean annual SSTs using a modern analogue technique (MAT) that includes reference to 1223 SH core top samples (SH0911C2, www.ncdc.noaa.gov/paleo/paleo.html; Cortese et al., 2013; Suppl. Fig. 4.7). The MAT finds faunas in the training set that most closely match that in the core set. The mean SST from the five most similar training set faunas is assigned to each test sample in the core set (using Chord coefficient of similarity). A measure of accuracy of these SST estimates is given as the range of SST values of the five most similar training set faunas. Equivalent MAT-based estimates of SSTs (five most similar) are also provided for MD06-2986 (Hayward et al., 2012; Suppl. Fig. 4.8), situated ~210 km south-west of the MD06-2991 core-site (Fig. 1.5), as the estimates of SST derived from MD06-2991 have not yet been calculated beyond 138 kyr.

Additional SST estimates were calculated using the same census data following the methods of Cortese et al. (2013) by George Scott (GNS) who used the Random Forest model (C2RF500). This is an ensemble decision tree tool (n=500 runs) that has been applied to core-top planktonic foraminiferal faunas from the SH0911C2 training set which are calibrated to modern SSTs, and computed using the Random Forest package (http://cran.r-project.org/web/packages/randomForest/). They show that the MAT method is the best predictor for error tolerances between 0–1°C, while the RF method replaces the MAT where error tolerances exceed this range. Cortese et al. (2013) concluding that RF is the best predictor over the full training set. All Random Forest-based SST estimates for the 18-9 ka period are within the uncertainty of the MAT-based estimates, with the 95% confidence interval for each predicted SST, computed from the 500 estimates (Suppl. Fig. 4.9).

4.2.4 MD06-2991 $CaCO_3$ and siliciclastic sediment content

The absolute abundance of pollen is usually reported in terms of grains per gram of sediment, however, the variability of pollen abundances in marine sediments could simply reflect variable dilution by biogenic $CaCO_3$ over time, rather than representing inherent changes in pollen production on land. To allow us to correct for these changes in absolute pollen

concentrations $CaCO_3$ content was measured at NIWA by Helen Bostock and Ashley Pocock on 56 samples collected at 20 cm spacing from MD06-2991 using a vacuum-gasometric system based on the principals of Presley (1975) and Jones and Kaiteris (1983). For a standard mass of powdered AR grade standard equivalent to a $CaCO_3$ content of "100%" the analytical reproducibility was ±2%. The $CaCO_3$ content for palynomorph samples lying between these measured points was estimated using linear interpolation. Assuming the sediment at MD06-2991 is comprised of only $CaCO_3$ and terrigenous siliciclastic material (and ignoring any contribution from biogenic silica), the terrigenous component of each sample can be estimated by the difference in $CaCO_3$ from 100%. The absolute abundance of pollen is therefore reported in terms of grains per gram ($gr.g^{-1}$) of dry terrigenous sediment using the following formula.

$$Abundance = pollen_counted \times \left(\frac{Total_exotic_Lycopods}{Lycopods_exotic_counted} \right) \div dry_sed_wgt(g) \times \left(1 - \frac{\%CaCO_3}{100} \right)$$

4.2.5 Okarito bog chronology and palynology (153-9.5 kyr)

The terrestrial palynological record developed from Okarito Bog is a composite of cores OKA1 (10-561 cm, n=116 samples) and 913 (601-968 cm, initially n=46 samples). An additional 20 "fill in" samples were taken from Okarito core OKA1-913 over the LIG (810-852.9 cm, total n=66 samples) and examined by Xun Li and Marcus Vandergoes (GNS Science) to improve the temporal resolution from ~2000 years as published in Newnham et al. (2007a) to ~520 years for this study. Chronological constraint for the palynological record established by Vandergoes et al. (2005) was achieved via radiocarbon dating, luminescence ages, and correlation of Kawakawa/Oruanui Tephra from OKA1 and nearby cores 0004, 0113, 0212, 0212b, and 0112b.

The Okarito Bog record is presented in two sections. The topmost section is chronologically constrained by ^{14}C dating and covers the interval 27-9.5 kyr (~275-390 cm, T-I). This captures a period of significant environmental change from the LGCP to the LGIT, and in conjunction with other Westland sites was used to provide estimates of the source-to-sink residence time of independently dated terrestrial palynomorphs and tephric material transported from Westland to the ^{14}C section of MD06-2991 (Chapter 3). The conclusion that the palynomorph residence time is negligible and remained constant over this interval suggests that the well-established MD06-2991 stratigraphy can be transferred to the lowermost section (i.e. below ~390 cm) of the Okarito Bog sequence by aligning 'palynomorph events' common to both cores.

In detail, 21 palynomorph events noted in the regional step-wise succession in the relative abundance of pollen flora recorded over MIS 6-5c (~153–98 ka) at MD06-2991 are correlated to similar events revealed at Okarito Bog (Fig. 4.4; Suppl. Fig. 4.10-4.15). Consequently, it is the variation in these taxa which define the palynomorph calibration point (hereinafter termed 'palynostratigraphic calibration points'; PCPs) and not the relative abundance attained in each record, with 18 taxa in total used. Whilst being well-represented in the MD06-2991 pollen record, fluctuations in the relative abundance of *Fuscospora* were excluded for the development of palynostratigraphic marker horizons in this study for two reasons. First, it is considered typically over-representative in treeless landscapes (Macphail and McQueen, 1983; Moar et al., 2011), and second, it is current not present in the study area (Wardle, 1984). This represents a revision of the approach taken by Ryan et al. (2012).

This period of palynostratigraphic correlation (MIS 6-5c) encapsulates the penultimate glacial-interglacial transition (PGIT), and displays a vegetation succession which resembles the Last Glacial-Interglacial Transition (Newnham et al., 2007a). Out of necessity, the palynomorph source-to-sink residence time to MD06-2991 during the last interglacial period was assumed to be similar to that calculated for the Last Glacial Coldest Period and Last Glacial-Interglacial Transition. Support for this assumption stems from the observation that both terminations exhibit similar magnitudes of global eustatic sea level (and thus shoreline) change (Thompson and Goldstein, 2005; Rohling et al., 2014). Three additional PCPs constrain the Okarito Bog record between 98-28 ka by aligning variations of *Dacrydium cupressinum* (535 cm = 67.9 ka; 645 cm = 84.9 ka; 665 cm = 85.9 ka).

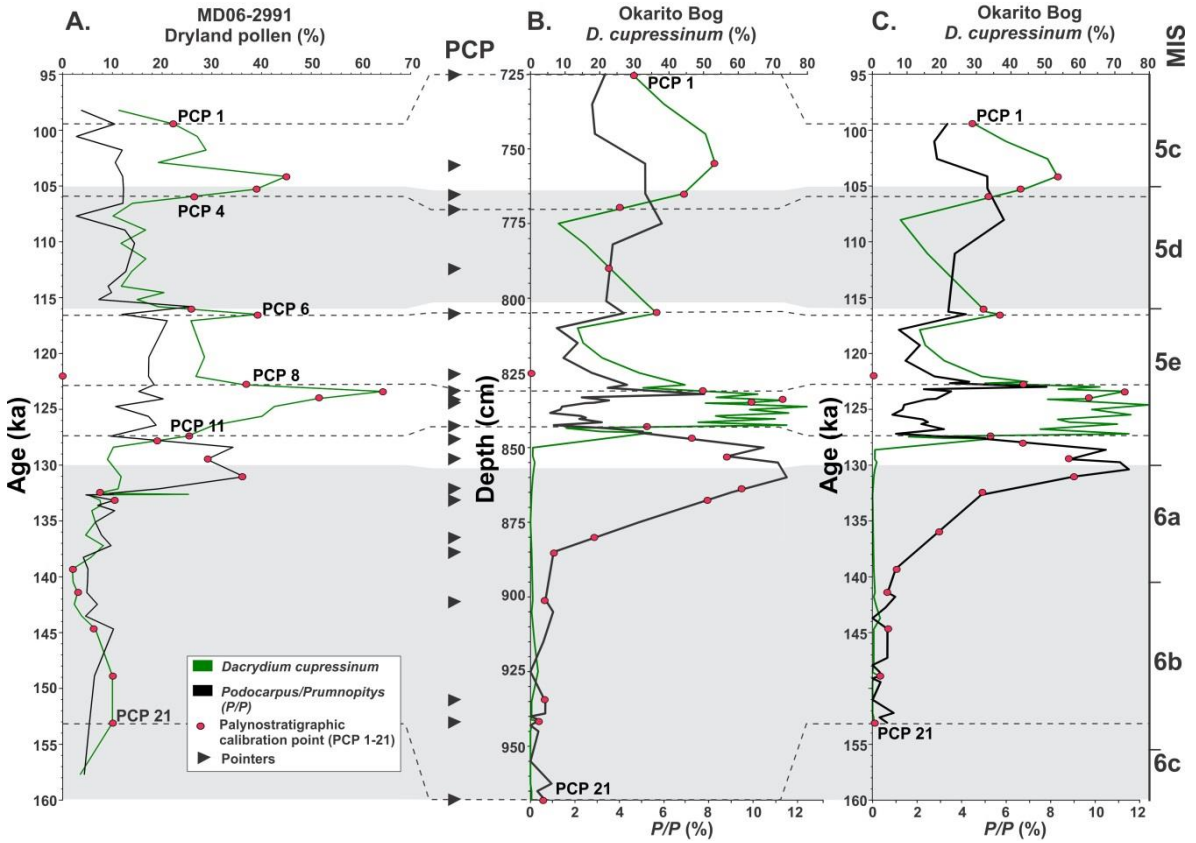

Fig. 4.4: Chronostratigraphic correlation of event based palynomorph calibration points (PCPs) between MD06-2991 and Okarito Bog over the interval 160-95 ka (MIS 6c to 5c). From left to right; **A.** MD06-2991 dryland pollen percentages for *Dacrydium cupressinum* (dark green) and *Podocarpus/Prumnopitys (P/P,* black) and the position of 21 PCPs generated from variations in the relative abundance of up to 18 taxa (Table 4.2 and visually illustrated in Suppl. Fig. 4.13-4.14). Pointers (black triangles) and guidelines (PCP 1, 4, 6, 8, 11, and 21) display where PCPs are aligned to **B.** the Okarito Bog depth profile (Vandergoes et al., 2005) dryland pollen percentages for *Dacrydium cupressinum* (dark green) (Vandergoes; unpublished data). **C.** The dryland percentages of these taxa are displayed for Okarito Bog realigned to the MD06-2991 age model, with differences in the relative proportions between sites (secondary x-axis). Glacial and stadial boundaries are displayed in grey shading (Lisiecki and Raymo, 2005; Railsback et al., 2015). The re-dated depth age relationship for Okarito Bog is shown in Suppl. Table 4.2.

Table 4.2: MD06-2991 palynostratigraphic calibration points (PCPs) to Okarito Bog

Tie-point	Identifying featues of palynomorph event based age tie points	MD age (ka)	Okarito depth (cm)	MIS
1	*Dacrydium cupressinum* decline.	99.45	725	**5c**
2	*D. cupressinum* peak, with an increase in *Cyathea* spp. Decline in *Lophozonia menziesii* values.	104.15	755	**5c**
3	*D. cupressinum* rise, increasing *Cyathea* spp.	105.23	765	**5d**
4	Mid-point in rising *D. cupressinum* values, declining Asteraceae and *Coprosma.*	105.89	770	**5d**
5	Decreased *D. cupressinum* and increasing *Halocarpus.*	115.81	791.5	**5d**
6	Increasing *D. cupressinum* and *P/P* values.	116.5	805	**5e**
7	*Ascarina lucida* absent.	122.05	825	**5e**
8	Decreasing *D. cupressinum,* with a simultaneous increase in *Coprosma* , *Nestegis* present.	122.79	831	**5e**
9	*Ascarina lucida* decline, high *D. cupressinum* values present.	123.4	834.2	**5e**
10	Low *Ascarina lucida* and Poaceae, with high *D. cupressinum* values.	124.07	835	**5e**
11	Mid-point in rising *D. cupressinum.*	127.41	843	**5e**
12	Transition point between declining *P/P* and increasing *D. cupressinum.*	127.9	847.5	**5e**
13	Max. in *Dacrycarpus dacrydioides* . Declining proportions of *Cyathea* spp., and *P/P.*	129.48	852.9	**5e**
14	Peak *Cyathea* spp., with high P/P and rising *Diksonia squarossa* values. Mid-point in declining *Coprosma* values, with low Asteraceae.	131.04	865	**6**
15	Peak *Coprosma* proportions, with increasing P/P and *Cyathea spp.*	132.67	875	**6**
16	Mid-point rise in *Coprosma* values. Asteraceae and Poaceae decline, with low proportions of *Cyathea* spp.	133.15	880	**6**
17	High Poaceae (peak in OB) and Asteraceae values, with low proportions of *Coprosma.*	139.31	885	**6**
18	High Asteraceae and Poaceae, *Nestegis* and *Dacrycarpus dacrydioides* present.	141.42	901	**6**
19	Low proportions of Asteraceae, Poaceae and *Lophozonia menziesii* .	144.68	935	**6**
20	*Metrosideros* , *D. cupressinum and Cyathea* spp decline. Asteraceae and Poaceae and *Lophozonia menziesii* increase.	148.88	941.5	**6**
21	Tall tree and tree fern taxa of *D. cupressinum, Metrosideros* and *Cyathea* spp are present, prior to increasing proportions of *Halocarpus.*	153.08	968	**6**

Note: *Podocarpus/Prumnopitys* abbreviated to *(P/P).*

PCPs were used to align Okarito Bog (725-968 cm) to the MD06-2991 chronology. To do this, two points near the ends of the Okarito depth profile were fixed. The points at 99 ka and 149 ka were chosen following several trials, after the Okarito Bog sedimentation rate and the least difference between both sets of pollen spectra were evaluated. These enable the MD06-2991 record and the Okarito Bog record to be viewed on a common depth-scale, normalised to [0 1] between the fixed points. This method provides an objective alignment of the two records. Groups of PCPs (1-4, 5-6, 7-16, 17-20), between which the sedimentation rate is relatively uniform, were identified and selected from this age-scale. The ages of the Okarito Bog pollen samples situated between PCPs were determined by linear interpolation. The uncertainty of Okarito sample ages was estimated by considering the alignment of PCPs. Okarito Bog ages had uncertainties assigned to them from the MD06-2991 age model and interpolated age errors. The age uncertainty for PCPs assigned to the Okarito Bog record is derived from the ages of the bracketing pollen samples in the MD06-2991 record, except at the two end PCPs of the record which are assumed to have symmetric errors. The uncertainties for interpolated Okarito Bog depths (i.e., non PCPs) are the means of the errors at the bracketing PCPs, i.e., equal to the average of the errors of the two depth/age points for which they were calculated. The age uncertainties are the interval between the bracketing sample points, which are (slightly) greater than 95% confidence points for a uniform distribution, and therefore conservative.

4.2.6 CONISS and Regional Pollen Assemblage Zones (RPAZ)

In order to facilitate comparison of the pollen records presented here with other published New Zealand climate records, a stratigraphically constrained cluster analysis (CONISS), with a square-root transformation, was performed on the MD06-2991 pollen profile (Grimm, 1987). This analysis included all dryland pollen taxa and the relative abundance of tree ferns, excluding values <2%. Over the period constrained by ^{14}C dating, CONISS pollen zonations for MD06-2991 are consistent with the pollen-based New Zealand-INTIMATE climate event stratigraphy (Barrell et al., 2013). Beyond ^{14}C timescales, CONISS pollen zonations guided the establishment of equivalent regional pollen assemblage zones (RPAZ) between land-sea records and provide evaluation of climatic events within the context of MIS subdivisions.

4.2.7 Okarito mean annual air temperature reconstruction (MAAT)

Mean annual air temperatures (MAAT) were reconstructed for the entire Okarito Bog sequence (~150-0 ka) using a pollen-climate calibration model that is based on a pre-

anthropogenic disturbance New Zealand-wide pollen database (Wilmshurst et al., 2007). Two tools provide past temperature estimates, one using a partial least squares (PLS) regression transfer function, and the other using a weighted average modern analogue technique (MAT) of ten closest analogues. Following the removal of outliers, the PLS transfer function had a root mean square error of prediction (RMSEP) of 1.5°C, and a similar performance in the MAT with RMSEP of 1.51°C (Wilmshurst et al., 2007). Estimates of MAAT (PLS and MAT) are specifically shown for MIS 6-5 (158-98 ka) and MIS 2-1 (27-9.5 ka) based on results generated by Janet Wilmshurst (Landcare Research Ltd). These included the 20 additional unpublished samples spanning MIS 6-5e provided by Marcus Vandergoes. Reconstructed MAATs using the modern analogue technique method for T-I are revised from those previously published by Newnham et al. (2012), and contain a more comprehensive data set of the taxa lists of pollen and plants.

One measure of the accuracy of the models is the difference between the modern measured MAAT, derived from Okarito Forest (11.3°C), and the temperature estimates modelled for the period immediately before anthropogenic vegetation disturbance (i.e., prior to~750 cal yr BP; Wilmshurst et al., 2007) identified from the Okarito core. Undertaking this comparison, PLS estimates produced a MAAT of 9.8 ± 1.51°C and MAT based estimates produced 8.8 ± 1.5°C. Pre anthropogenic disturbance PLS based estimates were therefore within the uncertainty of modern measured temperatures, whereas those reconstructed from the modern analogue technique and their uncertainties fall below modern measured temperatures by an additional 1°C. MAT estimates may be underestimated at Okarito Bog due to the low number of low altitude sites from Westland represented in the pre-deforestation database. Additionally, the large diameter (1 km^2) of Okarito Bog likely has captured a greater component of regional pollen rain than that which is of local origin (Fig. 2.1; Chapter 2; Jacobson and Bradshaw, 1981). Therefore, smaller sites used in the training set may potentially reflect more local vegetation signals. If these explanations are correct then the trend in the temperature reconstructions should be valid, although the absolute magnitude may be compromised (Wilmshurt et al., 2007). Alternatively, the climate of Westland may have been dissimilar during the 13th century than that of the present-day, however a tree ring climate reconstruction by Cook et al. (2006) suggests similarity in the climate between the two intervals.

4.3 Results

4.3.1 MD06-2991 (Sedimentation, $CaCO_3$, $\delta^{18}O$, SST, pollen)

Once aligned with the LR04 stack, the age depth profile of MD-2991 shows sedimentation rates were between 4.6-10.6 cm.kyr^{-1} (average 7 cm.kyr^{-1}) with the highest rates occurring during glacial and stadial periods MIS 2, 4 and 5b and the lowest during the MIS 5e interglacial and MIS 3 interstadial (Fig. 4.3; Suppl. Table 4.1). $CaCO_3$ content varies between 15 to 39% down-core but with no systematic changes over G-I cycles (Suppl. Fig. 4.15). Similarly, when calculated on a $CaCO_3$-free basis, dryland pollen displays no systematic changes in absolute abundance down-core (Suppl. Fig. 4.15). In contrast, $\delta^{18}O$, faunal census-derived SST, and the proportion of arboreal pollen taxa and tree fern spores vary in concert with G-I cycles (Suppl. Fig. 4.15-4.16), and show broadly similar trends across T-I and T-II. A total of nine common regional pollen assemblage zones (RPAZ 2a-2i) are compared between MD06-2991 and Okarito Bog between 158-98 ka.

SSTs during glacial periods were of similar magnitude ~10-10.5ºC. Interglacial SSTs reached SSTs 16-18ºC, and increased relatively synchronous with a progressive decrease in $\delta^{18}O$. Higher resolution analysis of T-II displays a divergence between $\delta^{18}O$ and SST estimates at 127.5 ka. SST attain the highest values in the MD06-2991 record over ~2 kyr between 129-127.5 ka and precede decreasing $\delta^{18}O_{planktonic}$ and $\delta^{18}O_{benthic}$ measurements by 1 and 2 kyr, respectively.

4.3.2 Pollen and SST change from southwestern New Zealand

Palynomorph assemblages at MD06-2991 and Okarito Bog profiles display broadly similar changes in the composition of regionally dispersed pollen over the LGCP and LGIT (18-9 cal kyr BP), and exhibit strong similarities to those previously recorded in this region for the last two glacial cycles by Ryan et al. (2012). Variations in palynomorph content between land-sea profiles are discussed in the timeframes outlined in the New Zealand-INTIMATE climate event (NZce) stratigraphy from 18-9 cal kyr BP (Barrell et al., 2013), and in the context of MIS subdivisions for the Penultimate glacial until MIS 5c (158-98 ka).

Termination I (18-9 cal ka BP)

18–15.6 cal ka BP (NZce-5)

The onset of the LGIT at MD06-2991 is characterised by a steady increase in the relative abundance of podocarp-hardwood taxa, while an increase in montane-subalpine tree and

shrub taxa is displayed at Okarito Bog (Fig. 4.5-4.6). Herb taxa decline in both records over this interval, with an associated increase in reconstructed MAAT largely mirroring this decline at Okarito Bog (Fig. 4.6; Table. 4.2). A pronounced rise in SST commenced at 18.6 cal ka BP at MD06-2991 and almost approaches modern values at 15.4 cal ka BP (15°C), and MAAT estimates show a continued warming during NZce-5.

NZce-4 (15.6–13.74 cal ka BP) and NZce-3 (13.7-12.55 cal ka BP) Lateglacial period

A shift in the dominance of tall tree taxa from pioneer species (e.g. *Podocarpus/Prumnopitys, Metrosideros*) to that dominated by *Dacrydium cupressinum* and *Fuscospora* occurs over NZce-4 at MD06-2991. Montane-subalpine tree and shrub pollen (Asteraceae and *Coprosma*) display a brief resurgence during NZce-3, with Poaceae increasing at the culmination of the climate event. Rising podocarp-hardwood taxa (primarily *Metrosideros*) similarly characterise NZce-4 at Okarito Bog, and lead to the highest estimates of MAAT (9.5°C) for the Last Glacial-Interglacial Transition (LGIT) at 14.5 ka (Fig. 4.6; Table 4.3). In contrast, SSTs from MD06-2991 reach their lowest values over the LGIT at 14.7 cal ka BP, and remain up to 2°C lower than present conditions until 12.78 ± 1.16 cal ka BP. A sustained trend of increasing montane-subalpine tree and shrub pollen at Okarito Bog commenced from 14.5 ka (approximately mid NZce-4), and steadily increase to values of 80% between 13.79–12.96 cal ka BP. This is marked by a lithostratigraphic change from brown organic silt to coarser lighter coloured silts, with a concomitant decline in MAAT (Fig. 4.6).

NZce-2 (12.55–11.88 cal ka BP)

In both MD06-2991 and Okarito Bog, tall tree podocarp-hardwoods, largely dominated by *Podocarpus/Prumnopitys*, gradually increase over NZce-2 as montane-subalpine shrubs simultaneously decline. An increase in the abundance of montane subalpine taxa of *Phyllocladus* spp. (presumably *P. alpinus*) and *Halocarpus*, which exhibit strong correlations with MAAT in the New Zealand pollen-vegetation database (r=-0.65 and -0.59 respectively; Wilmshurst et al., 2007), produce low MAATs (6.7-7.1°C) following the onset of NZce-2 at 12.34 ± 1.2 cal ka BP (Table 4.3, Fig. 4.6). *Cyathea* tree fern spores and *Podocarpus/Prumnopitys* attain their highest values over the LGIT near the culmination of the episode at 11.96 ± 0.3 cal ka BP, and are coupled with the highest SSTs (RF-based) of the LGIT over 16°C.

NZce-1 (11.88–9 cal ka BP)

Podocarpus/Prumnopitys proportions remain high (~40%) at both sites following the NZce-1 onset. These taxa contribute to a gradual increase in MAAT, while in the adjacent ocean

Random Forest-based SSTs are ~1°C higher than present, with Okarito Bog sediment transitioning from coarse to organic-rich silt marking this change at 11.69 ± 1.4 cal ka BP. Pollen of *D. cupressinum* becomes the dominant tall tree conifer taxon in both records after ~10.88 ± 1.08 cal ka BP, where it attains maximum values over the entire 27-9 kyr interval at 10.5 ± 1.3 cal ka BP at MD06-2991. A difference of ~1.1 kyr occurs between the period of initial dominance of *Podocarpus/Prumnopitys* (defined by the primary peak at 11.96 ± 0.3 cal ka BP) and the succeeding rapid rise in *D. cupressinum* (defined by the mid-point at ~10.88 ± 1.08 cal ka BP). This change in pollen content is reflected in MAATs which peak in the early Holocene to 10.2°C between 10.8–9.5 cal kyr BP, while SSTs (RF-based) decline to modern values over the same interval. In the two records examined it takes ~3.8 kyr between the early dominance of podocarp-hardwood pollen and MAAT increase in NZce-4 to that of the *D. cupressinum* rise to dominance during NZce-1.

Table 4.3: Comparison and summary of the primary palynomorph changes at MD06-2991 and Okarito Bog, and the respective estimates of sea surface temperature (SST) and mean annual air temperature (MAAT) across Termination I (T-I).

		MD06-2991		Okarito Bog	
NZ-INTIMATE EVENT	**Age range (cal kyr BP)**	**Pollen-based vegetation change**	**SST estimates**	**Pollen-based vegetation change**	**Air temperature estimates (MAAT)**
NZce-1	**11.88–9**	Initial increase in *P/P* followed by increasing *D. cupressinum.*	**MAT:** Increases from 14.4–15.5°C (modern SST). **RF:** Declines from 16.2–~15.5°C.	Initial increase in *P/P* , followed by *D. cupressinum*. Montane-subalpine shrubs decline throughout.	**MAT:** Increases from 7.1–9.3°C **PLS:** Increases from 7.1–10°C
NZce-2	**12.55–11.88**	Increasing podocarp-hardwood taxa, dominated by increasing *P/P.* Montane-subalpine shrubs simultaneously decline.	**MAT:** Between 14.4–14.5°C. **RF:** Declines to 14.8, rises to 16.3°C.	Increasing podocarp-hardwood taxa, dominated by increasing *P/P.* Largely declining montane-subalpine shrubs.	**MAT:** Between 7.1–7.9 **PLS:** Between 6.7–7.9°C
NZce-3	**13.74–12.55**	Transitional between increasing herbs, montane-subalpine shrubs and podocarp-hardwood taxa.	**MAT:** Increases to 15.4°C **RF:** Between 14.5–15.7°C	Increasing montane-subalpine shrub taxa followed by increasing podocarp-hardwood taxa.	**MAT:** Declining from ~8–6.8°C **PLS:** Decling from ~8–7°C
NZce-4	**15.6–13.74**	Decreasing *P/P and* increasing *D. cupressinum.* A late increase of montane-subalpine shrubs.	**MAT:** Declines to 14.1-14.8°C. **RF:** Declines to 13.4°C, rises to 15.2°C.	Increasing podocarp-hardwood taxa, with decreasing montane-subalpine shrubs and Poaceae which reverses at the end of Nzce-4.	**MAT:** Between 7.4–9.6°C **PLS:** Between 7.5–9.5°C
NZce-5	**18–15.6**	Increasing podocarp-hardwood taxa, decreasing *Coprosma* and Poaceae.	**MAT:** Increases from 11–15.3°C. **RF:** Increases from 11.5–15.3°C	Increasing proportions of montane-subalpine shrubs, particlarily *Myrsine,* with decreasing Poaceae.	**MAT:** Increases from 7.7–7.9°C **PLS:** Increases from 6.9–8.3°C

Note: *Podocarpus/Prumnopitys* is abbreviated to *(P/P),* and *Dacrydium cupressinum* abbreviated to *D. cupressinum.*

MD06-2991

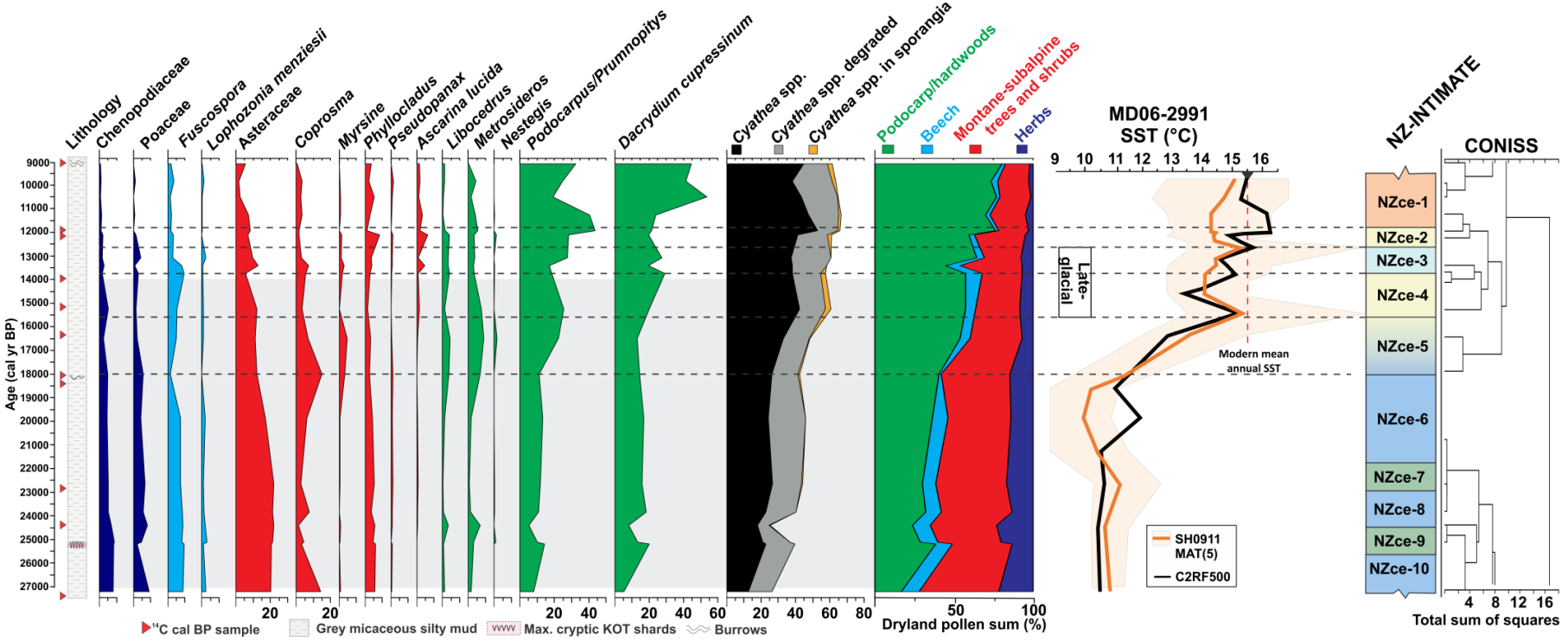

Fig. 4.5: Partial percentage pollen diagram showing the prominent dryland pollen taxa for MD06-2991 over 27-9 cal ka BP. Left-right; core stratigraphy and location of the calibrated AMS ^{14}C ages (red triangles) and the position of the maximum concentration of KOT glass shards. Colour coded individual and grouped dryland pollen taxa and *Cyathea* fern spores. SH0911C2 MAT (five nearest analogues and uncertainty) and Random Forest (C2RF500) based sea surface temperature (SST) estimates for MD06-2991 follow the pollen diagram, with the modern (from 1981-2010) mean annual SST (15.5°C) outlined. The NZ INTIMATE climate event stratigraphy from Barrell et al. (2013) is shown with the colour scheme schematically illustrating characteristic atmospheric temperatures (orange = warmest, blue = coldest). Black dashed lines for each subdivision are shown across the diagram, with MIS 2 displayed in grey shading (Lisiecki and Raymo, 2005). The CONISS zonation developed for the MD06-2991 dryland pollen taxa and tree fern spores broadly matches zonations to that defined in the NZ-CES.

Okarito Bog

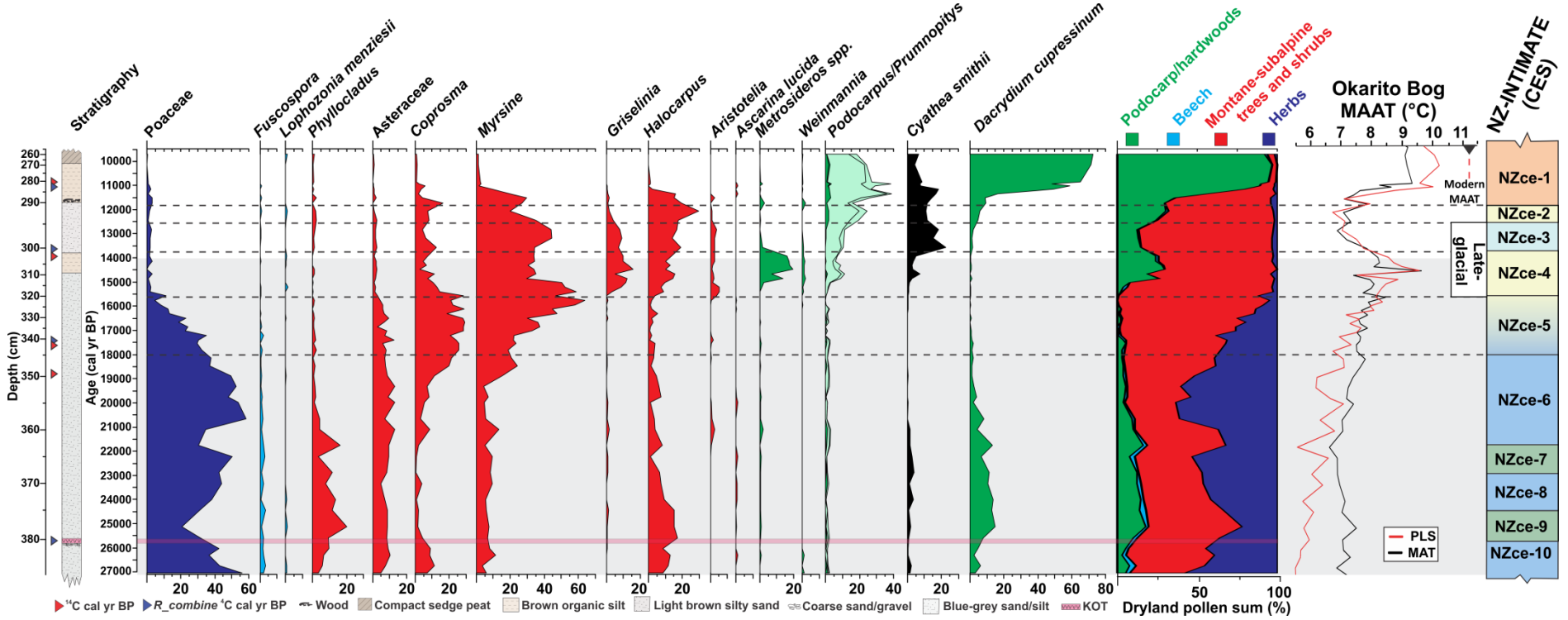

Fig. 4.6: Partial percentage pollen diagram showing the prominent dryland pollen taxa for Okarito Bog over 27-9.5 cal ka BP. Left-right, core stratigraphy and location of the calibrated AMS ^{14}C ages (red triangles) and KOT. Colour coded individual and grouped dryland pollen taxa and *Cyathea* fern spores. Note *Podocarpus*/*Prumnopitys* are grouped with *Podocarpus* and podocarpoid (green), while *Prumnopitys ferruginea* and *Prumnopitys taxifolia* (both light green) are differentiated by a black line. MAT (black line) and PLS-based (red line) estimates of MAAT are displayed with the modern mean MAAT of 11.3°C for Okarito indicated by a black triangle and red dashed line (Whitehead et al., 2002). The NZ INTIMATE CES from Barrell et al. (2013) is depicted with the colour scheme schematically illustrating characteristic atmospheric temperatures (orange = warmest, blue = coldest). Black dashed lines for each subdivision are shown across the diagram, with MIS 2 displayed in grey shading behind the pollen diagram (Lisiecki and Raymo, 2005).

Termination II (158-98 ka)

MIS 6c-6b (158–~140.5 ka) RPAZ 2a-2b

Podocarp-hardwood taxa and *Cyathea* tree fern spores increase at MD06-2991 over the transition from MIS 6c-6b, with the highest tall tree taxa attained for both substages at 153 ka. Basal sediment at Okarito Bog are assigned that age, although the equivalent taxa occur in lower proportions, and precede the age of 148 ka previously assigned to this horizon via the palynostratigraphic correlation to TAN0513-14 by ~6 kyr (Suppl. Fig. 4.17). Proportions of *Fuscospora* greatly contrast between Okarito Bog (~40-55%) and MD06-2991 (~10%) for this interval.

Herb pollen abundances increase over two steps while *Cyathea* tree fern spores overall decrease during MIS 6b at MD06-2991, with comparable changes at Okarito Bog (Table 4.4). The initial inflection in herb pollen at 149 ka is accompanied by a change in lithology from olive-grey to grey micaceous silt at MD06-2991. Similarly, a lithological change from laminated blue-grey sandy silt to uniform blue grey silt occurs at ~941.5 cm composite core depth at Okarito Bog (core 913), and is assigned to PCP 20 (~149 ka). MAATs reach their highest values for the period assigned to MIS 6b between herb advances (~RPAZ 2a/2b boundary), where taxa which are significantly correlated to warmer temperatures in the New Zealand pollen database occur in trace amounts (e.g. *D. cupressinum*, *Nestegis*, *Ascarina lucida*). SSTs from the nearby MD06-2986 record peak in the upper part of RPAZ-2a and then decline towards the culmination of RPAZ-2b/MIS 6b (Hayward et al., 2012).

MIS 6a (140.5–130 ka) RPAZ 2c-2d

Tall tree taxa reach their lowest proportions over the entire 160 kyr MD06-2991 record at the base of RPAZ-2c/MIS 6a at 139 ka. Poaceae and the montane-subalpine shrub Asteraceae simultaneously rise in both MD06-2991 and Okarito Bog, and the latter attains the highest proportions at MD06-2991. These taxa are significantly correlated to cool mean annual temperatures in the New Zealand pollen database (Wilmshurst et al., 2007), and consequently display the lowest MAATs in the lower part of the Okarito Bog record until MIS 4-2 (PLS based). Reconstructions of SST from MD06-2991 also reach their lowest values in RPAZ-2c. Tall tree taxa and SSTs simultaneously increase over the remainder of RPAZ-2c and 2d at MD06-2991, but are twice briefly punctuated by advances in montane-subalpine shrub taxa and declining SSTs from ~137-136 ka and 134-133.5 ka. This corresponding interval at Okarito Bog has been sampled at low resolution, although the

timing of increasing montane-subalpine shrubs, in particular increases in *Coprosma* and *Myrsine*, and rising MAATs can be defined between 139.3-132.5 ka.

A distinctive step-wise progression of arboreal pollen defines the onset of RPAZ-2d in both pollen profiles, with the end of the zone synchronous with the MIS 6-5 termination boundary (Fig. 4.7-4.8). Rising *Coprosma* and *Myrsine* give way to a brief dominance of *Griselinia* and tree ferns (*Cyathea* spp., *Dicksonia squarrosa*), which are followed by an increase in a variety of podocarp-hardwood taxa. The succession revealed in the pollen spectra is synchronous with increasing SSTs, where the highest relative abundance of *Podocarpus/Prumnopitys* and *Cyathea* for the entire MD06-2991 record occurs at 131 ka when SSTs are within 0.5°C of the modern environment. This complementary rise in SST and *Podocarpus/Prumnopitys* taxa is analogous to that which occurs during the early Holocene NZce-2-1.

MIS 5e (130–116 ka) RPAZ 2e-2g

The last interglacial (MIS 5e) is categorized into three regional pollen assemblage zones (2e-2g). The first, RPAZ-2e, is initially characterised by the greatest relative abundance of *Dacrycarpus dacrydioides* in both profiles, with those reflected at Okarito Bog (71%) far exceeding those at MD06-2991 (5%). This prominent rise is responsible for the greatest increase in PLS-based MAAT since the onset of the Okarito Bog record reaching 10.3°C at 129.5 ka, exceeding early Holocene estimates (~10°C). A brief ~1.5-2 kyr resurgence in montane-subalpine shrubs (*Phyllocladus* and *Halocarpus*) occurs in the upper part of RPAZ-2e and corresponds with an MAAT decline of 1.5-2°C, and is similar to that displayed during mid NZce-4 to 3 of T-I (*Coprosma, Myrsine, Asteraceae, Ascarina lucida*). *Dacrydium cupressinum* rises at the culmination of RPAZ-2e in MD06-2991 and Okarito Bog, with the mid-point of this rise occurring 3.6 kyr after the initial dominance of *Podocarpus/Prumnopitys* (defined by the primary peak at 131 ka). This exceeds the equivalent successional lag calculated for T-I from the same two taxa (1.1 cal kyr BP), but is similar to that which occurs between the early dominance of podocarp-hardwoods during NZce-4 and 2 (~3.8 kyr).

The notable escalation in *D. cupressinum* values, characteristic of RPAZ-2f, occur as modern mean annual SSTs at MD06-2991 are surpassed by 0.5°C. The mid-point of rising *D. cupressinum* (127.4 ka) is synchronous with the highest SSTs (16.8–18°C) for the entire MD06-2991 record, occurring at the RPAZ-2e/2f boundary. Pollen taxa which have strong positive correlations with MAAT, namely *Ascarina lucida*, *Dodonaea viscosa*, *Nestegis* and *Dacrydium cupressinum*, occur in both records at this time. *D. cupressinum* values at Okarito

extend to ~80% in RPAZ 2f (and MIS 5e), and exceed previous low resolution MIS 5e values of ~62% and early Holocene values of 73% (Vandergoes et al., 2005; Newnham et al., 2007a). Maximum MAATs of ~0.5-1.5°C greater than the temperature estimates modelled for the pre anthropogenic period in the Okarito core are relatively synchronous with rising SST. These persist above the modern reconstructed estimates until ~123.5 ka, despite SSTs declining to modern mean annual values (Fig. 4.7-4.8). *D. cupressinum* rapidly declines at 122.8 ka in both MD06-2991 and Okarito Bog as montane-subalpine shrubs and herbs simultaneously increase. This defines the onset of RPAZ-2g and is paralleled by declining SST (MAT based) and MAAT estimates. Proportions of *D. cupressinum* steady between 122-117 ka at MD06-2991 (RPAZ-2g), while Okarito Bog values display a greater decline at the expense of montane-subalpine taxa. This is accompanied by the lowest MAATs for MIS 5e, which remain marginally higher than the coolest MIS 6 values. SST reconstructions contrast between 122-117 ka, with both estimates rising to modern values at 116 ka in the uppermost RPAZ-2g (MIS 5e). This is coeval with a short-lived increase in podocarp-hardwood proportions in both records and rising MAATs (PLS-based), with a rapid deposition of organic material at Okarito Bog of 18 cm/kyr.

MIS 5d (116–105 ka) RPAZ 2h

Podocarp-hardwood taxa decline over early-mid MIS 5d to their lowest proportions since MIS 6 at ~115 ka and 108 ka, as montane-subalpine shrubs increase at both sites. Nothofagaceae (*Fuscospora, Lophozonia menziesii*) is recorded in greater values at MD06-2991 in RPAZ-2h, and is succeeded by rising *Podocarpus/Prumnopitys* and then *D. cupressinum* abundance in the uppermost part of the stadial. SSTs similarly display a gradual decline over the stadial, with the lowest values since MIS 6 (<5°C below modern) occurring at ~109 ka. Random Forest-based SSTs rise to exceed modern values at the culmination of MIS 5d, with a concomitant rise in MAAT.

MIS 5c (105–98 ka) RPAZ 2i

In both MD06-2991 and Okarito Bog, pollen of podocarp-hardwoods and reconstruction of MAATs attain their greatest values for MIS 5c early in the interstadial at 104 kyr (RPAZ-2i). These proportions and the MAAT values are lower than those of MIS 5e (RPAZ-2f). Podocarp-hardwoods decline over the remainder of the interstadial in both profiles, as additional vegetation categories of montane-subalpine shrubs and beech increase, with a concomitant decline in SST and MAAT.

Table 4.4: Comparison between vegetation changes recorded at MD06-2991 and Okarito Bog, and their respective estimates of SST and MAAT.

			MD06-2991			Okarito Bog	
RPAZ	**MIS**	**Age range (kyr)**	**Tie Points**	**Vegetetion succession**	**SST estimates**	**Vegetetion succession**	**Air temperature estimates (MAAT)**
RPAZ-2i	**5c**	**105–98**	**2-1**	*D. cupressinum* and *Cyathea* fern spores increase until 104.2 ka, and decline as montane-subalpine shrubs, Nothofagaceae and herbs increase.	**MAT:** Between 14–14.4°C. **RF:** Decreasing from 15.7–14.5°C.	*D. cupressinum* and *Cyathea* fern spores increase at the beginning of the zone, and decline with increasing montane-subalpine shrubs Nothofagaceae and herb pollen.	**MAT and PLS:** Increases to 9°C, declines to ~7.6°C.
RPAZ-2h	**5d**	**116–105**	**5-3**	Declining *D. cupressinum,* with increasing montane-subalpine shrubs (Asteraceae, *Coprosma, Phyllocladus*) and Nothofagaceae. These taxa decline after 108 ka as podocarp-hardwoods increase.	**MAT:** Between 15.1–11.5°C. **RF:** Between 15.6–10.6°C.	Declining *D. cupressinum,* with increasing montane-subalpine shrubs (Asteraceae, *Coprosma, Phyllocladus)* . These taxa decline after 108 ka as podocarp-hardwoods increase.	**MAT:** Increases to 8.1°C. **PLS:** Declines to 6.6°C then increases to 8.3°C.
RPAZ-2g	**5e**	**122.8–116**	**8-6**	*D. cupressinum* declines with a simultaneous increase in Asteraceae, *Coprosma, Phyllocladus,* Poaceae, *Fuscospora* and the hardwoods of *Libocedrus* and *Metrosideros. D. cupressinum* increases at 118 ka.	Increases from 14.8°C in both reconstructions at 122.8 ka. **MAT:** Between 14.2–15.5°C . **RF:** Highest 16.2°C.	*D. cupressinum* declines with a simultaneous increase in *Halocarpus, Phyllocladus,* and the hardwoods of *Libocedrus, Metrosideros. D. cupressinum* increases at 118 ka.	**MAT:** Between 7.2–8.5°C. **PLS:** Between 6.2–7.8°C.
RPAZ-2f	**5e**	**127.4–122.8**	**11-8**	*D. cupressinum* steadily rises to attain the highest proportions in the entire record. *Ascarina lucida, Nestegis* and *Phyllocladus* are present with decreasing Poaceae and *Coprosma.*	**MAT:** Declines to 14.7 before rising to 15.2°C (124.1 ka). **RF:** Declines to 15.2°C before rising to 15.8°C (124.1 ka).	*D. cupressinum* steadily rises to attain the highest proportions in the entire record. *Ascarina lucida, Quintinia, Phyllocladus,* and *Nestegis* are present with decreasing *Coprosma* and low Poaceae.	**MAT:** Between 8.5–10.1°C. **PLS:** Increase to 10.8°C, declines to ~8.2°C.
RPAZ-2e	**5e**	**130–127.4**	**13-11**	*Phyllocladus* increases, followed by increases in *D. cupressinum* and *Metrosideros* at the expense of declining *P/P.*	**MAT:** Increases from 14.5–18°C. **RF:** Increases from 15.5–16.8°C.	*Dacrycarpus dacydioides* declines with a resurgence in *Myrsine, Phllocladus* and *Quintinia. D. cupressinum* and *Metrosideros* similarily increase.	**MAT:** Declines from 9.2–8.2°C **PLS:** Declines from 10.3–8.2°C
RPAZ-2d	**6a**	**132.7–130**	**15-14**	Poaceae and the montane-subalpine shrubs (*Coprosma, Myrsine)* decline. A concomitant increase is reflected in Cyathea tree ferns, *P/P, Metrosideros, Dacrycarpus dacrydioides,* and *D. cupressinum.*	**MAT:** Between 11.1–15°C. **RF:** Increases from 13.2–15.5°C.	Poaceae and montane-subalpine shrubs (*Coprosma, Myrsine)* decline. A step-wise increase occurs in *Griselinia* , tree ferns, *P/P* , *Metrosideros* , *Elaeocarpus* , *Weinmannia* , and *Dacrycarpus dacydioides* .	**MAT:** Increases from 8–9.6°C. **PLS:** Increases from 8–8.8°C
RPAZ-2c	**6a**	**140.8–132.7**	**17-15**	Initial increase followed by a gradual decline in Poaceae and Asteraceae. Gradual increase in montane-subalpine shrubs (*Coprosma, Myrisne),* podocarp-hardwoods and tree fern spores.	**MAT:** Between 10–11.7°C. **RF:** Increases from 10.5–13.2°C.	Initial increase followed by a gradual decline in Poaceae and Asteraceae. Gradual increase in montane-subalpine shrubs (*Coprosma, Myrisne).*	**MAT:** Increases from 7.5–8°C. **PLS:** Increases from 6.1–8°C
RPAZ-2b	**6b**	**144.7–140.8**	**19-18**	Podocarp-harwood taxa declines, particularily *D. cupressinum* , while Poaceae simultaneously increases.	**MD06-2986: MAT:** Declines to 10.5 °C at 141.8 kyr	Increasing proportions of Poaceae and Asteraceae with declining *Fuscospora* .	**MAT:** Declines from 8.3-7.3°C. **PLS:** Declines from 7.7-6.1°C
RPAZ-2a	**6c-6b**	**158–144.7**	**21-19**	Increasing tall tree taxa of *D. cupressinum, Libocedrus* , *Cyathea* tree ferns, with decreasing Asteraceae between 153-148.8 kyr. A respective decline and increase occurs in both until 144.7 ka.	**MD06-2986: MAT:** Increases from 10.9–13.1°C, followed by a decline to 11.2°C.	*Cyathea smithii,* podocarp-hardwood and herb taxa are persistent until 148.8 ka, with high *Fuscospora* recorded. Poaceae and Asteraceae rapidly decline from 147.9 ka.	**MAT:** Between 7.5–8.3°C. **PLS:** Between 6.1–7.7°C

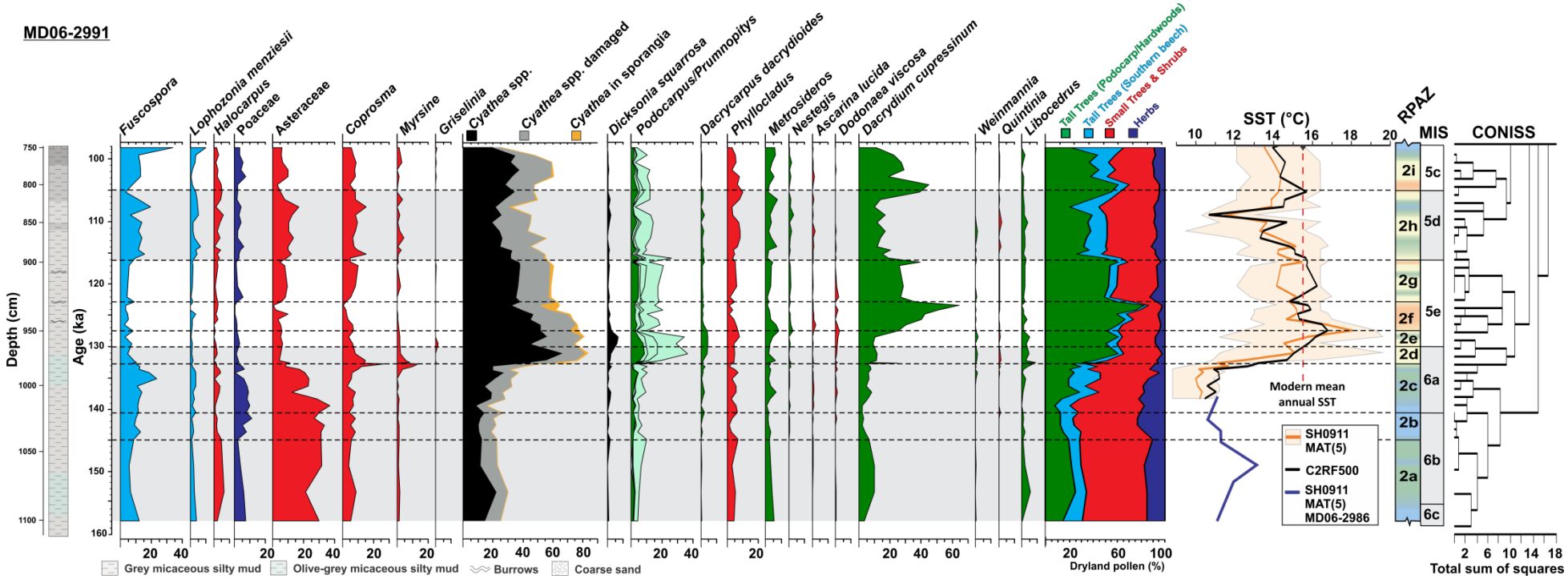

Fig. 4.7: Partial percentage pollen diagram showing the prominent dryland pollen taxa for T-II to MIS 5c at MD06-2991. Colour-coded individual and grouped dryland pollen (excl. spores) taxa and *Cyathea* fern spores. *Podocarpus*/*Prumnopitys* are grouped with *Podocarpus* (green) and undifferentiated *Podocarpus*/*Prumnopitys* (light green), while *Prumnopitys ferruginea* and *Prumnopitys taxifolia* (both light green) are differentiated by a black line. Note the distinctive succession between the *Fuscospora* peak at 144.7 ka, through grassland-shrub taxa, tree fern spores and tall tree taxa as the termination progresses. SH0911C2 MAT (five most similar training set faunas and accuracy) and Random Forest (C2RF500) based SSTs for MD06-2991 follow the pollen diagram, with the modern mean annual SST (15.5°C) for MD06-2991 (1981-2010). MAT-based SSTs for the interval 158-137 kyr are provided from the nearby MD06-2986 record. Regional pollen assemblage zones (RPAZ 2a–2i) aided by constrained cluster analysis (CONISS) are defined. The colour scheme schematically illustrates characteristic changes in regional atmospheric temperatures (orange = warmest, blue = coldest), and follows that produced for the NZ-CES over the LGIT by Barrell et al. (2013). Glacial and stadial boundaries (MIS 6 and 5d) are displayed in grey shading and black dashed lines (Lisiecki and Raymo, 2005, with large >30% increases in the proportion of *Dacrydium cupressinum* pollen occurring during MIS 5e and 5c.

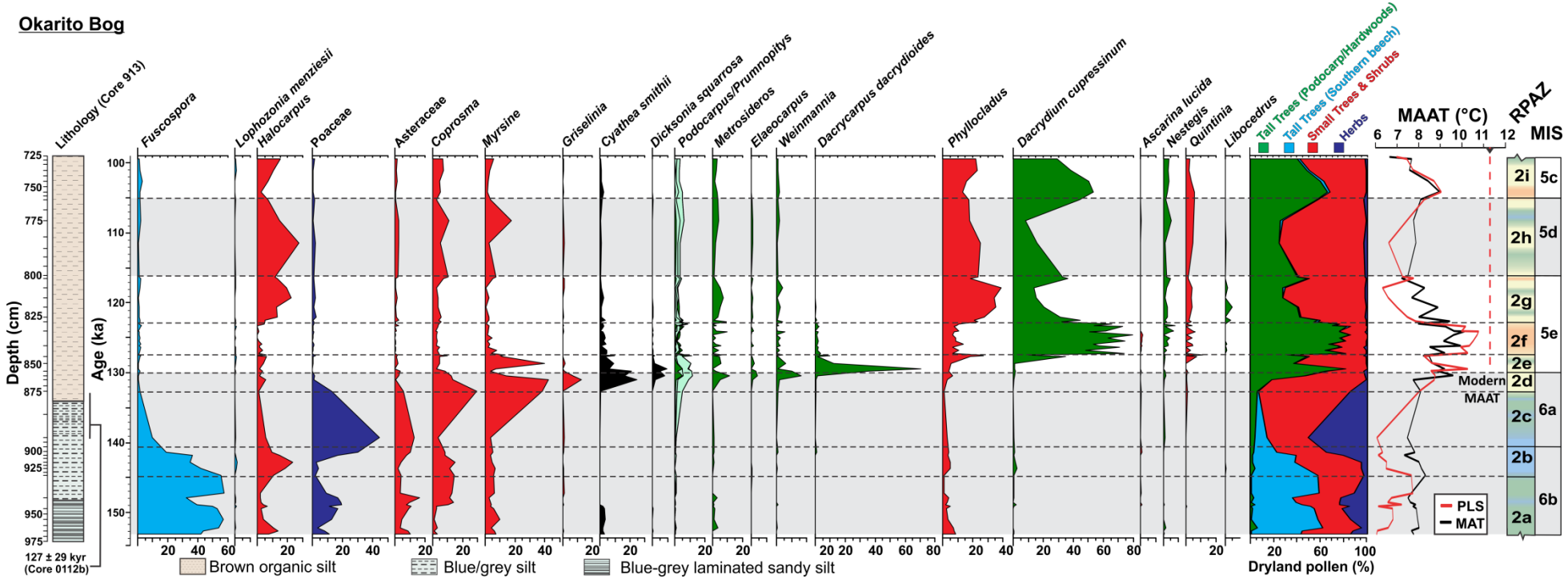

Fig. 4.8: Partial percentage pollen diagram showing the prominent dryland pollen taxa for T-II to MIS 5c at Okarito Bog (aligned to the MD06-2991 chronology). Left-right; the Okarito Bog core stratigraphy from core 913 and associated pollen analysis, with the position of an independent derived pooled weighted mean IRSL age of 127 ± 29 kyr (1σ) from core 0112b (Vandergoes et al., 2005; Newnham et al., 2007a). As for MD-2991, note the distinctive succession from the *Fuscospora* peak at 144.7 ka (143.7–147.3, 95% HPDF), through grassland-shrub taxa, tree fern spores and tall tree taxa as the termination progresses. *Podocarpus*/*Prumnopitys* are displayed grouped, although their respective relative percentages are distinguished as *Podocarpus* and podocarpoid (green), *Prumnopitys ferruginea* and *Prumnopitys taxifolia* (light green with line separator). Past MAAT estimates (MAT and PLS) are displayed with the modern MAAT of 11.3°C for Okarito (Whitehead et al., 2002) indicated by a black triangle and red line. Regional pollen assemblage zones (RPAZ) are depicted where the colour scheme schematically illustrates characteristic changes in regional atmospheric temperatures (orange = warmest, blue = coldest). Glacial and stadial boundaries (MIS 6 and 5d) are displayed in grey shading and black dashed lines (Lisiecki and Raymo, 2005, with large >30% increases in the proportion of *Dacrydium cupressinum* pollen occurring during MIS 5e and 5c. The complete pollen diagram and mean MAATs for the entire Okarito Bog record (153-0 ka) is displayed in Suppl. Fig. 4.18.

4.4 Discussion

MD06-2991 is the first integrated continuous record of regional vegetation and SST change developed from the East Tasman Sea. This terrestrial palynomorph record in a marine setting provides unequivocal evidence for a closely coupled ocean-atmosphere system from southwestern New Zealand for the last two G-I cycles, consequently circumventing potential chronological uncertainties which may arise when comparing discrete land-sea paleoclimate records. Inferences about the timing and magnitude of ocean and atmospheric (vegetation) changes are based on the best constrained age model yet developed in the Southern Hemisphere mid-high latitudes for a long paired marine/terrestrial record from MD06-2991 and Okarito Bog. Uncertainties are addressed for 1) the alignment to the LR04 $\delta^{18}O$ reference stack (Lisiecki and Raymo, 2005); 2) the stack itself via correlation of isotope profiles from U/Th dated Chinese speleothems (Caballero-Gill et al., 2012a); 3) the residence time between pollen production and delivery to the East Tasman Sea over the Last Glacial-Interglacial Transition; and 4) the transfer of the MD06-2991 age model to the Okarito Bog sequence prior to ^{14}C age control.

The pattern of vegetation changes recorded from south-west New Zealand land-sea pollen sequences are broadly similar for the last two G-I transitions, with both environments essentially recording the same regional pollen rain. Across the G-I transition, both the marine and terrestrial records indicate a progressive step-wise development from a shrubland-grassland mosaic, into a mix of shrubs and conifers, then finally into a landscape dominated by tall conifer trees as the termination progresses to completion. These similarities in vegetation change occur despite that T-II being characterised by a higher rate and variation (5% higher) of insolation forcing than T-I as a result of differences in orbital configuration (Berger, 1978; Berger and Loutre, 1997; Laskar et al., 2004), which ultimately altered the rate and amplitude of temperature change, CO_2 and sea level rise (Clark et al., 2009; Landais et al., 2015). For example, ~70% of the G-I sea-level change over the Penultimate Glacial-Interglacial Transition occurred during HS-11 within MIS 6a (135 ± 1 to 130 ± 2 ka, 2σ; Grant et al., 2014; Marino et al., 2015), while 75% of the sea level rise followed HS-1 during the Last Glacial-Interglacial Transition (Carlson and Clark, 2012). The timing and magnitude of vegetation changes in MD06-2991 and Okarito Bog are assessed relative to these climate drivers for TI and T-II in sections 4.4.4–4.4.7.

4.4.1 Palynomorph taphonomy, representivity, and paleovegetation reconstruction

The similarity between land-sea records is attributed to the short source-to-sink pathway of palynomorphs, their negligible residence time, high rates of sediment delivery, and relatively minor variation in the size of the palynomorph collection area over a G-I cycle. Importantly, it enables the alignment of the pre ^{14}C interval of the Okarito Bog profile with the MD06-2991 chronology, and provides some confidence for interpreting preceding interglacials which have no adjacent terrestrial equivalents (see Chapter 5). Nevertheless, marine-terrestrial comparisons must take into account the various taphonomic processes (discussed in Chapter 2 and 3) that have distorted the relationship between pollen representivity and abundance of the parent plant compared to traditional terrestrial lake and bog profiles (e.g. Moss et al., 2005; Wilmshurst and McGlone, 2005). This makes the standard method of quantitative climate reconstruction of limited utility in marine pollen records. Consequently, the combined palynomorph records developed from MD06-2991 and Okarito Bog provide a basis for precise assessment of quantitative land-sea estimates of temperature change over the last 160 kyr.

Key differences between both pollen profiles are outlined as follows.

1) Tall tree pollen (podocarp-hardwood and southern beech) are over-represented at MD06-2991 through MIS 6, 4 and 2 compared to onshore equivalents (Suppl. Fig. 4.15 and 4.18). This preservation bias is recognised in other New Zealand sequences where marine sediments deposited over the last glacial cycle are matched to proximal terrestrial counterparts (Heusser and van de Geer, 1994; Wright et al., 1995; Wilmshurst et al., 1999; McGlone, 2001; Carter et al., 2002; Mildenhall, 2003; Mildenhall et al., 2004; Mildenhall and Orpin, 2010; Ryan et al., 2012). The selective yet important preservation of bisaccate gymnosperm pollen at MD06-2991 may result from their superior hydrodynamic performance, meaning that they stay afloat longer than other pollen morphologies and are thus increasingly dominant in samples further offshore (Chaloner and Muir, 1968; Mudie, 1982; Smirnov et al., 1996; Traverse, 2007; Crouch et al., 2010; Luo et al., 2014). Alternatively, enhanced tall tree pollen at MD06-2991 may result from the survival of forest refugia along the coastal fringe seaward of Westland such as that considered for glacial maxima over the Late Pleistocene (Fig. 4.2; Leschen and Michaux, 2005; Leschen et al., 2008; Hill et al., 2009; Marske et al., 2009; Marske et al., 2011; Marshall et al., 2012; Marske et al., 2012).

2) Unfavourable conditions likely prevented the continual persistence of pure stands of podocarp-hardwoods at Okarito during lowstand sea-level, with the site at ~200 masl,

proximal to ice cover, and exposed to cold air drainage (Wardle, 1979; Newnham et al., 2007a). Nonetheless, brief expansions of tall trees are seen in the Okarito record over the LGM. These are considered to reflect a response of the local vegetation to climate amelioration over decades to centuries, and attest to the survival of remnant stands of podocarp trees in the region (Newnham et al., 2013; Vandergoes et al., 2013a). Despite these differences, reconstructed vegetation changes from these land and sea records are consistent with a shrubland-grassland mosaic, with rare conifers in inland areas and patches of beech likely persisting either side of the contemporary Biotic Gap (Norris, 1978; Moar, 1980; McGlone et al., 2010c).

3) Southern beech (*Fuscospora*) is reflected in high numbers in modern and fossil marine sediments adjacent to Westland, despite the region being devoid of these trees. This may result from the redistribution of palynomorphs by coast-parallel ocean currents either side of the central Westland 'Biotic Gap' (Fig. 4.2; Ryan et al., 2012). Their low representivity in modern terrestrial surface samples is due to the absence of these trees in this zone (Moar, 1970). High proportions of beech pollen in pre last interglacial horizons (Newnham et al., 2007a; Ryan et al., 2012), coupled with genetic studies of modern fungus beetles (Leschen et al., 2008), suggest that the trees may have occupied this region prior to that time. Nonetheless, its reduction in pollen profiles from southwestern New Zealand following T-II, and to a lesser degree T-I, are consistent with a progressive outpacing and rapid expansion of competitive podocarp-hardwood species during phases of climate amelioration (Cockayne, 1926; Willett, 1950; Wardle, 1963; Burrows, 1965; Baylis, 1980; McGlone, 1985; McGlone et al., 1996; Trewick and Wallis, 2001; Newnham et al., 2007a).

4) Differences in palynomorph taphonomy exhibited between these land and sea profiles is additionally influenced by the durability of grains during transport until their final resting place. Less durable grains (i.e., Poaceae), may become degraded during fluvial transport to the marine realm (Mudie, 1982). Robust grains such as Asteraceae and tree fern spores, which can be readily washed into streams and rivers by surface runoff over a wide altitudinal range (Wilmshurst et al., 1999; McGlone, 2001; Moar et al., 2011), are represented in greater numbers at MD06-2991. In contrast, relatively small numbers of these grains occur at Okarito, and together with the geomorphology of the site, suggest the basin received little fluvial input sourced from high alpine regions.

4.4.2 The onset of Okarito Bog sedimentation

The lower inorganic laminated silts retrieved from the base of Okarito Bog are proposed to have been rapidly deposited in an ice-scoured depression in front of a retreating glacier soon after deposition (Newnham et al., 2007a). The sediments were tentatively assigned a penultimate glacial age via an independent pooled weighted mean infrared stimulated luminescence (IRSL) age of 127 ± 30 ka obtained ~1 m up core (Vandergoes et al., 2005). Constraining the basal Okarito strata via palynostratigraphic core correlation to East Tasman Sea records is problematic prior to ~139 ka, where the abundance of *Fuscospora* pollen is mismatched between the two records, and far greater proportions are recognised onshore (Ryan et al., 2012).

In this study, the alignment of palynomorph taxa from MD06-2991 to Okarito Bog constrains the basal age of sediment deposition to 153 ka, extending previous estimates for the age of this sediment via correlation to TAN0513-14 by Ryan et al. (2012) by ~6 kyr. Under this scenario, the deposition of sediment into the Okarito basin commenced during a mild period of less cold climate (interstadial) in the SH during MIS 6b. This would suggest that the moraine enclosing the site was emplaced during MIS 6c. Tall tree taxa expanded across the central South Island during this climate transition, as detected in the marine pollen records of MD06-2991 and DSDP Site 594 (Fig. 4.2; Heusser and van de Geer, 1994; Suppl. Fig. 4.19). This commenced as SSTs in the surrounding and Southern Ocean rose (Pahnke et al., 2003; Pelejero et al., 2006; Barrows et al., 2007a; Hayward et al., 2008; Hayward et al., 2012), and coincides with a subdued warming and CO_2 rise in Antarctica (Jouzel et al., 2007; Bazin et al., 2013; Veres et al., 2013; Bereiter et al., 2015). Warming in the SH mid-high latitudes at this time is consistent with evidence for a weak bipolar temperature see-saw mechanism (Margari et al., 2014). NH ice sheet melt led to the deposition of IRD in the North Atlantic (McManus et al., 1999; Eynaud et al., 2007; Toucanne et al., 2009), generating the coldest SSTs in the NH mid-latitudes for the last 160 kyr (Martrat et al., 2007; Margari et al., 2014). These conditions may have facilitated the southward displacement of the Intertropical Convergence Zone and climatic boundaries, resulting in a strengthening of the westerly wind intensity and relative humidity similar to that proposed in Westland during Heinrich Events 1-6 over MIS 4-2 (Whittaker et al., 2011). Shifting wind patterns may have aerially transported *Fuscospora* pollen which is capable of long distance transport (Moar, 1970; Pocknall, 1978; Holt et al., 2010; Moar et al., 2011), from trees living adjacent to, within, or outside of the contemporary Biotic Gap along New Zealand's west coast over this period of environmental change (Newnham et al., 2007a). This would promote this taxon to appear

locally dominant in the open, relatively treeless landscape which is typical of glacial environments proximal to ice cover (McGlone et al., 1993).

An alternative hypothesis for the pre 139 ka section of Okarito Bog considers that the high proportions of *Fuscospora* represent deposition during the MIS 7 interglacial (Vandergoes, 18 Oct. 2015; pers. comm.). This interpretation is not inconsistent with previous vegetation reconstructions from the East Tasman Sea (Ryan et al., 2012). Estimates of MAAT for MIS 7 are several degrees lower than the following two interglacial stages, and are consistent with a cool MIS 7 derived from pollen and beetle records around New Zealand (Heusser and van de Geer, 1994; Bussell and Pillans, 1997; Marra et al., 2006). These opposing interpretations for the basal age of the sequence may be advanced by surface exposure dating of the moraine enclosing the bog, or by independently dating basal sediment at Okarito. Additional insights into the biogeography of southern beech in Westland may be improved by the re-examination of interglacial peat at Blue Spur Road in central Westland (Moar and Suggate, 1973; Moar, 1984), which contain high southern beech proportions and was previously assigned to the last interglacial and is now considered of ~MIS 7 age (Almond, 23 July 2011; pers. comm.). Whilst the methodology for tie-points assumes the first scenario, the existence of these two competing hypotheses prevents a detailed examination of the pre ~139 ka section at Okarito Bog.

4.4.3 Climate event stratigraphy and chronological uncertainty for MIS 6-5 from southwestern New Zealand

The alignment of measurements of $\delta^{18}O_{benthic}$ from MD06-2991 to the reference LR04 $\delta^{18}O_{benthic}$ stack revises a similar approach undertaken on $\delta^{18}O_{planktonic}$ measurements in this region (Ryan et al., 2012). Measurements of $\delta^{18}O_{planktonic}$ are considered more sensitive to SST variations and non-glacioeustatic sea water $\delta^{18}O$ from melt water input and local changes in precipitation (Govin et al., 2015). Warm episodes in southwestern New Zealand, as distinguished by maxima in *D. cupressinum* forest pollen and high MAATs, are coeval with depleted $\delta^{18}O_{benthic}$ measurements. These vary with NH ice volume minima (Lisiecki and Raymo, 2005), and hence were typically in phase climatically with northern summer insolation, consistent with previous studies in this region (Ryan et al., 2012). The five-fold subdivision for MIS 5 (130-71 ka) displayed in the pollen content of Westland sequences defines the local Kaihinu Interglacial (Suggate, 1990; Moar and Suggate, 1996). Williams et al. (2015) restrict this period to MIS 5e from 128-117 ka (Fig. 4.9), on the basis that reduced forest phases and glacier advance in Southern Alps during the MIS 5d and 5b stadials reflect

significant climate deterioration and thus cannot be considered as interglacial (Preusser et al., 2005; Sutherland et al., 2007; Ryan et al., 2012; Rother et al., 2014). The terminology of Williams et al. (2015) is adopted here for the MIS 5e, although evidence exists for cooling between 130-128 ka and 123-117.5 ka from MD06-2991 and Okarito Bog, and are labelled the LIG climate reversal and LIG stadial II, respectively.

The greatest uncertainties in the MD06-2991 chronology likely result from $\delta^{18}O$ variability between the Atlantic and the Pacific ocean basins, which are offset by ~1.6 kyr (2σ) respectively during T-II (Lisiecki and Raymo, 2009). Individual points of uncertainty in the LR04 stack are defined relative to key southwestern New Zealand vegetation-climate events in order to provide constraint (Fig. 4.9). Uncertainty for the T-II onset at 138.6 ± 1.6 kyr (2σ) was determined via alignment to a rapid increase of calcite $\delta^{18}O$ in the Sanbao Cave speleothem record (Wang et al., 2008; Cheng et al., 2009; Caballero-Gill et al., 2012a). This occurs at the midpoint between northern and southern summer insolation extrema (Schulz and Zeebe, 2006), and is consistent with an early ice retreat during melt water pulse-2A and North Atlantic cooling dated at 139 ±1 kyr (2σ) (c.f. Marino et al., 2015). Two phases of lowland podocarp-hardwood forest development occur over T-II. The first occurs between 139-133 ka and defines the T-II amelioration in MD06-2991 (Fig. 4.7), with the second occurring as ocean-atmosphere temperatures rapidly rose in southwestern New Zealand between 133-130 ka, and defines the Penultimate glacial mild episode. The latter is synchronous with the onset of the last interglacial as defined in the EDC ice core record by >-403‰ δD, and spans from ~132.5-116 ka (EPICA Community Members, 2004), preceding the last interglacial as defined in this region from Williams et al. (2015) and Ryan et al. (2012) by 4.5 kyr. The absolute age uncertainty of that period is~1.8 kyr (1σ), when placed on the most coherent ice and gas age timescale reference chronology, AICC2012 (Bazin et al., 2013; Veres et al., 2013; Govin et al., 2015). Warming in the SH mid-high latitudes over T-II is synchronous in southwestern New Zealand and Antarctic ice core records, while records from the North Atlantic display cooling over HS-11 (135 ± 1 to 130 ± 2 ka, 2σ; Grant et al., 2014), with the mid-point of sea level rise occurring at 133.6 ± 1 ka (2σ) during melt water pulse-2a (Marino et al., 2015).

The MIS 6-5 boundary is defined in the LR04 stack at 130 ka and has an associated age uncertainty of ± 1 kyr (2σ)(Fig. 4.9; Wang et al., 2008; Caballero-Gill et al., 2012a). This boundary is followed by an advance in shrub taxa in southwestern New Zealand which interrupts rising tall tree taxa and is inferred to represent a reduction in temperature and is

termed the early LIG climate reversal (~130-128 ka; spanning RPAZ-2e; Fig. 4.9). A ~5-6 kyr LIG thermal optimum follows this from ~128-122 ka and is consistent with the 'acme' of LIG values from the EDC ice core record between 129.4-120.3 ka as defined by Govin et al. (2015). The demise in thermophilous vegetation over southwestern New Zealand which follows this episode defines the LIG stadial II, and is consistent with more enriched $\delta^{18}O$ measurements in LR04 at 122 ka ± 1 ka (2σ) (Caballero-Gill et al., 2012a). The culmination of the LIG at 116 ka in the vegetation-climate event stratigraphy is consistent with that defined as the last glacial inception from the EDC ice core record (Bazin et al., 2013; Veres et al., 2013).

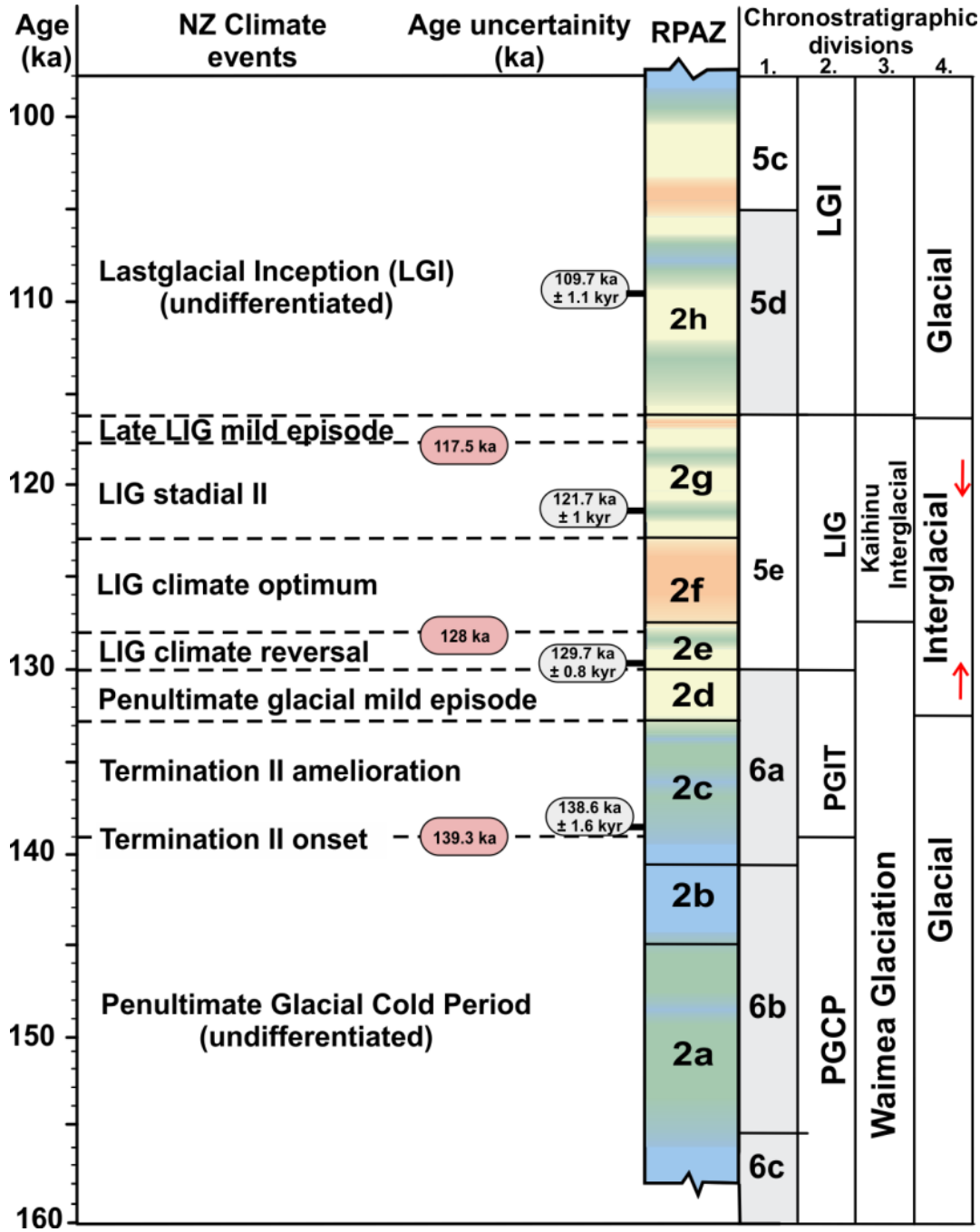

Fig. 4.9: Southwestern New Zealand climate event stratigraphy. Ages follow those of relative pollen assemblage zones (RPAZ), with additional datum in red circles. The colour scheme for the RPAZ schematically illustrates characteristic atmospheric temperatures (orange = warmest, blue = coldest). Chronostratigraphic schemes are: **1.** global marine-oxygen isotope scale (MIS) stages (Lisiecki and Raymo, 2005; Railsback et al., 2015), with independent age uncertainty estimates (2σ) for the LR04 stack in grey circles (Caballero-Gill et al., 2012a); **2.** Climate phases in southwestern New Zealand; **3.** NZ climate-based time-stratigraphic stages (Suggate, 1990; Moar and Suggate, 1996); **4.** Last interglacial (LIG) defined in EDC δD ice record/surface temperature record (Jouzel et al., 2007) as defined by EPICA Community Members (2004) to the AICC2012 timescale (Bazin et al., 2012; Veres et al., 2013), where arrows indicate the onset and demise of the LIG "acme" of Govin et al. (2015).

4.4.4 Radiocarbon chronology of Termination I in southwest New Zealand

The Last Termination amelioration (18-15.6 cal ka BP; NZce-5)

The contraction in grassland observed in these land and sea records from southwestern New Zealand reflects a change in atmospheric conditions during the last termination climate amelioration. Forest and shrubs advanced along the exposed Westland continental margin and piedmont from 17.8 ± 0.2 cal ka BP, and persisted until 15.6 cal ka BP (Fig. 4.10). Trees intolerant of dry air, drought and low rainfall, including *D. cupressinum*, *Weinmannia* and tree ferns at MD06-2991, slowly spread in the Westland lowlands far from the influence of ice. This is consistent with evidence for increasingly wetter conditions interpreted in Westland speleothem isotope profiles from 17 ka (Hellstrom et al., 1998; Whittaker et al., 2011). The upslope migration of vegetation zones corresponds to 1.5°C of warming at Okarito, and is consistent with that identified in biotic (pollen/chironomid) proxies within the SH mid-latitudes including elsewhere in New Zealand (Vandergoes et al., 2008; Barrell et al., 2013), Tasmania (Rees and Cwynar, 2010), and in southern South America (Fig. 4.1; Moreno et al., 2015).

In addition to the climate signature for T-I amelioration reflected in biotic proxies described above, those derived from past glacier positions across the Southern Alps highlight important although contrasting contributions to the style of mountain glacier retreat initiating ~18.7-17.4 cal ka BP, until the onset of the Lateglacial (NZce-4) at 15.6 cal ka BP (Sutherland et al., 2007; Putnam et al, 2013a, 2013b; Barrows et al., 2013; Rother et al., 2014; Kelley et al., 2014; Doughty et al., 2015). The first scenario is that glacier retreat occurred rapidly with an inferred warming of ~4°C (Fig 4.10; Putnam et al, 2013a, 2013b). The second scenario is that up to 70% of LGM ice survived until 15.8 ka (Rother et al., 2014), with lake calving influencing ice retreat dynamics in the first scenario. Despite these contrasting models, southwestern New Zealand profiles reveal that warming on land over NZce-5 (~18-15.6 ka) was synchronous with that of the adjacent ocean (~4°C), which may have been caused by a southwards migration of the position of the Subtropical Front from 42-44°S (Fig. 4.11; Pelejero et al., 2006; Barrows et al., 2007a, 2007b; Calvo et al., 2007; De Deckker et al., 2012; Hayward et al., 2012; Barrows et al., 2013; Bostock et al., 2013; 2015). This contrasts to cooler climate conditions revealed in the North Atlantic during Heinrich Stadial (HS) 1 from 17.8–14.7 cal ka BP (Bard et al., 2000; Cheng et al., 2009; Putnam et al., 2013a), and is consistent with the bipolar ocean-atmosphere temperature seesaw mechanism.

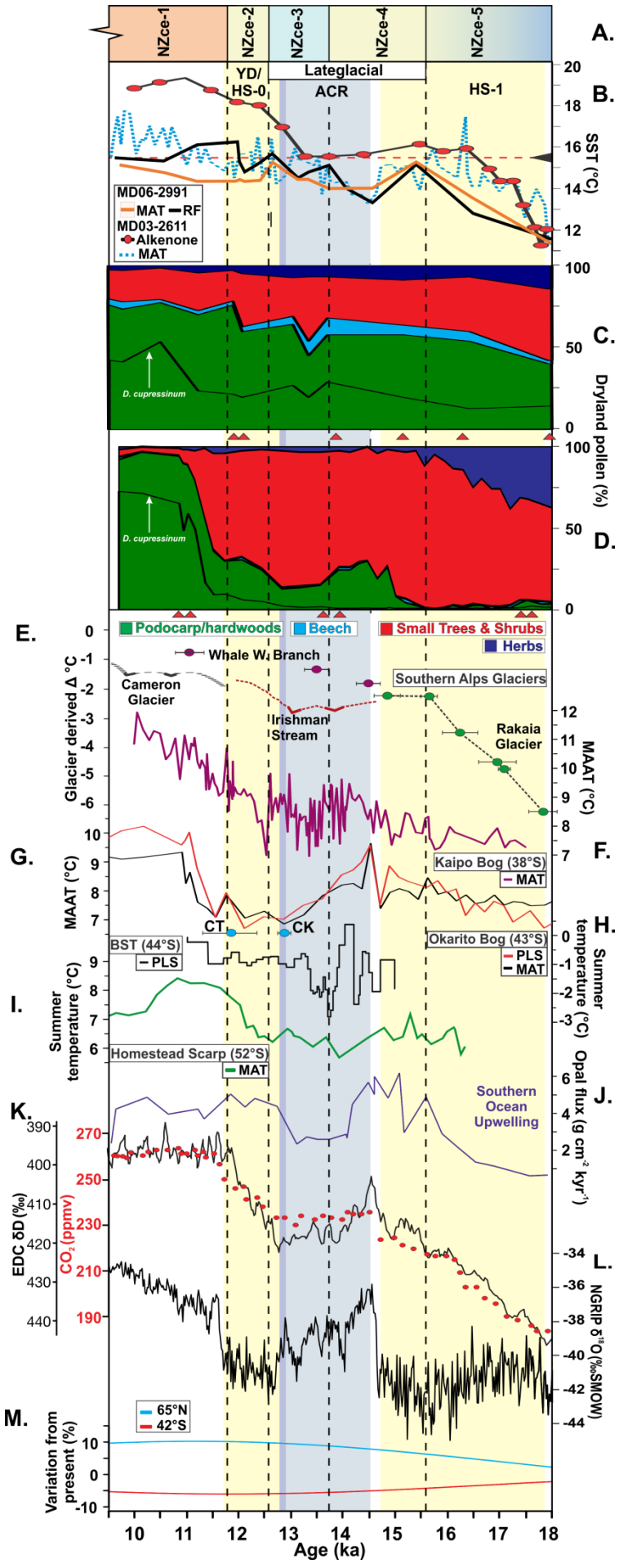
NZce-1
NZce-2
NZce-3
NZce-4
NZce-5
A.
Lateglacial
YD/
HS-0
ACR
HS-1
B.
SST (°C)
MD06-2991
MAT
RF
MD03-2611
Alkenone
MAT
C.
D. cupressinum
Dryland pollen (%)
D.
D. cupressinum
E.
Podocarp/hardwoods
Beech
Small Trees & Shrubs
Herbs
Whale W. Branch
Cameron Glacier
Southern Alps Glaciers
Irishman Stream
Rakaia Glacier
Glacier derived Δ °C
MAAT (°C)
F.
G.
MAAT (°C)
Kaipo Bog (38°S)
MAT
CT
CK
BST (44°S)
PLS
Okarito Bog (43°S)
PLS
MAT
H.
Summer temperature (°C)
I.
Summer temperature (°C)
Homestead Scarp (52°S)
MAT
Southern Ocean Upwelling
J.
Opal flux (g cm-2 kyr-1)
K.
EDC δD (‰)
CO2 (ppmv)
L.
NGRIP δ18O (‰SMOW)
M.
65°N
42°S
Variation from present (%)
Age (ka)

Fig. 4.10: Integration of Ice, Marine and Terrestrial (INTIMATE) records from 18-9.5 cal ka BP. Top to bottom; **A.** NZ-INTIMATE climate event stratigraphy (Barrell et al., 2013) including the Lateglacial period outlined by Lowe et al. (2013). The timing of HS-1, ACR and the Younger Dryas (YD)/HS-0 chronozones are displayed (Barker et al., 2009; Putnam et al., 2010b; Kaplan et al., 2013). **B.** foraminiferal MAT (orange), and RF (black)-based SST estimates from MD06-2991 compared with foraminiferal MAT and alkenone derived SST estimates from MD03-2611 (Calvo et al., 2007; De Deckker et al., 2012). Modern mean annual SST for MD06-2991 is indicated by red dashed line and black triangle (15.5°C), and is similar to that illustrated for the MD03-2611 site (Fig. 4.11). **C.** Cumulative dryland pollen diagram for MD06-2991. **D.** Cumulative dryland pollen diagram for Okarito Bog. The relative abundances of *D. cupressinum* are indicated (black line). Red triangles underlying each diagram represent the position of ^{14}C dates constraining each respective record. **E.** Right to left; glacier derived temperature change from eastern South Island locations including the Rakaia (green circles; Putnam et al., 2013a), west Whale Branch Stream (purple circles; Kaplan et al., 2013), Irishman Stream (red line, Kaplan et al., 2010; Doughty et al., 2013), and Cameron Glacier (black line, Putnam et al., 2012). Solid lines represent where age control is known, while dashed lines represent inferences. Reconstructed temperature estimates increasing plotted with increasing latitude south; **F.** Kaipo Bog weighted modern analogue technique annual air temperatures (MAAT) from Newnham et al. (2012) are aligned to the age model of Lowe et al. (2013); **G.** Okarito Bog (revised from Newnham et al., 2012) using the reconstructions of Wilmshurst et al. (2007); **H**. Reconstructed chironomid based temperature change (PLS) from Boundary Stream Tarn (BST, Vandergoes et al., 2008; Doughty et al., 2013); **I.** Pollen based summer temperature estimates from Homestead Bog from McGlone et al. (2010a). Re-calibrated ^{14}C ages (SHCal13; Hogg et al., 2013) of wood from CK (Canavans Knob) by Turney et al. (2007) and Cropp Till (CT) by Basher and McSaveney (1989) are illustrated (Supplementary Fig. 4.20). **J.** Southern Ocean upwelling signal (Anderson et al., 2009). **K.** CO_2 (Lourantou et al., 2010) and δD (Lemieux-Dudon et al., 2010) from EPICA Dome C (EDC). **L.** NGRIP $\delta^{18}O$ on AICC2012 timescale (Rasmussen et al., 2006; Veres et al., 2013). **M.** Summer insolation anomaly for 42°S (21 Dec., red) and 65°N (21 June, blue) (Laskar et al., 2004; Paillard et al., 1996).

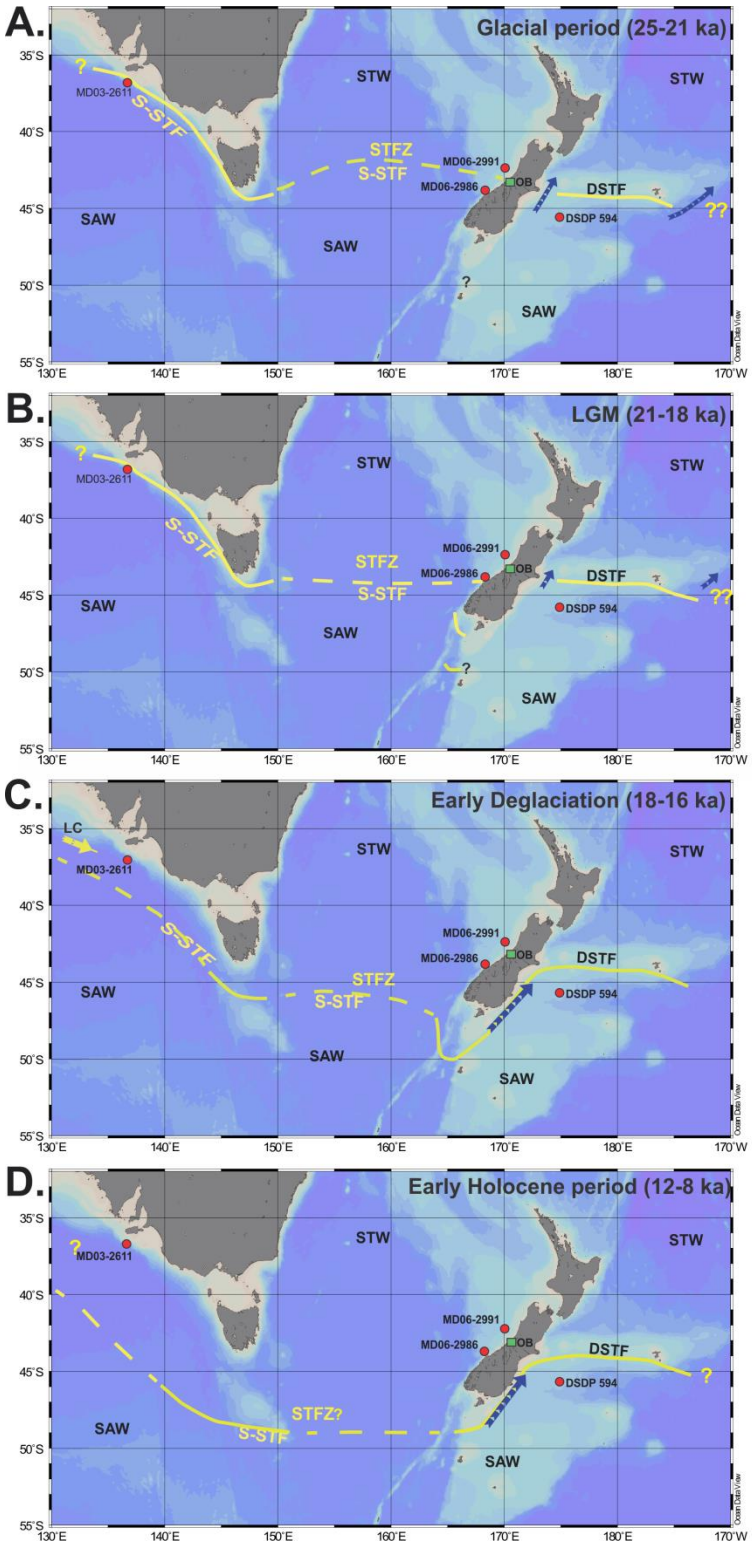

Fig. 4.11: Four reconstructions of the Southern Subtropical Front–S-STF (yellow line) and Dynamical Subtropical Front–DSTF for the southwest Pacific Ocean reproduced following that of Bostock et al. (2015) in Ocean Data View (Schlitzer, 2009). The dashed yellow line indicates regions where there are no cores to constrain the location of the S-STF. STW: Subtropical Water, SAW: Subantarctic Water, LC: Leeuwin Current. **A.** Glacial period (25-21 ka), **B.** LGM: Last Glacial Maximum (21–18 ka), **C.** early deglaciation (18–16 ka), **D.** early Holocene period (12–8 ka). Core locations discussed in this study are shown by red dots, with Okarito Bog (OB) outlined by a green square.

This process of events is consistent with rising boreal summer insolation intensity during T-I inducing a southward shift of the earth's thermal equator, the marine Intertropical Convergence Zone and the Southern Hemisphere westerly wind belt (Cheng et al., 2009; Denton et al., 2010; Whittaker et al., 2011). This disrupted the stratification of the Southern Ocean (Anderson et al., 2009), leading to upwelling and the outgassing of atmospheric CO_2 as reflected in the EDC ice core (Fig. 4.10), thus triggering further ice retreat in Antarctica and the SH mid-latitudes (Lemieux-Dudon et al., 2010; Parrenin et al., 2013). Whether these processes were amplified or driven by lengthened summers and shortening of winters in southern latitudes remains a topic open to debate (Huybers and Denton, 2008; De Deckker et al., 2012).

The Lateglacial period (15.6–12.5 cal ka BP; NZce4-2)

Regional vegetation-climate reconstructions from southwest New Zealand pollen records display wet and warm conditions during the Lateglacial mild episode (NZce-4), with wet and cooler than the present conditions during the succeeding Lateglacial cool episode (NZce-3) from ~13.7 ka. A similar pattern of vegetation-climate change is also recorded further north at Kaipo Bog, North Island, New Zealand (Lowe et al., 1999; Newnham and Lowe, 2000; Hajdas et al., 2006; Newnham et al., 2012; Barrell et al., 2013).

Tall tree podocarp-hardwoods, intolerant to low rainfall and cool temperatures, progressed up onto the Westland piedmont from 15.6 to 14.5 ka, with a reconstructed MAAT increase of 1.5°C over that period from Okarito Bog. Within dating uncertainties of ±0.5- ka (2σ) for both MD06-2991 and Okarito, this lags near modern surface temperatures in the Tasman Sea by at least 1.1 ka (Fig. 4.10; Calvo et al., 2007; De Deckker et al., 2012; Bostock et al., 2015). This arose at the time of the suggested "rapid demise" of Southern Alps glaciers after 15.8 ka (Rother et al., 2014), and enhanced moisture in Westland implied from speleothem isotope profiles (Whittaker et al., 2011). Modern temperatures are similarly reflected in western Tasmania (Rees and Cwynar, 2009), while in Antarctica, temperature, the atmospheric CO_2 content, and iceberg flux reach their Last Glacial-Interglacial Transition maxima (Clark et al., 2009; Lemieux-Dudson et al., 2010; Lourantou et al., 2010; Weber et al., 2014). Ocean-atmosphere warming over the Lateglacial mild episode is synchronous with the upper part of HS-1, and is consistent with the bipolar temperature seesaw mechanism.

Despite warming occurring near synchronously over New Zealand during the Lateglacial, there remains a distinct regional difference in the timing in the development of lowland

podocarp-hardwood forest between northern and southwestern New Zealand. Forest expansion precedes the deposition of the Rotorua Tephra (15.6 cal ka BP) in northern sites (Sandiford et al., 2001; 2003; Newnham et al., 2003; Sikes et al., 2013), with the tephra providing constraint for the onset of the Lateglacial mild episode (Barrell et al., 2013; Lowe et al., 2013). As such, southwestern New Zealand lowland forest growth trails northern sites by 1-2 kyr, and is greater than the uncertainty derived from comparison of different age models. Variables such as soil conditions, geographic barriers to landscape readjustment, in combination with climatic variables such as drought, wind intensity, frost, and seasonality likely suppressed the growth of these trees on the central Westland piedmont (McGlone et al 1988; Newnham et al., 1989; Moar et al., 1996; McGlone, 2001; Newnham et al., 2003).

Lateglacial cool period/Antarctic Cold Reversal (ACR)

Evidence for a cool Lateglacial episode in New Zealand pollen records is registered in some records (Turney et al., 2003; McGlone et al., 2004; Hajdas et al., 2006; Wilmshurst et al., 2007; McGlone et al., 2010a), but is absent or not easily recognisable in others (Singer et al., 1998; Sandiford et al., 2003; Turney et al., 2003; Alloway et al., 2007a). This may arise due to local site characteristics, or from latitudinal variations in climate, such as seasonality which may influence the extent to which the Antarctic pattern is registered (Sikes et al., 2013; Pedro et al., 2015). Newnham et al. (2012) quantify past land surface temperatures for records of vegetation change over New Zealand (Okarito, Kaipo, Pukaki) using the pollen calibration model of Wilmshurst et al. (2007) and suggest a latitudinal displacement may exist for the timing of ACR/Lateglacial cooling over the New Zealand archipelago, with its occurrence first reflected in the southern site of Okarito Bog. Lateglacial cooling is arguably best represented in southwestern New Zealand vegetation by a resurgence in montane-subalpine shrubs at Okarito Bog (Vandergoes and Fitzsimons, 2003; Newnham et al., 2007a). The site's large (~1 km) diameter and location on the lowland Westland piedmont, fortuitously distant from the influence of inflowing streams, potentially sourced up to 85% of the regional pollen rain and thus was better placed to capture this millennial scale climate fluctuation (Fig. 2.1; Jacobson and Bradshaw, 1981). An advance in montane-subalpine shrubs place between 14.5 ± 0.8 to 13 ± 1 cal ka BP, with a cooling of 3°C relative to present, and overlaps with the entire ACR chronozone ca. 14.6-12.8 cal ka BP (following Moreno et al., 2009; Putnam et al., 2010b; Lemieux-Dudson et al., 2010; Garcia et al., 2012), and the Lateglacial cool episode (13.7-12.5 cal ka BP).

Cooling in the East Tasman Sea (within dating uncertainties) is synchronous with the ACR. This is consistent with evidence for strongly coupled millennial scale fluctuations in ocean-atmosphere conditions recorded in additional independent land and sea records over the last glacial cycle from the New Zealand region (Barrows et al., 2007a; Kelley et al., 2014; Doughty et al., 2015). East Tasman Sea surface temperature reconstructions remain up to 2°C lower than present between 14.6-~12.9 ka, and are consistent with cooling in regional, South Australian and Southern Ocean records (Pahnke et al., 2003; Barrows et al., 2007b; Calvo et al., 2007; De Deckker et al., 2012; Hayward et al., 2012). Surface conditions in the East Tasman Sea were likely influenced by the northwards transport of cool watermasses derived from the Southern Ocean, and decreased warm water advection across the Tasman Sea (Carter et al., 2008; Hayward et al., 2012; Bostock et al., 2013; Putnam et al., 2013a; Pedro et al., 2015). Model based reconstructions reveal cooling in the New Zealand/Tasman Sea region was similar between winter and summer, and is an exception to the winter dominated cooling throughout most of the SH (Pedro et al., 2015). SST cooling is consistent with mountain glacier advance in the Southern Alps and the central North Island between ~14.1 to ~12.9 ka (Denton and Hendy, 1994; Turney et al., 2007; Putnam et al., 2010b; Applegate et al., 2012; Kaplan et al., 2013; Eaves, 2015; Suppl. Fig. 4.20). Glacier and biotic proxy records display temperatures ~2.5-3°C cooler than present over the New Zealand archipelago, spanning a wide latitudinal range of 37-53°S (Vandergoes et al., 2008; Newnham et al., 2012; Doughty et al., 2013; Sikes et al., 2013; Eaves, 2015). Following the revision of the Okarito and Kaipo Bog chronologies (Fig. 4.10), in combination with a revision of the MAAT reconstruction (MAT-based) from Okarito Bog from Newnham et al. (2012) to include a more comprehensive data set of the taxa lists of pollen and plants (section 4.2.7), there is insufficient evidence to support a latitudinal displacement for the timing of ACR/Lateglacial cooling over the New Zealand archipelago. The vegetation records and reconstructed MAATs from Okarito and Kaipo now show coeval cooling over this interval.

Several proxies invoke enhanced moisture in Westland between ~14-11 ka, attributed to a strengthening/northwards expansion of the Southern Hemisphere westerly wind belt (Fletcher and Moreno, 2011; Whittaker et al., 2011). Hydrophilous taxa, e.g. tree ferns, *Acarina lucida*, and *Lophozonia menziesii* (Wardle, 1979; Wilmshurst et al., 2007), increase in southwestern New Zealand land and sea profiles between ~13.7-12.9 ka, and support this hypothesis. A lithostratigraphic change to lighter, coarser inorganic silts at Okarito Bog accompanies the onset of this interval, and may reflect increased surface erosion and subsequent in-wash of the high moraine ridges surrounding the site (Vandergoes and

Fitzsimons, 2003). In addition, high values of aquatic taxa (60-25%) displayed at the site from 14-11 ka led Fletcher and Moreno (2011) to suggest that moisture levels increased due to enhanced Southern Hemisphere westerly wind flow, although this signal is likely complicated due to the terrestrialisation of the site over that interval (Newnham et al., 2007a). Lastly, speleothem isotope profiles reflect wetter conditions between 14.5-13 ka (Whittaker et al., 2011), and are associated with a steep meridional temperature gradient from an inferred northern position of the Intertropical Convergence Zone, Polar Front and Subtropical Front (Carter et al., 2008; Bostock et al., 2013; Putnam et al., 2010b).

Late deglacial/Early Holocene (12.5-9.5 cal ka BP; NZce 2-1)

Synchronised pollen and SST measurements at MD06-2991 provide unequivocal evidence for ocean-atmosphere coupling in southwestern New Zealand over the pre-Holocene climate amelioration ((defined by Barrell et al. (2013) as NZce-2; from 12.55±0.14 ka to 11.88±0.18 ka)). The growth of emergent podocarp-hardwood forest tolerable of mild climate conditions occurs from ~12.5-11.2 cal ka BP, at the same time as SSTs are higher than present levels by up to 1°C. Both SSTs and emergent conifers climax for the Last Glacial-Interglacial Transition at 11.87 ± 0.3 cal ka BP (2σ) and is consistent in time with the onset of the Holocene Interglacial defined in North Island New Zealand (NZce-1; 11.88 cal ka BP). Evidence of warm ocean temperatures for the early Holocene are reflected in previous studies from New Zealand (Pahnke et al., 2003; Pahnke and Sachs, 2006; Barrows et al., 2007a; Barrows et al., 2007b; Bostock et al., 2013), and the distant SH mid-high latitudes (Lamy et al., 2004; Barrows et al., 2007a; Calvo et al., 2007; De Deckker et al., 2012). Ocean warming in these regions is consistent with a southwards shift of the Subtropical and Polar Fronts and a wholesale meridional southward shift of the Southern Hemisphere westerly wind belt (Fig. 4.11; Pahnke et al., 2003; Sikes et al., 2009; Bostock et al., 2015). Ocean-atmosphere warming of southwestern New Zealand between 12.5-11.2 ka is coeval with the timing of the Younger Dryas (YD) chron/HS-0 (~12.9-11.7 cal ka BP), as characterised in records from the North Atlantic Region (Rasmussen et al., 2006; Brauer et al., 2009), and are consistent with the bipolar temperature seesaw pattern previously noted for HS-1 (Broecker, 1998; García et al., 2012; Newnham et al., 2012; Putnam et al., 2013a; Putnam et al., 2013b). Despite evidence for forest growth reflected at MD06-2991 and Okarito Bog over the pre Holocene amelioration and early Holocene, reconstructed mean annual land surface temperatures are diminished despite warm mean annual temperatures displayed in the adjacent ocean. Consequently MAAT reconstructions for Okarito are up to 8°C lower than those of the surrounding ocean (16°C), and may reflect reduced terrestrial seasonality

(McGlone et al., 2010a; McGlone and Basher, 2012). Rainfall is not considered a limiting factor as it likely exceeded that required for plant growth in this highly oceanic environment, with wetter conditions interpreted from regional speleothem isotope profiles attributed to the southwards displacement of the Intertropical Convergence Zone (Whittaker et al., 2011). A reduced seasonality regime of cooler summers and warm winters is considered to have restricted forest at high altitudes and latitudes (Körner and Paulsen, 2004; McGlone et al., 2010a; 2010b), and permitted glacier advance in the upper Hokitika catchment at 11.9 ± 0.6 cal ka BP (Fig. 4.10; Basher and McSaveney, 1989; McGlone and Basher, 2012). Cool summers would have disproportionately affected tall tree conifers on the Westland lowlands (Newnham et al., 2007a); while relatively warm winters would permit the survival of the frost and drought sensitive lowland understory shrub *Ascarina lucida* as reflected in MD06-2991. Enhanced winter warmth over New Zealand is proposed from model based studies, where strong NH cooling during the YD/HS-0 weakened the South Pacific Jet, allowing the penetration of tropical airmasses southwards with a concomitant southwards shift of the Subtropical Front (Chiang et al., 2014). The southwards shift of ocean-atmosphere circulation systems is proposed to have facilitated the wind driven upwelling of deep water from the high southern latitudes between 12.4-11.6 ka (Toggweiler et al., 2006; Fletcher and Moreno, 2011), and raised atmospheric CO_2 above the threshold to sustain interglacial conditions (Anderson et al., 2009; Denton et al., 2010; Lourantou et al., 2010). Increased atmospheric CO_2 warmed Antarctica (Lemieux-Dudson et al., 2010) with major ice sheet recession commencing by ~12 ka (Mackintosh et al., 2014), and is equivalent in time with glacier recession in the eastern Southern Alps (Kaplan et al., 2010; Putnam et al., 2010b; Putnam et al., 2012; Kaplan et al., 2013).

The subsequent development of *D. cupressinum* after 10.8 ka across southwestern New Zealand, resulting in a 1°C MAAT rise above reconstructions for the modern setting at Okarito Bog, peaks ~1 kyr after SST maxima at MD06-2991. This apparent decoupling is considered to reflect the time taken for this species to reach ecological climax with interglacial conditions (James and Norton, 2002), and follows its initial suppression under a reduced seasonality regime (McGlone and Basher, 2012). Overall, this pattern of vegetation change is consistent with pollen sequences from the central Westland lowlands and the adjacent ocean (McGlone 1988; Moar and Suggate, 1996; Vandergoes and Fitszimons, 2003; Newnham et al., 2007a; Moar et al., 2008; Callard, 2011; Ryan et al., 2012). Similar increases in MAAT to 1-1.5°C above modern take place over New Zealand between ~12.5-9.5 ka (Fig. 4.10; Hajdas et al., 2006; McGlone et al., 2010a; McGlone et al., 2010b; Newnham et

al., 2012). A similar pattern of vegetation change occurs on the opposite side of the Pacific Ocean in north-western Patagonia (40°S), where thermophilous trees increased gradually between 12.6-11 cal ka BP, and rapidly expanded thereafter (Moreno et al., 2009; Moreno et al., 2015).

4.4.5 The 'local' Penultimate Glacial maxima

The culmination of cold climate conditions during the penultimate glacial, ending one of the most extensive glaciations of the Late Quaternary, occurred in southwestern New Zealand and the East Tasman Sea at ~140-139 ka (Fig. 4.12, marker 1). Its timing coincides with NH summer insolation intensity minima and suggests regional climate was influenced by global changes in the ocean-atmosphere circulation system. In Westland, grassland-shrubland expansion represents an inferred treeline depression, corresponding to a reduction in temperatures of ~5°C cooler than present. Glaciers extended as far as the contemporary Westland shoreline (Norris, 1978; Barrell et al., 2005; Sutherland et al., 2007; Barrell, 2011; Barrell et al., 2011), although fortuitously did not over-run the Okarito basin (Newnham et al., 2007a). Surface exposure ages of moraines representing glacier advance to the west (138 ± 5.9 ka; Sutherland et al., 2007) and east (138 ± 10.6 ka; Putnam et al., 2013b) of the Southern Alps, revised to local production rates (Putnam et al., 2010a), show good correspondence with vegetation change. Comparative estimates of atmosphere cooling derived from those rare MIS 6 glacial deposits was not evaluated due to site specific topographic, tectonic and geomorphic influences, as they would bias younger glacials to smaller amplitudes under identical climate forcing (Schaefer et al., 2015).

The timing and magnitude of cooling from South Island pollen and glacial records at the culmination of the local penultimate glacial maxima (140-139 ka) parallel equivalent proxy records during the concluding cold episode of the Last Glacial Coldest Period (Otira Glaciation Stadial A) at ~22-18 ka cal BP (Barrell et al., 2013; Barrows et al., 2013; Vandergoes et al., 2013a). Both glacial maxima are characterised by similar minimum SSTs in the surrounding ocean (Fig. 4.13), and low atmospheric CO_2 which likely facilitated strong onshore cooling (Pahnke et al., 2003; Barrows et al., 2007a; Hayward et al., 2008; Doughty et al., 2015). Reconstructions of vegetation change from MD06-2991 and Okarito records add to the dearth of proxy climate data which capture the culmination of the penultimate glacial cooling in the SH mid-latitudes.

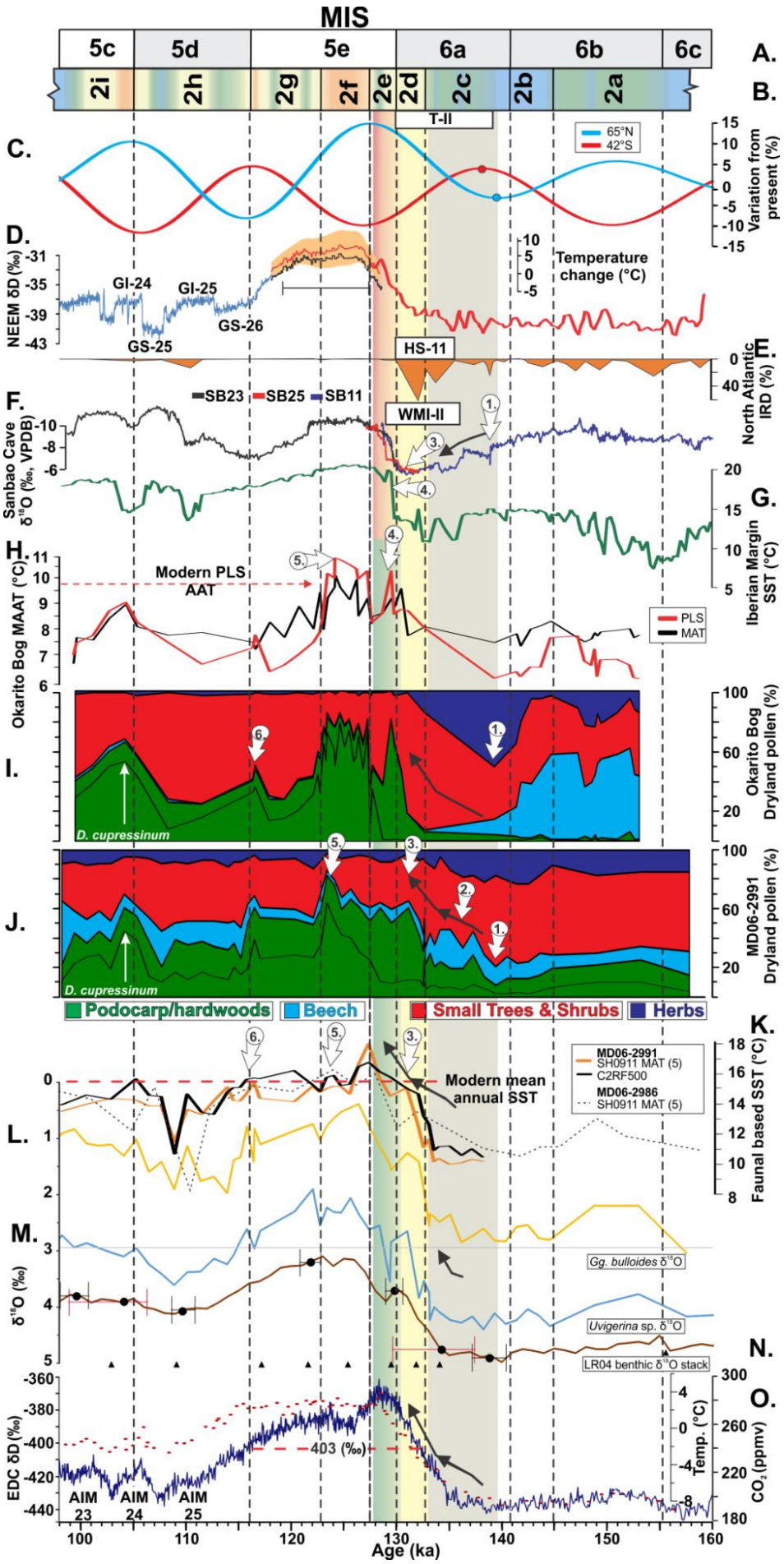
MIS
5c
5d
5e
6a
6b
6c
2i
2h
2g
2f
2e
2d
2c
2b
2a
A.
B.
C.
D.
E.
F.
G.
H.
I.
J.
K.
L.
M.
N.
O.
T-II
65°N
42°S
Variation from present (%)
NEEM δD (‰)
GI-24
GI-25
GS-25
GS-26
Temperature change (°C)
HS-11
North Atlantic IRD (%)
SB23
SB25
SB11
WMI-II
Sanbao Cave δ18O (‰, VPDB)
Iberian Margin SST (°C)
Okarito Bog MAAT (°C)
Modern PLS AAT
PLS
MAT
Okarito Bog Dryland pollen (%)
D. cupressinum
MD06-2991 Dryland pollen (%)
Podocarp/hardwoods
Beech
Small Trees & Shrubs
Herbs
MD06-2991
SH0911 MAT (5)
C2RF500
MD06-2986
SH0911 MAT (5)
Modern mean annual SST
Faunal based SST (°C)
Gg. bulloides δ18O
Uvigerina sp. δ18O
LR04 benthic δ18O stack
EDC δD (‰)
403 (‰)
AIM 23
AIM 24
AIM 25
Temp. (°C)
CO2 (ppmv)
Age (ka)

Fig. 4.12: Integration of key Ice, Marine and Terrestrial (INTIMATE) records from 160-98 ka. Numbers (1-6) inside of markers refer to key points of discussion. **A.** MIS boundaries (Lisiecki and Raymo, 2005; Railsback et al., 2015). **B.** Regional pollen assemblage zones (RPAZ; this study). **C.** Summer insolation anomaly for 42°S (21 Dec) and 65°N (21 June) (Paillard et al., 1996; Laskar et al., 2004), with extrema for T-II in circles. **D.** NGRIP ice $\delta^{18}O$ (blue, North Greenland Ice Core Project members, 2004) displayed on the AICC2012 ice timescale, NEEM ice $\delta^{18}O$ (black) on and EDC3 timescale (NEEM Community Members, 2013) and reconstruction of temperature change with surface melt interval displayed through the LIG. The Greenland synthetic curve (GL_T_syn) predates the LIG and is tuned to Sanbao Cave speleothem ages (Barker et al., 2011). Greenland Interstadials/Stadials numbering follows Rasmussen et al. (2014). **E.** Ice rafted debris (IRD) from ODP 980 (McManus et al., 1999) tuned to Sanbao cave with Heinrich Stadial 11 (HS-11) shown (Wang et al., 2008; Cheng et al., 2009; Barker et al., 2011; Marino et al., 2015). **F.** Sanbao Cave $\delta^{18}O$ calcite, with the weak monsoon interval II (WM-II) displayed (Wang et al., 2008; Cheng et al., 2009), transitioning to red over the culmination of T-II in NH records (Landais et al., 2013). Grey vertical box is the T-II amelioration, with the yellow box representing the Penultimate glacial mild episode, where both overlap with HS-11/WMI-II. The transition to green following T-II represents the early LIG climate reversal. **G.** Alkenone based SST estimates off the Iberian Margin from MD01-2444 (Martrat et al., 2014; Barker et al., 2011). **H.** MAAT estimates for Okarito Bog. **I & J.** Cumulative dryland pollen diagrams for MD06-2991 and Okarito Bog (aligned to MD06-2991), with the relative abundance of *D. cupressinum* outlined within the podocarp/hardwood category by a black line. **K.** SST estimates for MD06-2991 and MD06-2986 (Hayward et al., 2012). **L.** MD06-2991 $\delta^{18}O$ measurements on *Globigerina bulloides* and **M.** *Uvigerina peregrina* aligned to **N.** the reference LR04 benthic $\delta^{18}O$ isotope stack with associated uncertainties displayed (Caballero-Gill et al., 2012a). **O.** δD from EDC (Jouzel et al., 2007) and CO_2 composite record (red circles; Luthi et al., 2008; Schneider et al., 2013) on AICC2012 chronology (Bazin et al., 2013; Veres et al., 2013; Bereiter et al., 2015), with Antarctic Isotope Maxima (AIM) events 25-23 shown (Veres et al., 2013). The LIG is defined by red dashed line at -403‰ δD between 132.5-116.3 ka (EPICA Community Members, 2004).

4.4.6 The penultimate glacial-interglacial transition (PGIT)

The penultimate termination amelioration (139-133 ka)

The advance of tall tree forest and understory shrubs in southwestern New Zealand, coupled with rising SSTs in the adjacent ocean, is represented over two phases during the penultimate glacial-interglacial transition and reflects improving climate conditions. The T-II amelioration is characterised by cool but progressively improving conditions from 139-133 ka (Fig. 4.12, marker 1-2). The onset of climate improvement as recorded in the pollen record from MD06-2991 occurred at 139-138.5 ka, as arboreal pollen increased from MIS 6 minima. At much the same time (140-139 ka), subdued warming is detected in other ocean-atmosphere records from SH mid-high latitudes (Barrows et al., 2007a; Jouzel et al., 2007; Masson-Delmotte et al., 2010), and atmospheric CO_2 steadily rises (Fig. 4.12O; Bazin et al., 2012; Landais et al., 2013; Schneider et al., 2013; Bereiter et al., 2015). These environmental changes coincided with boreal summer insolation rise and were accompanied by an early phase of ice sheet retreat (Marino et al., 2015), and concomitant North Atlantic SST cooling (Fig. 4.12G; McManus et al., 1999; Martrat et al., 2014). These changes precede the rapid collapse of NH ice sheets and widespread cooling of the ocean-atmosphere in the NH by ~3-4 kyr (Marino et al., 2015). A distinct increase of calcite $\delta^{18}O$ in Sanbao Cave (Fig. 4.12F), likely reflects an early southwards shift of the Intertropical Convergence Zone (Cheng et al., 2009). This early warming in the SH ocean-atmosphere circulation systems displays similarity to its T-I counterpart at ~19 ka (Pedro et al., 2011; Pedro et al., 2012), and the sequence of climate events which follow are consistent with the essential elements of a termination outlined by Denton et al. (2010).

The expansion of arboreal pollen from 139-133 ka suggest trees likely continued to contract landwards from the southwestern New Zealand continental shelf as relative sea level rose from -90 to -60 m lower than the present (Grant et al., 2014; Marino et al., 2015). At higher elevations (up to 150 m), montane-subalpine trees and shrubs colonised recently deglaciated sites. Even though reconstructions of temperature are limited for this interval, the 1.5°C rise in pollen-based MAAT from Okarito Bog is equal to post Termination amelioration values (Fig. 4.10; Barrell et al., 2013). Despite this, the composition and proportion of tall trees for the two periods are dissimilar (Fig. 4.13). T-II is comprised of a mixed podocarp-hardwood (~20%) and southern beech (20%) community at MD06-2991, while the post Termination amelioration (NZce-5) is dominated by podocarp-hardwood forest (60%). Greater southern beech during T-II may reflect its dominance in a substantially alpine environment which,

despite gradual warming, may have been characterised by a harsher local climate and stronger winds than during T-I.

In addition, the gradual amelioration in climate over T-II is punctuated by two episodic minor advances in the grassland-shrubland community at MD06-2991 which are coupled with declining SSTs at ~137-136 ka and 134-133 ka, respectively. The latter of these vegetation changes, occurring during HS-11, is recognised by cooling in the ocean-atmosphere circulation systems in SH mid-high latitudes such as the Southern Ocean from marine sediment cores 64PE-174P13 (Scussolini et al., 2015) and MD02-2488 (Govin et al., 2012), and in Antarctica at EDC (Jouzel et al., 2007; Bereiter et al., 2015). These are antiphased with short-lived SST warming in the North Atlantic Ocean (Fig. 4.12G; Barker et al., 2011; Martrat et al., 2014), and inferred northward shifts of the Intertropical Convergence Zone during a brief multi-centennial wet interstadial phase (Fig. 4.12F; Wang et al., 2004; Wang et al., 2008; Cheng et al., 2009). While a higher resolution sampling strategy is required in the MD06-2991 and Okarito records to support these findings, these initial results suggest that millennial scale hemispheric asynchrony occurred during T-II.

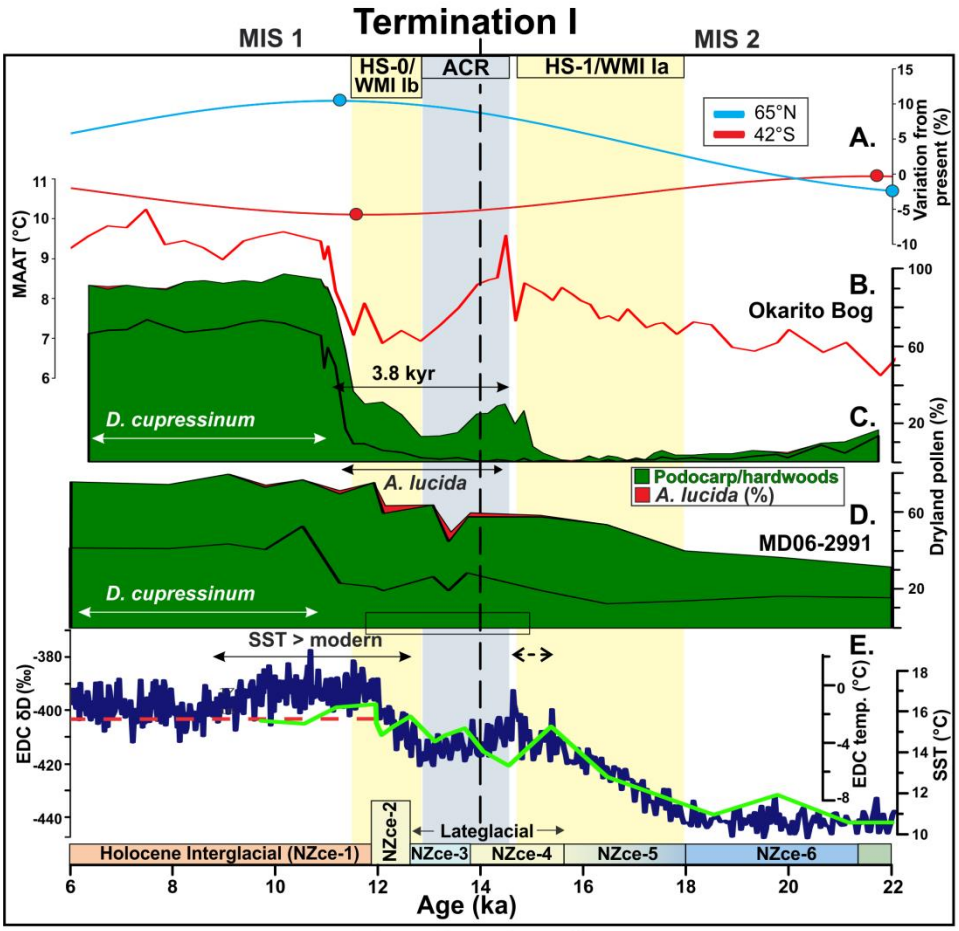
Termination I
MIS 1
MIS 2
HS-0/ WMI Ib
ACR
HS-1/WMI Ia
65°N
42°S
A.
Variation from present (%)
MAAT (°C)
B.
Okarito Bog
3.8 kyr
D. cupressinum
C.
Dryland pollen (%)
A. lucida
Podocarp/hardwoods
A. lucida (%)
D.
MD06-2991
D. cupressinum
SST > modern
E.
EDC δD (‰)
EDC temp. (°C)
SST (°C)
NZce-2
Lateglacial
Holocene Interglacial (NZce-1)
NZce-3
NZce-4
NZce-5
NZce-6
Age (ka)

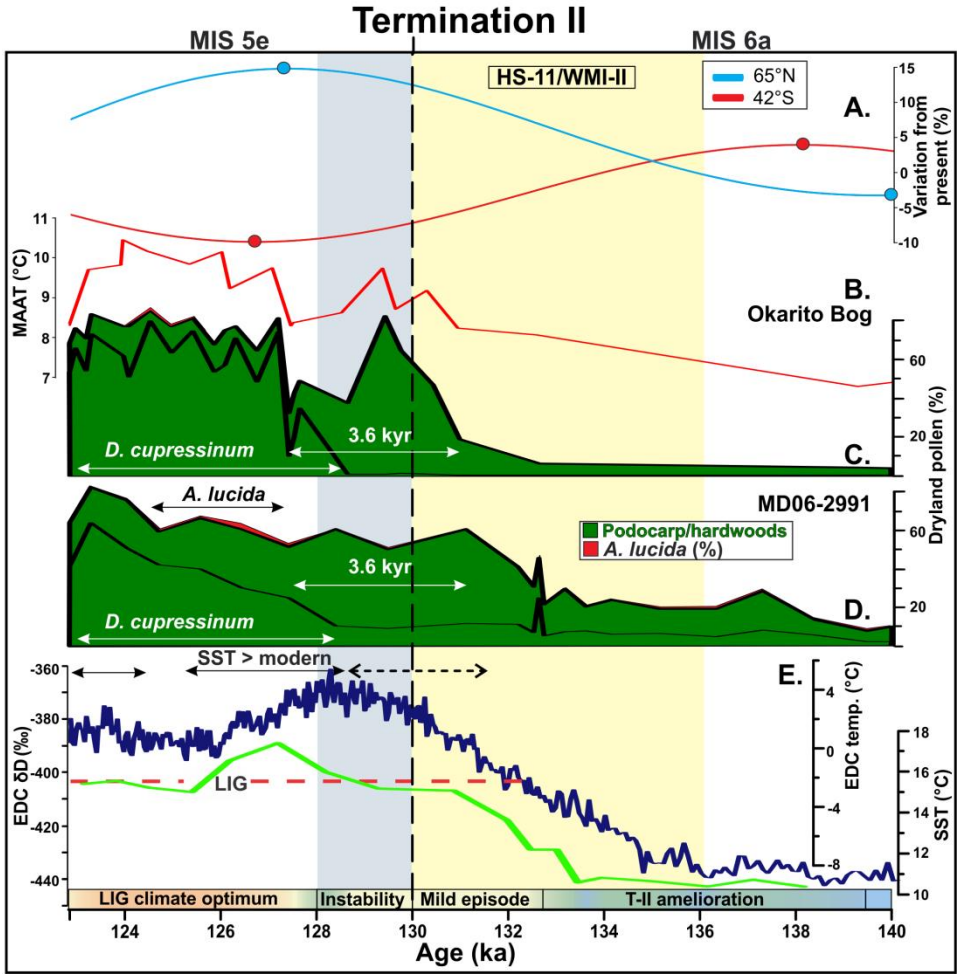
Termination II
MIS 5e
MIS 6a
HS-11/WMI-II
65°N
42°S
A.
Variation from present (%)
MAAT (°C)
B.
Okarito Bog
3.6 kyr
D. cupressinum
C.
Dryland pollen (%)
A. lucida
MD06-2991
Podocarp/hardwoods
A. lucida (%)
3.6 kyr
D. cupressinum
D.
SST > modern
E.
EDC δD (‰)
LIG
EDC temp. (°C)
SST (°C)
LIG climate optimum
Instability
Mild episode
T-II amelioration
Age (ka)

Fig. 4.13: Comparison between T-I and T-II. **A.** Summer insolation anomaly for 42°S (21 Dec) and 65°N (21 June) (Paillard et al., 1996; Laskar et al., 2004), with extrema in circles. **B.** Mean of MAAT estimates (PLS and MAT based) for Okarito Bog. **C.** & **D**. Relative abundance of podocarp-hardwoods and *Ascarina lucida* for the respective Okarito Bog (aligned to MD06-2991) and MD06-2991 records, with *D. cupressinum* values outlined by a black line in both. Time intervals between mixed podocarp-hardwood growth and *D. cupressinum* expansion are of similar duration (>3.6 kyr). **E.** δD (blue) from EDC (Jouzel et al., 2007) on AICC2012 chronology (Bazin et al., 2013; Veres et al., 2013; Bereiter et al., 2015). The onset of the Holocene Interglacial and LIG is defined by δD values of -403‰ (red dashed line) (EPICA Community Members, 2004). This red line also similarly defines the modern SST value adjacent to southwestern New Zealand of 15.5°C. Average SST estimates from RF and MAT approaches are displayed in light green. Windows where SSTs exceed modern from MD06-2991 and regional estimates are indicated by solid black arrows above the plot, with conditions 0.5°C from modern indicated by a dashed line (Barrows et al., 2007a; 2007b; Hayward et al., 2012). The boundaries of MIS 2-1 and 6-5 are displayed by a black vertical dashed line at 14 and 130 ka, respectively (Lisiecki and Raymo, 2005). The colour scheme for the RPAZ schematically illustrates characteristic atmospheric temperatures (orange = warmest, blue = coldest). The timing of the respective climate events are defined by; HS-1 (Putnam et al., 2013a); ACR (Putnam et al., 2010b); YD/HS-0 (Rasmussen et al., 2006) NZCe-4; (Barrell et al., 2014); HS-11/WMI-II (Cheng et al., 2009; Marino et al., 2015).

The Penultimate glacial mild episode (133-130 ka)

Phase two of the penultimate glacial-interglacial transition is characterised by rapid improvement of climate conditions in southwestern New Zealand between ~133–130 ka, and is termed the Penultimate glacial mild episode. Tall tree podocarp-hardwood forests likely colonised higher sites on the piedmont previously occupied by montane-subalpine shrubs, as adjacent ocean temperatures in the East Tasman Sea rapidly rose close to modern values (Fig. 4.12, marker 3; Suppl. Fig. 4.21-4.22; Moar and Suggate, 1996; Moar and McKellar, 2001). This transpired as the continental shelf flooded during a rapid sea level rise to modern conditions by ~130 ka (Marino et al., 2015), and is considered to have suppressed southern beech advance in central Westland (Leathwick, 1998; Hall and McGlone, 2006; Newnham et al., 2007c). Ocean-atmosphere change over the penultimate glacial mild episode resembles those of the Lateglacial mild episode and the pre-Holocene amelioration (Fig. 4.13), with the character and rate of organic sediment deposition at Okarito Bog also similar between T-I and T-II (Suppl. Fig. 4.10-11; Newnham et al., 2007a). Minor dissimilarities in vegetation composition and MAATs between these episodes during T-I and T-II are attributed to the duration of improving conditions over the SH mid-latitudes over HS-11 and HS-1 (~5 kyr and ~3 kyr, respectively). In this regard, the composition of podocarp-hardwood forest displayed at the culmination of HS-11 is more similar to that which followed HS-1 and HS-0/YD.

This rapid amelioration in the ocean-atmosphere precedes that which follows HS-11 in the NH mid-high latitudes by ~2-3 kyr (Sánchez Goñi et al., 1999; Sánchez Goñi et al., 2012; Capron et al., 2014; Martrat et al., 2014; Govin et al., 2015; Marino et al., 2015). The sequence of climate events associated with this interval of the glacial termination is consistent with the processes outlined for a termination by Denton et al. (2010). It follows that rapidly rising summer NH insolation variation triggered the collapse of NH ice sheets and resulted in melt water pulse-2b. This instigated the breakdown of the Atlantic meridional overturning current leading to North Atlantic cooling over HS-11 (McManus et al., 1999; Skinner and Shackleton, 2006; Martrat et al 2014). The marine Intertropical Convergence Zone moved southwards during Weak Monsoon Interval (WMI)-II (Fig. 4.12; Wang et al., 2008; Cheng et al., 2009; Landais et al., 2013; Jacobel et al., 2016), allowing tropical airmasses and the Subtropical Front to penetrate southwards (Urrego et al., 2015). Proxy and model reconstructions of ocean-atmosphere conditions from the SH mid-high latitudes are consistent with this pattern of early SST warming relative to 125 ka (Pahnke et al., 2003; Barrows et al., 2007a; Turney and Jones, 2010; Govin et al., 2012; Hayward et al., 2012; Cortese et al., 2013; Capron et al.,

2014; Langebroek and Nisancioglu, 2014). Early warming preceding the last interglacial in the study region is not inconsistent with that inferred for the southern South Island by Cortese et al. (2013), who considered this to result from a strengthening of the South Pacific Gyre which may have enhanced the East Australian Current (EAC), resulting in the transport of warm water across the Tasman Sea. These variations occurred in synchrony (within chronological uncertainty) with rapidly rising atmospheric CO_2 concentrations, and increasing temperatures in EDC (Jouzel et al., 2007; Masson-Delmotte et al., 2010), marking the onset of the last interglacial in that record (Fig. 4.12; EPICA Community Members, 2004; Landais et al., 2013). Half of the G-I release of CO_2 occurred during HS-11, and is considered to have resulted from the southwards shift of the Southern Hemisphere westerly wind belt and outgassing from the Southern Ocean (Toggweiler, 2009; Anderson et al., 2009).

Early last interglacial (LIG) climate reversal (~130-128 ka)

The culmination of the Penultimate Glacial-Interglacial Transition in southwestern New Zealand land and sea palynomorph profiles is indicated by a distinctive shift from mixed forest to forest almost exclusively dominated by *D. cupressinum*. This transition is interrupted by a short lived ~1.5−2 kyr expansion in cool climate taxa and adjacent ocean temperatures, and in this regard displays strong similarities to the New Zealand Lateglacial cool episode (Fig. 4.13; Newnham et al., 2007a; Moreno et al., 2009; Putnam et al., 2010b; Lemieux-Dudson et al., 2010; Garcia et al., 2012). The curtailment of forest taxa is more pronounced on land at Okarito Bog than at sea at MD06-2991 for both periods, despite both environments being regional recorders of the pollen rain (Suppl. Fig. 4.13). MAATs reconstructed from Okarito show that atmospheric cooling (1.5-2°C, Fig. 4.12, marker 4) and the duration of both events are remarkably similar, although the late glacial reversal is ~2.8°C cooler than that of the early last interglacial interval. Similarly, surface cooling of the East Tasman Sea is less pronounced during the early last interglacial than for the late glacial at MD06-2991 and other records (Barrows et al., 2007a; Calvo et al., 2007; Pelejero et al., 2007; Hayward et al., 2008), despite a positive excursion in $\delta^{18}O$ values over both intervals. This may result from a weaker meridional temperature gradient than that inferred for the ACR (Whittaker et al., 2011).

This period of climate instability is coeval within chronological uncertainty (±1 ka, 2σ) with a strong enhancement of the low-latitude hydrological cycle at the culmination of the Weak Monsoon Interval (WMI)-II (Cheng et al., 2009; Landais et al., 2013; Scussolini et al., 2015; Jacobel et al., 2016), as perihelion moved from alignment with the NH spring equinox to the

summer solstice (132-126 ka). An intensification of the Atlantic meridional overturning current, is postulated to have decoupled the climate system from the carbon cycle, as reflected by the highest concentrations of CO_2 in EDC at 128.5 ka (Masson-Delmotte et al., 2010; Landais et al., 2013). An equatorial migration of the Southern Hemisphere westerly wind belt, similar to that over the early Holocene at ~9 kyr (Anderson et al., 2009; McGlone et al., 2010a), would have increased the wind driven Ekman current transport of cool water northwards into the East Tasman Sea. These processes would have altered regional wind stresses and precipitation (Rojas et al., 2009), and may partly explain the suppression of tall tree growth. This in combination with a reduced terrestrial seasonality regime akin to that proposed for the pre-Holocene amelioration (McGlone et al., 2010a; McGlone and Basher, 2012), supressed tall tree *D. cupressinum* growth on the Westland lowlands and favoured the expansion of cool climate taxa (Wilmshurst et al., 2007). However, enhanced westerly wind flow is in contrast to persistent or more frequent La Niña like conditions proposed for this region at this time by Pelejero et al. (2003), which if similar to the present would have enhanced subtropical easterly flow and resulted in a warm-dry climate in southwestern New Zealand (Kidston et al., 2009). Nonetheless, both scenarios may have limited the growth of moisture loving taxa on the Westland lowlands. The attendant curtailment of vegetation in New Zealand is asynchronous with rapid warming in environmental records from the NH mid-high latitudes (Fig 4.14; Tzedakis et al., 2003; Drysdale et al., 2005; Müller et al., 2005; Brauer et al., 2007; Allen and Huntley, 2009; Barker et al., 2011; Milner et al., 2012; Milner et al., 2013; Rasmussen et al., 2013), and the onset of the LIG (Eemian) occurring around ~129-127 ka. This is consistent with the bipolar temperature seesaw mechanism similarly reflected in paleoenvironmental records for T-I (Denton et al., 2010; Putnam et al., 2013a).

4.4.7 The timing and duration of the last interglacial (LIG) in southwestern New Zealand (~128-116 ka)

Widespread evidence for warm, mesic conditions are evident in reconstructions in vegetation change over the LIG from New Zealand (Bussell, 1990; 1992; Heusser and Van de Geer, 1994; Mildenhall, 1995; Carter, 2000, 2002; Okuda et al., 2002; Marra, 2003; Newnham and Alloway, 2004; Ryan et al., 2012; Williams et al., 2015), with forest species extending further south beyond their contemporary ranges (Moar and Suggate, 1996; Moar and McKellar, 2001; Marra, 2003; Newham et al., 2007a). However, the timing and duration of these changes identified in terrestrial sequences typically remain poorly constrained (i.e., Suppl. Fig. 4.21-4.22).

The rapid expansion of podocarp-hardwood forest, dominated by *D. cupressinum* between ~128-123 ka (Fig. 4.12, marker 5), defines the climate optimum of the LIG. The onset of forest expansion is strongly coupled with rising SSTs in the East Tasman Sea from ~128 ka. This interval is consistent with warm-wet conditions described in regional vegetation-climate reconstructions from marine sequences and speleothem isotope profiles, occurring between 128-122 ka (Ryan et al., 2012; Williams et al., 2015). This is also coeval with the culmination of peat deposition from the long paleoenvironmental record at Lake Poukawa, eastern North Island, (Carter, 2002; Okuda et al., 2002), at ~123 ± 8 ka, with slightly warmer drier conditions suggesting possible regional differences in climate which is similar to that of present patterns (McGlone et al., 2002). The LIG climate optimum in southwestern New Zealand is synchronous with that in NH pollen records, which is similarly defined by the expansion of thermophilous taxa, and occurs between ~128-122 ka (Brauer et al., 2007; Allen and Huntley, 2009; Milner et al., 2013). There is also evidence to suggest that millennial scale variability extended throughout this period with the resumption of cool conditions in the North Atlantic between 127-125 ka (Barker et al., 2011; 2015).

This rise in *D. cupressinum* forest at the onset of the LIG thermal optimum follows the expansion of mixed podocarp-hardwood forest during the Penultimate glacial mild episode by ~3-4 kyr. Despite dissimilar rates and variations of orbital forcing, this is equivalent to that highlighted between the Lateglacial mild episode and the subsequent rise in *D. cupressinum* in Westland during the Holocene Interglacial from 11.2–10.9 cal ka BP (Fig. 4.13). This lag arises despite land-sea temperatures achieving near modern values during both mild episodes at ~130 ka and 14.5 ka (Fig. 4.13). This delayed response of thermophilous vegetation to climate amelioration in southwestern New Zealand may reflect the influence of strong winds, reduced terrestrial seasonality, and topographic controls which inhibited the southward spread of northern taxa into this geographically isolated region. Similarly the >30 km wide Cook Straight undoubtedly acted as a coastal barrier for the migration of northern species during the LIG (Marra 2003), with global sea level rising from modern to 6-9 m higher than the present from ~130-125ka (Kopp et al., 2009; Dutton and Lambeck, 2012; Dutton et al., 2015a; Dutton et al., 2015b).

Proportions of *D. cupressinum* persist at levels above 20% over MIS 5e from 128-116 ka in MD06-2991. This ~12 kyr period is akin to that of ~11 kyr produced from the low resolution pollen record of TAN0513-14 situated in the same submarine canyon setting (Ryan et al., 2012). Williams et al. (2015) apply the local Kaihinu interglacial to this period, based on

extensive cooling revealed in glacier and pollen records during MIS 5d and 5b. However, following the pronounced thermal optimum for MIS 5e, vegetation reconstructions from MD06-2991 and Okarito Bog display an increase in cool climate taxa from 123-118 ka and decrease of these taxa from 118-116 ka, respectively (Fig. 4.12). Vegetation based reconstructions from this region suggest that the LIG was highly variable in character with evidence for millennial scale climate oscillations during warmer-than-present times. The culmination of the LIG in southwestern New Zealand matches that of the thermal optimum defined in Greenland at 117.3ka (Rasmussen et al., 2013), while NH vegetation records indicate stadial conditions took place much later at ~111 ka (Shackleton et al., 2003; Brauer et al., 2007; Sánchez Goñi et al., 2012).

4.4.8 The amplitude of LIG temperature change and seasonality

The LIG climate optimum

Few well constrained quantitative estimates of terrestrial temperature are generated for the LIG in the SH mid-latitudes (Turney and Jones, 2010; Capron et al., 2014). Compiled proxy data display a strong latitudinal gradient to warming, with warming greater at high latitudes (>60°) than tropical regions (0-30°), and global temperatures on average ~1.5°C higher than relative to AD 1961-1990 (Turney and Jones, 2010). Further, model reconstructions attempting to quantify the nature and timing of land-sea warmth exhibit dissimilarities (Lunt et al., 2013; Otto-Bliesner et al., 2013; Capron et al., 2014; Langebroek and Nisancioglu, 2014). This emphasises the necessity for generating quantifiable temperature estimates over the LIG from records with robust chronological control. Until now, no such quantitative records exists from South Island New Zealand over the LIG, and the early warming identified which preceded it, while records from the adjacent ocean surrounding New Zealand display distinct regional differences to warming over the interval from 132-120 ka (Cortese et al., 2013). Highly resolved quantitative estimates of ocean-atmosphere temperatures from adjacent land-sea records presented here provide unequivocal evidence of coupling in southwestern New Zealand over the LIG, and advance previous attempts to reconcile whether a LIG thermal optimum existed in this region (c.f. Ryan et al., 2012).

Thermophilous and drought sensitive species, consisting of *D. cupressinum, Ascarina lucida* and *Dodonaea viscosa,* inhabited forests of the Westland lowlands during the thermal optimum. These species flourished once East Tasman Sea surface temperatures surpassed modern conditions, where maxima of +1.3 to 2.5°C above modern were reached from 128-127.5 ka. Ocean temperature warmth during the LIG climate optimum aligns closely with the broad

regional warming trend in southwestern New Zealand for the MIS 5e window (132-120 ka) of Cortese et al. (2013), and is higher than that which occurs at ~125 ka, with a similar conclusion displayed in modelling studies (Fig. 4.14., Capron et al., 2014).

Forest development over the LIG climate optimum corresponds to an MAAT increase of 0.5-1.5°C higher than pre New Zealand forest disturbance values, exceeding early Holocene estimates by ~0.75°C. These temperatures lag the highest adjacent East Tasman Sea estimates by 0.5-3 kyr, similar to the Holocene interglacial (Fig. 4.13). This apparent decoupling of ocean-atmosphere circulation systems in this maritime climate setting is considered to reflect the time taken for vegetation to reach ecological climax with interglacial conditions. In addition, the persistence of thermophilous taxa over the LIG climate optimum in southwestern New Zealand occurs during a reduced seasonality regime (Berger and Loutre, 1991). Warm SSTs in the East Tasman Sea, which at the time were at least at modern conditions, likely reduced the amplitude of the seasonal cycle (Sutton and Roemmich, 2001). Akin to the early Holocene, this may have generated milder, cloudier climates, reducing terrestrial seasonal contrasts, with longer growing seasons compensating for cooler summer temperatures (McGlone et al., 2010b; McGlone and Basher, 2012). Warmer winters on the western coastline of New Zealand are considered to have facilitated the growth and survival of the frost intolerant *Ascarina lucida*, consistent with the conditions proposed to result from a strengthening of the East Asian monsoonal system under strong NH summer insolation forcing (Chiang et al., 2014).

At Okarito a parallel pattern in hydrology between 5e and the early Holocene may have emerged, with evidence for shallowing of the lake basin. The wetland macrophyte *Isoetes* decreases at Okarito from 124-122 ka (becoming temporarily absent at 123 ka), in combination with a concomitant increase in the wetland shrub *Leptospermum*, and may indicate reduced water levels with the site becoming more akin to the swamp which has existed since the early Holocene, although not as significant as the terrestrialisation which occurred over the later period (Newnham et al., 2007a). Alternatively, these changes may result from ecological or physical mechanisms, which may be directly or indirectly related to climate. Other comparisons between these two interglacials however suggest there was less hydrological variability during LIG compared to the Holocene, possibly the result of warmer temperatures during the LIG (Mackay et al., 2013). Perhaps a more comparable analogue to that of T-I is considered to be T-V (MIS 12-11 transition), with similar relatively low magnitude insolation fluctuations (Berger, 1978).

Distinct regional differences in New Zealand warming may result from variability in warm water conveyed across the Tasman Sea (Cortese et al., 2013), via a postulated southwards extension of the East Australian Current (EACe). Conditions in the western North Island at south Taranaki (Bussell, 1990), which is presently ~2°C warmer annually than Westland, similarly reflect warm-wet conditions from peat considered to represent the LIG, with proportions of *Ascarina lucida* there reaching ~20%. Evidence for warmer winters (2.3–3.2°C) and summers relative to modern (1.6–2.5°C) are inferred from beetle remains from the southern position of New Zealand's North Island (Marra, 2003). These species are more similar to that which occur in contemporary forests ~700 km north, and likely suggest they extended further south during the LIG climate optimum. Slightly warmer yet drier conditions are interpreted from pollen/phytolith profiles of peat deposited during the LIG climate optimum in the eastern North Island at Lake Poukawa (Carter, 2002; Okuda et al., 2002), with evidence for reduced lake sizes than for the remainder of MIS 5, and are equivalent to early Holocene levels (Harper and Collen, 2002). McGlone (2002) proposes that rainfall may have been reduced during the early Holocene due to more NW airflow, with similar conditions during the LIG (Okuda et al., 2002). In the adjacent ocean, Cortese et al. (2013) show ocean surface temperatures were ~2.5°C greater than modern at ~125 ka, with enhanced warmth supported by the presence of the extinct temperate-tropical estuarine mollusc *Anadara trapezia* (Murray-Wallace et al., 2000). Warm-wet conditions are similarly reflected across the Tasman Sea at Lake Wangoom, South Australia, with a higher proportion of rainforest pollen taxa (~25%) than the MIS 1 community (Harle et al., 2002; Harle et al., 2004). Further south in Tasmania and the same latitude as southwestern New Zealand, pollen based estimates of MAAT from Lake Selina (516 m) similarly display a temperature increase of ~1°C higher than modern between 130-122 ka during MIS 5e (Fletcher and Thomas, 2010). Enhanced MAAT estimates are consistent with those modelled by Capron et al. (2014), who display simulated MAATs at ~125 ka which are 1-1.5°C higher than at 130 ka (Fig. 4.14).

The extent of warming outlined during the LIG climate optimum provides a past analogue into anticipated future climate change. By the end of the century, atmospheric warming is projected to raise global mean surface temperatures 0.3-4.8°C above pre-industrial values (Meinshausen et al., 2011; Stocker et al., 2013). An unprecedented warming and shift in the surface ocean off South Australia to 45°S (Cowan et al., 2014), far exceeding global mean values (Hill et al., 2011; Wu et al., 2012; Oliver and Holbrook, 2014), displays similarities to

those outlined for the LIG (Cortese et al., 2013). This is considered to be the result of an intensification of the flow and accelerated warming in the East Australian Current (EAC) (Ridgway and Hill, 2012), shifting 50-80 km over the last 40 years (Moore et al., 1999), with climate model simulations anticipating this trend to accelerate over the next 100 years (Oliver et al., 2015). The progressive warming further south may in turn accelerate ice melt from Antarctica (Golledge et al., 2015), and may be similar to that which occurred during the LIG where ~5 m of global eustatic sea level rise was produced from the WAIS with a contribution from the EAIS (Dahl-Jensen et al., 2013; Pol et al., 2014; Dutton et al., 2015b).

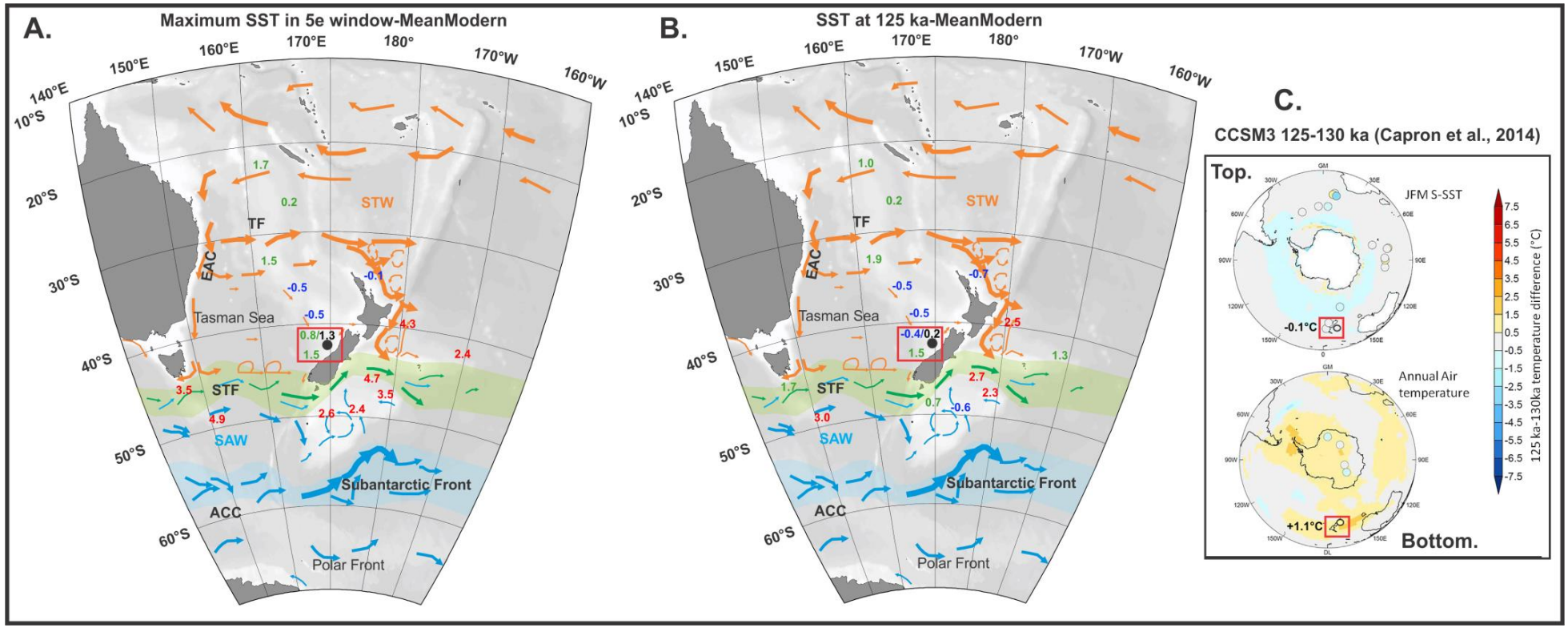

Fig. 4.14: A. Map of anomalies in degrees centigrade (highest SST value recorded between the **A.** the MIS 5e window 132-120 ka minus Modern mean annual SST and **B.** the SST value recorded at 125 ka minus Modern mean annual SST, with all sites investigated by Cortese et al. (2013). The magnitude of the anomalies is colour coded as blue (negative), green (0 to 2°C), and red (>2°C). The MD06-2991 site and SST value is displayed in black with RF- based SSTs calculated following Cortese et al. (2013). SSTs are 1.3 and 0.2°C higher than the modern SST (15.5°C) at MD06-2991 (Locarnini et al., 2013) in each respective plot. The generalized ocean circulation and shortenings are the same for each time interval and follow Fig. 2.x, with the study region indicated by a red box. Map plotted in Ocean Data View v.4.6.4 (Schlitzer, 2012). **C.** Temperature difference between climatic conditions at 125 ka and 130 ka recorded in Antarctic ice core and marine sediment data which was simulated by CCSM3 from Capron et al. (2014). **Top.** Simulated Summer SST calculated as a temperature average over the months JFM for the Southern Hemisphere. Annual MD06-2991 SST shows little change between time-frames and was averaged for RF and MAT estimates. **Bottom.** Simulated annual land surface temperatures are compared with air temperature anomalies inferred from Antarctic ice cores. MAAT calculated for Okarito Bog shows a +1.1°C change between time-frames and was averaged for both PLS and MAT estimates.

LIG stadial II and the late LIG mild episode

Following the marked thermal maximum of the LIG climate optimum, montane-subalpine trees and shrubs associated with cooler climates advanced rapidly at the expense of the tall lowland conifer *Dacrydium cupressinum* and thermophilous understory shrubs (LIG stadial II; 123-118 ka). *D. cupressinum* experiences minimal growth below 8.5°C and optimal growth at 17°C (Whitehead et al., 2002). Reconstructed atmospheric cooling of 2-3°C from modern estimates is considered to have been detrimental to the growth of this species. This is sufficiently greater than adjacent SST estimates (~1°C reduction below modern values), with minor variations in atmospheric CO_2, and requires explanation. Ryan et al. (2012) consider that frost tolerant taxa would benefit in a regime dominated by changes in the magnitude and frequency of extreme events, as may occur for this period of increasing seasonality. This pattern of vegetation change displays similarity with the late Holocene in New Zealand (McGlone et al., 2010b; Jara et al., 2015), and is reflected at MD06-2991 (Fig. 3.5). The reduction of the frost-sensitive *Ascarina lucida* from lowland forests along western New Zealand and central North Island (McGlone and Moar, 1977; McGlone et al., 1992) from ~6 ka has previously been considered to have resulted from the shortening of summers (warming) and lengthening winters (cooling) (McGlone et al., 2011). As *A. lucida* declined alpine trees are considered to have replaced low growing shrubland in winter over the mid-late Holocene (McGlone and Basher, 2012).

The cessation of cool conditions in southwestern New Zealand at ~118 ka is consistent in time with the onset of cooling observed in the GIS record (North Greenland Ice Core Project members, 2004; Rasmussen et al., 2013), declining SST estimates from the North-Atlantic Ocean and a minor pulse of IRD (C-25) between ~116-113 ka (Chapman et al., 1999). This cooling, similarly reflected in terrestrial records from the NH mid-latitudes between ~117-115 ka (Allen and Huntley, 2009; Milner et al., 2012; Pickarski et al., 2015), facilitated a disruption of the Atlantic meridional overturning current (Müller et al., 2005; Milner et al., 2012), and shifted the Intertropical Convergence Zone southward (Wang et al., 2008; Cheng et al., 2009; Groot et al., 2011), with concomitant southward penetration of the NH westerlies into central Asia (Mackay et al., 2013). This mechanism provides evidence for hemispheric asynchrony at the culmination of the LIG and matches that previously identified from polar regions at this time (Wolff et al., 2009).

Evidence for warm-wet conditions at the culmination of the LIG in southwestern New Zealand is observed from ~117.5-116 ka, with a brief expansion in *D. cupressinum* (Fig. 4.12,

marker 6), Random Forest-based SST and depleted $\delta^{18}O$ measurements. This coincides with the highest rate of sediment accumulation at Okarito Bog (~18 cm/kyr), considered to result from the rapid influx of organic material during this rapid phase of climate amelioration. A re-expansion of *D. cupressinum* is also reflected in the less resolved TAN0513-14 record from southwestern New Zealand (Fig. 2.3; Ryan et al., 2012). Additional evidence for warm conditions at this time are reported from the southern North Island (Marra, 2003), and from the highest proportions of *D. cupressinum* at DSDP Site 594 (Heusser and van de Geer, 1994), which may reflect a change in the moisture source to eastern regions or a longer adjustment of LIG vegetation than that revealed in Westland records. These records of mid-latitude climate reflect conditions which are more variable than those from Antarctic ice cores (Bazin et al., 2012; Veres et al., 2012) although sharp 1‰ positive $\delta^{18}O$ excursions are observed in the EDML ice core (Fig. 4.1; Stenni et al., 2010). Evidence for warming in southwestern New Zealand is consistent with modelled summer temperatures from Antarctica which display increased summer temperatures during the LIG at 115 ka (Langebroeck and Nisancioglu, 2014) and occur during perihelion in the SH summer solstice at 116 ka. Warmer surface oceans coupled with melting under the surface of Antarctic ice sheets are considered to have contributed to a sea level rise of 3-9 m during this time (Siddall et al., 2010; Caballero-Gill et al., 2012b; O'Leary et al., 2013).

These rapid inflections in podocarp-hardwood taxa at Okarito Bog are similarly repeated during MIS 5b and during the LGM when perihelion occurs in the SH summer solstice. Vandergoes et al. (2005) proposed that the later advance in forest taxa may have been due to "local" insolation forcing of SH mid-latitude vegetation, and provide a plausible alternative to the bipolar seesaw. The revised Okarito Bog record shows that while this may be significant, the bipolar temperature seesaw mechanism is an important contributor of heat to the SH mid and polar latitudes.

The last glacial inception (<116 ka)

The expansion of montane subalpine shrubs and southern beech on the Westland lowlands reflects climate deterioration through MIS 5d. Southern beech is considered to have recolonized into the Hokitika catchment, where an increased dominance is similarly reflected in terrestrial sites positioned ~15 km (Chesterfield), ~25 km (Candle Light) and 50 km (Shultz Creek) north-east of Hokitika (Moar and Suggate 1996; Moar et al., 2008; Suppl. Fig. 4.22 and 4.23). These trees likely persisted at favourable inland sites and on the recently exposed continental shelf with relative-sea level reconstructions between -20 to -50 m lower

than present (Grant et al., 2014). This resurgence in southern beech is considered to have been via its current northern limit of the central Westland Biotic Gap, due to low traces of this pollen at Okarito Bog. Evidence of a resurgence of Southern Alps glaciers between 110-108 ka (Preusser et al., 2005; Rother et al., 2014), are not inconsistent with declining SSTs from this region (Barrows et al., 2007a; Hayward et al., 2012). A similar advance in montane-subalpine shrubs and herbs in eastern regions of New Zealand is observed at DSDP Site 594 (Heusser and van de Geer, 1994), with a coeval cooling in SSTs and increased terrigenous material considered to represent increased glacial erosion (Nelson et al., 1986; Hayward et al., 2008; Suppl. Fig. 4.19). This pattern of cooling in the ocean-atmosphere circulation systems is coeval with the coldest temperatures in EDC (Jouzel et al., 2007), and likely suggests that similar processes were involved in transmitting this hemispheric signal.

The vegetation progression over MIS 5d/5c in MD06-2991 displays similarities with that outlined for T-II, with both occurring during rising NH insolation intensity. A mixed shrubland podocarp-hardwood community progresses into one dominated by *D. cupressinum*, as SSTs increase to modern values. This is synchronous with Antarctic Isotope Maxima (AIM) 24 in EDC δD measurements (Fig. 4.12), and precedes warming in the NH mid-latitudes. In a similar fashion to expansion of *D. cupressinum* in MIS 5e, the climax of forest development commences subsequent (up to 1 kyr) to SSTs reaching modern conditions. However, this lag is considerably less than that displayed during T-II (3-4 kyr), and points to the survival of podocarp-hardwoods in the region during the MIS 5d stadial, and provided a platform for expansion as the climate ameliorated. The advance of cool climate montane-subalpine shrubs and declining *D. cupressinum* and declining SST from MD06-2991 over MIS 5d displays similarity to cooling exhibited in Antarctica at the culmination of AIM 24 and 23 (Fig. 4.12), and display an asynchronous pattern to that in the NH mid-high latitudes.

4.5 Conclusion

Combined reconstructions of ocean-atmosphere change spanning the last two glacial-interglacial cycles from southwestern New Zealand and adjacent East Tasman Sea offer new insights into the nature, timing, magnitude and duration of past climate change in the SH mid-latitudes. The key outcomes of this study are:

1. Vegetation change in southwestern New Zealand is broadly synchronous between land and sea records and driven by orbital forcing. Superimposed on these trends are sub-millennial scale patterns which are typically antiphased from NH records. Vegetation is strongly coupled to SST variability, suggesting coastal air temperature varies synchronously with SST, except at the culmination of terminations where *D. cupressinum* lags the SST maxima.

2. Vegetation reconstructions display a subdued warming for MIS 6c/6b each side of the Southern Alps, with coeval ocean-atmosphere warming displayed adjacent to and south of New Zealand. This is not explained by local summer insolation intensity and supports a weak bipolar temperature seesaw. It is plausible that coeval glacial retreat formed the Okarito Basin, with sediment infill commencing from ~153 ka, although this may represent deposition during the penultimate MIS 7 interglacial.

3. An expansion in grassland-shrubland at the culmination of penultimate glacial cold period (139 ka) is coeval with advance of Southern Alps glaciers. This is in phase with NH summer insolation intensity minima and is similar in timing and magnitude to the vegetation changes which occurred at the conclusion of the Last Glacial Coldest Period.

4. The steady growth of tall tree vegetation persists from 139-133 ka and is matched by early warming in the ocean and atmosphere at mid-high SH latitudes. This precedes the rapid collapse of NH ice sheets and widespread ocean-atmosphere cooling in the NH by ~3-4 kyr, commencing at the onset of HS-11. These conditions and processes evident for T-II support the termination paradigm outlined by Denton et al. (2010) based on T-I, where heat stored in the NH is transferred to the SH via the ocean-atmosphere (bipolar temperature seesaw, Intertropical Convergence Zone), facilitating outgassing of CO_2 which in the southern ocean which further amplified

the rate and magnitude of terminations I and II globally and synchronously. Cool episodes briefly punctuate this SH warming and were antiphased with warming in the NH mid-latitudes.

5. A rapid succession of vegetation changes associated with warmer MAATs and a concomitant 4-5°C rise in SSTs in the East Tasman Sea occurs over T-II between 133-130 ka, with coeval warming displayed south of New Zealand. This precedes NH mid-latitude warming by at least 2 kyr, with cool conditions persisting over the remainder of HS-11/T-II. This may have been initiated by a southward transport of warm EAC water down the eastern Australian coastline and across the East Tasman Sea, by an intensification of the Southwest Pacific Gyre due to a southwards shift/intensification of the Southern hemisphere westerly wind belt. A similar pattern of ocean warming is emerging from the East Australian Current under present warming. Southern beech was likely competitively excluded during recolonisation inland from coastal refugia and rapid sea level rise during this time, perhaps giving rise to the early formation of the "Biotic Gap Zone" in central-south Westland.

6. A distinct curtailment in tall tree vegetation (early LIG climate reversal) follows HS-11 and persists for ~2 kyr. This is synchronous with a rapid decline in the Agulhas leakage, the northward migration of the Intertropical Convergence Zone and a SST rise of >5°C in the NH mid-latitudes. This displays similarities with the ACR, matching the duration (~1.8 kyr), and amplitude (~1.5-2°C) of MAAT cooling, although cooling during the ACR is ~2.8°C cooler than T-II. The signal is more pronounced in the high resolution Okarito Bog sequence than marine archives. SST cooling is more distinct during NZce-3 ~1–2°C lower than present than that at ~129.5 ka.

7. Afforestation of Westland by *D. cupressinum* occurred at the culmination of the early LIG climate reversal (127.4 ka), coeval with the warmest SSTs in the adjacent ocean (+1.3–2.5°C above modern). These conditions likely encouraged conditions favourable for growth, lagging the initial climax of podocarp-hardwood taxa by ~2 kyr, and is akin to that of T-I (3.8 kyr). Local factors such as ice cover, topographic and edaphic barriers, and prevalence of cool-conditions were likely responsible for inhibiting the development of this species in this region earlier.

8. The progression of vegetation changes are comparable between T-I and T-II, despite the rate of insolation, CO_2 rise, and sea level greatly contrasting. Dissimilarities between the timing and magnitude of environmental changes over each termination are explained by variants in these forcing mechanisms.

9. The thermal optimum in the terrestrial environment during MIS 5e occurs between 128-123 ka, with the attainment of modern estimated MAATs in the Okarito Bog record, and are coeval with or lag SST maxima by 3 kyr. This lag is partly explained by vegetation requiring time to reach equilibrium with interglacial climate, with reduced seasonality also favouring the spread of drought-frost intolerant *Ascarina lucida* on the Westland piedmont, rather than a decoupling of land and sea temperatures in this maritime environment.

10. Marked brief ~2kyr expansions in tall tree conifers occur during high austral summer insolation, and relatively low CO_2 forcing (late MIS 5e, 116 ka; mid MIS 5b, 93 ka; early MIS 4, 71 ka; MIS 3, 46 ka). These are largely synchronous with warming in ocean-atmosphere proxy records from the SH, and asynchronous with those derived from proxy records from the NH, consistent with the bipolar seesaw mechanism.

4.6 Contributions

MTR Writing, ideas and figures shown in this manuscript and supplementary information. Pollen processing and analysis for MD06-2991. Sampling, washing and picking of benthic and planktonic foraminifera for $\delta^{18}O$ analysis and SST estimates for the high resolution section MIS 6-5a. Calculation of RF based SST uncertainties Correlation of $\delta^{18}O$ depth measurements to LR04 reference curve to develop a high resolution $\delta^{18}O$ chronology. Alignment of all proxies undertaken on MD06-2991 to the respective age model. Construction of PCP's from MD06-2991 to Okarito Bog. Revision of figures generated from EGCS. Recalibration of radiocarbon dates from sites including Canavans Knob, Cropp Basin Till, and the revision of the Okarito Bog age model. Alignment of Kaipo Bog MAATs to age model of Lowe et al. (2013). Alignment of all proxies generated by other authors to revised Okarito Bog age model.

All additional work provided by other parties for this chapter:

RMN Project guidance. Partial funding of SST determinations for MD06-2991 and (with MJV) provision of MAAT data determined from Okarito Bog.

GBD Project guidance.

MJV Project guidance. Pollen analysis and ^{14}C sampling for Okarito Bog. Initial pollen counting of Okarito Bog. Provision of new pollen data and MAAT data determined from Okarito Bog.

EGCS Development of statistical uncertainty between marine-terrestrial comparisons. Calculation of level of fit between LR04 and MD06-2991. Liner interpolation of age-depth points to Okarito Bog. Calculation of sedimentation rate at MD06-2991 using interpolated points.

HB and **HLN** Picking, processing and analysis of benthic and planktonic foraminifera for developing a $\delta^{18}O$ chronology, and SST estimates for the 20 cm section of samples from MD06-2991. $CaCO_3$ analysis.

XL High resolution pollen analysis of MIS 5e for Okarito Bog.

JW MAT and PLS based MAAT estimates for the Okarito Bog record.

ABHR Provided guidance in OxCal for the depositional modelling of Okarito Bog and MD06-2991 (50% contribution).

ATS MD06-2991 planktonic foraminiferal census data for developing SST estimates.

BWH Generation of MAT-based SST estimates using the MAT SH0911 method.

GHS Random Forest SST estimates from the analysis of data provided by BH and AS.

BVA Analysis of KOT glass shards from MD06-2991 (following Chapter 3).

Chapter Five

5. Ocean-atmosphere reconstructions over MIS 11 from southwestern New Zealand

Abstract:

There is considerable interest in using past analogues to provide insight into vegetation responses to predicted future climate warming. Little is known about how mid-latitude Southern Hemisphere (MLSH) terrestrial vegetation responded to climatic forcing during the warmer phases of the Quaternary, especially those preceding the last interglacial (LIG). Terrestrial palynological records of earlier interglacial periods are commonly fragmentary and poorly-dated. These problems have been circumvented for this study by direct correlation of terrestrial (pollen) and marine climate indicators from the eastern Tasman Sea, ~100 km west of New Zealand's South Island, revealing the phase relationships between central-western South Island vegetation, sea surface temperatures in this region and ice volume during MIS 12-10. These sequences are chronologically constrained by $\delta^{18}O$, with additional independent control provided by the identification of the ~345 ka widespread silicic Rangitawa Tephra, sourced from the central North Island, which provides an important interregional marker bed between land-sea records at the onset of Termination (T)-IV.

Termination-V is characterised palynologically by a rapid increase in emergent forest taxa, and shows a similar pattern to T-II and T-I, where warming is antiphased with cooling in the Northern Hemisphere mid-high latitudes. The development of tall trees and the persistence of the thermophilous shrub *Ascarina lucida* define interglacial conditions between ~428-396 ka (32 ka duration), with several warm-cold cycles of sub orbital timescale reflected on land and ocean following the climatic optimum of MIS 11c. Surface ocean warming in the East Tasman Sea reaches ~1.5-2°C warmer than present during the interglacial, and occurs in two stages from 435 ka (MIS 12a) to ~426 ka (early MIS 11e), and from 417-407 ka. The vegetation composition in this highly humid region, between ~426 and 407 ka, shows a notable expansion and dominance of *Ascarina lucida*, and contrasts markedly with the modern interglacial assemblage in the region which is dominated by the tall tree conifer *Dacrydium cupressinum*. The assemblage is more akin to that displayed during the early Holocene climatic

optimum (11.5-9 ka) in west-central North Island, ~4 degrees of latitude north of the study region, where mean annual temperatures are on average ~3°C greater today and occur under a reduced terrestrial seasonality regime. Likewise the vegetation structure differs from LIG reconstructions, the most recent period of enhanced global warmth, which is more similar to the Holocene. Vegetation change over the MIS 11 interglacial likely reflects a prolonged period of higher land surface temperatures following extreme cold of the MIS 12 glacial which transformed the composition of the forests of southwestern New Zealand. Biogeographic barriers most likely inhibited the migration of species from more northerly latitudes better adapted to warmer climatic conditions. Comparison to vegetation changes revealed at DSDP Site 594, located ~300 km east of the South Island, suggests tall tree podocarps colonised eastern regions by as much as ~10 kyr later than their western equivalents. There is no evidence for a central Westland 'Biotic Gap' that characterises the region today, suggesting that this developed during the subsequent glacial-interglacial cycles.

5.1 Introduction

Past interglacials with climates warmer than the present are regularly studied as a means of gaining insight into the impact of future climatic warming on ecologic and geomorphic systems (Meinshausen et al., 2011; Stocker et al., 2013). Over the past 800,000 years two interglacial periods stand out as potential climate analogues for a future, warmer earth (Imbrie and Imbrie, 1980; Loutre et al., 2003; EPICA Community Members, 2004; Rodrigues et al., 2011; Yin and Berger, 2012, 2015). The greatest attention has focused on the climate optimums of the last integlacial (LIG) between 132-120 ka (Kukla et al., 2002; Cortese et al., 2013; Capron et al., 2014), and MIS 11c between ~417-396 ka (Berger and Loutre, 2002; Droxler et al., 2003; Tzedakis, 2010). These periods emerge as being globally distinctive with evidence for warmer conditions than the present interglacial (Tzedakis et al., 2009b; Lang and Wolff, 2011; Past Interglacials Working Group of PAGES, 2016), with slightly higher average atmospheric CO_2 concentrations (20 and 22 ppmv, respectively) than the pre-industrial period (Lüthi et al., 2008; Schneider et al., 2013).

The MIS 11 interglacial is seen as a particularly appealing natural analgoue for future climate condtions on earth because it is characterised by similar-to-Holocene insolation (Fig. 1.1), with low eccentricity and precession (Berger and Loutre, 1991; Howard, 1997; Berger and Loutre, 2002; Herold et al., 2012). Atmospheric CO_2 concentrations from the EPICA Dome C (EDC) ice core reached 286 ppm during MIS 11 (Siegenthaler et al., 2005; Lüthi et al., 2008), and were greater than pre-industrial concentrations (before 1750) of 278 ppm (Rubino et al., 2013), but are less than the current anthropogenically enhanced CO_2 levels which reached ~409 ppm during April 2016 (Keeling et al., 2016). Interglacial conditions were sustained over a protracted length (~28-32 kyr) during MIS 11e-c (Bazin et al., 2013; Railsback et al., 2015), and spanned two insolation peaks (Tzedakis, 2010), while the current interglacial (~12 kyr) has spanned one so far (Loutre and Berger, 2000; Loutre et al., 2003). The largest peak occurred during the climate optimum at ~410 ka and occurs late within the stage relative to the insolation minimum of the preceding MIS 12 glacial at ca. 437 ka (Candy et al., 2014). This makes the deglacial termination (T-V) the longest deglacial of the past 450 ka (Imbrie et al., 1984; Lisiecki and Raymo, 2005; Tzedakis, 2005) as well as one of the largest amplitude climate changes over the last million years (Droxler et al., 2003). One standout record of reconstructed climate change for MIS 11 regularly used in comparison to the Holocene is from EDC, with evidence for a dynamic and complex climate containing sub-millennial to millennial scale climate oscillations (Pol et al., 2011), and temperatures +3°C warmer than present (EPICA Community Members, 2004; Jouzel et al., 2007).

Proxy and simulated climate data display higher annual and seasonal air-ocean temperatures than MIS 1, and reach up to ~1.5-2°C warmer than present (Milker et al., 2013; Yin and Berger, 2015). Extremely warm conditions represented in high Northern Hemisphere latitudes over MIS 11c, with maximum summer temperatures and annual precipitation values (~4°C and 300 mm) higher than MIS 1 and MIS 5e, has led to MIS 11 considered as a "super interglacial" (Melles et al., 2012). However, such extreme warmth is not captured in paleoclimate simulations from greenhouse gas and astronomical forcing alone (+0.5°C), with amplifying feedbacks and far field linkages such as major deglaciation events in Antarctica, which are considered critical for these discrepancies (Melles et al., 2012; Coletti et al., 2015). The protracted duration of global and regional warmth is considered to have played a role in ice sheet melting in Greenland and West Antarctica which contributed to global sea levels 6-13 m above present (Rohling et al., 2010; Raymo and Mitrovica, 2012; Reyes et al., 2014). This has important implications for future sea level predictions, where atmospheric warming of the same order (1.5-2°C) produces an unstoppable contribution to sea level rise resulting from the collapse of polar ice sheets in climate models (Golledge et al., 2015).

Importantly, with the exception of climate reconstructions developed from ice cores, there remains a distinct paucity of paleoclimate and paleoenvironmental analysis from terrestrial sequences containing T-V and the MIS 11 climatic optimum in the mid-high Southern Hemisphere latitudes (Milker et al., 2013; Candy et al., 2014). As a result there is limited opportunity for empirical support of model simulations of past climate or ecological change in this region (Kleinen et al., 2014). This paucity in part results from the difficulty of finding and dating long terrestrial records that span multiple glacial-interglacial cycles. In this chapter, marine paleoclimate data from MIS 12-10 (456-338 ka) that are chronologically constrained by $\delta^{18}O$ stratigraphy are developed from MD06-2990 and MD06-2991 cores. These two nearby sites were analysed to explore the nature of T-V (Fig. 5.1), however, only MD06-2990 contains an undisturbed MIS 12-10. These sequences provide a rare opportunity to combine terrestrial and ocean climate indicators to investigate the phase relationships between ocean and atmosphere temperature regimes and ice volume over this important interval.

As there are no terrestrial sequences in the New Zealand region containing T-V and the climatic optimum of MIS 11, it is necessary to turn to Holocene records from more northern (~39°S) latitudes (western North Island) for modern analogues. Presently mean annual land surface temperatures at those sites are ~3°C warmer than for southwestern New Zealand,

and provide useful insight into how vegetation may have responded during enhanced warmth in this region (Crundwell et al., 2008; Hayward et al., 2012; Prebble et al., 2016). In addition, a similarly long pollen and SST record from DSDP Site 594, situated ~300 km east of South Island, New Zealand, offers an equally useful insight into regional climate variability over South Island from late MIS 12-10. Identification of the regionally widespread ~345 ka Rangitawa Tephra (RtT) (Lowe et al., 2008) in MD06-2990, 2991 and DSDP Site 594 strengthens the $\delta^{18}O$-based age models and provides an important interregional marker bed in paleoenvironmental studies at the time of deposition (Pillans et al., 1996; Alloway et al., 2005).

The strengths of extracting terrestrial palynomorphs from marine sequences are utilised over this interval to overcome their respective shortcomings and are used here to specifically address the following questions:

1. What is the sequence of vegetation and climate events associated with glacial termination V and the full MIS 11 interglacial from southwestern New Zealand?

2. How do the timing and magnitude of climate events during MIS 12-10 across southern South Island relate to climate forcing, and how do they compare with existing observations and paradigms of glacial terminations such as that outlined by Denton et al. (2010), and subsequent climate optimums during the LIG and the Holocene?

5.2 Environmental framework:

The climate and vegetation of southwestern New Zealand is described in Chapter 2 and 3. MD06-2990 is situated on the north bank of the Hokitika submarine canyon system, ~10 km NW of MD06-2991, with both cores analysed in this study. The location of marine and terrestrial sites discussed in text is displayed in Fig. 5.1 with proxy information, such as vegetation and SST reconstructions and the occurrence of tephra from them detailed in Suppl. Table 5.1. Cores from these sites span from the MIS 12 glacial, locally termed the Kawhaka glacial (Suggate, 1990; Suggate and Waight, 1999; Barrell, 2011), until the MIS 10 glacial (Neomona glacial), with all sites containing the MIS 11 interglacial.

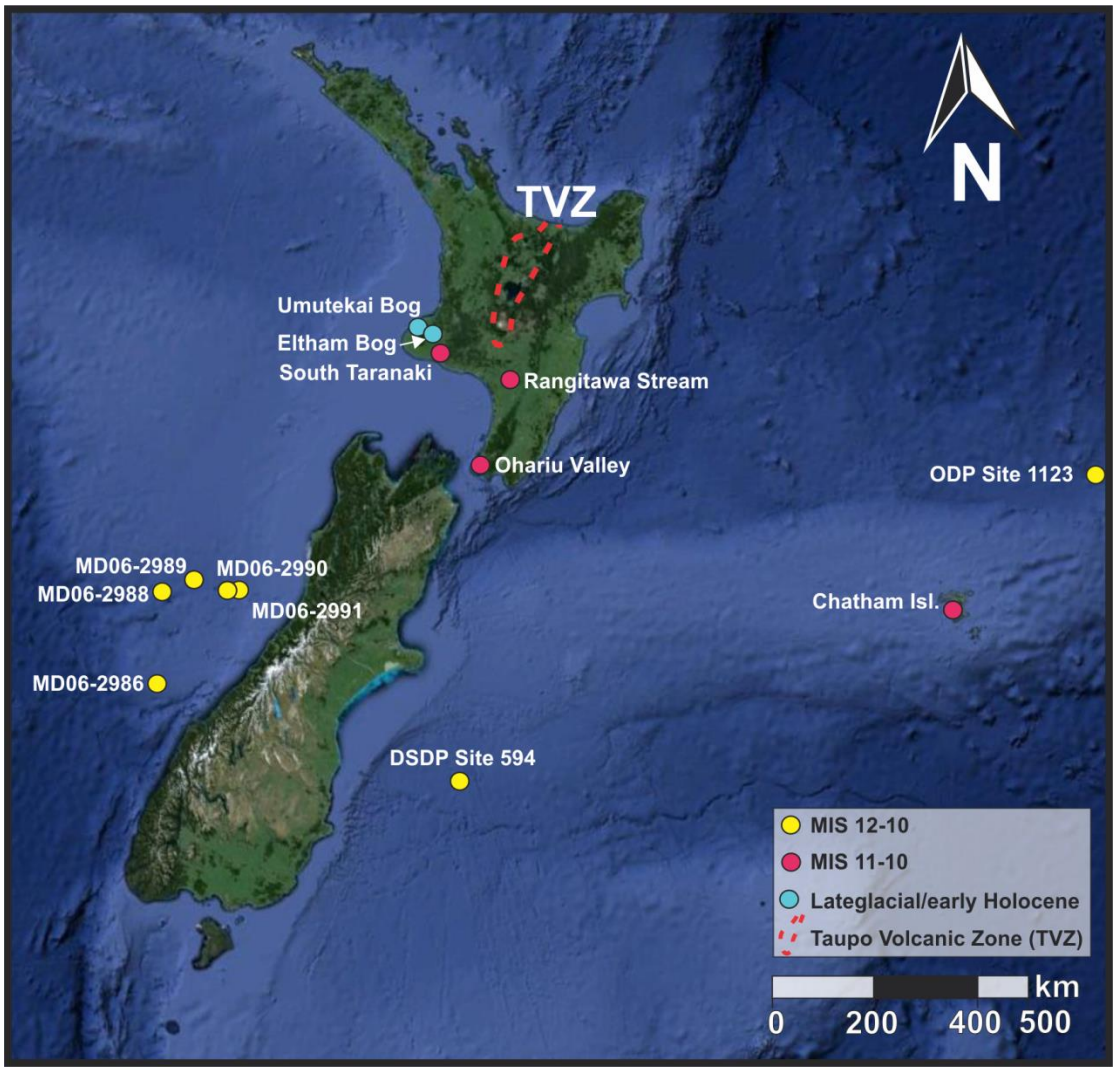

Fig. 5.1: Location of all land and sea records which encompass the MIS 11 interglacial discussed in text. Pollen records developed from MD06-2990/2991 (yellow) form the primary focus of this study. Rangitawa Tephra (RtT), erupted from the Taupo Volcanic Zone (TVZ), occurs in all records, except MD06-2986, 2988 and 2989 and ODP Site 1123 (Crundwell et al., 2008; Hayward et al., 2012; Prebble et al., 2016). The Lateglacial terrestrial palynomorph record from Umutekai Bog (blue) is discussed as an analogue for potential vegetation and climate changes in Westland under enhanced global/regional temperatures than the present. Source: Google Earth.

5.2.1 Umutekai Bog (early Holocene analogue)

Umutekai Bog (90 masl), situated ~5 km inland of the Taranaki coastline on the west coast of North Island (Fig. 5.1), contains a sequence of mud, peat and tephra which encompass the late glacial-early Holocene climatic optimum (Newnham, 1990; Newnham and Alloway, 2001; Newnham and Alloway, 2004). This sequence was selected for inclusion here as the early Holocene interval (~11-9 cal ka BP) at this locality represents wet and warm conditions potentially analagous to the MIS 11 found in cores MD2990/1 further south. Presently the climate of north Taranaki coastline is temperate with a mean monthly maximum of ~17.5°C (~22°C in February the warmest month), and a monthly minimum of 10°C (5.8°C July; the coolest month),~13 frost days per year and relatively high rainfall (900-1600 mm) which is distributed evenly throughout the year. Offshore mean annual SSTs are 16°C (Locarnini et al., 2013). Early Holocene conditions in the Taranaki region are characterised by podocarp-angiosperm forest and abundant tree ferns, with high levels of *Dacrydium cupressinum* and the thermophilous *Ascarina lucida*, which is rare or not found in Taranaki today (Alloway et al., 1992; McGlone and Neall, 1994; Newnham and Alloway, 2001; Newnham and Alloway, 2004). These species are associated with warm-wet conditions in the New Zealand pre-deforestation database, with reconstructed vegetation based temperature reconstructions for the early Holocene from Eltham Bog in Taranaki (Fig. 5.1), slightly warmer (0.4°C) than present conditions (McGlone and Neall, 1994; Wilmshurst et al., 2007).

5.2.2 Rangitawa Tephra (RtT)

Rangitawa Tephra has been geochemically and chronologically linked to one of the largest super-eruptions of the Late Quaternary (Froggatt et al., 1986; Kohn et al., 1992; Lowe et al., 2001; Alloway et al., 2005). Rhyolitic ignimbrites and their co-eruptive fall deposits (>2000 km^3 dense-rock equivalent; DRE) originated from Whakamaru Caldera, Taupo Volcanic Zone (TVZ), central North Island of New Zealand, 630 km to the northeast of Westland, and represent one of the largest eruptions known to have occurred in New Zealand (Briggs, 1976; Wilson et al., 1986; Brown et al., 1998; Matthews et al., 2012; Downs et al., 2014). Widespread ash fall out (~700 km^3) from this eruption provides an important New Zealand interregional marker bed in paleoenvironmental studies for the mid-Pleistocene, occurring within terrestrial and adjacent marine sedimentary sequences assigned to the MIS 10 glacial (Kohn et al., 1992; Hesse, 1994; Heusser and van de Geer, 1994; Palmer and Pillans, 1996; Holt et al., 2010). The tephra may have also extended as far south as the Antarctic margin (Froggatt et al., 1986; Pillans et al., 1996).

Approximately 54 independent numerical age estimates exist for Rangitawa Tephra. These were obtained by fission-track (glass and zircon), thermoluminescence, infrared stimulated luminescence, K/Ar and single crystal $^{40}Ar/^{39}Ar$ analysis, and orbital tuning via matching to $\delta^{18}O$ stratigraphy of ocean sediments (Pillans et al., 1996; Shane et al., 1996; Lowe et al., 2001; Holt et al., 2010; Downs et al., 2014). Pillians et al. (1996) show there is relatively good correspondence between the weighted mean of fission track ages (345 ± 12 ka, 1σ) and that of 340 ± 7 ka produced from astronomical tuning variations in $\delta^{18}O$ from two marine sediment cores adjacent to New Zealand (Nelson et al., 1985; Black et al., 1988; Shackleton et al., 1990). Downs et al. (2014) present the most recent weighted mean age ($^{40}Ar/^{39}Ar$) of the correlative Whakamaru Eruption to 349±4 ka (2σ). The identification of RtT in highly resolved marine sediment archives with $\delta^{18}O$ chronologies and a strong terrestrial influence adjacent to South Island New Zealand in this study offers insight between the background state of climate in the SH mid-high latitudes at onset of T-IV.

5.3 Materials and methods

5.3.1 Core information and sampling and chronology

Piston cores MD06-2991 (33 m long, 886 mbsl, 42°21´S, 169°59´E) and MD06-2990 (33.55 m long, 943 mbsl, 42°19'S, 169°55'E) were retrieved from the northern levee bank of the Hokitika submarine canyon system by a Calypso piston corer deployed from the R.V *Marion Dufresne* (Proust et al., 2006; Proust et al., 2008). Sediment recovered at each site consisted of a greenish grey foraminifera-rich mud, with no turbidites observed.

MD06-2991

For the purpose of establishing a core chronology, samples of sediment from MD06-2991 were analysed every 10 to 20 cm (0.5-1 cm thick slices) from the working half of the core between 33.2-21.6 m core depth. Bulk samples were washed and foraminifera from each sample were picked for stable isotopes ($\delta^{18}O$ and $\delta^{13}C$) at NIWA by Helen Neil and Helen Bostock, and follow the methods outlined in Chapter 2, which follow those of Neil et al. (2004). The age models adopted for all southwestern New Zealand cores presented in this study were constrained by matching down-core benthic foraminiferal $\delta^{18}O$ to the reference LR04 benthic $\delta^{18}O$ stack by the author (Lisiecki and Raymo, 2005; Fig. 5.2 and Fig. 5.3). The basal ~4 m of core (33.2-28.6 m) have depleted $\delta^{18}O$ measurements interpreted to reflect an over thickened sequence of ~MIS 11 age (Fig. 5.2; Neil, 2008). Forty-two samples (4-15 g dry weight) between 28.6-21.6 m (MIS 11-10; 404-338 ka), situated within 1 cm of the above-mentioned, were treated following palynological methods described in previous chapters. The addition of a *Lycopodium* tablet (20,848 grains, s.d. 1546) to each sample was used for determining the absolute abundance of pollen and volcanic glass shards. Rates of deposition at MD06-2991 are greatest during MIS 11c and MIS 11b (~25 and 14 $cm.kyr^{-1}$ respectively), with a rate of ~8.5-10 $cm.kyr^{-1}$ until MIS 10 (Suppl. Table 5.2). The average sample resolution is 1 sample per 1.6 kyr, with an average of 244 dryland pollen grains (range 112-329 grains) per sample.

MD06-2990

The age model adopted for MD06-2990 is based on high (2 cm) resolution benthic foraminiferal isotope analyses ($\delta^{18}O$ and $\delta^{13}C$) down to 19.48 m by Silke Steph at the Alfred Wegener Institute in Germany. The sampling procedure follows that taken for the top 13.5 m of core outlined in Ronge et al. (2015). Each sample consisted of approximately four specimens of the benthic foraminifera *Cibicidoides wuellerstorfi*, or three specimens of *Uvigerina*

peregrina in samples lacking sufficient amount of *C. wuellerstorfi*. Stable isotope measurements were conducted using a Finnigan MAT 253 mass spectrometer with a Kiel IV Carbonate Device. The internal precision (within a run) of standard measurements was better than ±0.06‰ for $\delta^{13}C$ and ±0.08‰ for $\delta^{18}O$ (Ronge et al., 2015).

Thirty-six sediment samples (14-28 g dry weight) were taken from the archive half of the MD06-2990 core at 1 cm thick slices over 10-20 cm intervals between 14-9 m (MIS 12-10; 456-339 ka). These samples were processed for palynology following the methods described in Chapter 3.3.4. The coarse fraction (>150 μm) was retained for planktonic foraminiferal assemblage counting (n=20 samples) to generate co-existing SST reconstructions from the same sample (see 5.2.3). The sedimentation rate over this interval averages 4.3 $cm.kyr^{-1}$ (1 palynological sample per 3 kyr), with an average of 257 dryland pollen grains (range 130-288 grains). Sedimentation is greatest (>6 $cm.kyr^{-1}$) during the glacial and stadial episodes of MIS 12, 11b and 10, and is lowest (2-2.5 $cm.kyr^{-1}$) during MIS 11c and 11d (Fig. 5.3; Suppl. Table 5.1). An additional <1g of dry weight of bulk sediment was taken at 1 cm resolution from 953-922 cm and spiked with a *Lycopodium* tablet to better constrain the distrubtion of RtT glass shards in the core (Blockley et al., 2005). Dryland pollen and non-dryland palynomorphs were grouped according to that outlined in Chapter 3. In order to facilitate comparison of the pollen records presented, a stratigraphically constrained cluster analysis (CONISS), with a square-root transformation was performed on the MD06-2990 and MD06-2991 pollen profiles (Grimm, 1987), and excluded all dryland pollen taxa that never reach 2% in any sample.

5.3.2 Chronological uncertainty

For reasons of stratigraphic integrity, reconstructions of vegetation and marine and terrestrial climate changes over MIS 12-10 are based on core MD06-2990 as $\delta^{18}O$ variability for MIS 11 is poorly resolved in MD06-2991 (Fig. 5.2). Orbital tuning of chronologies over MIS 11 are considered less secure than other warm stages due to the subtle shifts in oxygen isotope values which provide fewer "tie points" (Desprat et al., 2005). Nonetheless, there is a strong correlation (r=0.92) between down-core MD06-2990 $\delta^{18}O$ variability and the LR04 $\delta^{18}O$ stack as determined in Analyseries 2.0 (Paillard et al., 1996). Age uncertainties in the LR04 $\delta^{18}O$ reference curve may be compounded by a degree of subjectivity in the fit (i.e., 'wiggle-match'). Age uncertainty associated with wiggle-matching is discussed in detail in supplementary material associated with Chapter 4. The time offset which gives the best fit between the LR04 benthic $\delta^{18}O$ stack and the MD06-2990 $\delta^{18}O$ stratigraphy over the 500-

0 ka time interval is 0.2 kyr (± 6 kyr, 95% level of confidence; Suppl. Fig. 5.1-5.2), and suggests good agreement between the subjective matching of MD06-2990 to the LR04 stack.

With all sources of errors incorporated, Lisiecki and Raymo (2005) suggest their widely used LR04 $\delta^{18}O$-age reference curve has an uncertainty of up to 4 kyr at any point in time over the last million years. This is potentially compounded by regional differences in the timing of $\delta^{18}O$ change (Skinner and Shackleton, 2005). For example, Lisiecki and Raymo (2009) suggest that $\delta^{18}O$ changes in the Atlantic precede those in the Pacific by an average of 1.6 kyr for the last five terminations. The timing and uncertainty during MIS 10 at 350 ka and at T-IV at 335 ka in the LR04 stack has been constrained in the Pacific basin by Caballero-Gill et al. (2012a) to be ~1 kyr (2σ), via matching their benthic $\delta^{18}O$ record from ODP 1146 in the South China Sea to the nearby independently U/Th dated speleothem SB11 from Sanbao Cave (Cheng et al., 2009).

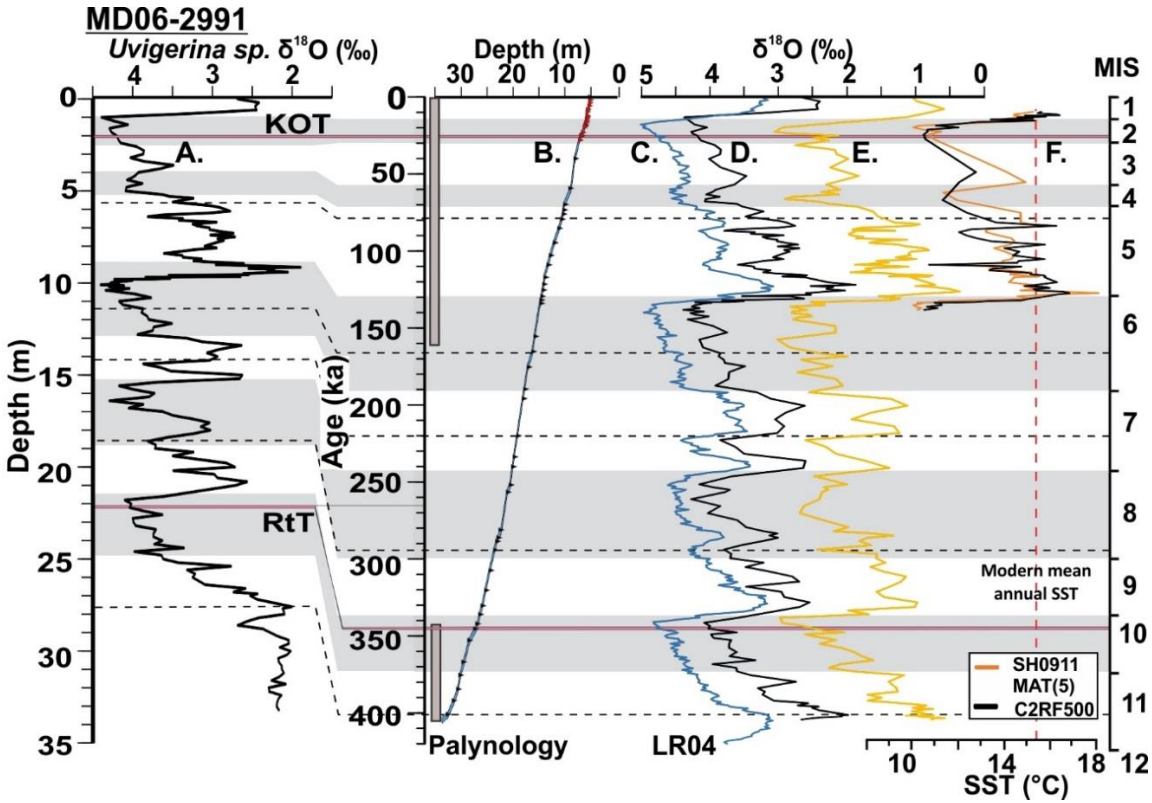

Fig. 5.2: MD06-2991 age model and SST reconstruction. **A.** Down-core benthic $\delta^{18}O$ stratigraphy of MD06-2991 *Uvigerina peregrina*. **B.** Age-depth model with calibrated ^{14}C dates (red triangles, n=15) on planktonic foraminifera, and $\delta^{18}O$ tie-points (black triangles) which align down-core $\delta^{18}O$ measurements from MD06-2991 to; **C.** the reference LR04 benthic $\delta^{18}O$ stack (Lisiecki and Raymo, 2005). Guidelines (dashed lines) illustrate this procedure, with MIS glacial boundaries displayed in grey (Lisiecki and Raymo, 2005). **D & E**. MD06-2991 oxygen isotope records for the benthic and planktic species *Uvigerina peregrina* and *Globigerina bulloides*. **F.** SST estimates from planktic foraminifera based on the modern analogue technique (MAT) using the SH training set (SH0911C2) and a random forest ensemble (C2RF500) based SST for the same foraminiferal counts. The maximum concentration of Kawakawa/Oruanui Tephra (KOT) and RtT glass shards is displayed in pink at 201 cm (25.1 ka) and 22.2 cm (346 ka), respectively. The pollen sequence examined in this chapter is the lower shaded section (405-345 ka).

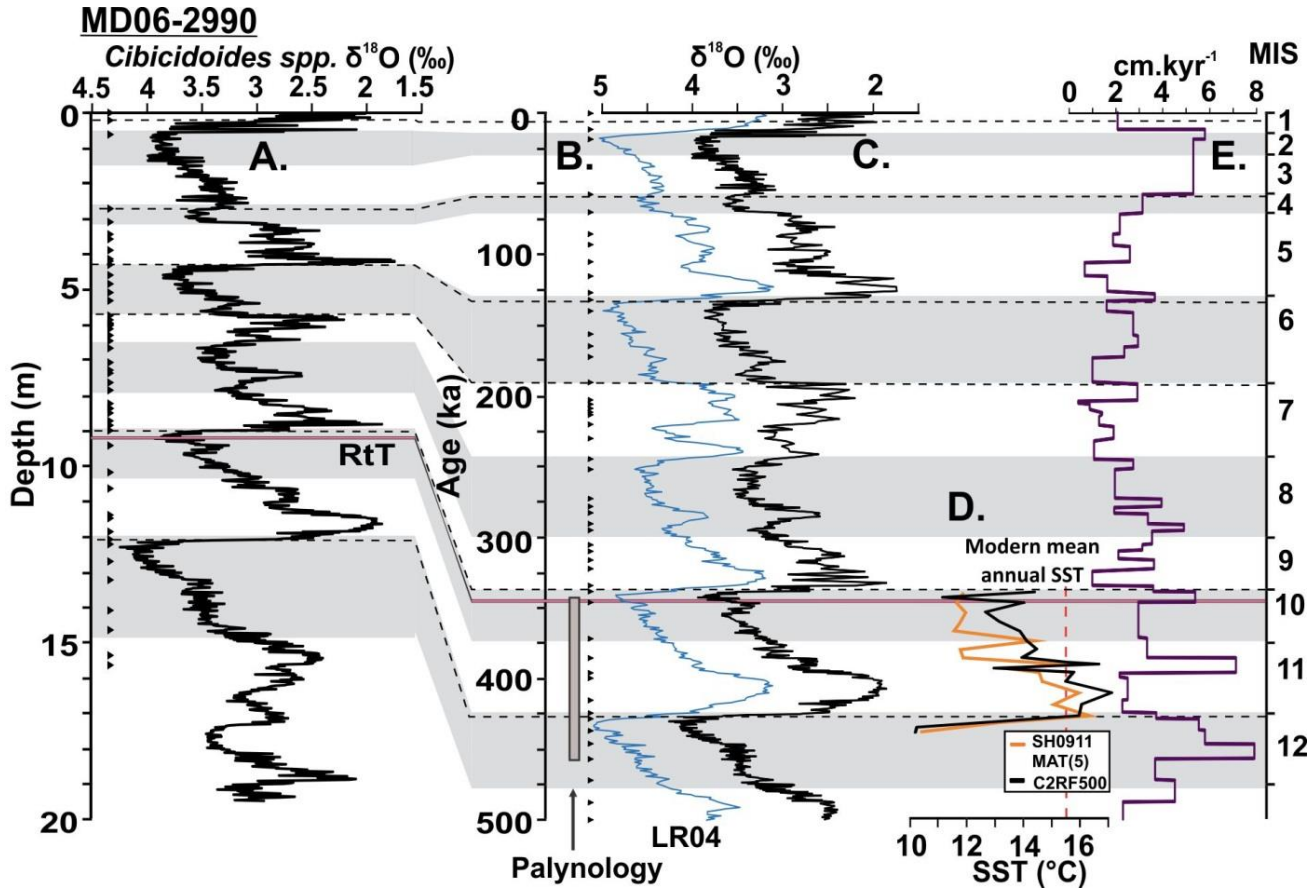

Fig. 5.3: MD06-2990 age model and SST reconstruction. **A.** Down-core benthic $\delta^{18}O$ stratigraphy of MD06-2990 (*Cibicidoides wuellerstorfi*) with corresponding $\delta^{18}O$ tie-points (black triangles) and guidelines (dashed lines) to **B.** the reference LR04 benthic $\delta^{18}O$ stack with MIS glacial boundaries are displayed in grey (Lisiecki and Raymo, 2005). **C.** The benthic $\delta^{18}O$ stratigraphy of MD06-2990. **D.** SST estimates from planktonic foraminifera based on the modern analogue technique (MAT) using the SH training set (SH0911C2) and a random forest ensemble (C2RF500) based SST for the same foraminiferal counts. The maximum concentration of RtT glass shards is displayed in pink at 931.5 cm and 344.5 ka, respectively. The pollen sequence examined in this study is indicated from 456-342 ka.

5.3.3 Rangitawa Tephra (RtT)

Additional independent tephrochronological control is achieved from the presence of volcanic glass geochemically correlative with the RtT, which occurs cryptically in marine cores MD06-2990/2991, and as a discrete ~10 cm thick bed in DSDP-594, situated ~300 km east of South Island, New Zealand (Fig. 5.1). Glass shards were separated by density from bulk sediment with 2.0 s.g. sodium-polytungstate at 22.21 mbsf from MD06-2991. Macroscopic glass was picked directly from bulk sediment at 36.5 mbsf from DSDP 594. The separated fractions were sieved through 63-μm meshes and glass shards in the >63 μm fraction were analysed for major elements with a JEOL Superprobe (JXA-8230) at Victoria University of Wellington by Brent Alloway. All analyses were corrected using the ZAF method. Analyses were performed using an accelerating voltage of 15 kV under a static electron beam operating at 8 nA. The electron beam was defocused to yield a spot size between 10 and 20 μm. The abundance of all elements was calculated on a water-free basis, with H_2O by difference from 100%. Total Fe was expressed as FeO_t and all samples were normalised against glass standards ATHO-G (Jochum et al., 2000) and/or VG-568 (Jarosewich et al., 1980). To confirm the presence of RtT in marine cores adjacent to southwestern New Zealnd where it was not present macroscopically, the abundance of glass shards >50 μm in size were counted in palynological slides (Suppl. Fig. 5.3-5.4) from depths bracketing the reported age of 345 ± 12 ka (1σ) for RtT determined by Pillans et al (1996). This equates to depths of 2260-2140 cm for MD06-2991, 960-900 cm for MD06-2990 and 24.34 m for MD06-2986.

5.3.4 MD06-2990 sea surface temperature (SST) estimates

SST estimates for MIS 12-10 are based on planktic foraminiferal faunal assemblages undertaken by Ashwaq Sabaa and Bruce Hayward (Geomarine Research Ltd) and follow the methods of Hayward et al. (2012) and Cortese et al. (2013). The >150 μm size fraction from 20 samples jointly processed for palynology was repeatedly split until approximately 300 (range 218-447) whole or nearly whole planktic foraminiferal tests remained, which were identified and counted. Eighteen species of planktic foraminiferal taxa were discriminated, with most being used in the reconstruction of mean annual SSTs using a modern analogue technique (MAT) that includes reference to 1223 SH core top samples (SH0911C2, www.ncdc.noaa.gov/paleo/paleo.html; Cortese et al., 2013). The MAT finds faunas in the training set that most closely match that in the core set. The mean SST from the five most similar training set faunas is assigned to each test sample in the core set (using Chord

coefficient of similarity), with 2σ uncertainty (Suppl. Fig. 5.5). A measure of accuracy of these SST estimates is given as the range of SST values of the five most similar training set faunas.

Additional SST estimates were calculated using the same census data following the methods of Cortese et al. (2013) by George Scott (GNS) who used the Random Forest model (C2RF500). This is an ensemble decision tree tool (n=500 runs) that has been applied to core-top planktonic foraminiferal faunas from the SH0911C2 training set which are calibrated to modern SSTs, and computed using the Random Forest package (http://cran.r-project.org/web/packages/randomForest/). Cortese et al. (2013) find that that the MAT method is the best predictor for error tolerances between 0-1°C, followed by Random Forests (RF). The Random Forest method replaces the MAT where error tolerances exceed this range, with Cortese et al. (2013) concluding that RF is the best predictor over the full training set. All RF-based SST estimates for the 437-338.5 ka period are within the uncertainty of the MAT-based estimates, with the 95% confidence interval for each predicted SST, computed from the 500 estimates (Suppl. Fig. 5.5).

5.4 Results

5.4.1 Southwestern New Zealand profiles (palynology and SST)

In general, sediment colour, $\delta^{18}O$, faunal census-derived SST, and arboreal pollen proportions in southwestern New Zealand profiles vary in concert with G-I cycles and MIS subdivisions (Suppl. Fig. 5.6 and 5.7). The palynological record from MD06-2990 captures the T-V transition and MIS 12-10 sequence and is the first to represent these periods in detail from New Zealand (Fig. 5.4). This record is summarised in Table 1 and is presented alongside the MD06-2991 pollen record (Fig. 5.5), which displays similar temporal trends in the relative abundance of dryland pollen.

The pollen assemblages for glacial periods periods MIS 12 and 10 are similar, and are characterised by the highest abundance of herb taxa (~20%), while Asteraceae (shrub) pollen is typically common to abundant (10-40%). SST reconstructions in MD06-2990 during MIS 12 are ~10.2ºC, similar to MIS 6 and MIS 2 values in MD06-2991 (10.4ºC, Chapter 4). Slightly higher SST values are observed for MIS 10 (11–11.5ºC). The pollen content and degree of cooling in SST estimates during MIS 12 and 10 were significantly cooler than brief stadials (i.e., MIS 11b), where prominent increases in subalpine shrub and herb taxa occur coeval with declining SSTs of up to 1-3°C. The lowland-montane forest shrub *Ascarina lucida* is largely absent during these cooler periods.

A distinctive step-wise progression of arboreal pollen occurs over the major climate transitions from MIS 12a-11e and MIS 10a-9e (i.e., terminations T-V and T-IV, respectively). Various montane-subalpine shrubs replace herbs, with an increase in tree ferns and podocarp-hardwood forest taxa over T-V and T-IV. Both intervals are marked by a distinctive change in the colour of micaceous silty mud from dark to light grey in MD06-2990. The shift in vegetation across T-V and T-IV appears to coincide with a 4°C increase in SSTs, and slightly precede the pronounced progressive decrease in $\delta^{18}O_{benthic}$ (Fig. 5.3). The onset of the MIS 11 and MIS 9 interglacials (428 and 338 ka, respectively) are marked by high abundances of tree ferns and tall tree taxa (up to 50 and 55%, respectively). The lowland shrub *Ascarina lucida* also increases in lower MIS 11e from >3% and reaches to ~15% in MIS 11c, forming an important component of the lowland forest assemblage. Interestingly these values are trhe highest yet recorded of *A. lucida* in southwestern New Zealand profiles (Suppl. Fig. 4.17 and 4.20), and exceed the relative abundances for interglacials MIS 5e and MIS 1 (Chapter 4). The interglacial succession over MIS 11 culminates with *Dacrydium cupressinum* becoming the dominant lowland conifer (~25%) during MIS 11c (414-

409 ka), as SSTs increase up to ~1.6°C greater than present. Southern beech is recorded in greater numbers during MIS 11 than subsequent warm interglacials and is variable after 406 ka in both southwestern New Zealand profiles, increasing to up to 17-30%. SSTs are sustained at levels equivalent to modern or above modern over the entire MIS 11e-c period in RF based reconstructions, with more variability in MAT based reconstructions. RF-based SST estimates more closely resemble the associated benthic isotope curve than MAT-based estimates (Fig. 5.3), and are preferred for comparison with SST estimates for preceding interglacials and other records of MIS 11 which use artificial neural network models (ANN). A quasi-steady demise of tall tree taxa and SSTs characterises MIS 11b-10b.

Table 5.1: Summary of the key palynomorph changes and their vegetation inferences drawn for southwestern New Zealand from MD06-2990/2991, in relation to MIS determined from the $\delta^{18}O$ for this core and SST estimates.

		Southwestern NZ	
MIS	**Age range (ka)**	**Description of key palynomorphs and inferred vegetation**	**SST estimates**
10a	346-338	Podocarp-hardwoods increase (20-40%) following the deposition of RtT at 346 ka until the culmination of MIS 10 at ~338 ka. Tree ferns and *Ascarina lucida* similarly rise from 343 ka.	**MAT:** Steady increase to 11.9°C. **RF:** Rapid decline to ~11°C at 343 ka, rising to 14.4°C at 339 ka
10b	354–346	A distinctive rise in podocarp-hardwood taxa to 35% is displayed in the higher reolution MD06-2991 record at 352 ka. This is similar to those which occur during MIS 11a, although is of smaller magnitude.	**MAT:** Slight decline from 12-11.6°C. **RF:** Increase from 12.7–14°C at 346 ka.
10c	365–354	Tall tree taxa decline to <35% in southwestern NZ profiles, with low values of *Dacrydium cupressinum* (<10%), relative to an expansion of montane-sublapine shrubs and herbs.	Values between 12-12.7°C.
11a	390–365	Characterised by minor fluctuations between podocarp-hardwood forest, montane-subalpine shrubs, and alpine herbs. With an overall trend of decreaing tall tree pollen and tree ferns.	**MAT:** Declines to 11.5°C, with a brief increase to 14.4°C at 373ka. **RF:** Gradual decline to 13.9°C.
11b	396–390	Podocarp-hardwood forest pollen, tree ferns, and *A. lucida* decline between ~395-392 ka in southwestern NZ profiles. Subalpine shrub taxa and herbs increase.	Rapid decline to 13-13.5°C in both reconstructions at 392 ka, and rises to rises to 15.5-16.7 at the onset of MIS 11a.
11c	417–396	A distinct shift in the composition of lowland forest taxa (*P/P*, *Dacrycarpus dacrydiodes*, and *A. lucida*) takes place at 413 ka. *D. cupressinum* attains peak abundance, with proportions reaching interglacial values (>25%). *Fuscospora* and *Phyllocladus* briefly increase at 405ka, while *A. lucida* remains present in southwestern NZ profiles.	**MAT:** Rises to 16°C (109.5 ka) and declines to 14.7°C. **RF:** Rises to 17.1°C and declines to modern values.
11d	420–417	Tall tree taxa remain dominant in this interval (60%), with a slight increase in beech. *A. lucida* reaches the highest values in the record (~15%).	MAT based estimates decline to 15°C, with RF estimates at 16°C.
11e	428–420	Podocarp-hardwood forest and tree ferns decline at the onset of MIS 11e, as the montane-subalpine shrub of Asteraceae increases. *A. lucida,* podocarp-hardwoods (particularly *P/P* and *Dacrycarpus dacrydiodes*), and tree ferns follow this rise and attain dominace at 422 ka.	Rising from 15°C to 16-16.4°C at 426 ka, before remaining steady or falling to 15.5°C (MAT)
12a	436–428	This interval is marked by a distinctive step wise transition from herbs, through shrub taxa of Asteraceae, *Coprosma* and *Myrsine*. The interval culminates with an expansion of lowland podocarps (*P/P*) and tree ferns, and the appearance of the frost and drought intolerant shrub *A. lucida*.	Both estimates increase from ~10.2 to 14.5°C.
12b	456–436	This period is characterised by relatively high levels of herb taxa (10-20%), and montane-subalpine shrubs (Asteraceae, *Coprosma*). Arboreal pollen (and tree ferns) decline to ~27%, with beech increasing at the end of the substage to <30%.	**MD06-2986: MAT:** Declines to 8.5°C at 450 ka as tree pollen declines, and increase at the end of the substage.

Note: *Podocarpus/Prumnopitys* is abbreviated to *(P/P)*.

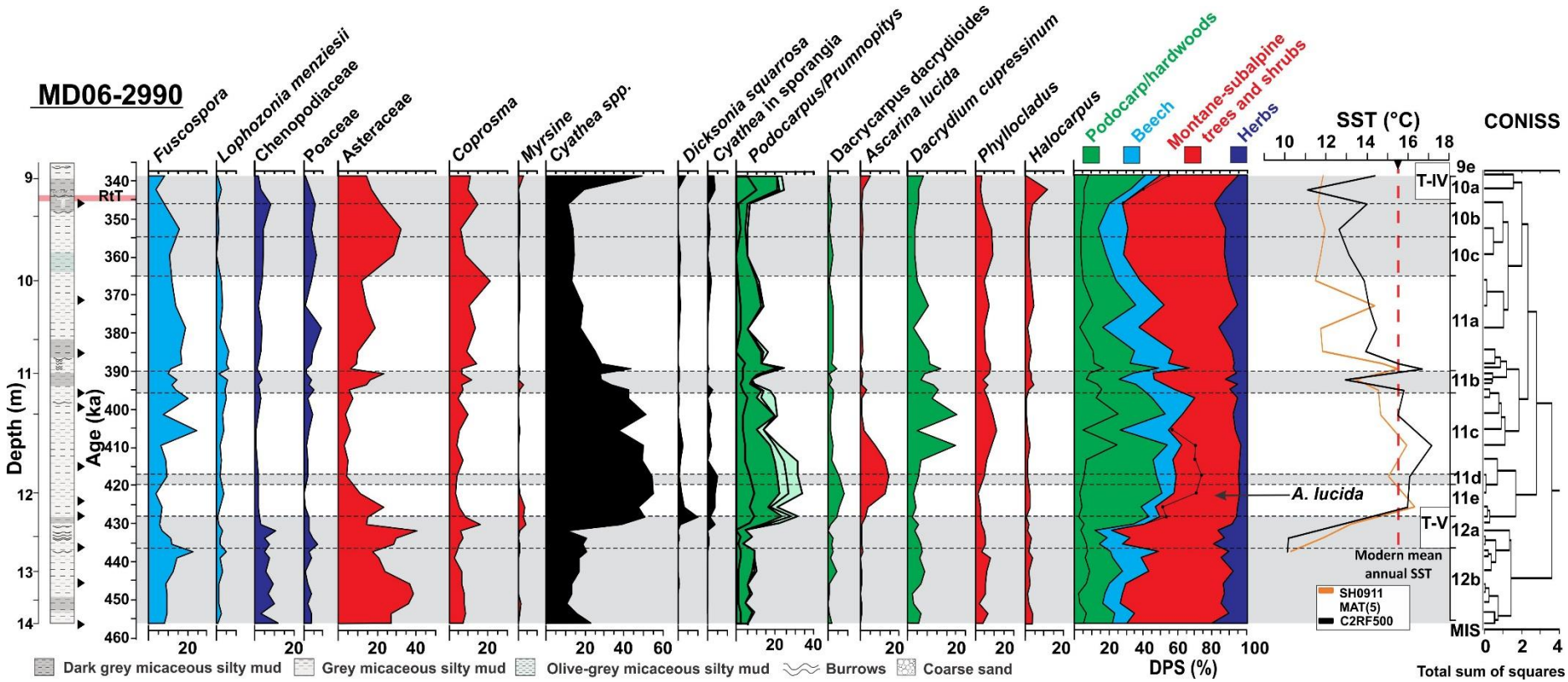

Fig. 5.4: Core stratigraphy, age model and partial percentage pollen diagram showing the prominent dryland pollen taxa from T-V to T-IV for MD06-2990. Colour-coded individual and grouped dryland pollen taxa and *Cyathea* fern spores. Note the distinctive succession between the *Fuscospora* peak at 437 ka, through grassland-shrub taxa, tree fern spores, and tall tree taxa as T-V progresses to completion. *Podocarpus/Prumnopitys* are grouped with *Podocarpus* (green) and undifferentiated *Podocarpus/Prumnopitys* (light green), while *Prumnopitys ferruginea* and *Prumnopitys taxifolia* (both light green) are differentiated by a black line. MIS 11 is dominated by *Ascarina lucida* (up to 20%), also outlined in the cumulative diagram in the montane trees category, and is replaced by *D. cupressinum* at 410 ka. SSTs for MD06-2990 follow the pollen diagram, with the modern mean annual SST (15.5°C) for the core site (1981-2010) indicated (red dashed line). Constrained cluster analysis (CONISS) is shown and broadly aligns with the MIS stratigraphy, with glacial and stadial boundaries displayed in grey shading and black dashed lines following Railsback et al. (2015). The maximum concentration of cryptic RtT is shown at ~342 ka, with concentrations counted in samples displayed with yellow circles.

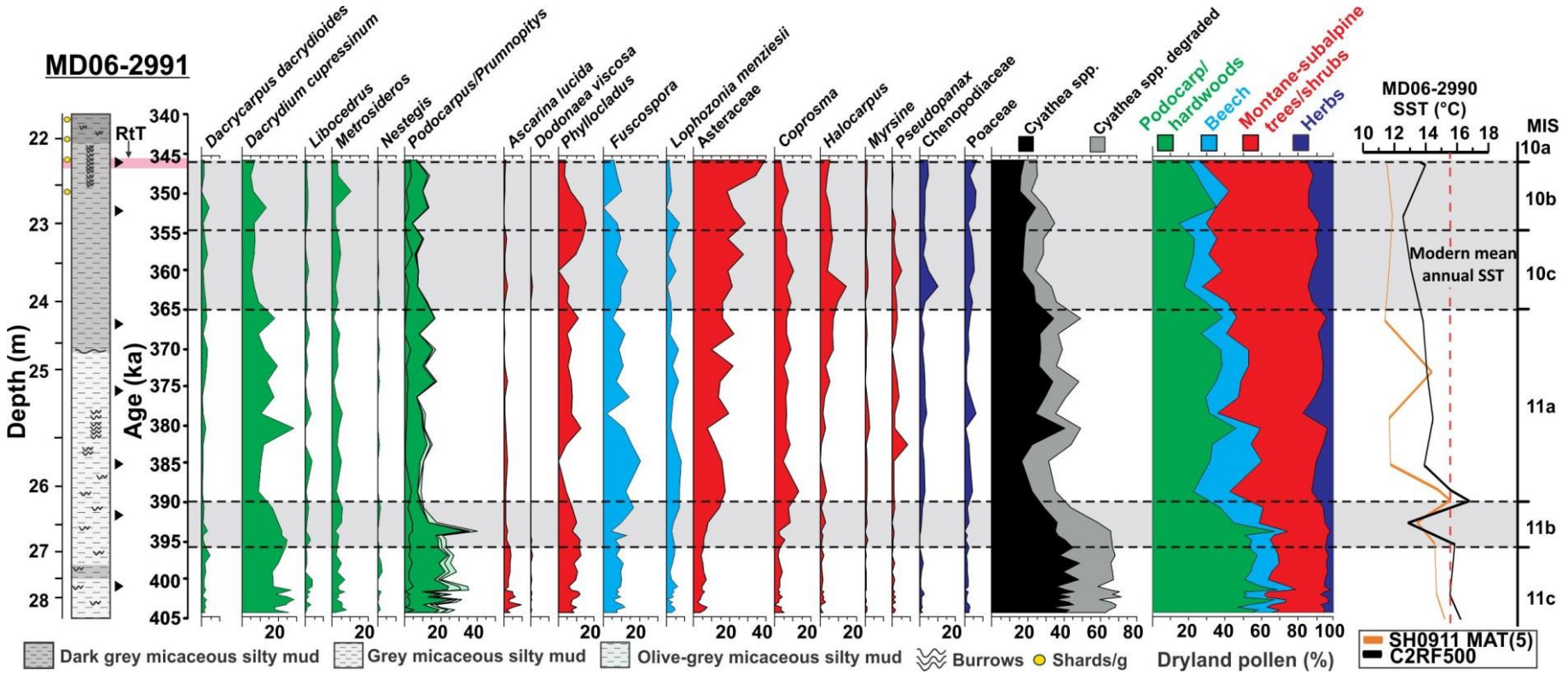

Fig. 5.5: Core stratigraphy, age model and partial percentage pollen diagram showing the prominent dryland pollen taxa from MIS 11-10 for MD06-2991. Colour-coded individual and grouped dryland pollen taxa and *Cyathea* fern spores. *Podocarpus/Prumnopitys* are grouped with *Podocarpus* (green) and undifferentiated *Podocarpus/Prumnopitys* (light green), while *Prumnopitys ferruginea* and *Prumnopitys taxifolia* (both light green) are differentiated by a black line. MIS 11 is dominated by tall tree taxa with *Ascarina lucida* present (5-10%). SSTs for MD06-2990 follow the pollen diagram, with the modern mean annual SST (15.5°C) for the core site (1981-2010) indicated (red dashed line).Constrained cluster analysis (CONISS) is shown and broadly aligns with the MIS stratigraphy, with glacial and stadial boundaries displayed in grey shading and black dashed lines (Lisiecki and Raymo, 2005; Railsback et al., 2015). The maximum concentration of cryptic RtT is shown at ~346 ka, with concentrations counted in samples displayed with yellow circles.

5.4.2 Rangitawa Tephra

Glass shard major element chemistry and stratigraphic position unambigously confirm the persence of the RtT for the first time adjacent to southwestern New Zealand (Fig. 5.6; Supp. Table 5.3). The maximum concentration of RtT glass shards recorded at MD06-2991 occurs at 22.21 mbsf (350 shards/g), corresponding to 346 ka. A distinct dark vertical burrow identified between 22.52-22.13 m core depth suggests bioturbation may have dispersed shards over this range, despite a relatively high sedimentation rate (~15 cm.kyr^{-1}). At MD06-2990, RtT glass shards are distributed between 346-342 ka (944-928 cm). The concentration is greater than at MD06-2991, with the maximum occurrence at 344.5 ka (931.5 cm; ~6500 shards/g), with cuboid and pseudo-hexagonal structures in the volcanic glass recognized (Suppl. Fig. 5.4). Light coloured burrows noted in this interval occur as the rate of deposition increased to 5.3 cm.kyr^{-1} (Proust et al., 2006), and may reflect tephra infill of bioturbation hollows. No shards were observed at 344.4 ka at MD06-2986, situated ~210 km south of the Hokitika Canyon cores. The revised age of RtT from DSDP 594 at 36.55-36.45 m corresponds to 345 ka when aligned to the LR04 stack (Suppl. Fig. 5.8), placing it at the onset of MIS 10a (~346-338 ka), 4 kyr older than previously suggested (Black et al., 1988; Nelson, 1988).

The stratigraphic position of RtT at MD06-2991, MD06-2990 and DSDP-594 is internally consistent in terms of their respective isotope-derived chronologies and pollen stratigraphy. Their associated ages and age uncertainties of 0-4 ka (1σ) for the LR04 stack (Lisiecki and Raymo, 2005) are consistent with the weighted mean age for RtT (345 ± 12 ka, 1σ) of Pillans et al. (1996), and the weighted mean age (^{40}Ar/^{39}Ar) of 349 ± 4 ka (2σ) defined for the precursory Whakamaru Eruption (Downs et al., 2014). The location of these cryptotephras therefore provides independent support to the existing chronologies.

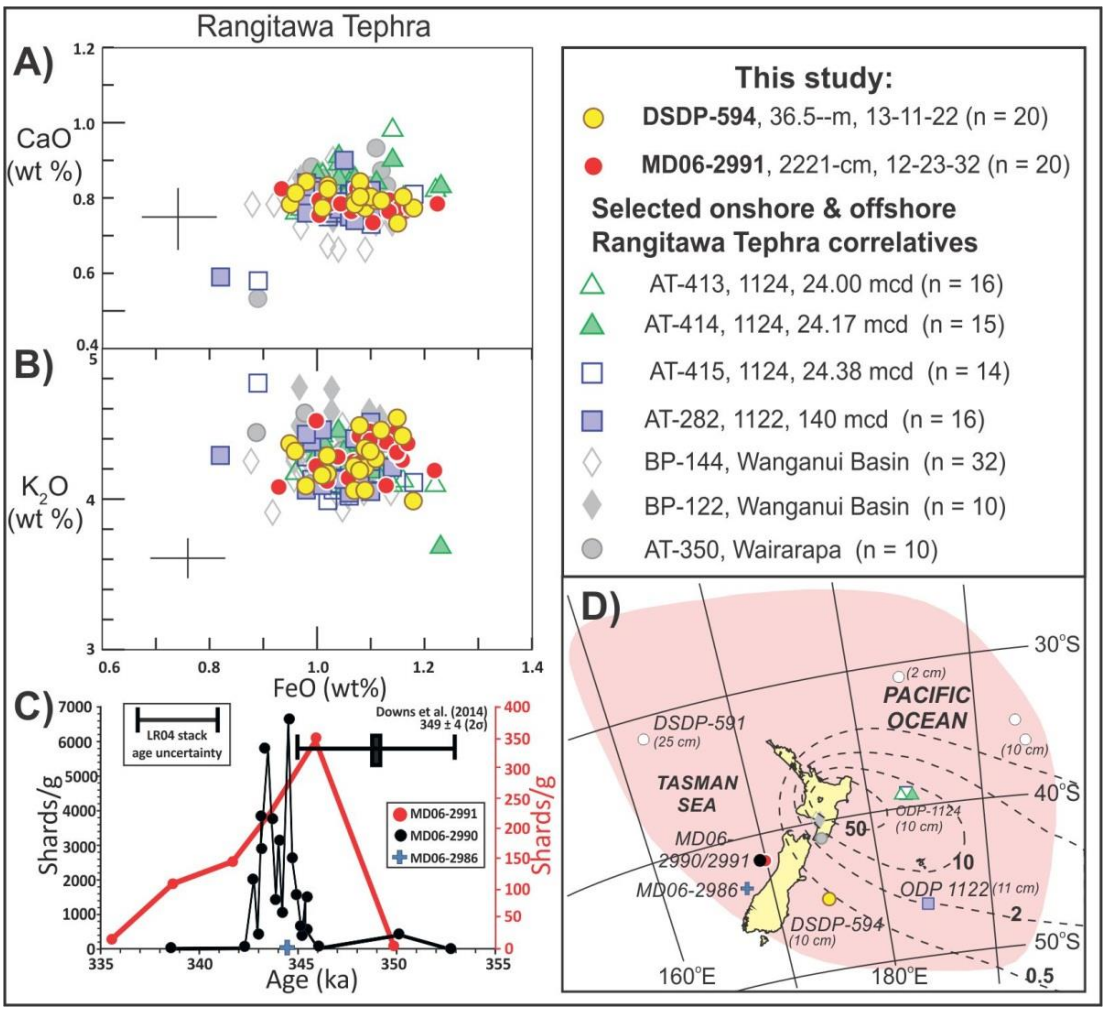

Fig. 5.6: Major element bivariate plots of **A)** CaO vs FeO (wt %) and **B)** K_2O vs FeO (wt %) for glass shards from 22.21 mbsf of MD06-2991 (n=20) and 36.5 mbsf of DSDP 594 (n=20). These are compared to seven sets of published elemental analyses of Rangitawa Tephra (RtT) presented in Alloway et al. (2005), with all electron microprobe (EMP) analyses conducted by Brent Alloway. This glass composition data is presented in Suppl. Table 5.3. Crosses represent the 2σ error on individual analyses. **C)** Glass shards per gram with the maximum for MD06-2990 shown at 344.5 ka (black, left Y-axis), and at 346 ka from MD06-2991 (red, right Y-axis), spanning the weighted mean age range for RtT (345 ± 12 ka) of Pillans et al. (1996). **D)** Regional distribution of RtT (Froggatt et al., 1986; Shane, 2000; Alloway et al., 2007b; Mildenhall and Alloway, 2008) and modelled tephra isopach of Matthews et al. (2012), with site locations used in EMP analysis and glass concentrations displayed.

5.5 Discussion

Marine records of terrestrial vegetation change adjacent to South Island, New Zealand, offer insight into the nature of T-V and the MIS 11c climate optimum in the dearth of adjacent terrestrial counterparts from this region and the wider Southern Hemisphere mid-high latitudes. The notable absence of MIS 11 proxy sequences is clear in recent compilations of such records and paleoclimate models for interglacial conditions (Milker et al., 2013; Candy et al., 2014; Kleinen et al., 2014). Reconstructions of terrestrial vegetation and ocean temperature changes from MD06-2990, southwestern New Zealand, provides unequivocal evidence for a closely coupled ocean-atmosphere system over MIS 12-10, and consequently circumvents potential chronological uncertainties which may arise when comparing discrete land-sea paleoclimate records. The broad similarity of regional vegetation changes from land-sea pollen sequences in this region over the last two G-I transitions provide a rationale for investigating periods for which there remain no terrestrial equivalents. Chapter 4 highlighted the similarity between the pattern of vegetation change over T-I and T-II despite differences in orbital forcing, the rate and amplitude of temperature change, CO_2 and sea level rise (Clark et al., 2009; Landais et al., 2013). The vegetation cover over the early part of T-V (MIS 11e) in southwestern New Zealand is initially similar to that of the Lateglacial (T-I) in this region, whereas the flora which characterises the early MIS 11c climate optimum is more analogous to that which arose at more northerly latitudes (i.e. as far as Taranaki) during the early Holocene climatic optimum (Newnham and Alloway, 2001). In this regard this does not fit the vegetation succession described for southwestern New Zealand for the interglacial conditions following T-I and T-II, where *D. cupressinum* is the dominant taxon at MD06-2991 and Okarito Bog, while during the MIS 11 interglacial the forest composition contains more *Ascarina lucida* (>10%). In combination with SST data over the MIS 11c climate optimum, these pollen data provide an unprecedented glimpse into a super-warm, super humid environment in this region.

5.5.1 The MIS 12 glacial

MIS 12 was one of the most extensive periods of glaciation of the last million years (Shackleton, 1987), with the lowest global sea level minima for the last 500 ka (Rohling et al., 2014) and inferred terrestrial temperature minima for the New Zealand Late Pleistocene (Carter, 2005). Conditions were coldest in southwestern New Zealand between 450-448 ka and 436-432 ka (Fig. 5.7), with vegetation reflecting a landscape dominated by grassland-shrubland mosaic, beech and rare conifers. The structure of vegetation is likened to

conditions displayed during the cold periods of the penultimate and last glacial from MD06-2991. The coldest land surface temperatures are considered to have emerged during MIS 12 and MIS 6, followed by MIS 2. This is suggested by lower proportions of podocarp-hardwood pollen during MIS 12 and MIS 6 (15%) than MIS 2 (20%), while those of the cool-climate subalpine shrub Asteraceae are greater during MIS 12 and MIS 6 (>35%) than MIS 2 (~25%). SSTs are similarly cold (10°C) in the adjacent ocean between MIS 12b-12a in MD06-2990, and has been associated with a northward migration of the STF (Prebble et al., 2016). Parallel cool climate conditions are reflected in the one million year-long composite SST record from East Tasman Sea cores MD06-2989/2986, where foraminiferal based reconstructions of cooling (artificial neural network method) persist at a minima of 9.5-10°C during the coldest phases of MIS 12, the coldest period for the last 500 ka (Hayward et al., 2012).

Environmental change during this extremely cold glacial period has been linked with a widespread population level extinction and/or bottlenecking of South Island insect fauna of forest beetles, stick insects and cicada from ~450-430 ka (Hill et al., 2009; Marske et al., 2009; Buckley et al., 2010; Marshall et al., 2012). During the coldest phases of MIS 12, proportions of the thermophilous tall tree taxon *Dacrydium cupressinum* fall to below 3% in MD06-2990, with little growth as the climate improved until early MIS 11c. It is likley the afforementioned flora and fauna were gradually reduced and/or excluded from the study region over MIS 12 due to harsh environmental conditions, surviving further north at favourable sites. In contrast, environmental reconstructions for the Last Glacial coldest Period, a period with a greater range and amount of available records, attest to the survival of remnant stands of podocarp-hardwoods containing *D. cupressinum* in the study region (Buckley et al., 2010; Marske et al., 2011, 2012; Newnham et al., 2013; Vandergoes et al., 2013b). For example, pollen percentages of *D. cupressinum* do not fall below ~5% and rise to 15% by the onset of climate amelioration at ~18 ka in MD06-2991 (Fig. 5.8, marker 1). These are greater values than for MIS 12, supporting the view that MIS 12 was an extremely cold glacial period that eliminated these thermophilous forest elements from this region.

5.5.2 Climate amelioration over Termination V in southwestern New Zealand

T-V (~346-427 ka) is characterised by an initially subdued and then prominent vegetation change reflecting climate amelioration of southwestern New Zealand which occurred in synchrony with variations reflected in Antarctic temperature (δD) and atmospheric CO_2 concentrations (Petit et al., 1999; Siegenthaler et al., 2005; Jouzel et al., 2007; Bereiter et al.,

2015). Cool-climate subalpine shrubs gradually replaced herbs between 435-432 ka, with an upsurge of emergent forest dwelling species, initially comprising of tree ferns, emergent podocarp-hardwood taxa (*Podocarpus/Prumnopitys*, *Dacrycarpus dacrydioides*) and the understory shrubs of *Coprosma* and *Myrsine* occurring after 432 ka. Surface ocean temperatures in the ETS rose by ~6°C from 435 ka (MIS 12a) to ~426 ka (early MIS 11e), and exceeded modern values by up to 1°C. The magnitude and timing of SST rise is consistent with foraminiferal and dinocyst assemblage changes in this region, with Subantarctic Surface Water replaced by Subtropical Water (Hayward et al., 2012; Prebble et al., 2016). Surface waters off eastern South Island remained cool at DSDP Site 594 up to 423 ka (Schaefer et al., 2005; Hayward et al., 2008; Prebble et al., 2016), with onshore conditions harsher (cooler and drier) than to the west probably inhibiting the spread of tall tree conifers (Suppl. Fig. 5.8). Their establishment in eastern South Island may have occurred via a west-east trans-alpine migration direction through the Southern Alps similar to that proposed for the last deglacial, as revealed from DNA sequencing of contemporary South Island insect fauna (Hill et al., 2009; Marske et al., 2009; 2011; 2012; Marshall et al., 2012).

In the Antarctic EDC ice core record, a prominent rise of δD above -403‰ marks the onset of the 31 ka duration MIS 11 interglacial from ~427-396 ka (Fig. 5.7; Bazin et al., 2013). This amelioration is associated with half of the inferred G-I sea level rise (Rohling et al., 2010; Elderfield et al., 2012), and reflects a strong non-linear responses of the global climate system during T-V (Past Interglacials Working Group of PAGES, 2016). The sequence of climate events associated with the exceptionally long T-V climate amelioration in southwestern New Zealand is consistent with the processes outlined for the last termination by Denton et al. (2010) which are outlined in Chapter 4. It follows that rapidly rising summer NH insolation variation triggered the collapse of large NH ice sheets, with evidence for increased IRD deposition and polar foraminifera in marine records from the mid-high NH latitudes during a stadial phase that is considered more intense and longer lasting than HS-1 of the last deglacial (McManus et al., 1999; McManus et al., 2003; Vázquez Riveiros et al., 2013; Barker et al., 2015). Declining SSTs associated with an exceptionally long collapse of the Atlantic meridional overturning current (AMOC) during this period are assigned to Heinrich type (Ht) events 5 and 4 (Voelker et al., 2010; Rodrigues et al., 2011; Vázquez Riveiros et al., 2013; Newton et al., 2016). The marine Intertropical Convergence Zone transitioned southwards in a similar manner to that displayed for Weak Monsoon Intervals (WMI) for the previous four terminations (Cheng et al., 2009), as interpreted from speleothem (Meckler et al., 2012; Meckler et al., 2015), and marine sediment records (Dickson et al., 2010). This enabled

tropical airmasses and the Subtropical Front to penetrate southwards into southwestern New Zealand and the East Tasman Sea, warming the ocean-atmosphere circulation system of the SH mid-high latitudes. Sea ice cover was likely reduced south of the Polar Front (Schneider Mor et al., 2012) which increased the available region to be influenced by Southern Hemisphere westerly winds, which in turn allowed degassing of atmospheric CO_2 similar to the last termination (Anderson et al., 2009; Barker et al., 2009; Skinner et al., 2010). This injection of greenhouse gases into the atmosphere reflected in EDC eventually enabled deglaciation (Fig. 5.7). Warming of the ocean-atmosphere in southwestern New Zealand at ~432 ka, as illustrated by marker one (Fig. 5.7), precedes the prominent equivalent warming in the NH mid-high latitudes by ~5-6 kyr, with those records similarly constrained to the LR04 $\delta^{18}O$ benthic stack (Voelker et al., 2010; Rodrigues et al., 2011; Barker et al., 2015). This delay is greater than that of 3.5 kyr displayed between T-I (18-14.5 cal ka BP) and T-II (133-129.5 ka).

The composition of emergent podocarp-hardwood forest displayed in southwestern New Zealand during Ht 5 and 4 (T-V) is broadly similar to that at the culmination of HS-11 (T-II) and HS-1/HS-0 (T-I). While the rapid growth of *Dacrydium cupressinum* follows those Heinrich events in all cases, the presence of the frost and drought intolerant understory shrub *Ascarina lucida* displays variability between each interglacial. Conditions were favourable for *Ascarina* growth at ~428 ka during T-V with reduced terrestrial seasonality and ocean- land surface temperatures near modern values in the East Tasman Sea and Antarctica. Similar to ~14.5 ka during T-I, *Ascarina* re-establishes its presence in southwestern New Zealand land-sea pollen profiles under comparable ocean- land surface temperatures (Chapter 4). During T-II, *Ascarina* growth largely occurred in concert with the thermophilous tall tree conifer *D. cupressinum* during warm-wet conditions of the LIG optimum from 128 ka (Fig. 4.13). Another distinctive difference between all three interglacials is the delay between the early expansion of podocarp-hardwoods and *D. cupressinum*. This is broadly similar between the culmination of T-I and T-II where the time offset was up to 3.8 kyr (Fig. 4.13), but is protracted during MIS 11 by up to ~10 kyr (Fig. 5.8). This may result from the initial exclusion of *D. cupressinum* from the region during the preceding cold MIS 12 glacial, and subsequent delayed afforestation resulting from harsher local climate conditions, forest disturbances, changing seasonality and competition, as discussed further in section 5.5.3.

The dominance of tall tress (podocarp hardwoods and southern beech) and the interglacial climate indicator taxon *Ascarina lucida* (Newnham and Alloway, 2004), defines interglacial

conditions in southwestern New Zealand between ~428-396 ka (MIS 11e-c). This follows similar techniques used to define climate episodes, where tree pollen exceeds that of grasses and shrubs (e.g. Moar, 1973). Further, interglacial conditions are characterised by $\delta^{18}O$ minima of benthic foraminifera which indicate substantially reduced global ice volumes (Fig. 5.7; Lisiecki and Raymo, 2005; Railsback et al., 2015), consistent with interglacial conditions of 32 ka duration reflected at EDC (Petit et al., 1999; Siegenthaler et al., 2005; Pol et al., 2011; Bazin et al., 2013), SST proxies (McManus et al., 2003; Rodrigues et al., 2012) and from pollen records in the mid-high NH latitudes (Desparat et al., 2005; Tzedakis, 2010).

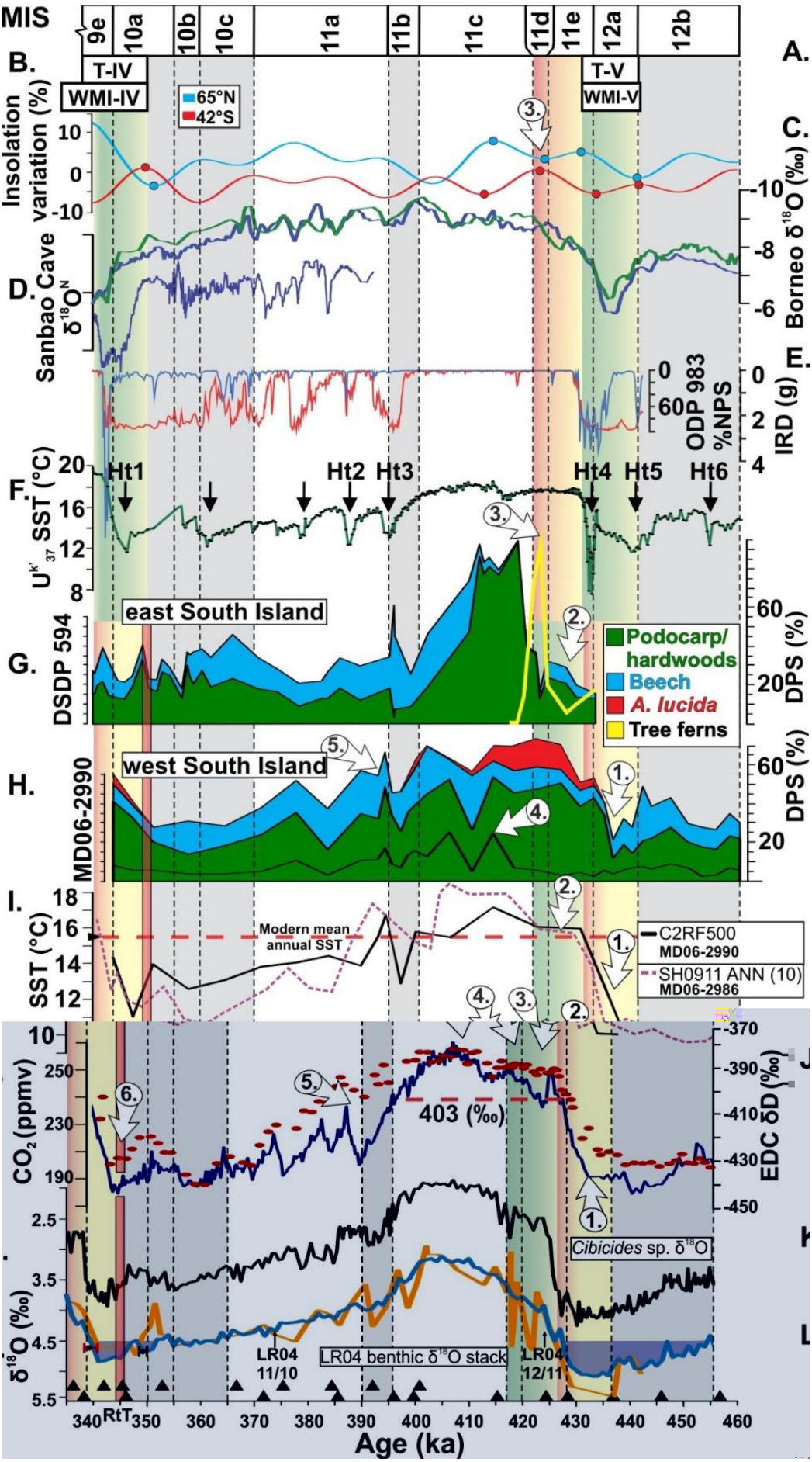
MIS
9e
10a
10b
10c
11a
11b
11c
11d
11e
12a
12b
A.
B.
T-IV
WMI-IV
T-V
WMI-V
65°N
42°S
Insolation variation (%)
C.
Borneo δ18O (‰)
D.
Sanbao Cave δ18ON
E.
ODP 983 %NPS
IRD (g)
F.
Ht1
Ht2
Ht3
Ht4
Ht5
Ht6
U k' 37 SST (°C)
east South Island
G.
DSDP 594
Podocarp/ hardwoods
Beech
A. lucida
Tree ferns
DPS (%)
west South Island
H.
MD06-2990
I.
SST (°C)
Modern mean annual SST
C2RF500 MD06-2990
SH0911 ANN (10) MD06-2986
CO2 (ppmv)
403 (‰)
EDC δD (‰)
Cibicides sp. δ18O
δ18O (‰)
LR04 benthic δ18O stack
LR04 11/10
LR04 12/11
RtT
Age (ka)

Fig. 5.7: (Previous page). Integration of key Ice, Marine and Terrestrial records from 460-335 ka, with numbers inside of the markers referring to key points of discussion. (**A**) MIS boundaries and substages, outlined in grey vertical boxes (Lisiecki and Raymo, 2005; Railsback et al., 2015). **B.** Summer insolation anomaly for 42°S (21 Dec) and 65°N (21 June) (Paillard et al., 1996; Laskar et al., 2004), with extrema in circles. **C & D.** $\delta^{18}O$ calcite isotope profiles from Borneo (Meckler et al., 2012) and Sanbao Cave (Cheng et al., 2009). Weak Monsoon Intervals (WMI) of T-IV and T-V are indicated, with coloured vertical boxes illustrating characteristic ocean atmosphere temperatures (yellow-red= warming, green = cooling) over the G-I transition. **E.** Ice rafted debris (IRD) >150 μm (000's) and percentage of the polar planktonic foraminifera *Neogloboquadrina pachyderma* (%NPS) from ODP 983 (Barker et al., 2015). **F.** Alkenone based SST from the western Iberian Margin from MD03-2699 from Rodrigues et al. (2011). **G** & **H.** Cumulative dryland pollen sum (DPS) for DSDP Site 594 and MD06-2990 (this study), with the relative abundance of *D. cupressinum* outlined within the podocarp/hardwood category by a black line. Tree fern proportions are displayed for DSDP-Site 594. **I.** Foraminiferal based SST estimates for C2RF500 from MD06-2990, and ANN model estimates for MD06-2986 (Hayward et al., 2012). **J.** δD from EDC (Jouzel et al., 2007) and CO_2 composite record (red circles; Petit et al., 1999; Siegenthaler et al., 2015) on AICC2012 chronology (Bazin et al., 2013). The interglacial is defined by red dashed line at -403‰ δD between 427-396 ka (EPICA Community Members, 2004). **K.** $\delta^{18}O$ measurements on *Cibicides wuellerstorfi* from MD06-2990 (black) and on *Uvigerina* spp. from DSDP-Site 594 (orange) aligned to; **L.** the reference LR04 benthic $\delta^{18}O$ isotope stack with associated uncertainties displayed (Caballero-Gill et al., 2012). Calibration points between MD06-2990 and LR04 are displayed (black triangles).

Fig. 5.8: (following page). Comparison between T-I and T-V. **A.** Summer insolation anomaly for 42°S (21 Dec) and 65°N (21 June) (Paillard et al., 1996; Laskar et al., 2004), with extrema in circles. **B.** Mean of MAAT estimates (PLS and MAT based) for Okarito Bog. **C-D & F**. Relative abundance of podocarp-hardwoods and *Ascarina lucida* for the respective Okarito Bog (aligned to MD06-2991), MD06-2991 and MD06-2990 records, with *D. cupressinum* values outlined by a black line in the podocarp-hardwood category for both. Time intervals between mixed podocarp-hardwood growth and *D. cupressinum* expansion differ in duration from 3.8 kyr (T-I) to 10 kyr during T-V. **E.** δD (blue) from EDC (Jouzel et al., 2007) on AICC2012 chronology (Bazin et al., 2013; Bereiter et al., 2015). Interglacial values are defined by δD values of -403‰ (red dashed line) (EPICA Community Members, 2004), which doubles as the modern SST value adjacent to southwestern New Zealand of 15.5°C. RF based SSTs from MD06-2991 (top) and MD06-2990 (bottom) are displayed in light green. Windows where SSTs exceed modern in each core and from regional estimates are indicated by solid black arrows above the plot, with conditions 0.5°C from modern indicated by a dashed line (Barrows et al., 2007a; Barrows et al., 2007b; Hayward et al., 2012). The boundaries of MIS 2-1 and 12-11 are displayed by a black vertical dashed line at 14 and 428 ka, respectively (Lisiecki and Raymo, 2005; Railsback et al., 2015). The colour scheme for New Zealand climate events (NZce) schematically illustrates characteristic atmospheric temperatures (orange = warmest, blue = coldest) and follows Barrell et al. (2013). The timing of the respective climate events are defined by HS-1 (Putnam et al., 2013a); ACR (Putnam et al., 2010a); YD/HS-0 (Rasmussen et al., 2006; Brauer et al., 2009); New Zealand Climate events; "Heinrich type" (Ht) events 4-5 (Rodrigues et al., 2011); and Weak Monsoon Intervals (WMI) I (Cheng et al., 2009) and V (Meckler et al., 2012).

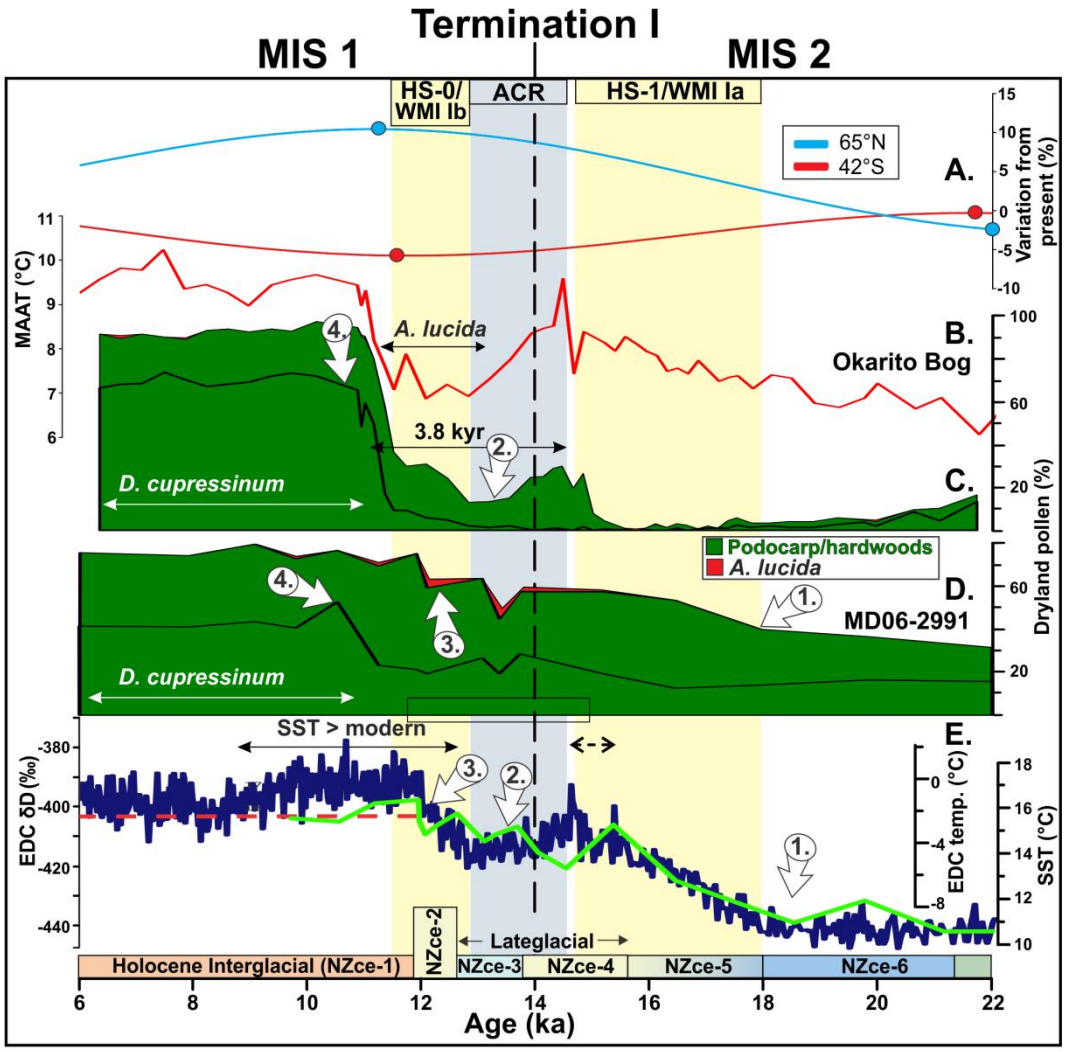
Termination I
MIS 1
MIS 2
HS-0/ WMI Ib
ACR
HS-1/WMI Ia
65°N
42°S
A.
Variation from present (°C)
MAAT (°C)
A. lucida
B.
Okarito Bog
3.8 kyr
D. cupressinum
C.
Dryland pollen (%)
Podocarp/hardwoods
A. lucida
D.
MD06-2991
SST > modern
E.
EDC δD (‰)
EDC temp. (°C)
SST (°C)
NZce-2
Lateglacial
Holocene Interglacial (NZce-1)
NZce-3
NZce-4
NZce-5
NZce-6
Age (ka)

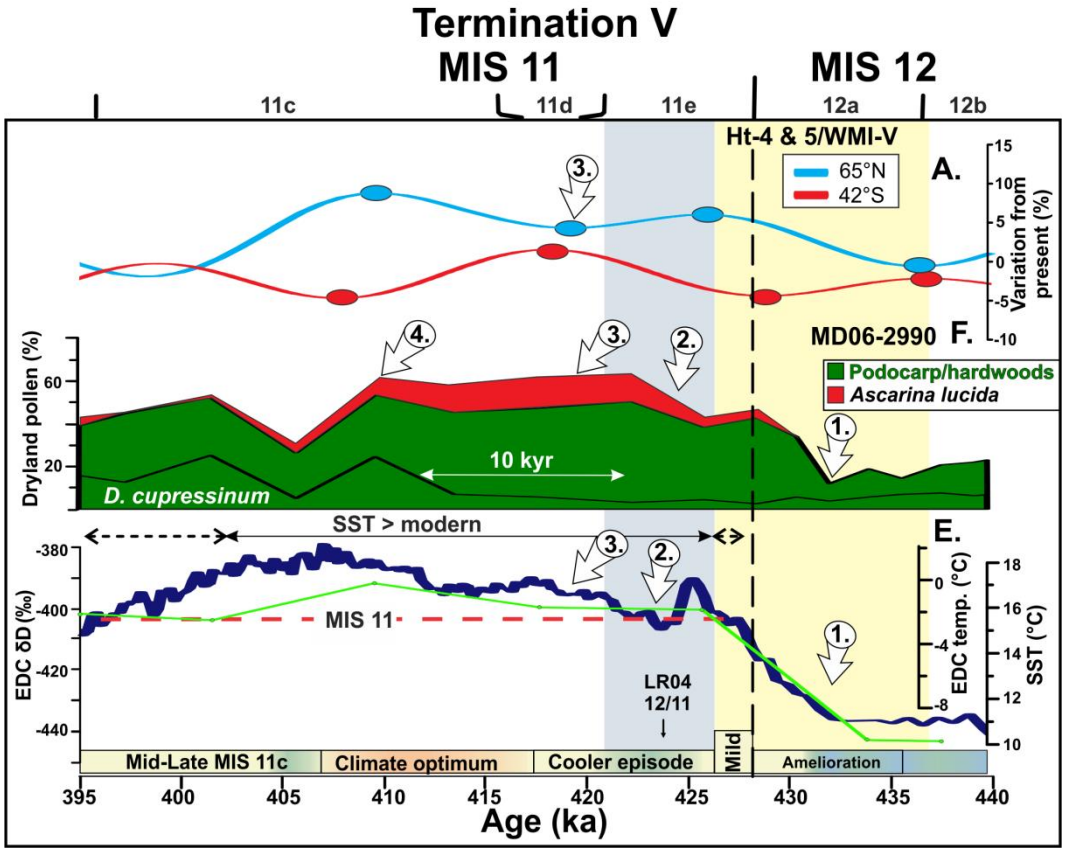
Termination V
MIS 11
MIS 12
11c
11d
11e
12a
12b
Ht-4 & 5/WMI-V
65°N
42°S
A.
Variation from present (°C)
MD06-2990
F.
Podocarp/hardwoods
Ascarina lucida
Dryland pollen (%)
10 kyr
D. cupressinum
SST > modern
E.
EDC δD (‰)
MIS 11
LR04
12/11
EDC temp. (°C)
SST (°C)
Mid-Late MIS 11c
Climate optimum
Cooler episode
Mild
Amelioration
Age (ka)

5.5.3 South Island vegetation change during early MIS 11(e-d)

Two distinctive phases of vegetation change occur in South Island New Zealand over this interval (Fig. 5.7, markers 2 & 3). The first phase reflects cooler conditions within the lower part of MIS 11e between 426-422 ka, as reflected by increasing values of the subalpine shrub Asteraceae west of the Southern Alps at MD06-2990, while at the same time herb proportions rise and tree ferns decline in eastern South Island at DSDP Site 594 (Fig. 5.7; Suppl. 4.19). The second phase suggests continued warming between 422-417 ka, with an increase in the relative abundance of tall trees and the lowland shrub *Ascarina lucida* in western South Island, and a notable peak in tree ferns and podocarp-hardwoods in DSDP Site 594. A two-step warming interval, warming in lower MIS11e, cooling and then warming again into MIS 11d. This trend of initially subdued before increasing temperatures (δD) is reflected at EDC over both phases, and displays some resemblance with temperature variability over T-I (HS-1; ACR and HS-0) (Fig. 5.8; Jouzel et al., 2007; Bazin et al., 2013). This trend takes longer during MIS 11 than the T-I interval.

In the ocean, both South Island records of MD06-2990 and DSDP Site 594 (Suppl. Fig. 5,8) display enrichments in $\delta^{18}O_{benthic}$ over both phases. Foraminiferal based reconstructions of SST from the East Tasman Sea are ~0.5°C above modern in both Random Forest (MD06-2990) and artificial neural network (MD06-2986) methods over both phases (Fig. 5.7), whereas modern analogue techniques show temperatures as much as 0.5°C colder than present at MD06-2990 during the top of MIS 11e. Stronger cooling (1.5°C below present) is reflected over the first phase in dinocyst estimates from MD06-2988 (Prebble et al., 2016), and is interpreted to reflect a brief incursion of Subantarctic Surface Water into the region. This is consistent in time with cooler surface ocean conditions displayed at higher latitudes in the deep South Atlantic Ocean (Vázquez Riveiros et al., 2010). Reconstructed SST estimates from foraminiferal and dinocyst assemblages diverge at DSDP 594 over both phases. During the first phase, foraminiferal estimates remain cold (~3°C) while dinocyst estimates rapidly rise to modern (Suppl. Fig. 8). These dissimilarities may represent differences in seasonal growth, or that there are insufficient modern dinocyst assembladge analogues (Prebble et al., 2013; Prebble et al., 2016). Both estimates reach modern values at the culmination of these two phases. Overall, both phases are at least double the length of their T-I counterparts, which has been attributed to the strong resumption of the Atlantic meridional overturning current and increased northwards heat transport in NH mid-high latitudes (Hodell et al., 2008; Stein et al., 2009; Voelker et al., 2010; Vázquez Riveiros et al., 2013; Sánchez Goñi et al., 2016). This occurred as boreal insolation intensity reached maxima

(Laskar et al., 2004), with a subsequent northwards migration of the Intertropical Convergence Zone over 2-5 kyr (Dickson et al., 2011; Meckler et al., 2012).

Vegetation change over the second phase of early MIS 11 (422-417 ka) in Westland is characterised by an increase in tall trees of *Podocarpus/Prumnopitys* followed by southern beech, and relatively common *Ascarina lucida* that attains a peak in abundance at ~417 ka (Fig. 5.7; marker 3). This occurs as the insolation budget shifted to a regime of increased terrestrial seasonality, with relatively low magnitude insolation fluctuations due to low eccentricity modulating precession (Fig. 5.7 and 5.8, marker 3). The response of tall trees and montane-subalpine shrubs during 422-417 ka is similar although less subdued than those shown over the mid-late Holocene at MD06-2991 (Fig. 3.5) and over New Zealand (McGlone and Moar, 1977; McGlone et al., 1992; McGlone et al., 2010b; Jara et al., 2015). For example, from 9.5 ka to present MD06-2991 displays an increase in southern beech from 5-10%, while increasing montane subalpine shrubs are characterised by cool-climate taxon of *Coprosma* and Asteraceae, and a decline in podocarp-hardwood proportions.

An increase in the magnitude and frequency of extreme events such as storms may have generated windthrow and, in combination with slightly higher SSTs and relatively humid conditions, would have promoted the growth of *Ascarina* over other shrubs in disturbed forests (Marin and Ogden, 2002). Disturbances of podocarp-hardwood forest would have similarly favoured the advance of southern beech forest following its presence in the region during MIS 12 into the contemporary Biotic Gap zone of central Westland where it is devoid today (Wardle, 1984, 1988). This is advocated by enhanced proportions of southern beech over early MIS 11, which constantly exceed 10% from mid MIS 11e-10 a, and are almost constantly double the values represented for the peak of the last two interglacials at MD06-2991 when it was considered to be absent (Moar and Suggate, 1996; Newnham et al., 2007a; Leschen et al., 2008; Ryan et al., 2012). The slow and steady rise of eustatic sea level over MIS 11 (Rohling et al., 2010; Koutsodendris et al., 2012; Raymo and Mitrovica, 2012), which likely reached modern values by ~410 ka, may have similarly favoured the progression of southern beech in this region in contrast to the rapid sea level rise accompanying its exclusion from central Westland during T-II (Newnham et al., 2007a).

Marked changes in vegetation cover are similarly reflected over phase 2 (422-417 ka) from DSDP Site 594, where a very prominent peak in tree fern spores accompanied by rising *Podocarpus/Prumnopitys* occurred as SSTs increased. Dinocyst-based estimates at that site were

~2°C warmer than present, with foraminiferal based SSTs rising to modern values by ~416 ka, lagging the equivalent levels achieved in the East Tasman Sea by ~10 and 7 kyr respectively (Hayward et al., 2012; Prebble et al., 2016). Rising temperatures are reflected further south in Antarctica over this period (Jouzel et al., 2007). There is little evidence for warming in the ocean surface from the North Atlantic (Rodrigues et al., 2011), and of the adjacent Iberian Peninsula as reconstructed from proportions of temperate tree taxa until 418 ka (Tzedakis et al., 2009b; Sánchez Goñi et al., 2016).

In summary, following ice retreat from extensive MIS 12 glacial limits (Barrell et al. 2011), *A. lucida* rapidly colonised disturbed soils in sheltered locations on the Westland piedmont in association with tree ferns and emergent podocarp-hardwoods (Fig. 5.7). The initial establishment and persistence of *A. lucida* in the region over the first phase of MIS 11e is likened to its occurrence over the Lateglacial and pre-early Holocene amelioration (Fig. 5.8; marker 2), although conditions in MIS 11 are considered to have been even more favourable (i.e., relatively frost and drought free) due to warmer temperatures under enhanced CO_2 conditions. Despite evidence of cooling between ~426-422 ka, ocean and atmosphere temperatures remained up to ~2°C greater during MIS 11e than over the ACR and pre-early Holocene amelioration for T-I, as represented in estimates of East Tasman Sea surface temperatures (foraminiferal) and Antarctic land surface temperatures (Jouzel et al., 2007; Bazin et al., 2013). A combination of a higher CO_2, a relatively warmer ocean, a reduced temperature seasonality regime (warmer winters and cooler summers), and a northerly position of the Intertropical Convergence Zone and Southern Hemipshere Westerly wind belt, similar to that proposed for the ACR (Whittaker et al., 2011; Pedro et al., 2015), likely enhanced moisture over Westland which enabled *Ascarina* to flourish on the Westland lowlands.

5.5.4 The timing and amplitude of the MIS 11c climatic optimum (417-407 ka)

The long MIS 11 interglacial is one of the strongest globally warm interglacials of the last 800,000 years (Masson-Delmotte et al., 2010; Lang and Wolff, 2011; Yin and Berger, 2015; Past Interglacials Working Group of PAGES, 2016). The strong global warmth occurred over MIS 11c and is considered difficult to explain by orbital parameters alone (Yin and Berger, 2012), as it occurred during a time of reduced eccentricity modulation of precession (Imbrie and Imbrie, 1980; Vázquez Riveiros et al., 2013). High greenhouse gas (GHG) concentrations are seen as critical for this prolonged warmth (Loutre and Berger, 2003; Yin and Berger, 2012), with maximum concentrations directly comparable to MIS 5e (Dutton et

al., 2015a). Both these interglacials are considered to be the warmest of the last 450,000 years, and despite some heterogeneity, provide analogues to future climate warmth under an enhanced CO_2 regimes (Past Interglacials Working Group of PAGES, 2016).

In southwestern New Zealand and the East Tasman Sea, the warmest conditions during the MIS 11c climate optimum, as reflected from the pollen content and co-existing SSTs at MD06-2990, arose during ~417-403 ka. In the vegetation record, this is initially associated with a widespread rise in pollen of *D. cupressinum* between ~417-407 ka (Fig. 5.7–5.8, marker 4). This displays similarities to the early Holocene climatic optimum in New Zealand and is discussed throughout this section (5.5.4). Variations in temperate tree taxa from ~407-403 ka may result from an increase in the magnitude and frequency of extreme events under a period of increasing seasonality, and displays similarity to vegetation changes in this region and New Zealand over the mid-late Holocene (McGlone and Moar, 1977; McGlone et al., 2010b; Jarra et al., 2015).

The advance of *D. cupressinum* on the Westland lowlands concludes the prolonged vegetation succession of T-V, with this taxon similarly characterising the forest climax following T-II and T-I in this region. The preceding proliferation of *Ascarina lucida* over T-V ensured it remained a dominant component of the lowland vegetation cover, with climate conditions likely to be super-humid, with high rainfall and reduced seasonality ensuring few droughts or frosts. SSTs in the adjacent East Tasman Sea mirror this trend, where modern values are surpassed by ~1.6°C (17.1°C, 410 ka) in Random Forest based reconstructions, and are greater than those developed from this method for the early Holocene and the last interglacial in this region (Table 5.2). Whilst these estimates from MD06-2990 fail to reproduce the +3°C warming reflected in SST proxies from additional sites within this region (Hayward et al., 2012; Prebble et al., 2016), they remain consistent with an inferred southwards shift of watermasses and the position of the Subtropical Front. Surface temperatures in MIS 11c in the East Tasman Sea remain higher than for the eastern South Island from DSDP Site 594 which also displays notable warming; where an overall increase in ocean- land surface temperatures and moisture encouraged the rapid expansion of tall tree podocarp-hardwoods across both regions. These proportions reach up to 90% for this time in DSDP Site 594 (Prebble, 2012), slightly higher than for MIS 5e (75%) and the early Holocene (80%) from the same core (Heusser and van de Geer, 1994), and may reflect increased land surface temperatures over South Island during MIS 11c.

Table 5.2: Comparison of Random Forest (*) and artificial neural network (") foraminiferal and dinocyst (red) based reconstructions of maximum SSTs adjacent to South Island New Zealand for the warm interglacial periods

Site	Mean annual SST	Early Holocene	LIG (MIS 5e)	MIS 11c
MD06-2990	15.5°C	—	—	+1.6°C*
MD06-2991	15.5°C	+0.8°C*	+1.3°C*	—
MD06-2986	15°C	+0.6°C"	1.4°C*/+3°C"	+3.6°C"
MD06-2988	15.5°C	—	—	+3.1°C"
MD06-2989	15.5°C	—	—	+3.3°C"
DSDP Site 594	11°C	+0.5°C"	4°C*/+4.5°C"	+4.1°C"

Vegetation-climate inferences over the early Holocene climatic optimum from northern latitudes provide useful analogues for assessing the magnitude of warmth in the Westland terrestrial environment in the absence of terrestrial sequences that span the MIS 11c climate optimum. These comparisons with the early Holocene also help to reconcile differences in the magnitude of enhanced warmth between SST proxies from the East Tasman Sea. The lowland forest cover revealed from southwestern New Zealand is most similar to the Taranaki region during the early Holocene climatic optimum, with both displaying high values of the thermophilous taxa *Ascarina lucida* and *D. cupressinum* (Newnham, 1990; Alloway et al., 1992; McGlone and Neall, 1994; Newnham and Alloway, 2001). These taxa characterise full interglacial conditions with temperature and precipitation optima (Newnham and Alloway, 2004). For example, vegetation reconstructions from Umutekai Bog, North Taranaki, situated ~4°N of southwestern New Zealand (Fig. 5.1), display similarities with MIS 11c, where thermophilous taxa peak as NH insolation reaches maxima (Suppl. Fig. 5.9-5.10). North Taranaki presently experiences MAATs which are ~3°C greater than southwestern New Zealand, implying that the MIS 11c climate optimum was at least as warm or in excess of peak Holocene estimates further south. Further, vegetation based temperature reconstructions for the early Holocene from the nearby Eltham Bog in Taranaki display slightly warmer (0.4°C) than present conditions (McGlone and Neall, 1994; Wilmshurst et al., 2007). Similarly, early-mid Holocene records from Wanganui (Bussell, 1988) and from Pauatahanui Inlet, Wellington Region (Mildenhall, 1979), show *A. lucida* at levels of ~15%.

Using this approach, the combined magnitude of MAAT warming may have been as much as ~3.4°C (3°C + 0.4°C) greater than present (Taranaki example), and is of a similar values to ANN (foraminifera and dinocysts) based reconstructions of SST from East Tasman Sea (Table 5.2). These values are not unique in the SH mid-high latitudes over this time, with a ~+3°C annual temperature warming estimated from EDC (Jouzel et al., 2007). Warmer

annual temperatures, coupled with a low seasonal contrast in the distribution of insolation over the SH, have been hypothesised to be at the origin of a particularly large sea-level rise during MIS-11 (Coletti et al., 2015; Yin and Berger, 2015).

Vegetation and SST data over the MIS 11 climate optimum provides an unprecedented glimpse into a super-warm, super humid environment from southwestern New Zealand. Longer growing seasons resulting from warmer winters may have compensated for cooler summer temperatures in the SH during MIS 11c, with reduced frosts under a high CO_2 regime, and are consistent with model predictions (Milker et al., 2013; Kleinen et al., 2014). Early warmth of ocean- land surface temperatures in the SH mid-latitudes between 417-410 ka may precede that reflected in NH mid-high latitudes, where cooler SSTs span from 57-37.5°N during this time (c.f. Candy et al., 2014), and pollen records show reduced temperate tree taxa (Tzedakis et al., 2009b; Tzedakis, 2010; Koutsodendris et al., 2010; Prokopenko et al., 2010). This early southern warming during MIS 11c is not inconsistent with that expressed in transient climate simulations of Yin and Berger (2015), where SH mid and high latitudes experience maximum annual mean temperature several thousand years earlier than in NH, due to the antiphased nature of obliquity maximum and precession minimum during MIS 11.

This protracted warmth spanning MIS 11d-11c may have been responsible for the southern migration of northern forest elements into the Taranaki and Wanganui region (Bussell, 1988; Kohn et al., 1992), with potential northern species extended as far as the southern position of New Zealand's North Island such as that indicated for MIS 5e and other Mid Pleistocene interglacials (Mildenhall, 1995; Marra, 2002). One such species is the coniferous tree *Agathis australis,* with its current distribution restricted north of 38°S in the North Island. While records of MIS 11 recovered from terrestrial New Zealand are considered to have been deposited subsequent to peak warmth (i.e., South Taranaki and Rangitawa Stream), there nonetheless remains evidence of a climate slightly warmer or as warm as today (McQueen, 1953). Kohn et al. (1992) suggested northern taxa may have been able to thrive further south due to edaphic and climatic conditions. They suggest that a subdued topography resulting from the absence of Central Plateau and Taranaki volcanoes may have resulted in stable soils with unimpeded warm and moist conditions from more northerly weather systems. The temperate marine mollusc of *Anadara trapezia*, a species currently locally extinct in New Zealand, is recorded in Rangitawa Stream sediments attributed to represent late MIS 11c, suggesting that ocean temperatures were warmer than present at the same latitude (Bussell,

1990). In addition, the site is more southerly than its occurrence in New Zealand during MIS 5e and supports that warmer than present ocean temperatures were sustained in the East Tasman Sea during the protracted MIS 11 than for preceding interglacials (Murray-Wallace et al., 2000). In addition, *Ascarina lucida* is similarly shown to grow with or at the expense of *D. cupressinum* in far northern regions, where temperatures are considered to have been 1-2°C warmer than present during the early Holocene (Newnham, 1990, Elliot et al., 2005). In this regard, far northern taxa in a warmer climate responded similarly to that reflected in southwestern New Zealand. However this signal is considered complex, with a paucity of *Ascarina lucida* possibly arising from low relief, with few sites receiving precipitation as high as the western New Zealand localities (Newnham, 1990).

Warm conditions during the MIS 11 climate optimum occur in synchrony with warmer winters and higher mean annual temperatures reconstructed from proxies and paleoclimate models (Milker et al., 2013; Kleinen et al., 2014), and similar atmospheric CO_2 levels relative to the preindustrial between 416-405 ka (Siegenthaler et al., 2015). Revised reconstructions of global sea level are 6-13 m higher between ~410-400 ka (Rohling et al., 2010; Raymo and Mitrovica, 2012; Roberts et al., 2012; Dutton et al., 2015a), with proxy and model studies indicating a 4.5-6 m above present contribution from the Greenland Ice Sheet (Willerslev et al., 2007; de Vernal and Hillaire-Marcel, 2008; Reyes et al., 2014). Other estimates invoke the collapse of the WAIS and minor contribution from EAIS, possibly also originating from warm winters and moderately cool summers in mid-high Southern Hemisphere latitudes expressed in climate simulations (Yin and Berger, 2015). Collapse of the GIS is considered to have not occurred in equilibrium with peak warming at 410 ka (Reyes et al., 2014), with maximum ice loss possibly delayed until ~403 ka. This requires that a climate/ice-sheet stability threshold was crossed during MIS 11 to generate complete GIS melting. Coupled climate/ice sheet models predict this threshold of warming to be between ~1.7-2°C relative to pre-industrial temperatures (Ridley et al., 2010; Robinson et al., 2012). Estimated ocean-land surface temperatures for southwestern New Zealand are within this threshold, and similarly provide evidence for a reduced seasonality regime which is one mechanism proposed to have pushed the GIS beyond the stability threshold (Reyes et al., 2014). Alternatively, Reyes et al. (2014) suggest the GIS may have responded fully to the protracted warmth during MIS 11 with similar temperatures as the early Holocene and the last interglacial, but for a prolonged interval. These temperature estimates are comparable to the 1.5-2°C of warming above present proposed by Golledge et al. (2015) to facilitate a major

collapse of the Antarctic ice shelves which would lead to an unstoppable contribution to future sea-level rise.

5.5.5 Progressive cooling and sub-orbital climate variability from MIS 11b-10a

The concomitant advance of grassland/shrubland taxa and declining SSTs from southwestern New Zealand and the East Tasman Sea reflects a progressive synchronous cooling on land and ocean from MIS 11b to MIS 10a. Random Forest based SSTs decline by 2.5°C from present in this region over MIS 11b. A strong ~5°C cooling is similarly reflected in the Antarctic EDC δD measurements (Jouzel et al., 2007; Bazin et al., 2013; Railsback et al., 2015), and suggests ocean and atmosphere circulation systems cooled synchronously over the SH mid-high latitudes during MIS 11b.

Several prominent sub-orbital scale advances in tall trees and rising SSTs interrupt this trend of cooling. The most striking is that which occurs at the MIS 11b/a transition, where surface ocean temperatures in the East Tasman Sea rise by 2.5-3.5°C to reach modern values and tall tree expansion occurs in MD06-2990 and DSDP Site 594. Forest expansion to the west consisted of tree ferns and conifers which included *Dacrydium cupressinum* and beech pollen (Fig. 5.8, marker 5), while afforestation of eastern South Island is comprised of southern beech and conifers characteristic of drier conditions than western equivalents. This response of local vegetation to climate amelioration attests to the survival of trees in each region during the overall cool period MIS 11b. An increase to more positive δD measurements in EDC similarly reflects warmer conditions in Antarctica between 390-387 ka and is within chronological and sampling uncertainty of warming each side of the South Island. These variations appear antiphased with ocean-atmosphere temperatures from the NH mid-high latitudes over Heinrich type-3 which display cooling over this period (Desparat et al., 2005; Rodrigues et al., 2011; Barker et al., 2015; Fletcher et al., 2015).

Variation in the boreal summer solar radiation budget between 396-385 ka (27 W/m^2) over MIS 11b is similar to the amount displayed over T-V (30 W/m^2). However, the response of the Northern Hemisphere ice sheets to this orbital forcing is less comprehensive during MIS 11b than MIS 12 (Rodrigues et al., 2013; Barker et al., 2015), as ice sheet size was more reduced during MIS 11b due to sustained high CO_2 concentrations (Loutre and Berger, 2003; Tzedakis et al., 2009a).

Tall tree taxa and SSTs progressively decline over South Island, with an increasing reduction or absence of the thermophilous taxa *D. cupressinum* and *Ascarina lucida* until the MIS10 a/9e boundary defined at ~338 ka by Railsback et al. (2015). Reconstructions of vegetation change from terrestrial sequences in western North Island reveal an equivalent progressive decline in tall trees from their high values assigned to the late stages of the MIS 11(c) interglacial, until the deposition of RtT at the onset of MIS 10a (see section 5.5.6). This is characteristic of harsh climate conditions, and is estimated to reflect a temperature lowering from present by at least 4°C (Fig. 5.7; Bussell, 1986; Kohn et al., 1992), which matches estimated cooling in the East Tasman Sea. The reduction and absence of thermophilous taxa from ~390-340 ka from southwestern New Zealand suggest conditions deteriorated with frequent disturbance and episodic drought. The start of this timing is similarly reflected from the last apperance of *Ascarina lucida* in the low resolution reconstruction of vegetation change from ODP Site 1123, 1100 km offshore from eastern New Zealand at ~400 ka (Fig. 5.1; Mildenhall, 2003; Mildenhall et al., 2004). Over South Island, New Zealand, tall trees similarly switch in dominance from podocarp to beech, a feature also reflected in the context of long distance pollen reaching Chatham Island (Holt et al., 2010), ~900 km east of South Island, New Zealand. Minor advances in tall trees identified from South Taranaki sequences are interpreted to reflect milder interstadial conditions (Kohn et al., 1992), although their limited chronological constraint prevents further investigation at present. Quantitative estimates of air temperature from such sequences may provide insight into the magnitude of cooling during the MIS 10 (Nemona) glacial and climate conditions leading into T-IV and the MIS 9 interglacial.

5.5.6 The deposition of Rangitawa Tephra (RtT) and its significance for T-IV

The interregionally widespread deposition of Rangitawa Tephra (RtT) provides an isochronous climatostratigraphic marker which allows land-sea paleoenvironmental records to be compared in New Zealand, and as far as the Antarctic margin 10,000 km from source (Froggatt et al., 1986; Pillans et al., 1996; Lowe et al., 2011). The dispersal of large volumes of fine ash and volatiles over New Zealand potentially disturbed vegetation, while their ejection into the stratosphere may have caused a significant and widespread disruption of the atmosphere and climate of the South Pacific and Southern Hemisphere (Froggatt et al., 1986; Matthews et al., 2012). Its provenance has been geochemically linked to the Whakamaru super eruption, with the age of ignimbrites associated with the eruption constrained to 349 $\pm$ 4 ka (2σ) (Downs et al., 2014). Three independently $\delta^{18}O$ dated marine cores adjacent to South Island provide an internally consistent age of the tephra to 345 ka, which is within

uncertainty of that constrained in terrestrial sequences (Pillans et al., 1996, Holt et al., 2010; Downs et al., 2014). The occurrence of RtT as a cryptotephra in southwestern New Zealand most likely resulted from its location upwind of the modelled main dispersion axis of air fall to the south-east (Matthews et al., 2012). Distinct differences in glass shard concentrations between MD06-2990/2991 likely results from the rate of sedimentation and settling at the core site (Manville and Wilson, 2004), with sediments influenced by the variability of terrigenous siliciclastic material or marine plankton over time (Jarrett, 1985), and effects of bioturbation (Lowe et al., 2011; Griggs et al., 2014).

Reconstructions of vegetation change from marine cores MD06-2990 and DSDP-Site 594 offer insight into the background state of climate in the SH mid-high latitudes at the time of RtT deposition. Both records display a prominent advance in tall tree pollen 2 kyr and <1 kyr following the maximum shard concentrations at ~345 ka, and suggest climate improved in this region, as has been suggested from a pollen record from the southern North Island (Ohariu Valley, Fig. 5.1) that also contains RtT (Mildenhall et al., 1977). This is coeval with a distinct shift to more positive values in speleothem isotope profiles from Borneo and China inferred to represent a weakening phase of the east Asian Monsoon (WMI-IV; Fig. 5.7; Cheng et al., 2009; Meckler et al., 2012), in response to strong cooling in the NH mid-high latitudes. This follows a rise in boreal summer insolation intensity at 346 ka, with local insolation (-42°S) at a maximum for that period. As shown for T-V, T-II and T-I, strong cooling of the NH mid-high latitudes is postulated to have caused a southwards displacement of the Intertropical Convergence Zone and Southern Hemipshere westerly wind belt and warmed southwestern New Zealand in an antiphased manner, consistent with the essential elements of a termination outlined by Denton et al. (2010). Similar to the vegetation patterns outlined for T-V, tall trees in southwestern New Zealand continue to rise over T-IV (MIS 10a) without a concomitant response from eastern South Island, as conditions may have been harsher in that region. Regional temperatures in the East Tasman Sea surface and in Antarctica remained cool until ~343 ka, and were followed by warming over T-IV (Jouzel et al., 2007). Potential identification of Rangitawa Tephra or volatiles released from the eruption in Antarctic ice cores (Pillans et al., 1996), may enable stronger correlation between records across the mid-high latitudes as well as help to determine its influence on hemispheric and global climate at the onset of T-IV.

Conclusion:

Reconstructions of ocean-atmosphere change for MIS 12-10 from southwest New Zealand and adjacent East Tasman Sea offer new insights into the nature, timing, magnitude and duration of past climate change in the SH mid-latitudes over an interval for which few terrestrial archives exist. This research aims to a) determine the sequence of vegetation and climate events associated with glacial termination V and the full MIS 11 interglacial from southern South Island; and b) investigate how climate events over MIS 12-10 relate to external forcing and existing paradigms during T-V and the climate optimums of the last interglacial and Holocene interglacial. The key outcomes of this chapter are:

1. Changing ocean-air and temperatures over southwestern New Zealand and East Tasman Sea over MIS 12-10 are driven by orbital forcing, with sub-orbital patterns superimposed on these trends that display antiphasing to NH records. Vegetation in southwest New Zealand during this time is strongly coupled to SST variability.

2. Ocean- land surface temperatures in southwestern New Zealand and the East Tasman Sea were the coldest during MIS 12 for the last ~500 ka. Climate amelioration in southwestern New Zealand over T-V is marked by a transition from a landscape dominated by grassland-shrubland to that comprised of emergent podocarp-hardwoods containing the thermophilous understorey shrub *Ascarina lucida*. This occurred in synchrony with a steady then prominent rise in SSTs over 435-426 ka to exceed modern values by ~1°C. The succesion of vegetation is broadly similar to that reflected over T-II and T-I, with rising tall trees and *Ascarina lucida* defining the MIS 11 interglacial in this region between 428-396 ka (~32 ka duration). The length of the MIS 11 interglacial is associated with a 400 kyr long period eccentricity orbital geometry similar to that existing in the Holocene, with the pattern of ocean-atmopheres changes shown during MIS 11 consistent with warm temperatures in EDC ice core in Antarctica (δD peak), and from the few available mid-high latitude SH records (Vázquez Riveiros et al., 2013).

3. Ocean-land surface temperatures from southwestern New Zealand display evidence for antiphasing to those in the mid-high Northern Hemisphere. The onset of the prominent ocean (>6°C) and atmopshere warming at ~432 ka preceeds that of LR04 $\delta^{18}O$ dated mid-high NH records at 426 ka (Voelker et al., 2010; Rodrigues et al., 2011; Barker et al., 2015). This is greater than the comparable 3.5 kyr delay illustrated for T-I (18-14.5 cal ka BP) and T-II (133-129.5 ka). Slightly cooler ocean- land

surface temperatures in mid-high latitude Southern Hemisphere records over 426-422 ka which follow Ht-4 are synchronous with a SST warming (~10°C) in the NH mid-latitudes. The length of that episode is double that of the ACR (T-I) and the cool episode which follows HS-11 (T-II) in the study region.

4. Differences in the timing and magnitude of environmental changes between the exceptionally long T-V in comparison to T-II and T-I are explained by variants in forcing mechanisms such as the rate of insolation change and CO_2 rise. The sequence of climate events and vegetation changes in southwestern New Zealand associated with the T-V climate amelioration is consistent with the conditions and processes outlined for a termination by Denton et al. (2010), where heat stored in the Northern Hemisphere is transferred south via the ocean-atmosphere circulation systems during Heinrich Stadial events, facilitating outgassing of CO_2. Cooler conditions in southwestern New Zealand and NH warming following each Heinrich event is consistent with a northward migration of the Intertropical Convergence Zone (Cheng et al., 2012; Meckler et al., 2012).

5. There are distinct differences in the composition of tall trees that follow T-V in comparison to T-I and T-II. Afforestation of *Dacrydium cupressinum* was prolonged by up to 10 kyr subsequent to emergent podocarps in early MIS 11, with a smaller and comparable delay of 3.8 kyr for T-I and T-II. *D. cupressinum* may have been excluded from the region during MIS 12, with its expansion delayed by harsher local climate conditions, forest disturbances, changing seasonality and competition (southern beech and *Ascarina lucida*). Enhanced southern beech pollen over MIS 11 points toward its survival in the contemporary 'Biotic Gap zone' over that time. Mild and moist conditions during early MIS 11(e-d) supported the proliferation of *A. lucida,* forming a dominant component of the lowland vegetation cover under full interglacial conditions during MIS 11c more so than during MIS 5e and MIS 1.

6. The thermal optimum in the terrestrial environment during MIS 11c occurs between 417-407 ka, and provides an unprecedented glimpse into an increasingly warmer world in the SH mid-latitudes such as that projected for the future. Dominance of tree and shrub species of *D. cupressinum* and *Ascarina* are more analogous to pollen records recovered from more northerly latitudes in western North Island during the early Holocene climatic optimum (11.5-9 cal ka BP). North Taranaki presently

experiences annual land surface temperatures which are ~3°C warmer than southwestern South Island implying that the MIS 11c climate optimum was at least as warm or in excess of peak Holocene estimates further south. SSTs reached their highest values during MIS 11c, exceeding modern values by 1.6°C, and as much as 3°C warmer from records each side of the South Island. The prominent expansion of conifers and tree ferns in eastern South Island (DSDP Site-594) follows that in the west (MD06-2990) by as much as 10 kyr. This is consistent with similar delays revealed in SSTs (Prebble et al., 2016), and reveals distinct regional differences to the pattern of climate amelioration. The magnitude and protracted length of warmth revealed for MIS 11c are consistent with that required for the complete collapse of the Greenland Ice Sheet, with possible Antarctic Ice Sheet melt contributing to sea levels between 6-13 m higher than present.

7. Deposition of the ~345 ka Rangitawa Tephra is identified for the first time in marine sediment archives adjacent to Westland, New Zealand, and is consistent with the most recent onshore eruption age of the 349 ± 4 ka (2σ) Whakamaru Ignimbrite (Downs et al., 2014). Its timing is synchronous with the onset of rising NH insolation during T-IV, highlighting its potential role as a widespread marker for this critical paleoclimate event.

5.6 Contributions

MTR: Writing, ideas and figures shown in this manuscript and supplementary information. Pollen processing, analysis and glass shard concentrations for MD06-2990/1. Sampling, washing for SST estimates from MD06-2990. Calculation of Random Forest based SST uncertainties. Correlation of $\delta^{18}O$ depth measurements to LR04 reference curve to develop a high resolution $\delta^{18}O$ chronology for MD06-2990/1. Sampling and washing of 21 new $\delta^{18}O$ measurements for DSDP 594. Revision of figures generated from EGCS. Age modelling of Umutekai Bog (50% contribution).

All additional work provided by other parties for this chapter:

RMN Project guidance. Pollen analysis and ^{14}C sampling for Umutekai Bog.

GBD Project guidance.

MJV Project guidance.

BVA Preparation and analysis of EMP mounts as well as acquisition and processing of major element compositional data of RtT glass shards from MD06-2991 and DSDP Site 594. Preparation of Fig. 5.6 (50% contribution) and Suppl. Table 5.3.

EGCS Calculation of level of fit between LR04 and MD06-2990 and preparation of Suppl. Fig. 5.1 and 5.2.

ABHR Provided guidance in OxCal for the depositional modelling of Umutekai Bog (50% contribution).

AS MD06-2990 planktonic foraminiferal census data for developing SST estimates.

BH Generation of MAT-based SST estimates using the MAT SH0911 method.

GHS Random Forest SST estimates from the analysis of data provided by BH and AS.

HB and **HLN** Picking, processing and analysis of benthic and planktonic foraminifera for developing the $\delta^{18}O$ chronology for MD06-2991. Picking of benthic and planktonic foraminifera of 21 new $\delta^{18}O$ measurements from DSDP-594.

RT Supplying downcore benthic $\delta^{18}O$ measurements for MD06-2990.

JP Supplied dryland pollen data for MIS 12-11 from DSDP 594. Correlation of $\delta^{18}O$ depth measurements to LR04 reference curve for DSDP-Site 594.

SS Picking, processing and analysis of benthic and planktonic foraminifera for developing the $\delta^{18}O$ chronology for MD06-2990.

Chapter Six

6. Synthesis

This thesis presents well constrained Late Quaternary records of terrestrial vegetation change and marine climate conditions for southwestern New Zealand and the East Tasman Sea. The records investigated provide an insight into terminations (T) I, II and V and their subsequent warm interglacials of MIS 11, 5e and 1. The relative forcing mechanisms of these terminations are discussed. The following synthesis revisits the aims that were introduced in Chapter 1, and presents key findings.

6.1 What is the source-to-sink residence time (RT) of terrestrial pollen deposited offshore Westland, New Zealand?

Terrestrial pollen is transported offshore to the adjacent East Tasman Sea (ETS), primarily by fluvial transport and once deposited onto the continental shelf, sediment bearing terrestrial pollen is likely to be efficiently transported down the adjacent submarine canyon systems (Proust et al., 2008). Past vegetation changes reconstructed from marine sedimentary sequences in the Westland region assumed that the lag between pollen release and final deposition on the seafloor, referred to as the source-to-sink residence time (RT) of terrestrial palynomorphs, was negligible (Ryan et al., 2012).

In Chapter 3, RT of terrestrial palynomorphs from Westland to the ocean floor of the East Tasman Sea was investigated using two approaches (Ryan et al., 2016). The first involved radiocarbon dating of fluvially transported organic matter from Westland rivers draining a variety of catchments, and found that RT ranged from negligible (i.e., -57 ± 22 cal yr BP) to thousands of years (3583 ± 188 cal yr BP). This lag between release and deposition could be even longer in regions lacking the high soil production and erosion rates that characterise Westland. This variability suggests that similar tests of terrestrial–marine RT should be conducted before assumptions of zero or negligible lags are invoked.

The second approach for investigating RT focused on paleodepositional setting, specifically over the Last Glacial Coldest Period and Last Glacial-Interglacial Transition in Westland (~28-10 ka). RT was approximated using the timing of four regional palynomorph events

and the Kawakawa/Oruanui Tephra (KOT) between marine core MD06-2991 and four terrestrial sediment records (Okarito Bog, Galway Tarn, Gillespies Beach Rd, Manks Tarn). Comparison of marine and terrestrial records was based on succession of vegetation changes over the Last Glacial-Interglacial Transition rather than absolute palynomorph abundance, which is influenced by taphonomic processes. Overall, the RT of Late Pleistocene palynomorph events appears to be negligible, as estimated using the independently dated marine and terrestrial records.

The Kawakawa/Oruanui Tephra (KOT) provides a third chronological link between marine and terrestrial sequences in this region during the Last Glacial Coldest Period (Pillans et al., 1993; Carter et al., 1995; Wilson, 2001; Manville and Wilson, 2004; Vandergoes et al., 2013b). I argue that the bulk of tephric material is delivered to MD06-2991 by the same processes as terrestrial palynomorphs, rather than by aerial deposition, meaning that the KOT also has an RT that can be estimated. The highest concentration of cryptic volcanic glass shards in MD06-2991 occurs at 25,142 ± 786 cal yr BP (2σ), based on the age-depth model, an age estimate that is statistically indistinguishable from calculated eruption ages of the Oruanui Ignimbrite (25,590 ± 72 cal yr BP, (2σ) (this study), and 25,360 ± 162 cal yr BP, (2σ) (Vandergoes et al., 2013b)). Despite major environmental changes that took place between the Last Glacial Coldest Period and the Last Glacial-Interglacial Transition, the synchronicity persists throughout and suggests RT remained negligible. Future insights into vegetation and sediment residence times over G-I cycles could be gained using 234U/238U activity ratios of fine (<50 μm) material in the MD06-2991 record.

The conclusions of Chapter 3 are; (1) that terrestrial palynomorphs, considered alongside marine proxy records of SST and $\delta^{18}O$, enable direct to ocean-land comparisons to be confidently made, and (2) that the terrestrial palynomorph record of MD06-2991 can be used to transfer its independently derived $\delta^{18}O$ chronology to terrestrial sequences in Westland, beyond the period datable by radiocarbon, by alignment of palynomorph events common to both records. The vegetation and climate records from MD06-2991 and Okarito Bog are placed on a rigorously constructed common timescale in Chapter 4 to examine in detail the relative phasing of environmentally significant events (both local and global) influencing each record.

6.2 What is the sequence of environmental changes for terminations I, II and V and their subsequent warm interglacials (MIS 1, 5e, 11) from southwestern New Zealand? How do their timing and magnitude relate to climate forcing, paradigms of terminations, and existing climate observations?

A central objective of this research was to determine the sequence of climate events during the selected past terminations I, II, and V and their subsequent warm interglacials from southwestern New Zealand. This was undertaken in collaboration with scientists from VUW, GNS, NIWA, AWI, Geomarine Research, Landcare Research. Producing the best constrained age models possible for marine sediment cores from this region was crucial for investigating the timing and magnitude of past environmental changes with respect to termination paradigms and existing climate observations. The sequence of climate events is best constrained for the most recent termination (T-I) and Holocene interglacial from both marine and terrestrial sequences on the western and eastern side of the South Island New Zealand (Barrell et al., 2013; Bostock et al., 2013; 2015; Putnam et al., 2013a).

However, few sequences from the SH mid-latitudes firmly constrain the sequence of vegetation and climate events for periods beyond ^{14}C dating, as records are commonly fragmentary, poorly-dated or are not reported (Moar and Suggate, 1996; Candy et al., 2014). Generating marine and terrestrial paleoclimate indictors from the same sequence circumvents potential chronological uncertainties that may arise from comparing discrete land and sea paleoclimate records, such as previously undertaken in the region for T-I and T-II (Ryan et al., 2012; Putnam et al., 2013a). Nonetheless, there is still some uncertainty related to correlation of the terrestrial signal in the MD06-2991 marine core to the terrestrial record in Okarito Bog. The broad similarity of regional vegetation changes from terrestrial and marine pollen sequences in this region over the last two G-I transitions provides a rationale for assessing pollen-vegetation-climate relationships in older periods for which there remain no terrestrial equivalents (i.e., T-V/MIS 11).

6.2.1 The termination of glacial conditions during MIS 12, 6 and 2 in southwestern New Zealand and the ETS

Reconstructions of vegetation change and SST from marine cores MD06-2990/1 constrain the timing and extent of regional cooling at the onset of T-V (~436 ka), T-II (~139 ka) and T-I (~18 ka). Each termination was characterised by expansion of grassland and shrubland with common to frequent beech and conifers representing treeline depression. Each coincided with or occurred near minima in NH summer insolation intensity (Fig. 6.1),

regional SSTs and atmospheric CO_2. The regional climate of southwestern New Zealand and the East Tasman Sea was influenced by global changes in the ocean-atmosphere circulation system. Cooling of surface temperatures in the East Tasman Sea was greatest during MIS 12 and MIS 6 (~10°C), reaching ~6°C cooler than present (Fig. 6.1), and facilitated strong onshore cooling as reflected in vegetation and MAAT reconstructions. This is consistent with a northward migration of the Subtropical Front ~3-5° north of its present position and located over the MD06-2990/1 core sites (Hayward et al., 2012; Prebble et al., 2016). A similar northward migration of the front is inferred to have occurred during MIS 2 (Fig. 6.2). Pollen based MAATs at Okarito Bog were ~4-5°C cooler than present during MIS 6 and 2 (unpublished data provided from M.J. Vandergoes). The timing of the aforementioned vegetation changes in southwestern New Zealand for MIS 2 and MIS 6, shows good correspondence with surface exposure age dating of moraines representing glacier advance to the west and east of the Southern Alps (Sutherland et al., 2007; Putnam et al., 2013b).

While no quantitative estimates of air temperature for MIS 12 presently exist, this period is considered here to reflect extreme cold conditions, where *Dacrydium cupressinum* may have been excluded from the study region. This environmental change during MIS 12 is coeval with a proposed widespread population level extinction of South Island insect fauna from ~450-430 ka (Hill et al., 2009; Marske et al., 2009; Buckley et al., 2010; Marshall et al., 2012). Overall, these data contribute to the sparse record of proxy climate data beyond the last glacial from the SH mid-latitudes.

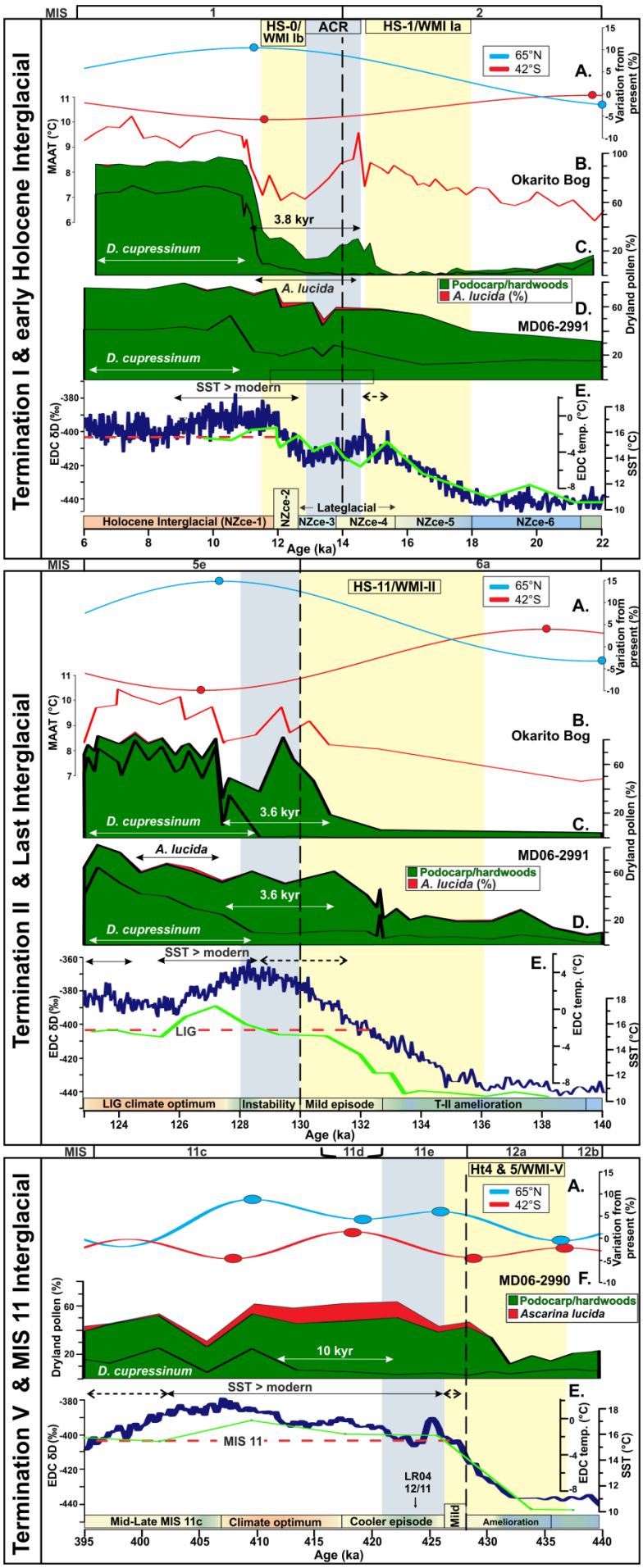
Termination I & early Holocene Interglacial
MIS
1
2
HS-0/ WMI Ib
ACR
HS-1/WMI Ia
65°N
42°S
A.
Variation from present (°C)
MAAT (°C)
B.
Okarito Bog
3.8 kyr
D. cupressinum
C.
Dryland pollen (%)
A. lucida
Podocarp/hardwoods
A. lucida (%)
D.
MD06-2991
SST > modern
E.
EDC δD (‰)
EDC temp. (°C)
SST (°C)
NZce-2
Lateglacial
Holocene Interglacial (NZce-1)
NZce-3
NZce-4
NZce-5
NZce-6
Age (ka)
Termination II & Last Interglacial
5e
6a
HS-11/WMI-II
LIG
LIG climate optimum
Instability
Mild episode
T-II amelioration
Termination V & MIS 11 Interglacial
11c
11d
11e
12a
12b
Ht4 & 5/WMI-V
MD06-2990
F.
Ascarina lucida
10 kyr
MIS 11
LR04
12/11
Mid-Late MIS 11c
Climate optimum
Cooler episode
Mild
Amelioration

Fig. 6.1: Comparison between T-I, T-II, and T-V. **A.** Summer insolation anomaly for 42°S (21 Dec) and 65°N (21 June) (Paillard et al., 1996; Laskar et al., 2004), with extrema in circles. **B.** Mean of MAAT estimates (PLS and MAT based) for Okarito Bog (MJ Vandergoes, unpublished). **C-D & F**. Relative abundance of podocarp-hardwoods and *Ascarina lucida* for the respective Okarito Bog (aligned to MD06-2991), MD06-2991 and MD06-2990 records, with *D. cupressinum* values outlined by a black line in the podocarp-hardwood category for both. Time intervals between mixed podocarp-hardwood growth and *D. cupressinum* expansion differ in duration from <4 kyr (T-I and T-II) to 10 kyr (T-V). **E.** δD (blue) from EDC (Jouzel et al., 2007) on AICC2012 chronology (Bazin et al., 2013; Bereiter et al., 2015). Interglacial values are defined by δD values of -403‰ (red dashed line) (EPICA Community Members, 2004), which doubles as the modern SST value adjacent to southwestern New Zealand of 15.5°C. RF based SSTs from MD06-2991 (top) and MD06-2990 (bottom) are displayed in light green. Windows where SSTs exceed modern in each core and from regional estimates are indicated by solid black arrows above the plot, with conditions 0.5°C from modern indicated by a dashed line (Barrows et al., 2007a; Barrows et al., 2007b; Hayward et al., 2012). The boundaries of MIS 2-1, 6-5, and 12-11 are displayed by a black vertical dashed line at 14, 130 and 428 ka, respectively (Lisiecki and Raymo, 2005; Railsback et al., 2015). The colour scheme for New Zealand climate events (NZce) schematically illustrates characteristic atmospheric temperatures (orange = warmest, blue = coldest) and follows Barrell et al. (2013). The timing of the respective climate events are defined by HS-1 (Putnam et al., 2013a); ACR (Putnam et al., 2010a); YD/HS-0 (Rasmussen et al., 2006; Brauer et al., 2009); New Zealand Climate events; HS-11 (Cheng et al., 2009; Marino et al., 2015); "Heinrich type" (Ht) events 4-5 (Rodrigues et al., 2011); Weak Monsoon Intervals (WMI) I and II (Cheng et al., 2009) and T-V (Meckler et al., 2012), with coloured vertical boxes illustrating characteristic ocean/atmosphere temperatures (yellow=warm/grey=cool).

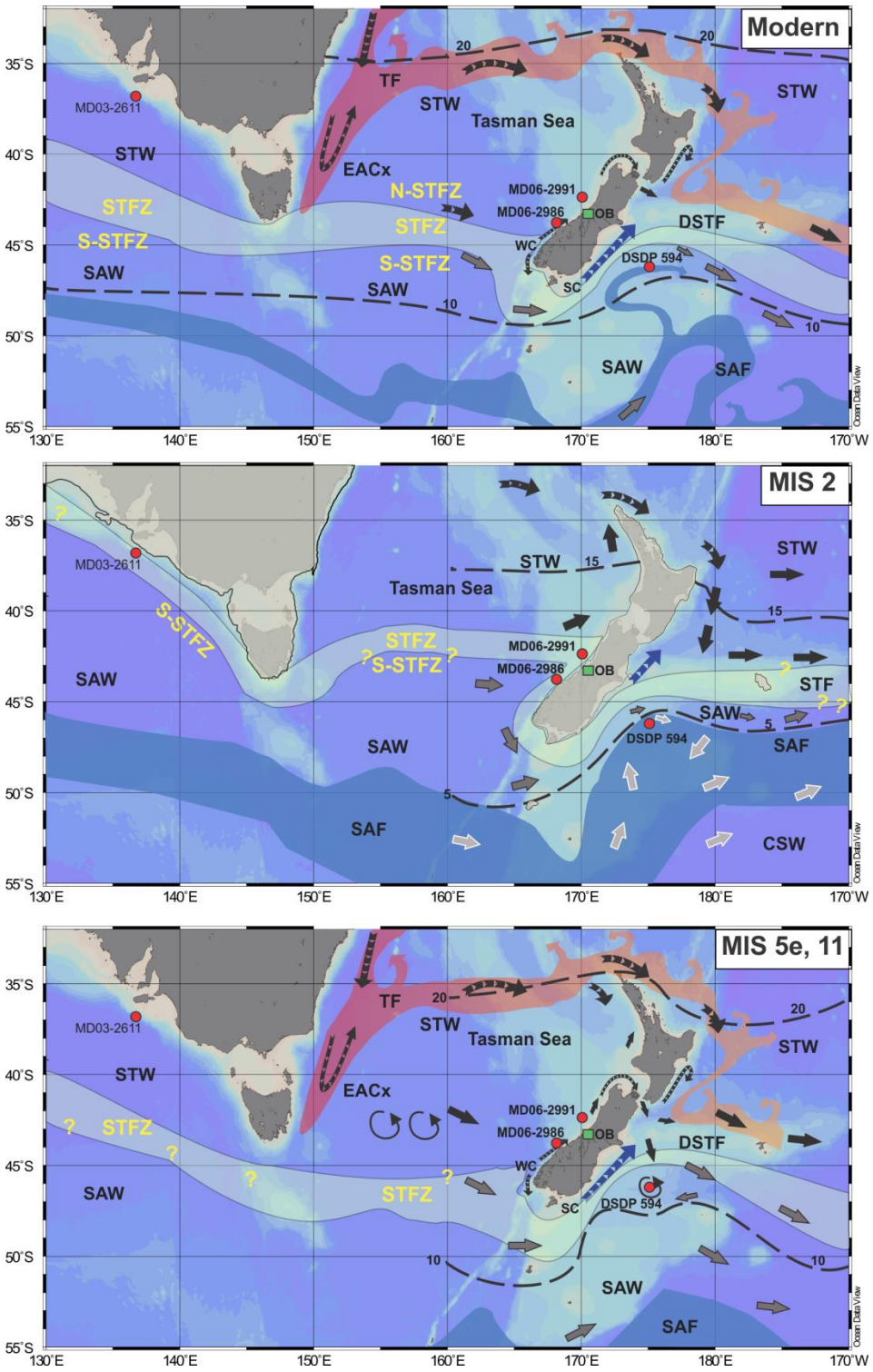

Fig. 6.2: Paleoceanographic reconstructions around New Zealand during: (a) modern, (b) interglacials MIS 11 and 5e, (c) MIS 2 (following Neil et al., 2004; Hayward et al., 2008; 2012; Cortese et al., 2013; Bostock et al., 2013; 2015). Small numerals are the SST (°C). CSW = Circumpolar Surface Water, SAF = Subantarctic Front, SAW = Subantarctic Surface Water, SC = Southland Current, STF = Subtropical Front, STW = Subtropical Surface Water, TF= Tasman Front, PF= Polar Front and flow pathways (arrows) across the southwest Pacific. The positions of East Australian Current (EAC), including its southernmost extension (EACe), the Westland Current (WC) and the Southland Current (SC) are labelled, along with the position of paleoclimate records discussed in this study.

6.2.2 Climate amelioration over land and ocean in southwestern New Zealand and the East Tasman Sea during terminations

Vegetation changes at MD06-2990/1 over T-I, T-II, and T-V in southwestern New Zealand are initially characterised by a transition from dominant grassland-shrubland to emergent podocarp-hardwoods. Each progression is shown to be coupled with rising SSTs in the East Tasman Sea, resulting from southwards migration of the Subtropical Front, which suggests a close coupling of atmosphere and ocean temperatures in this region. Ocean-atmosphere conditions over each termination are driven by orbital forcing, and display similar trends despite differences in orbital parameters (Fig. 6.1), the rate and amplitude of temperature change, CO_2 and rates of sea level rise.

Southern warming during terminations is asynchronous with the NH mid-high latitudes, and occurs as boreal summer insolation intensity rises. This is consistent with the conditions and processes of the termination paradigm of Denton et al. (2010) based on T-I, where heat stored in the NH is transferred to the SH via the ocean-atmosphere circulation systems (bipolar temperature seesaw, Intertropical Convergence Zone) during Heinrich Stadial events (HS-0/1, HS-11, Ht-4/5), facilitating outgassing of CO_2. Differences in the timing and magnitude of these environmental changes between terminations are explained by variation in forcing mechanisms (rate of insolation change and CO_2 rise). For example, warming in southwestern New Zealand associated with the long T-V climate amelioration at ~432 ka displayed in this study precedes the equivalent warming in the NH mid-high latitudes by ~5-6 kyr (Voelker et al., 2010; Rodrigues et al., 2011; Barker et al., 2015). This delay is greater than that of T-I (18-14.5 cal ka BP) and T-II (133-129.5 ka). Furthermore, interglacial conditions were reached during MIS 11 and MIS 5e over one prominent transition each (Fig. 6.1), with a similar pattern revealed in Antarctic ice cores (Jouzel et al., 2007; Bazin et al., 2013). The transition between glacial and interglacial in MIS 1 was charcterised by initial warming, interupted by the Antarctic Cold Reversal (ACR), and followed by warming again bringing the termination to completeion, and is consistent with a similar pattern revealed in Antarctic ice cores.

The ~345 ka Rangitawa Tephra (RtT) provides an important marker in marine cores MD06-2990/1 and DSDP Site 594, strengthening $\delta^{18}O$-based age models (Pillans et al., 1996; Alloway et al., 2005). RtT is recognised for the first time adjacent to southwestern New Zealand in this study. Its timing is synchronous with the onset of rising NH insolation during

T-IV, and an inferred weakening phase of the east Asian Monsoon Weak Monsoon Interval (WMI)-IV in response to NH cooling (Cheng et al., 2009; Meckler et al., 2012).

6.2.3 Does each termination register the appearance of millennial scale climate reversals as noted globally for T-I?

Marine and terrestrial records offer valuable insights into climate events during terminations (McManus et al., 1999; Tzedakais et al., 2009a; 2009b; Cheng et al., 2009). Pollen and SST data from southwestern New Zealand and the ETS, in combination with existing paleoclimate data over the New Zealand archipelago spanning a wide latitudinal range (38-52°S), display evidence for climate deterioration over land and ocean between ~14.5-12.8 cal ka BP (Vandergoes et al., 2008; Doughty et al., 2013; Newnham et al., 2012; Sikes et al., 2013). East Tasman Sea surface temperature reconstructions remain up to 2°C lower than present, with a similar 2-3°C of MAAT cooling from pollen and glacier derived estimates from New Zealand (Fig. 4.10). These changes are coeval with the Antarctic Cold Reversal (ACR), with strong cooling reflected in all regions south of 40°S (Pedro et al., 2015).

A similar distinctive reduction in tall tree vegetation, characterised by increasing cool-climate taxa, is reflected in marine and terrestrial pollen records for southwestern New Zealand from 130-128 ka. This signal is more pronounced on land at Okarito Bog (Newnham et al., 2007a). This cool episode punctuates Southern Hemisphere warming and occurs once interglacial conditions have been reached for the last interglacial, as defined for southwestern New Zealand and from EDC at 132 ka (Fig. 4.9; Govin et al., 2015). This cooling is antiphased with prominent SST warming (>5°C) in the NH mid-latitudes. The early LIG climate reversal contrasts with the ACR in that it follows the attainment of interglacial conditions, although displays a similar duration (~2 kyr) and amplitude (1.5-2°C) of cooling as reflected in MAATs at Okarito Bog. Cooler ocean- land surface temperatures also characterise early MIS 11 at MD06-2990 between 426-422 ka and are consistent with cooler temperatures at EDC (more negative δD values) between 425-421 ka (Jouzel et al., 2007; Bazin et al., 2013). Cooling of the mid-high SH latitudes follows Heinrich type 'Ht" event 4 in the NH mid-latitudes (Rodrigues et al., 2011), and is asynchronous with prominent SST warming (~10°C) in the NH mid-latitudes. Despite similar orbital configurations to that of T-I, this episode of cooling is twice the length of both the ACR (T-I) and the early LIG climate reversal which follows HS-11 (T-II) in the study region. Such millennial-scale climate asynchrony between the hemispheres is most likely a result of a systematic, but non-linear, re-organisation of the ocean-atmosphere circulation system in response to orbital forcing.

6.2.4 Is the pattern of climate amelioration between land and sea synchronous for all three interglacials or is there evidence for lags in the climate system?

Section 6.22 highlighted the synchronous nature of changes between vegetation in southwestern New Zealand and SST from the East Tasman Sea. However, there is evidence for lags in the climate system following terminations, where the rise to dominance of *Dacrydium cupressinum* follows the initial development of emergent podocarps and also SST maxima (Fig. 6.1). Afforestation of *D. cupressinum* was prolonged by up to 10 kyr subsequent to emergent podocarps in early MIS 11, with a smaller and comparable delay of 3.8 kyr for T-I and T-II. *D. cupressinum* was likely excluded far from the region during the preceding cold MIS 12 glacial, with its expansion delayed by competition from the thermophilous shrub *Ascarina lucida* and southern beech. The delayed afforestation of *D. cupressinum* results in an apparent "decoupling" of ocean-atmosphere circulation systems in this maritime climate setting, where reconstructed MAATs from Okarito Bog lag the East Tasman Sea surface temperature maxima by between ~0.5–3 kyr for T-I and T-II. This is considered to reflect the time taken for vegetation to reach ecological climax with interglacial conditions. Similar lags are revealed from the colonisation of tall tree podocarps to eastern regions to their western equivalents over MIS 11 at DSDP Site 594, located ~300 km east of the South Island.

6.2.5 Are vegetation changes in the southwestern New Zealand during interglacials of similar character and magnitude?

The palynological records presented here from marine sediment cores adjacent to South Island, New Zealand suggest that the vegetation composition varies between post mid-Brunhes Event interglacials (i.e., MIS 1, 5e, 7a-7c, 7e, 9e, 11c; Fig. 1.1) – i.e., that the same "interglacial flora" are included although can vary between each interglacial.

While expansion of *D. cupressinum* in the East Tasman Sea follows T-I, T-II and T-V in all cases (Fig. 6.1), the frost and drought intolerant understory shrub *Ascarina lucida* is more variable in its climate response. During early MIS 11(e-d) *A. lucida* proliferated, favoured by mild, moist conditions, and eventually forming a dominant component of the lowland vegetation cover under full interglacial conditions during MIS 11c, much more so than during MIS 1 and MIS 5e. Southern beech also proliferated during MIS 11c, compared to the last two interglacial climate optima. During MIS 11 it may have survived in the

contemporary central Westland 'Biotic Gap zone' where it is absent today (Wardle, 1984, 1988).

6.2.6 Were past interglacials (MIS 1, 5e and 11) in southwestern New Zealand warmer than present, and what do they tell us about future climate in a warming world?

Direct comparisons of vegetation change and SST from East Tasman Sea cores have enabled the scale and timing of past climatic changes to be assessed for MIS 1 and 5e, and 11. In addition, transfer of the MD06-2991 chronology to the Okarito Bog sequence has enabled air and ocean temperatures to be quantified for a common time scale to reconcile whether there was evidence for past warmth over the last two interglacial climatic optima (building on the work of Vandergoes et al., 2005 and Ryan et al., 2012).

Early Holocene climate optimum (~12-9.5 ka)

Synchronised pollen and SST measurements at MD06-2991 provide unequivocal evidence for ocean-atmosphere coupling in southwestern New Zealand over the pre-Holocene climate amelioration. SSTs and emergent conifers tolerable of mild climate conditions both peak at 11.87 ± 0.3 cal ka BP (2σ) coeval with the onset of the Holocene Interglacial defined in North Island New Zealand (NZce-1; 11.88 cal ka BP). SSTs exceeded present levels by up to 1°C, with an equivalent rise in MAAT reconstructions from Okarito Bog lagging SST maxima by ~1 kyr, and concurrent expansion of *D. cupressinum* in Westland.

Last interglacial (LIG) climate optimum (~128-123 ka)

Thermophilous and drought sensitive species inhabited forests of the Westland lowlands during the last interglacial (LIG) climate optimum (128-123 ka). These species flourished once surface temperatures in the East Tasman Sea surpassed modern conditions. MAATs were ~0.5-1.5°C greater than their modern reconstructed values for the LIG climate optimum, and exceeded early Holocene estimates by ~0.75°C (M.J.V unpublished data). These higher SST and MAAT estimates are consistent with previous regional estimates derived from paleoclimate modelling (Capron et al., 2014), terrestrial proxy data (Marra, 2003; Fletcher and Thomas, 2010), and marine SST records (Murray-Wallace et al., 2000; Barrows et al., 2007a; Hayward et al., 2012; Cortese et al., 2013). Previous conclusions for a marked warming exhibited off southwest New Zealand over the LIG climate optimum propose that warm water was conveyed across the Tasman Sea by a southwards extension of the warm East Australian Current (EACe) (Fig. 6.2), resulting from a southwards

shift/intensification of the Southern Hemisphere westerly wind belt (Cortese et al. (2013). This resulted in a southward shift of the STF in the East Tasman Sea (Hayward et al., 2012).

By the end of the century, atmospheric warming is projected to raise global mean surface temperatures 0.3-4.8°C above pre-industrial values (Meinshausen et al., 2011; Stocker et al., 2013). An unprecedented warming and shift in the surface ocean off South Australia to 45°S (Cowan et al., 2014), far exceeding global mean values (Hill et al., 2011; Wu et al., 2012; Oliver and Holbrook, 2014), displays similarities to those outlined for the LIG (Cortese et al., 2013). This is considered to be the result of an intensification of the flow and accelerated warming in the East Australian Current (EAC) (Ridgeway and Hill, 2012), shifting 50-80 km over the last 40 years (Moore et al 1999), and climate model simulations anticipate that this trend will accelerate over the next 100 years (Oliver et al., 2014; Oliver et al., 2015). The progressive warming further south may in turn accelerate ice melt from Antarctica (Golledge et al., 2015), and may be similar to that which occurred during the LIG where ~5 m of global eustatic sea level rise was produced from the WAIS with a contribution from the EAIS (Dahl-Jensen et al., 2013; Pol et al., 2014; DeConto and Pollard, 2015; Dutton et al., 2015b).

MIS 11c climate optimum (~417-407 ka)

The thermal optimum in the terrestrial environment during MIS 11c occurs between 417-407 ka, and provides an unprecedented glimpse into the kind of conditions in the Southern Hemisphere mid-latitudes that are projected for the future. The dominance of tree and shrub species, *D. cupressinum* and *Ascarina lucida* in MIS11c is analogous to pollen records recovered from more northerly latitudes in western North Island during the early Holocene climatic optimum (11.5-9 cal ka BP). North Taranaki presently experiences annual land surface temperatures which are ~3°C warmer than southwestern South Island, implying that the MIS 11c climate optimum was at least as warm or in excess of peak Holocene estimates further south. This composition contrasts markedly with the dominance of *D. cupressinum* for the Holocene (MIS 1) and last interglacial (MIS 5e) assemblage in southwestern New Zealand, with biogeographic barriers proposed to have inhibited the migration of better adapted species from more northerly latitudes to warmer climatic conditions over MIS 5e and MIS 11. The prominent expansion of conifers and tree ferns in eastern South Island (DSDP 594) lags that from the west (MD06-2990) by as much as 10 kyr. This is consistent with similar delays revealed in SSTs (Prebble et al., 2016), and reveals distinct regional differences to the pattern of climate amelioration.

SSTs each side of the South Island were on average ~3°greater than present (Table 5.2), with the STF situated further south than present (Fig. 5.2), and an equivalent ~+3°C of annual warming estimated from EDC in Antarctica (Jouzel et al., 2007). The protracted duration of global and regional warmth for MIS 11c, coupled with low terrestrial seasonality (Coletti et al., 2015; Yin and Berger, 2015), are mechanisms considered to have played roles in ice sheet melting in Greenland and West Antarctica which contributed to global sea levels ~6-13 m above present (Rohling et al., 2010; Raymo and Mitrovica, 2012; Reyes et al., 2014). This has important implications for future sea level predictions, where atmospheric warming of the same order (1.5-2°C) produces an unstoppable contribution to sea level rise resulting from the collapse of polar ice sheets in climate models (Golledge et al., 2015).

6.3 Summary

This thesis has established a high-resolution chronostratigraphic framework from marine and terrestrial and marine climate conditions from southwestern New Zealand and the East Tasman Sea over the past 450 ka. This has permitted investigations of regional and global climate forcing, specifically during termination I, II and V, and their following interglacials 1, 5e and 11.

References

Abe-Ouchi, A., Saito, F., Kawamura, K., Raymo, M.E., Okuno, J.i., Takahashi, K., Blatter, H., 2013. Insolation-driven 100,000-year glacial cycles and hysteresis of ice-sheet volume. Nature 500, 190-193.

Ahn, J., Brook, E.J., 2008. Atmospheric CO_2 and climate on millennial time scales during the last glacial period. Science 322, 83-85.

Allen, J.R.M., Brandt, U., Brauer, A., Hubberten, H.-W., Huntley, B., Keller, J., Kraml, M., Mackensen, A., Mingram, J., Negendank, J.F., 1999. Rapid environmental changes in southern Europe during the last glacial period. Nature 400, 740-743.

Allen, J.R.M., Huntley, B., 2009. Last Interglacial palaeovegetation, palaeoenvironments and chronology: a new record from Lago Grande di Monticchio, southern Italy. Quaternary Science Reviews 28, 1521-1538.

Alley, R.B., Agustsdottir, A.M., Fawcett, P.J., 1999. Ice-core evidence of late-Holocene reduction in North Atlantic Ocean heat transport. Mechanisms of Global Climate Change at Millennial Time Scales, In: Clark, P.U., Webb, R.S., Keigwin, L.D. (Eds.), Mechanisms of Global Climate Change at Millennial Time Scales. American Geophysical Union., Geophysical Monograph Series, pp. 301-312.

Alloway, B.V., Lowe, D.J., Barrell, D.J.A., Newnham, R.M., Almond, P.C., Augustinus, P.C., Bertler, N.A.N., Carter, L., Litchfield, N.J., McGlone, M.S., Shulmeister, J., Vandergoes, M.J., Williams, P.W., NZ-INTIMATE-members, 2007a. Towards a climate event stratigraphy for New Zealand over the past 30,000 years (NZ-INTIMATE project). Journal of Quaternary Science 22, 9-35.

Alloway, B.V., Larsen, G., Lowe, D.J., Shane, P.A.R., Westgate, J.A., 2007b. Tephrochronology, In: Elias, S.A (Ed.), Encyclopaedia of Quaternary Science. , Elsevier, London, pp. 2869-2898.

Alloway, B. V., McGlone, M. S., Neall, V. E., & Vucetich, C. G. (1992). The role of Egmont-sourced tephra in evaluating the paleoclimatic correspondence between the bio-and soil-stratigraphic records of central Taranaki, New Zealand. Quaternary international, 13, 187-194.

Alloway, B.V., Neall, V.E., Vucetich, C.G., 1995. Late Quaternary (post 28,000 year B.P.) tephrostratigraphy of northeast and central Taranaki, New Zealand. Journal of the Royal Society of New Zealand 25, 385-458.

Alloway, B.V., Pillans, B.J., Carter, L., Naish, T.R., Westgate, J.A., 2005. Onshore-offshore correlation of Pleistocene rhyolitic eruptions from New Zealand: implications for TVZ eruptive history and paleoenvironmental construction. Quaternary Science Reviews 24, 1601-1622.

Almond, P.C., Moar, N.T., Lian, O.B., 2001. Reinterpretation of the glacial chronology of South Westland, New Zealand. New Zealand Journal of Geology and Geophysics 44, 1-16.

Anderson, R.F, Ali, S., Bradtmiller, L.I, Nielsen, S.H.H, Fleisher, M.Q, Anderson, B.E, Burckle, L.H, 2009. Wind-driven upwelling in the Southern Ocean and the deglacial rise in atmospheric CO_2. Science 323, 1443-1448.

Applegate, P.J., Lowell, T.V., Alley, R.B., 2008. Comment on "Absence of cooling in New Zealand and the adjacent ocean during the Younger Dryas chronozone". Science 320, 746d-746d.

Aubry, M.-P., Van Couvering, J.A., Christie-Blick, N., Pratt, R., Owen, D.E., Ferrusquía, I.-v., 2009. Terminology of geological time: Establishment of a community standard. Stratigraphy 6 (2), 100-105.

Bard, E., Rostek, F., Turon, J.-L., Gendreau, S., 2000. Hydrological impact of Heinrich events in the subtropical Northeast Atlantic. Science 289, 1321-1324.

Barker, S., Chen, J., Gong, X., Jonkers, L., Knorr, G., Thornalley, D., 2015. Icebergs not the trigger for North Atlantic cold events. Nature 520, 333-336.
Barker, S., Diz, P., Vautravers, M.J., Pike, J., Knorr, G., Hall, I.R., Broecker, W.S., 2009. Interhemispheric Atlantic seesaw response during the last deglaciation. Nature 457, 1097-1102.
Barker, S., Knorr, G., Edwards, R.L., Parrenin, F., Putnam, A.E., Skinner, L.C., Wolff, E., Ziegler, M., 2011. 800,000 years of abrupt climate variability. Science 334, 347-351.
Barrell, D.J.A., 2011. Quaternary Glaciers of New Zealand, In: Ehlers, J., Gibbard, P.L., Hughes, P.D. (Eds.), Developments in Quaternary Science. Quaternary glaciations: extent and chronology - a closer look. Elsevier Ltd, Amsterdam, The Netherlands, pp. 1047-1064.
Barrell, D.J.A., Alloway, B.V., Shulmeister, J., Newnham, R., 2005. Towards a climate event stratigraphy for New Zealand over the past 30,000 years. GNS Science Report, SR 2005/07 (includes poster).
Barrell, D.J.A., Almond, P.C., Vandergoes, M.J., Lowe, D.J., Newnham, R.M., 2013. A composite pollen-based stratotype for inter-regional evaluation of climatic events in New Zealand over the past 30,000 years (NZ-INTIMATE project). Quaternary Science Reviews 74, 4-20.
Barrell, D.J.A., Andersen, B.G., Denton, G.H., 2011. Glacial geomorphology of the central South Island, New Zealand. GNS Science Monograph 27, 81 pp. + map (5 sheets) + legend (1 sheet). Lower Hutt, New Zealand. GNS Science.
Barrows, T.T., Almond, P., Rose, R., Keith Fifield, L., Mills, S.C., Tims, S.G., 2013. Late Pleistocene glacial stratigraphy of the Kumara-Moana region, West Coast of South Island, New Zealand. Quaternary Science Reviews 74, 139-159.
Barrows, T.T., Juggins, S., De Deckker, P., Calvo, E., Pelejero, C., 2007a. Long term sea surface temperature and climate change in the Australian-New Zealand region. Paleoceanography 22, 1-17. PA 2215.
Barrows, T.T., Lehman, S.J., Fifield, L.K., De Deckker, P., 2007b. Absence of cooling in New Zealand and the adjacent ocean during the Younger Dryas chronozone. Science 318, 86-89.
Basher, L., McSaveney, M., 1989. An early Aranuian glacial advance at Cropp River, central Westland, New Zealand. Journal of the Royal Society of New Zealand. 19, 263-268.
Batten, D., 1996. Palynofacies and environmental interpretation, In: Jansonius, J., McGregor, D.C. (Eds.), Palynology: Principles and Applications. American Association of Stratigraphic Palynologists Foundation, Dallas.
Baylis, G., 1980. Mycorrhizas and the spread of beech. New Zealand Journal of Ecology 3, 151-153.
Bazin, L., Landais, A., Lemieux-Dudon, B., Toyé Mahamadou Kele, H., Veres, D., Parrenin, F., Martinerie, P., Ritz, C., Capron, E., Lipenkov, V., 2013. An optimized multi-proxy, multi-site Antarctic ice and gas orbital chronology (AICC2012): 120-800 ka. Climate of the Past 9, 1715-1731.
Bender, M., Sowers, T., Dickson, M.-L., Orchardo, J., Grootes, P., Mayewski, P.A., Meese, D.A., 1994. Climate correlations between Greenland and Antarctica during the past 100,000 years. Nature 372, 663-666.
Bereiter, B., Eggleston, S., Schmitt, J., Nehrbass-Ahles, C., Stocker, T.F., Fischer, H., Kipfstuhl, S., Chappellaz, J., 2015. Revision of the EPICA Dome C CO_2 record from 800 to 600 kyr before present. Geophysical Research Letters 42, 542-549.
Berger, A., 1978. Long-term variations of caloric insolation resulting from the Earth's orbital elements. Quaternary Research 9, 139-167.
Berger, A., Loutre, M.F., 1991. Insolation values for the climate of the last 10 million years. Quaternary Science Reviews 10, 297-317.

Berger, A., Loutre, M.F., 1997. Palaeoclimate sensitivity to CO_2 and insolation. Ambio 26, 32-37.
Berger, A., Loutre, M.F., 2002. An exceptionally long interglacial ahead? Science 297, 1287-1288.
Berger, G.W., Almond, P.C., Pillans, B.J., 2001. Luminescence dating and glacial stratigraphy in Westland, New Zealand. New Zealand Journal of Geology and Geophysics 44, 25-35.
Berger, W.H., 1999. The 100-kyr ice-age cycle; international oscillation or inclinational forcing? International Journal of Earth Sciences, 88, 305-316.
Berger, W.H., Jansen, E., 1994. Fourier stratigraphy; spectral gain adjustment of orbital ice mass models as an aid in dating late Neogene deep-sea sediments. Paleoceanography 9 (5), 693-703.
Birks, H.H., Birks, H.J.B., 2006. Multi-proxy studies in palaeolimnology. Vegetation History and Archaeobotany 15, 235-251.
Black, K.P., Nelson, C.S., Hendy, C.H., 1988. A spectral analysis procedure for dating Quaternary deep-sea cores and its application to a high-resolution Brunhes record from the Southwest Pacific. Marine Geology 83, 21-30.
Blunden, J., Arndt, D.S., 2016. State of the Climate in 2015. Bulletin of the American Meteorological Society 97 (8), 1-275.
Bond, G.C., Heinrich, H., Broecker, W.S., Labeyrie, L.D., McManus, J., Andrews, J., Huon, S., Jantschik, R., Clasen, S., Simet, C., Tedesco, K., Klas, M., Bonani, G., Ivy, S., 1992. Evidence for massive discharges of icebergs into the North Atlantic ocean during the last glacial period. Nature 360, 245-249.
Bostock, H.C., Barrows, T.T., Carter, L., Chase, Z., Cortese, G., Dunbar, G., Ellwood, M., Hayward, B., Howard, W., Neil, H., 2013. A review of the Australian–New Zealand sector of the Southern Ocean over the last 30 ka (Aus-INTIMATE project). Quaternary Science Reviews 74, 35-57.
Bostock, H.C., Hayward, B.W., Neil, H.L., Sabaa, A.T., Scott, G.H., 2015. Changes in the position of the Subtropical Front south of New Zealand since the last glacial period. Paleoceanography 30 (7), 824-844.
Bouttes, N., Paillard, D., Roche, D., 2010. Impact of brine-induced stratification on the glacial carbon cycle. Climate of the Past 6, 575-589.
Bradford-Grieve, J.M., Probert, K.P., Lewis, K.B., Sutton, P., Zeldis, J., Orpin, A.R., 2006. New Zealand shelf region (31, S). In: Robinson, A.R., Brink, K. (Eds.), The sea. The global ocean: interdisciplinary regional studies and synthesis. Harvard University Press., Cambridge, MA, pp. 1451-1492.
Bradford, J.M., 1983. Physical and chemical oceanographic observations off Westland, New Zealand, June 1979. New Zealand Journal of Marine and Freshwater Research 17, 71-81.
Brasier, M.D., 1980. Microfossils. George Allen & Unwin London, pp. 59-77.
Brauer, A., Allen, J.R., Mingram, J., Dulski, P., Wulf, S., Huntley, B., 2007. Evidence for last interglacial chronology and environmental change from Southern Europe. Proceedings of the National Academy of Sciences 104, 450-455.
Brauer, A., Dulski, P., Mangili, C., Mingram, J., Liu, J., 2009. The potential of varves in high-resolution paleolimnological studies. PAGES News 17, 96-98.
Briggs, N.D., 1976. Recognition and correlation of subdivisions within the Whakamaru Ignimbrite, central North Island, New Zealand. New Zealand Journal of Geology and Geophysics 19, 463-501.
Broecker, W.S., 1998. Paleocean circulation during the last deglaciation; a bipolar seesaw? Paleoceanography 13, 119-121.
Broecker, W.S., 2000. Abrupt climate change; causal constraints provided by the paleoclimate record. Earth-Science Reviews 51, 137-154.
Broecker, W.S., Bond, G.C., Klas, M., Clark, E.A., McManus, J., 1992. Origin of the northern Atlantic's Heinrich events. Climate Dynamics 6, 265-273.

Broecker, W.S., Denton, G.H., 1990. The role of ocean-atmosphere reorganizations in glacial cycles. Quaternary Science Reviews 9, 305-341.
Broecker, W.S., Donk, J., 1970. Insolation changes, ice volumes, and the O^{18} record in deep-sea cores. Reviews of Geophysics and Space Physics 8, 169-198.
Broecker, W.S., Peteet, D.M., Rind, D.H., 1985. Does the ocean-atmosphere system have more than one stable mode of operation? Nature 315, 21-26.
Bronk Ramsey, C., 2008. Deposition models for chronological records. Quaternary Science Reviews 27, 42-60.
Bronk Ramsey, C., 2009a. Dealing with outliers and offsets in radiocarbon dating. Radiocarbon 51, 1023-1045.
Bronk Ramsey, C., 2009b. Bayesian analysis of radiocarbon dates. Radiocarbon 51, 337-360.
Bronk Ramsey, C., Lee, S., 2013. Recent and planned developments of the program OxCal. Radiocarbon 55, 720-730.
Brown, S.J.A, Wilson, C.J.N, Cole, J.W, Wooden, J., 1998. The Whakamaru group ignimbrites, Taupo Volcanic Zone, New Zealand: evidence for reverse tapping of a zoned silicic magmatic system. Journal of Volcanology and Geothermal Research 84, 1-37.
Buckley, T.R., Marske, K., Attanayake, D., 2010. Phylogeography and ecological niche modelling of the New Zealand stick insect Clitarchus hookeri (White) support survival in multiple coastal refugia. Journal of Biogeography 37, 682-695.
Burrows, C., 1965. Some discontinuous distributions of plants within New Zealand and their ecological significance. Part II: Disjunctions between Otago-Southland and Nelson-Marlborough and related distribution patterns. Tuatara 13, 9-29.
Bussell, M.R., 1988. Mid and late Holocene pollen diagrams and Polynesian deforestation, Wanganui District, New Zealand. New Zealand Journal of Botany 26, 431-451.
Bussell, M.R., 1990. Palynology of oxygen isotope Stage 6 and Substage 5e from the cover beds of a marine terrace, Taranaki, New Zealand. Quaternary Research 34, 86-100.
Bussell, M.R., 1992. Late Pleistocene palynology of terrestrial cover beds at the type section of the Rapanui Terrace, Wanganui, New Zealand. Journal of the Royal Society of New Zealand 22, 77-90.
Bussell, M.R., Pillans, B., 1997. Vegetational and climatic history during oxygen isotope stage 7 and early stage 6, Taranaki, New Zealand. Journal of the Royal Society of New Zealand 27, 419-438.
Caballero-Gill, R.P., Clemens, S.C., Prell, W.L., 2012a. Direct correlation of Chinese speleothem $\delta^{18}O$ and South China Sea planktonic $\delta^{18}O$: Transferring a speleothem chronology to the benthic marine chronology. Paleoceanography 27 (2), PA2203.
Caballero-Gill, R.P., Clemens, S.C, Prell, W.L, 2012b. Antarctic Isotope Maxima events 24 and 25 identified in benthic marine $\delta^{18}O$. Paleoceanography 27, doi.org/10.1029/2011PA002269.
Cahill, M., Middleton, J., Stanton, B., 1991. Coastal-trapped waves on the west coast of South Island. New Zealand Journal of Physical Oceanography 21, 541–557.
Callard, S.L., 2011. The Last Glacial Maximum and deglaciation in southern New Zealand: new pollen-climate reconstructions. PhD thesis. School of Geography, Environment and Earth Sciences, Victoria University of Wellington.
Calvo, E., Pelejero, C., De Deckker, P., Logan, G.A., 2007. Antarctic deglacial pattern in a 30 kyr record of sea surface temperature offshore South Australia. Geophysical Research Letters 34(13), 1-6.
Candy, I., Schreve, D.C., Sherriff, J., Tye, G.J., 2014. Marine Isotope Stage 11: Palaeoclimates, palaeoenvironments and its role as an analogue for the current interglacial. Earth-Science Reviews 128, 18-51.
Capron, E., Govin, A., Stone, E.J., Masson-Delmotte, V., Mulitza, S., Otto-Bliesner, B., Rasmussen, T.L., Sime, L.C., Waelbroeck, C., Wolff, E.W., 2014. Temporal and spatial

structure of multi-millennial temperature changes at high latitudes during the Last Interglacial. Quaternary Science Reviews 103, 116-133.
Carlson, A.E., Clark, P.U., 2012. Ice sheet sources of sea level rise and freshwater discharge during the last deglaciation. Reviews of Geophysics 50(4), RG4007. doi.org/10.1029/2011rg000371.
Carter, J.A., 2002. Phytolith analysis and paleoenvironmental reconstruction from Lake Poukawa Core, Hawkes Bay, New Zealand. Global and Planetary Change 33, 257-267.
Carter, J.A., Lian, O.B., 2000. Palaeoenvironmental reconstruction from the last interglacial using phytolith analysis, southeastern North Island, New Zealand. Journal of Quaternary Science 15, 733-743.
Carter, L., 1975. Sedimentation on the continental terrace around New Zealand; a review. Marine Geology 19, 209-237.
Carter, L., Heath, R.A., 1975. Role of mean circulation, tides, and waves in the transport of bottom sediment on the New Zealand continental shelf. New Zealand Journal of Marine and Freshwater Research 9, 423-448.
Carter, L., Manighetti, B., 2006. Glacial/interglacial control of terrigenous and biogenic fluxes in the deep ocean off a high input, collisional margin: A 139 kyr-record from New Zealand. Marine Geology 226, 307-222.
Carter, L., Manighetti, B., Elliot, M., Trustrum, N., Gomez, B., 2002. Source, sea level and circulation effects on the sediment flux to the deep ocean over the past 15 ka off eastern New Zealand. Global and Planetary Change 33(3), 339-355.
Carter, L., Manighetti, B., Ganssen, G., Northcote, L., 2008. Southwest Pacific modulation of abrupt climate change during the Antarctic Cold Reversal–Younger Dryas. Palaeogeography, Palaeoclimatology, Palaeoecology 260, 284-298.
Carter, L., Nelson, C.S., Neil, H.L., Froggatt, P.C., 1995. Correlation, dispersal, and preservation of the Kawakawa Tephra and other late Quaternary tephra layers in the Southwest Pacific Ocean. New Zealand Journal of Geology and Geophysics 38, 29-46.
Carter, R.M., 2005. A New Zealand climatic template back to c. 3.9 Ma: ODP Site 1119, Canterbury Bight, south-west Pacific Ocean, and its relationship to onland successions. Journal of the Royal Society of New Zealand 35, 9-42.
Carter, R.M., Carter, L., Johnson, D.P., 1986. Submergent shorelines in the SW Pacific; evidence for an episodic post-glacial transgression. Sedimentology 33, 629-649.
Chaloner, W.G., Muir, M., 1968. Spores and floras, In: Murchison, D.G., Westoll, T.S. (Eds.), Coal and coal-bearing strata. Oliver and Boyd, Edinburgh, pp. 127-146.
Cheng, H., Edwards, R.L., Broecker, W.S., Denton, G.H., Kong, X., Wang, Y., Zhang, R., Wang, X., 2009. Ice age terminations. Science 326, 248-252.
Chiang, J.C., Lee, S.-Y., Putnam, A.E., Wang, X., 2014. South Pacific Split Jet, ITCZ shifts, and atmospheric North–South linkages during abrupt climate changes of the last glacial period. Earth and Planetary Science Letters 406, 233-246.
Chiswell, S.M., Bostock, H.C., Sutton, P.J., Williams, M.J., 2015. Physical oceanography of the deep seas around New Zealand: a review. New Zealand Journal of Marine and Freshwater Research 49, 286-317.
Clark, P.U., Alley, R.B., Pollard, D., 1999. Northern Hemisphere ice-sheet influences on global climate change. Science 286, 1104-1111.
Clark, P.U., Dyke, A.S., Shakun, J.D., Carlson, A.E., Clark, J., Wohlfarth, B., Mitrovica, J.X., Hostetler, S.W., McCabe, A.M., 2009. The last glacial maximum. Science 325, 710-714.
Cockayne, L., 1926. Monograph on the New Zealand beech forests. Part 1, The ecology of the forests and taxonomy of the beeches. New Zealand Forest Bulletin, 4-71.
Cogez, A., Meynadier, L., Allègre, C., Limmois, D., Herman, F., Gaillardet, J., 2015. Constraints on the role of tectonic and climate on erosion revealed by two time series analysis of marine cores around New Zealand. Earth and Planetary Science Letters 410, 174-185.

Coletti, A., DeConto, R., Brigham-Grette, J., Melles, M., 2015. A GCM comparison of Pleistocene super-interglacial periods in relation to Lake El'gygytgyn, NE Arctic Russia. Climate of the Past 11, 979-989.
Cook, E.R., Buckley, B.M., Palmer, J.G., Fenwick, P., Peterson, M.J., Boswijk, G., Fowler, A., 2006. Millennia-long tree-ring records from Tasmania and New Zealand: a basis for modelling climate variability and forcing, past, present and future. Journal of Quaternary Science 21, 689-700.
Cortese, G., Dunbar, G.B, Carter, L., Scott, G., Bostock, H., Bowen, M., Crundwell, M., Hayward, B.W, Howard, W., Martínez, J.I, Moy, A., Neil, H., Sabaa, A., Sturm, A., 2013. Southwest Pacific Ocean response to a warmer world: insights from Marine Isotope Stage 5e. Paleoceanography 28, 585-598, doi:10.1002/palo.20052
Cowan, T., Purich, A., Perkins, S., Pezza, A., Boschat, G., Sadler, K., 2014. More frequent, longer, and hotter heat waves for Australia in the twenty-first century. Journal of Climate 27, 5851-5871.
Crouch, E.M, Mildenhall, D.C, Neil, H.L, 2010. Distribution of organic-walled marine and terrestrial palynomorphs in surface sediments, offshore eastern New Zealand. Marine Geology 270, 235-256.
Crowley, T.J., 1992. North Atlantic Deep Water cools the Southern Hemisphere. Paleoceanography 7, 489-497.
Crundwell, M., Scott, G., Naish, T., Carter, L., 2008. Glacial-interglacial ocean climate variability from planktonic foraminifera during the Mid-Pleistocene transition in the temperate Southwest Pacific, ODP Site 1123. Palaeogeography, Palaeoclimatology, Palaeoecology 260, 202-229.
Cundill, P.R., Austin, W.E.N., Davies, S.E., 2006. Modern pollen from the catchment and surficial sediments of a Scottish sea loch (fjord). Grana 45, 230 - 238.
Cushing, E., 1967. Evidence for differential pollen preservation in late Quaternary sediments in Minnesota. Review of Palaeobotany and Palynology 4, 87-101.
Dahl-Jensen, D. and NEEM community members., 2013. Eemian interglacial reconstructed from a Greenland folded ice core. Nature 493, 489-494.
De Deckker, P., Moros, M., Perner, K., Jansen, E., 2012. Influence of the tropics and southern westerlies on glacial interhemispheric asymmetry. Nature Geoscience 5, 266-269.
Delusina, I., 2007. Selective Preservation and the Interpretation of Pollen Data from Hypoxic Marine Conditions: Evidence from Cariaco Basin Core MD03-2620. AGU Fall Meeting Abstracts, Volume 1, 06.
Denton, G.H., Alley, R.B., Comer, G.C., Broecker, W.S., 2005. The role of seasonality in abrupt climate change. Quaternary Science Reviews 24, 1159-1182.
Denton, G.H., Anderson, R.F., Toggweiler, J.R., Edwards, R.L., Schaefer, J.M., Putnam, A.E., 2010. The last glacial termination. Science 328, 1652-1656.
Denton, G.H., Hendy, C.H., 1994. Younger Dryas age advance of Franz Josef Glacier in the Southern Alps of New Zealand. Science 264, 1434-1437.
Denton, G.H., Heusser, C.J., Lowell, T.V., Moreno, P.I., Andersen, B.G., Heusser, L.E., Schluechter, C., Marchant, D.R., 1999. Interhemispheric linkage of paleoclimate during the last glaciation. Geografiska Annaler. Series A: Physical Geography 81, 107-153.
Denton, G.H., Hughes, T.J., 1983. Milankovich theory of ice ages; hypothesis of ice-sheet linkage between regional insolation and global climate. Quaternary Research 20, 125-144.
Desprat, S., Goñi, M.S., Turon, J.-L., McManus, J., Loutre, M.-F., Duprat, J., Malaize, B., Peyron, O., Peypouquet, J.-P., 2005. Is vegetation responsible for glacial inception during periods of muted insolation changes? Quaternary Science Reviews 24, 1361-1374.
Dickson, A.J., Leng, M.J., Maslin, M.A., Röhl, U., 2010. Oceanic, atmospheric and ice-sheet forcing of South East Atlantic Ocean productivity and South African monsoon intensity during MIS-12 to 10. Quaternary Science Reviews 29, 3936-3947.

Dosseto, A., Hesse, P., Maher, K., Fryirs, K., Turner, S., 2010. Climatic and vegetation control on sediment dynamics during the last glacial cycle. Geology 38, 395-398.
Doughty, A.M., Anderson, B.M., Mackintosh, A.N., Kaplan, M.R., Vandergoes, M.J., Barrell, D.J., Denton, G.H., Schaefer, J.M., Chinn, T.J., Putnam, A.E., 2013. Evaluation of Lateglacial temperatures in the Southern Alps of New Zealand based on glacier modelling at Irishman Stream, Ben Ohau Range. Quaternary Science Reviews 74, 160-169.
Doughty, A.M., Schaefer, J.M., Putnam, A.E., Denton, G.H., Kaplan, M.R., Barrell, D.J., Andersen, B.G., Kelley, S.E., Finkel, R.C., Schwartz, R., 2015. Mismatch of glacier extent and summer insolation in Southern Hemisphere mid-latitudes. Geology 43, 407-410.
Downs, D.T., Wilson, C.J.N., Cole, J.W, Rowland, J.V., Calvert, A.T., Leonard, G.S., Keall, J.M., 2014. Age and eruptive center of the Paeroa subgroup ignimbrites (Whakamaru group) within the Taupo Volcanic Zone of New Zealand. Geological Society of America Bulletin 126, 1131-1144.
Droxler, A.W., Alley, R.B., Howard, W.R., Poore, R.Z., Burckle, L.H., 2003. Unique and exceptionally long interglacial Marine Isotope Stage 11; window into Earth warm future climate. In: Droxler, A.W, Poore, R.Z., Burckle, L.H. (Eds.), Earth's Climate and Orbital Eccentricity: The Marine Isotope Stage 11 Question, Geophysical Monograph 137, American Geophysical Union, Washington, DC (2003), 1–14.
Drysdale, R.N., Zanchetta, G., Hellstrom, J.C., Fallick, A.E., Zhao, J.X., 2005. Stalagmite evidence for the onset of the Last Interglacial in southern Europe at 129±1 ka. Geophysical Research Letters 32(24), doi:10.1029/2005GL024658.
Dudley, W.C., Nelson, C.S., 1994. The influence of non-equilibrium isotope fractionation on the Quaternary calcareous nannofossil stable isotope signal in the Southwest Pacific Ocean, DSDP Site 594. Marine Micropaleontology 24, 3-27.
Dunbar, G.B., Dickens, G.R., Carter, R.M., 2000. Sediment flux across the Great Barrier Reef shelf to the Queensland Trough over last 300 ky. Sedimentary Geology 133, 49-92.
Dunbar, G.B., McLea, B., Goff, J.R., 1997. Holocene pollen stratigraphy and sedimentation, Wellington Harbour, New Zealand. New Zealand Journal of Geology and Geophysics 40, 325-333.
Dupont, L.M, Wyputta, U., 2003. Reconstructing pathways of aeolian pollen transport to the marine sediments along the coastline of SW Africa. Quaternary Science Reviews 22, 157-174.
Dutton, A., Carlson, A.E., Long, A.J., Milne, G.A., Clark, P.U., DeConto, R., Horton, B.P., Rahmstorf, S., Raymo, M.E., 2015a. Sea-level rise due to polar ice-sheet mass loss during past warm periods. Science 349, aaa4019.
Dutton, A., Lambeck, K., 2012. Ice volume and sea level during the last interglacial. Science 337, 216-219.
Dutton, A., Webster, J.M., Zwartz, D., Lambeck, K., Wohlfarth, B., 2015b. Tropical tales of polar ice: Evidence of last interglacial polar ice sheet retreat recorded by fossil reefs of the granitic Seychelles islands. Quaternary Science Reviews 107, 182-196.
Eaves, S. R., 2015. The glacial history of Tongariro and Ruapehu volcanoes, New Zealand, PhD thesis, Victoria University of Wellington.
Elderfield, H., Ferretti, P., Greaves, M., Crowhurst, S., McCave, I.N., Hodell, D., Piotrowski, A.M., 2012. Evolution of ocean temperature and ice volume through the mid-Pleistocene climate transition. Science 337, 704-709.
EPICA Community Members, 2004. Eight glacial cycles from an Antarctic ice core. Nature 429, 623-628.
EPICA Community Members, 2006. One-to-one coupling of glacial climate variability in Greenland and Antarctica. Nature 444, 195-198.
Eynaud, F., Zaragosi, S., Scourse, J., Mojtahid, M., Bourillet, J.-F., Hall, I.R., Penaud, A., Locascio, M., Reijonen, A., 2007. Deglacial laminated facies on the NW European continental margin: The hydrographic significance of British-Irish Ice Sheet deglaciation

and Fleuve Manche paleoriver discharges. Geochemistry, Geophysics, Geosystems 8(6), doi:10.1029/2006GC001496.
Faegri, K., Iversen, J., 1989. Textbook of pollen analysis., 4 ed. Wiley, Chichester.
Fletcher, M.-S., Moreno, P.I., 2011. Zonally symmetric changes in the strength and position of the Southern Westerlies drove atmospheric CO_2 variations over the past 14 ky. Geology 39, 419-422.
Fletcher, M.-S., Thomas, I., 2010. A quantitative Late Quaternary temperature reconstruction from western Tasmania, Australia. Quaternary Science Reviews 29, 2351-2361.
Fogwill, C.J., Turney, C.S.M., Hutchinson, D.K., Taschetto, A.S., England, M.H., 2015. Obliquity control on Southern Hemisphere climate during the Last Glacial. Scientific Reports 5, doi: 10.1038/srep11673.
Froggatt, P.C., Nelson, C.S., Carter, L., Griggs, G., Black, K.P., 1986. An exceptionally large late Quaternary eruption from New Zealand. Nature 319, 578-582.
Gage, M., Suggate, R.P., 1958. Glacial chronology of the New Zealand Pleistocene. Geological Society of America Bulletin 69, 589-598.
Galaasen, E.V., Ninnemann, U.S., Irvalı, N., Kleiven, H.K.F., Rosenthal, Y., Kissel, C., Hodell, D.A., 2014. Rapid reductions in North Atlantic Deep Water during the peak of the last interglacial period. Science 343, 1129-1132.
García, J.L., Kaplan, M.R., Hall, B.L., Schaefer, J.M., Vega, R.M., Schwartz, R., Finkel, R., 2012. Glacier expansion in southern Patagonia throughout the Antarctic cold reversal. Geology 40, 859-862.
Garnier, B., 1958. The climate of New Zealand: a geographic survey. Edward Arnold, London.
Golledge, N.R., Kowalewski, D.E., Naish, T.R., Levy, R.H., Fogwill, C.J., Gasson, E.G.W., 2015. The multi-millennial Antarctic commitment to future sea-level rise. Nature 526, 421-425.
Govin, A., Braconnot, P., Capron, E., Cortijo, E., Duplessy, J.-C., Jansen, E., Labeyrie, L., Landais, A., Marti, O., Michel, E., Mosquet, E., Risebrobakken, B., Swingedouw, D., Waelbroeck, C., 2012. Persistent influence of ice sheet melting on high northern latitude climate during the early Last Interglacial. Climate of the Past 8, 483-507.
Govin, A., Capron, E., Tzedakis, P.C., Verheyden, S., Ghaleb, B., Hillaire-Marcel, C., St-Onge, G., Stoner, J.S., Bassinot, F., Bazin, L., Mosquet, E., Risebrobakken, B., Swingedouw, D., Waelbroeck, C., Blunier, T., Combourieu-Nebout, N., El Ouahabi l, A., Genty, D., Gersonde, R., Jimenez-Amat, P., Landais, A., Martrat, B., Masson-Delmotte, V., Parrenin, F., Seidenkrantz, M.-S., Veres, D., Waelbroeck, C., Zahn, R., 2015. Sequence of events from the onset to the demise of the Last Interglacial: Evaluating strengths and limitations of chronologies used in climatic archives. Quaternary Science Reviews 129, 1-36.
Grant, K.M., Rohling, E.J., Ramsey, C.B., Cheng, H., Edwards, R.L., Florindo, F., Heslop, D., Marra, F., Roberts, A.P., Tamisiea, M.E., Williams, F., 2014. Sea-level variability over five glacial cycles. Nature communications 5, doi: 10.1038/ncomms6076
Griffiths, G.A., McSaveney, M.J., 1983a. Hydrology of a basin with extreme rainfalls- Cropp River, New Zealand. New Zealand Journal of Science 26, 293-306.
Griffiths, G.A., McSaveney, M.J., 1983b. Distribution of mean annual precipitation across some steepland regions of New Zealand. . New Zealand Journal of Science. 26, 197-209.
Grimm, E.C., 1987. CONISS: a FORTRAN 77 program for stratigraphically constrained cluster analysis by the method of incremental sum of squares. Computers & Geosciences 13, 13-35.
Groot, M.H.M., Bogotā, R.G., Lourens, L.J., Hooghiemstra, H., Vriend, M., Berrio, J.C., Tuenter, E., Plicht, J., Van Geel, B, Ziegler, M., Weber, S.L.., Betancourt, A., Contreras, L., Gaviria, S., Giraldo, C., Gonzālez, N., Jansen, J. H. F., Konert, M., Ortega, D., Range, O., Sarmiento, G., Vandenberghe, J., Van der Hammen, T., Van der Linden, M.,

Westerhoff, W., 2011. Ultra-high resolution pollen record from the northern Andes reveals rapid shifts in montane climates within the last two glacial cycles. Climate of the Past 7, 299-316.
Haase, P., 1990. Environmental and floristic gradients in Westland, New Zealand, and the discontinuous distribution of *Nothofagus*. New Zealand Journal of Botany 28, 25-40.
Hajdas, I., Lowe, D.J., Newnham, R.M., Bonani, G., 2006. Timing of the late-glacial climate reversal in the Southern Hemisphere using high-resolution radiocarbon chronology for Kaipo bog, New Zealand. Quaternary Research 65, 340-345.
Hall, G.M.J., McGlone, M.S., 2006. Potential forest cover of New Zealand as determined by an ecosystem process model. New Zealand Journal of Botany 44, 211-232.
Harle, K.J., Heijnis, H., Chisari, R., Kershaw, A.P., Zoppi, U., Jacobsen, G., 2002. A chronology for the long pollen record from Lake Wangoom, western Victoria (Australia) as derived from uranium/thorium disequilibrium dating. Journal of Quaternary Science 17, 707-720.
Harle, K.J., Kershaw, A.P., Clayton, E., 2004. Patterns of vegetation change in southwest Victoria (Australia) over the last two glacial/interglacial cycles: evidence from Lake Wangoom. Proceedings of the Royal Society of Victoria 116, 107-139.
Harper, M.A., Collen, J.D., 2002. Glaciations, interglaciations and reworked microfossils in Poukawa Basin, New Zealand. Global and Planetary Change 33, 243-256.
Harrison, S., Sánchez Goñi, M.F., 2010. Global patterns of vegetation response to millennial-scale variability and rapid climate change during the last glacial period. Quaternary Science Reviews 29, 2957-2980.
Hays, J.D., Imbrie, J., Shackleton, N.J., 1976. Variations in the Earth's orbit; pacemaker of the ice ages. Science 194, 1121-1132.
Hayward, B.W., Grenfell, H.R., Sabaa, A.T., Neil, H., Buzas, M.A., 2010. Recent New Zealand deep-water benthic foraminifera: taxonomy, ecologic distribution, biogeography, and use in paleoenvironmental assessment. Institute of Geological and Nuclear Sciences monograph 26
Hayward, B.W., Sabaa, A.T., Kolodziej, A., Crundwell, M.P., Steph, S., Scott, G.H., Neil, H.L., Bostock, H.C., Carter, L., Grenfell, H.R., 2012. Planktic foraminifera-based sea-surface temperature record in the Tasman Sea and history of the Subtropical Front around New Zealand, over the last one million years. Marine Micropaleontology 82-83, 13-27.
Hayward, B.W., Scott, G.H., Crundwell, M., Kennett, J., Carter, L., Neil, H., Sabaa, A., Wilson, K., Rodger, J., Schaefer, G., 2008. The effect of submerged plateaux on Pleistocene gyral circulation and sea-surface temperatures in the Southwest Pacific. Global and Planetary Change 63, 309-316.
He, F., Shakun, J.D., Clark, P.U., Carlson, A.E., Liu, Z., Otto-Bliesner, B.L., Kutzbach, J.E., 2013. Northern Hemisphere forcing of Southern Hemisphere climate during the last deglaciation. Nature 494, 81-85.
Heath, R.A., 1985. A review of the physical oceanography of the seas around New Zealand—1982. New Zealand Journal of Marine and Freshwater Research 19, 79-124.
Heenan, P.B., Smissen, R.D., 2013. Revised circumscription of *Nothofagus* and recognition of the segregate genera *Fuscospora*, *Lophozonia*, and *Trisyngyne* (Nothofagaceae). Phytotaxa 146, 1-31.
Heinrich, H., 1988. Origin and consequences of cyclic ice rafting in the northeast Atlantic Ocean during the past 130,000 years. Quaternary Research 29, 142-152.
Hellstrom, J., McCulloch, M., Stone, J., 1998. A detailed 31,000-year record of climate and vegetation change, from the isotope geochemistry of two New Zealand speleothems. Quaternary Research 50, 167-178.
Hemleben, C., Spindler, M., Anderson, O.R., 1989. Taxonomy and species features, modern planktonic foraminifera. Springer-Verlag, New York, 363 pp. doi:10.1007/978-1-4612-3544-6

Hemming, S.R., 2004. Heinrich events: Massive late Pleistocene detritus layers of the North Atlantic and their global climate imprint. Reviews of Geophysics 42(1), RG1005, doi:10.1029/2003RG000128 .

Herold, N., Yin, Q.Z., Karami, M.P., Berger, A., 2012. Modelling the climatic diversity of the warm interglacials. Quaternary Science Reviews 56, 126-141.

Hesse, P.P., 1994. The record of continental dust from Australia in Tasman Sea sediments. Quaternary Science Reviews 13, 257-272.

Heusser, L.E., 1990. Northeast Asian pollen records for the last 150,000 years from deep-sea cores V28-304 and RC14-99 taken off the Pacific coast of Japan. Review of Palaeobotany and Palynology 65, 1-8.

Heusser, L.E., van de Geer, G., 1994. Direct correlation of terrestrial and marine paleoclimate records from four glacial-interglacial cycles; DSDP Site 594, Southwest Pacific. Quaternary Science Reviews 13, 273-282.

Hicks, D.M., Shankar, U., McKerchar, A.I., Basher, L., Lynn, I., Page, M., Jessen, M., 2011. Suspended sediment yields from New Zealand rivers. Journal of Hydrology (New Zealand) 50, 81-142.

Hill, K.B., Simon, C., Marshall, D.C., Chambers, G.K., 2009. Surviving glacial ages within the biotic gap: phylogeography of the New Zealand cicada *Maoricicada campbelli*. Journal of Biogeography 36, 675-692.

Hill, K.L., Rintoul, S.R., Ridgway, K.R., Oke, P.R., 2011. Decadal changes in the South Pacific western boundary current system revealed in observations and ocean state estimates. Journal of Geophysical Research: Oceans 116. C01009.

Hodell, D.A., Channell, J.E., Curtis, J.H., Romero, O.E., Röhl, U., 2008. Onset of "Hudson Strait" Heinrich events in the eastern North Atlantic at the end of the middle Pleistocene transition (~ 640 ka)? Paleoceanography 23, PA4218. doi:10.1029/ 2008PA001591.

Hogg, A.G., Hua, Q., Blackwell, P.G., Niu, M., Buck, C.E., Guilderson, T.P., Heaton, T.J., Palmer, J.G., Reimer, P.J., Reimer, R.W., 2013. SHCal13 Southern Hemisphere calibration, 0–50,000 years cal BP. Radiocarbon 55, 1889-1903.

Hogg, A.G., Lowe, D.J., Hendy, C.H., 1987. University of Waikato radiocarbon dates I. Radiocarbon 29, 263-301.

Holmes, P., 1994. Studies of palynosedimentation in modern enivronments. Palynomorph sedimentation. In: Traverse, A. (Ed.), Sedimentation of organic particles. Cambridge Univeristy Press.

Holt, K.A., Wallace, R.C., Neall, V.E., Kohn, B.P., Lowe, D.J., 2010. Quaternary tephra marker beds and their potential for palaeoenvironmental reconstruction on Chatham Island, east of New Zealand, southwest Pacific Ocean. Journal of Quaternary Science 25, 1169-1178.

Hope, G., Kershaw, A.P., van der Kaars, S., Xiangjun, S., Liew, P.M., Heusser, L.E., Takahara, H., McGlone, M.S., Miyoshi, N., Moss, P.T., 2004. History of vegetation and habitat in the Austral-Asian region. . Quaternary International, 103-126.

Horrell, G.A., McKerchar, A.M., Griffiths, G.M., Griffiths, G.A., 2012. South Island storms and floods of December 2010. Journal of Hydrology (New Zealand) 51(1), 63.

Howard, W.R., 1997. Palaeoclimatology: A warm future in the past. Nature 388, 418-419.

Howarth, J.D., Fitzsimons, S.J., Jacobsen, G.E., Vandergoes, M.J., Norris, R.J., 2013. Identifying a reliable target fraction for radiocarbon dating sedimentary records from lakes. Quaternary Geochronology 17, 68-80.

Hua, Q., Barbetti, M., Rakowski, A.Z., 2013. Atmospheric radiocarbon for the period 1950–2010. Radiocarbon 55, 2059-2072.

Husson, F., Josse, J., Le, S., Mazet, J., 2013. FactoMineR: multivariate exploratory data analysis and data mining with R. R package version 1, 102-123.

Huybers, P., 2004. On the origins of the ice ages: insolation forcing, age models, and nonlinear climate change. PhD thesis. Department of Earth, Atmospheric and Planetary Sciences. Massachusetts Institute of Technology.

Huybers, P., 2007. Glacial variability over the last two million years: an extended depth-derived age model, continuous obliquity pacing, and the Pleistocene progression. Quaternary Science Reviews 26, 37-55.

Huybers, P., 2009. Pleistocene glacial variability as a chaotic response to obliquity forcing. Climate of the Past 5, 481-488.

Huybers, P., 2011. Combined obliquity and precession pacing of late Pleistocene deglaciations. Nature 480, 229-232.

Huybers, P., Denton, G.H., 2008. Antarctic temperature at orbital timescales controlled by local summer duration. Nature Geoscience 1, 787-792.

Huybers, P., Wunsch, C., 2005. Obliquity pacing of the late Pleistocene glacial terminations. Nature 434, 491-494.

Imbrie, J., Berger, A., Boyle, E.A., Clemens, S.C., Duffy, A., Howard, W.R., Kukla, G., Kutzbach, J., Martinson, D.G., McIntyre, A., Mix, A.C., Molfino, B., Morley, J.J., Peterson, L.C., Pisias, N.G., Prell, W.L., Raymo, M.E., Shackleton, N.J., Toggweiler, J.R., 1993. On the structure and origin of major glaciation cycles; 2, The 100,000-year cycle. Paleoceanography 8, 698-735.

Imbrie, J., Boyle, E.A., Clemens, S.C., Duffy, A., Howard, W.R., Kukla, G., Kutzbach, J., Martinson, D.G., McIntyre, A., Mix, A.C., Molfino, B., Morley, J.J., Peterson, L.C., Pisias, N.G., Prell, W.L., Raymo, M.E., Shackleton, N.J., Toggweiler, J.R., 1992. On the structure and origin of major glaciation cycles; 1, Linear responses to Milankovitch forcing. Paleoceanography 7(6), 701-738.

Imbrie, J., Hays, J.D., Martinson, D.G., McIntyre, A., Mix, A., Morley, J.J., Pisias, N.G., Prell, W., Shackleton, N.J., 1984. The orbital theory of Pleitocene climate: support from a revised chronology of the marine $\delta^{18}O$ record. In: Berger, A., Hays, J., Kukla, G., Salzman, B. (Eds.), Milankovitch and Climate. Reidel, Dordrecht, Holland pp. 269-305.

Imbrie, J., Imbrie, J.Z., 1980. Modeling the climatic response to orbital variations. Science 207, 943-953.

IPCC, 2014: Climate Change 2014: Synthesis Report. Contribution of Working Groups I, II and III to the Fifth Assessment Report of the Intergovernmental Panel on Climate Change [Core Writing Team, R.K. Pachauri and L.A. Meyer (eds.)]. IPCC, Geneva, Switzerland, 151 pp.

Jacobel, A.W., McManus, J.F., Anderson, R.F., Winckler, G., 2016. Large deglacial shifts of the Pacific Intertropical Convergence Zone. Nature communications 7. doi: 10.1038/ncomms10449.

Jacobson, G.L., Bradshaw, R.H.W., 1981. The selection of sites for paleovegetational studies. Quaternary Research 16, 80-96.

James, I.L., Norton, D.A., 2002. Helicopter-based natural forest management for New Zealand's rimu (*Dacrydium cupressinum*, Podocarpaceae) forests. Forest Ecology and Management 155, 337-346.

Jara, I.A., Newnham, R.M., Vandergoes, M.J., Foster, C.R., Lowe, D.J., Wilmshurst, J.M., Moreno, P.I., Renwick, J.A., Homes, A.M., 2015. Pollen–climate reconstruction from northern South Island, New Zealand (41°S), reveals varying high-and low-latitude teleconnections over the last 16 000 years. Journal of Quaternary Science 30, 817-829.

Jarosewich, E., Nelen, J., Norberg, J.A., 1980. Reference Samples for Electron Microprobe Analysis*. Geostandards Newsletter 4, 43-47.

Jarrett, G.R., 1985. Late Cenozoic Lithostratigraphy of DSDP Site 594, Southwestern Chatham Rise, New Zealand, with emphasis on the paleoenvironmental significance of the Late Quaternary Sequence. M.Sc. thesis. University of Waikato, Hamilton, New Zealand.

Jarzen, D. M. and D. J. Nichols. 1996. Pollen. p. 261–292. In J. Jansonius and D. C. McGregor (eds.) Palynology: Principles and Applications. American Association of Stratigraphic Palynologists Foundation, Volume 1. Publishers Press, Salt Lake City, UT, USA.

Jochum, K.P., Dingwell, D.B., Rocholl, A., Stoll, B., Hofmann, A.W., Becker, S., Besmehn, A., Bessette, D., Dietze, H.J., Dulski, P., 2000. The preparation and preliminary characterisation of eight geological MPI-DING reference glasses for in-situ microanalysis. Geostandards Newsletter 24, 87-133.

Jones, G.A., Kaiteris, P., 1983. A vacuum-gasometric technique for rapid and precise analysis of calcium carbonate in sediments and soils. Journal of Sedimentary Research 53, 655.

Jouzel, J., Masson-Delmotte, V., Cattani, O., Dreyfus, G., Falourd, S., Hoffmann, G., Minster, B., Nouet, J., Barnola, J.M., Chappellaz, J., 2007. Orbital and millennial Antarctic climate variability over the past 800,000 years. Science 317, 793.

Kaplan, M.R., Schaefer, J.M., Denton, G.H., Barrell, D.J.A., Chinn, T.J.H., Putnam, A.E., Andersen, B.G., Finkel, R.C., Schwartz, R., Doughty, A.M., 2010. Glacier retreat in New Zealand during the Younger Dryas stadial. Nature 467, 194-197.

Kaplan, M.R., Schaefer, J.M., Denton, G.H., Doughty, A.M., Barrell, D.J., Chinn, T.J., Putnam, A.E., Andersen, B.G., Mackintosh, A., Finkel, R.C., 2013. The anatomy of long-term warming since 15 ka in New Zealand based on net glacier snowline rise. Geology 41, 887-890.

Kawamura, K., Parrenin, F., Lisiecki, L., Uemura, R., Vimeux, F., Severinghaus, J.P., Hutterli, M.A., Nakazawa, T., Aoki, S., Jouzel, J., 2007. Northern Hemisphere forcing of climatic cycles in Antarctica over the past 360,000 years. Nature 448, 912-916.

Keeling, R.F., Walker, S.J., Piper, S.C., Bollenbacher, A.F., 2016. Atmospheric CO_2 concentrations (ppm) derived from in situ air measurements, (1958-2016). Scripps Institution of Oceanography, UC San Diego.

Kelley, S.E., Kaplan, M.R., Schaefer, J.M., Andersen, B.G., Barrell, D.J., Putnam, A.E., Denton, G.H., Schwartz, R., Finkel, R.C., Doughty, A.M., 2014. High-precision ^{10}Be chronology of moraines in the Southern Alps indicates synchronous cooling in Antarctica and New Zealand 42,000 years ago. Earth and Planetary Science Letters 405, 194-206.

Kidston, J., Renwick, J.A., McGregor, J., 2009. Hemispheric-scale seasonality of the Southern Annular Mode and impacts on the climate of New Zealand. Journal of Climate 22, 4759-4770.

Kistler, R., Collins, W., Saha, S., White, G., Woollen, J., Kalnay, E., Chelliah, M., Ebisuzaki, W., Kanamitsu, M., Kousky, V., 2001. The NCEP-NCAR 50-year reanalysis: Monthly means CD-ROM and documentation. Bulletin of the American Meteorological Society 82, 247-267.

Kleinen, T., Hildebrandt, S., Prange, M., Rachmayani, R., Müller, S., Bezrukova, E., Brovkin, V., Tarasov, P.E., 2014. The climate and vegetation of Marine Isotope Stage 11–model results and proxy-based reconstructions at global and regional scale. Quaternary International 348, 247-265.

Knutti, R., Stocker, T.F., Joos, F., Plattner, G.-K., 2002. Constraints on radiative forcing and future climate change from observations and climate model ensembles. Nature 416, 719-723.

Kohn, B.P., Pillans, B., McGlone, M.S., 1992. Zircon fission track age for middle Pleistocene Rangitawa Tephra, New Zealand; stratigraphic and paleoclimatic significance. Palaeogeography, Palaeoclimatology, Palaeoecology 95, 73-94.

Kopp, R.E., Simons, F.J., Mitrovica, J.X., Maloof, A.C., Oppenheimer, M., 2009. Probabilistic assessment of sea level during the last interglacial stage. Nature 462, 863-867.

Körner, C., Paulsen, J., 2004. A world-wide study of high altitude treeline temperatures. Journal of Biogeography 31, 713-732.

Koutsodendris, A., Brauer, A., Pälike, H., Müller, U.C., Dulski, P., Lotter, A.F., Pross, J., 2011. Sub-decadal-to decadal-scale climate cyclicity during the Holsteinian interglacial (MIS 11) evidenced in annually laminated sediments. Climate of the Past 7, 987-999.

Koutsodendris, A., Pross, J., Müller, U.C., Brauer, A., Fletcher, W.J., Kühl, N., Kirilova, E., Verhagen, F.T., Lücke, A., Lotter, A.F., 2012. A short-term climate oscillation during the Holsteinian interglacial (MIS 11c): An analogy to the 8.2 ka climatic event? Global and Planetary Change 92, 224-235.

Kukla, G.J., 2000. The last interglacial. Science 287, 987-988.

Kukla, G.J., Bender, M.L., de Beaulieu, J.-L., Bond, G.C., Broecker, W.S., Cleveringa, P., Gavin, J.E., Herbert, T.D., Imbrie, J., Jouzel, J., Keigwin, L.D., Knudsen, K.-L., McManus, J.F., Merkt, J., Muhs, D.R., Mueller, H., Poore, R.Z., Porter, S.C., Seret, G., Shackleton, N.J., Turner, C., Tzedakis, P.C., Winograd, I.J., 2002. Last interglacial climates. Quaternary Research 58, 2-13.

Lamy, F., Kaiser, J., Ninnemann, U., Hebbeln, D., Arz, H.W., Stoner, J., 2004. Antarctic timing of surface water changes off Chile and Patagonian ice sheet response. Science 304, 1959-1962.

Landais, A., Dreyfus, G., Capron, E., Jouzel, J., Masson-Delmotte, V., Roche, D.M., Prié, F., Caillon, N., Chappellaz, J., Leuenberger, M., 2013. Two-phase change in CO_2, Antarctic temperature and global climate during Termination II. Nature Geoscience 6, 1062-1065.

Landais, A., Masson-Delmotte, V., Stenni, B., Selmo, E., Roche, D.M., Jouzel, J., Lambert, F., Guillevic, M., Bazin, L., Arzel, O., 2015. A review of the bipolar see–saw from synchronized and high resolution ice core water stable isotope records from Greenland and East Antarctica. Quaternary Science Reviews 114, 18-32.

Lang, N., Wolff, E.W., 2011. Interglacial and glacial variability from the last 800 ka in marine, ice and terrestrial archives. Climate of the Past 7, 361-380.

Langebroek, P.M., Nisancioglu, K.H., 2014. Simulating last interglacial climate with NorESM: role of insolation and greenhouse gases in the timing of peak warmth. Climate of the Past 10, 1305-1318.

Large, M.F., Braggins, J.E., 1991. Spore atlas of New Zealand ferns and fern allies. A supplement to the New Zealand Journal of Botany. SIR Publishing, Wellington.

Larsen, I.J., Almond, P.C., Eger, A., Stone, J.O., Montgomery, D.R., Malcolm, B., 2014. Rapid soil production and weathering in the Southern Alps, New Zealand. Science 343, 637-640.

Laskar, J., Robutel, P., Joutel, F., Gastineau, M., Correia, A.C.M., Levrard, B., 2004. A long-term numerical solution for the insolation quantities of the Earth. Astronomy and Astrophysics 428, 261-285.

Leathwick, J.R., 1998. Are New Zealand's Nothofagus species in equilibrium with their environment? Journal of Vegetation Science 9, 719-732.

Leschen, R.A.B., Buckley, T.R., Harman, H.M., Shulmeister, J., 2008. Determining the origin and age of the Westland beech (*Nothofagus*) gap, New Zealand, using fungus beetle genetics. Molecular Ecology 17, 1256-1276.

Leschen, R.A.B., Michaux, B., 2005. Biogeography and evolution of New Zealand Priasilphidae (Coleoptera: Cucujoidea). New Zealand Entomologist 28, 55-64.

Li, Z., Moore, T.A., Weaver, S.D., 2001. Leaching of inorganics in the Cretaceous Greymouth coal beds, South Island, New Zealand. International Journal of Coal Geology 47, 235-253.

Lisiecki, L.E., Raymo, M.E., 2005. A Pliocene-Pleistocene stack of 57 globally distributed benthic $\delta^{18}O$ records. Paleoceanography 20, PA1003, doi:1010.1029/2004PA001071.

Lisiecki, L.E., Raymo, M.E., 2009. Diachronous benthic $\delta^{18}O$ responses during late Pleistocene terminations. Paleoceanography 24(3). PA3210, doi:10.1029/2009PA001732, 2009.

Locarnini, R., Mishonov, A., Antonov, J., Boyer, T., Garcia, H., Baranova, O., Zweng, M., Paver, C., Reagan, J., Johnson, D., 2013. World ocean atlas 2013, volume 1: temperature. NOAA Atlas NESDIS 73, 40.

Lourantou, A., Lavrič, J.V., Köhler, P., Barnola, J.M., Paillard, D., Michel, E., Raynaud, D., Chappellaz, J., 2010. Constraint of the CO_2 rise by new atmospheric carbon isotopic measurements during the last deglaciation. Global Biogeochemical Cycles 24. GB2015.

Loutre, M.F., Berger, A., 2000. Future climatic changes; are we entering an exceptionally long interglacial? Climatic Change 46, 61-90.

Loutre, M.F., Berger, A., 2003. Marine Isotope Stage 11 as an analogue for the present interglacial. Global and Planetary Change 36, 209-217.

Lowe, D.J., 1988. Late Quaternary volcanism in New Zealand; towards an integrated record using distal airfall tephras in lakes and bogs. Journal of Quaternary Science 3, 111-120.

Lowe, D.J., Blaauw, M., Hogg, A.G., Newnham, R.M., 2013. Ages of 24 widespread tephras erupted since 30,000 years ago in New Zealand, with re-evaluation of the timing and palaeoclimatic implications of the Lateglacial cool episode recorded at Kaipo bog. Quaternary Science Reviews 74, 170-194.

Lowe, D.J., Shane, P.A.R., Alloway, B.V., Newnham, R.M., 2008. Fingerprints and age models for widespread New Zealand tephra marker beds erupted since 30,000 years ago: a framework for NZ-INTIMATE. Quaternary Science Reviews 27, 95-126.

Lowe, D.J., Tippett, J.M., Kamp, P.J.J., Liddell, I.J., Briggs, R.M., Horrocks, J.L., 2001. Ages on weathered Plio-Pleistocene tephra sequences, western North Island, New Zealand, In: Juvigne, E.T., Raynal, J.-P. (Eds.), Tephras: Chronology, Archaeology, pp. 45-60.

Lunt, D., Abe-Ouchi, A., Bakker, P., Berger, A., Braconnot, P., Charbit, S., Fischer, N., Herold, N., Jungclaus, J.H., Kohn, V., 2013. A multi-model assessment of last interglacial temperatures. Climate of the Past 9, 699-717.

Luo, C., Chen, M., Xiang, R., Liu, J., Zhang, L., Lu, J., Yang, M., 2014. Modern pollen distribution in marine sediments from the northern part of the South China Sea. Marine Micropaleontology 108, 41-56.

Lüthi, D., Le Floch, M., Bereiter, B., Blunier, T., Barnola, J.-M., Siegenthaler, U., Raynaud, D., Jouzel, J., Fischer, H., Kawamura, K., 2008. High-resolution carbon dioxide concentration record 650,000–800,000 years before present. Nature 453, 379-382.

Mackay, A.W., Swann, G.E., Fagel, N., Fietz, S., Leng, M.J., Morley, D., Rioual, P., Tarasov, P., 2013. Hydrological instability during the Last Interglacial in central Asia: a new diatom oxygen isotope record from Lake Baikal. Quaternary Science Reviews 66, 45-54.

Mackintosh, A.N., Verleyen, E., O'Brien, P.E., White, D.A., Jones, R.S., McKay, R., Dunbar, R., Gore, D.B., Fink, D., Post, A.L., 2014. Retreat history of the East Antarctic Ice Sheet since the last glacial maximum. Quaternary Science Reviews 100, 10-30.

Macphail, M.K., McQueen, D.R., 1983. The value of New Zealand pollen and spores as indicators of Cenozoic vegetation and climates. Tuatara 26, 37-59.

Manville, V., Wilson, C.J.N., 2004. Vertical density currents: a review of their potential role in the deposition and interpretation of deep-sea ash layers. Journal of the Geological Society 161, 947-958.

Margari, V., Skinner, L.C., Hodell, D.A., Martrat, B., Toucanne, S., Grimalt, J.O., Gibbard, P.L., Lunkka, J., Tzedakis, P., 2014. Land-ocean changes on orbital and millennial time scales and the penultimate glaciation. Geology 42, 183-186.

Marino, G., Rohling, E.J., Rodríguez-Sanz, L., Grant, K.M., Heslop, D., Roberts, A.P., Stanford, J.D., Yu, J., 2015. Bipolar seesaw control on last interglacial sea level. Nature 522, 197-201.

Marra, M.J., 2003. Last interglacial beetle fauna from New Zealand. Quaternary Research 59, 122-131.

Marra, M.J., Alloway, B.V., Newnham, R.M., 2006. Paleoenvironmental reconstruction of a well-preserved Stage 7 forest sequence catastrophically buried by basaltic eruptive deposits, northern New Zealand. Quaternary Science Reviews 25, 2143-2161.
Marshall, D.C., Hill, K.B., Marske, K.A., Chambers, C., Buckley, T.R., Simon, C., 2012. Limited, episodic diversification and contrasting phylogeography in a New Zealand cicada radiation. BMC evolutionary biology 12, 177. doi:10.1186/1471-2148-12-177.
Marske, K.A., Leschen, R.A., Barker, G.M., Buckley, T.R., 2009. Phylogeography and ecological niche modelling implicate coastal refugia and trans-alpine dispersal of a New Zealand fungus beetle. Molecular Ecology 18, 5126-5142.
Marske, K.A., Leschen, R.A., Buckley, T.R., 2011. Reconciling phylogeography and ecological niche models for New Zealand beetles: looking beyond glacial refugia. Molecular Phylogenetics and Evolution 59, 89-102.
Marske, K.A., Leschen, R.A., Buckley, T.R., 2012. Concerted versus independent evolution and the search for multiple refugia: comparative phylogeography of four forest beetles. Evolution 66, 1862-1877.
Martin, T.J., Ogden, J., 2005. Experimental studies on the drought, waterlogging, and frost tolerance of *Ascarina lucida* Hook. f (Chloranthaceae) seedlings. New Zealand Journal of Ecology 29, 53-59.
Martrat, B., Jimenez-Amat, P., Zahn, R., Grimalt, J.O., 2014. Similarities and dissimilarities between the last two deglaciations and interglaciations in the North Atlantic region. Quaternary Science Reviews 99, 122-134.
Masson-Delmotte, V., Schulz, M., Abe-Ouchi, A., Beer, J., Ganopolski, A., González Rouco, J.F., Jansen, E., Lambeck, K., Luterbacher, J., Naish, T., Osborn, T., Otto-Bliesner, B., Quinn, T., Ramesh, R., Rojas, M., Shao, X., Timmermann, A., 2013. Information from paleoclimate archives, In: Stocker, T.F., Qin, D., Plattner, G.-K., Tignor, M., Allen, S.K., Boschung, J., Nauels, A., Xia, Y., Bex, V., Midgley, P.M. (Eds.), Climate Change 2013: The Physical Science Basis. Contribution of Working Group I to the Fifth Assessment Report of the Intergovernmental Panel on Climate Change Cambridge University Press, Cambridge, United Kingdom and New York, NY, USA., pp. 383-464.
Masson-Delmotte, V., Stenni, B., Pol, K., Braconnot, P., Cattani, O., Falourd, S., Kageyama, M., Jouzel, J., Landais, A., Minster, B., 2010. EPICA Dome C record of glacial and interglacial intensities. Quaternary Science Reviews 29, 113-128.
Matthews, N.E., Smith, V.C., Costa, A., Durant, A.J., Pyle, D.M., Pearce, N.J., 2012. Ultra-distal tephra deposits from super-eruptions: examples from Toba, Indonesia and Taupo Volcanic Zone, New Zealand. Quaternary International 258, 54-79.
McDonald, J.E., 1962. Collection and washout of airborne pollens and spores by raindrops. Science 135, 435.
McGlone, M.S., 1985. Plant biogeography and the late Cenozoic history of New Zealand. New Zealand Journal of Botany 23, 723-749.
McGlone, M.S., 2001. A late Quaternary pollen record from marine core P69, southeastern North Island, New Zealand. New Zealand Journal of Geology and Geophysics 44, 69-77.
McGlone, M.S., 2002. A Holocene and latest Pleistocene pollen record from Lake Poukawa, Hawke's Bay, New Zealand. Global and Planetary Change 33, 283-299.
McGlone, M.S., Basher, L., 2012. Holocene vegetation change at treeline, Cropp Valley, Southern Alps, New Zealand. Peopled landscapes: Archaelogcial and biogeographic approaches to landscapes. Terra Australis 34, 343-358.
McGlone, M.S., Hall, G.M., Wilmshurst, J.M., 2010b. Seasonality in the early Holocene: Extending fossil-based estimates with a forest ecosystem process model. The Holocene, 21, 517-526.
McGlone, M.S., Kershaw, A.P., Markgraf, V., 1992. El Nin/Southern Oscillation climatic variability in Australasian and South American paleoenvironmental records. In: Diaz,

H.F., Markgraf, V. (Eds.). El Nino; historical and paleoclimatic aspects of the Southern Oscillation, pp. 435-462.
McGlone, M.S., Mildenhall, D.C., Pole, M.S., 1996. History and paleoecology of New Zealand *Nothofagus* forests. In: Veblen, T.V., Hill, R.S., Read, J. (Eds.). The ecology and biogeography of *Nothofagus* forests. Yale University Press, pp. 83-130.
McGlone, M.S., Moar, N.T., 1977. The Ascarina decline and post-glacial climatic change in New Zealand. New Zealand Journal of Botany 15, 485-489.
McGlone, M.S., Neall, V., 1994. The late Pleistocene and Holocene vegetation history of Taranaki, North Island, New Zealand. New Zealand Journal of Botany 32, 251-269.
McGlone, M.S., Newnham, R.M., Moar, N.T., 2010c. The vegetation cover of New Zealand during the Last Glacial Maximum: Do pollen records under-represent woody vegetation? In: Haberle, S.G., Stevenson, J., Prebble, M. (Eds.), Altered Ecologies: Fire, Climate and Human Influence on Terrestrial Landscapes. Terra Australis, vol. 32. ANU E Press, Australian National University, Canberra, Australia, pp. 49-68.
McGlone, M.S., Salinger, M.J., Moar, N.T., Wright, H.E., Jr., 1993. Paleovegetation studies of New Zealand's climate since the last glacial maximum, In: Wright, H.E., Jr., Kutzbach, J.E., Webb III, T., Ruddiman, W.F., Street-Perrott, F.A., Bartlein, P.J. (Eds.), Global climates since the Last Glacial Maximum. University of Minnesota Press, London, pp. 294-317.
McGlone, M.S., Topping, W.W., 1973. Late Otiran/early Aranuian vegetation in the Tongariro area, central North Island. New Zealand Journal of Botany 11, 283-290.
McGlone, M.S., Turney, C.S.M., Wilmshurst, J.M., 2004. Late-glacial and Holocene vegetation and climatic history of the Cass Basin, central South Island, New Zealand. Quaternary Research 62, 267-279.
McGlone, M.S., Turney, C.S.M., Wilmshurst, J.M., Renwick, J., Pahnke, K., 2010a. Divergent trends in land and ocean temperature in the Southern Ocean over the past 18,000 years. Nature Geoscience 3, 622-626.
McGlone, M.S., Wardle, P., Worthy, T., 2003. Environmental Change since the Last Glaciation, In: Darby, J., Fordyce, R., Mark, A., Probert, K., Townsend, C. (Eds.). The Natural History of Southern New Zealand, pp. 105-118.
McManus, J.F., Oppo, D.W., Cullen, J.L., 1999. A 0.5-million-year record of millennial-scale climate variability in the North Atlantic. Science 283, 971-975.
McManus, J., Oppo, D., Cullen, J., Healey, S., 2003. Marine Isotope Stage 11 (MIS 11): analog for Holocene and future climate? In: Droxler, A., Poore, R., Burckle, L., Osterman, L. (Eds.), Earth's Climate and Orbital Eccentricity, The Marine Isotope Stage II Question, vol. 137. American Geophysical Union, pp. 69–85.
Meckler, A.N., Affolter, S., Dublyansky, Y.V., Krüger, Y., Vogel, N., Bernasconi, S.M., Frenz, M., Kipfer, R., Leuenberger, M., Spötl, C., 2015. Glacial–interglacial temperature change in the tropical West Pacific: A comparison of stalagmite-based paleo-thermometers. Quaternary Science Reviews 127, 90-116.
Meckler, A.N., Clarkson, M.O., Cobb, K.M., Sodemann, H., Adkins, J.F., 2012. Interglacial hydroclimate in the tropical West Pacific through the Late Pleistocene. Science 336, 1301-1304.
Meinshausen, M., Smith, S.J., Calvin, K., Daniel, J.S., Kainuma, M., Lamarque, J., Matsumoto, K., Montzka, S., Raper, S., Riahi, K., 2011. The RCP greenhouse gas concentrations and their extensions from 1765 to 2300. Climatic Change 109, 213-241.
Melles, M., Brigham-Grette, J., Minyuk, P.S., Nowaczyk, N.R., Wennrich, V., DeConto, R.M., Anderson, P.M., Andreev, A.A., Coletti, A., Cook, T.L., 2012. 2.8 million years of Arctic climate change from Lake El'gygytgyn, NE Russia. Science 337, 315-320.
Mew, G., Hunt, J.L., Froggatt, P.C., Eden, D.N., Jackson, R.J., 1986. An occurrence of Kawakawa Tephra from the Grey River valley, South Island, New Zealand. New Zealand Journal of Geology and Geophysics 29, 315-322.

Mildenhall, D.C., 1979. Holocene pollen diagrams from Pauatahanui Inlet, Porirua, New Zealand. New Zealand Journal of Geology and Geophysics 22, 585-591.
Mildenhall, D.C., 1995. Pleistocene palynology of the Petone and Seaview drillholes, Petone, lower Hutt Valley, North Island, New Zealand. Journal of the Royal Society of New Zealand 25, 207-262.
Mildenhall, D.C., 2003. Deep-sea record of Pliocene and Pleistocene terrestrial palynomorphs from offshore eastern New Zealand (ODP Site 1123, Leg 181). New Zealand Journal of Geology and Geophysics 46, 343-361.
Mildenhall, D.C., Alloway, B.V., 2008. A widespread ca. 1.1 Ma TVZ silicic tephra preserved near Wellington, New Zealand: implications for regional reconstruction of mid-Pleistocene vegetation. Quaternary International 178, 167-182.
Mildenhall, D.C., Hollis, C.J., Naish, T.R., 2004. Orbitally-influenced vegetation record of the mid-Pleistocene climate transition, offshore eastern New Zealand (ODP Leg 181, Site 1123). Marine Geology 205, 87-111.
Mildenhall, D.C., Orpin, A.R., 2010. Terrestrial palynology from marine cores as an indicator of environmental change for the Waipaoa Sedimentary System and north-eastern New Zealand. Marine Geology 270, 227-234.
Milker, Y., Rachmayani, R., Weinkauf, M., Prange, M., Raitzsch, M., Schulz, M., Kucera, M., 2013. Global and regional sea surface temperature trends during Marine Isotope Stage 11. Climate of the Past 9, 2231-2252.
Milner, A.M., Collier, R.E., Roucoux, K.H., Müller, U.C., Pross, J., Kalaitzidis, S., Christanis, K., Tzedakis, P.C., 2012. Enhanced seasonality of precipitation in the Mediterranean during the early part of the Last Interglacial. Geology 40, 919-922.
Milner, A.M., Müller, U.C., Roucoux, K.H., Collier, R.E., Pross, J., Kalaitzidis, S., Christanis, K., Tzedakis, P.C., 2013. Environmental variability during the Last Interglacial: a new high-resolution pollen record from Tenaghi Philippon, Greece. Journal of Quaternary Science 28, 113-117.
Moar, N.T., 1969. Possible long-distance transport of pollen to New Zealand. New Zealand Journal of Botany 7, 424-426.
Moar, N.T., 1970. Recent pollen spectra from three localities in the South Island, New Zealand. New Zealand Journal of Botany 8, 210-221.
Moar, N.T., 1973. Contributions to the Quaternary History of the New Zealand Flora 7. Two Aranuian Pollen Diagrams from Central South Island New Zealand Journal of Botany 11, 291-304.
Moar, N.T., 1980. Late Otiran and early Aranuian grassland in central South Island. New Zealand Journal of Ecology 3, 4-12.
Moar, N.T., 1984. *Nestegis* (Oleaceae) pollen in coastal sites in Westland. New Zealand Journal of Botany 22, 169-171.
Moar, N.T., 1993. Pollen grains of New Zealand dicotyledonous plants. Manaaki Whenua Press Lincoln, Canterbury, New Zealand, 200 pp.
Moar, N.T., McKellar, I.C., 2001. Interglacial vegetation in South Westland, South Island, New Zealand. New Zealand Journal of Geology and Geophysics 44, 17-24.
Moar, N.T., Suggate, R.P., 1973. Pollen analysis of late Otiran and Aranuian sediments at Blue Spur Road (S51), north Westland. New Zealand Journal of Geology and Geophysics. IX INQUA Congress Issue 16, 333-344.
Moar, N.T., Suggate, R.P., 1996. Vegetation history from the Kaihinu (last) interglacial to the present, West Coast, South Island, New Zealand. Quaternary Science Reviews 15, 521-547.
Moar, N.T., Suggate, R.P., Burrows, C., 2008. Environments during the Kaihinu Interglacial and Otira Glaciation, coastal north Westland, New Zealand. New Zealand Journal of Botany 46, 49-63.

Moar, N.T., Wilmshurst, J., McGlone, M.S., 2011. Standardizing names applied to pollen and spores in New Zealand Quaternary palynology. New Zealand Journal of Botany 49, 201-229.

Molloy, G., 1970. The case for production forestry in Westland. New Zealand Forest Service, 196-203.

Monnin, E., Indermühle, A., Dällenbach, A., Flückiger, J., Stauffer, B., Stocker, T.F., Raynaud, D., Barnola, J.-M., 2001. Atmospheric CO_2 concentrations over the last glacial termination. Science 291, 112-114.

Moore, J.K., Abbott, M.R., Richman, J.G., 1999. Location and dynamics of the Antarctic Polar Front from satellite sea surface temperature data. Journal of Geophysical Research: Oceans 104, 3059-3073.

Moore, M.I., Murdoch, R.C., 1993. Physical and biological observations of coastal squirts under nonupwelling conditions. Journal of Geophysical Research-Oceans 98, 20,043-020,061.

Moreno, P.I., Kaplan, M.R., François, J.P., Villa-Martínez, R., Moy, C.R., Stern, C.M., Kubik, P.W., 2009. Renewed glacial activity during the Antarctic cold reversal and persistence of cold conditions until 11.5 ka in southwestern Patagonia. Geology 37, 375-378.

Moreno, P.I., Denton, G.H., Moreno, H., Lowell, T.V., Putnam, A.E., Kaplan, M.R., 2015. Radiocarbon chronology of the last glacial maximum and its termination in northwestern Patagonia. Quaternary Science Reviews 122, 233-249.

Moss, P.T, Kershaw, A.P., 2000. The last glacial cycle from the humid tropics of northeastern Australia: comparison of a terrestrial and a marine record. Palaeogeography, Palaeoclimatology, Palaeoecology 155, 155-176.

Moss, P.T., Dunbar, G.B., Dickens, G., Jacobsen, G., 2007. Comparative ages of pollen and foraminifera in the ODP 820 marine core, 15th Australian Conference on Nuclear and Complementary Techniques of Analysis and 9th Vacuum Society of Australia Congress, 21st – 23rd November, Melbourne, Australia: University of Melbourne.

Moss, P.T., Kershaw, A.P., Grindrod, J., 2005. Pollen transport and deposition in riverine and marine environments within the humid tropics of northeastern Australia. Review of Palaeobotany and Palynology 134, 55-69.

Mudie, P.J., 1982. Pollen distribution in recent marine sediments, eastern Canada. Canadian Journal of Earth Sciences 19, 729-747.

Mudie, P.J., McCarthy, F.M.G., 1994. Late Quaternary pollen transport processes, western North Atlantic: data from box models, cross-margin and NS transects. Marine Geology 118, 79-105.

Mudie, P.J., McCarthy, F.M.G., 2006. Marine palynology: potentials for onshore—offshore correlation of Pleistocene—Holocene records. Transactions of the Royal Society of South Africa 61, 139-157.

Müller, U.C., Klotz, S., Geyh, M.A., Pross, J., Bond, G.C., 2005. Cyclic climate fluctuations during the last interglacial in central Europe. Geology 33, 449-452.

Murray-Wallace, C.V., Beu, A.G., Kendrick, G.W., Brown, L.J., Belperio, A.P., Sherwood, J.E., 2000. Palaeoclimatic implications of the occurrence of the arcoid bivalve *Anadara trapezia* (Deshayes) in the Quaternary of Australasia. Quaternary Science Reviews 19, 559-590.

Neil, H.L., 2008. Sediment conduits to the deep Tasman: two contrasting large canyons-channel complexes from the West Coast, South Island, New Zealand, Geological Society of New Zealand, New Zealand Geophysical Society and New Zealand Geochemical & Mineralogical Society Joint Annual Conference, Miscellaneous Publication 124A, Page 234.

Neil, H.L., Carter, L., Morris, M.Y., 2004. Thermal isolation of Campbell Plateau, New Zealand, by the Antarctic Circumpolar Current over the past 130kyr. Paleoceanography 19, doi:10.1029/2003PA000975.

Nelson, C.S., 1988. Revised age of a late Quaternary tephra at DSDP Site 594 off eastern South Island and some implications for correlation. Newsletter - Geological Society of New Zealand 82, 35-40.
Nelson, C.S., Cooke, P.J., Hendy, C.H., Cuthbertson, A.M., 1993. Oceanographic and climatic changes over the past 160,000 years at Deep Sea Drilling Project Site 594 off southeastern New Zealand, Southwest Pacific Ocean. Paleoceanography 8, 435-458.
Nelson, C.S., Hendy, C.H., Jarrett, G.R., Cuthbertson, A.M., 1985. Near-synchroneity of New Zealand alpine glaciations and Northern Hemisphere continental glaciations during the past 750 kyr. Nature 318, 361-363.
Nelson, F.E., Wilson, G.S., Neil, H.L., 2013. Marine magnetic signature of the Last Glacial Maximum and last deglaciation from the Southern Hemisphere mid-latitudes. Marine Geology 346, 246-255.
Newnham, R.M., 1990. Late Quaternary palynological investigations into the history of vegetation and climate in northern New Zealand. PhD thesis. University of Auckland.
Newnham, R.M., Alloway, B.V., 2001. The last interglacial/glacial cycle in Taranaki, western North Island, New Zealand; a palynostratigraphic model. Proceedings of the IX international palynological congress, In: Goodman, D.K., Clarke, R.T. (Eds.), Proceedings - International Palynological Conference, Houston, TX, United States, pp. 411-422.
Newnham, R.M., Alloway, B.V., 2004. A terrestrial record of last interglacial climate preserved by voluminous debris avalanche inundation in Taranaki, New Zealand. Journal of Quaternary Science 19, 299-314.
Newnham, R.M., McGlone, M.S., Moar, N.T., Wilmshurst, J., Vandergoes, M., 2013. The vegetation cover of New Zealand at the last glacial maximum. Quaternary Science Reviews 74, 202-214.
Newnham, R.M., Vandergoes, M.J., Hendy, C.H., Lowe, D.J., Preusser, F., 2007a. A terrestrial palynological record for the last two glacial cycles from southwestern New Zealand. Quaternary Science Reviews 26, 517-535.
Newnham, R.M., Vandergoes, M.J., Garnett, M.H., Lowe, D.J., Prior, C., Almond, P.C., 2007b. Test of AMS ^{14}C dating of pollen concentrates using tephrochronology. Journal of Quaternary Science 22, 37-51.
Newnham, R.M., Lowe, D.J., Giles, T.M., Alloway, B.V., 2007c. Vegetation and climate of Auckland, New Zealand since ca 32,000 cal yr ago: support for an extended LGM. Journal of Quaternary Science 22, 517-534.
Newnham, R.M., Vandergoes, M.J., Sikes, E., Carter, L., Wilmhurst, J.M., Lowe, D.J., McGlone, M.S., Sandiford, A., 2012. Does the bipolar seesaw extend to the terrestrial southern mid-latitudes? Quaternary Science Reviews 36, 214-222.
Newton, A.M., Huuse, M., Brocklehurst, S.H., 2016. Buried iceberg scours reveal reduced North Atlantic Current during the stage 12 deglacial. Nature Communications 7, doi:10.1038/ncomms10927
Nicol, A., VanDissen, R., Vella, P., Alloway, B., Melhuish, A., 2002. Growth of contractional structures during the last 10 my at the southern end of the emergent Hikurangi forearc basin, New Zealand. New Zealand Journal of Geology and Geophysics 45, 365-385.
NIWA, 2013. The environmental information browser: New Zealand, Hokitika River flow data (2003-2013). NIWA.
NIWA, 2014a. The national climate database; New Zealand, Ivory Coast Glacier (2009-2014). http://cliflo.niwa.co.nz/doc/terms.html.
NIWA, 2014b. The national climate database; New Zealand, Hokitika Aero site (1981-2014). http://cliflo.niwa.co.nz/doc/terms.html.
Norris, R.M., 1978. Late Cenozoic geology of the west coast shelf between Karamea and the Waiho River, South Island, New Zealand. New Zealand Oceanographic Institute.

North Greenland Ice Core Project members, 2004. High-resolution record of Northern Hemisphere climate extending into the last interglacial period. Nature 431, 147-151.
Norton, D.A., Herbert, J.W., Beveridge, A.E., 1988. The ecology of *Dacrydium cupressinum*: a review. New Zealand Journal of Botany 26, 37-62.
O'Leary, M.J., Hearty, P.J., Thompson, W.G., Raymo, M.E., Mitrovica, J.X., Webster, J.M., 2013. Ice sheet collapse following a prolonged period of stable sea level during the last interglacial. Nature Geoscience 6, 796-800.
Oksanen, J., Kindt, R., Legendre, P., O'Hara, B., Simpson, G.L., Solymos, P., Stevens, M.H.H., Wagner, H., 2014. The vegan Package. Community ecology package Version 2.0-9.
Okuda, M., Shulmeister, J., Flenley, J.R., 2002. Vegetation changes and their climatic implication for the late Pleistocene at Lake Poukawa, Hawkes Bay, New Zealand. Global and Planetary Change 33, 269-282.
Oliver, E.C., Holbrook, N.J., 2014. Extending our understanding of South Pacific gyre "spin-up": Modeling the East Australian Current in a future climate. Journal of Geophysical Research: Oceans 119, 2788-2805.
Oliver, E.C., O'Kane, T.J., Holbrook, N.J., 2015. Projected changes to Tasman Sea eddies in a future climate. Journal of Geophysical Research: Oceans 120, 7150-7165.
Oliver, E.C., Wotherspoon, S.J., Chamberlain, M.A., Holbrook, N.J., 2014. Projected Tasman Sea extremes in sea surface temperature through the twenty-first century. Journal of Climate 27, 1980-1998.
Oppo, D.W., McManus, J.F., Cullen, J.L., 1998. Abrupt climate events 500,000 to 340,000 years ago; evidence from subpolar North Atlantic sediments. Science 279, 1335-1338.
Oppo, D.W., McManus, J.F., Cullen, J.L., 2006. Evolution and demise of the Last Interglacial warmth in the subpolar North Atlantic. Quaternary Science Reviews 25, 3268-3277.
Otto-Bliesner, B.L., Rosenbloom, N., Stone, E.J., McKay, N.P., Lunt, D.J., Brady, E.C., Overpeck, J.T., 2013. How warm was the last interglacial? New model–data comparisons. Philosophical Transactions of the Royal Society of London A: Mathematical, Physical and Engineering Sciences 371, 20130097.
Pahnke, K., Sachs, J.P., 2006. Sea surface temperatures of southern midlatitudes 0–160 kyr BP. Paleoceanography 21.
Pahnke, K., Zahn, R., 2005. Southern Hemisphere water mass conversion linked with North Atlantic climate variability. Science 307, 1741-1746.
Pahnke, K., Zahn, R., Elderfield, H., Schultz, M., 2003. 340,000-Year Centennial Scale Marine record of Southern Hemisphere Climatic Oscillation. Science 301, 948-952.
Paillard, D., 1998. The timing of Pleistocene glaciations from a simple multiple-state climate model. Nature 391, 378-381.
Paillard, D., Labeyrie, L., Yiou, P., 1996. Macintosh program performs time-series analysis. Eos, Transactions American Geophysical Union 77, 379-379.
Palmer, A.S., Pillans, B.J., 1996. Record of climatic fluctuations from ca. 500 ka loess deposits and Paleosols near Wanganui, New Zealand. Tephra, loess, and Paleosols; an integration, In: Lowe, D.J (Ed.), International inter-INQUA field conference and workshop on Tephrochronology, loess, and paleopedology, Hamilton, New Zealand, pp. 155-162.
Parrenin, F., Masson-Delmotte, V., Köhler, P., Raynaud, D., Paillard, D., Schwander, J., Barbante, C., Landais, A., Wegner, A., Jouzel, J., 2013. Synchronous change of atmospheric CO_2 and Antarctic temperature during the last deglacial warming. Science 339, 1060-1063.
Past Interglacials Working Group of PAGES, 2016. Interglacials of the last 800,000 years. Reviews of Geophysics 54, 162–219.
Peakall, J., McCaffrey, B., Kneller, B., 2000. A process model for the evolution, morphology, and architecture of sinuous submarine channels. Journal of sedimentary Research 70, 434-448.

Peck, R.M., 1973. Pollen budget studies in a small Yorkshire catchment, In: Birks, H.J.B., West, R.G. (Eds.), Quaternary Plant Ecology. Blackwell, pp. 43-59.

Pedro, J.B., Bostock, H.C., Bitz, C.M., He, F., Vandergoes, M.J., Steig, E.J., Chase, B.M., Krause, C.E., Rasmussen, S.O., Markle, B.R., 2015. The spatial extent and dynamics of the Antarctic Cold Reversal. Nature Geoscience. doi: 10.1038/NGEO2580

Pedro, J.B., Rasmussen, S.O., van Ommen, T.D., 2012. Tightened constraints on the time-lag between Antarctic temperature and CO_2 during the last deglaciation. Climate of the Past 8, 1213-1221.

Pedro, J.B., Rasmussen, S.O., van Ommen, T.D., Morgan, V.I., Chappellaz, J., Moy, A.D., Masson-Delmotte, V., Delmotte, M., 2011. The last deglaciation: timing the bipolar seesaw. Climate of the Past 7, 671–683. doi:10.5194/cp-7-671-2011.

Pelejero, C., Calvo, E., Barrows, T.T., Logan, G.A., De Deckker, P., 2006. South Tasman Sea alkenone palaeothermometry over the last four glacial/interglacial cycles. Marine Geology 230, 73-86.

Pelejero, C., Calvo, E., Logan, G.A., De Deckker, P., 2003. Marine isotopic stage 5e in the Southwest Pacific: similarities with Antarctica and ENSO inferences. Geophysical Research Letters 30, 2185.

Petit, J.R., Jouzel, J., Raynaud, D., Barkov, N.I., Barnola, J., Basile, I., Bender, M., Chappellaz, J.M., Davis, M., Delaygue, G., Delmotte, M., Kotlyakov, V.M., Legrand, M., Lipenkov, V. Y., Lorius, C., Pepin, L., Ritz, C., Saltzmann, E., Stievenard, M., 1999. Climate and atmospheric history of the past 420,000 years from the Vostok ice core, Antarctica. Nature 399, 429-436.

Pickarski, N., Kwiecien, O., Langgut, D., Litt, T., 2015. Abrupt climate and vegetation variability of eastern Anatolia during the last glacial. Climate of the Past 11, 1491-1505.

Pillans, B., Kohn, B.P., Berger, G.W., Froggatt, P.C., Duller, G., Alloway, B.V., Hesse, P., 1996. Multi-method dating comparison for mid-Pleistocene Rangitawa Tephra, New Zealand. Quaternary Science Reviews 15, 641-653.

Pillans, B., McGlone, M.S., Palmer, A., Mildenhall, D.C., Alloway, B.V., Berger, G., 1993. The Last Glacial Maximum in central and southern North Island, New Zealand; a paleoenvironmental reconstruction using the Kawakawa Tephra formation as a chronostratigraphic marker. Palaegeography, Palaeoclimatology, Palaeoecology 101, 283-304.

Pocknall, D., 1978. Relative pollen representation in relation to vegetation composition, Westland, New Zealand. New Zealand Journal of Botany 16, 379-386.

Pocknall, D., 1981a. Pollen morphology of *Phyllocladus* LC et A. Rich. New Zealand Journal of Botany 19, 259-266.

Pocknall, D., 1981b. Pollen morphology of the New Zealand species of *Dacrydium* Solander, *Podocarpus* L'Heritier, and *Dacrycarpus* Endlicher (*Podocarpaceae)*. New Zealand Journal of Botany 19, 67-95.

Pol, K., Debret, M., Masson-Delmotte, V., Capron, E., Cattani, O., Dreyfus, G., Falourd, S., Johnsen, S., Jouzel, J., Landais, A., 2011. Links between MIS 11 millennial to sub-millennial climate variability and long term trends as revealed by new high resolution EPICA Dome C deuterium data–A comparison with the Holocene. Climate of the Past 7, 437-450.

Pol, K., Masson-Delmotte, V., Cattani, O., Debret, M., Falourd, S., Jouzel, J., Landais, A., Minster, B., Mudelsee, M., Schulz, M., 2014. Climate variability features of the last interglacial in the East Antarctic EPICA Dome C ice core. Geophysical Research Letters 41, 4004-4012.

Prebble, J.G., 2012. Ocean and terrestrial response to a Pleistocene warm interglacial (MIS 11) as revealed by pollen and dinoflagellates from marine sediment cores, South Island, New Zealand. PhD thesis. School of Geography, Environment and Earth Sciences. Victoria University of Wellington.

Prebble, J.G., Crouch, E.M., Carter, L., Cortese, G., Bostock, H., Neil, H., 2013. An expanded modern dinoflagellate cyst dataset for the Southwest Pacific and Southern Hemisphere with environmental associations. Marine Micropaleontology 101, 33-48.

Prebble, J.G., Crouch, E.M., Cortese, G., Carter, L., Neil, H., Bostock, H., 2016. Southwest Pacific sea surface conditions during Marine Isotope Stage 11–results from dinoflagellate cysts. Palaeogeography, Palaeoclimatology, Palaeoecology 446, 19-31.

Presley, B.J., 1975. A simple method for determining calcium carbonate in sediment samples. Journal of Sedimentary Research 45, 745-746.

Preusser, F., Andersen, B.G., Denton, G.H., Schlüchter, C., 2005. Luminescence chronology of Late Pleistocene glacial deposits in north Westland, New Zealand. Quaternary Science Reviews 24, 2207-2227.

Proust, J.N, Lamarche, G., Migeon, S., Neil, H.L., Shipboard-party, 2006. Tectonic and climatic controls on sediment budget. MD152/MATACORE on *R.V. Marion-Dufresne*, pp. 1-107.

Proust, J.N., Lamarche, G., Migeon, S., Neil, H.L, 2008. Climate and tectonic changes in the ocean around New Zealand. Eos, Transactions American Geophysical Union 89, 277-278.

Putnam, A.E., Schaefer, J.M., Barrell, D.J.A, Vandergoes, M.J., Denton, G.H., Kaplan, M.R., Finkel, R.C., Schwartz, R., Goehring, B.M., Kelley, S.E, 2010a. In situ cosmogenic ^{10}Be production-rate calibration from the Southern Alps, New Zealand. Quaternary Geochronology 5, 392-409.

Putnam, A.E., Denton, G.H., Schaefer, J.M., Barrell, D.J.A., Andersen, B.G., Finkel, R.C., Schwartz, R., Doughty, A.M., Kaplan, M.R., Schlüchter, C., 2010b. Glacier advance in southern middle-latitudes during the Antarctic Cold Reversal. Nature Geoscience 3, 700-704.

Putnam, A.E., Schaefer, J.M., Denton, G.H., Barrell, D.J., Andersen, B.G., Koffman, T.N., Rowan, A.V., Finkel, R.C., Rood, D.H., Schwartz, R., 2013a. Warming and glacier recession in the Rakaia valley, Southern Alps of New Zealand, during Heinrich Stadial 1. Earth and Planetary Science Letters 382, 98-110.

Putnam, A.E., Schaefer, J.M., Denton, G.H., Barrell, D.J., Birkel, S.D., Andersen, B.G., Kaplan, M.R., Finkel, R.C., Schwartz, R., Doughty, A.M., 2013b. The Last Glacial Maximum at 44° S documented by 10Be moraine chronology at Lake Ohau, Southern Alps of New Zealand. Quaternary Science Reviews 62, 114-141.

Putnam, A.E., Schaefer, J.M., Denton, G.H., Barrell, D.J., Finkel, R.C., Andersen, B.G., Schwartz, R., Chinn, T.J., Doughty, A.M., 2012. Regional climate control of glaciers in New Zealand and Europe during the pre-industrial Holocene. Nature Geoscience 5, 627-630.

R-Core Team, 2014. A Language and Environment for Statistical Computing. R foundation for statistical computing, Vienna, Austria.

Radford, J., 2012. Shelf-to-canyon sedimentation on the South Westland Continental Margin, Westland, New Zealand. M.S.c thesis. University of Canterbury.

Railsback, L.B., Gibbard, P.L., Head, M.J., Voarintsoa, N.R.G., Toucanne, S., 2015. An optimized scheme of lettered marine isotope substages for the last 1.0 million years, and the climatostratigraphic nature of isotope stages and substages. Quaternary Science Reviews 111, 94-106.

Rasmussen, S.O., Abbott, P.M., Blunier, T., Bourne, A.J., Brook, E., Buchardt, S.L., Buizert, C., Chappellaz, J., Clausen, H.B., Cook, E., Dahl-Jensen, D., Davies, S. M., Guillevic, M., Kipfstuhl, S., Laepple, T., Seierstad, K., Severinghaus, J.P., Steffensen, J.P., Stowasser, C., Svensson, A., Vallelonga, P., Vinther, B.M., Wilhelms, F., Winstrup, M., 2013. A first chronology for the North Greenland Eemian Ice Drilling (NEEM) ice core. Climate of the Past 9, 2713-2730. doi:10.5194/cp-9-2713-2013.

Rasmussen, S.O., Andersen, K.K., Svensson, A.M., Steffensen, J.P., Vinther, B.M., Clausen, H.B., Siggaard-Andersen, M.L., Johnsen, S.J., Larsen, L.B., Dahl-Jensen, D., D., Bigler, M., Röthlisberger, R., Fischer, H., Goto-Azuma, K., Hansson, M.E., Ruth, 2006. A new Greenland ice core chronology for the last glacial termination. Journal of Geophysical Research: Atmospheres 111, D06102.

Raymo, M.E., 1997. The timing of major climate terminations. Paleoceanography 12, 577-585.

Raymo, M.E., Huybers, P., 2008. Unlocking the mysteries of the ice ages. Nature 451, 284-285.

Raymo, M.E., Lisiecki, L.E., Nisancioglu, K.H., 2006. Plio-Pleistocene Ice Volume, Antarctic Climate, and the Global $\delta^{18}O$ Record. Science 313, 492-495.

Raymo, M.E., Mitrovica, J.X., 2012. Collapse of polar ice sheets during the stage 11 interglacial. Nature 483, 453-456.

Rees, A.B., Cwynar, L.C., 2010. Evidence for early postglacial warming in Mount field National Park, Tasmania. Quaternary Science Reviews 29, 443-454.

Reif, A., Allen, R.B., 1988. Plant communities of the steepland conifer-broadleaved hardwood forests of central Westland, South Island, New Zealand. Phytocoenologia 16, 145-224.

Reimer, P.J., Bard, E., Bayliss, A., Beck, J.W., Blackwell, P.G., Ramsey, C.B., Buck, C.E., Cheng, H., Edwards, R.L., Friedrich, M., 2013. IntCal13 and Marine13 radiocarbon age calibration curves 0–50,000 years cal BP. Radiocarbon 55, 1869-1887.

Renwick, J., Hurst, R., Kidson, J., 1998. Climatic influences on the survival of southern gemfish (*Rexea solandri*, Gempylidae) in New Zealand waters. International Journal of Climatology 18, 1655-1667.

Reyes, A.V., Carlson, A.E., Beard, B.L., Hatfield, R.G., Stoner, J.S., Winsor, K., Welke, B., Ullman, D.J., 2014. South Greenland ice-sheet collapse during Marine Isotope Stage 11. Nature 510, 525-528.

Ridgway, K.R., Hill, K.L., 2012. East Australian Current. A Marine Climate Change Impacts and Adaptation Report for Australia, 1-16.

Rodrigues, T., Voelker, A.H.L, Grimalt, J.O., Abrantes, F., Naughton, F., 2011. Iberian Margin sea surface temperature during MIS 15 to 9 (580–300 ka): Glacial suborbital variability versus interglacial stability. Paleoceanography 26(1). doi:10.1029/2010PA001927

Rohling, E.J., Braun, K., Grant, K., Kucera, M., Roberts, A.P., Siddall, M.E., Trommer, G., 2010. Comparison between Holocene and Marine Isotope Stage-11 sea-level histories. Earth and Planetary Science Letters 291, 97-105.

Rohling, E.J., Foster, G.L., Grant, K.M., Marino, G., Roberts, A.P., Tamisiea, M.E., Williams, F., 2014. Sea-level and deep-sea-temperature variability over the past 5.3 million years. Nature 508, 477-482.

Rohling, E.J., Grant, K., Bolshaw, M., Roberts, A.P., Siddall, M., Hemleben, C., Kucera, M., 2009. Antarctic temperature and global sea level closely coupled over the past five glacial cycles. Nature Geoscience 2, 500-504.

Rojas, M., Moreno, P.I., Kageyama, M., Crucifix, M., Hewitt, C., Abe-Ouchi, A., Ohgaito, R., Brady, E.C., Hope, P., 2009. The Southern Westerlies during the last glacial maximum in PMIP2 simulations. Climate Dynamics 32, 525-548.

Ronge, T.A., Steph, S., Tiedemann, R., Prange, M., Merkel, U., Nürnberg, D., Kuhn, G., 2015. Pushing the boundaries: Glacial/interglacial variability of intermediate and deep waters in the southwest Pacific over the last 350,000 years. Paleoceanography 30, 23-38.

Rother, H., Fink, D., Shulmeister, J., Mifsud, C., Evans, M., Pugh, J., 2014. The early rise and late demise of New Zealand's last glacial maximum. Proceedings of the National Academy of Sciences 111, 11630-11635.

Ryan, M.T., 2010. A palynological record of the vegetation and climate of Westland since 210 ka. M.S.c thesis. School of Geography, Environment and Earth Sciences. Victoria University of Wellington, 188 pp.

Ryan, M.T., Dunbar, G.B., Vandergoes, M.J., Neil, H.L., Hannah, M.J., Newnham, R.M., Bostock, H., Alloway, B.V., 2012. Vegetation and climate in Southern Hemisphere mid-latitudes since 210 ka: new insights from marine and terrestrial pollen records from New Zealand. Quaternary Science Reviews 48, 80-98.

Ryan, M.T., Newnham, R.M., Dunbar, G.B., Vandergoes, M.J., Rees, A.B., Neil, H., Callard, S.L., Alloway, B.V., Bostock, H., Hua, Q., 2016. Exploring the source-to-sink residence time of terrestrial pollen deposited offshore Westland, New Zealand. Review of Palaeobotany and Palynology 230, 37-46.

Sakai, A., Wardle, P., 1978. Freezing resistance of New Zealand trees and shrubs. New Zealand Journal of Ecology 1, 51-61.

Sánchez Goñi, M.F., Bakker, P., Desprat, S., Carlson, A.E., Van Meerbeeck, C.J., Peyron, O., Naughton, F., Fletcher, W.J., Eynaud, F., Rossignol, L., 2012. European climate optimum and enhanced Greenland melt during the Last Interglacial. Geology 40, 627-630.

Sánchez Goñi, M.F., Bard, E., Landais, A., Rossignol, L., d'Errico, F., 2013. Air-sea temperature decoupling in western Europe during the last interglacial-glacial transition. Nature Geoscience 6, 837-841.

Sánchez Goñi, M.F., Eynaud, F., Turon, J.L., Shackleton, N.J., 1999. High resolution palynological record off the Iberian margin: direct land-sea correlation for the Last Interglacial complex. Earth and Planetary Science Letters 171, 123-137.

Sánchez Goñi, M.F., Llave, E., Oliveira, D.A., Naughton, F., Desprat, S., Ducassou, E., Hodell, D., Herñandez-Molina, F.G., 2016. Climate changes in south western Iberia and Mediterranean Outflow variations during two contrasting cycles of the last 1 Myrs: MIS 31-MIS 30 and MIS 12-MIS 11. Global and Planetary Change 136, 18-29.

Sandiford, A., Newnham, R.M., Alloway, B.V., Ogden, J., 2003. A 28 000-7600 cal yr BP pollen record of vegetation and climate change from Pukaki Crater, northern New Zealand. Palaeogeography, Palaeoclimatology, Palaeoecology 201, 235-247.

Schaefer, G., Rodger, J.S., Hayward, B.W., Kennett, J.P., Sabaa, A.T., Scott, G.H, 2005. Planktic foraminiferal and sea surface temperature record during the last 1 Myr across the Subtropical Front, Southwest Pacific. Marine Micropaleontology 54, 191-212.

Schaefer, J.M., Putnam, A.E., Denton, G.H., Kaplan, M.R., Birkel, S., Doughty, A.M., Kelley, S., Barrell, D.J., Finkel, R.C., Winckler, G., 2015. The Southern Glacial Maximum 65,000 years ago and its unfinished termination. Quaternary Science Reviews 114, 52-60.

Schlitzer, R., 2012. Ocean data view. odv. awi. de.

Schneider Mor, A., Yam, R., Bianchi, C., Kunz-Pirrung, M., Gersonde, R., Shemesh, A., 2012. Variable sequence of events during the past seven terminations in two deep-sea cores from the Southern Ocean. Quaternary Research 77, 317-325.

Schneider, R., Schmitt, J., Köhler, P., Joos, F., Fischer, H., 2013. A reconstruction of atmospheric carbon dioxide and its stable carbon isotopic composition from the penultimate glacial maximum to the last glacial inception. Climate of the Past 9, 2507-2523.

Schulz, K.G., Zeebe, R.E., 2006. Pleistocene glacial terminations triggered by synchronous changes in Southern and Northern Hemisphere insolation: The insolation canon hypothesis. Earth and Planetary Science Letters 249, 326-336.

Scussolini, P., Marino, G., Brummer, G.-J.A., Peeters, F.J., 2015. Saline Indian Ocean waters invaded the South Atlantic thermocline during glacial termination II. Geology 43, 139-142.

Shackleton, N.J., 1987. Oxygen isotopes, ice volume and sea level. Quaternary Science Reviews 6, 183-190.

Shackleton, N.J., 2000. The 100,000-year ice-age cycle identified and found to lag temperature, carbon dioxide, and orbital eccentricity. Science 289, 1897-1902.
Shackleton, N.J., Berger, A., Peltier, W.A., 1990. An alternative astronomical calibration of the lower Pleistocene timescale based on ODP Site 677. Transactions of the Royal Society of Edinburgh: Earth Sciences 81, 251-261.
Shackleton, N.J., Sánchez-Goñi, M.F., Pailler, D., Lancelot, Y., 2003. Marine isotope substage 5e and the Eemian interglacial. Global and Planetary Change 36, 151-155.
Shakun, J.D., Clark, P.U., He, F., Marcott, S.A., Mix, A.C., Liu, Z., Otto-Bliesner, B., Schmittner, A., Bard, E., 2012. Global warming preceded by increasing carbon dioxide concentrations during the last deglaciation. Nature 484, 49-54.
Shane, P.A.R., 2000. Tephrochronology: a New Zealand case study. Earth Science Reviews 49, 223-259.
Shane, P.A.R., Black, T.M., Alloway, B.V., Westgate, J.A., 1996. Early to middle Pleistocene tephrochronology of North Island, New Zealand; implications for volcanism, tectonism, and paleoenvironments. Geological Society of America Bulletin 108, 915-925.
Shulmeister, J., Soons, J.M., Berger, G.W., Harper, M., Holt, S., Moar, N.T., Carter, J.A., 1999. Environmental and sea-level changes on Banks Peninsula (Canterbury, New Zealand) through three glaciation–interglaciation cycles. Palaeogeography, Palaeoclimatology, Palaeoecology 152, 101-127.
Siddall, M., Kaplan, M.R., Schaefer, J.M., Putnam, A., Kelly, M.A., Goehring, B., 2010. Changing influence of Antarctic and Greenlandic temperature records on sea-level over the last glacial cycle. Quaternary Science Reviews 29, 410-423.
Siegenthaler, U., Monnin, E., Kawamura, K., Spahni, R., Schwander, J., Stauffer, B., Stocker, T.F., Barnola, J.M., Fischer, H., 2005. Supporting evidence from the EPICA Dronning Maud Land ice core for atmospheric CO_2 changes during the past millennium. Tellus B 57, 51-57.
Sikes, E.L., Cook, M.S., Guilderson, T.P., 2016. Reduced deep ocean ventilation in the Southern Pacific Ocean during the last glaciation persisted into the deglaciation. Earth and Planetary Science Letters 438, 130-138.
Sikes, E.L., Medeiros, P.M., Augustinus, P., Wilmshurst, J.M., Freeman, K.R., 2013. Seasonal variations in aridity and temperature characterize changing climate during the last deglaciation in New Zealand. Quaternary Science Reviews 74, 245-256.
Sikes, E.L., Samson, C.R., Guilderson, T.P., Howard, W.R., 2000. Old radiocarbon ages in the southwest Pacific Ocean during the last glacial period and deglaciation. Nature 405, 555-559.
Sime, L.C., Wolff, E.W., Oliver, K.I.C., Tindall, J.C., 2009. Evidence for warmer interglacials in East Antarctic ice cores. Nature 462, 342-345.
Singer, C., Shulmeister, J., McLea, B., 1998. Evidence against a significant Younger Dryas cooling event in New Zealand. Science 281, 812-814.
Skinner, L.C., Fallon, S., Waelbroeck, C., Michel, E., Barker, S., 2010. Ventilation of the deep Southern Ocean and deglacial CO_2 rise. Science 328, 1147-1151.
Skinner, L.C., Shackleton, N.J., 2005. An Atlantic lead over Pacific deep-water change across Termination I: implications for the application of the marine isotope stage stratigraphy. Quaternary Science Reviews 24, 571-580.
Smirnov, A., Chmura, G.L., Lapointe, M.F., 1996. Spatial distribution of suspended pollen in the Mississippi River as an example of pollen transport in alluvial channels. Review of Palaeobotany and Palynology 92, 69-81.
Smith, R.O., Vennell, R., Bostock, H.C., Williams, M.J., 2013. Interaction of the subtropical front with topography around southern New Zealand. Deep Sea Research Part I: Oceanographic Research Papers 76, 13-26.
Stanton, B.R., 1976. Circulation and hydrology off the west coast of the South Island, New Zealand. . New Zealand Journal of Marine and Freshwater Research 10, 445-467.

Steig, E.J., Huybers, K., Singh, H.A., Steiger, N.J., Frierson, D.M., Popp, T., White, J.W., 2015. Combined ice core and climate-model evidence for the collapse of the West Antarctic Ice Sheet during Marine Isotope Stage 5e, EGU General Assembly Conference Abstracts, p. 2609.

Stein, R., Hefter, J., Grützner, J., Voelker, A., Naafs, B.D.A., 2009. Variability of surface water characteristics and Heinrich-like events in the Pleistocene midlatitude North Atlantic Ocean: Biomarker and XRD records from IODP Site U1313 (MIS 16–9). Paleoceanography 24.

Stenni, B., Masson-Delmotte, V., Selmo, E., Oerter, H., Meyer, H., Röthlisberger, R., Jouzel, J., Cattani, O., Falourd, S., Fischer, H., Hoffmann, G., Iacumin, P., Johnsen, S.J., Minster, B., Udisti, R., 2010. The deuterium excess records of EPICA Dome C and Dronning Maud Land ice cores (East Antarctica). Quaternary Science Reviews 29, 146-159.

Stocker, T.F., 2000. Past and future reorganizations in the climate system. Quaternary Science Reviews 19, 301-319.

Stocker, T.F, Qin, D., Plattner, G., Tignor, M., Allen, S., Boschung, J., Nauels, A., Xia, Y., Bex, B., Midgley, B., 2013. IPCC, 2013: climate change 2013: the physical science basis. Contribution of working group I to the fifth assessment report of the intergovernmental panel on climate change; Cambridge University Press, Cambridge, United Kingdom and New York, USA, 2013.

Stuart, S.J., 2009. Influence of synoptic climate upon near-surface temperature lapse rates in the region of Franz Joseph Glacier and Aoraki Mount Cook. GradDipSc. School of Geography, Environment and Earth Sciences. University of Wellington.

Sturman, A.P., Tapper, N.J., 2006. The weather and climate of Australia and New Zealand. Oxford University Press, Melbourne, 476 pp.

Suggate, R.P., 1961. The upper boundary of the Hawera series. Transactions of the Royal Society of New Zealand, Geology 1, 11-16.

Suggate, R.P., 1990. Late Pliocene and Quaternary glaciations of New Zealand. Quaternary Science Reviews 9, 175-197.

Suggate, R.P., Almond, P.C., 2005. The Last Glacial Maximum (LGM) in western South Island, New Zealand: implications for the global LGM and MIS 2. Quaternary Science Reviews 24, 1923-1940.

Suggate, R.P., Waight, T.E., 1999. Geology of the Kumara-Moana area, sheets J32 and part K32, scale 1: 50,000.

Sutherland, R., Kim, K., Zondervan, A., McSaveney, M., 2007. Orbital forcing of mid-latitude Southern Hemisphere glaciation since 100 ka inferred from cosmogenic nuclide ages of moraine boulders from the Cascade Plateau, southwest New Zealand. Geological Society of America Bulletin 119, 443-451.

Sutton, P.J.H., Roemmich, D., 2001. Ocean temperature climate off North-east New Zealand. New Zealand Journal of Marine and Freshwater Research 35, 553-565.

Thompson, W.G., Goldstein, S.L., 2006. A radiometric calibration of the SPECMAP timescale. Quaternary Science Reviews 25, 3207-3215.

Timmermann, R., Danilov, S., Schröter, J., Böning, C., Sidorenko, D., Rollenhagen, K., 2009. Ocean circulation and sea ice distribution in a finite element global sea ice–ocean model. Ocean Modelling 27, 114-129.

Toggweiler, J.R., 2009. Shifting westerlies. Science 323, 1434-1435.

Toucanne, S., Zaragosi, S., Bourillet, J.-F., Cremer, M., Eynaud, F., Van Vliet-Lanoë, B., Penaud, A., Fontanier, C., Turon, J.L., Cortijo, E., 2009. Timing of massive 'Fleuve Manche'discharges over the last 350 kyr: insights into the European ice-sheet oscillations and the European drainage network from MIS 10 to 2. Quaternary Science Reviews 28, 1238-1256.

Traverse, A., 2007. Paleopalynology, 2 ed. Kluwer Academic Pub, Springer. 600 pp.

Trewick, S., Wallis, G., 2001. Bridging the " beech-gap": New Zealand invertebrate phylogeography implicates Pleistocene glaciation and Pliocene isolation. Evolution, 2170-2180.

Turney, C.S.M., Jones, R.T., 2010. Does the Agulhas Current amplify global temperatures during super-interglacials? Journal of Quaternary Science 25, 839-843.

Turney, C.S.M., Kershaw, A.P., Lowe, D.J., van der Kaars, S., Johnston, R., Rule, S., Moss, P., Radke, L., Tibby, J., McGlone, M.S., Wilmshurst, J.M., Vandergoes, M.J., Fitzsimons, S.J., Bryant, C., James, S., Branch, N.P., Cowley, J., Kalin, R.M., Ogle, N., Jacobsen, G., Fifield, L.K., 2006. Climatic variability in the southwest Pacific during the Last Termination (20-10 kyr BP). Quaternary Science Reviews 25, 886-903.

Turney, C.S.M., McGlone, M.S., Wilmshurst, J.M., 2003. Asynchronous climate change between New Zealand and the North Atlantic during the last deglaciation. Geology (Boulder) 31, 223-226.

Turney, C.S.M., Roberts, R., De Jonge, N., Prior, C., Wilmshurst, J., McGlone, M., Cooper, J., 2007. Redating the advance of the New Zealand Franz Josef Glacier during the Last Termination: evidence for asynchronous climate change. Quaternary Science Reviews 26, 3037-3042.

Tzedakis, P.C., 2005. Towards an understanding of the response of southern European vegetation to orbital and suborbital climate variability. Quaternary Science Reviews 24, 1585-1599.

Tzedakis, P.C., 2010. The MIS 11–MIS 1 analogy, southern European vegetation, atmospheric methane and the" early anthropogenic hypothesis". Climate of the Past 6, 131-144.

Tzedakis, P.C., Hooghiemstra, H., Pälike, H., 2006. The last 1.35 million years at Tenaghi Philippon: revised chronostratigraphy and long-term vegetation trends. Quaternary Science Reviews 25, 3416-3430.

Tzedakis, P.C., McManus, J.F., Hooghiemstra, H., Oppo, D.W., Wijmstra, T.A., 2003. Comparison of changes in vegetation in northeast Greece with records of climate variability on orbital and suborbital frequencies over the last 450 000 years. Earth and Planetary Science Letters 212, 197-212.

Tzedakis, P.C., Pälike, H., Roucoux, K.H, de Abreu, L., 2009a. Atmospheric methane, southern European vegetation and low-mid latitude links on orbital and millennial timescales. Earth and Planetary Science Letters 277, 307-317.

Tzedakis, P.C., Raynaud, D., McManus, J.F., Berger, A., Brovkin, V., Kiefer, T., 2009b. Interglacial diversity. Nature Geosci 2, 751-755.

Tzedakis, P.C., Roucoux, K., De Abreu, L., Shackleton, N., 2004. The duration of forest stages in southern Europe and interglacial climate variability. Science 306, 2231-2235.

Tziperman, E., Raymo, M., Huybers, P., Wunsch, C., 2006. Consequences of pacing the Pleistocene 100 kyr ice ages by nonlinear phase locking to Milankovitch forcing. Paleoceanography 21, PA4206, doi:10.1029/2005PA001241.

Urrego, D.H, Sánchez Goñi, M.S., Daniau, A.L., Lechevrel, S., Hanquiez, V., 2015. South-western Africa vegetation responses to atmospheric and oceanic changes during the last climatic cycle. Climate of the Past Discussions 11, 345-376.

van der Kaars, S., 2001. Pollen distribution in marine sediments from the south-eastern Indonesian waters. Palaeogeography, Palaeoclimatology, Palaeoecology 171, 341-361.

Van Der Kaars, S., De Deckker, P., 2003. Pollen distribution in marine surface sediments offshore Western Australia. Review of Palaeobotany and Palynology 124, 113-129.

Van Eaton, A.R., Harper, M.A., Wilson, C.J.N, 2013. High-flying diatoms: Widespread dispersal of microorganisms in an explosive volcanic eruption. Geology 41, 1187-1190.

Vandergoes, M.J., 2000. A High Resolution Record of Late Quaternary Vegetation and Climate Change, South Westland, New Zealand. PhD thesis. Department of Geography. Otago University. 189 pp.

Vandergoes, M.J., Dieffenbacher-Krall, A.C., Newnham, R.M., Denton, G.H., Blaauw, M., 2008. Cooling and changing seasonality in the southern Alps, New Zealand during the Antarctic cold reversal. Quaternary Science Reviews 27, 589-601.

Vandergoes, M.J., Fitzsimons, S.J., 2003. The last glacial–interglacial transition (LGIT) in south Westland, New Zealand: Paleoecological insight into mid-latitude Southern Hemisphere climate change. Quaternary Science Reviews 22, 1461-1476.

Vandergoes, M.J., Newnham, R.M., Denton, G.H., Blaauw, M., Barrell, D.J., 2013a. The anatomy of Last Glacial Maximum climate variations in south Westland, New Zealand, derived from pollen records. Quaternary Science Reviews 74, 215-229.

Vandergoes, M.J., Hogg, A.G., Lowe, D.J., Newnham, R.M., Denton, G.H., Southon, J., Barrell, D.J., Wilson, C.J.N, McGlone, M.S., Allan, A.S., 2013b. A revised age for the Kawakawa/Oruanui tephra, a key marker for the Last Glacial Maximum in New Zealand. Quaternary Science Reviews 74, 195-201.

Vandergoes, M.J., Newnham, R.M., Preusser, F., Hendy, C.H., Lowell, T.V., Fitzsimons, S.J., Hogg, A.G., Kasper, H.U., Schlüchter, C., 2005. Regional insolation forcing of late Quaternary climate change in the Southern Hemisphere. Nature 436, 242-245.

Vandergoes, M.J., Prior, C.A., 2003. AMS dating of pollen concentrates; a methodological study of late Quaternary sediments from south Westland, New Zealand. Radiocarbon 45, 479-491.

Vázquez Riveiros, N., Waelbroeck, C., Skinner, L., Duplessy, J.-C., McManus, J.F., Kandiano, E.S., Bauch, H.A., 2013. The "MIS 11 paradox" and ocean circulation: Role of millennial scale events. Earth and Planetary Science Letters 371, 258-268.

Vázquez Riveiros, N., Waelbroeck, C., Skinner, L., Roche, D.M., Duplessy, J.-C., Michel, E., 2010. Response of South Atlantic deep waters to deglacial warming during Terminations V and I. Earth and Planetary Science Letters 298, 323-333.

Veres, D., Bazin, L., Landais, A., Toyé Mahamadou Kele, H., Lemieux-Dudon, B., Parrenin, F., Martinerie, P., Blayo, E., Blunier, T., Capron, E., Chappellaz, J., Rasmussen, S.O., Severi, M., Svensson, A., Vinther, B., Wolff, E.W., 2013. The Antarctic ice core chronology (AICC2012): an optimized multi-parameter and multi-site dating approach for the last 120 thousand years. Climate of the Past 9, 1733-1748. doi:10.5194/cp-9-1733-2013.

Villamor, P., Van Dissen, R., Alloway, B.V., Palmer, A.S., Litchfield, N., 2007. The Rangipo fault, Taupo rift, New Zealand: An example of temporal slip-rate and single-event displacement variability in a volcanic environment. Geological Society of America Bulletin 119, 529.

Voelker, A.H., Rodrigues, T., Billups, K., Oppo, D.W., McManus, J.F., Stein, R., Hefter, J., Grimalt, J.O., 2010. Variations in mid-latitude North Atlantic surface water properties during the mid-Brunhes (MIS 9–14) and their implications for the thermohaline circulation.

WAIS Divide Project Members, 2013. Onset of deglacial warming in West Antarctica driven by local orbital forcing. Nature 500, 440-444.

WAIS Divide Project Members, 2015. Precise interpolar phasing of abrupt climate change during the last ice age. Nature 520, 661-665.

Wang, X., Auler, A.S., Edwards, R.L., Cheng, H., Cristalli, P.S., Smart, P.L., Richards, D.A., Shen, C.-C., 2004. Wet periods in northeastern Brazil over the past 210 kyr linked to distant climate anomalies. Nature 432, 740-743.

Wang, Y.J., Cheng, H., Edwards, R.L., An, Z.S., Wu, J.Y., Shen, C.C., Dorale, J.A., 2001. A high-resolution absolute-dated late Pleistocene monsoon record from Hulu Cave, China. Science 294, 2345-2348.

Wang, Y.J., Cheng, H., Edwards, R.L., Kong, X., Shao, X., Chen, S., Wu, J., Jiang, X., Wang, X., An, Z., 2008. Millennial-and orbital-scale changes in the East Asian monsoon over the past 224,000 years. Nature 451, 1090-1093.

Wanner, H., Solomina, O., Grosjean, M., Ritz, S.P., Jetel, M., 2011. Structure and origin of Holocene cold events. Quaternary Science Reviews 30, 3109-3123.
Wardle, J., 1984. The New Zealand beeches: ecology, utilisation, and management. New Zealand Forest Service. Christchurch: Caxton Press, 447 pp.
Wardle, P., 1963. Evolution and distribution of the New Zealand flora, as affected by Quaternary climates. New Zealand Journal Botany 1, 3-17.
Wardle, P., 1979. Plants and landscape in Westland National Park. National Parks scientific series 3. National Parks Authority, Wellington.
Wardle, P., 1988. Effects of glacial climates on floristic distribution in New Zealand. 1. A review of the evidence. New Zealand Journal of Botany 26, 541-555.
Wardle, P., 1991. Vegetation of New Zealand. Cambridge University Press, Cambridge, England.
West, R.G., 1971. Studying the past by pollen analysis. Oxford University Press.
Whitehead, D., Hall, G.M., Walcroft, A.S., Brown, K.J., Landsberg, J.J., Tissue, D.T., Turnbull, M.H., Griffin, K.L., Schuster, W.S., Carswell, F.E., 2002. Analysis of the growth of rimu (*Dacrydium cupressinum*) in South Westland, New Zealand, using process-based simulation models. International journal of biometeorology 46, 66-75.
Whittaker, T.E., Hendy, C.H., Hellstrom, J.C., 2011. Abrupt millennial-scale changes in intensity of Southern Hemisphere westerly winds during marine isotope stages 2-4. Geology 39, 455.
Willett, R.W., 1950. The New Zealand Pleistocene snow line, climatic conditions, and suggested biological effects. New Zealand journal of science and technology 32, 18-48.
Williams, P.W., McGlone, M., Neil, H., Zhao, J.-X., 2015. A review of New Zealand palaeoclimate from the Last Interglacial to the global Last Glacial Maximum. Quaternary Science Reviews 110, 92-106.
Wilmshurst, J.M., Eden, D.N., Froggatt, P.C., 1999. Late Holocene forest disturbance in Gisborne, New Zealand: a comparison of terrestrial and marine pollen records. New Zealand Journal of Botany 37(3), 523-540.
Wilmshurst, J.M., McGlone, M.S., 2005. Origin of pollen and spores in surface lake sediments: comparison of modern palynomorph assemblages in moss cushions, surface soils and surface lake sediments. Review of Palaeobotany and Palynology 136, 1-15.
Wilmshurst, J.M., McGlone, M.S., Leathwick, J.R., Newnham, R.M., 2007. A pre-deforestation pollen-climate calibration model for New Zealand and quantitative temperature reconstructions for the past 18 000 years BP. Journal of Quaternary Science 22, 535-547.
Wilson, C.J.N., 2001. The 26.5 ka Oruanui eruption, New Zealand: an introduction and overview. Journal of Volcanology and Geothermal Research 112, 133-174.
Wilson, C.J.N., Gravley, D.M., Leonard, G.S., Rowland, J.V., 2009. Volcanism in the central Taupo Volcanic Zone, New Zealand: tempo, styles and controls. Studies in Volcanology: The Legacy of George Walker. Special Publications of IAVCEI 2, 225-247.
Wilson, C.J.N., Houghton, B.F., Lloyd, E.F., 1986. Volcanic history and evolution of the Maroa-Taupo area, central North Island. Late Cenozoic Volcanism in New Zealand. Royal Society of New Zealand Bulletin 23, 194-223.
Wolff, E.W., Fischer, H., Fundel, F., Ruth, U., Twarloh, B., Littot, G.C., Mulvaney, R., Röthlisberger, R., De Angelis, M., Boutron, C.F., 2006. Southern Ocean sea-ice extent, productivity and iron flux over the past eight glacial cycles. Nature 440, 491-496.
Wolff, E.W., Fischer, H., Röthlisberger, R., 2009. Glacial terminations as southern warmings without northern control. Nature Geoscience 2, 206-209.
Wright, I.C., McGlone, M.S., Nelson, C.S., Pillans, B.J., 1995. An integrated latest Quaternary (Stage 3 to present) paleoclimatic and paleoceanographic record from offshore northern New Zealand. Quaternary Research 44, 283-293.

Wu, L., Cai, W., Zhang, L., Nakamura, H., Timmermann, A., Joyce, T., McPhaden, M.J., Alexander, M., Qiu, B., Visbeck, M., 2012. Enhanced warming over the global subtropical western boundary currents. Nature Climate Change 2, 161-166.

Yin, Q.Z., Berger, A., 2012. Individual contribution of insolation and CO_2 to the interglacial climates of the past 800,000 years. Climate Dynamics 38, 709-724.

Yin, Q.Z., Berger, A., 2015. Interglacial analogues of the Holocene and its natural near future. Quaternary Science Reviews 120, 28-46.

Appendix One Supplementary Figures

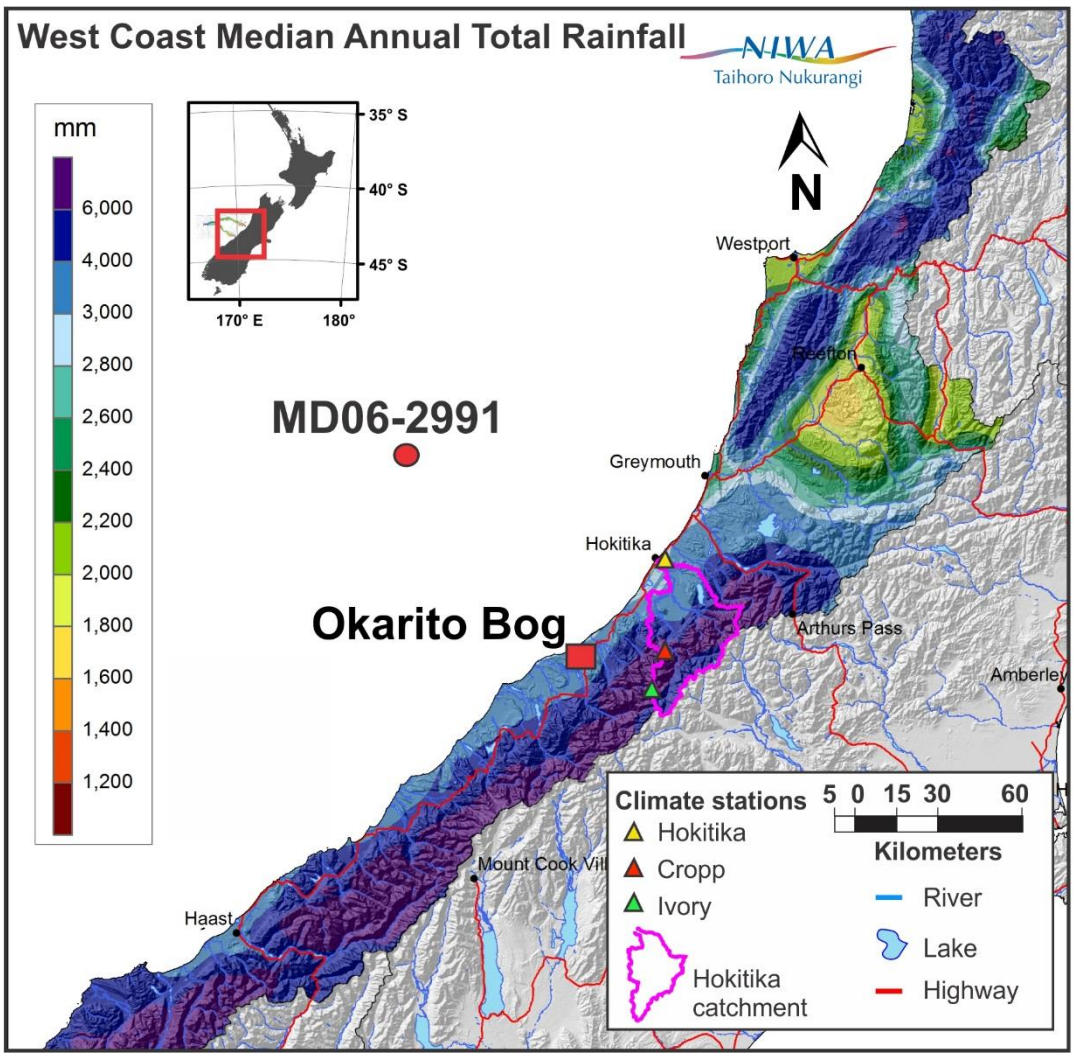

Supplementary Fig. 2.1: Median annual total rainfall for West Coast, South Island, New Zealand, based on the 30-year period (1981-2010). Rainfall is ~2900 mm/yr^{-1} in coastal regions such as the Hokitika Aero climate station 39 masl (metres above sea level) (NIWA, 2014a) and rises to 11,200 mm/yr^{-1} at altitude (902 masl; Cropp climate station, Hicks et al., 2011). The Hokitika catchment (magenta) is a primary source of the palynomorphs deposited into the Hokitika submarine channel, and eventually to the MD06-2991 core-site situated in the East Tasman Sea. The location of Okarito Bog is illustrated. This map is modified from NIWA (2012) to include sites outlined in text.

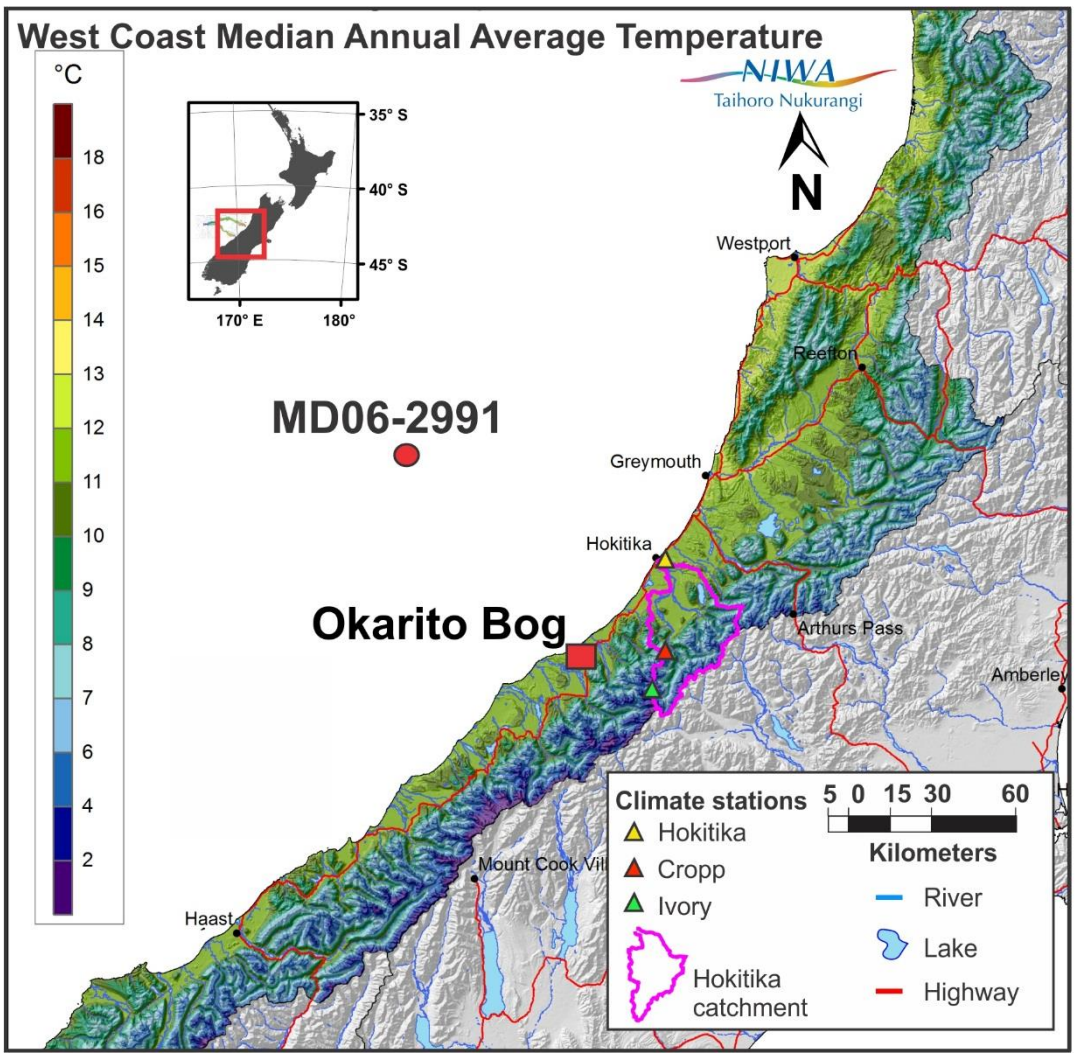

Supplementary Fig. 2.2: Median annual temperature (°C) for West Coast, South Island, New Zealand, based on the 30 year period (1981-2010). The map shows temperature reaches ~11.5°C in coastal regions such as that recorded at the Hokitika Aero climate station 39 masl (metres above sea level) (NIWA 2014a) and declines to 4.1°C at altitude (1400 masl; Ivory climate station, NIWA 2012b). The composition of native flora in the Westland region strongly reflects the altitudinal relationship with temperature (Wardle 1991). The Hokitika catchment (magenta) is a primary source of the palynomorphs deposited into the Hokitika submarine channel, and eventually to the MD06-2991 core-site situated in the East Tasman Sea. The location of Okarito Bog is illustrated. This map is modified from NIWA (2012) to include sites outlined in text.

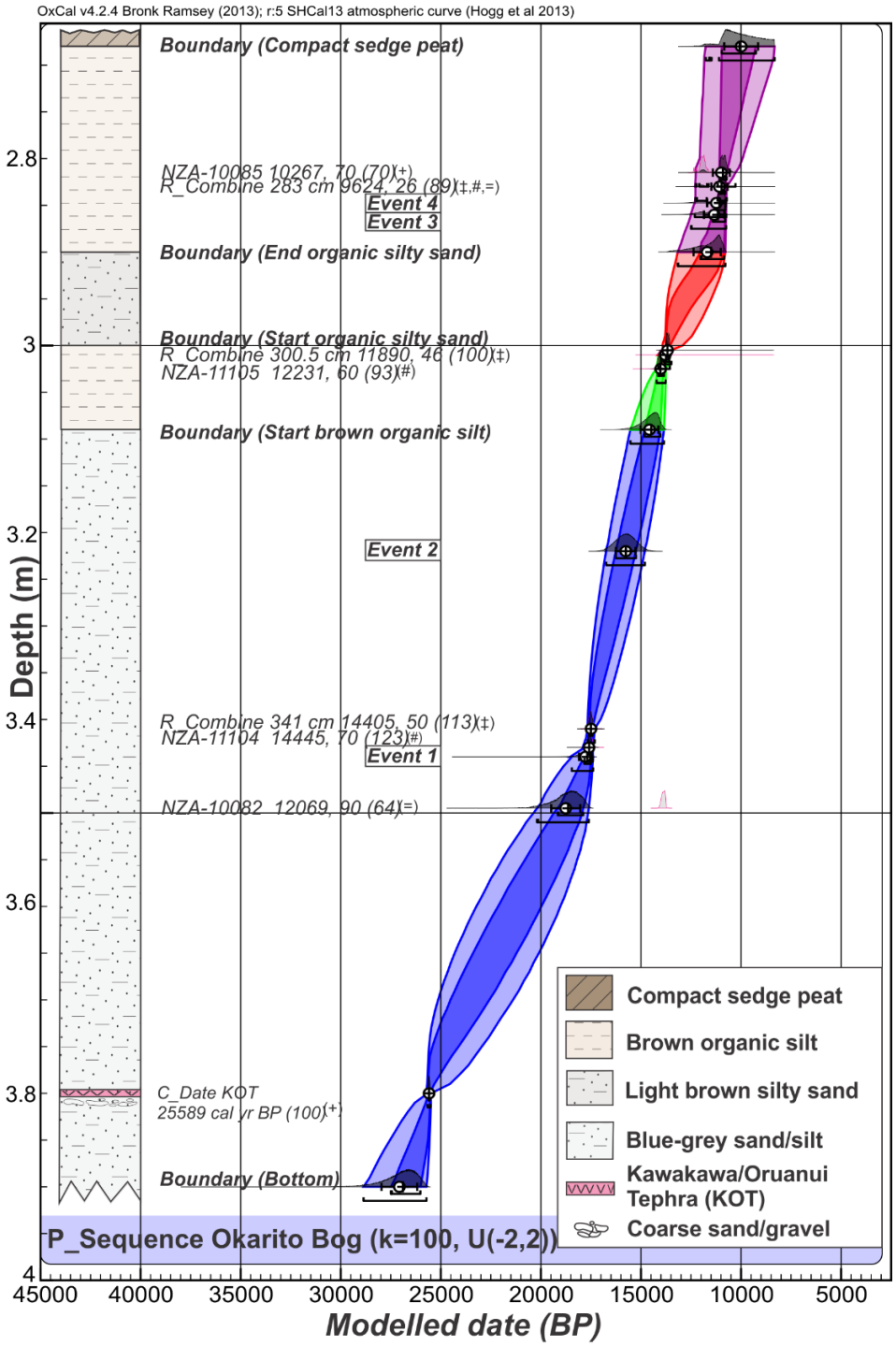

Supplementary Fig. 3.1: Age-depth model and stratigraphy for the Okarito Bog record based on fourteen of seventeen ^{14}C dates (i.e., three dates were rejected as outliers) published in Vandergoes et al. (2005). *R_combine* ages were calculated for horizons where multiple ^{14}C dates were obtained (283, 300.5 and 341 cm), and an outlier was detected in each horizon. The remodelled KOT (2σ) was assigned to 3.80 m core depth. A variable k value of 100 was applied, producing a final Amodel of 80.3 from the fourteen ^{14}C dates. The 68% and the 95% levels of confidence are shown, along with calendar age likelihood in dark pink, and posterior probability density functions in dark grey. The laboratory number, followed by ^{14}C date, 1σ error, and sample agreement indexes (in parentheses) are listed by each radiocarbon sample. The mean (white circle) and median (vertical line in circle) values of the calibration distributions are also shown. Stratigraphic boundaries in the depositional model are represented by changes in colour from blue, green, red and purple.

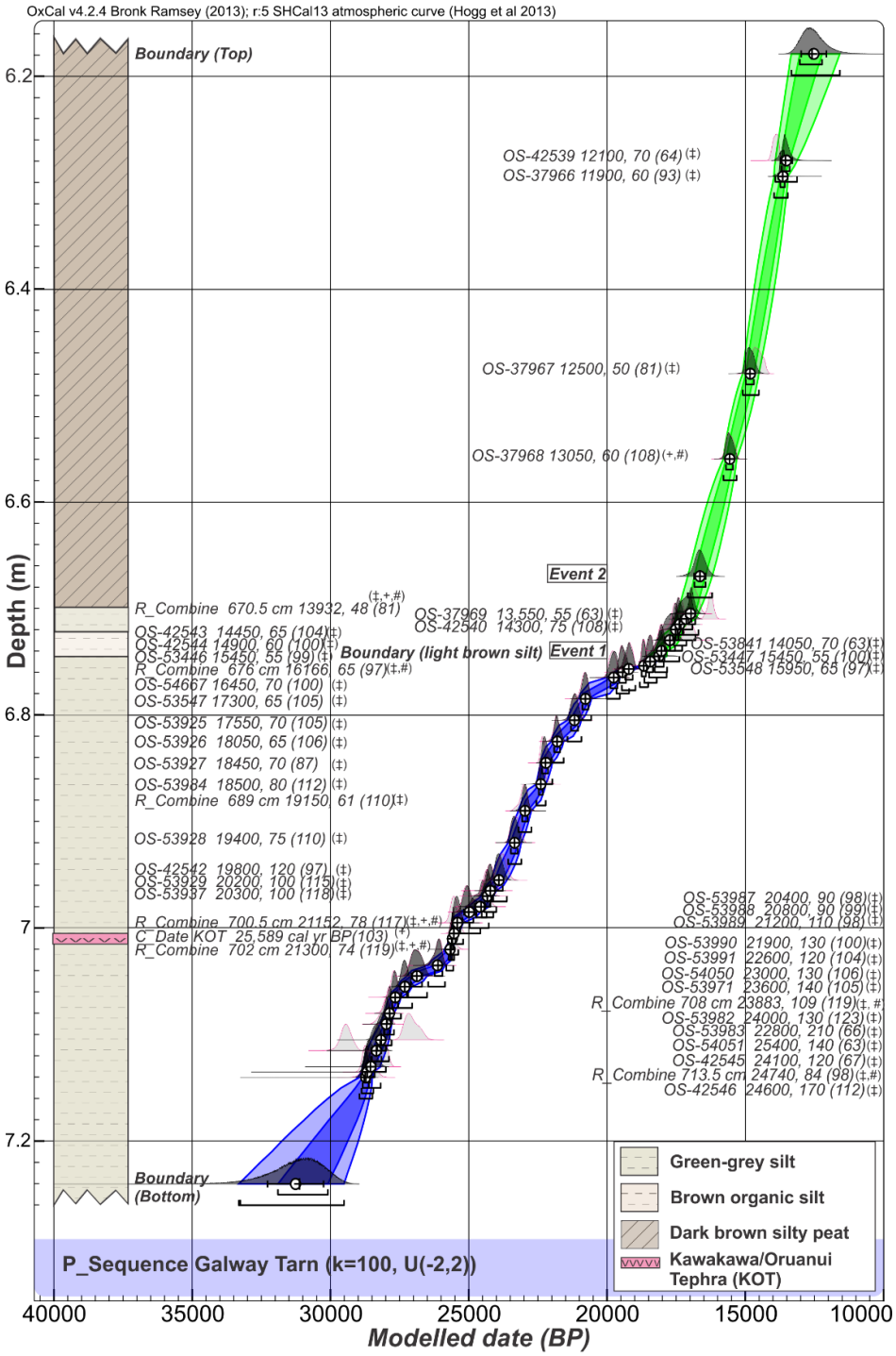

Supplementary Fig. 3.2: Age-depth model and core stratigraphy for the Galway tarn record based on forty-eight of fifty ^{14}C dates (i.e., two dates were rejected as outliers) revised from Vandergoes et al. (2013a). Material was dated from organic sediment concentrates (<90-10 µm, ‡), wood (+), and sieved organic material (>90 µm, #). The recalibrated age of the KOT (2σ) was assigned to 7.01 m. A variable k value of 100 was applied, producing an Amodel of 78.6. The 68% and the 95% levels of confidence are shown, along with calendar age likelihood in dark pink, and posterior probability density functions in dark grey. The laboratory number, followed by ^{14}C date, 1σ error, and sample agreements (in parentheses) are listed by each radiocarbon sample. The mean (white circle) and median (vertical line in circle) values of the calibration distributions are also pictured. The lithological change from green-grey silt to dark brown silty peat is represented in the depositional model by a colour change from blue to green.

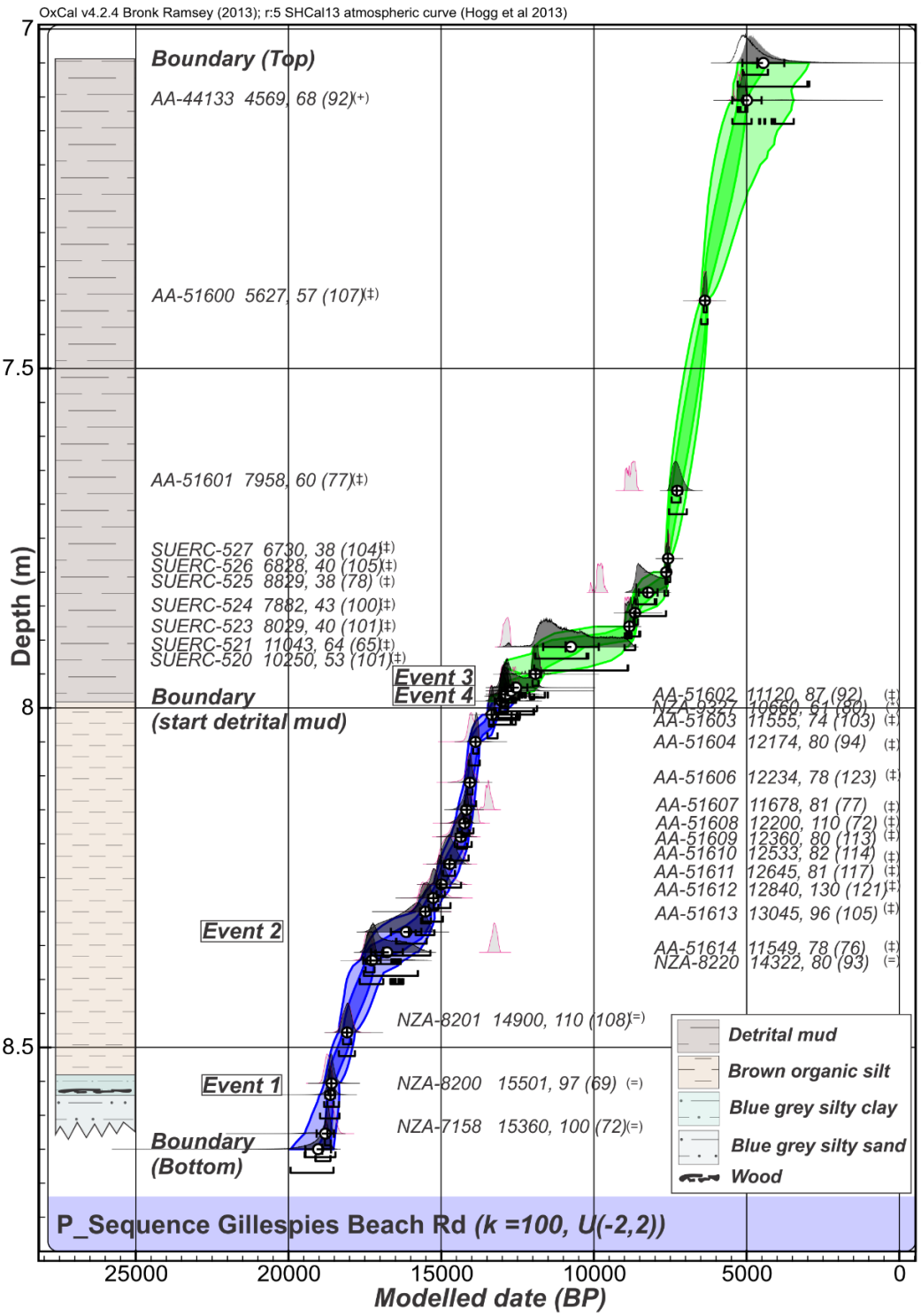

Supplementary Fig. 3.3: Age-model and core stratigraphy for the Gillespies Beach Rd (GBR) record based on twenty-seven of twenty-eight ^{14}C dates (i.e., one date was rejected as an outlier). Sixteen dates were comprised of pollen concentrates (<63 µm, ‡), three of bulk sediment (=), and one of wood and leaves (+). A variable k value of 100 was applied, producing an Amodel of 65.7. The 68% and the 95% levels of confidence are shown, along with calendar age likelihood in dark pink, and posterior probability density functions in dark grey. The laboratory number, followed by ^{14}C date, 1σ error, and sample agreements (in parentheses) are listed by each radiocarbon sample. The mean (white circle) and median (vertical line in circle) values of the calibration distributions are also pictured. The lithological change from brown organic silt to detrital mud is represented in the depositional model by a colour change from blue to green.

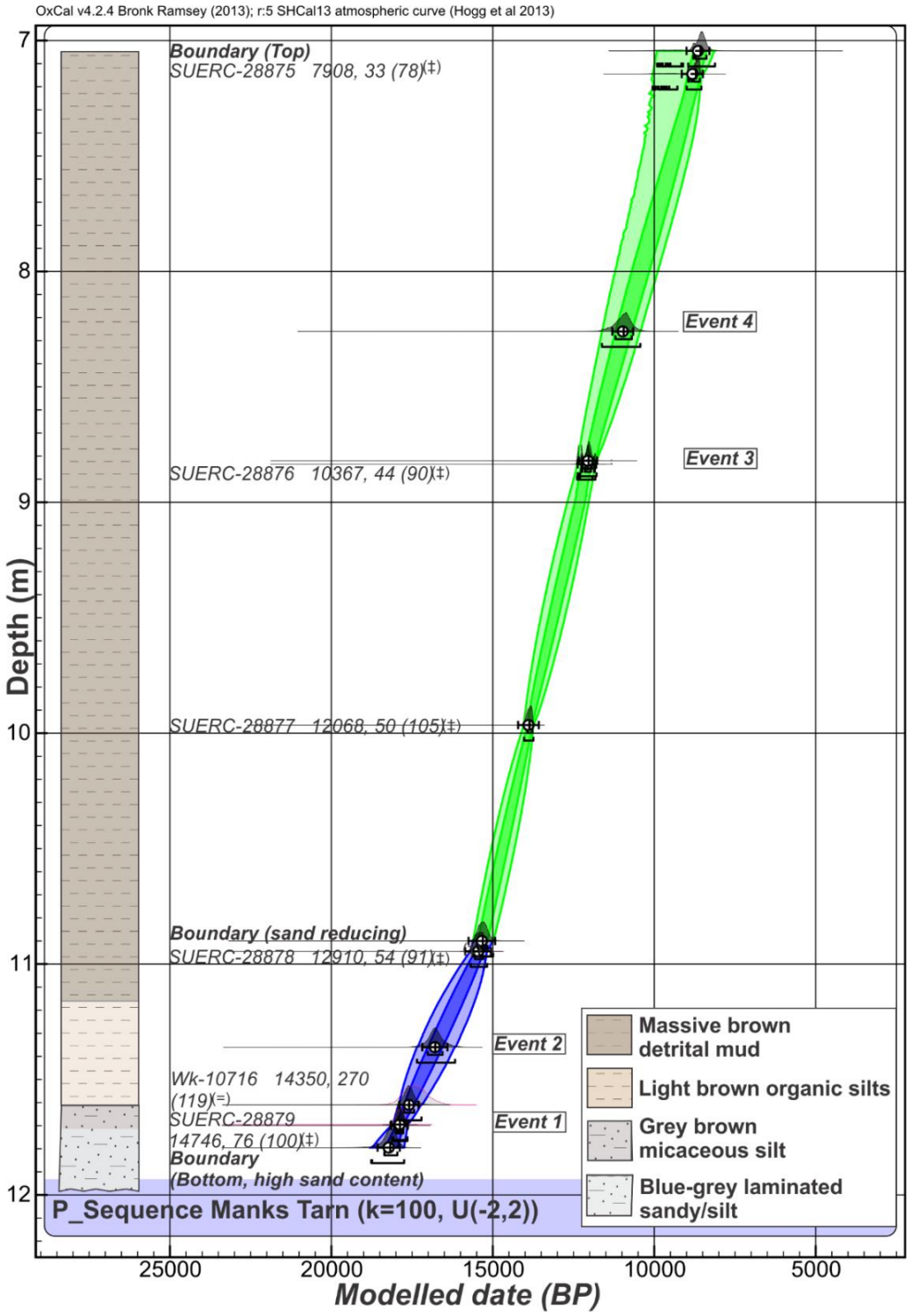

Supplementary Fig. 3.4: Age-depth model for the Manks Tarn record based on six ^{14}C dates from pollen concentrates (n=5, ‡) and bulk sediment (n=1, =); no outliers were identified. A k value of 100 was applied, producing an Amodel of 93.5. The 68% and the 95% levels of confidence are shown, along with calendar age likelihood in dark pink, and posterior probability density functions in dark grey. The laboratory number, followed by ^{14}C date, 1σ error, and sample agreements (in parentheses) are listed by each radiocarbon sample. The mean (white circle) and median (vertical line in circle) values of the calibration distributions are also pictured. Particle size analysis revealed a marked reduction in sand (~18-7%) between 1090-810 cm within the massive brown detrital mud (Callard, 2011). This defines a lithologic boundary shown from blue to green in the depositional model.

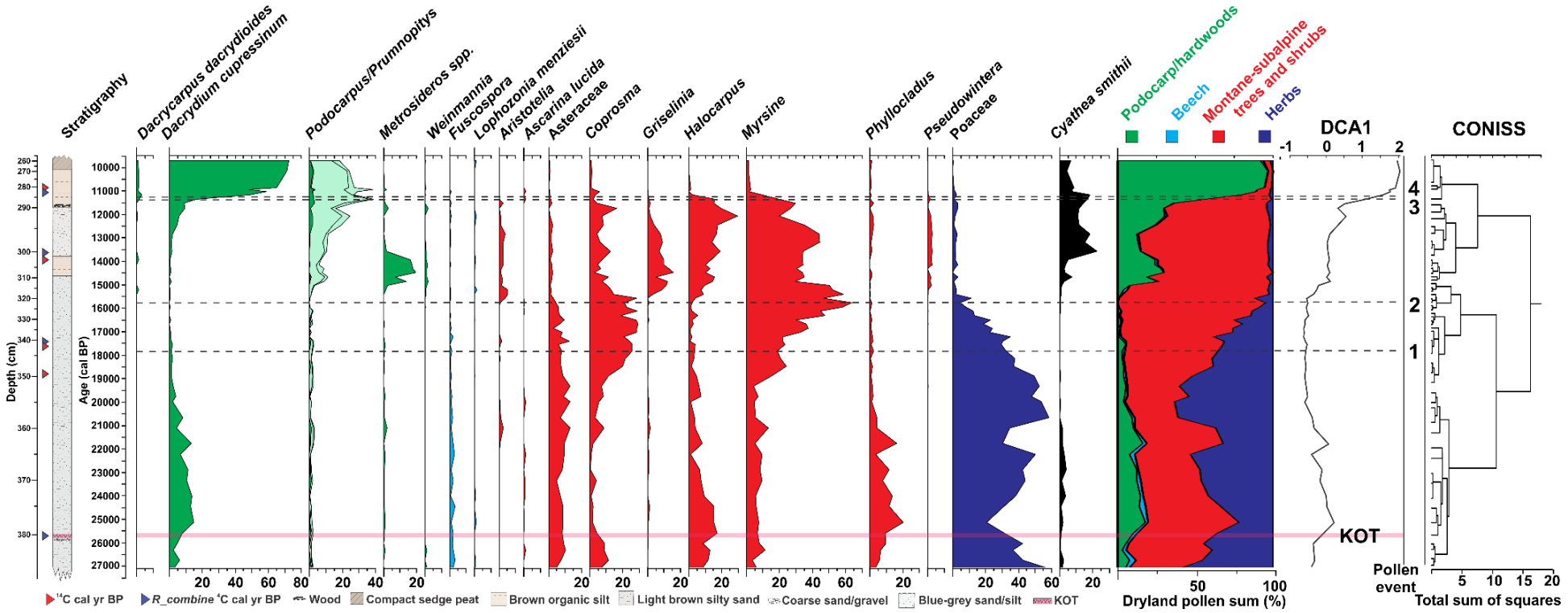

Supplementary Fig. 3.5: Summary pollen diagram for Okarito Bog. Stratigraphy and location of the calibrated AMS ^{14}C ages (red triangles) and *R_combine* ages (blue triangles) are shown on the left. The relative percentages of main dryland pollen taxa are shown from left to right and are grouped into a cumulative dryland pollen plot. This includes podocarp-hardwoods, beech, montane-subalpine trees and shrubs, and herbs. *Podocarpus/Prumnopitys* are grouped, although their respective relative percentages are distinguished as *Podocarpus* and podocarpoid (green), *Prumnopitys ferruginea* and *Prumnopitys taxifolia* (light green with line separator). The palynomorph events depicted for all records are indicated by dashed lines and event numbers. Kawakawa/Oruanui Tephra (KOT) shown in pink. DCA axis 1 scores and CONISS zonation results are shown (far right).

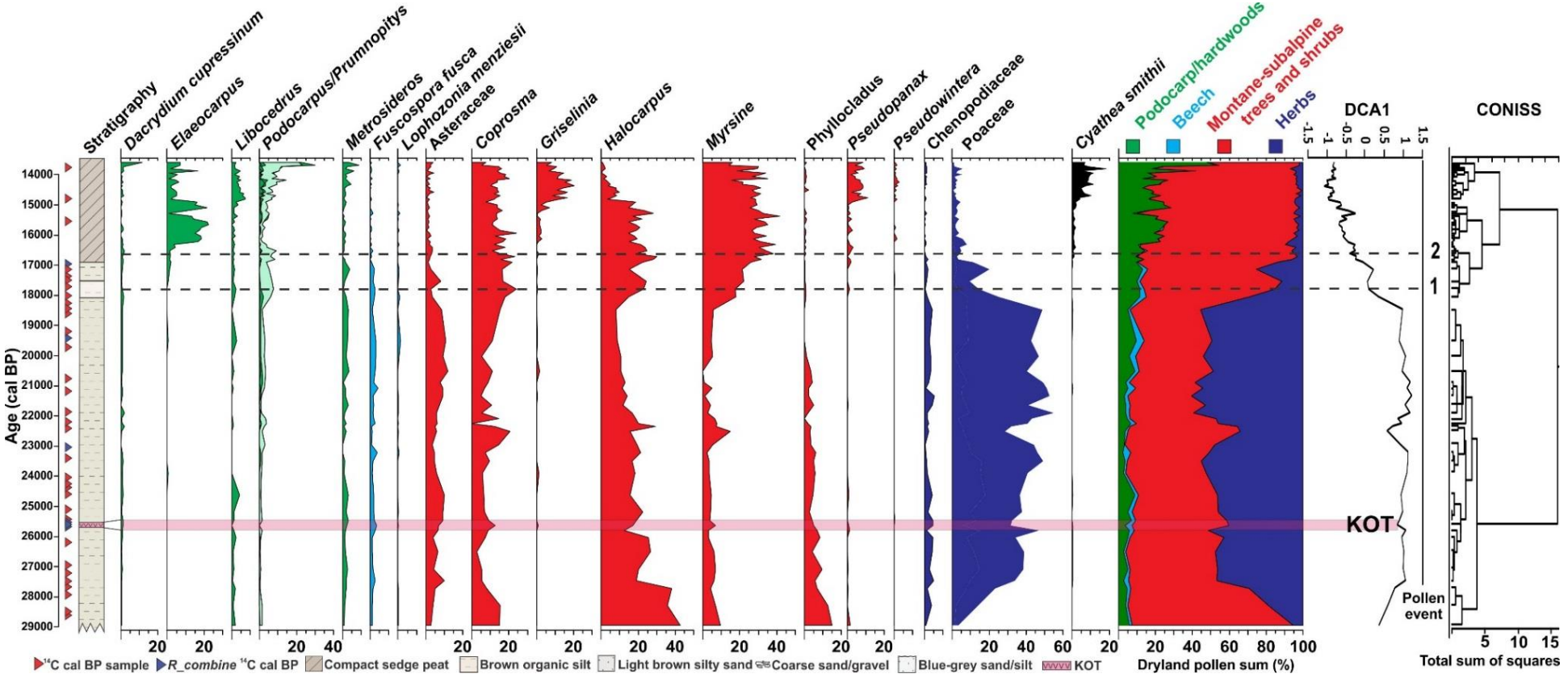

Supplementary Fig. 3.6: Summary pollen diagram for Galway tarn. Stratigraphy and location of the calibrated AMS ^{14}C ages (red triangles) are shown on the left. The relative percentages of main dryland pollen taxa are shown from left to right and are grouped into a cumulative dryland pollen diagram, which includes podocarp-hardwoods, beech, montane-subalpine trees and shrubs, and herbs. *Podocarpus*/*Prumnopitys* are displayed grouped, although their respective relative percentages are distinguished as *Podocarpus* (dark green) and *Prumnopitys* sp. (light green). The palynomorph events depicted for all records are indicated by dashed lines and event numbers, with the position of the KOT also presented. DCA axis 1 scores and CONISS zonation results are shown (far right).

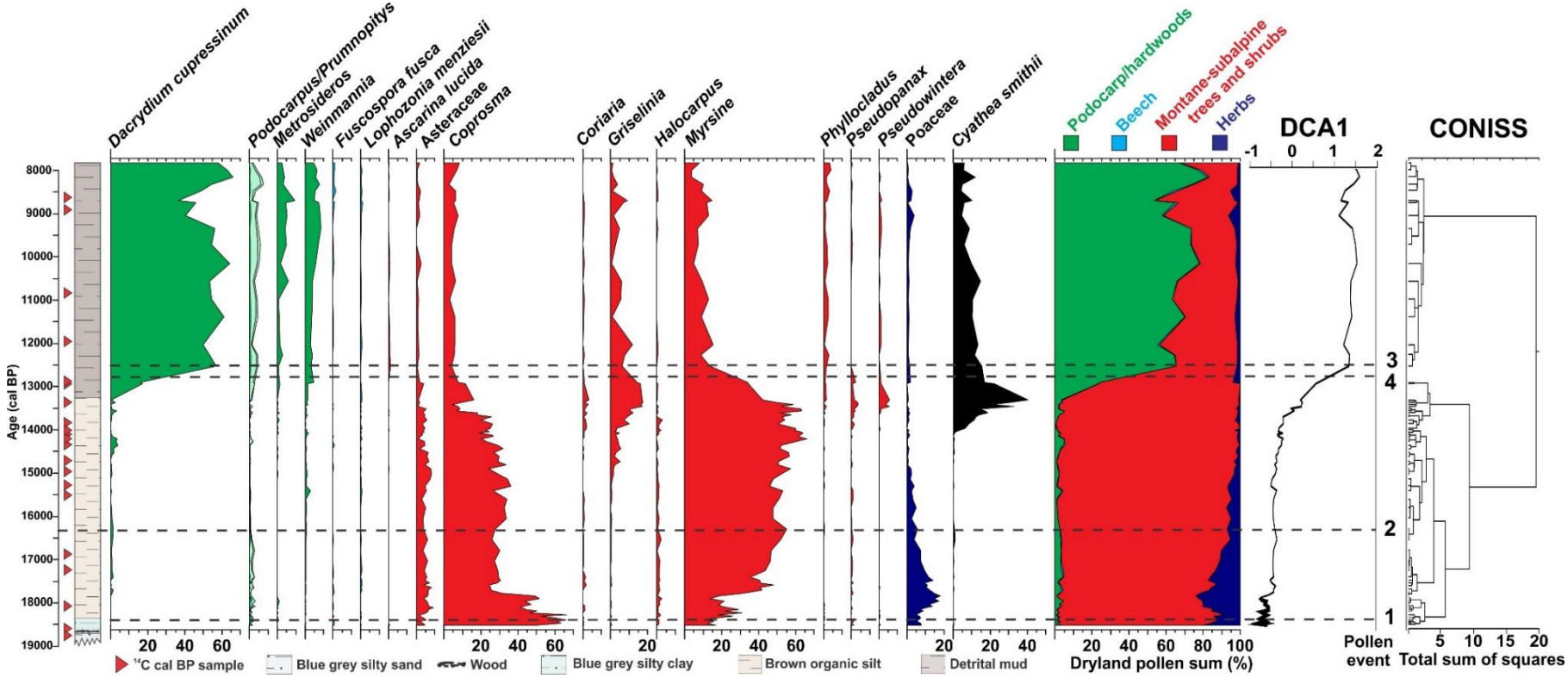

Supplementary Fig. 3.7: Summary pollen diagram for Gillespies Beach Rd. The core stratigraphy and location of the calibrated AMS ^{14}C ages (red triangles) are shown on the left. The relative percentages of main dryland pollen taxa are shown from left to right and are grouped into a cumulative dryland pollen diagram, which includes podocarp-hardwoods, beech, montane-subalpine trees and shrubs, and herbs. *Podocarpus*/*Prumnopitys* are displayed grouped, although their respective relative percentages are distinguished as *Podocarpus* (dark green) and *Prumnopitys* sp. (light green). The palynomorph events depicted for all records are indicated by dashed lines and event numbers. Palynomorph events 3 and 4 are reversed in order, as the mid-point of *D. cupressinum* (event four) occurs prior to the highest amount of podocarp-hardwood taxa (event 3). This likely reflects a local signal, as *D. cupressinum* is better able to survive in boggy substrates that characterise GBR. DCA axis 1 scores and CONISS zonation results are shown (far right).

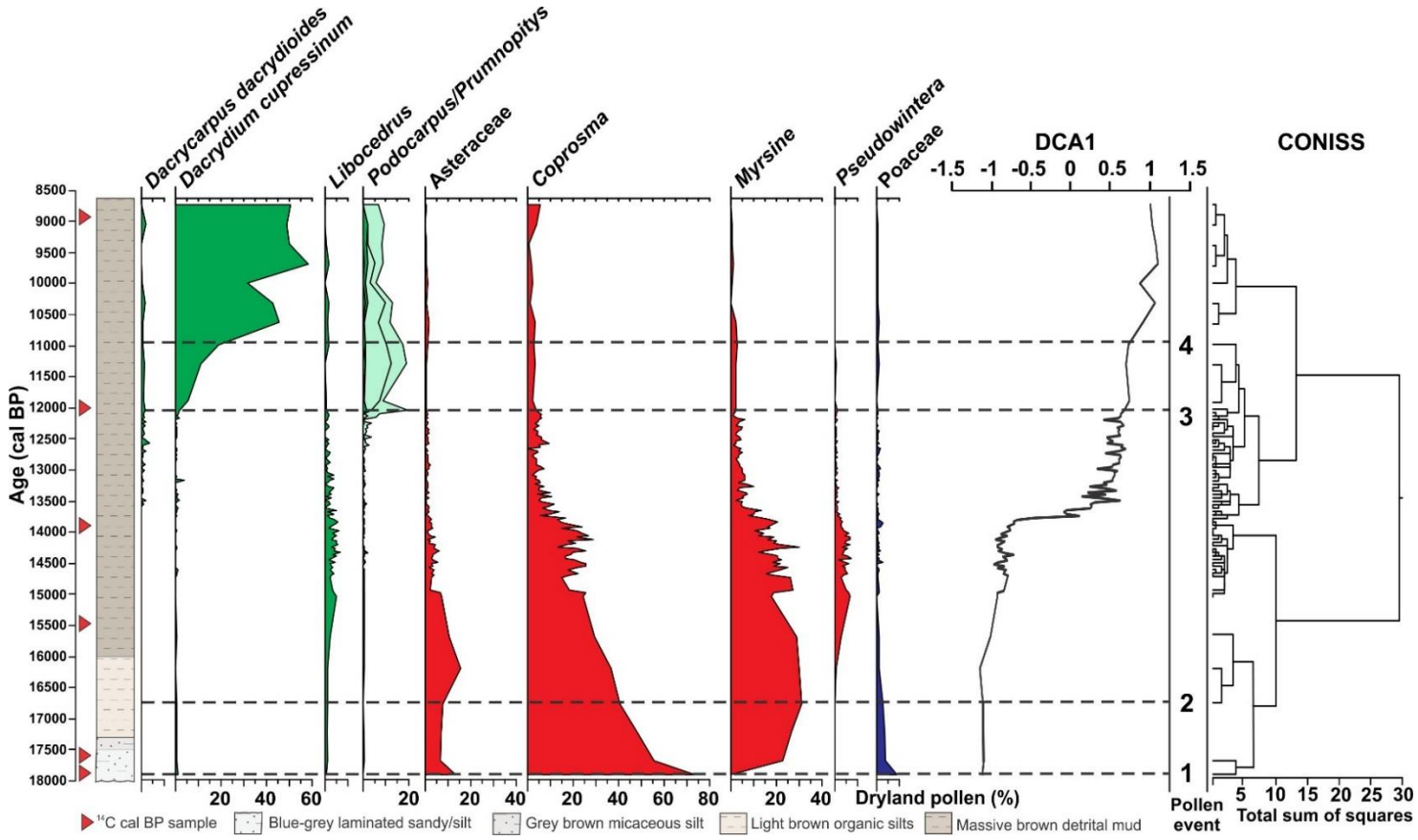

Supplementary Fig. 3.8: Summary pollen diagram for Manks Tarn. Stratigraphy and location of the calibrated AMS ^{14}C ages (red triangles) are shown on the left. The relative percentages of main dryland pollen taxa are shown from left to right. *Podocarpus/Prumnopitys* are displayed grouped, although their respective relative percentages are distinguished as *Podocarpus* and Podocarpoid (green), with *Prumnopitys ferruginea* and *Prumnopitys taxifolia* distinguished by a colour change and a line (light green). The palynomorph events depicted for all records are indicated by dashed lines and event numbers. DCA axis 1 scores and CONISS zonation results are shown (far right).

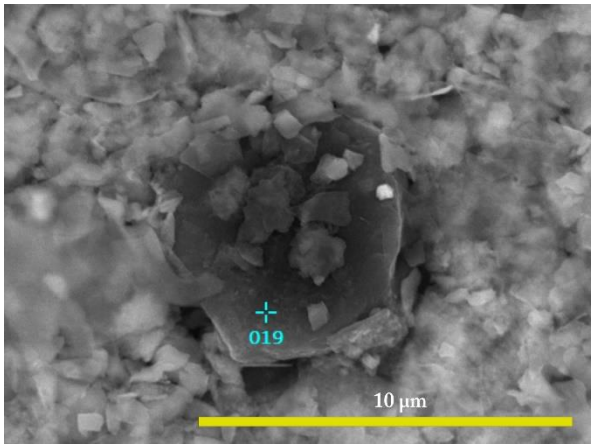

Element	C	O	Na	Mg	Al	Si	
EDS (wt%)	63.69	18.28	0.54	0.1	0.61	15.05	Total (Mass%)
Cl	K	Ca	Fe	Ba	W	Pt	100
0.19	0.18	0.09	0.17	0	0	1.1	

Appendix Fig. 3.9: An organic particle from 230-231 cm core depth (10-50 µm, 1.6 s.g. sink) from MD06-2991 under a field emission scanning electron microprobe (FESEM). Results (tabled directly above) indicate this grain has a high proportion of carbon similar to that of West Coast lignite shown in Li et al. (2001). This supplementary figure was not included in manuscript resulting from this chapter.

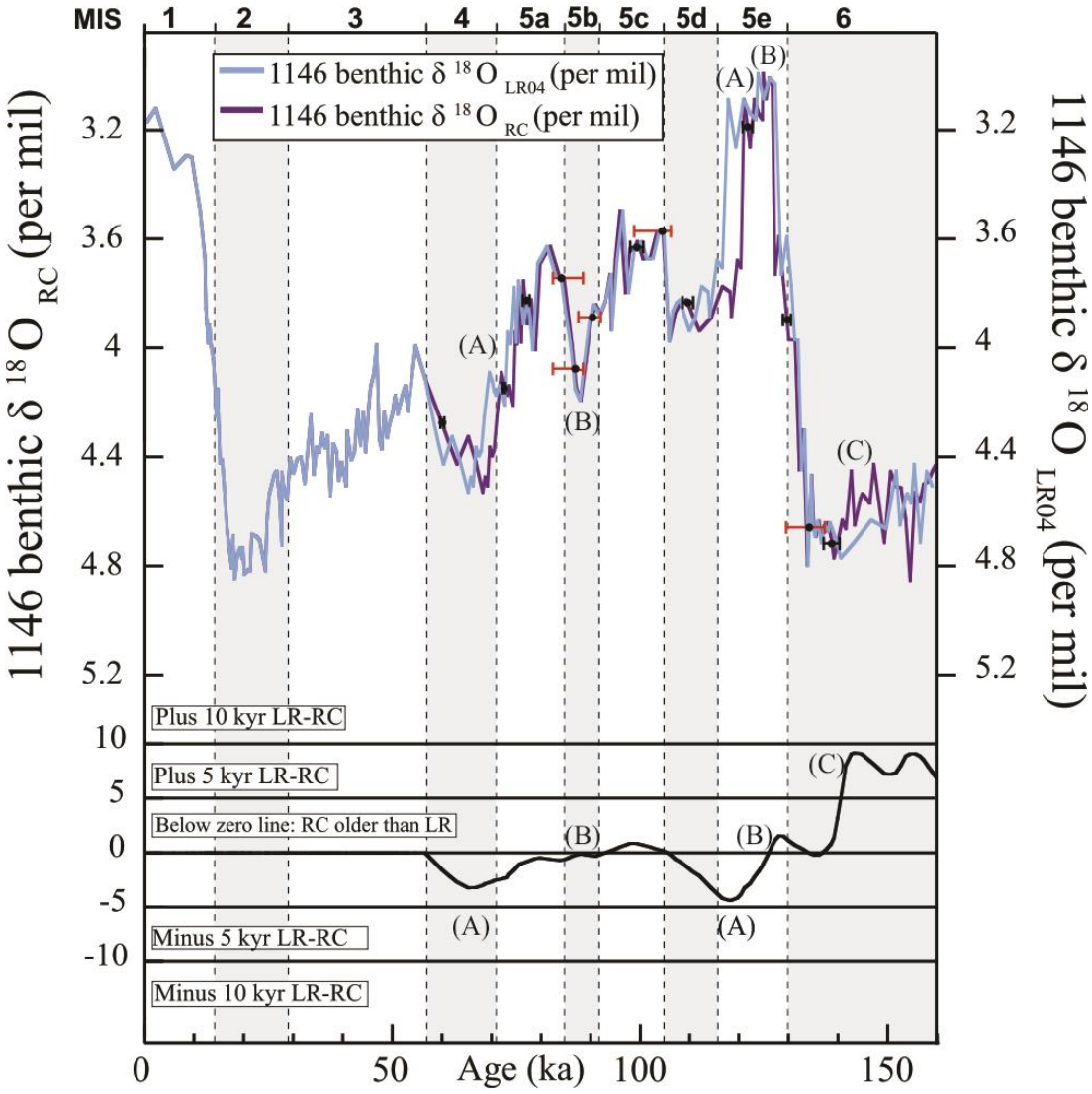

Supplementary Fig. 4.1: The comparison of the orbitally tuned benthic $\delta^{18}O$ record from ODP 1146 (light blue) to the LR04 benthic $\delta^{18}O$ stack (Lisiecki and Raymo, 2005), vs. that tuned to a $\delta^{18}O$ radiometric U/Th chronology composite record from Sanbao and Hulu Caves (Wang et al., 2001; 2008; Cheng et al., 2009). The bottom of the plot shows the age difference between the benthic $\delta^{18}O$ ODP 1114 record (aligned to the LR04 stack, LR) and the radiometrically calibrated (RC) age models. The example shows how a systematic bias in each direction can occur between the LR04 benthic $\delta^{18}O$ stack and the radiometrically constrained speleothem record. Examples include; A) where the RC chronology is older than LR; B) where there is no systematic offset between both records; C) where RC is younger than LR. Figure modified from Caballero-Gill et al. (2012a).

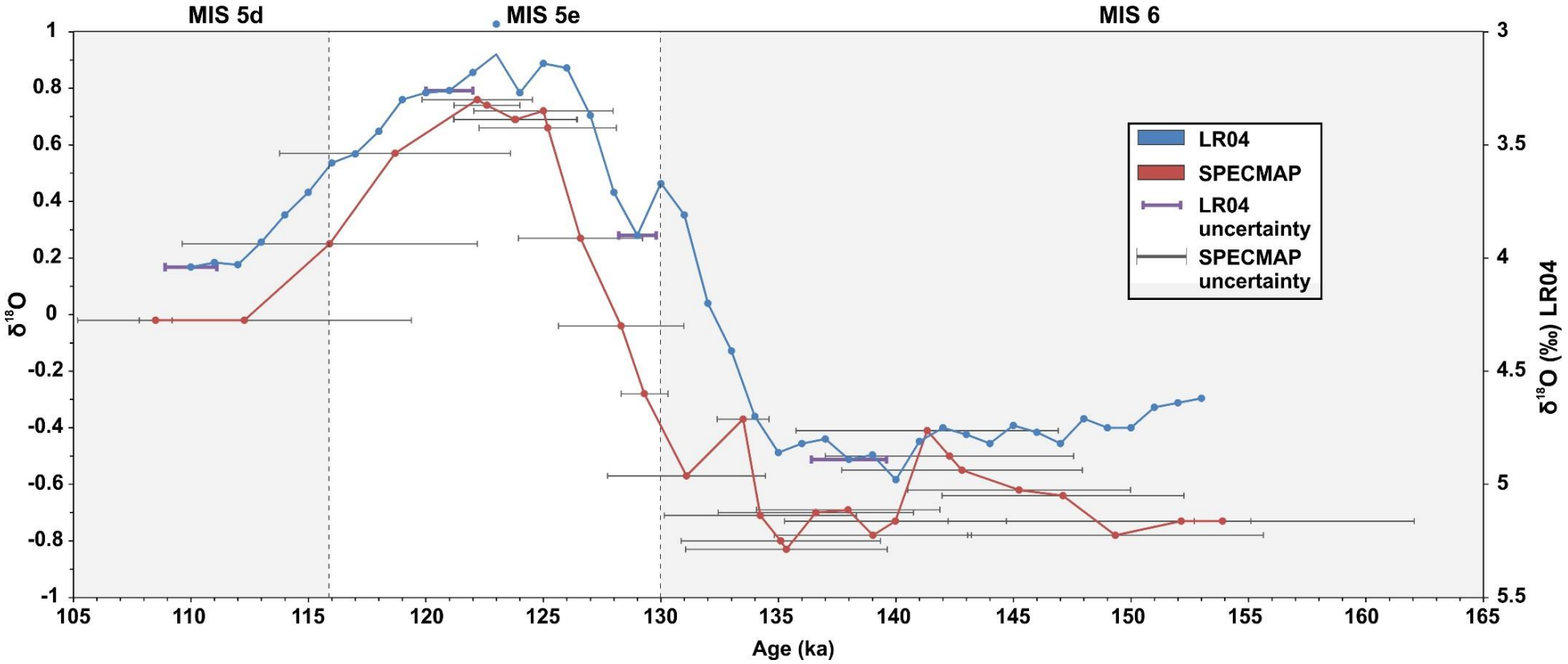

Supplementary Fig. 4.2: Comparison between the LR04 benthic $\delta^{18}O$ record of Lisiecki and Raymo (2005) with associated error uncertainties from Caballero-Gill et al. (2012a), to that of the normalised SPECMAP $\delta^{18}O$ isotope record (Martinson et al., 1987) with error uncertainties provided by Thompson and Goldstein (2006). The MIS substage boundaries are here assigned to that of Lisiecki and Raymo (2005).

Evaluating the accuracy of matching $\delta^{18}O$ from MD06-2991 to LR04 for the interval 158-28 ka.

We have measurements (MD06-2991) O_j of $\delta^{18}O$ at 97 depths d_j. These have been matched to a reference $\delta^{18}O$-age model (LR04), O^0_k , which has $\delta^{18}O$ values at uniform 1000 year spacing. The objective is to determine an overall mean misfit between the times t_j, and the uncertainty of that estimate.

Both O_j and O^0_k are noisy. We assume each set of data points have independent Gaussian errors with variances σ^2 and $\sigma^{0\,2}$ respectively. Since LR04 results from the stack of a number of different datasets, $\sigma^{0\,2} << \sigma^{2}$. The possibility of biases in the LR04 model is not considered.

The method we will use will determine the optimum offset value Δ which minimises the integrated square error ISE (Δ):

$$ISE(\Delta) = \int_a^b [\, O(t-\Delta) - O^0(t) \,]^2 \, dt \qquad (1)$$

This optimum value, Δ_{opt}, is the overall mean offset, or bias, between the two timescales. We will infer the uncertainty of Δ by showing that ISE (Δ)/ ISE $(\Delta)_{min}$ has approximately a χ^2 distribution. To calculate the ISE (Δ) both datasets have to be resampled (by linear interpolation) at a set of times which include the 1ky times of LR04, to ensure a maximum number of independent reference data points for matching. This means that resampling interval must be 1/n kyr where e.g. n=5 or 10. The original and resampled curves are shown in supplementary figure 4.3.

The interpolated data points are not independent of each other. The two resulting time-series to be compared have a number of independent data not less than the smaller of the numbers of data points in the original datasets (before resampling). For the comparison of 2991 and LR04 between 158 and 28 ka, the number of data are 131 and 85 respectively. Thus the resampled data points will have at least 85 degrees of freedom.

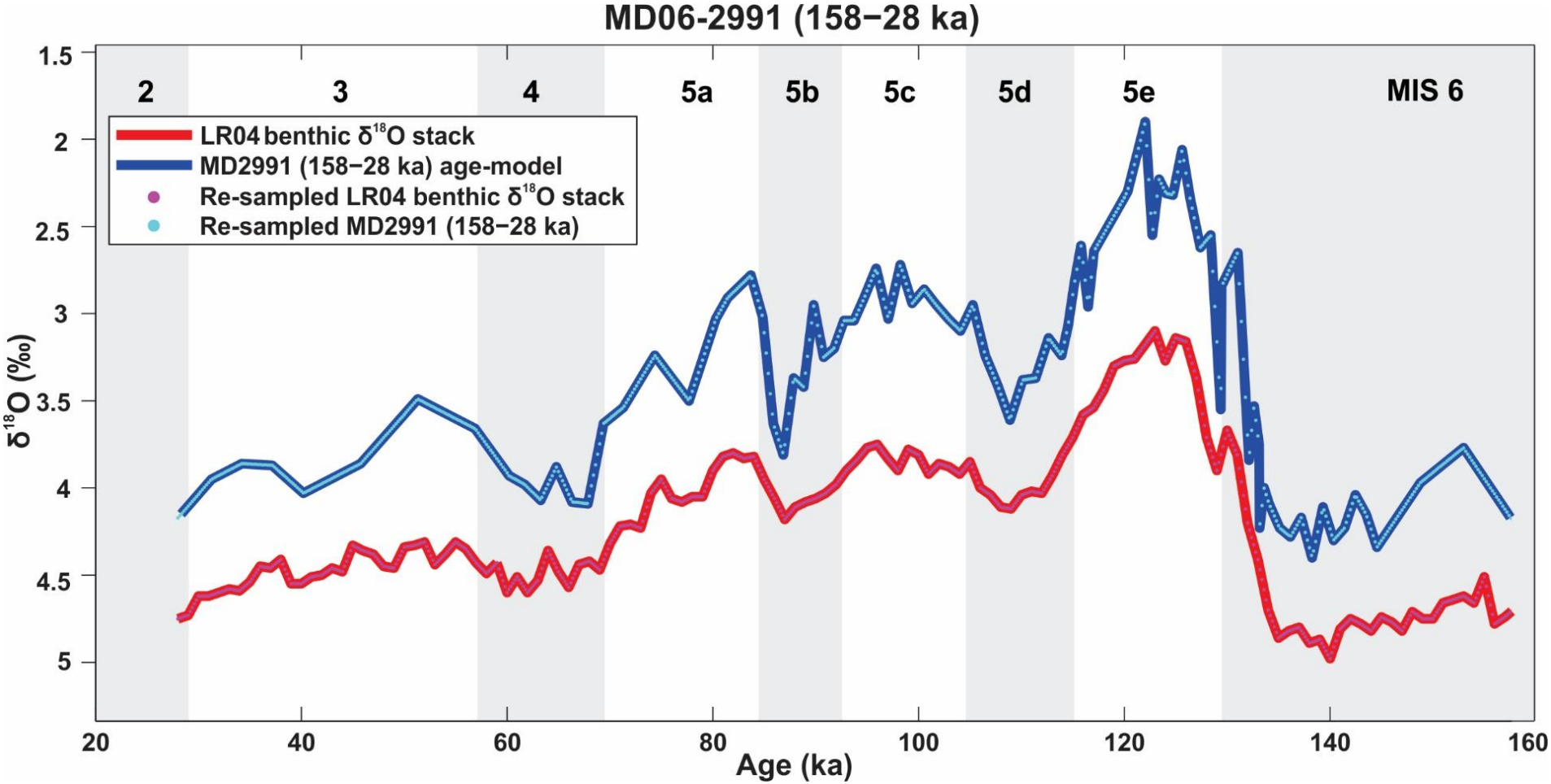

Supplementary Fig. 4.3: Original and resampled ^{18}O curves for LR04 (red, bottom) and MD2991 (blue, top) for the interval 158-28 ka.

Uncertainties

ISE (Δ) is calculated by summing over the N resampled times t_j :

$$ISE(\Delta) = \Sigma_1^{\ N} [\ O_j(t-\Delta) - O^0_j(t)\ ]^2 \qquad (2)$$

We assume that for the value of Δ, Δ_{opt}, which minimises ISE (Δ), the remaining discrepancy between the curves is random noise.

Each term is a difference of two Gaussian variables with variances σ^2 and $\sigma^{0\,2}$ so the variance of their difference is $\sigma^2 + \sigma^{0\,2}$. ISE (Δ_{opt}) is therefore a sum of the squares of N (non-independent) Gaussian variables, and so has a χ^2 distribution, with at least 85 degrees of freedom (df) in the example presented here.

This means that an estimate of $\sigma^2 + \sigma^{0\,2}$ is provided by ISE (Δ_{opt})/df. The upper 95% confidence limit for a χ^2 distribution with 85 df is 107.5 so the upper limit for ISE (Δ_{opt})/df is 107.5/85 = 1.265 (Supplementary Fig. 4.4). Thus values ISE (Δ)/df ≤ 1.265 ISE (Δ_{opt})/df are not significant at the 95% level, and so this provides 95% uncertainty limits for Δ.

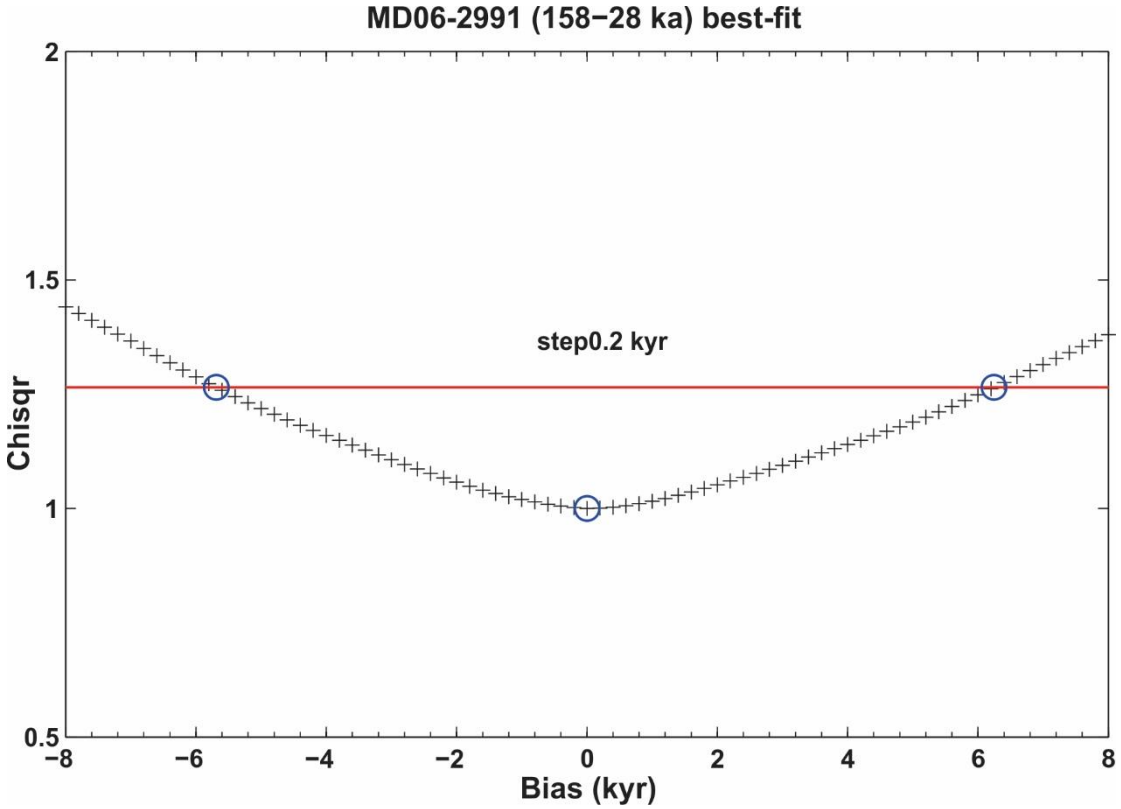

Supplementary Fig. 4.4: Evaluation of the fit between the MD06-2991 $\delta^{18}O$ stratigraphy and the LR04 benthic $\delta^{18}O$ stack over the 158-28 kyr time interval (ISE (Δ)/ISE(Δ_{opt}) vs. offset Δ). The optimum, Δ_{opt}, and 95% confidence intervals for Δ_{opt} are shown as circles. The red line is drawn at χ^2 (95%,85df)/ 85 = 1.265. The optimum offset Δ_{opt} = 0 kyr, with a confidence interval of ± 6 kyr.

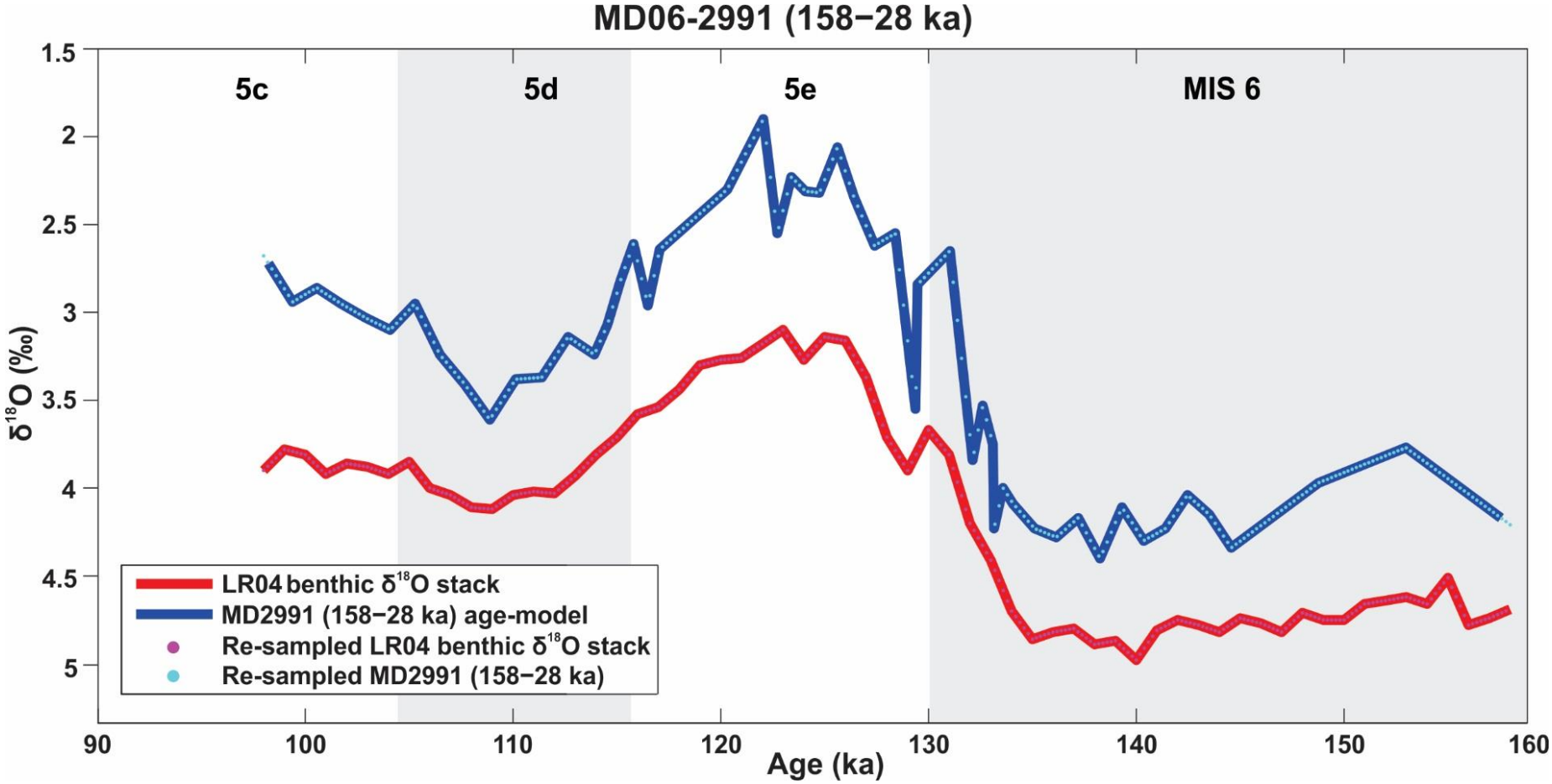

Supplementary Fig. 4.5: Original and resampled ^{18}O curves for LR04 (red, bottom) and MD2991 (blue, top) for the higher resolution interval 158-98 ka.

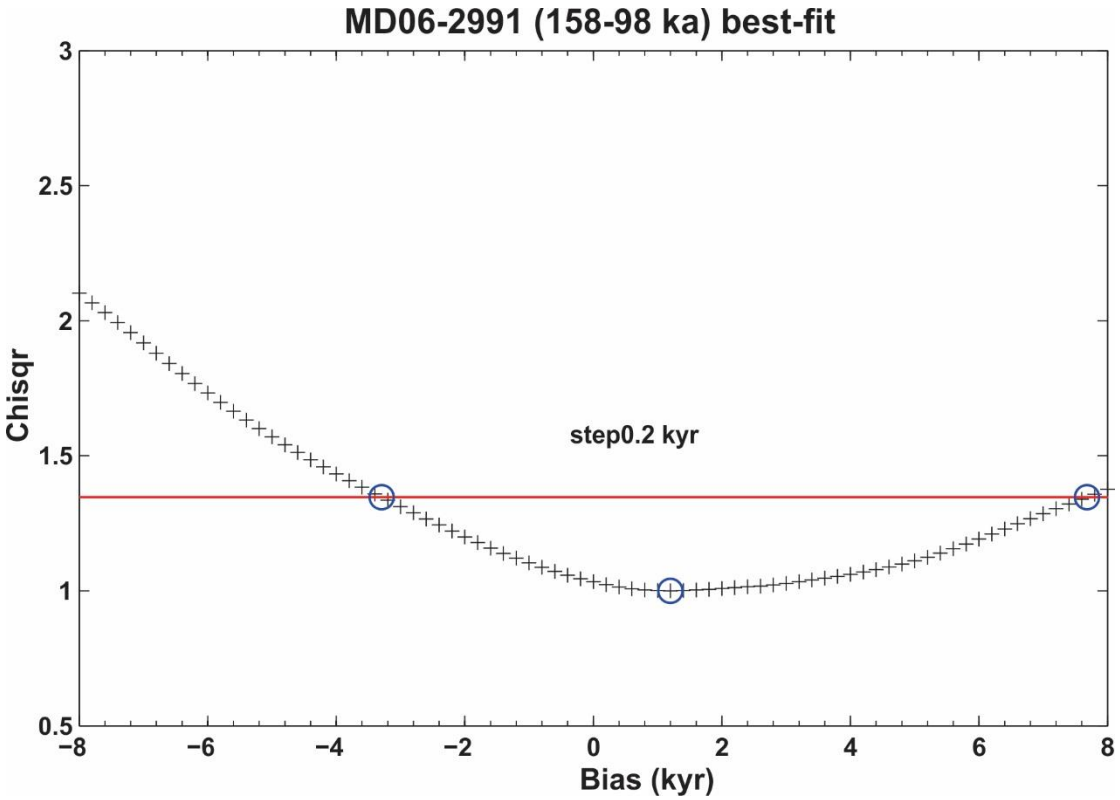

Supplementary Fig. 4.6. As for supplementary fig. 4.4 for MD06-2991 for 158-98 ka. The optimum offset is 1.2 kyr (95% CI, + 7 kyr -5 kyr). The bias is not significantly different from 0. Here the red line is drawn at χ^2 (95%, 85df)/ 85 = 1.265.

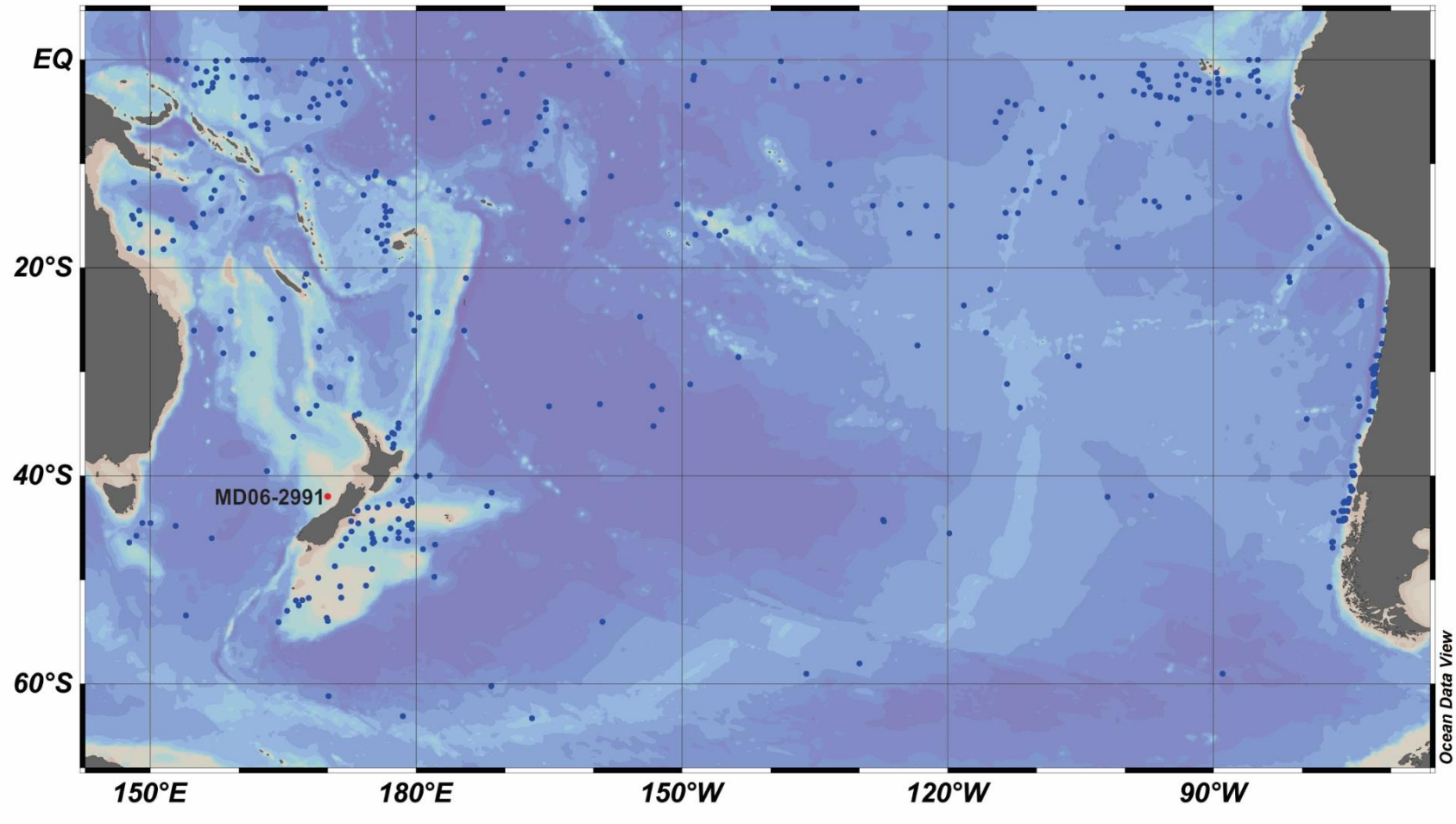

Supplementary Fig. 4.7: Distribution of faunal foraminiferal-based core top samples from the Pacific region (479 analogues), contributing to 1223 samples applied in the SH0911 database (Cortese et al., 2013). The location of MD06-2991 is displayed.

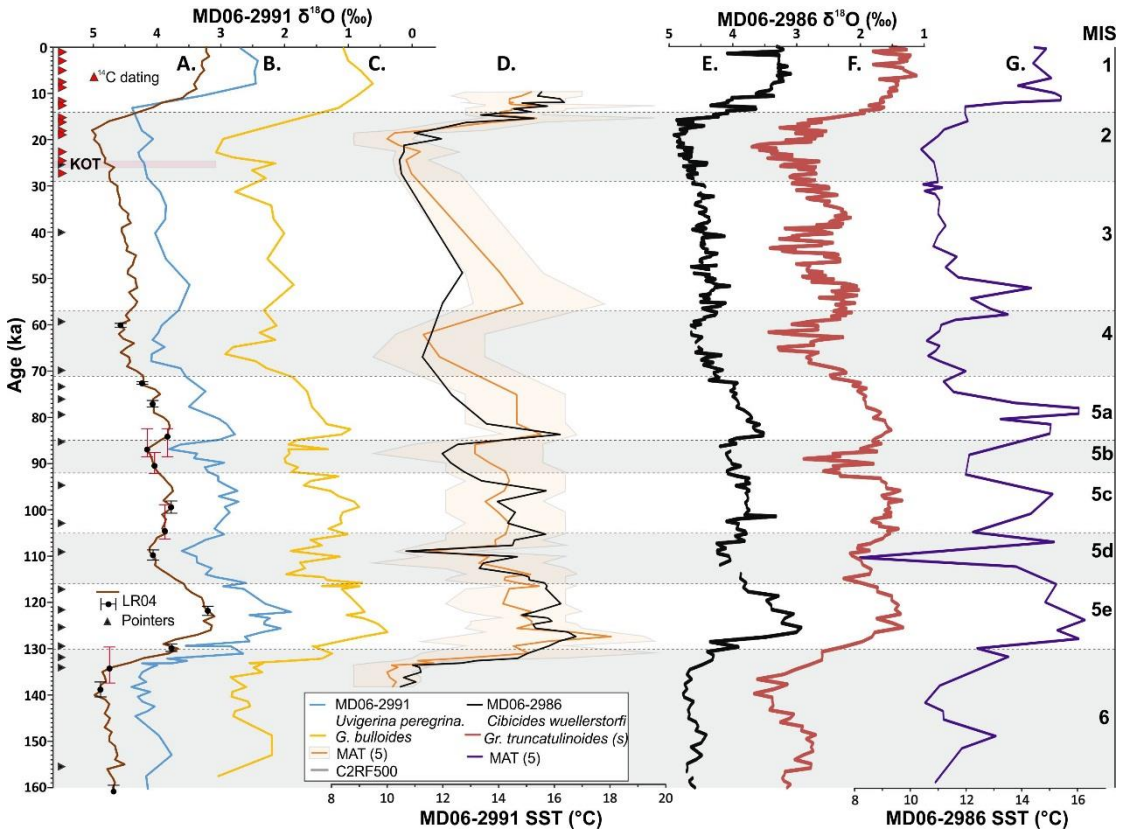

Supplementary Fig. 4.8: Comparison of MD06-2991 and MD06-2986 age model and SST estimates. Location of calibrated ^{14}C dates (red triangles, n=15) on planktonic foraminifera, the maximum concentration of KOT glass shards in MD06-2991, and $\delta^{18}O$ tie-points (black triangles) which align down-core $\delta^{18}O$ measurements from MD06-2991 to; **A.** the reference LR04 benthic $\delta^{18}O$ stack (Lisiecki and Raymo, 2005). Age uncertainties for the LR04 stack determined by Caballero-Gill et al. (2012a) are displayed. **B** & **C.** MD06-2991 oxygen isotope records for *Uvigerina peregrina* and *Globigerina bulloides*; **D.** SST estimates from planktic foraminifera based on the modern analogue technique (MAT) using the SH training set (SH0911C2) with an associated uncertainty envelope, and a random forest ensemble (C2RF500) based SST for the same foraminiferal counts. MD06-2986 oxygen isotope records for; **E.** *Cibicides spp.* and; **F.** *Gr* (*Globorotalia*) *truncatulinoides* (sinistral), with the MAT (5 nearest analogues) revised from Hayward et al. (2012). The MIS boundaries of the LR04 stack follow the subdivision of Railsback et al. (2015), where the MIS glacial stages and the stadial sub-stages are represented in grey shading.

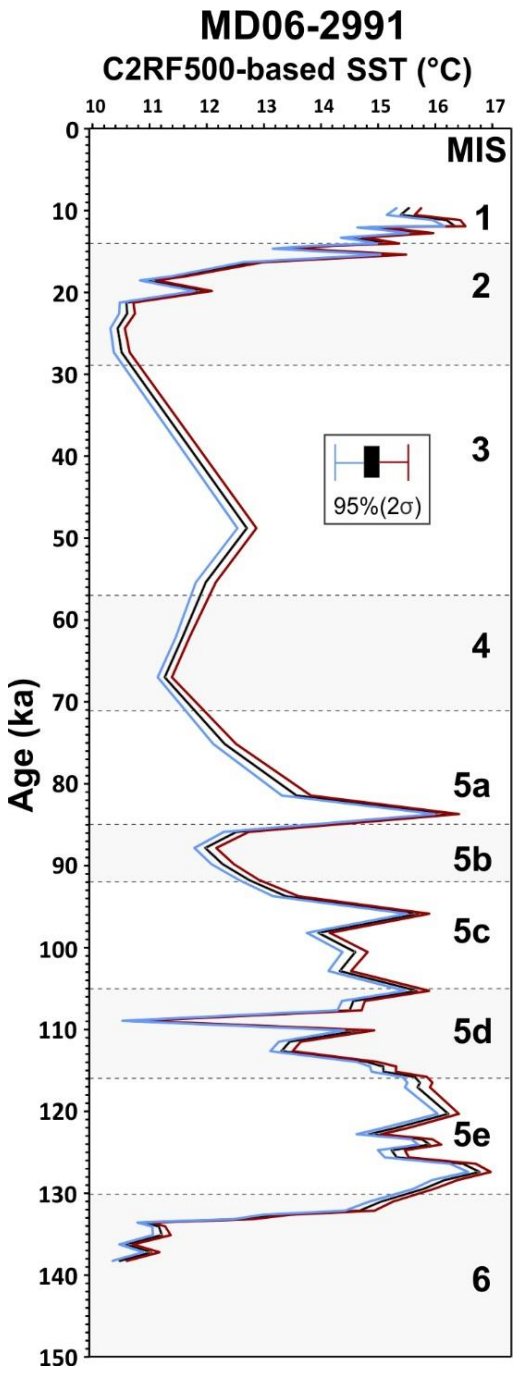

Supplementary Fig. 4.9: The 95% confidence interval for the mean C2RF500 estimates was calculated using the equation supplied by Cortese et al. (2013): 95% C.I = x± tcrit * (σ/sqrt (n)), where x = the average SST (for each sample, this average is based on the values provided by the 500 Random Forests trees we generated); σ = the standard deviation of this average; the tcrit value (obtained from a table of the t distribution, based on a 95% confidence level, two tails, for 499° of freedom, corresponding to 1.96), and the square root of n = the number of observations (in our case 22.36, which is the square root of 500). The MIS boundaries of the LR04 benthic $\delta^{18}O$ stack of Lisiecki and Raymo (2005) are shown, where the MIS glacial stages (6, 4 and 2) and the sub-stages (MIS 5d and 5b) are represented in grey shading. These are potentially an underestimate of the true error, with the down-core error assumed to be larger due to factors including post depositional affects (dissolution, winnowing), and potential non-analogues (Cortese, 31 Oct. 2014).

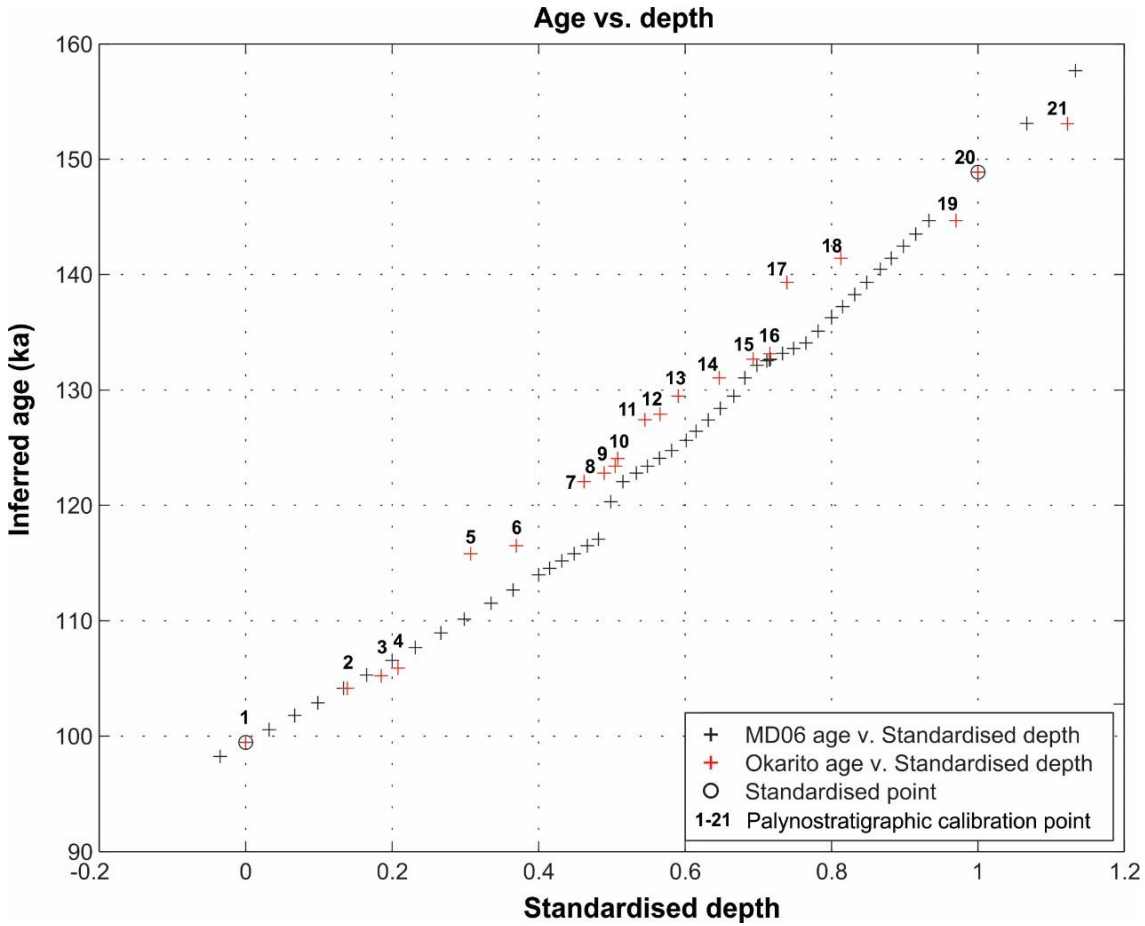

Supplementary Fig. 4.10: Illustration of the twenty-one palynostratigraphic calibration points (red) used to transfer the MD06-2991 age model to the Okarito Bog depth profile. Points were fixed close to either end of the Okarito depth profile were used to align the MD06-2991 chronology to the Okarito depth scale, producing a common, normalised depth scale [0 1] between the fixed points.

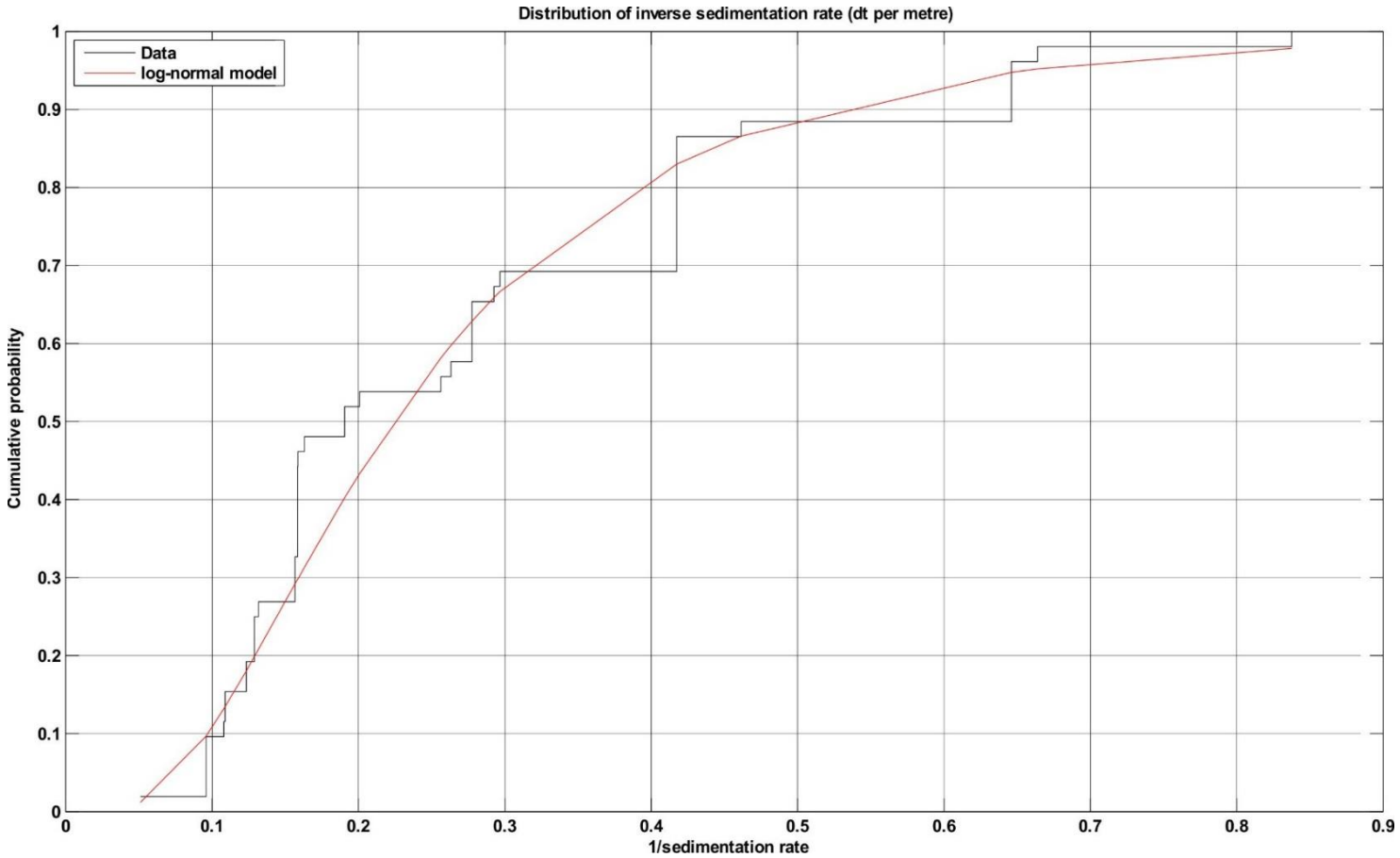

Supplementary Fig. 4.11: Distribution of the inverse sedimentation rate (dt per metre) for Okarito Bog. The data are well fitted by a log-normal model (red line). The largest sedimentation rate ~18 cm/kyr (lowest 1/sedimentation rate; ~0.05 in the fig) occurs at 805 cm (116.5 ka) and is determined substantially by the mid-point age calibration point 6 (115.8 ka, 791.5 cm). This represents <1% of the data and is, by inspection of the figure, consistent with the rest of the data.

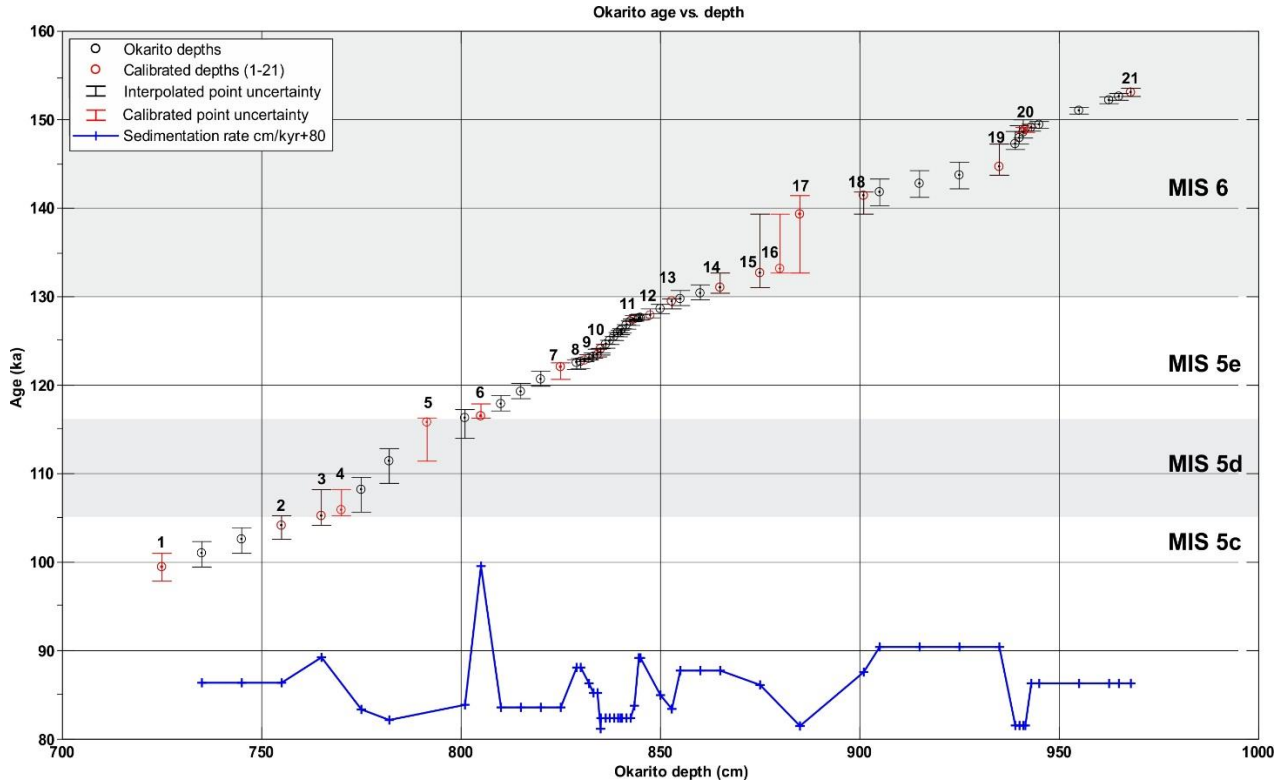

Supplementary Fig. 4.12: Age-depth model and associated age uncertainty for pollen sample depths from the Okarito Bog pollen profile. Twenty-one palynostratigraphic calibration points (red circles) from the MD06-2991 palynomorph profile were aligned to corresponding changes in the Okarito Bog palynomorph depth profile (Suppl. Fig. 4.13). The ages of Okarito Bog pollen depths situated between calibration points were determined by linear interpolation (black circles). The age uncertainty for calibration points assigned to the Okarito Bog record is derived from the ages of the bracketing pollen samples in the MD06-2991 record, except at the two end calibration points of the record where the errors are taken to be symmetric. The uncertainty for interpolated Okarito Bog depths (i.e. non calibration points) are the means of the errors at the bracketing calibration points, i.e. equal to the average of the errors of the two depth/age points for which they were calculated. The sedimentation rate (cm/kyr+80) is presented for Okarito Bog along the bottom of the plot (blue line).

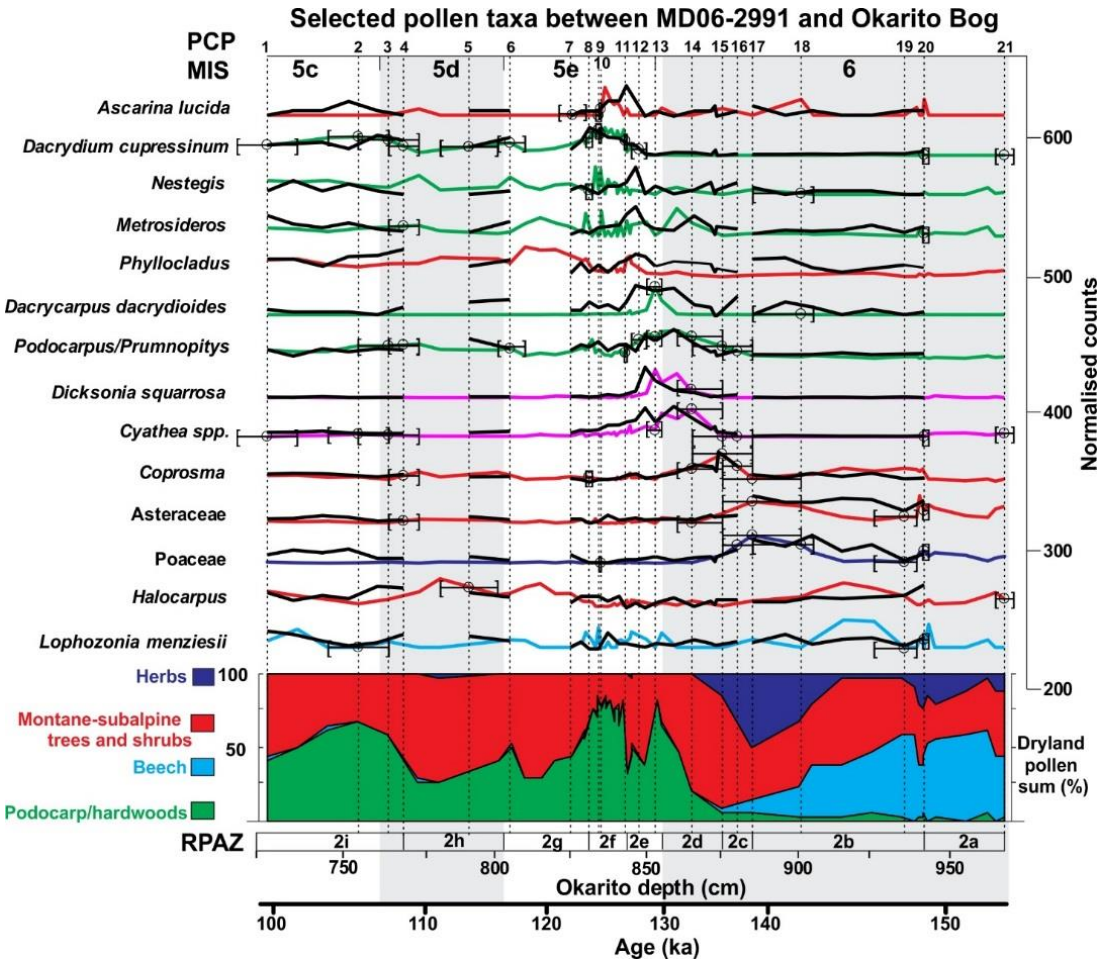

Supplementary Fig. 4.13: (previous page). Depth error bar model and comparison of palynomorph taxa between Okarito Bog and MD06-2991. The positions of the twenty-one palynostratigraphic calibration points (PCPs) used to transfer the MD06-2991 chronology to the Okarito Bog stratigraphy are numbered (top) and are displayed on the Okarito Bog taxa (black open circles). Okarito Bog pollen taxa are coloured to each dryland pollen category in the dryland pollen sum. MD06-2991 taxa (black line) are standardised to the Okarito depth record (968-725 cm), with each record's taxa normalised to 1 over this sequence. This period is equivalent to 153-98 ka. Groups of PCPs (1-4, 5-6, 7-16, 17-20), with approximately uniform sedimentation rates were selected from this timescale. Uncertainties (black cross hairs) are conservative estimate of the 95% C.I. MIS boundaries follow Lisiecki and Raymo (2005), with the MIS 6 glacial and MIS 5d stadial outlined in grey. Regional pollen assemblage zones (RPAZ) 2c-2e are displayed.

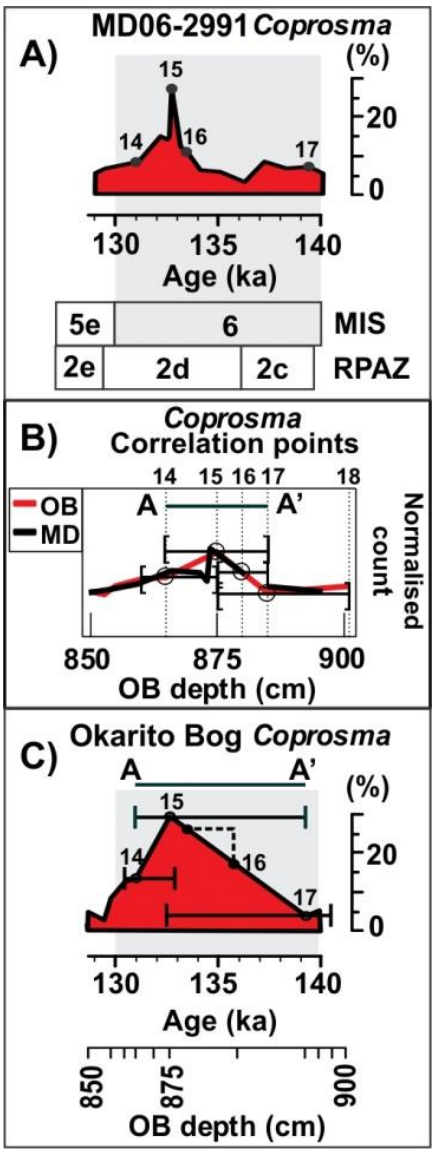

Supplementary Fig. 4.14: Schematic displaying the transfer of PCPs from MD06-2991 (MD) to generate the chronology and uncertainty for Okarito Bog (OB) over ~T-II. **A.** The relative abundance of *Coprosma* in MD, PCPs 14-18, MIS boundaries (Lisiecki and Raymo, 2005), and RPAZ's; **B.** enlarged representation of the depth error bar model and comparison of the relative abundance of *Coprosma* between OB and MD (normalised to 1 over the complete 968-725 cm OB sequence) from Suppl. Fig. 4.10. PCP 14-17 are displayed with open black circles. Points 16 and 17 (red circles and uncertainties) mark the boundaries between two groups of PCPs (7-16 and 17-20) and is associated with an increase in the sediment accumulation rate in OB (Suppl. Fig 4.11-4.12). Uncertainties are the intervals between the bracketing OB sample points for PCP 14, 15 and 17, and the bracketing points of change for midpoints e.g. 16. For example, if the location of a peak in the relative abundance (i.e. calibration point 15) between OB data points (in this instance, PCP 14 and 17) is assumed a uniform random variable, then on the interval A-A', the 95% confidence interval for the peak is calculable, but is very close to points A-A'. So conservatively we have taken it to be points and A-A'; **C.** OB chronology and depth scale. Additional of Okarito Bog between PCP 15-17 in OB would help constrain the position of calibration point 16, as it presently is offset from that identified in the MD06-2991 record as it is a mid-point (dashed line identifies the offset).

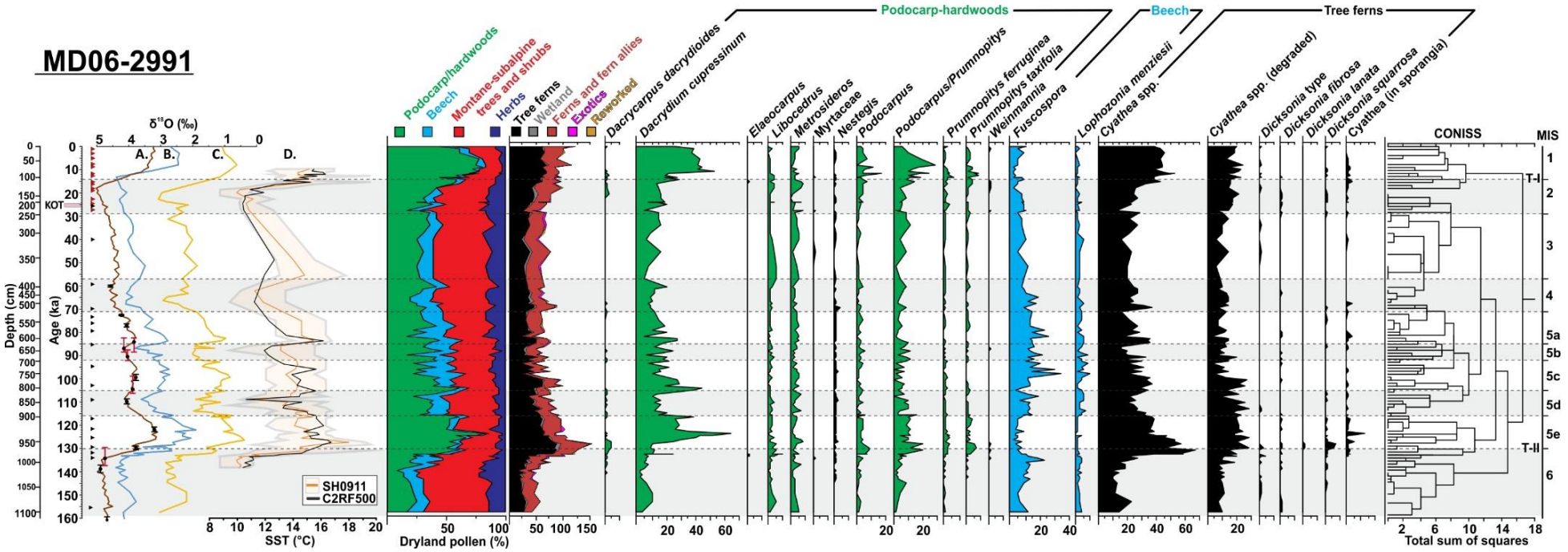

Supplementary Fig. 4.15: MD06-2991 chronology, SST estimates and palynology. **A.** Reference LR04 benthic $\delta^{18}O$ stack (Lisiecki and Raymo, 2005), and corresponding tie-points (black triangles) applied to; **B.** benthic $\delta^{18}O$ stratigraphy of MD06-2991. This aligns **C.** planktonic $\delta^{18}O$ curve; and **D.** faunal-SST estimates from MAT (1σ error) and RF-based approaches. The pollen diagram is shown in three parts: (1) trees; (2) shrubs and herbs; (3) wetland, aquatics, exotics, reworked taxa, ferns and fern allies. The CONISS zonation and the MIS glacial and stadial boundaries including terminations are displayed. The top section 28-0 ka of the MD06-2991 record is constrained by ^{14}C dating (red triangles), with the maximum position of the KOT shown.

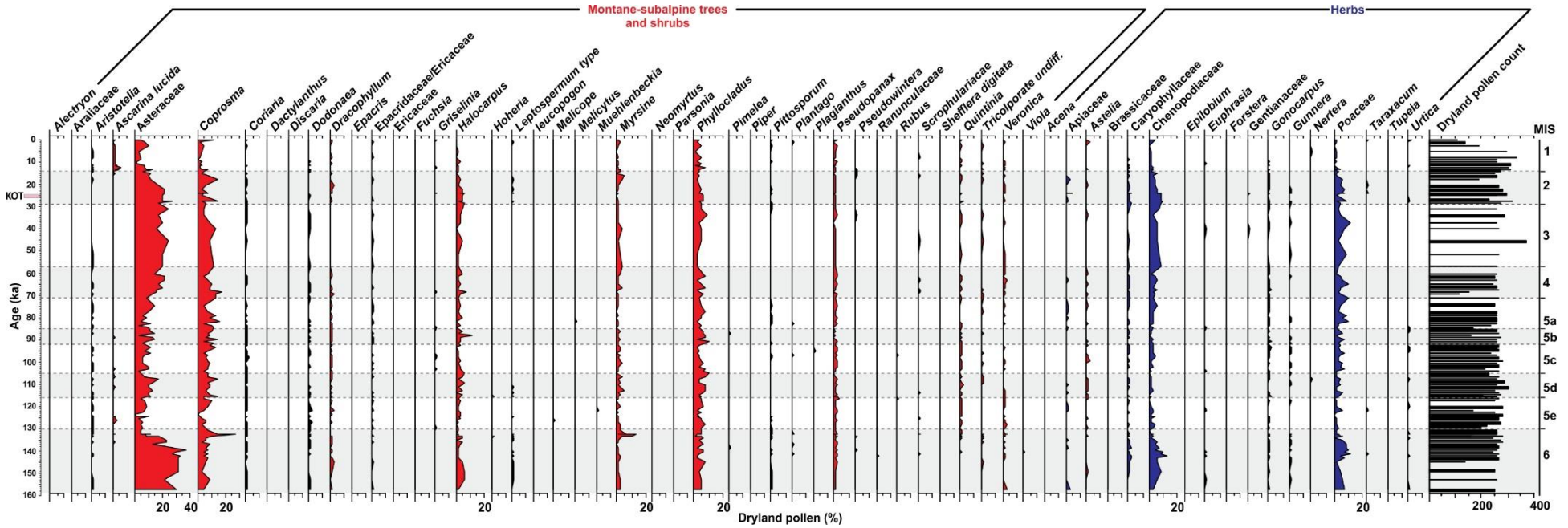

Supplementary Fig. 4.15. (*Continued*)

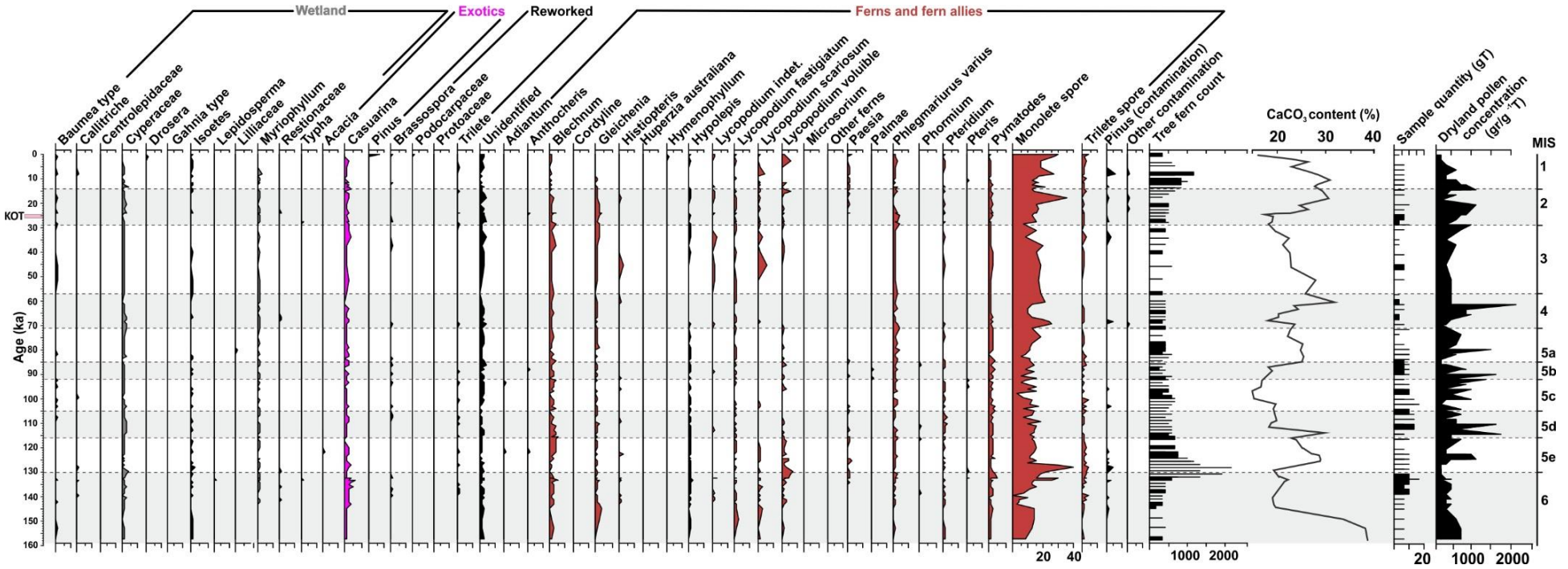

Supplementary Fig. 4.15. (*Continued*). The $CaCO_3$ content is excluded from the quantity of sample, producing the dryland pollen concentration in grains per gram of terrigenous sediment ($gr/g^{-1}T$).

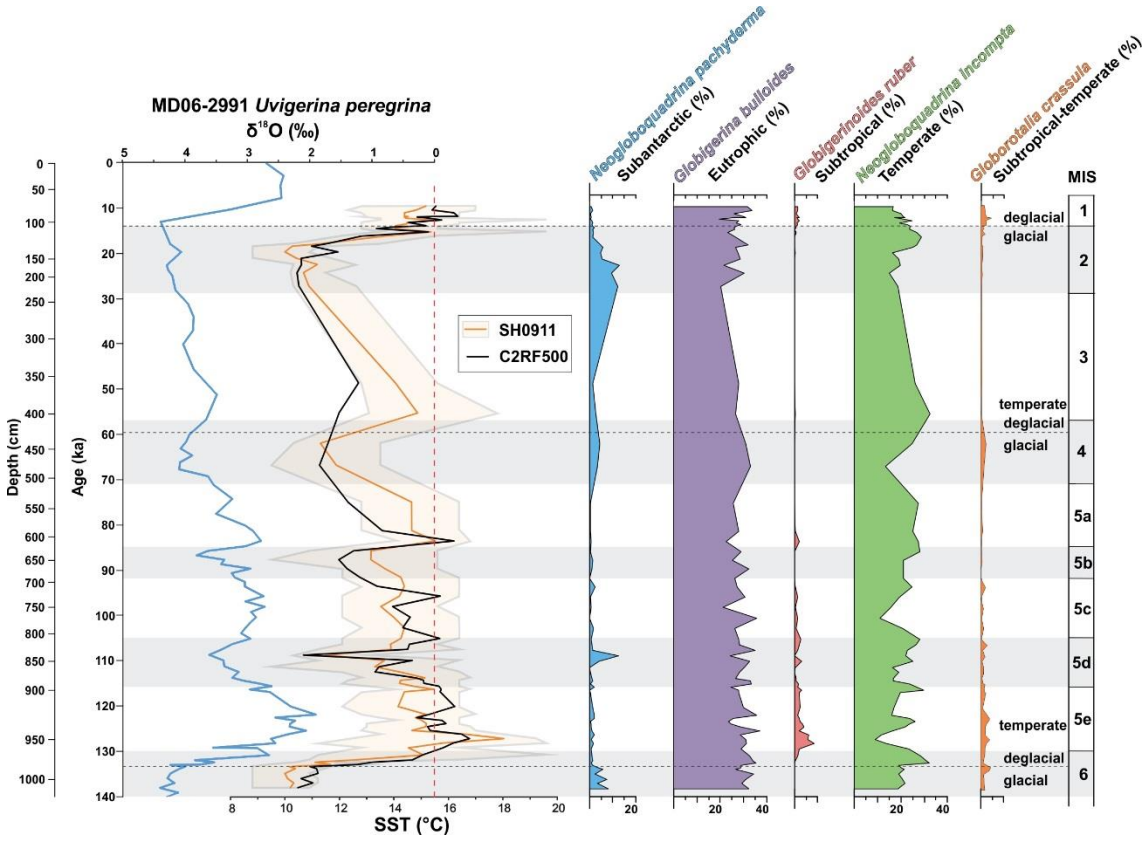

Supplementary Fig. 4.16: Variability in the dominant species in the biogeographic groups of Subantarctic taxa *(Neogloboquadrina pachyderma*), eutrophic (*Globigerina bulloides*), subtropical (*Globigeriniodes ruber*), temperate *(Neogloboquadrina incompta)*, and subtropical-temperate *(Globorotalia crassula)* across MIS 6-1. The blue line represents the benthic $\delta^{18}O$ for MD06-2991; the orange (MAT-5 of the 5 nearest analogues) and grey (C2RF500) lines represent the SST reconstructions from MD06-2991. The red-dashed line is the present mean annual SST at the MD06-2991 core site. The dominant species in each group follows that of Crundwell et al. (2008), with deglacial boundaries defined by variations in the transition of taxa, and the MIS boundaries of the LR04 benthic $\delta^{18}O$ stack (Lisiecki and Raymo, 2005) depicted (far right).

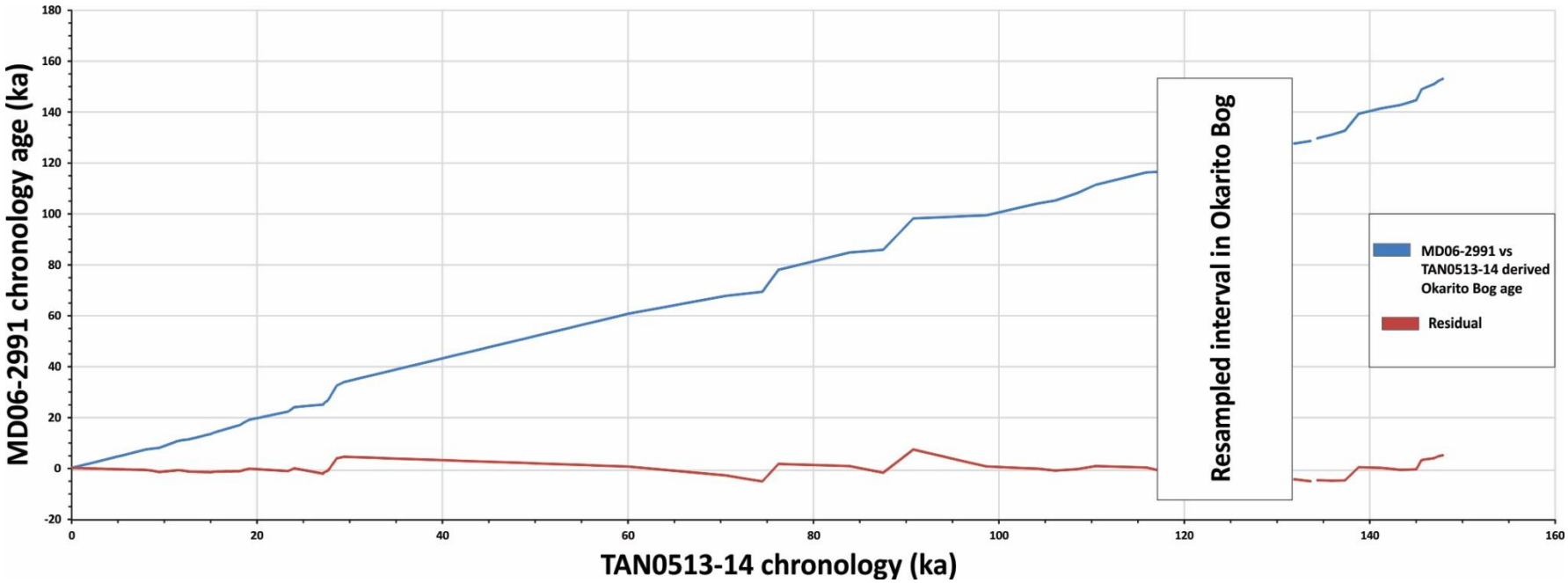

Supplementary Fig. 4.17: Comparison of Okarito Bog (OB) age models derived by palynostratigraphic approaches from the $\delta^{18}O$ dated MD06-2991 record (this study) and that from TAN0513-14 (Ryan et al., 2012). Positive residuals (red line) indicates that the MD06-2991 derived OB record is older than the TAN0513-14 derived OB record. Absent data points represent additional OB pollen samples subsequently calibrated to the MD06-2991 chronology.

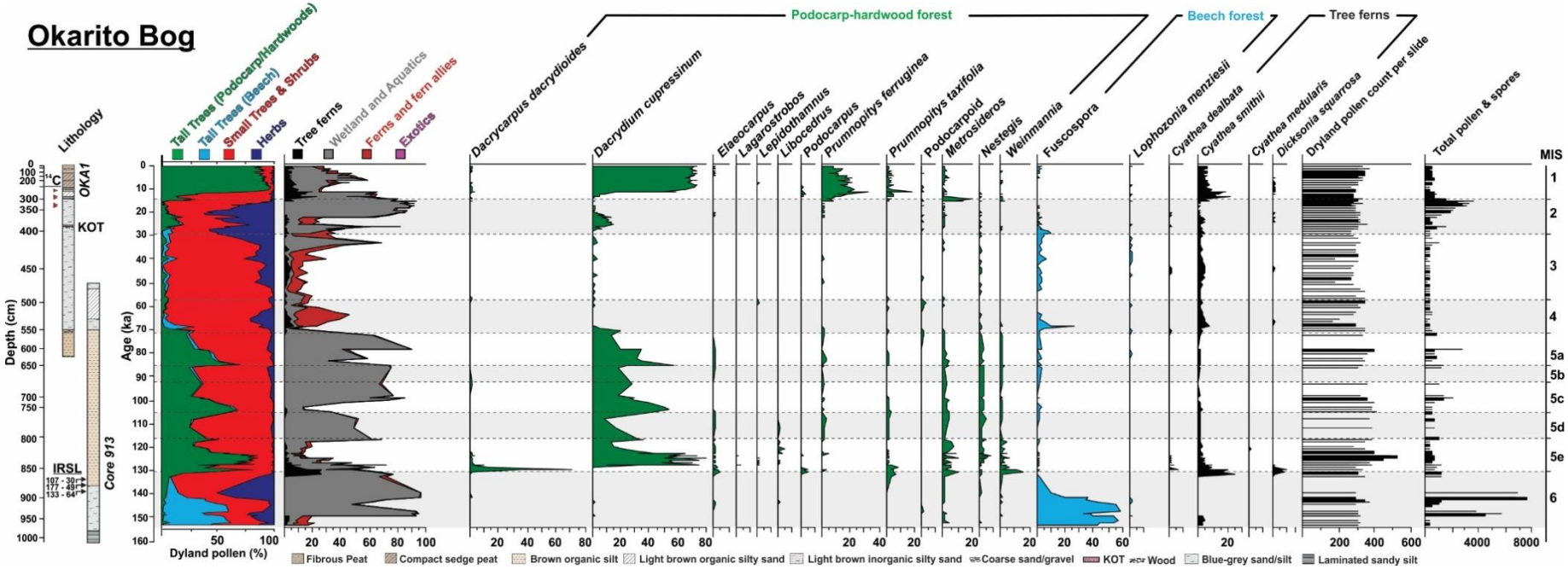

Supplementary Fig. 4.18: Revised Okarito Bog pollen percentage diagram in three parts: (a) trees; (b) shrubs and herbs; (c) wetland, aquatics, fern and fern allies. The depth scale is a composite of two pollen profiles developed from cores OKA1 and 913. The four red triangles located adjacent to the stratigraphy from core OKA1 represent ^{14}C dates which constrain the Okarito Bog chronology from 283 cm (10.93 ± 0.2 cal ka BP, 2σ) down to the location of the KOT at ~380 cm at which has been assigned the age of the Oruanui Eruption (25.62 ± 0.16 cal ka BP, 2σ). The topmost section (above 283 cm) is constrained by linear interpolation. Palynostratigraphic calibration points are applied to the MD06-2991 chronology in two sections; between 98-28 kyr and between 153-98 kyr (PCP 1-21), where the latter are discussed in text (Table 3.1). Independent chronological control for the lowermost brown organic silts and blue-grey sandy-silt was generated from infra-red stimulated luminescence (IRSL) and was translated to core 913 by Vandergoes et al. (2005), and contributes to a pooled weighted mean age of 127 ± 30 ka. This portion occurs between 133-139 ka from that of the MD06-2991 $\delta^{18}O$ stratigraphy. The MIS boundaries of Lisiecki and Raymo, (2005) are illustrated.

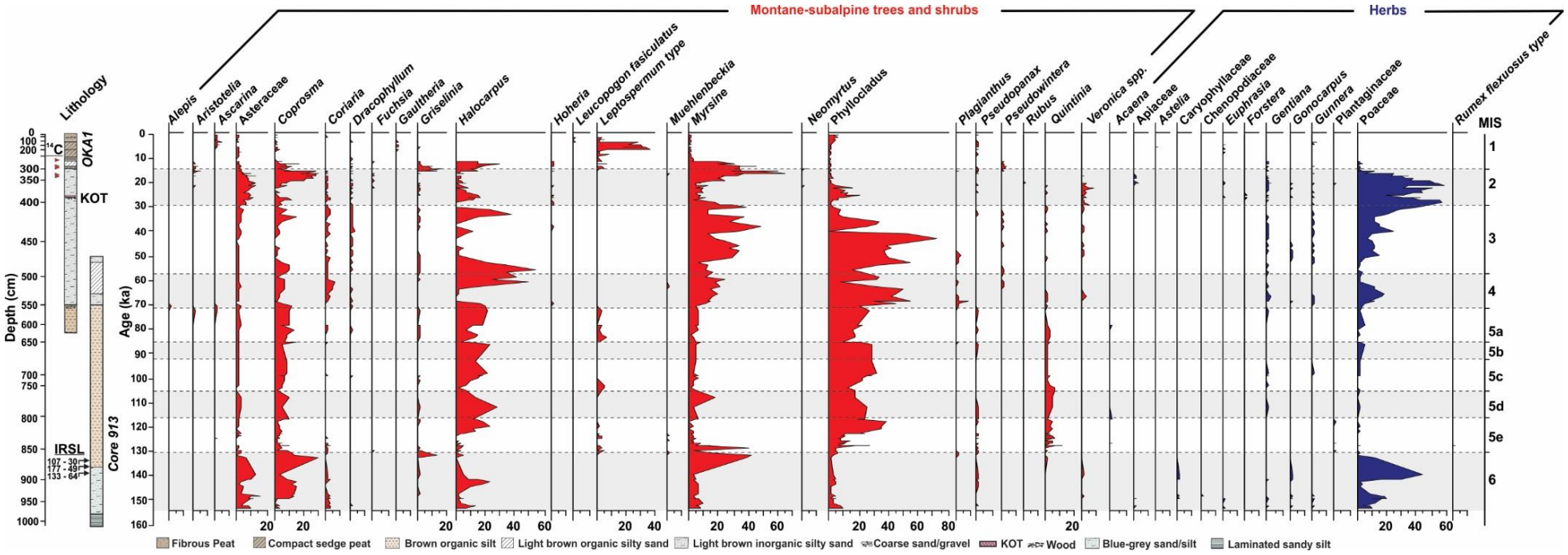

Supplementary Fig. 4.18: *(Continued).*

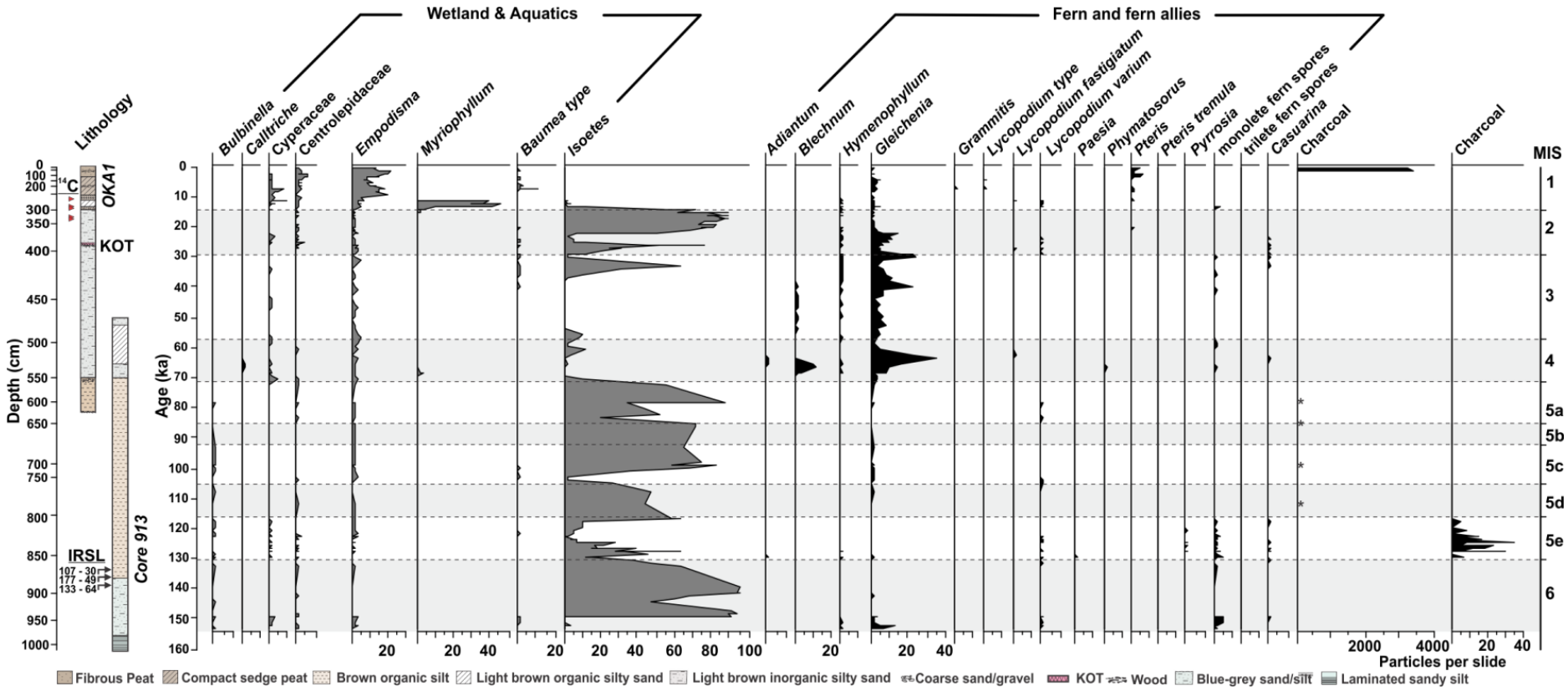

Supplementary Fig. 4.18: *(Continued).* Traces of charcoal for lower portion of the record indicated by asterisk.

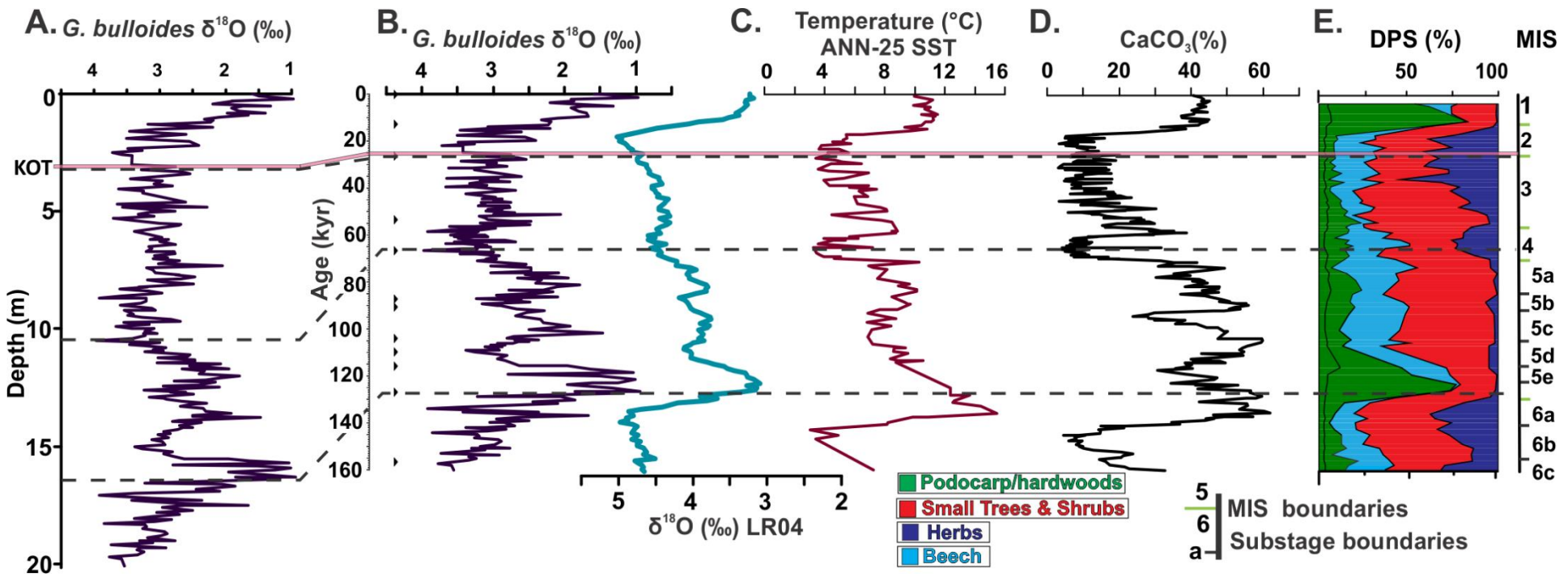

Supplementary Fig. 4.19: Revised age model for DSDP-594 and additional proxies following Ryan (2010). **A.** DSDP 594 $\delta^{18}O$ measurements on *Globigerina bulloides* from Nelson et al. (1993), and Dudley and Nelson (1994) against depth. **B.** The $\delta^{18}O$ measurements for DSDP Site 594 are tied to the reference LR04 $\delta^{18}O$ stack (light blue) of Lisiecki and Raymo (2005), with tie-points indicated by small black triangles. **C.** SST estimates of Hayward et al. (2008). **D.** $CaCO_3$ record of Nelson et al. (1986). **E.** Cumulative dryland pollen diagram with dryland pollen categories. Proportions of *Dacrydium cupressinum* are outlined by a black line in the podocarp-hardwood category.

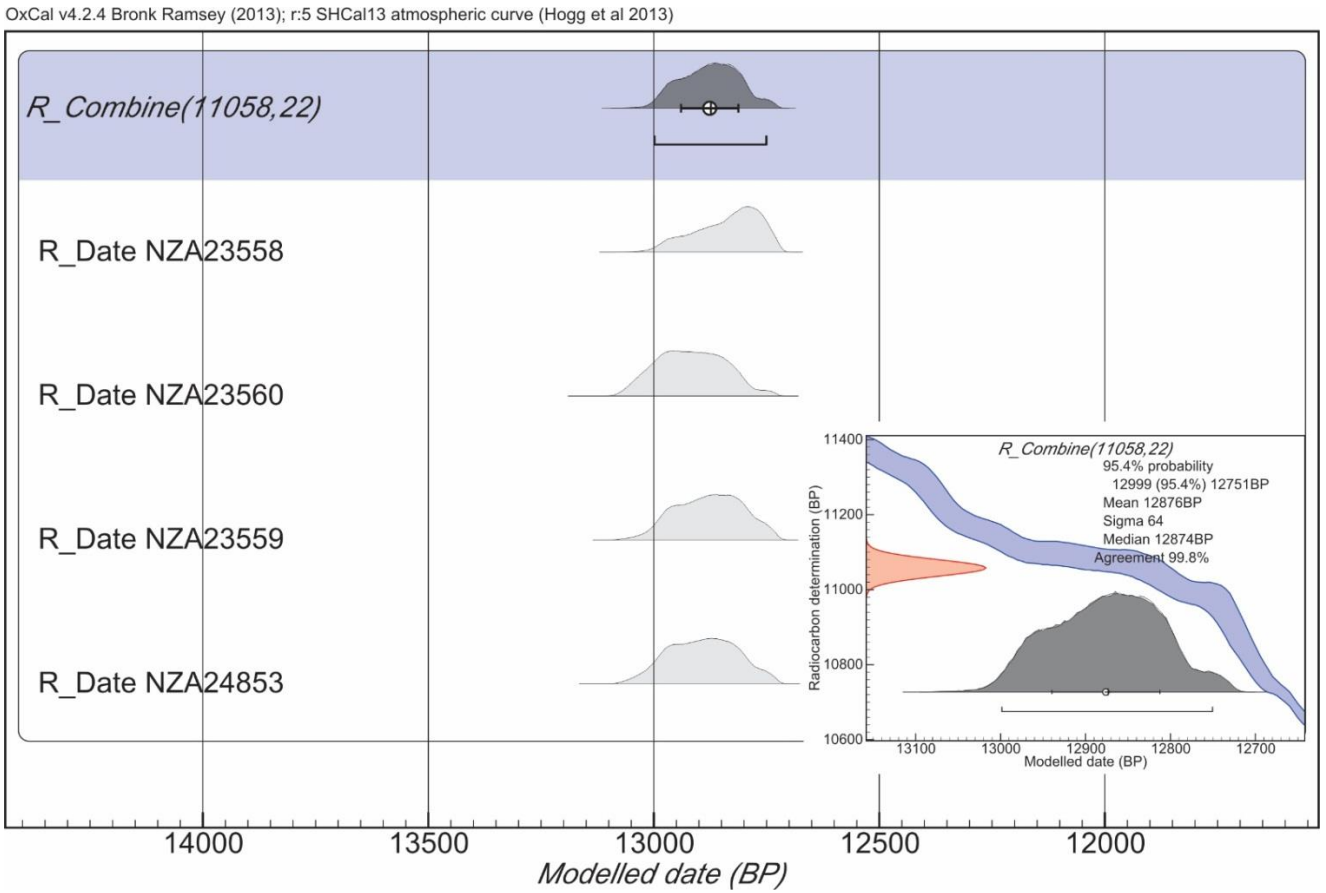

Supplementary Fig. 4.20: Probability distributions of calibrated radiocarbon (^{14}C) ages of wood (*Metrosideros cf. umbellata*) from glacial sediments preserved at Canavans Knob (Turney et al., 2007) using an *R_combine* function the calibration curve SHCal13 (Hogg et al., 2013) in OxCal v4.2.3 (Bronk Ramsey, 2009a). A general outlier model with a Student's *t* distribution with 5 degrees of freedom was performed (Bronk Ramsey, 2009a), with an agreement index of 60% as the rejection threshold. No samples were rejected, producing an age of 12876 ± 128 (2σ) cal yr BP.

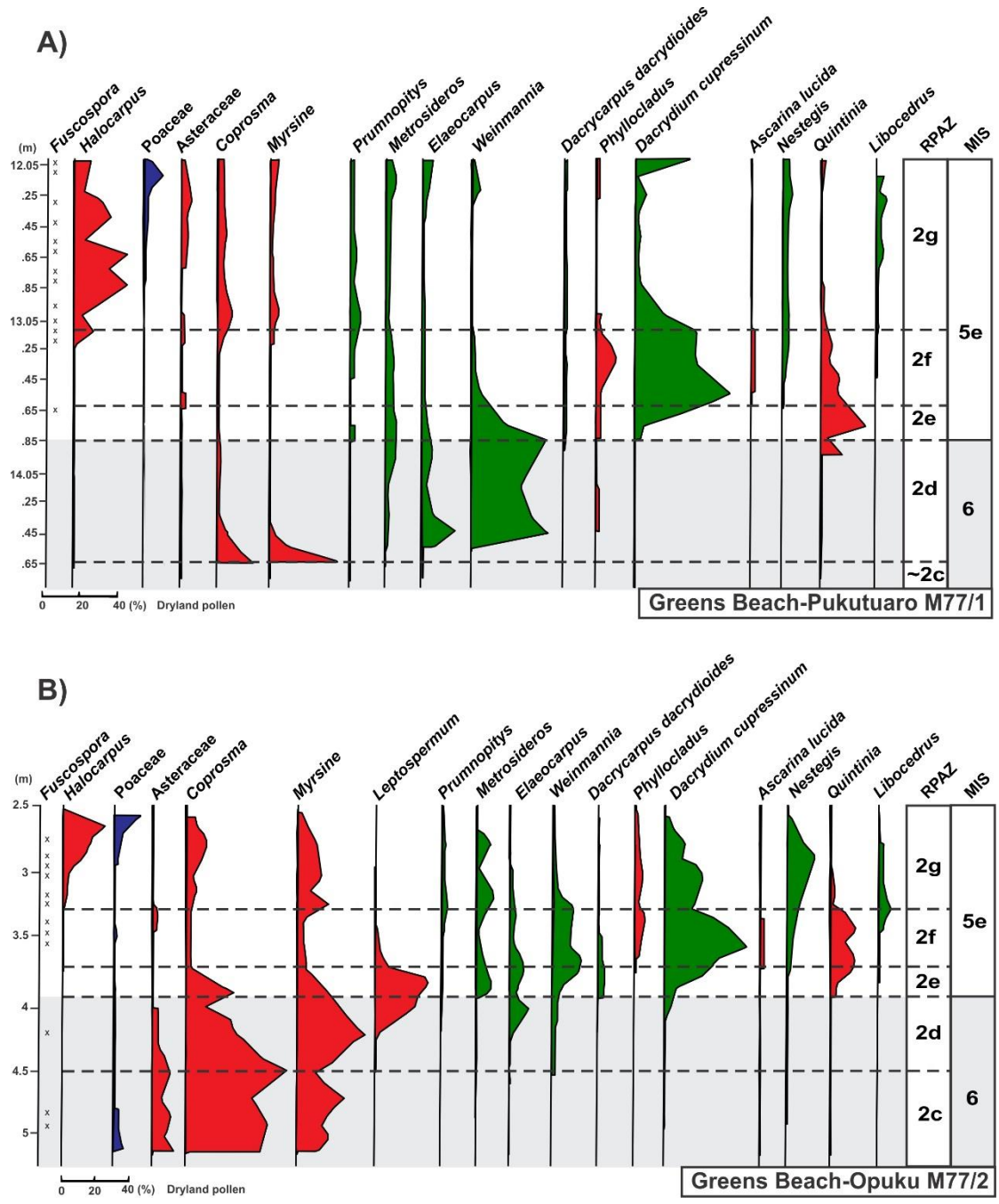

Supplementary Fig. 4.21: Partial percentage pollen diagram showing the prominent pollen taxa for **A.** Pukutuaro (M77/1) at the southern end of Greens Beach and **B.** Opuku (M77/2) at the northern end of Greens Beach (Fig. 4.2), modified from Moar and McKellar (2001). The relative positions of the regional pollen zones and tentative position of the MIS 6-5e boundary corresponding to 130 ka is displayed for each.

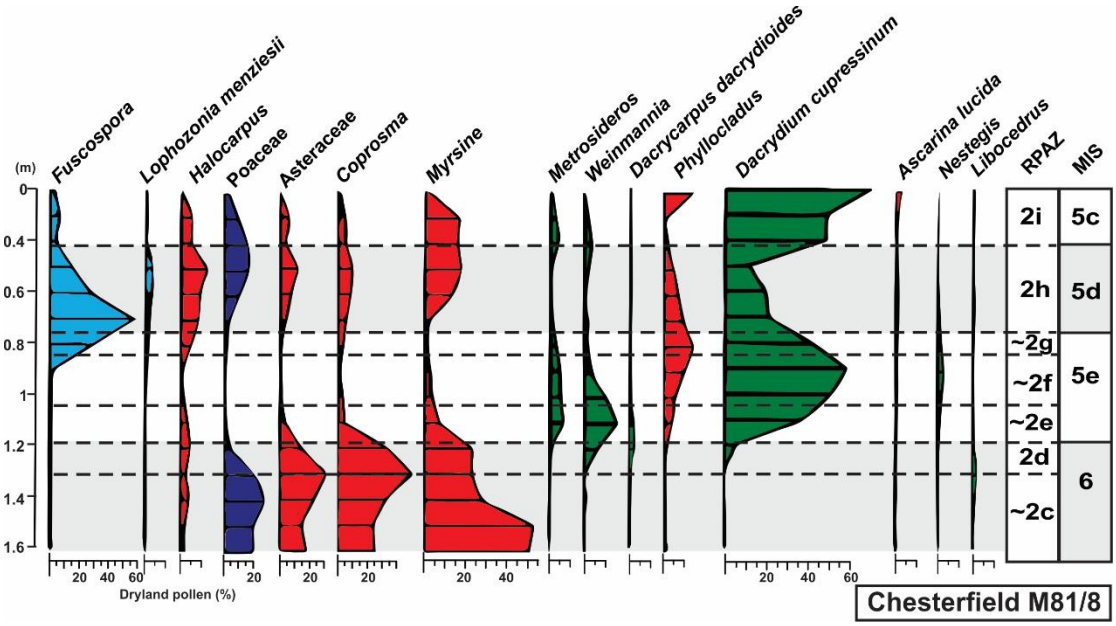

Supplementary Fig. 4.22: Pollen diagram showing the prominent dryland pollen taxa at Chesterfield (M81/1), situated 15 km NE of Hokitika on the lower Waimea (MIS 6) terrace (Fig. 4.2), modified from Moar and Suggate (1996). The profile contains no breaks in the record, with the relative positions of the regional pollen zones from RPAZ-2c-2g displayed. The glacial and stadial boundaries of MIS 6 (130 ka) and 5d (116-105 ka) of Lisiecki and Raymo (2005) are displayed in grey shading.

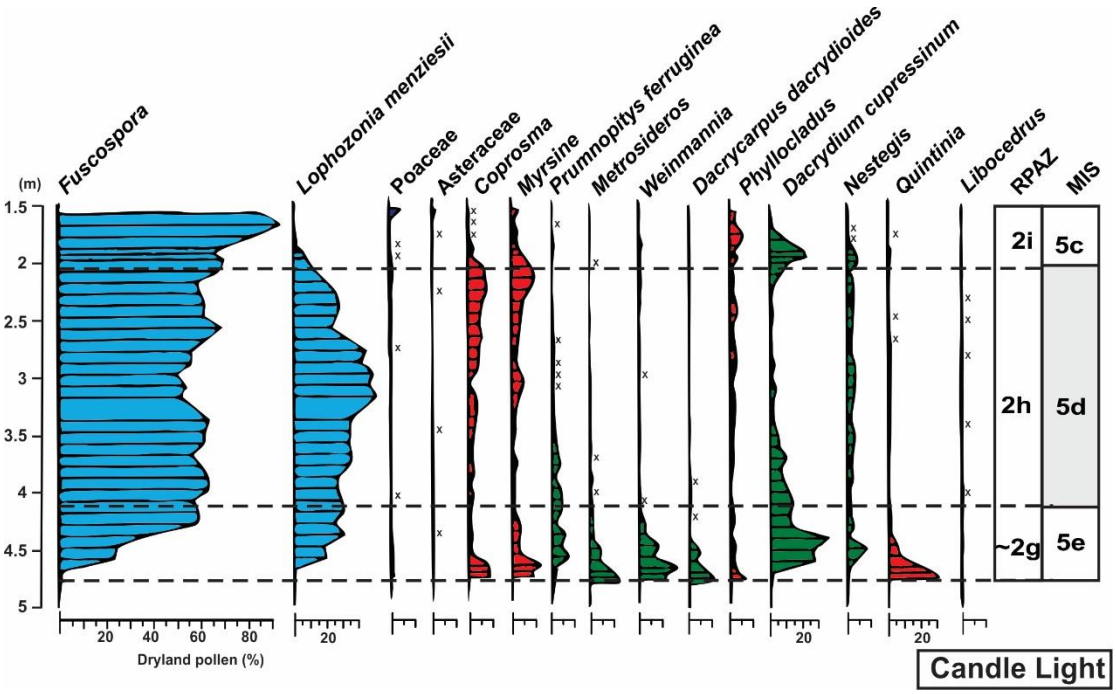

Supplementary Fig. 4.23 Pollen diagram showing the prominent dryland pollen taxa at Candle Light, situated ~25 km NE of Hokitika in a beach sand hollow following high sea level shoreline retreat, modified from Moar and Suggate (1996). The relative positions of the regional pollen zones from RPAZ-2c-2g displayed. The stadial boundary of MIS 5d (116-105 ka) of Lisiecki and Raymo (2005) is displayed in grey shading.

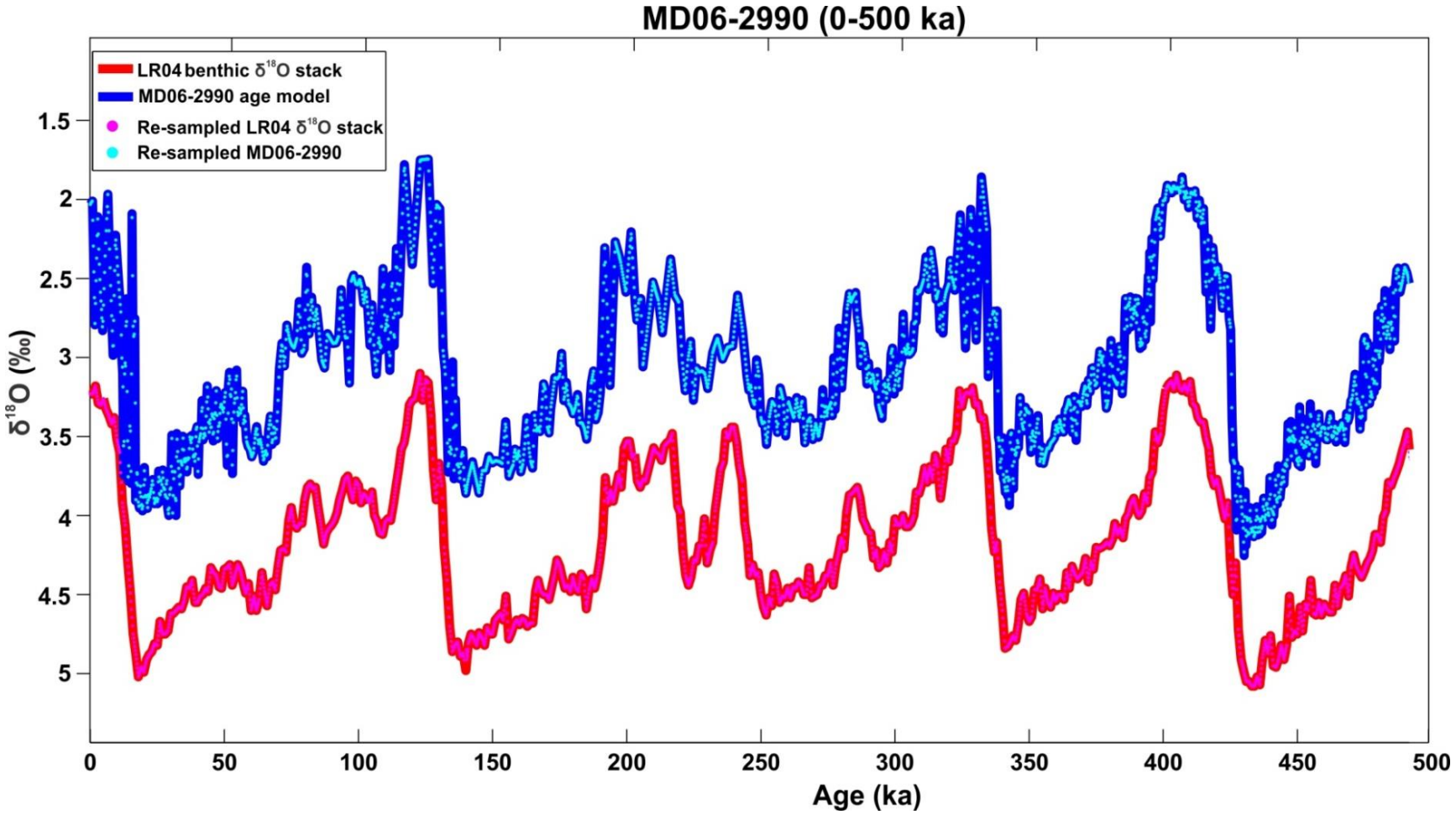

Supplementary Fig. 5.1: Original and resampled ^{18}O curves for LR04 (red, bottom) and MD06-2990 (blue, top) for the interval ~500-0 ka. The number of data points for MD06-2990 and LR04 are 770 and 496 respectively. Thus the resampled data points have at least 496 degrees of freedom.

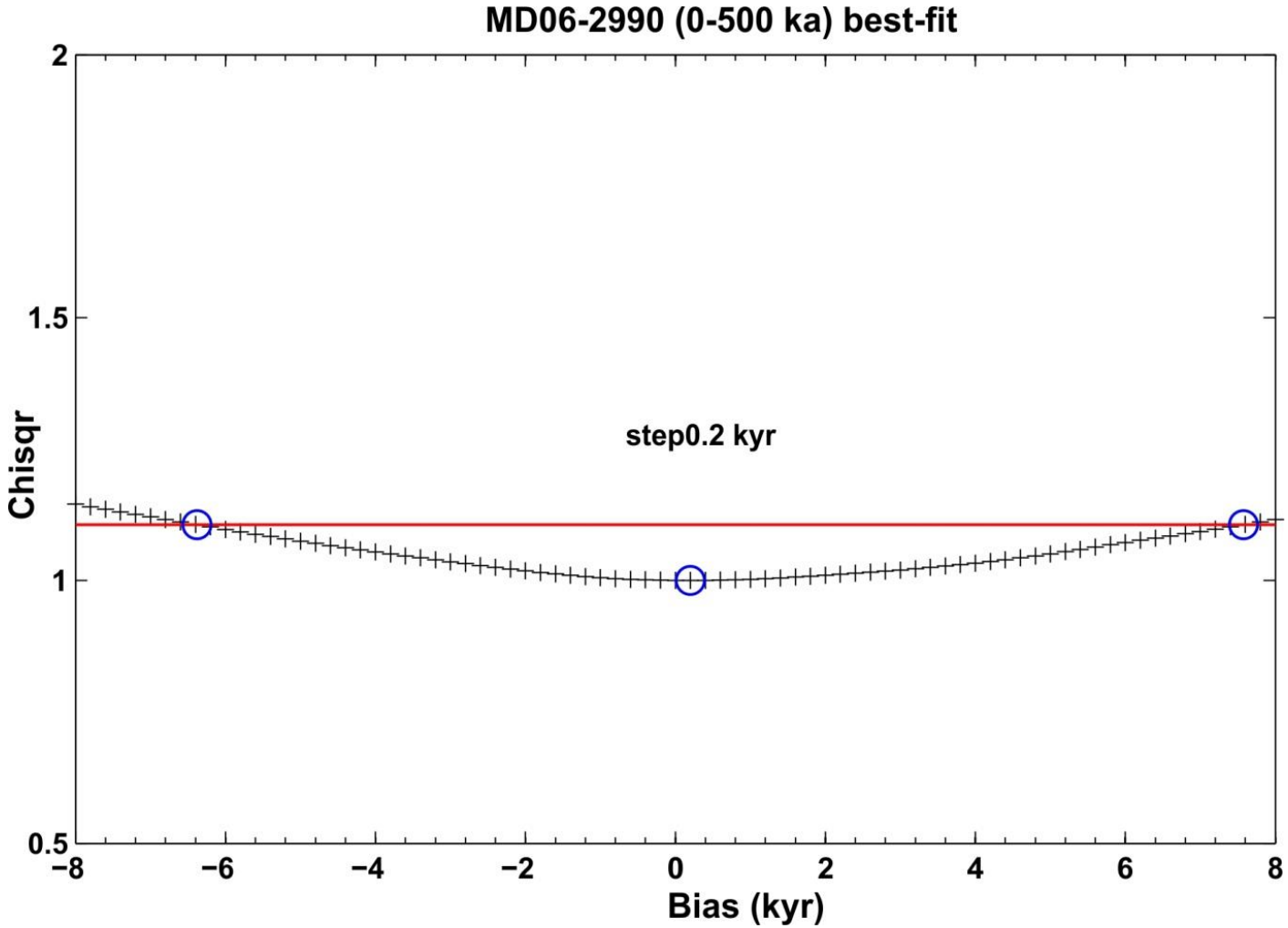

Supplementary Fig. 5.2. The optimum offset is 0.2 kyr (95% CI, ± 6 kyr). The bias is not significantly different from 0. Here the red line is drawn at χ^2 (95%, 496df)/496 = 1.11.

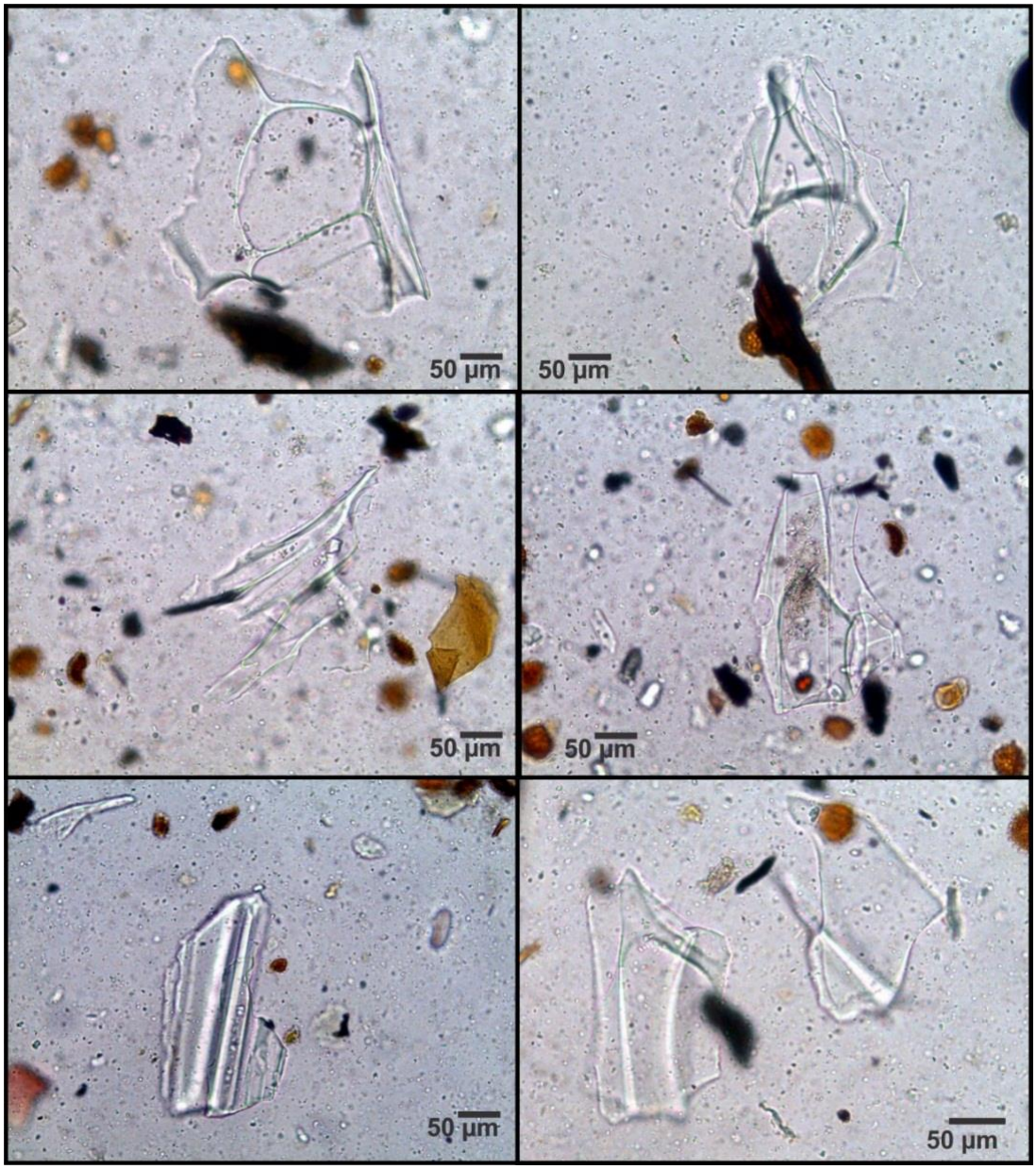

Supplementary Fig. 5.3: Colourless and vesicular cuspate Rangitawa Tephra (RtT) glass shards in palynological slides (<2.0 g cm^3) from 2200.5-2201 cm core depth MD06-2991. This sample has the highest concentration (~350 shards/g^{-1}) of >50 µm glass shards and correspond to an age of 346 ka.

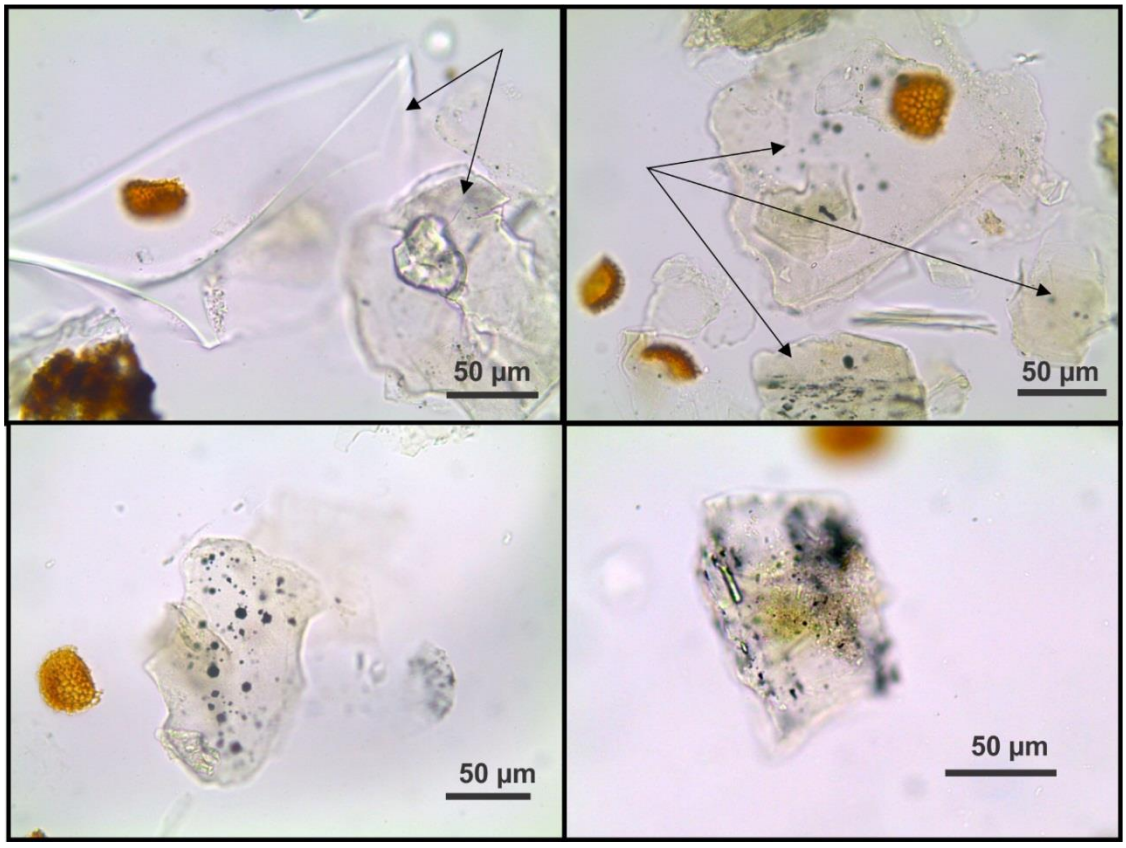

Supplementary Fig. 5.4: Glass shards containing mineral inclusions are assigned to Rangitawa Tephra (RtT) in palynological slides (<2.0 g cm^3) from 932-931 cm at MD06-2990. The highest concentration (>6000 shards/g^{-1}) of >50 µm glass shards occurs at this depth and corresponds to 344.5 ka. Cuboid and pseudo-hexagonal structures are profuse at this depth, and likely represent titanomagnetite and ilmenite, respectively.

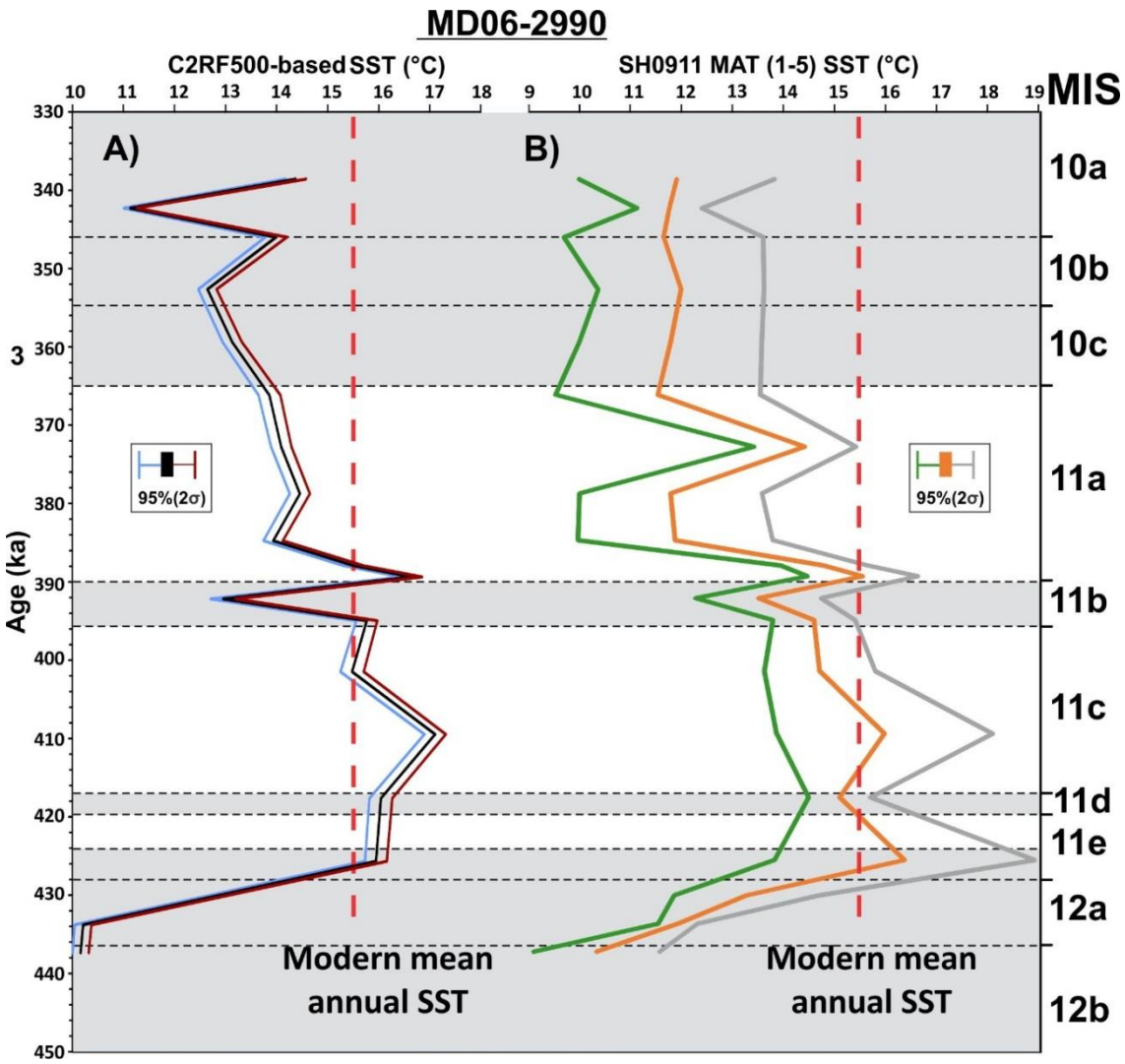

Supplementary Fig. 5.5: Uncertainty calculated for SST estimates for MD06-2990. **A.** The 95% confidence interval for the mean C2RF500 estimates was calculated using the equation supplied by Cortese et al. (2013): 95% C.I = x± tcrit * (σ/sqrt (n)), where x = the average SST (for each sample, this average is based on the values provided by the 500 Random Forests trees we generated); σ = the standard deviation of this average; the tcrit value (obtained from a table of the t distribution, based on a 95% confidence level, two tails, for 499° of freedom, corresponding to 1.96), and the square root of n = the number of observations (in our case 22.36, which is the square root of 500). These are potentially an underestimate of the true error, with the down-core error assumed to be larger due to factors including post depositional affects (dissolution, winnowing), and potential non-analogues (Cortese personnel communication, 2014). **B.** Mean SST from the five most similar training set faunas assigned to each test sample in the core set (using Chord coefficient of similarity), with 2σ uncertainty. The MIS boundaries of the LR04 benthic $\delta^{18}O$ stack of Lisiecki and Raymo, (2005) are shown, where the MIS glacial stages (12 and 10) and the sub-stages (MIS 11d and 11b) are represented in grey shading (Railsback et al., 2015).

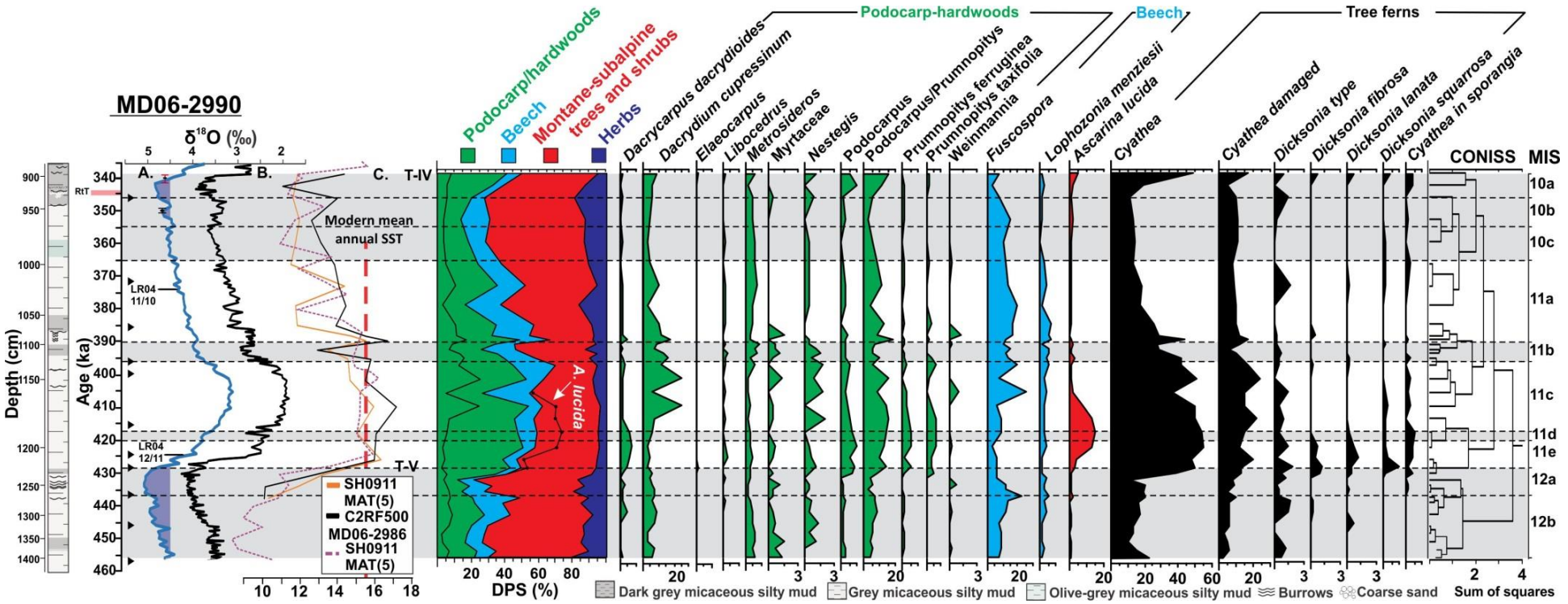

Supplementary Fig. 5.6: MD06-2990 chronology, SST estimates and palynology. **A.** Reference LR04 benthic $\delta^{18}O$ stack (Lisiecki and Raymo, 2005), with corresponding tie-points (black triangles) applied to; **B.** benthic $\delta^{18}O$ stratigraphy of MD06-2990. This aligns; **C.** faunal-SST estimates from MAT and RF-based approaches. The MD06-2986 SST estimates are displayed for comparison (Hayward et al., 2012). The maximum position of Rangitawa Tephra (RtT) is shown (far left). The pollen diagram is shown in three parts: (1) trees, including the shrub *Ascarina lucida*, with relative abundances outlined for MIS 11e-11c on the cumulative percentage diagram; (2) shrubs and herbs; (3) wetland, aquatics, exotics, reworked taxa, ferns and fern allies. The CONISS zonation and the MIS glacial and stadial boundaries including terminations T-V and T-IV are displayed following Railsback et al. (2015), with the intervals of "excess ice" of Raymo (1997) considered necessary to achieve a termination are shown (purple shading, >4.5‰). Uncertainties for the topmost section of the LR04 stack provided (Caballero-Gill et al., 2012a).

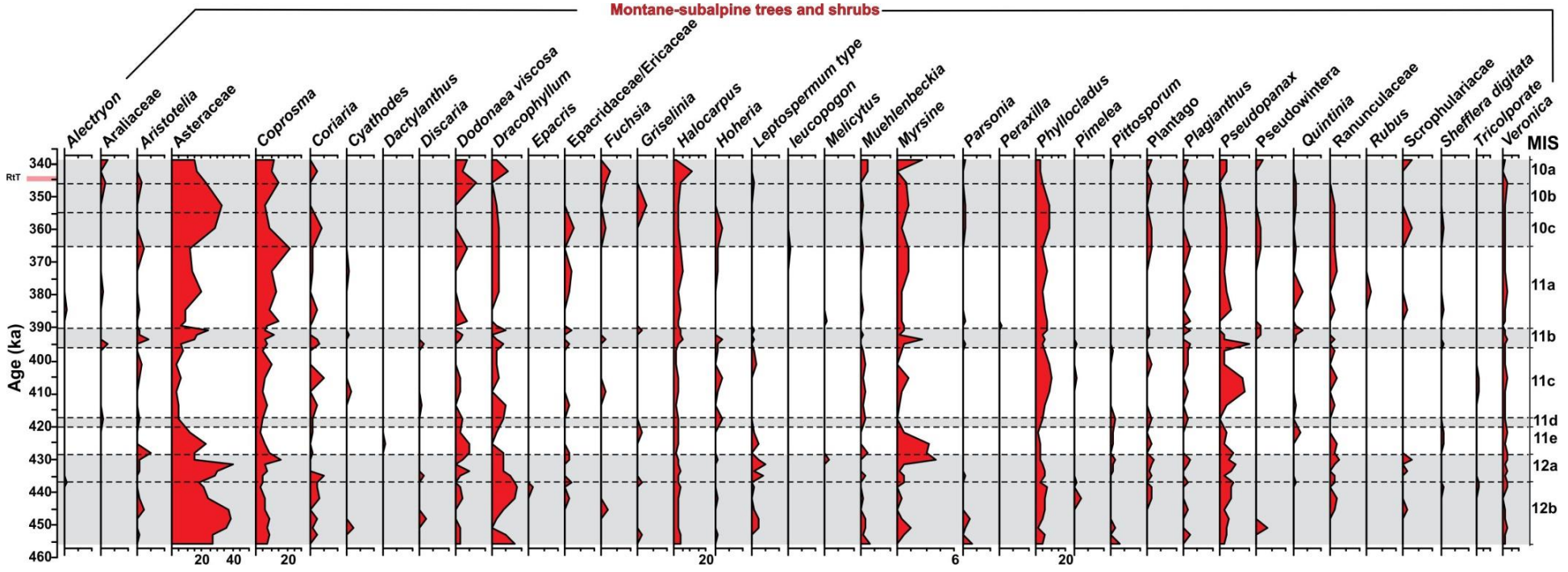

Supplementary Fig. 5.6: (*Continued*).

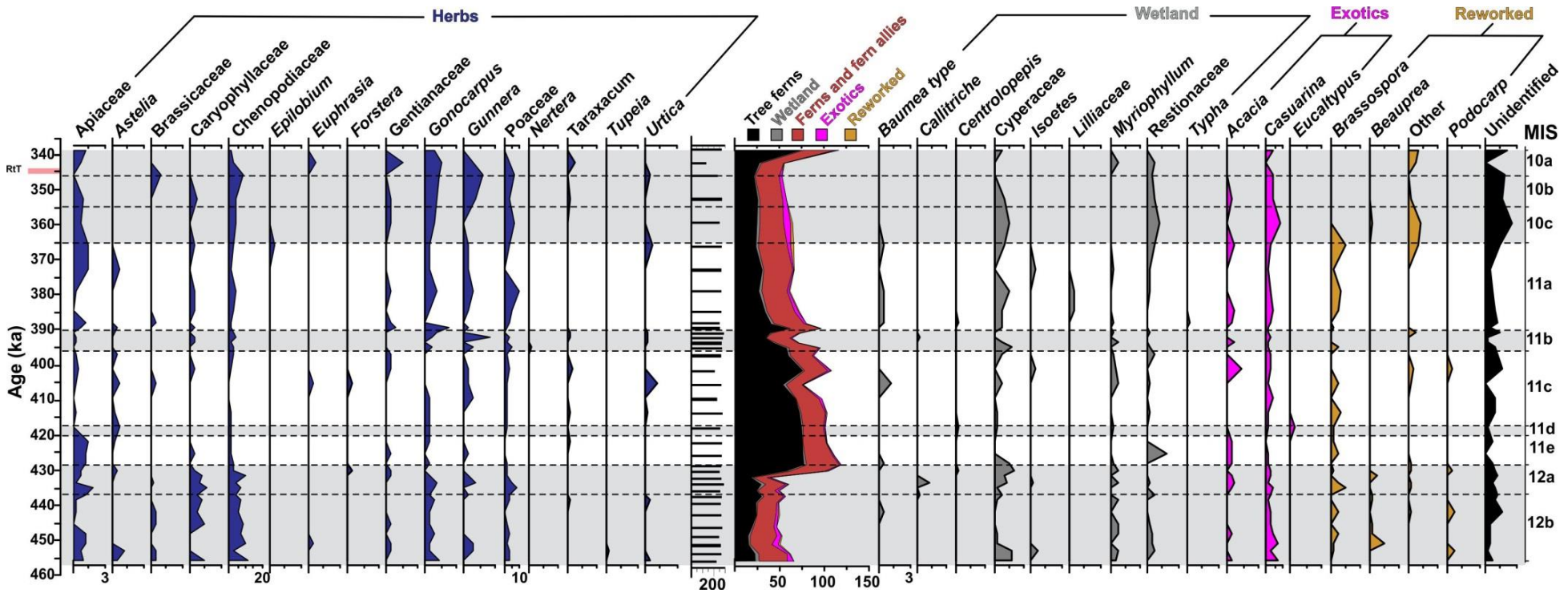

Supplementary Fig. 5.6: (*Continued*).

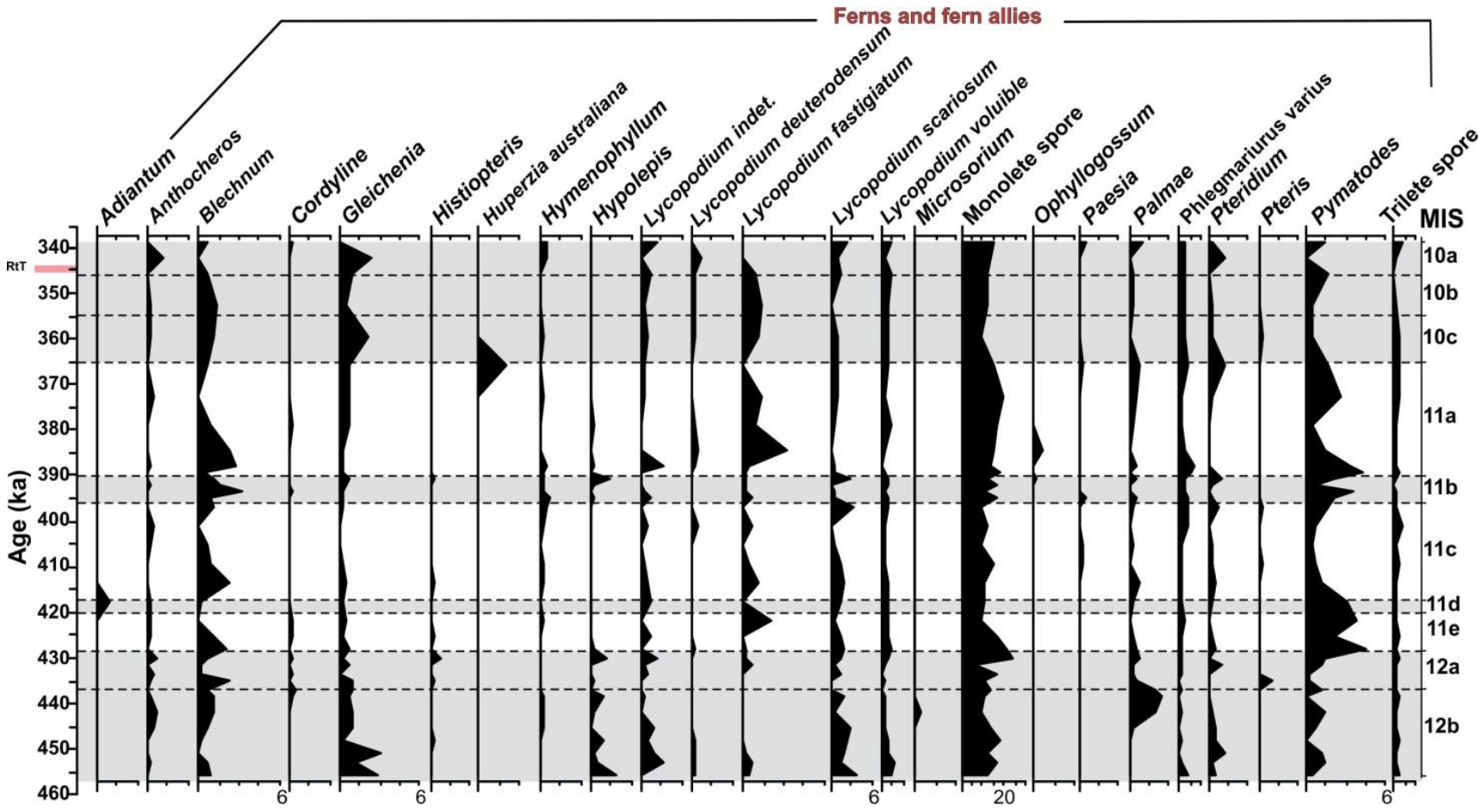

Supplementary Fig. 5.6: (*Continued*).

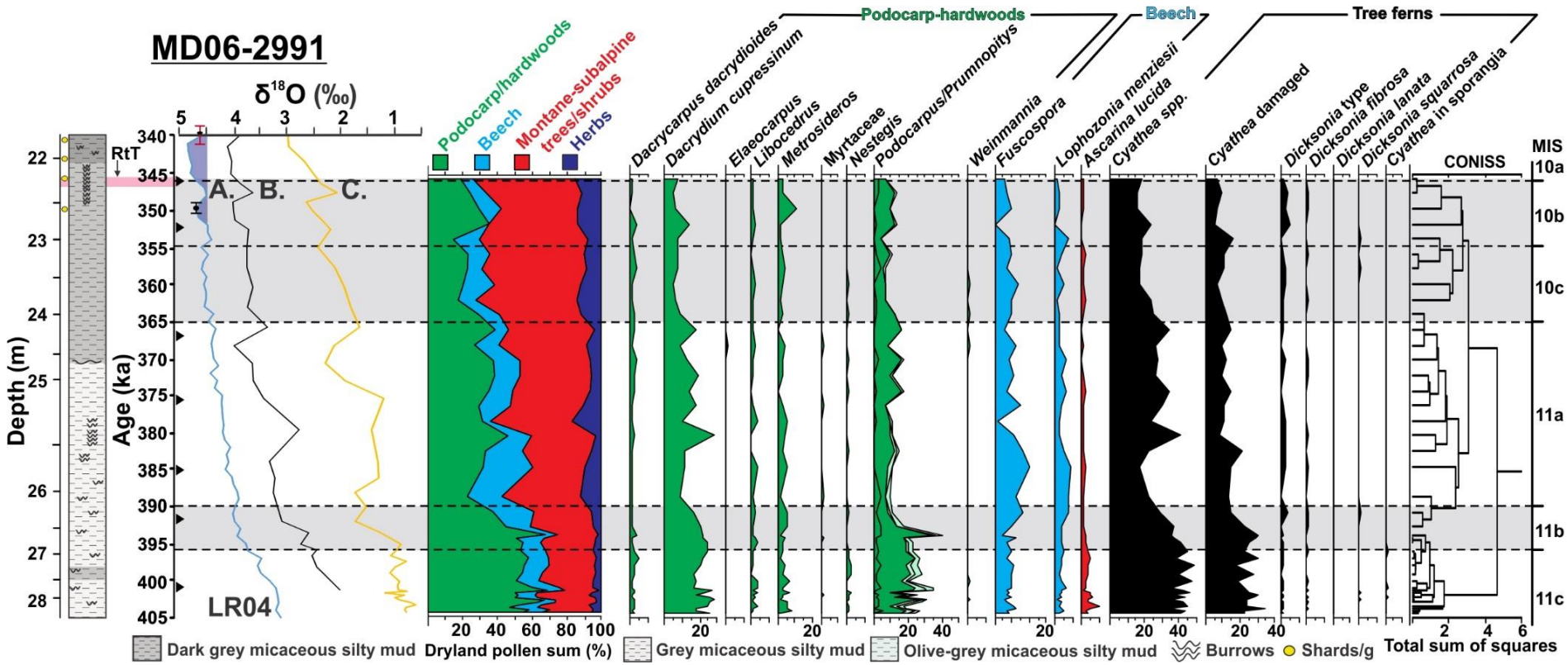

Supplementary Fig. 5.7: MD06-2991 chronology, SST estimates and palynology. **A.** Reference LR04 benthic $\delta^{18}O$ stack (Lisiecki and Raymo, 2005), with corresponding tie-points (black triangles) applied to; **B.** benthic $\delta^{18}O$ stratigraphy of MD06-2990. This aligns **C.** planktonic $\delta^{18}O$ stratigraphy and the pollen diagram which is displayed in three parts: (1) trees, including the shrub *Ascarina lucida*, (2) shrubs and herbs; (3) wetland, aquatics, exotics, reworked taxa, ferns and fern allies. *Podocarpus/Prumnopitys* are grouped with *Podocarpus* (green) and undifferentiated *Podocarpus/Prumnopitys* (light green), while *Prumnopitys ferruginea* and *Prumnopitys taxifolia* (both light green) are differentiated by a black line. The CONISS zonation and the MIS glacial and stadial boundaries are displayed following Railsback et al. (2015). Uncertainties for the topmost section of the LR04 stack are provided (Caballero-Gill et al., 2012a), with the intervals of "excess ice" of Raymo (1997) considered necessary to achieve a termination are shown (purple shading, >4.5‰).

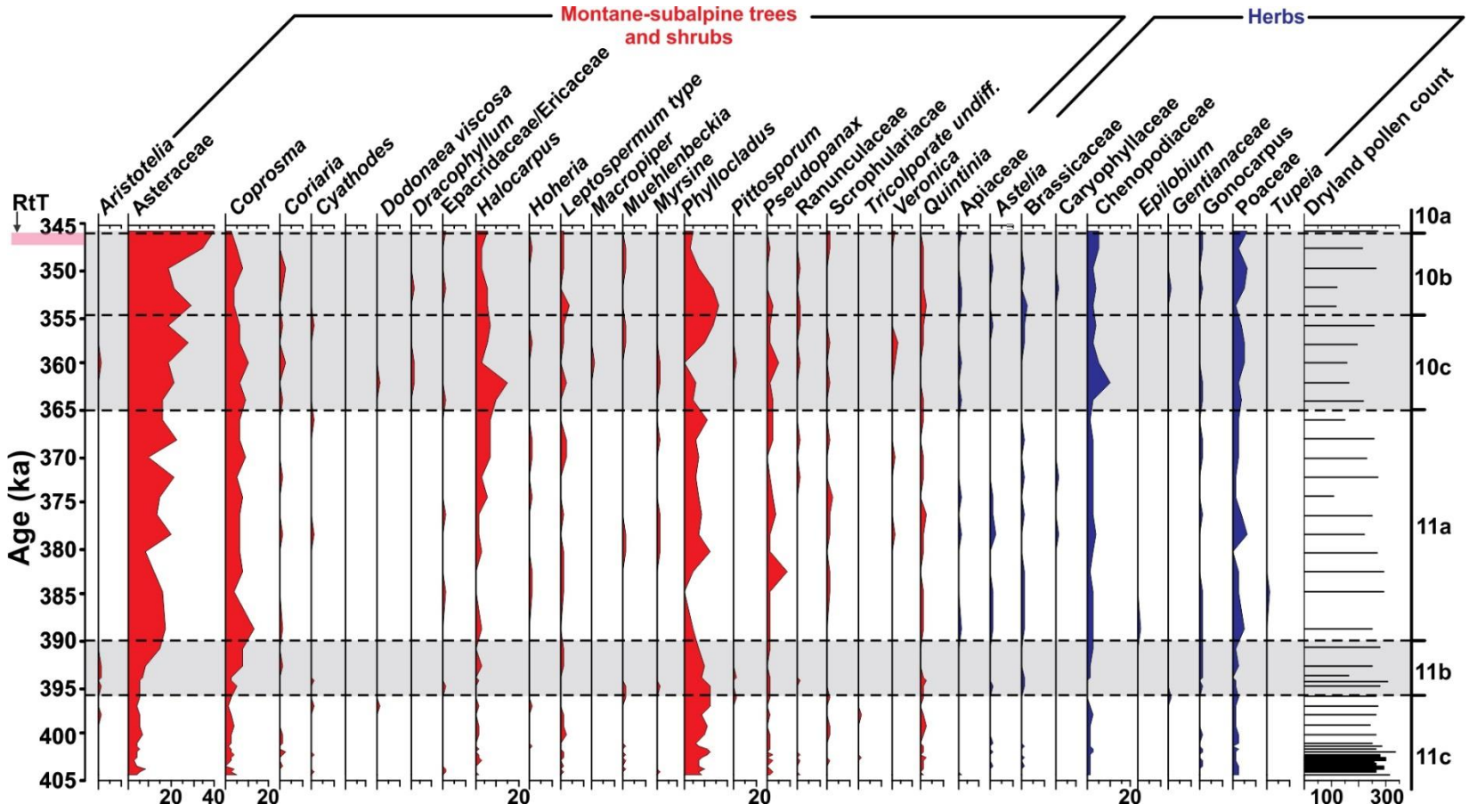

Supplementary Fig. 5.7: (*Continued*)

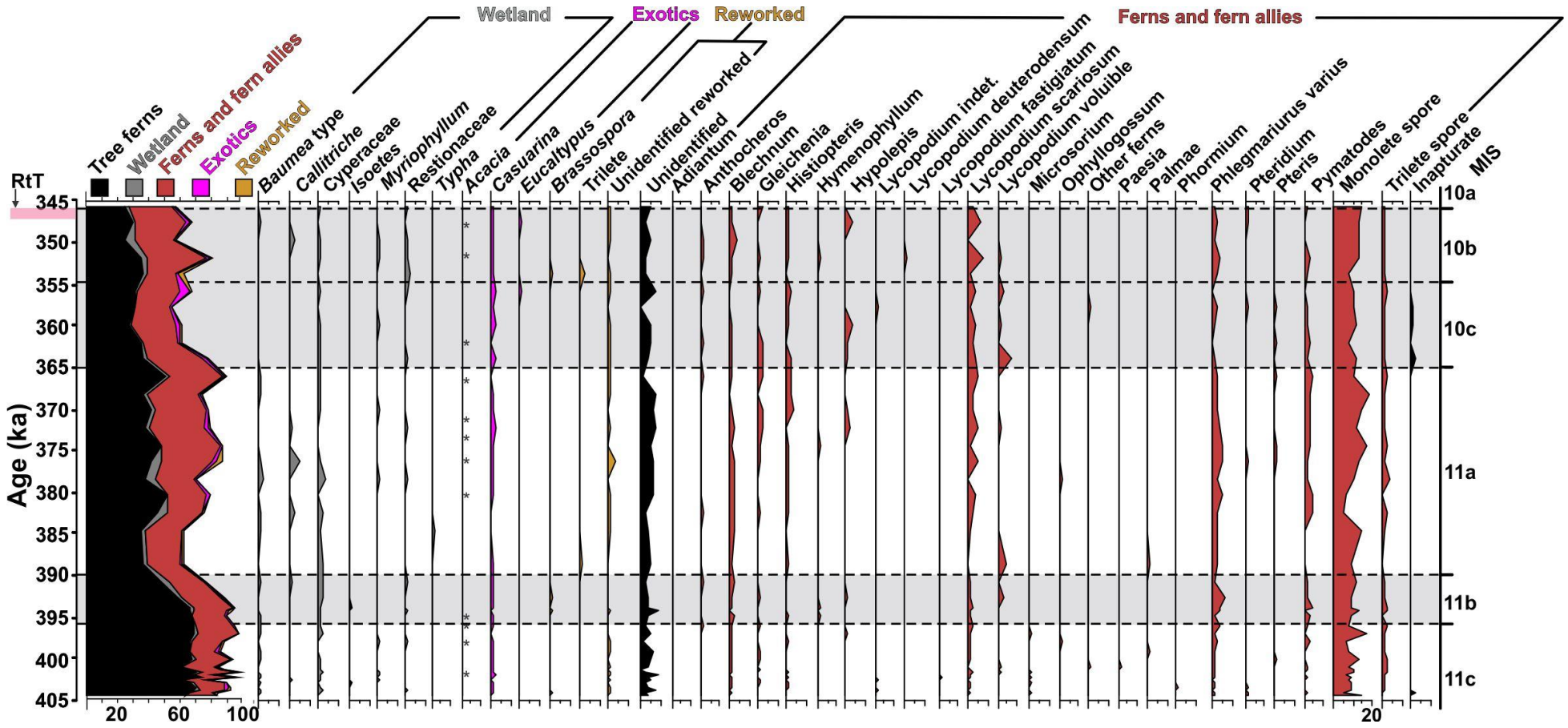

Supplementary Fig. 5.7: (*Continued*). (*) rare taxa.

Revision of DSDP Site 594 age model

In order to facilitate a robust comparison with the long joint pollen and SST record developed from DSDP-594 from the eastern South Island for MIS 12-10 (Hayward et al., 2012; Prebble et al., 2016), 21 *Uvigerina peregrina* samples and 39 samples of *Globigerina bulloides* from 47.87-32.95 mbsf were processed by the author. These were picked by Helen Neil, who conducted stable isotope ($\delta^{18}O$) measurements on 3-4 tests of foraminifera in each sample at NIWA. These samples greatly improve the temporal resolution compared to the existing low resolution $\delta^{18}O$ record (Nelson et al., 1993; Dudley and Nelson, 1994), to ~1 sample/2.3 ka for benthics between 442 and 338 ka (Suppl. Fig. 5.8; Suppl. Table 5.4). These data are presented alongside SST reconstructions for this interval by Prebble et al. (2016). DSDP Site 594 displays a similar pattern of high sediment rates during MIS 12 and MIS 10 as MD06-2990 with 25 and 17 $cm.kyr^{-1}$ respectively, which decreases to 15-17 $cm.kyr^{-1}$ during MIS 11 (Suppl. Table 5.2). High sedimentation rates during glacial periods have been considered to represent an influx of terrigenous material derived from extensive glaciation in the Southern Alps (Nelson et al., 1985), with low $CaCO_3$ content at those times supporting that view (Jarrett, 1985). Associated pollen data from 38.5 and 30 mbsf (Heusser and van de Geer, 1994) and from 49.3-36.9 mbsf (Prebble, 2012) are placed on this revised age model (Fig. 5.8).

Pollen data from DSDP Site 594 from Heusser and van de Geer (1994) and Prebble (2012) from 49-30 mbsf are placed on the revised age model (Fig. 5.8). The base of the pollen data is from late MIS 12a (428.5 ka) and is 18 kyr younger than that previously presented (Prebble, 2012). The transition from MIS 12a-MIS 11e is charcterised by rising podocarp-hardwoods as montane-subalpine shrubs (Asteraceae) decline, a sharp 1.5‰ decrease in $\delta^{18}O$, with a minor rise in foraminiferal-based SST. Tree fern spores, herb taxa and the montane-subalpine shrub *Coprosma* increase over MIS 11e-d, with a concomitant increase in dinocyst-based SSTs to modern values at 420 ka (Prebble et al., 2016). This follows rising SSTs in the ETS by ~5 kyr. Foraminiferal-based SSTs rise by 8°C to reach modern levels between 420-417 kyr (MIS 11c), and are associated with a rapid rise in podocarp-hardwood taxa to reach their highest values for the entire record (95%). Podocarp-hardwood pollen reduces rapidly from 405 ka, with herb taxa progressively increasing following MIS 11c (396 ka) to reach their greatest proportions over MIS 10a, and then decline as arboreal pollen rises over MIS 9e (Heusser and van de Geer, 1994).

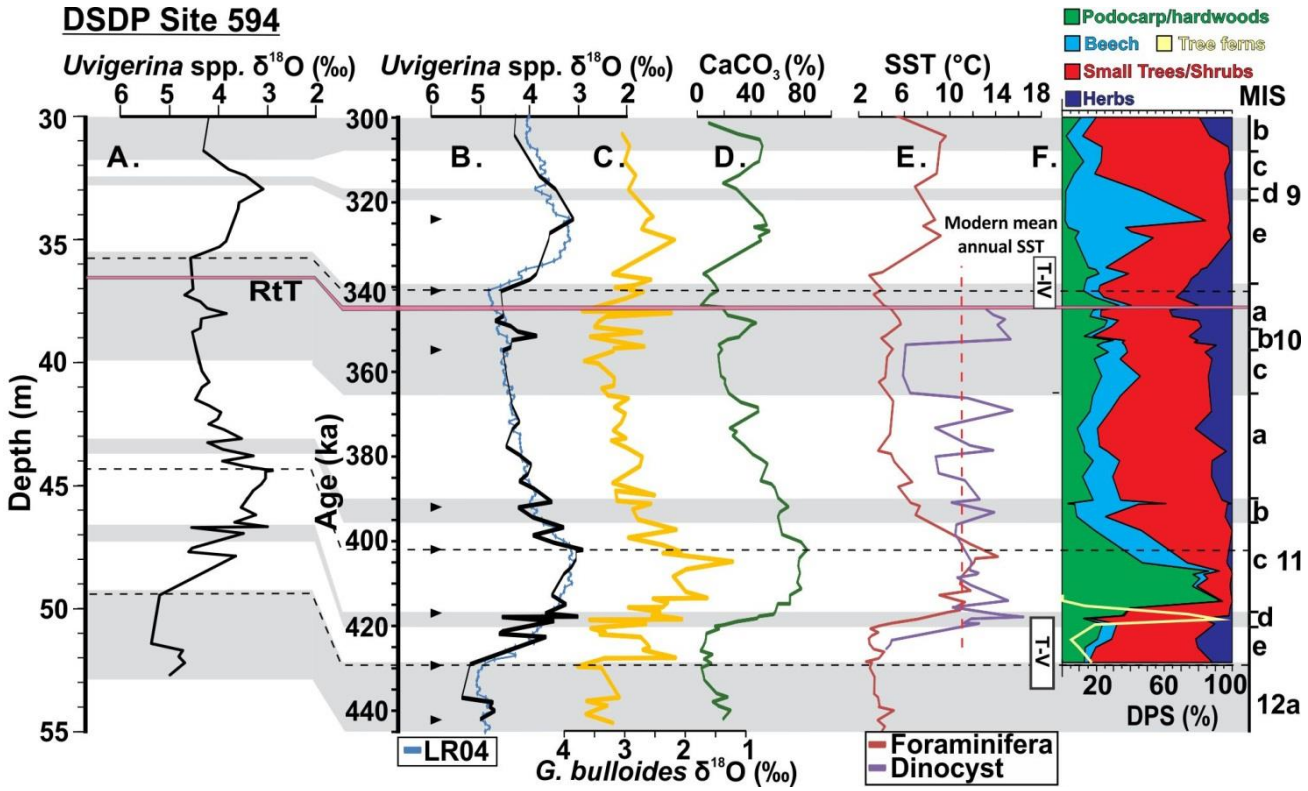

Supplementary Fig. 5.8: The revision of the DSDP-594 age model over the MIS 12-10 interval, and additional core properties. **A.** Down-core benthic $\delta^{18}O$ stratigraphy of DSDP-594 *Uvigerina* spp*;* **B.** $\delta^{18}O$ tie-points (black triangles) which align the down-core benthic $\delta^{18}O$ measurements from DSDP-594 to the reference LR04 benthic $\delta^{18}O$ stack in blue (Lisiecki and Raymo, 2005). Guidelines (dashed lines) illustrate this procedure; with MIS glacial boundaries displayed in grey (Railsback et al., 2015). The maximum concentration of RtT glass shards is displayed in pink at 36.5 cm (345 ka). **C.** $\delta^{18}O$ measurements for the planktic species *Globigerina bulloides*. **D.** $CaCO_3$ data from Jarrett (1985) **E.** Comparison of SST estimates from planktic foraminifera based on the artificial neural network (ANN) from (Hayward et al., 2008) and of ANN dinocysts from the same core (Prebble et al., 2016). **F.** Cumulative dryland pollen diagram of Heusser and van de Geer (1994) and Prebble (2012) placed on the revised DSDP 594 age model. Tree ferns are highlighted for T-V, and remain <15% for the rest of the interval displayed.

Calibration of Umuketai Bog radiocarbon dates and chronology

A revised chronology from the palynological record from Umuketai Bog was developed for this study from that previously presented (Newnham, 1989; Newnham and Alloway; 2001; 2004). This was equally undertaken by Matt Ryan and Andrew Rees in an attempt to better constrain the early Holocene vegetation succession in this record.

The eight original radiocarbon dates from Umutekai sediments were recalibrated with SHCal13 (Hogg et al., 2013), and an age-depth model was developed using a P_Sequence model (Suppl. Fig. 5.9; Bronk Ramsey, 2008) with a variable k parameter (Bronk Ramsey and Lee, 2013) in OxCal v4.2.4 (Bronk Ramsey, 2009a). The record includes several important tephra marker beds that were provisionally identified by Vince Neall based on their visual appearance and stratigraphic order based on the knowledge of tephrostratigraphy of the region. These important marker beds support the independent radiocarbon chronology at this site, and were included in development of the Umutekai chronology. Two ^{14}C ages undertaken at proximal sites are assigned to the deposition model on the basis of co-occurrence of tephra. The first (Wk451, 11050 ± 130 ^{14}C yr) was undertaken on organic lacustrine sediment straddling the Mahoe Tephra at 10.2 m (Hogg et al., 1987; Lowe, 1988); with the second the second on peat 3 cm below the Konini Tephra bed A at Durham Rd (NZA-5410A, 10450±200 ^{14}C yr), ~15 km SSE of the site (Alloway et al., 1992; Alloway et al., 1995).

Thirteen *R_combine* ages were calculated for horizons where multiple ^{14}C dates were obtained from measurements on wood, peat or lake sediment immediately bracketing four tephra horizons, described from additional sites (Alloway et al., 1995; Lowe et al., 2013). From bottom to top the depths of the provisional tephra horizons and number of dates are; Konini Tephra Bed B (9.35 cm, n=3); Tariki Tephra (6.6 m; n=3); Korito Tephra (5.6 m; n=3); and Inglewood Tephra (5.15 m; n=4). OxCal identified two ages as outliers (11.25 m, NZA-114) and (2.75 m, NZA-7562); these dates were retained though down-weighted in the model to highlight uncertainty.

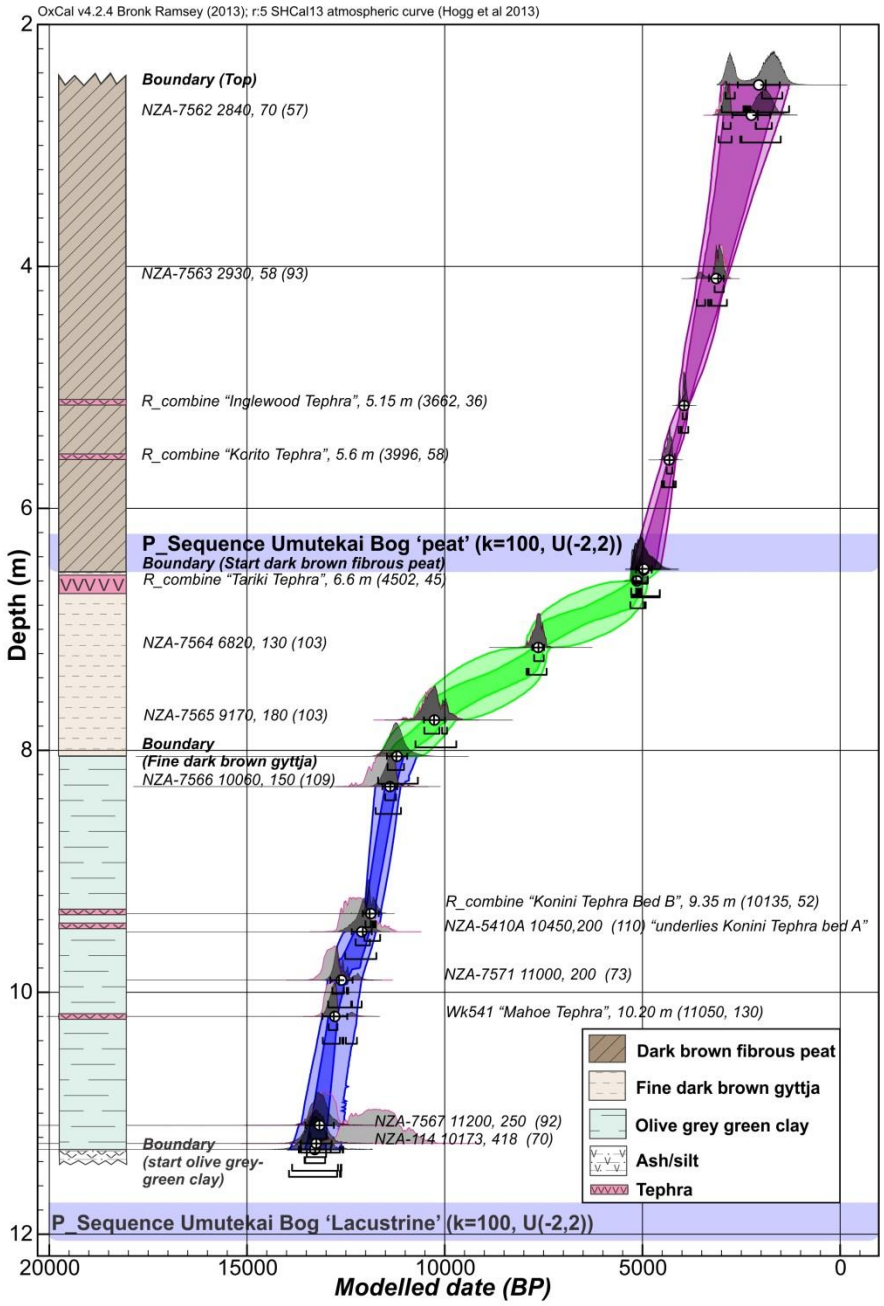

Supplementary Fig. 5.9: Age-model and core stratigraphy for the Umutekai Bog record based on twenty three ^{14}C dates from peat/lacustrine sediments. Eight ^{14}C ages are directly from the site, thirteen were measured immediately below and above four tephra horizons identified in other records (Konini bed B, Tariki, Korito and the Inglewood) with an *R_combine* produced for each. Two additional dates constrain the Mahoe Tephra and Konini Tephra bed A in nearby records, and were assigned to these tephra. A variable k value of 100 was applied, producing an A_{model} of 67%. The 68% and the 95% levels of confidence are shown, along with calendar age likelihood in dark pink and posterior probability density functions in dark grey. The laboratory number, followed by ^{14}C date, 1σ error, and sample agreements (in parentheses) are listed by each radiocarbon sample. The mean (white circle) and median ("bulls eye") values of the calibration distributions are pictured. The lithological change from olive grey green clay to fine dark brown gyttja is represented in the depositional model by a colour change from blue to green. A lithological change to dark brown fibrous peat marks a change in the sedimentation rate at the site and defines a second P_Sequence from lacustrine to peat deposition.

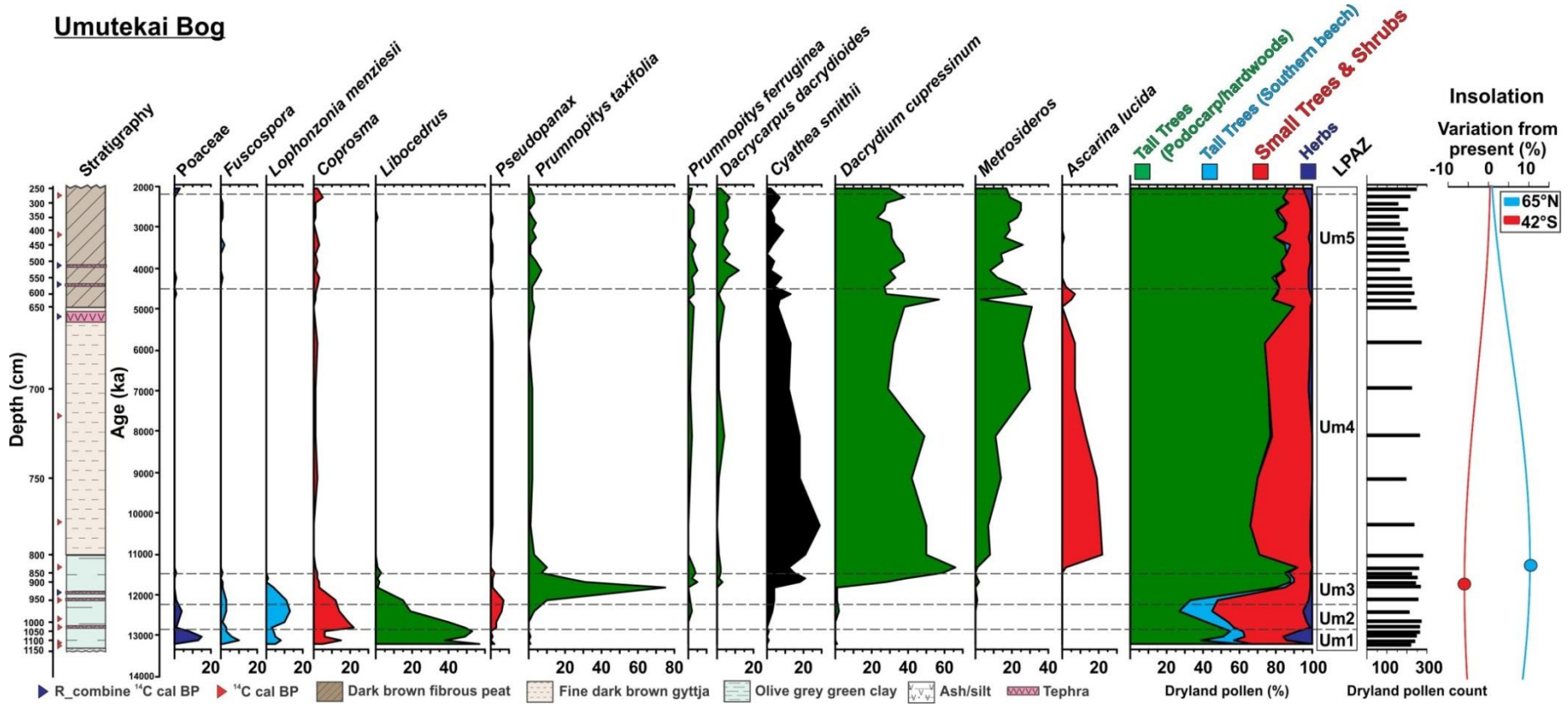

Supplementary Fig 5.10: Summary pollen diagram for selected taxa from Umutekai Bog for the late glacial to early Holocene (Newnham, 1989; Newnham and Alloway, 2001; 2004). The core stratigraphy for the 11.4 m record and location of ten calibrated AMS ^{14}C ages (red triangles) are shown on the left, with previously identified tephra horizons providing additional chronological control using their *R_combine* age (blue triangles) from additional sites. The relative percentages of main dryland pollen taxa are shown from left to right and are grouped into a cumulative dryland pollen diagram, which includes podocarp-hardwoods, beech, montane-subalpine trees and shrubs, and herbs. Notably high proportions of *Ascarina lucida* occur in the early Holocene under a reduced seasonality regime. The percentage of the tree fern *Cyathea smithii* is also shown, and is excluded from the dryland pollen sum. Dashed lines represent local pollen zones, which were established with CONISS. The insolation variation from present follows Laskar et al. (2004), with circles defining extrema

Appendix Two Supplementary Tables

Supplementary Table 3.1: Mean major element composition of glass shards from East Tasman Sea marine cores MD06-2991 and TAN0513-14 (Ryan et al., 2012), compared with selected South Island & offshore Kawakawa/Oruanui Tephra (KOT) correlatives

	SiO_2	Al_2O_3	TiO_2	FeO	MgO	MnO	CaO	Na_2O	K_2O	Cl	H_2O	*n*
MD06-2991 [a] (180.5 cm) (12-23-31; Nov 15th, 2012)	78.16 (0.15)	12.47 (0.10)	0.11 (0.02)	1.28 (0.06)	0.11 (0.01)	0.05 (0.02)	1.05 (0.07)	3.86 (0.13)	2.91 (0.11)	*nd* [b]	3.02 (0.54)	17
TAN0513-14 (43-47 cm) (11-5-1 to -3; May 18th, 2011)	78.50 (0.26)	12.55 (0.11)	0.12 (0.02)	1.19 (0.06)	0.12 (0.01)	0.05 (0.02)	1.00 (0.06)	3.42 (0.15)	3.07 (0.16)	*nd* [b]	3.87 (1.09)	46
Okarito Lagoon, south Westland [c]	78.04 (0.30)	12.65 (0.15)	0.14 (0.03)	1.13 (0.10)	0.13 (0.02)	0.06 (0.06)	1.02 (0.07)	3.34 (0.41)	3.27 (0.34)	0.20 (0.05)	5.05 (1.42)	20
Galway Tarn, south Westland [c]	77.75 (0.36)	12.59 (0.16)	0.13 (0.03)	1.13 (0.13)	0.13 (0.03)	0.08 (0.05)	1.04 (0.06)	3.79 (0.24)	3.06 (0.11)	0.23 (0.16)	4.40 (1.62)	20
31B, Motukarara, Banks Peninsula [a]	78.34 (0.17)	12.57 (0.10)	0.12 (0.02)	1.18 (0.05)	0.12 (0.02)	0.05 (0.02)	1.00 (0.06)	3.59 (0.12)	3.02 (0.12)	*nd*	4.60 (1.58)	23
AT-331, ODP Site 1123 1.01 mcd [d]	77.98 (0.29)	12.31 (0.12)	0.13 (0.03)	1.16 (0.08)	0.11 (0.02)	*nd*	1.07 (0.11)	3.98 (0.10)	3.05 (0.19)	0.15 (0.02)	4.23 (1.02)	15
Whangamata Road, TS [e] 50334-40 (T17/619830)	79.01 (0.38)	12.15 (0.30)	0.13 (0.03)	1.15 (0.19)	0.12 (0.02)	***nd***	1.05 (0.19)	3.31 (0.21)	3.07 (0.25)	*nd*	5.65 (1.62)	74

[a] All major element determinations were made on a JEOL Superprobe (JXA-8230) housed at Victoria University of Wellington, using the ZAF correction method. Analyses were performed using an accelerating voltage of 15 kV under a static electron beam operating at 8 nA. The electron beam was defocused to between 10 to 20 μm. All elements calculated on a water-free basis, with H_2O by difference from 100%. Total Fe expressed as FeO_t. Mean and ± 1 standard deviation (in parentheses), based on *n* analyses. All samples normalised against either glass standard VG-568 or ATHO-G. Analyst: B. V. Alloway. [b] Not determined or not available. Analyst and/or sources of analyses – [c] J.L. Horrocks in Newnham et al., 2007a; [d] Alloway et al. 2005; [e] P.C. Froggatt in Villamor et al. (Villamor et al., 2007).

Supplementary Table 4.1: Age-depth model and sampling resolution ($\delta^{18}O$ measurements, SST estimates and palynology) undertaken on MD06-2991.

MD06-2991						
MIS stage	**Age (kyr)**	**Depth (cm)**	**Sedimentation rate (cm/kyr)**	**$\delta^{18}O$ resolution**	**SST resolution**	**Palynology resolution**
1	14–0	105–0	7.5	2.3 kyr	0.4 kyr (top 9.7 kyr)	1.1 kyr
2	29–14	244–105	9.3	2.1 kyr	1.2 kyr	1.2 kyr
3	57–29	381–244	4.9	4 kyr	14 kyr	4 kyr
4	71–57	529–381	10.6	2 kyr	7 kyr	1.8 kyr
5a	85–71	622–529	6.6	1.8 kyr	3.5 kyr	1.5 kyr
5b	92–85	693–622	10.1	0.9 kyr	1.8 kyr	1 kyr
5c	105–92	808–693	8.8	1.2 kyr	2.6 kyr	1.2 kyr
5d	116–105	897–808	8.1	1 kyr	1 kyr	1 kyr
5e	130–116	962–897	4.6	0.9 kyr	1.1 kyr	1.1 kyr
6	158–130	1100–962	4.9	1.4 kyr	0.8 kyr (bottom 138 kyr)	1.3 kyr

Supplementary Table 4.2

Okarito Bog $\delta^{18}O$ chronology				
Okarito Bog depth (cm)	Okarito Bog age (ka)	lower age limit (ka)	upper age limit (ka)	sed. rate (cm/kyr)
725	99.5	97.9	101.0	0.00
735	101.0	99.5	102.3	6.38
745	102.6	101.0	103.9	6.38
755	104.2	102.6	105.2	6.38
765	105.2	104.2	108.0	9.26
775	108.0	105.3	109.4	3.55
782	111.1	108.4	112.4	2.32
801	116.3	113.8	117.2	3.65
805	116.5	116.3	117.9	17.39
810	117.9	117.1	118.8	3.60
815	119.3	118.5	120.2	3.60
820	120.7	119.9	121.6	3.60
825	122.1	120.7	122.5	3.60
829	122.5	121.8	122.9	8.11
830	122.7	121.9	123.0	8.11
832.1	123.0	122.8	123.4	6.31
833.2	123.2	123.1	123.6	5.25
834.2	123.4	123.2	124.1	5.25
835	124.1	123.4	124.1	1.19
835.1	124.1	123.7	124.2	2.40
836.3	124.6	124.2	124.7	2.40
837.3	125.0	124.6	125.1	2.40
838.4	125.5	125.1	125.5	2.40
839.4	125.9	125.5	126.0	2.40
840	126.2	125.7	126.2	2.40
840.4	126.3	125.9	126.4	2.40
841.5	126.8	126.3	126.8	2.40
842.5	127.2	126.8	127.2	2.40
843.5	127.5	127.2	127.9	3.80
844.6	127.6	127.3	128.0	9.18
845	127.6	127.4	128.0	9.18
850	128.6	128.1	129.1	4.98
852.9	129.5	128.6	129.8	3.42
855	129.8	129.0	130.7	7.76
860	130.4	129.6	131.3	7.76
865	131.0	130.4	132.7	7.76
875	132.7	131.0	139.3	6.13
885	139.3	132.7	141.4	1.51
901	141.4	139.3	141.8	7.58
905	141.8	140.3	143.3	10.43
915	142.8	141.2	144.2	10.43
925	143.7	142.2	145.2	10.43
935	144.7	143.7	147.3	10.43
939	147.3	146.6	148.7	1.55
940	147.9	147.3	149.3	1.55
941	148.6	147.9	150.0	1.55
941.5	148.9	148.6	149.1	1.55
943	149.1	148.7	149.5	6.31
945	149.4	149.0	149.8	6.31
955	151.0	150.6	151.4	6.31
962.5	152.2	151.8	152.6	6.31
965	152.6	152.2	153.0	6.31
968	153.1	152.6	153.6	6.31

Supplementary Table 5.1: Site location and analysis

Site	Location	Height (m)	RtT age (ka)	Proxy information	Reference
Marine records					
MD06-2990	42°19′S, 169°55′E	–943	345 ± 4	Pollen, SSTs, RtT	*This study*
MD06-2991	42°21´S, 169°59´E	–886	346 ± 4	Pollen, RtT	*This study*
MD06-2986	42°27´S, 167°54´E	-1477	absent	SSTs	Hayward et al., 2012
MD06-2988	42°21´S, 16°56´E	-1790	–	SSTs	Prebble et al., 2016
MD06-2989	42°06´S, 168°53´E	-1250	–	SSTs	Prebble et al., 2016
DSDP Site 594	45°31'S, 174°56'E	1204	344 ± 4	Pollen, SSTs, RtT	Prebble, 2012; Hayward et al., 2012, Prebble et al., 2016
ODP Site 1123	41°47'S, 171°30'W	-3290	absent	Pollen, SSTs	Mildenhall et al., 2004; Crundwell et al., 2008; Hayward et al., 2012
Terrestrial records					
Chatham Island	43°44’S, 176°17’E	16	350 ± 50 (1σ)	Pollen, RtT	Holt et al., 2010
Rangitawa Stream	40°07’S, 175°27’E	80	400 ± 90 (1σ)	Pollen, marine molluscs, plant macrofossils	McQueen, 1953;Seward, 1974; Bussell, 1986; Kohn et al., 1992
South Taranaki pollen site-1	39°30’S, 174°21’E	250	340 ± 30 (1σ)	Pollen, RtT	Kohn et al., 1992
Ohariu Valley	41°12’S, 174°46’E	80	220 ± 30 (1σ)	Pollen, RtT	Mildenhall et al., 1977
Umutekai Bog	39°5'S, 174° 8'E	90	N/A	Pollen, tephra	Newnham, 1990; Newnham and Alloway 2001; 2004
Climate Station					
New Plymouth Airport	39°0'S, 174°10'E	27	–	Cliamte data	NIWA, 2014c

Supplementary table 5.2: Sedimentation rate and sample resolution for marine cores

MD06-2990 (MIS 12-10)						
MIS stage	**Age (kyr)**	**Depth (cm)**	**Sedimentation rate (cm/kyr)**	**$\delta^{18}O$ resolution**	**SST resolution**	**Palynology resolution**
10a	346-338	940-898	6	0.3 kyr	4 kyr	4 kyr
10b	354–346	964-940	3	0.7 kyr	4 kyr	4 kyr
10c	365–354	997-964	3	0.7 kyr	11 kyr	11 kyr
11a	390–365	1095-997	4	0.5 kyr	4 kyr	4.2 kyr
11b	396–390	1137-1095	7	0.3 kyr	3 kyr	1.5 kyr
11c	417–396	1189-1137	2.5	0.8 kyr	10.5 kyr	4.2 kyr
11d	420–417	1195-1189	2	1 kyr	3 kyr	3 kyr
11e	428–420	1220-1195	3	0.6 kyr	8 kyr	2.7 kyr
12a	436–428	1264-1220	5.5	0.4 kyr	4 kyr	1.6 kyr
12b	456–436	1400-1264	6.8	0.3 kyr	1 sample	2.5 kyr

MD06-2991 (MIS 12-10)					
MIS stage	**Age (kyr)**	**Depth (cm)**	**Sedimentation rate (cm/kyr)**	**$\delta^{18}O$ resolution**	**Palynology resolution**
10a	346-338	2225-2160	8.7	2.7 kyr	2 kyr
10b	354–346	2300–2225	9.4	2 kyr	2.7 kyr
10c	365–354	2410–2300	10	1.8 kyr	1.8 kyr
11a	390–365	2630–2410	8.8	2.3 kyr	2.3 kyr
11b	396–390	2712–2630	13.7	1.2 kyr	1 kyr
11c	~404–396	2860–2712	24.6	0.5 kyr	0.5 kyr

DSDP 594 MIS (12-10)					
MIS stage	**Age (kyr)**	**Depth (cm)**	**Sedimentation rate (cm/kyr)**	**$\delta^{18}O$ resolution**	**Palynology resolution**
10	365–338	3998–3530	17.3	2.5 kyr	~2 kyr
11	428-365	4922-3998	14.7	2.2 kyr	~2.4 kyr
12	442–428	5271–4922	25	2.3 kyr	1 sample

Supplementary table 5.3: Mean major element composition of glass shards from MD06-2991 and DSDP-594, compared with selected offshore and onshore Rangitawa Tephra correlatives

	SiO_2	Al_2O_3	TiO_2	FeO	MgO	MnO	CaO	Na_2O	K_2O	Cl	H_2O	*n*
MD06-2991 [a], 2221-cm depth *(12-23-32; Nov 15th, 2012)*	77.47 (0.16)	12.44 (0.09)	0.14 (0.01)	1.09 (0.07)	0.10 (0.02)	0.03 (0.02)	0.78 (0.02)	3.67 (0.10)	4.28 (0.13)	*nd* [b]	2.23 (0.47)	20
DSDP-594, 36.5-m depth *(13-11-22; Sept 18th, 2013)*	77.86 (0.14)	12.38 (0.08)	0.14 (0.01)	1.07 (0.06)	0.10 (0.01)	0.04 (0.03)	0.79 (0.03)	3.33 (0.11)	4.27 (0.15)	0.02 (0.01)	3.96 (0.47)	20
ODP site 1124 [c], **24.00 mcd** (AT-413)	77.18 (0.24)	12.42 (0.14)	0.14 (0.04)	1.07 (0.07)	0.13 (0.04)	*nd* [b]	0.82 (0.05)	3.75 (0.08)	4.22 (0.10)	0.28 (0.03)	7.09 (0.51)	16
ODP site 1124 [c], **24.17 mcd** (AT-414)	78.47 (0.20)	12.43 (0.16)	0.12 (0.06)	1.07 (0.06)	0.12 (0.03)	*nd*	0.82 (0.04)	3.72 (0.16)	4.21 (0.17)	0.30 (0.03)	8.21 (0.51)	15
ODP site 1124 [c], **24.38 mcd** (AT-415)	78.76 (0.27)	12.35 (0.22)	0.14 (0.04)	1.05 (0.07)	0.11 (0.03)	*nd*	0.77 (0.06)	3.65 (0.14)	4.16 (0.19)	0.28 (0.03)	6.29 (0.59)	14
ODP site 1122 [c], **140 mcd** (AT-282)	77.75 (0.19)	12.34 (0.15)	0.13 (0.06)	1.03 (0.07)	0.11 (0.03)	*nd*	0.78 (0.06)	3.39 (0.07)	4.23 (0.16)	0.19 (0.02)	4.06 (0.47)	16
Chatham Islands [d] (KCh15)	77.32 (0.34)	12.14 (0.17)	0.19 (0.09)	1.00 (0.14)	0.09 (0.09)	0.06 (0.06)	0.78 (0.08)	3.65 (0.12)	4.51 (0.14)	0.25 (0.03)	6.39 (0.41)	16
Omahina Road [e], **Wanganui Basin** (BP-144)	78.03 (0.39)	12.13 (0.14)	0.15 (0.04)	1.03 (0.06)	0.12 (0.02)	*nd*	0.78 (0.06)	3.35 (0.22)	4.22 (0.15)	0.19 (0.04)	5.86 (0.14)	32
Rangitawa Stream TS [e], **Wanganui Basin** (BP-122)	77.34 (0.28)	12.21 (0.09)	0.14 (0.04)	1.04 (0.05)	0.12 (0.02)	*nd*	0.82 (0.03)	3.59 (0.17)	4.52 (0.16)	0.22 (0.02)	5.92 (0.61)	10
Foreman-Drury [f], **Wairarapa** (AT-350)	77.55 (0.25)	12.21 (0.08)	0.15 (0.07)	1.04 (0.08)	0.12 (0.03)	0.04 (0.04)	0.82 (0.11)	3.60 (0.10)	4.29 (0.15)	0.18 (0.03)	4.07 (0.59)	10
Glass Standards												
ATHO-G (Nov 15th, 2012)	75.59 (0.28)	12.20 (0.11)	0.23 (0.02)	3.27 (0.09)	0.09 (0.01)	0.11 (0.02)	1.70 (0.02)	3.75 (0.45)	2.64 (0.04)	*nd*	0.41 (0.66)	55
(Sept 18th, 2013)	75.61 (0.30)	12.18 (0.09)	0.24 (0.02)	3.29 (0.11)	0.10 (0.01)	0.10 (0.03)	1.70 (0.02)	3.73 (0.29)	2.64 (0.04)	*nd*	0.42 (0.44)	64

[a]All major element determinations were made on a JEOL Superprobe (JXA-8230) housed at Victoria University of Wellington, using the ZAF correction method. Analyses were performed using an accelerating voltage of 15 kV under a static electron beam operating at 8 nA. The electron beam was defocused between 10 and 20 μm. All elements calculated on a water-free basis, with H_2O by difference from 100%. Total Fe expressed as FeO_t. Mean and ± 1 standard deviation (in parentheses), based on *n* analyses. All samples normalised against glass standard ATHO-G. Analyst: B. V. Alloway. [b]Not determined or not available. Analyst and/or sources of analyses – [c] Alloway *et al.* 2005; [d] D.J. Lowe in Holt *et al*., 2010; [e] B.J. Pillans (*unpublished data*), and [f] Alloway in Nicol et al. (2002).

Supplementary table 5.4: DSDP Site 594 revised isotope stratigraphy

No:	Leg	Site	H	Cor	T	Sc	Top(cm)	Bot(cm)	Depth(mbsf)	Globigerina bulloides	Globigerina bulloides	Uvigerina spp	Uvigerina spp
										13/12-C	18/16-O	13/12-C	18/16-O
1	90	594	*	4	H	6	35	37	32.95	0.89	2.64	-0.73	3.08
2	90	594	*	4	H	6	63	65	33.23	0.69	2.72		
3	90	594	*	4	H	6	90	92	33.5	0.91	2.49	-0.02	3.57
4	90	594	*	4	H	6	115	117	33.75	0.63	2.18	-0.83	3.59
5	90	594	*	5	H	1	38	40	35.08	0.4	3.2	-0.41	3.84
6	90	594	*	5	H	1	60	62	35.3	0.66	2.57	-0.86	3.97
7	90	594	*	5	H	1	90	92	35.6	0.16	3.16		
8	90	594	*	5	H	1	140	142	36.1	0.48	2.98		
9	90	594	*	5	H	2	63	65	36.83	0.15	2.23		
10	90	594	*	5	H	3	10	12	37.8	0.44	2.72	-0.7	4.22
11	90	594	*	5	H	3	90	92	38.6	0.62	3.18	-0.77	4.36
12	90	594	*	5	H	3	140	142	39.1	0.11	3.44		
13	90	594	*	5	H	4	61	63	39.81	0.29	3.38		
14	90	594	*	5	H	4	90	92	40.1	0.55	2.94		
15	90	594	*	5	H	4	115	117	40.35	0.28	3.17	-1.15	4.33
16	90	594	*	5	H	5	10	12	40.8	1.07	3.06	-0.61	4.18
17	90	594	*	5	H	5	60	62	41.3	0.63	3.22		
18	90	594	*	5	H	6	10	12	42.3	0.59	3	-0.94	4.01
19	90	594	*	5	H	6	65	67	42.85	0.46	2.51		
20	90	594	*	5	H	6	90	92	43.1	0.3	2.57	-0.28	3.52
21	90	594	*	5	H	7	10	12	43.8	0.65	2.15	-0.28	3.28
22	90	594	A	1	H	3	10	12	44.4	0.41	2.07	-0.37	2.89
23	90	594	A	1	H	4	10	12	45.9	0.04	1.64	-0.43	3.53
24	90	594	A	1	H	4	25	27	46.05	-0.06	2.29		
25	90	594	A	1	H	4	40	42	46.2	0.34	2.37	-0.14	3.23
26	90	594	A	1	H	4	55	57	46.35	0.17	2.42		
27	90	594	A	1	H	4	70	72	46.5	0.31	2.55	0.29	3.66
28	90	594	A	1	H	4	88	90	46.68	0.06	2.06	-0.16	2.99
29	90	594	A	1	H	4	102	104	46.82	0.1	2.71		
30	90	594	A	1	H	4	115	117	46.95	-0.07	2.65	0.09	3.48
31	90	594	A	1	H	4	130	132	47.1	0.7	3.28		
32	90	594	A	1	H	5	10	12	47.4	-0.03	3.35		
33	90	594	A	1	H	5	25	27	47.55	0.24	3.41	-1.27	4.53
34	90	594	A	1	H	5	40	42	47.7	0	2.74	-1.16	4.6
35	90	594	A	1	H	5	85	87	48.15	0.33	2.62	-0.53	3.64
36	90	594	A	1	H	5	101	103	48.31	-0.1	2.59		
37	90	594	A	1	H	5	115	117	48.45	0.51	2.7		
38	90	594	A	1	H	6	10	12	48.9	0.33	2.16		
39	90	594	A	1	H	6	60	62	49.4	-0.37	3.78		

Appendix Three Exploring the source-to-sink residence time of terrestrial pollen deposited offshore Westland, New Zealand